

# SinCrys – a single crystal diffraction branch at DanMAX

*MASH session ID: maxiv\_sincrys\_00*

Peter Sondhauss

March 31, 2023

# Contents

<b>1</b>	<b>Introduction</b>	<b>39</b>
<b>2</b>	<b>Models used in the simulations</b>	<b>40</b>
2.1	Shadow heat flux . . . . .	40
2.2	Undulator scanning . . . . .	40
2.3	Thermoelastic model . . . . .	41
2.4	Boundary conditions . . . . .	42
2.4.1	Wet wall . . . . .	42
2.4.2	Solid-solid interface . . . . .	43
2.4.3	Free air convection . . . . .	43
2.4.4	Surface to ambient radiation . . . . .	43
2.4.5	Absorption of radiation . . . . .	43
2.5	Asymmetric diffraction focusing . . . . .	44
2.6	Autofocusing . . . . .	45
2.7	Lens design . . . . .	47
2.8	Transfocator . . . . .	49
2.8.1	Numbers of lens elements in thin lens approximation . . . . .	49
2.8.2	Transfocator as a thick lens . . . . .	51
2.8.3	An algorithm for design and optimization of transfocators . .	53
<b>I</b>	<b>Choice of beam splitter</b>	<b>55</b>
<b>3</b>	<b>Setup with Si333 beam splitter</b>	<b>56</b>
<b>4</b>	<b>Finite element analysis (FEA)</b>	<b>62</b>
4.1	Room temperature . . . . .	63
4.2	Cryogenic temperature . . . . .	67
<b>5</b>	<b>Parameter scan cases</b>	<b>73</b>
<b>6</b>	<b>Photon energy scan</b>	<b>75</b>
<b>7</b>	<b>Plots</b>	<b>77</b>
7.1	Statistics of incident irradiance . . . . .	77
7.2	Statistics of absorbed irradiance . . . . .	81
7.3	Statistics of temperature . . . . .	85
7.4	Statistics of mechanical stress (von Mises stress) . . . . .	86
7.5	Statistics of optical surface deformation . . . . .	86
7.6	Statistics of photon irradiance on optical surface . . . . .	87
7.7	Statistics of photon irradiance in beam cross section . . . . .	89
7.8	Absorbed irradiance on surface . . . . .	95
7.9	Incident spectral flux on surface . . . . .	100

7.10 Temperature on surface . . . . .	104
7.11 Mechanical stress (Von Mises stress) on surface . . . . .	106
7.12 Surface slope error in meridional direction (y) . . . . .	108
7.13 Incident photon irradiance on surface . . . . .	111
7.14 Photon irradiance in beam cross section . . . . .	114
7.15 Spectral photon flux in beam cross section . . . . .	115
<b>8 Setup with Si111 beam splitter</b>	<b>117</b>
<b>9 Finite element analysis (FEA)</b>	<b>123</b>
9.1 Room temperature . . . . .	123
9.2 Cryogenic temperature . . . . .	128
<b>10 Parameter scan cases</b>	<b>134</b>
<b>11 Photon energy scan</b>	<b>136</b>
<b>12 Plots</b>	<b>138</b>
12.1 Statistics of incident irradiance . . . . .	138
12.2 Statistics of absorbed irradiance . . . . .	139
12.3 Statistics of temperature . . . . .	140
12.4 Statistics of mechanical stress (von Mises stress) . . . . .	141
12.5 Statistics of optical surface deformation . . . . .	141
12.6 Statistics of photon irradiance on optical surface . . . . .	142
12.7 Statistics of photon irradiance in beam cross section . . . . .	144
12.8 Absorbed irradiance on surface . . . . .	150
12.9 Incident spectral flux on surface . . . . .	152
12.10 Temperature on surface . . . . .	153
12.11 Mechanical stress (Von Mises stress) on surface . . . . .	155
12.12 Surface slope error in meridional direction (y) . . . . .	157
12.13 Incident photon irradiance on surface . . . . .	160
12.14 Photon irradiance in beam cross section . . . . .	163
12.15 Spectral photon flux in beam cross section . . . . .	164
<b>13 Setup with diamond 111 beam splitter in Laue geometry</b>	<b>166</b>
<b>14 Finite element analysis (FEA)</b>	<b>172</b>
14.1 FEA with both 600 and 400 micron diamond filters in . . . . .	173
14.2 FEA with only 400 micron diamond filter in . . . . .	178
14.3 FEA with no diamond filters in . . . . .	183
<b>15 Parameter scan cases</b>	<b>189</b>
<b>16 Photon energy scan</b>	<b>192</b>
<b>17 Plots</b>	<b>197</b>
17.1 Statistics of incident irradiance . . . . .	197
17.2 Statistics of absorbed irradiance . . . . .	198
17.3 Statistics of temperature . . . . .	199
17.4 Statistics of mechanical stress (von Mises stress) . . . . .	200
17.5 Statistics of optical surface deformation . . . . .	200
17.6 Statistics of photon irradiance on optical surface . . . . .	201
17.7 Statistics of photon irradiance in beam cross section . . . . .	203
17.8 Absorbed irradiance on surface . . . . .	209
17.9 Incident spectral flux on surface . . . . .	212

17.10	Temperature on surface . . . . .	214
17.11	Mechanical stress (Von Mises stress) on surface . . . . .	217
17.12	Surface slope error in meridional direction (y) . . . . .	220
17.13	Incident photon irradiance on surface . . . . .	224
17.14	Photon irradiance in beam cross section . . . . .	229
17.15	Spectral photon flux in beam cross section . . . . .	233
<b>18</b>	<b>Setup with diamond 111 beam splitter in Bragg geometry</b>	<b>235</b>
<b>19</b>	<b>Finite element analysis (FEA)</b>	<b>241</b>
19.1	FEA with both 600 and 400 micron diamond filters in . . . . .	242
19.2	FEA with only 400 micron diamond filter in . . . . .	247
19.3	FEA with no diamond filters in . . . . .	252
<b>20</b>	<b>Parameter scan cases</b>	<b>258</b>
<b>21</b>	<b>Photon energy scan</b>	<b>259</b>
<b>22</b>	<b>Plots</b>	<b>264</b>
22.1	Statistics of incident irradiance . . . . .	264
22.2	Statistics of absorbed irradiance . . . . .	265
22.3	Statistics of temperature . . . . .	266
22.4	Statistics of mechanical stress (von Mises stress) . . . . .	267
22.5	Statistics of optical surface deformation . . . . .	267
22.6	Statistics of photon irradiance on optical surface . . . . .	268
22.7	Statistics of photon irradiance in beam cross section . . . . .	270
22.8	Absorbed irradiance on surface . . . . .	277
22.9	Incident spectral flux on surface . . . . .	280
22.10	Temperature on surface . . . . .	283
22.11	Mechanical stress (Von Mises stress) on surface . . . . .	287
22.12	Surface slope error in meridional direction (y) . . . . .	291
22.13	Incident photon irradiance on surface . . . . .	295
22.14	Photon irradiance in beam cross section . . . . .	299
22.15	Spectral photon flux in beam cross section . . . . .	302
<b>23</b>	<b>Discussion of results</b>	<b>304</b>
23.1	Silicon or diamond for the beam splitter . . . . .	304
23.2	Reduced filtering with diamond beam splitter . . . . .	304
23.3	Germanium or diamond for the second crystal . . . . .	305
<b>II</b>	<b>Beam splitters effect on main beam</b>	<b>306</b>
<b>24</b>	<b>Setup for the modelling of the transmitted main branch in the case of Laue geometry</b>	<b>307</b>
<b>25</b>	<b>Finite element analysis (FEA)</b>	<b>313</b>
25.1	FEA with both 600 and 400 micron diamond filters in . . . . .	313
25.2	FEA with only 400 micron diamond filter in . . . . .	318
25.3	FEA with no diamond filters in . . . . .	323
<b>26</b>	<b>Parameter scan cases</b>	<b>329</b>
<b>27</b>	<b>Photon energy scan</b>	<b>330</b>

<b>28 Plots</b>	<b>334</b>
28.1 Statistics of incident irradiance . . . . .	334
28.2 Statistics of absorbed irradiance . . . . .	335
28.3 Statistics of temperature . . . . .	336
28.4 Statistics of mechanical stress (von Mises stress) . . . . .	337
28.5 Statistics of optical surface deformation . . . . .	337
28.6 Statistics of photon irradiance on optical surface . . . . .	338
28.7 Statistics of photon irradiance in beam cross section . . . . .	343
28.8 Absorbed irradiance on surface . . . . .	354
28.9 Incident spectral flux on surface . . . . .	357
28.10 Temperature on surface . . . . .	359
28.11 Mechanical stress (Von Mises stress) on surface . . . . .	362
28.12 Surface slope error in meridional direction (y) . . . . .	365
28.13 Incident photon irradiance on surface . . . . .	368
28.14 Photon irradiance in beam cross section . . . . .	376
28.15 Spectral photon flux in beam cross section . . . . .	384
<b>29 Sharing the same harmonic in a Laue geometry beam splitter</b>	<b>388</b>
<b>30 Setup for the modelling of the transmitted main branch in the case of Bragg geometry</b>	<b>394</b>
<b>31 Finite element analysis (FEA)</b>	<b>400</b>
31.1 FEA with both 600 and 400 micron diamond filters in . . . . .	400
31.2 FEA with only 400 micron diamond filter in . . . . .	405
31.3 FEA with no diamond filters in . . . . .	410
<b>32 Parameter scan cases</b>	<b>416</b>
<b>33 Photon energy scan</b>	<b>417</b>
<b>34 Plots</b>	<b>421</b>
34.1 Statistics of incident irradiance . . . . .	421
34.2 Statistics of absorbed irradiance . . . . .	422
34.3 Statistics of temperature . . . . .	423
34.4 Statistics of mechanical stress (von Mises stress) . . . . .	424
34.5 Statistics of optical surface deformation . . . . .	424
34.6 Statistics of photon irradiance on optical surface . . . . .	425
34.7 Statistics of photon irradiance in beam cross section . . . . .	430
34.8 Absorbed irradiance on surface . . . . .	442
34.9 Incident spectral flux on surface . . . . .	445
34.10 Temperature on surface . . . . .	448
34.11 Mechanical stress (Von Mises stress) on surface . . . . .	452
34.12 Surface slope error in meridional direction (y) . . . . .	456
34.13 Incident photon irradiance on surface . . . . .	460
34.14 Photon irradiance in beam cross section . . . . .	469
34.15 Spectral photon flux in beam cross section . . . . .	477
<b>35 Discussion of results</b>	<b>481</b>
35.1 Absorption . . . . .	481
35.2 Refraction . . . . .	481

<b>III Focussing with CRLs</b>	<b>483</b>
<b>36 Focussing setup with beam splitter in Laue geometry</b>	<b>484</b>
<b>37 Parameter scan cases</b>	<b>494</b>
<b>38 Photon energy scan</b>	<b>497</b>
<b>39 Plots</b>	<b>500</b>
39.1 Statistics of incident irradiance . . . . .	500
39.2 Statistics of absorbed irradiance . . . . .	501
39.3 Statistics of temperature . . . . .	502
39.4 Statistics of mechanical stress (von Mises stress) . . . . .	503
39.5 Statistics of optical surface deformation . . . . .	503
39.6 Statistics of photon irradiance on optical surface . . . . .	504
39.7 Statistics of photon irradiance in beam cross section . . . . .	509
39.8 Absorbed irradiance on surface . . . . .	520
39.9 Incident spectral flux on surface . . . . .	521
39.10 Temperature on surface . . . . .	522
39.11 Mechanical stress (Von Mises stress) on surface . . . . .	523
39.12 Surface slope error in meridional direction (y) . . . . .	524
39.13 Incident photon irradiance on surface . . . . .	526
39.14 Photon irradiance in beam cross section . . . . .	530
39.15 Spectral photon flux in beam cross section . . . . .	532
<b>40 Focussing setup with beam splitter in Bragg geometry</b>	<b>535</b>
<b>41 Parameter scan cases</b>	<b>545</b>
<b>42 Photon energy scan</b>	<b>548</b>
<b>43 Plots</b>	<b>551</b>
43.1 Statistics of incident irradiance . . . . .	551
43.2 Statistics of absorbed irradiance . . . . .	552
43.3 Statistics of temperature . . . . .	553
43.4 Statistics of mechanical stress (von Mises stress) . . . . .	554
43.5 Statistics of optical surface deformation . . . . .	554
43.6 Statistics of photon irradiance on optical surface . . . . .	555
43.7 Statistics of photon irradiance in beam cross section . . . . .	560
43.8 Absorbed irradiance on surface . . . . .	572
43.9 Incident spectral flux on surface . . . . .	573
43.10 Temperature on surface . . . . .	575
43.11 Mechanical stress (Von Mises stress) on surface . . . . .	577
43.12 Surface slope error in meridional direction (y) . . . . .	579
43.13 Incident photon irradiance on surface . . . . .	581
43.14 Photon irradiance in beam cross section . . . . .	583
43.15 Spectral photon flux in beam cross section . . . . .	585
<b>44 Discussion of results</b>	<b>587</b>
44.1 Beam splitter in Laue geometry . . . . .	587
44.2 Beam splitter in Bragg geometry . . . . .	587

<b>IV Defocussing with CRLs</b>	<b>588</b>
<b>45 Focusing test setup with diamond 111 beam splitter in Laue geometry</b>	<b>589</b>
<b>46 Parameter scan cases</b>	<b>599</b>
<b>47 Photon energy scan</b>	<b>600</b>
<b>48 Plots</b>	<b>606</b>
48.1 Statistics of photon irradiance on optical surface . . . . .	606
48.2 Statistics of photon irradiance in beam cross section . . . . .	609
48.3 Incident photon irradiance on surface . . . . .	614
48.4 Photon irradiance in beam cross section . . . . .	616
48.5 Spectral photon flux in beam cross section . . . . .	619
<b>49 Focusing test setup with diamond 111 beam splitter in Bragg geometry</b>	<b>622</b>
<b>50 Parameter scan cases</b>	<b>632</b>
<b>51 Photon energy scan</b>	<b>633</b>
<b>52 Plots</b>	<b>639</b>
52.1 Statistics of photon irradiance on optical surface . . . . .	639
52.2 Statistics of photon irradiance in beam cross section . . . . .	642
52.3 Incident photon irradiance on surface . . . . .	647
52.4 Photon irradiance in beam cross section . . . . .	651
52.5 Spectral photon flux in beam cross section . . . . .	653
<b>53 Discussion of results</b>	<b>656</b>
53.1 Horizontal beam size . . . . .	656
53.2 Vertical beam size . . . . .	656
53.3 Flux . . . . .	656
<b>V High harmonic contamination</b>	<b>657</b>
<b>54 Higher harmonic test setup with diamond 111 beam splitter in Laue geometry</b>	<b>658</b>
<b>55 Parameter scan cases</b>	<b>667</b>
<b>56 Photon energy scan</b>	<b>669</b>
<b>57 Plots</b>	<b>671</b>
57.1 Flux at sample position with higher harmonic contamination . . . . .	671
<b>58 Higher harmonic test setup with diamond 111 beam splitter in Bragg geometry</b>	<b>672</b>
<b>59 Parameter scan cases</b>	<b>681</b>
<b>60 Photon energy scan</b>	<b>683</b>

<b>61</b>	<b>Plots</b>	<b>685</b>
61.1	Flux at sample position with higher harmonic contamination . . . . .	685
<b>62</b>	<b>Discussion of results</b>	<b>686</b>
62.1	Beam splitter in Laue geometry . . . . .	686
62.2	Beam splitter in Bragg geometry . . . . .	686

# List of Tables

3.1	Setup parameters common to all components. (*Glancing angle for mirrors, multilayers and crystals. Angle to surface normal otherwise.)	57
5.1	Parameter values for different cases in parameter scan	74
6.1	Scan values for different photon energies in energy scan	76
8.1	Setup parameters common to all components. (*Glancing angle for mirrors, multilayers and crystals. Angle to surface normal otherwise.)	118
10.1	Parameter values for different cases in parameter scan	135
11.1	Scan values for different photon energies in energy scan	137
13.1	Setup parameters common to all components. (*Glancing angle for mirrors, multilayers and crystals. Angle to surface normal otherwise.)	167
15.1	Parameter values for different cases in parameter scan	190
16.1	Scan values for different photon energies in energy scan	193
16.2	Scan values for different photon energies with diamond filters of 1000 micron total thickness in	194
16.3	Scan values for different photon energies with upstream diamond filter of 400 micron thickness in	195
16.4	Scan values for different photon energies with no upstream filters	196
18.1	Setup parameters common to all components. (*Glancing angle for mirrors, multilayers and crystals. Angle to surface normal otherwise.)	236
20.1	Parameter values for different cases in parameter scan	258
21.1	Scan values for different photon energies in energy scan	260
21.2	Scan values for different photon energies with diamond filters of 1000 micron total thickness in	261
21.3	Scan values for different photon energies with upstream diamond filter of 400 micron thickness in	262
21.4	Scan values for different photon energies with no upstream filters	263
24.1	Setup parameters common to all components. (*Glancing angle for mirrors, multilayers and crystals. Angle to surface normal otherwise.)	308
26.1	Parameter values for different cases in parameter scan	329
27.1	Scan values for different photon energies in energy scan	330

27.2	Scan values for different photon energies with diamond filters of 1000 micron total thickness in . . . . .	331
27.3	Scan values for different photon energies with upstream diamond filter of 400 micron thickness in . . . . .	332
27.4	Scan values for different photon energies with no upstream filters . . . . .	333
30.1	Setup parameters common to all components. (*Glancing angle for mirrors, multilayers and crystals. Angle to surface normal otherwise.)	395
32.1	Parameter values for different cases in parameter scan . . . . .	416
33.1	Scan values for different photon energies in energy scan . . . . .	417
33.2	Scan values for different photon energies with diamond filters of 1000 micron total thickness in . . . . .	418
33.3	Scan values for different photon energies with upstream diamond filter of 400 micron thickness in . . . . .	419
33.4	Scan values for different photon energies with no upstream filters . . . . .	420
36.1	Setup parameters common to all components. (*Glancing angle for mirrors, multilayers and crystals. Angle to surface normal otherwise.)	486
37.1	Parameter values for different cases in parameter scan . . . . .	495
38.1	Scan values for different photon energies in energy scan of setup without heat load . . . . .	498
38.2	Scan values for different photon energies in energy scan of setup with heat load . . . . .	499
40.1	Setup parameters common to all components. (*Glancing angle for mirrors, multilayers and crystals. Angle to surface normal otherwise.)	537
41.1	Parameter values for different cases in parameter scan . . . . .	546
42.1	Scan values for different photon energies in energy scan of setup without heat load . . . . .	549
42.2	Scan values for different photon energies in energy scan with heat load on the beam splitter. . . . .	550
45.1	Setup parameters common to all components. (*Glancing angle for mirrors, multilayers and crystals. Angle to surface normal otherwise.)	591
46.1	Parameter values for different cases in parameter scan . . . . .	599
47.1	Scan values for different photon energies in energy scan of case #1 (best focus) . . . . .	601
47.2	Scan values for different photon energies in energy scan of case #2 (5 × 5 microns) . . . . .	602
47.3	Scan values for different photon energies in energy scan of case #3 (15 × 15 microns) . . . . .	603
47.4	Scan values for different photon energies in energy scan of case #4 (100 × 100 microns) . . . . .	604
47.5	Scan values for different photon energies in energy scan of case #5 (unfocussed) . . . . .	605
49.1	Setup parameters common to all components. (*Glancing angle for mirrors, multilayers and crystals. Angle to surface normal otherwise.)	624

50.1 Parameter values for different cases in parameter scan . . . . .	632
51.1 Scan values for different photon energies in energy scan of case #1 (best focus) . . . . .	634
51.2 Scan values for different photon energies in energy scan of case #2 ( $5 \times 5$ microns) . . . . .	635
51.3 Scan values for different photon energies in energy scan of case #3 ( $15 \times 15$ microns) . . . . .	636
51.4 Scan values for different photon energies in energy scan of case #4 ( $100 \times 100$ microns) . . . . .	637
51.5 Scan values for different photon energies in energy scan of case #5 (unfocussed) . . . . .	638
54.1 Setup parameters common to all components. (*Glancing angle for mirrors, multilayers and crystals. Angle to surface normal otherwise.)	660
55.1 Parameter values for different cases in parameter scan . . . . .	667
56.1 Scan values for the 9th harmonic energy scan . . . . .	669
58.1 Setup parameters common to all components. (*Glancing angle for mirrors, multilayers and crystals. Angle to surface normal otherwise.)	674
59.1 Parameter values for different cases in parameter scan . . . . .	681
60.1 Scan values for different photon energies in energy scan . . . . .	683

# List of Figures

2.1	Point $S$ is a source point, points $A$ and $B$ are the points, where two rays originating from $S$ are reflected. $S'$ is the point where the symmetrically reflected rays appear to come from, i.e. a virtual source point. . . . .	44
2.2	Diffraction in Laue geometry from lattice planes perpendicular to the surface, which is strongly focusing. Diffraction in Laue geometry from lattice planes parallel to the surface is not possible, and hence always counts as asymmetric in a focusing context. . . . .	45
2.3	Beam phase diagram for a divergent beam, i.e. behind best focus. . . . .	46
2.4	Parabolic bi-concave lens element in CRL . . . . .	48
2.5	Cardinal points of an optical system with $N$ optical planes. . . . .	51
2.6	Simplified flowchart of the transfocator design and optimisation algorithm. . . . .	54
3.1	Schematic of optical setup . . . . .	57
4.1	Geometry [m] of optical element #03, for case #16, at 21800 eV photon energy setting. . . . .	63
4.2	Elastic boundary conditions on the surfaces of optical element #03, for case #16, at 21800 eV photon energy setting. Color legend: Blue: Surface can move freely in all directions. Cyan: Tension free kinematic mounting. Minimalistic constraint for three points in surface. One point is fixed, the second can move in one direction, and the third in two, in a fashion that defines angular orientation without introducing stress if the surface expands. . . . .	63
4.3	Thermal boundary conditions on the surfaces of optical element #03, for case #16, at 21800 eV photon energy setting. Color legend: Orange: No heat transfer at all. Blue: Heat transfer coefficient and temperature difference define heat current density, $j_q=h(T-T_{cool})$ . Red: Forced heat flux from e.g. absorbed X-rays. Cyan: Heat transfer coefficient and temperature difference define heat current density, $j_q=h*\Delta T$ (only at inner surfaces). . . . .	64
4.4	Heat transfer coefficient, $h$ [ $\text{W}/(\text{m}^2 \text{ K})$ ], on the surfaces of optical element #03, for case #16, at 21800 eV photon energy setting. . . . .	64
4.5	Absorbed irradiance, $p_{abs}$ [ $\text{W}/\text{m}^2$ ], on the surfaces of optical element #03, for case #16, at 21800 eV photon energy setting. . . . .	65
4.6	Temperature, $T$ [K], on the surfaces of optical element #03, for case #16, at 21800 eV photon energy setting. . . . .	65
4.7	Thermal conductivity, $\lambda$ [ $\text{W}/(\text{m K})$ ], on the surfaces of optical element #03, for case #16, at 21800 eV photon energy setting. . . . .	66
4.8	Von Mises stress, $\sigma$ [Pa], on the surfaces of optical element #03, for case #16, at 21800 eV photon energy setting. . . . .	66

4.9	Thermoelastic deformation, dz [m], on the surfaces of optical element #03, for case #16, at 21800 eV photon energy setting. . . . .	67
4.10	Geometry [m] of optical element #03, for case #26, at 21800 eV photon energy setting. . . . .	67
4.11	Elastic boundary conditions on the surfaces of optical element #03, for case #26, at 21800 eV photon energy setting. Color legend: Blue: Surface can move freely in all directions. Cyan: Tension free kinematic mounting. Minimalistic constraint for three points in surface. One point is fixed, the second can move in one direction, and the third in two, in a fashion that defines angular orientation without introducing stress if the surface expands. . . . .	68
4.12	Thermal boundary conditions on the surfaces of optical element #03, for case #26, at 21800 eV photon energy setting. Color legend: Orange: No heat transfer at all. Blue: Heat transfer coefficient and temperature difference define heat current density, $j_q=h(T-T_{cool})$ . Red: Forced heat flux from e.g. absorbed X-rays. Cyan: Heat transfer coefficient and temperature difference define heat current density, $j_q=h^*\Delta T$ (only at inner surfaces). . . . .	69
4.13	Heat transfer coefficient, h [W/(m <sup>2</sup> K)], on the surfaces of optical element #03, for case #26, at 21800 eV photon energy setting. . . . .	69
4.14	Absorbed irradiance, p_abs [W/m <sup>2</sup> ], on the surfaces of optical element #03, for case #26, at 21800 eV photon energy setting. . . . .	70
4.15	Temperature, T [K], on the surfaces of optical element #03, for case #26, at 21800 eV photon energy setting. . . . .	70
4.16	Thermal conductivity, lambda [W/(m K)], on the surfaces of optical element #03, for case #26, at 21800 eV photon energy setting. . . . .	71
4.17	Von Mises stress, sigma [Pa], on the surfaces of optical element #03, for case #26, at 21800 eV photon energy setting. . . . .	71
4.18	Thermoelastic deformation, dz [m], on the surfaces of optical element #03, for case #26, at 21800 eV photon energy setting. . . . .	72
7.1	Incident peak irradiance of screen #01 belonging to optical element #01. . . . .	77
7.2	Incident peak irradiance of screen #01 belonging to optical element #02 (Filter). . . . .	78
7.3	Incident peak irradiance of screen #02 belonging to optical element #02 (Filter). . . . .	78
7.4	Incident peak irradiance of optical element #03 (BS). . . . .	79
7.5	Incident flux of screen #01 belonging to optical element #01. . . . .	79
7.6	Incident flux of screen #01 belonging to optical element #02 (Filter). . . . .	80
7.7	Incident flux of screen #02 belonging to optical element #02 (Filter). . . . .	80
7.8	Incident flux of optical element #03 (BS). . . . .	81
7.9	Absorbed peak irradiance of screen #01 belonging to optical element #01. . . . .	81
7.10	Absorbed peak irradiance of screen #01 belonging to optical element #02 (Filter). . . . .	82
7.11	Absorbed peak irradiance of screen #02 belonging to optical element #02 (Filter). . . . .	82
7.12	Absorbed peak irradiance of optical element #03 (BS). . . . .	83
7.13	Absorbed flux of screen #01 belonging to optical element #01. . . . .	83
7.14	Absorbed flux of screen #01 belonging to optical element #02 (Filter). . . . .	84
7.15	Absorbed flux of screen #02 belonging to optical element #02 (Filter). . . . .	84

7.16	Absorbed flux of optical element #03 (BS). . . . .	85
7.17	Peak temperature of optical element #03 (BS). . . . .	85
7.18	Peak mechanical stress (Von Mises stress) of optical element #03 (BS). . . . .	86
7.19	Peak deformation of optical element #03 (BS). . . . .	86
7.20	Sagittal footprint diameter (FWHM) of optical element #04 (CM2). . . . .	87
7.21	Meridional footprint diameter (FWHM) of optical element #04 (CM2). . . . .	87
7.22	Incident photon flux on surface of optical element #04 (CM2). . . . .	88
7.23	Sagittal coordinate of footprint's centre of 'gravity' on surface of optical element #04 (CM2). . . . .	88
7.24	Meridional coordinate of footprint's centre of 'gravity' on surface of optical element #04 (CM2). . . . .	89
7.25	Sagittal beam diameter (FWHM) of optical element #04 (CM2). . . . .	89
7.26	Meridional beam diameter (FWHM) of optical element #04 (CM2). . . . .	90
7.27	Photon flux in beam cross section of optical element #04 (CM2). . . . .	90
7.28	Sagittal coordinate of beam's centre of 'gravity' in beam cross section of optical element #04 (CM2). . . . .	91
7.29	Meridional coordinate of beam's centre of 'gravity' in beam cross section of optical element #04 (CM2). . . . .	91
7.30	Sagittal beam divergence (FWHM) of optical element #04 (CM2). . . . .	92
7.31	Meridional beam divergence (FWHM) of optical element #04 (CM2). . . . .	92
7.32	Photon flux in beam cross section of optical element #04 (CM2). . . . .	93
7.33	Sagittal coordinate of beam's centre of 'gravity' in angle space of optical element #04 (CM2). . . . .	93
7.34	Meridional coordinate of beam's centre of 'gravity' in angle space of optical element #04 (CM2). . . . .	94
7.35	Bandwidth (FWHM) in beam cross section of optical element #04 (CM2). . . . .	94
7.36	Absorbed irradiance on surface of screen #01 belonging to optical element #01 for case #16 for 21800 eV photon energy setting. . . . .	95
7.37	Absorbed irradiance on surface of screen #01 belonging to optical element #01 for case #26 for 21800 eV photon energy setting. . . . .	95
7.38	Absorbed irradiance on surface of screen #01 belonging to optical element #02 (Filter) for case #16 for 21800 eV photon energy setting. . . . .	96
7.39	Absorbed irradiance on surface of screen #01 belonging to optical element #02 (Filter) for case #26 for 21800 eV photon energy setting. . . . .	96
7.40	Absorbed irradiance on surface of screen #02 belonging to optical element #02 (Filter) for case #16 for 21800 eV photon energy setting. . . . .	97
7.41	Absorbed irradiance on surface of screen #02 belonging to optical element #02 (Filter) for case #26 for 21800 eV photon energy setting. . . . .	97
7.42	Absorbed irradiance on surface of optical element #03 (BS) for case #16 for 21800 eV photon energy setting. . . . .	98
7.43	Absorbed irradiance on surface of optical element #03 (BS) for case #26 for 21800 eV photon energy setting. . . . .	99
7.44	Incident spectral flux on surface of screen #01 belonging to optical element #01 for case #16 for 21800 eV photon energy setting. . . . .	100
7.45	Incident spectral flux on surface of screen #01 belonging to optical element #01 for case #26 for 21800 eV photon energy setting. . . . .	100
7.46	Incident spectral flux on surface of screen #01 belonging to optical element #02 (Filter) for case #16 for 21800 eV photon energy setting. .	101
7.47	Incident spectral flux on surface of screen #01 belonging to optical element #02 (Filter) for case #26 for 21800 eV photon energy setting. .	101

7.48	Incident spectral flux on surface of screen #02 belonging to optical element #02 (Filter) for case #16 for 21800 eV photon energy setting.	102
7.49	Incident spectral flux on surface of screen #02 belonging to optical element #02 (Filter) for case #26 for 21800 eV photon energy setting.	102
7.50	Incident spectral flux on surface of optical element #03 (BS) for case #16 for 21800 eV photon energy setting. . . . .	103
7.51	Incident spectral flux on surface of optical element #03 (BS) for case #26 for 21800 eV photon energy setting. . . . .	103
7.52	Temperature on surface of optical element #03 (BS) for case #16 for 21800 eV photon energy setting. . . . .	104
7.53	Temperature on surface of optical element #03 (BS) for case #26 for 21800 eV photon energy setting. . . . .	105
7.54	Mechanical stress (Von Mises stress) on surface of optical element #03 (BS) for case #16 for 21800 eV photon energy setting. . . . .	106
7.55	Mechanical stress (Von Mises stress) on surface of optical element #03 (BS) for case #26 for 21800 eV photon energy setting. . . . .	107
7.56	Surface slope error in meridional direction (y) of optical element #03 (BS) for case #16 for 21800 eV photon energy setting. . . . .	108
7.57	Surface slope error in meridional direction (y) of optical element #03 (BS) for case #26 for 21800 eV photon energy setting. . . . .	109
7.58	Incident photon irradiance on surface of optical element #04 (CM2) for case #6 for 21800 eV photon energy setting. . . . .	111
7.59	Incident photon irradiance on surface of optical element #04 (CM2) for case #16 for 21800 eV photon energy setting. . . . .	112
7.60	Incident photon irradiance on surface of optical element #04 (CM2) for case #26 for 21800 eV photon energy setting. . . . .	113
7.61	Photon irradiance in beam cross section of optical element #04 (CM2) for case #6 for 21800 eV photon energy setting. . . . .	114
7.62	Photon irradiance in beam cross section of optical element #04 (CM2) for case #16 for 21800 eV photon energy setting. . . . .	114
7.63	Photon irradiance in beam cross section of optical element #04 (CM2) for case #26 for 21800 eV photon energy setting. . . . .	115
7.64	Spectral photon flux in beam cross section of optical element #04 (CM2) for case #6 for 21800 eV photon energy setting. . . . .	115
7.65	Spectral photon flux in beam cross section of optical element #04 (CM2) for case #16 for 21800 eV photon energy setting. . . . .	116
7.66	Spectral photon flux in beam cross section of optical element #04 (CM2) for case #26 for 21800 eV photon energy setting. . . . .	116
8.1	Schematic of optical setup . . . . .	118
9.1	Geometry [m] of optical element #03, for case #14, at 21800 eV photon energy setting. . . . .	123
9.2	Elastic boundary conditions on the surfaces of optical element #03, for case #14, at 21800 eV photon energy setting. Color legend: Blue: Surface can move freely in all directions. Cyan: Tension free kinematic mounting. Minimalistic constraint for three points in surface. One point is fixed, the second can move in one direction, and the third in two, in a fashion that defines angular orientation without introducing stress if the surface expands. . . . .	124

9.3	Thermal boundary conditions on the surfaces of optical element #03, for case #14, at 21800 eV photon energy setting. Color legend: Orange: No heat transfer at all. Blue: Heat transfer coefficient and temperature difference define heat current density, $j_q=h(T-T_{cool})$ . Red: Forced heat flux from e.g. absorbed X-rays. Cyan: Heat transfer coefficient and temperature difference define heat current density, $j_q=h^*\Delta T$ (only at inner surfaces). . . . .	125
9.4	Heat transfer coefficient, $h$ [W/(m <sup>2</sup> K)], on the surfaces of optical element #03, for case #14, at 21800 eV photon energy setting. . . . .	125
9.5	Absorbed irradiance, $p_{abs}$ [W/m <sup>2</sup> ], on the surfaces of optical element #03, for case #14, at 21800 eV photon energy setting. . . . .	126
9.6	Temperature, $T$ [K], on the surfaces of optical element #03, for case #14, at 21800 eV photon energy setting. . . . .	126
9.7	Thermal conductivity, $\lambda$ [W/(m K)], on the surfaces of optical element #03, for case #14, at 21800 eV photon energy setting. . . . .	127
9.8	Von Mises stress, $\sigma$ [Pa], on the surfaces of optical element #03, for case #14, at 21800 eV photon energy setting. . . . .	127
9.9	Thermoelastic deformation, $dz$ [m], on the surfaces of optical element #03, for case #14, at 21800 eV photon energy setting. . . . .	128
9.10	Geometry [m] of optical element #03, for case #24, at 21800 eV photon energy setting. . . . .	128
9.11	Elastic boundary conditions on the surfaces of optical element #03, for case #24, at 21800 eV photon energy setting. Color legend: Blue: Surface can move freely in all directions. Cyan: Tension free kinematic mounting. Minimalistic constraint for three points in surface. One point is fixed, the second can move in one direction, and the third in two, in a fashion that defines angular orientation without introducing stress if the surface expands. . . . .	129
9.12	Thermal boundary conditions on the surfaces of optical element #03, for case #24, at 21800 eV photon energy setting. Color legend: Orange: No heat transfer at all. Blue: Heat transfer coefficient and temperature difference define heat current density, $j_q=h(T-T_{cool})$ . Red: Forced heat flux from e.g. absorbed X-rays. Cyan: Heat transfer coefficient and temperature difference define heat current density, $j_q=h^*\Delta T$ (only at inner surfaces). . . . .	130
9.13	Heat transfer coefficient, $h$ [W/(m <sup>2</sup> K)], on the surfaces of optical element #03, for case #24, at 21800 eV photon energy setting. . . . .	130
9.14	Absorbed irradiance, $p_{abs}$ [W/m <sup>2</sup> ], on the surfaces of optical element #03, for case #24, at 21800 eV photon energy setting. . . . .	131
9.15	Temperature, $T$ [K], on the surfaces of optical element #03, for case #24, at 21800 eV photon energy setting. . . . .	131
9.16	Thermal conductivity, $\lambda$ [W/(m K)], on the surfaces of optical element #03, for case #24, at 21800 eV photon energy setting. . . . .	132
9.17	Von Mises stress, $\sigma$ [Pa], on the surfaces of optical element #03, for case #24, at 21800 eV photon energy setting. . . . .	132
9.18	Thermoelastic deformation, $dz$ [m], on the surfaces of optical element #03, for case #24, at 21800 eV photon energy setting. . . . .	133
12.1	Incident peak irradiance of optical element #03 (BS). . . . .	138
12.2	Incident flux of optical element #03 (BS). . . . .	139
12.3	Absorbed peak irradiance of optical element #03 (BS). . . . .	139
12.4	Absorbed flux of optical element #03 (BS). . . . .	140
12.5	Peak temperature of optical element #03 (BS). . . . .	140

12.6 Peak mechanical stress (Von Mises stress) of optical element #03 (BS). . . . .	141
12.7 Peak deformation of optical element #03 (BS). . . . .	141
12.8 Sagittal footprint diameter (FWHM) of optical element #04 (CM2). . . . .	142
12.9 Meridional footprint diameter (FWHM) of optical element #04 (CM2). . . . .	142
12.10 Incident photon flux on surface of optical element #04 (CM2). . . . .	143
12.11 Sagittal coordinate of footprint's centre of 'gravity' on surface of optical element #04 (CM2). . . . .	143
12.12 Meridional coordinate of footprint's centre of 'gravity' on surface of optical element #04 (CM2). . . . .	144
12.13 Sagittal beam diameter (FWHM) of optical element #04 (CM2). . . . .	144
12.14 Meridional beam diameter (FWHM) of optical element #04 (CM2). . . . .	145
12.15 Photon flux in beam cross section of optical element #04 (CM2). . . . .	145
12.16 Sagittal coordinate of beam's centre of 'gravity' in beam cross section of optical element #04 (CM2). . . . .	146
12.17 Meridional coordinate of beam's centre of 'gravity' in beam cross section of optical element #04 (CM2). . . . .	146
12.18 Sagittal beam divergence (FWHM) of optical element #04 (CM2). . . . .	147
12.19 Meridional beam divergence (FWHM) of optical element #04 (CM2). . . . .	147
12.20 Photon flux in beam cross section of optical element #04 (CM2). . . . .	148
12.21 Sagittal coordinate of beam's centre of 'gravity' in angle space of optical element #04 (CM2). . . . .	148
12.22 Meridional coordinate of beam's centre of 'gravity' in angle space of optical element #04 (CM2). . . . .	149
12.23 Bandwidth (FWHM) in beam cross section of optical element #04 (CM2). . . . .	149
12.24 Absorbed irradiance on surface of optical element #03 (BS) for case #14 for 21800 eV photon energy setting. . . . .	150
12.25 Absorbed irradiance on surface of optical element #03 (BS) for case #24 for 21800 eV photon energy setting. . . . .	151
12.26 Incident spectral flux on surface of optical element #03 (BS) for case #14 for 21800 eV photon energy setting. . . . .	152
12.27 Incident spectral flux on surface of optical element #03 (BS) for case #24 for 21800 eV photon energy setting. . . . .	152
12.28 Temperature on surface of optical element #03 (BS) for case #14 for 21800 eV photon energy setting. . . . .	153
12.29 Temperature on surface of optical element #03 (BS) for case #24 for 21800 eV photon energy setting. . . . .	154
12.30 Mechanical stress (Von Mises stress) on surface of optical element #03 (BS) for case #14 for 21800 eV photon energy setting. . . . .	155
12.31 Mechanical stress (Von Mises stress) on surface of optical element #03 (BS) for case #24 for 21800 eV photon energy setting. . . . .	156
12.32 Surface slope error in meridional direction (y) of optical element #03 (BS) for case #14 for 21800 eV photon energy setting. . . . .	157
12.33 Surface slope error in meridional direction (y) of optical element #03 (BS) for case #24 for 21800 eV photon energy setting. . . . .	158
12.34 Incident photon irradiance on surface of optical element #04 (CM2) for case #4 for 21800 eV photon energy setting. . . . .	160
12.35 Incident photon irradiance on surface of optical element #04 (CM2) for case #14 for 21800 eV photon energy setting. . . . .	161
12.36 Incident photon irradiance on surface of optical element #04 (CM2) for case #24 for 21800 eV photon energy setting. . . . .	162

12.37	Photon irradiance in beam cross section of optical element #04 (CM2) for case #4 for 21800 eV photon energy setting.	163
12.38	Photon irradiance in beam cross section of optical element #04 (CM2) for case #14 for 21800 eV photon energy setting.	163
12.39	Photon irradiance in beam cross section of optical element #04 (CM2) for case #24 for 21800 eV photon energy setting.	164
12.40	Spectral photon flux in beam cross section of optical element #04 (CM2) for case #4 for 21800 eV photon energy setting.	164
12.41	Spectral photon flux in beam cross section of optical element #04 (CM2) for case #14 for 21800 eV photon energy setting.	165
12.42	Spectral photon flux in beam cross section of optical element #04 (CM2) for case #24 for 21800 eV photon energy setting.	165
13.1	Schematic of optical setup	167
14.1	Geometry [m] of optical element #03, for case #16, at 21800 eV photon energy setting.	173
14.2	Elastic boundary conditions on the surfaces of optical element #03, for case #16, at 21800 eV photon energy setting. Color legend: Blue: Surface can move freely in all directions. Cyan: Tension free kine- matic mounting. Minimalistic constraint for three points in surface. One point is fixed, the second can move in one direction, and the third in two, in a fashion that defines angular orientation without introducing stress if the surface expands.	174
14.3	Thermal boundary conditions on the surfaces of optical element #03, for case #16, at 21800 eV photon energy setting. Color legend: Or- ange: No heat transfer at all. Blue: Heat transfer coefficient and temperature difference define heat current density, $j_q=h(T-T_{cool})$ . Red: Forced heat flux from e.g. absorbed X-rays. Cyan: Heat trans- fer coefficient and temperature difference define heat current density, $j_q=h^*\Delta_T$ (only at inner surfaces).	175
14.4	Heat transfer coefficient, $h$ [ $\text{W}/(\text{m}^2 \text{ K})$ ], on the surfaces of optical element #03, for case #16, at 21800 eV photon energy setting.	175
14.5	Absorbed irradiance, $p_{abs}$ [ $\text{W}/\text{m}^2$ ], on the surfaces of optical ele- ment #03, for case #16, at 21800 eV photon energy setting.	176
14.6	Temperature, $T$ [K], on the surfaces of optical element #03, for case #16, at 21800 eV photon energy setting.	176
14.7	Thermal conductivity, $\lambda$ [ $\text{W}/(\text{m K})$ ], on the surfaces of optical element #03, for case #16, at 21800 eV photon energy setting.	177
14.8	Von Mises stress, $\sigma$ [Pa], on the surfaces of optical element #03, for case #16, at 21800 eV photon energy setting.	177
14.9	Thermoelastic deformation, $dz$ [m], on the surfaces of optical element #03, for case #16, at 21800 eV photon energy setting.	178
14.10	Geometry [m] of optical element #03, for case #26, at 21800 eV photon energy setting.	178
14.11	Elastic boundary conditions on the surfaces of optical element #03, for case #26, at 21800 eV photon energy setting. Color legend: Blue: Surface can move freely in all directions. Cyan: Tension free kine- matic mounting. Minimalistic constraint for three points in surface. One point is fixed, the second can move in one direction, and the third in two, in a fashion that defines angular orientation without introducing stress if the surface expands.	179

14.12 Thermal boundary conditions on the surfaces of optical element #03, for case #26, at 21800 eV photon energy setting. Color legend: Orange: No heat transfer at all. Blue: Heat transfer coefficient and temperature difference define heat current density, $j_q=h(T-T_{cool})$ . Red: Forced heat flux from e.g. absorbed X-rays. Cyan: Heat transfer coefficient and temperature difference define heat current density, $j_q=h^*\Delta T$ (only at inner surfaces). . . . .	180
14.13 Heat transfer coefficient, $h$ [W/(m <sup>2</sup> K)], on the surfaces of optical element #03, for case #26, at 21800 eV photon energy setting. . . . .	180
14.14 Absorbed irradiance, $p_{abs}$ [W/m <sup>2</sup> ], on the surfaces of optical element #03, for case #26, at 21800 eV photon energy setting. . . . .	181
14.15 Temperature, $T$ [K], on the surfaces of optical element #03, for case #26, at 21800 eV photon energy setting. . . . .	181
14.16 Thermal conductivity, $\lambda$ [W/(m K)], on the surfaces of optical element #03, for case #26, at 21800 eV photon energy setting. . . . .	182
14.17 Von Mises stress, $\sigma$ [Pa], on the surfaces of optical element #03, for case #26, at 21800 eV photon energy setting. . . . .	182
14.18 Thermoelastic deformation, $dz$ [m], on the surfaces of optical element #03, for case #26, at 21800 eV photon energy setting. . . . .	183
14.19 Geometry [m] of optical element #03, for case #36, at 21800 eV photon energy setting. . . . .	183
14.20 Elastic boundary conditions on the surfaces of optical element #03, for case #36, at 21800 eV photon energy setting. Color legend: Blue: Surface can move freely in all directions. Cyan: Tension free kinematic mounting. Minimalistic constraint for three points in surface. One point is fixed, the second can move in one direction, and the third in two, in a fashion that defines angular orientation without introducing stress if the surface expands. . . . .	184
14.21 Thermal boundary conditions on the surfaces of optical element #03, for case #36, at 21800 eV photon energy setting. Color legend: Orange: No heat transfer at all. Blue: Heat transfer coefficient and temperature difference define heat current density, $j_q=h(T-T_{cool})$ . Red: Forced heat flux from e.g. absorbed X-rays. Cyan: Heat transfer coefficient and temperature difference define heat current density, $j_q=h^*\Delta T$ (only at inner surfaces). . . . .	185
14.22 Heat transfer coefficient, $h$ [W/(m <sup>2</sup> K)], on the surfaces of optical element #03, for case #36, at 21800 eV photon energy setting. . . . .	185
14.23 Absorbed irradiance, $p_{abs}$ [W/m <sup>2</sup> ], on the surfaces of optical element #03, for case #36, at 21800 eV photon energy setting. . . . .	186
14.24 Temperature, $T$ [K], on the surfaces of optical element #03, for case #36, at 21800 eV photon energy setting. . . . .	186
14.25 Thermal conductivity, $\lambda$ [W/(m K)], on the surfaces of optical element #03, for case #36, at 21800 eV photon energy setting. . . . .	187
14.26 Von Mises stress, $\sigma$ [Pa], on the surfaces of optical element #03, for case #36, at 21800 eV photon energy setting. . . . .	187
14.27 Thermoelastic deformation, $dz$ [m], on the surfaces of optical element #03, for case #36, at 21800 eV photon energy setting. . . . .	188
17.1 Incident peak irradiance of optical element #03 (BS). . . . .	197
17.2 Incident flux of optical element #03 (BS). . . . .	198
17.3 Absorbed peak irradiance of optical element #03 (BS). . . . .	198
17.4 Absorbed flux of optical element #03 (BS). . . . .	199
17.5 Peak temperature of optical element #03 (BS). . . . .	199

17.6 Peak mechanical stress (Von Mises stress) of optical element #03 (BS). . . . .	200
17.7 Peak deformation of optical element #03 (BS). . . . .	200
17.8 Sagittal footprint diameter (FWHM) of optical element #04 (CM2). . . . .	201
17.9 Meridional footprint diameter (FWHM) of optical element #04 (CM2). . . . .	201
17.10 Incident photon flux on surface of optical element #04 (CM2). . . . .	202
17.11 Sagittal coordinate of footprint's centre of 'gravity' on surface of optical element #04 (CM2). . . . .	202
17.12 Meridional coordinate of footprint's centre of 'gravity' on surface of optical element #04 (CM2). . . . .	203
17.13 Sagittal beam diameter (FWHM) of optical element #04 (CM2). . . . .	203
17.14 Meridional beam diameter (FWHM) of optical element #04 (CM2). . . . .	204
17.15 Photon flux in beam cross section of optical element #04 (CM2). . . . .	204
17.16 Sagittal coordinate of beam's centre of 'gravity' in beam cross section of optical element #04 (CM2). . . . .	205
17.17 Meridional coordinate of beam's centre of 'gravity' in beam cross section of optical element #04 (CM2). . . . .	205
17.18 Sagittal beam divergence (FWHM) of optical element #04 (CM2). . . . .	206
17.19 Meridional beam divergence (FWHM) of optical element #04 (CM2). . . . .	206
17.20 Photon flux in beam cross section of optical element #04 (CM2). . . . .	207
17.21 Sagittal coordinate of beam's centre of 'gravity' in angle space of optical element #04 (CM2). . . . .	207
17.22 Meridional coordinate of beam's centre of 'gravity' in angle space of optical element #04 (CM2). . . . .	208
17.23 Bandwidth (FWHM) in beam cross section of optical element #04 (CM2). . . . .	208
17.24 Absorbed irradiance on surface of optical element #03 (BS) for case #16 for 21800 eV photon energy setting. . . . .	209
17.25 Absorbed irradiance on surface of optical element #03 (BS) for case #26 for 21800 eV photon energy setting. . . . .	210
17.26 Absorbed irradiance on surface of optical element #03 (BS) for case #36 for 21800 eV photon energy setting. . . . .	211
17.27 Incident spectral flux on surface of optical element #03 (BS) for case #16 for 21800 eV photon energy setting. . . . .	212
17.28 Incident spectral flux on surface of optical element #03 (BS) for case #26 for 21800 eV photon energy setting. . . . .	212
17.29 Incident spectral flux on surface of optical element #03 (BS) for case #36 for 21800 eV photon energy setting. . . . .	213
17.30 Temperature on surface of optical element #03 (BS) for case #16 for 21800 eV photon energy setting. . . . .	214
17.31 Temperature on surface of optical element #03 (BS) for case #26 for 21800 eV photon energy setting. . . . .	215
17.32 Temperature on surface of optical element #03 (BS) for case #36 for 21800 eV photon energy setting. . . . .	216
17.33 Mechanical stress (Von Mises stress) on surface of optical element #03 (BS) for case #16 for 21800 eV photon energy setting. . . . .	217
17.34 Mechanical stress (Von Mises stress) on surface of optical element #03 (BS) for case #26 for 21800 eV photon energy setting. . . . .	218
17.35 Mechanical stress (Von Mises stress) on surface of optical element #03 (BS) for case #36 for 21800 eV photon energy setting. . . . .	219
17.36 Surface slope error in meridional direction (y) of optical element #03 (BS) for case #16 for 21800 eV photon energy setting. . . . .	220

17.37	Surface slope error in meridional direction (y) of optical element #03 (BS) for case #26 for 21800 eV photon energy setting.	221
17.38	Surface slope error in meridional direction (y) of optical element #03 (BS) for case #36 for 21800 eV photon energy setting.	222
17.39	Incident photon irradiance on surface of optical element #04 (CM2) for case #6 for 21800 eV photon energy setting.	224
17.40	Incident photon irradiance on surface of optical element #04 (CM2) for case #16 for 21800 eV photon energy setting.	225
17.41	Incident photon irradiance on surface of optical element #04 (CM2) for case #26 for 21800 eV photon energy setting.	226
17.42	Incident photon irradiance on surface of optical element #04 (CM2) for case #36 for 21800 eV photon energy setting.	227
17.43	Photon irradiance in beam cross section of optical element #04 (CM2) for case #6 for 21800 eV photon energy setting.	229
17.44	Photon irradiance in beam cross section of optical element #04 (CM2) for case #16 for 21800 eV photon energy setting.	230
17.45	Photon irradiance in beam cross section of optical element #04 (CM2) for case #26 for 21800 eV photon energy setting.	231
17.46	Photon irradiance in beam cross section of optical element #04 (CM2) for case #36 for 21800 eV photon energy setting.	232
17.47	Spectral photon flux in beam cross section of optical element #04 (CM2) for case #6 for 21800 eV photon energy setting.	233
17.48	Spectral photon flux in beam cross section of optical element #04 (CM2) for case #16 for 21800 eV photon energy setting.	233
17.49	Spectral photon flux in beam cross section of optical element #04 (CM2) for case #26 for 21800 eV photon energy setting.	234
17.50	Spectral photon flux in beam cross section of optical element #04 (CM2) for case #36 for 21800 eV photon energy setting.	234
18.1	Schematic of optical setup	236
19.1	Geometry [m] of optical element #03, for case #02, at 21800 eV photon energy setting.	242
19.2	Elastic boundary conditions on the surfaces of optical element #03, for case #02, at 21800 eV photon energy setting. Color legend: Blue: Surface can move freely in all directions. Cyan: Tension free kinematic mounting. Minimalistic constraint for three points in surface. One point is fixed, the second can move in one direction, and the third in two, in a fashion that defines angular orientation without introducing stress if the surface expands.	243
19.3	Thermal boundary conditions on the surfaces of optical element #03, for case #02, at 21800 eV photon energy setting. Color legend: Orange: No heat transfer at all. Blue: Heat transfer coefficient and temperature difference define heat current density, $j_q=h(T-T_{cool})$ . Red: Forced heat flux from e.g. absorbed X-rays. Cyan: Heat trans- fer coefficient and temperature difference define heat current density, $j_q=h^*\Delta T$ (only at inner surfaces).	244
19.4	Heat transfer coefficient, $h$ [ $\text{W}/(\text{m}^2 \text{ K})$ ], on the surfaces of optical element #03, for case #02, at 21800 eV photon energy setting.	244
19.5	Absorbed irradiance, $p_{abs}$ [ $\text{W}/\text{m}^2$ ], on the surfaces of optical ele- ment #03, for case #02, at 21800 eV photon energy setting.	245
19.6	Temperature, $T$ [K], on the surfaces of optical element #03, for case #02, at 21800 eV photon energy setting.	245

19.7 Thermal conductivity, lambda [W/(m K)], on the surfaces of optical element #03, for case #02, at 21800 eV photon energy setting. . . . .	246
19.8 Von Mises stress, sigma [Pa], on the surfaces of optical element #03, for case #02, at 21800 eV photon energy setting. . . . .	246
19.9 Thermoelastic deformation, dz [m], on the surfaces of optical element #03, for case #02, at 21800 eV photon energy setting. . . . .	247
19.10 Geometry [m] of optical element #03, for case #03, at 21800 eV photon energy setting. . . . .	247
19.11 Elastic boundary conditions on the surfaces of optical element #03, for case #03, at 21800 eV photon energy setting. Color legend: Blue: Surface can move freely in all directions. Cyan: Tension free kinematic mounting. Minimalistic constraint for three points in surface. One point is fixed, the second can move in one direction, and the third in two, in a fashion that defines angular orientation without introducing stress if the surface expands. . . . .	248
19.12 Thermal boundary conditions on the surfaces of optical element #03, for case #03, at 21800 eV photon energy setting. Color legend: Orange: No heat transfer at all. Blue: Heat transfer coefficient and temperature difference define heat current density, $j_q=h(T-T_{cool})$ . Red: Forced heat flux from e.g. absorbed X-rays. Cyan: Heat transfer coefficient and temperature difference define heat current density, $j_q=h^*\Delta T$ (only at inner surfaces). . . . .	249
19.13 Heat transfer coefficient, h [W/(m <sup>2</sup> K)], on the surfaces of optical element #03, for case #03, at 21800 eV photon energy setting. . . . .	249
19.14 Absorbed irradiance, p_abs [W/m <sup>2</sup> ], on the surfaces of optical element #03, for case #03, at 21800 eV photon energy setting. . . . .	250
19.15 Temperature, T [K], on the surfaces of optical element #03, for case #03, at 21800 eV photon energy setting. . . . .	250
19.16 Thermal conductivity, lambda [W/(m K)], on the surfaces of optical element #03, for case #03, at 21800 eV photon energy setting. . . . .	251
19.17 Von Mises stress, sigma [Pa], on the surfaces of optical element #03, for case #03, at 21800 eV photon energy setting. . . . .	251
19.18 Thermoelastic deformation, dz [m], on the surfaces of optical element #03, for case #03, at 21800 eV photon energy setting. . . . .	252
19.19 Geometry [m] of optical element #03, for case #04, at 21800 eV photon energy setting. . . . .	252
19.20 Elastic boundary conditions on the surfaces of optical element #03, for case #04, at 21800 eV photon energy setting. Color legend: Blue: Surface can move freely in all directions. Cyan: Tension free kinematic mounting. Minimalistic constraint for three points in surface. One point is fixed, the second can move in one direction, and the third in two, in a fashion that defines angular orientation without introducing stress if the surface expands. . . . .	253
19.21 Thermal boundary conditions on the surfaces of optical element #03, for case #04, at 21800 eV photon energy setting. Color legend: Orange: No heat transfer at all. Blue: Heat transfer coefficient and temperature difference define heat current density, $j_q=h(T-T_{cool})$ . Red: Forced heat flux from e.g. absorbed X-rays. Cyan: Heat transfer coefficient and temperature difference define heat current density, $j_q=h^*\Delta T$ (only at inner surfaces). . . . .	254
19.22 Heat transfer coefficient, h [W/(m <sup>2</sup> K)], on the surfaces of optical element #03, for case #04, at 21800 eV photon energy setting. . . . .	254
19.23 Absorbed irradiance, p_abs [W/m <sup>2</sup> ], on the surfaces of optical element #03, for case #04, at 21800 eV photon energy setting. . . . .	255

19.24Temperature, T [K], on the surfaces of optical element #03, for case #04, at 21800 eV photon energy setting. . . . .	255
19.25Thermal conductivity, lambda [W/(m K)], on the surfaces of optical element #03, for case #04, at 21800 eV photon energy setting. . . . .	256
19.26Von Mises stress, sigma [Pa], on the surfaces of optical element #03, for case #04, at 21800 eV photon energy setting. . . . .	256
19.27Thermoelastic deformation, dz [m], on the surfaces of optical element #03, for case #04, at 21800 eV photon energy setting. . . . .	257
 22.1 Incident peak irradiance of optical element #03 (BS). . . . .	264
22.2 Incident flux of optical element #03 (BS). . . . .	265
22.3 Absorbed peak irradiance of optical element #03 (BS). . . . .	265
22.4 Absorbed flux of optical element #03 (BS). . . . .	266
22.5 Peak temperature of optical element #03 (BS). . . . .	266
22.6 Peak mechanical stress (Von Mises stress) of optical element #03 (BS). . . . .	267
22.7 Peak deformation of optical element #03 (BS). . . . .	267
22.8 Sagittal footprint diameter (FWHM) of optical element #04 (CM2). . . . .	268
22.9 Meridional footprint diameter (FWHM) of optical element #04 (CM2). . . . .	268
 22.10Incident photon flux on surface of optical element #04 (CM2). . . . .	269
22.11Sagittal coordinate of footprint's centre of 'gravity' on surface of optical element #04 (CM2). . . . .	269
22.12Meridional coordinate of footprint's centre of 'gravity' on surface of optical element #04 (CM2). . . . .	270
22.13Sagittal beam diameter (FWHM) of optical element #04 (CM2). . . . .	270
22.14Meridional beam diameter (FWHM) of optical element #04 (CM2). . . . .	271
22.15Photon flux in beam cross section of optical element #04 (CM2). . . . .	271
22.16Sagittal coordinate of beam's centre of 'gravity' in beam cross section of optical element #04 (CM2). . . . .	272
22.17Meridional coordinate of beam's centre of 'gravity' in beam cross section of optical element #04 (CM2). . . . .	272
22.18Sagittal beam divergence (FWHM) of optical element #04 (CM2). . . . .	273
22.19Meridional beam divergence (FWHM) of optical element #04 (CM2). . . . .	273
22.20Photon flux in beam cross section of optical element #04 (CM2). . . . .	274
22.21Sagittal coordinate of beam's centre of 'gravity' in angle space of optical element #04 (CM2). . . . .	274
22.22Meridional coordinate of beam's centre of 'gravity' in angle space of optical element #04 (CM2). . . . .	275
22.23Bandwidth (FWHM) in beam cross section of optical element #04 (CM2). . . . .	275
22.24Absorbed irradiance on surface of optical element #03 (BS) for case #2 for 21800 eV photon energy setting. . . . .	277
22.25Absorbed irradiance on surface of optical element #03 (BS) for case #3 for 21800 eV photon energy setting. . . . .	278
22.26Absorbed irradiance on surface of optical element #03 (BS) for case #4 for 21800 eV photon energy setting. . . . .	279
22.27Incident spectral flux on surface of optical element #03 (BS) for case #2 for 21800 eV photon energy setting. . . . .	280
22.28Incident spectral flux on surface of optical element #03 (BS) for case #3 for 21800 eV photon energy setting. . . . .	280
22.29Incident spectral flux on surface of optical element #03 (BS) for case #4 for 21800 eV photon energy setting. . . . .	281

22.30	Temperature on surface of optical element #03 (BS) for case #2 for 21800 eV photon energy setting.	283
22.31	Temperature on surface of optical element #03 (BS) for case #3 for 21800 eV photon energy setting.	284
22.32	Temperature on surface of optical element #03 (BS) for case #4 for 21800 eV photon energy setting.	285
22.33	Mechanical stress (Von Mises stress) on surface of optical element #03 (BS) for case #2 for 21800 eV photon energy setting.	287
22.34	Mechanical stress (Von Mises stress) on surface of optical element #03 (BS) for case #3 for 21800 eV photon energy setting.	288
22.35	Mechanical stress (Von Mises stress) on surface of optical element #03 (BS) for case #4 for 21800 eV photon energy setting.	289
22.36	Surface slope error in meridional direction (y) of optical element #03 (BS) for case #2 for 21800 eV photon energy setting.	291
22.37	Surface slope error in meridional direction (y) of optical element #03 (BS) for case #3 for 21800 eV photon energy setting.	292
22.38	Surface slope error in meridional direction (y) of optical element #03 (BS) for case #4 for 21800 eV photon energy setting.	293
22.39	Incident photon irradiance on surface of optical element #04 (CM2) for case #1 for 21800 eV photon energy setting.	295
22.40	Incident photon irradiance on surface of optical element #04 (CM2) for case #2 for 21800 eV photon energy setting.	296
22.41	Incident photon irradiance on surface of optical element #04 (CM2) for case #3 for 21800 eV photon energy setting.	297
22.42	Incident photon irradiance on surface of optical element #04 (CM2) for case #4 for 21800 eV photon energy setting.	298
22.43	Photon irradiance in beam cross section of optical element #04 (CM2) for case #1 for 21800 eV photon energy setting.	299
22.44	Photon irradiance in beam cross section of optical element #04 (CM2) for case #2 for 21800 eV photon energy setting.	300
22.45	Photon irradiance in beam cross section of optical element #04 (CM2) for case #3 for 21800 eV photon energy setting.	301
22.46	Photon irradiance in beam cross section of optical element #04 (CM2) for case #4 for 21800 eV photon energy setting.	301
22.47	Spectral photon flux in beam cross section of optical element #04 (CM2) for case #1 for 21800 eV photon energy setting.	302
22.48	Spectral photon flux in beam cross section of optical element #04 (CM2) for case #2 for 21800 eV photon energy setting.	302
22.49	Spectral photon flux in beam cross section of optical element #04 (CM2) for case #3 for 21800 eV photon energy setting.	303
22.50	Spectral photon flux in beam cross section of optical element #04 (CM2) for case #4 for 21800 eV photon energy setting.	303
24.1	Schematic of optical setup	308
25.1	Geometry [m] of optical element #04, for case #02, at 16955 eV photon energy setting.	313
25.2	Elastic boundary conditions on the surfaces of optical element #04, for case #02, at 16955 eV photon energy setting. Color legend: Blue: Surface can move freely in all directions. Cyan: Tension free kinematic mounting. Minimalistic constraint for three points in surface. One point is fixed, the second can move in one direction, and the third in two, in a fashion that defines angular orientation without introducing stress if the surface expands.	314

25.3 Thermal boundary conditions on the surfaces of optical element #04, for case #02, at 16955 eV photon energy setting. Color legend: Orange: No heat transfer at all. Blue: Heat transfer coefficient and temperature difference define heat current density, $j_q=h(T-T_{cool})$ . Red: Forced heat flux from e.g. absorbed X-rays. Cyan: Heat transfer coefficient and temperature difference define heat current density, $j_q=h^*\Delta T$ (only at inner surfaces). . . . .	315
25.4 Heat transfer coefficient, $h$ [W/(m <sup>2</sup> K)], on the surfaces of optical element #04, for case #02, at 16955 eV photon energy setting. . . . .	315
25.5 Absorbed irradiance, $p_{abs}$ [W/m <sup>2</sup> ], on the surfaces of optical element #04, for case #02, at 16955 eV photon energy setting. . . . .	316
25.6 Temperature, $T$ [K], on the surfaces of optical element #04, for case #02, at 16955 eV photon energy setting. . . . .	316
25.7 Thermal conductivity, $\lambda$ [W/(m K)], on the surfaces of optical element #04, for case #02, at 16955 eV photon energy setting. . . . .	317
25.8 Von Mises stress, $\sigma$ [Pa], on the surfaces of optical element #04, for case #02, at 16955 eV photon energy setting. . . . .	317
25.9 Thermoelastic deformation, $dz$ [m], on the surfaces of optical element #04, for case #02, at 16955 eV photon energy setting. . . . .	318
25.10 Geometry [m] of optical element #04, for case #03, at 16955 eV photon energy setting. . . . .	318
25.11 Elastic boundary conditions on the surfaces of optical element #04, for case #03, at 16955 eV photon energy setting. Color legend: Blue: Surface can move freely in all directions. Cyan: Tension free kinematic mounting. Minimalistic constraint for three points in surface. One point is fixed, the second can move in one direction, and the third in two, in a fashion that defines angular orientation without introducing stress if the surface expands. . . . .	319
25.12 Thermal boundary conditions on the surfaces of optical element #04, for case #03, at 16955 eV photon energy setting. Color legend: Orange: No heat transfer at all. Blue: Heat transfer coefficient and temperature difference define heat current density, $j_q=h(T-T_{cool})$ . Red: Forced heat flux from e.g. absorbed X-rays. Cyan: Heat transfer coefficient and temperature difference define heat current density, $j_q=h^*\Delta T$ (only at inner surfaces). . . . .	320
25.13 Heat transfer coefficient, $h$ [W/(m <sup>2</sup> K)], on the surfaces of optical element #04, for case #03, at 16955 eV photon energy setting. . . . .	320
25.14 Absorbed irradiance, $p_{abs}$ [W/m <sup>2</sup> ], on the surfaces of optical element #04, for case #03, at 16955 eV photon energy setting. . . . .	321
25.15 Temperature, $T$ [K], on the surfaces of optical element #04, for case #03, at 16955 eV photon energy setting. . . . .	321
25.16 Thermal conductivity, $\lambda$ [W/(m K)], on the surfaces of optical element #04, for case #03, at 16955 eV photon energy setting. . . . .	322
25.17 Von Mises stress, $\sigma$ [Pa], on the surfaces of optical element #04, for case #03, at 16955 eV photon energy setting. . . . .	322
25.18 Thermoelastic deformation, $dz$ [m], on the surfaces of optical element #04, for case #03, at 16955 eV photon energy setting. . . . .	323
25.19 Geometry [m] of optical element #04, for case #04, at 16955 eV photon energy setting. . . . .	323

25.20Elastic boundary conditions on the surfaces of optical element #04, for case #04, at 16955 eV photon energy setting. Color legend: Blue: Surface can move freely in all directions. Cyan: Tension free kinematic mounting. Minimalistic constraint for three points in surface. One point is fixed, the second can move in one direction, and the third in two, in a fashion that defines angular orientation without introducing stress if the surface expands. . . . .	324
25.21Thermal boundary conditions on the surfaces of optical element #04, for case #04, at 16955 eV photon energy setting. Color legend: Orange: No heat transfer at all. Blue: Heat transfer coefficient and temperature difference define heat current density, $j_q=h(T-T_{cool})$ . Red: Forced heat flux from e.g. absorbed X-rays. Cyan: Heat transfer coefficient and temperature difference define heat current density, $j_q=h^*\Delta T$ (only at inner surfaces). . . . .	325
25.22Heat transfer coefficient, $h$ [W/(m <sup>2</sup> K)], on the surfaces of optical element #04, for case #04, at 16955 eV photon energy setting. . . . .	325
25.23Absorbed irradiance, $p_{abs}$ [W/m <sup>2</sup> ], on the surfaces of optical element #04, for case #04, at 16955 eV photon energy setting. . . . .	326
25.24Temperature, $T$ [K], on the surfaces of optical element #04, for case #04, at 16955 eV photon energy setting. . . . .	326
25.25Thermal conductivity, $\lambda$ [W/(m K)], on the surfaces of optical element #04, for case #04, at 16955 eV photon energy setting. . . . .	327
25.26Von Mises stress, $\sigma$ [Pa], on the surfaces of optical element #04, for case #04, at 16955 eV photon energy setting. . . . .	327
25.27Thermoelastic deformation, $dz$ [m], on the surfaces of optical element #04, for case #04, at 16955 eV photon energy setting. . . . .	328
 28.1 Incident peak irradiance of optical element #04 (BS). . . . .	334
28.2 Incident flux of optical element #04 (BS). . . . .	335
28.3 Absorbed peak irradiance of optical element #04 (BS). . . . .	335
28.4 Absorbed flux of optical element #04 (BS). . . . .	336
28.5 Peak temperature of optical element #04 (BS). . . . .	336
28.6 Peak mechanical stress (Von Mises stress) of optical element #04 (BS). . . . .	337
28.7 Peak deformation of optical element #04 (BS). . . . .	337
28.8 Sagittal footprint diameter (FWHM) of optical element #04 (BS). . . . .	338
28.9 Sagittal footprint diameter (FWHM) of optical element #05 (DanMAX). . . . .	338
28.10Meridional footprint diameter (FWHM) of optical element #04 (BS). . . . .	339
28.11Meridional footprint diameter (FWHM) of optical element #05 (DanMAX). . . . .	339
28.12Incident photon flux on surface of optical element #04 (BS). . . . .	340
28.13Incident photon flux on surface of optical element #05 (DanMAX). . . . .	340
28.14Sagittal coordinate of footprint's centre of 'gravity' on surface of optical element #04 (BS). . . . .	341
28.15Sagittal coordinate of footprint's centre of 'gravity' on surface of optical element #05 (DanMAX). . . . .	341
28.16Meridional coordinate of footprint's centre of 'gravity' on surface of optical element #04 (BS). . . . .	342
28.17Meridional coordinate of footprint's centre of 'gravity' on surface of optical element #05 (DanMAX). . . . .	342
28.18Sagittal beam diameter (FWHM) of optical element #04 (BS). . . . .	343
28.19Sagittal beam diameter (FWHM) of optical element #05 (DanMAX). . . . .	343
28.20Meridional beam diameter (FWHM) of optical element #04 (BS). . . . .	344

28.21	Meridional beam diameter (FWHM) of optical element #05 (DanMAX). . . . .	344
28.22	Photon flux in beam cross section of optical element #04 (BS). . . . .	345
28.23	Photon flux in beam cross section of optical element #05 (DanMAX). .	345
28.24	Sagittal coordinate of beam's centre of 'gravity' in beam cross section of optical element #04 (BS). . . . .	346
28.25	Sagittal coordinate of beam's centre of 'gravity' in beam cross section of optical element #05 (DanMAX). . . . .	346
28.26	Meridional coordinate of beam's centre of 'gravity' in beam cross section of optical element #04 (BS). . . . .	347
28.27	Meridional coordinate of beam's centre of 'gravity' in beam cross section of optical element #05 (DanMAX). . . . .	347
28.28	Sagittal beam divergence (FWHM) of optical element #04 (BS). . .	348
28.29	Sagittal beam divergence (FWHM) of optical element #05 (DanMAX). . . . .	348
28.30	Meridional beam divergence (FWHM) of optical element #04 (BS). .	349
28.31	Meridional beam divergence (FWHM) of optical element #05 (DanMAX). . . . .	349
28.32	Photon flux in beam cross section of optical element #04 (BS). . . . .	350
28.33	Photon flux in beam cross section of optical element #05 (DanMAX). .	350
28.34	Sagittal coordinate of beam's centre of 'gravity' in angle space of optical element #04 (BS). . . . .	351
28.35	Sagittal coordinate of beam's centre of 'gravity' in angle space of optical element #05 (DanMAX). . . . .	351
28.36	Meridional coordinate of beam's centre of 'gravity' in angle space of optical element #04 (BS). . . . .	352
28.37	Meridional coordinate of beam's centre of 'gravity' in angle space of optical element #05 (DanMAX). . . . .	352
28.38	Bandwidth (FWHM) in beam cross section of optical element #04 (BS). . . . .	353
28.39	Bandwidth (FWHM) in beam cross section of optical element #05 (DanMAX). . . . .	353
28.40	Absorbed irradiance on surface of optical element #04 (BS) for case #2 for 16955.9 eV photon energy setting. . . . .	354
28.41	Absorbed irradiance on surface of optical element #04 (BS) for case #3 for 16955.9 eV photon energy setting. . . . .	355
28.42	Absorbed irradiance on surface of optical element #04 (BS) for case #4 for 16955.9 eV photon energy setting. . . . .	356
28.43	Incident spectral flux on surface of optical element #04 (BS) for case #2 for 16955.9 eV photon energy setting. . . . .	357
28.44	Incident spectral flux on surface of optical element #04 (BS) for case #3 for 16955.9 eV photon energy setting. . . . .	357
28.45	Incident spectral flux on surface of optical element #04 (BS) for case #4 for 16955.9 eV photon energy setting. . . . .	358
28.46	Temperature on surface of optical element #04 (BS) for case #2 for 16955.9 eV photon energy setting. . . . .	359
28.47	Temperature on surface of optical element #04 (BS) for case #3 for 16955.9 eV photon energy setting. . . . .	360
28.48	Temperature on surface of optical element #04 (BS) for case #4 for 16955.9 eV photon energy setting. . . . .	361
28.49	Mechanical stress (Von Mises stress) on surface of optical element #04 (BS) for case #2 for 16955.9 eV photon energy setting. . . .	362
28.50	Mechanical stress (Von Mises stress) on surface of optical element #04 (BS) for case #3 for 16955.9 eV photon energy setting. . . .	363

28.51	Mechanical stress (Von Mises stress) on surface of optical element #04 (BS) for case #4 for 16955.9 eV photon energy setting. . . . .	364
28.52	Surface slope error in meridional direction (y) of optical element #04 (BS) for case #2 for 16955.9 eV photon energy setting. . . . .	365
28.53	Surface slope error in meridional direction (y) of optical element #04 (BS) for case #3 for 16955.9 eV photon energy setting. . . . .	366
28.54	Surface slope error in meridional direction (y) of optical element #04 (BS) for case #4 for 16955.9 eV photon energy setting. . . . .	367
28.55	Incident photon irradiance on surface of optical element #04 (BS) for case #1 for 16955.9 eV photon energy setting. . . . .	368
28.56	Incident photon irradiance on surface of optical element #04 (BS) for case #2 for 16955.9 eV photon energy setting. . . . .	369
28.57	Incident photon irradiance on surface of optical element #04 (BS) for case #3 for 16955.9 eV photon energy setting. . . . .	370
28.58	Incident photon irradiance on surface of optical element #04 (BS) for case #4 for 16955.9 eV photon energy setting. . . . .	371
28.59	Incident photon irradiance on surface of optical element #05 (Dan-MAX) for case #1 for 16955.9 eV photon energy setting. . . . .	372
28.60	Incident photon irradiance on surface of optical element #05 (Dan-MAX) for case #2 for 16955.9 eV photon energy setting. . . . .	373
28.61	Incident photon irradiance on surface of optical element #05 (Dan-MAX) for case #3 for 16955.9 eV photon energy setting. . . . .	374
28.62	Incident photon irradiance on surface of optical element #05 (Dan-MAX) for case #4 for 16955.9 eV photon energy setting. . . . .	375
28.63	Photon irradiance in beam cross section of optical element #04 (BS) for case #1 for 16955.9 eV photon energy setting. . . . .	376
28.64	Photon irradiance in beam cross section of optical element #04 (BS) for case #2 for 16955.9 eV photon energy setting. . . . .	377
28.65	Photon irradiance in beam cross section of optical element #04 (BS) for case #3 for 16955.9 eV photon energy setting. . . . .	378
28.66	Photon irradiance in beam cross section of optical element #04 (BS) for case #4 for 16955.9 eV photon energy setting. . . . .	379
28.67	Photon irradiance in beam cross section of optical element #05 (Dan-MAX) for case #1 for 16955.9 eV photon energy setting. . . . .	380
28.68	Photon irradiance in beam cross section of optical element #05 (Dan-MAX) for case #2 for 16955.9 eV photon energy setting. . . . .	381
28.69	Photon irradiance in beam cross section of optical element #05 (Dan-MAX) for case #3 for 16955.9 eV photon energy setting. . . . .	382
28.70	Photon irradiance in beam cross section of optical element #05 (Dan-MAX) for case #4 for 16955.9 eV photon energy setting. . . . .	383
28.71	Spectral photon flux in beam cross section of optical element #04 (BS) for case #1 for 16955.9 eV photon energy setting. . . . .	384
28.72	Spectral photon flux in beam cross section of optical element #04 (BS) for case #2 for 16955.9 eV photon energy setting. . . . .	384
28.73	Spectral photon flux in beam cross section of optical element #04 (BS) for case #3 for 16955.9 eV photon energy setting. . . . .	385
28.74	Spectral photon flux in beam cross section of optical element #04 (BS) for case #4 for 16955.9 eV photon energy setting. . . . .	385
28.75	Spectral photon flux in beam cross section of optical element #05 (DanMAX) for case #1 for 16955.9 eV photon energy setting. . . .	386
28.76	Spectral photon flux in beam cross section of optical element #05 (DanMAX) for case #2 for 16955.9 eV photon energy setting. . . .	386
28.77	Spectral photon flux in beam cross section of optical element #05 (DanMAX) for case #3 for 16955.9 eV photon energy setting. . . .	387

28.78Spectral photon flux in beam cross section of optical element #05 (DanMAX) for case #4 for 16955.9 eV photon energy setting. . . . .	387
29.1 . . . . .	389
29.2 . . . . .	390
29.3 . . . . .	390
29.4 . . . . .	391
29.5 Integral of the density ( $\propto$ irradiance) in DuMond diagram over angle coordinate in Fig. 29.4. This represents the <i>spectral distribution</i> of the radiation transmitted by the diamond beam splitter and subsequently reflected from the first crystal in the DanMAX monochromator. . . . .	392
29.6 Integral of the density ( $\propto$ irradiance) in DuMond diagram over wavelength coordinate in Fig. 29.4. This represents the <i>angular distribution</i> of the radiation transmitted by the diamond beam splitter and subsequently reflected from the first crystal in the DanMAX monochromator. . . . .	392
30.1 Schematic of optical setup . . . . .	395
31.1 Geometry [m] of optical element #04, for case #02, at 16955 eV photon energy setting. . . . .	400
31.2 Elastic boundary conditions on the surfaces of optical element #04, for case #02, at 16955 eV photon energy setting. Color legend: Blue: Surface can move freely in all directions. Cyan: Tension free kinematic mounting. Minimalistic constraint for three points in surface. One point is fixed, the second can move in one direction, and the third in two, in a fashion that defines angular orientation without introducing stress if the surface expands. . . . .	401
31.3 Thermal boundary conditions on the surfaces of optical element #04, for case #02, at 16955 eV photon energy setting. Color legend: Orange: No heat transfer at all. Blue: Heat transfer coefficient and temperature difference define heat current density, $j_q=h(T-T_{cool})$ . Red: Forced heat flux from e.g. absorbed X-rays. Cyan: Heat transfer coefficient and temperature difference define heat current density, $j_q=h^*\Delta T$ (only at inner surfaces). . . . .	402
31.4 Heat transfer coefficient, $h$ [ $W/(m^2 K)$ ], on the surfaces of optical element #04, for case #02, at 16955 eV photon energy setting. . . . .	402
31.5 Absorbed irradiance, $p_{abs}$ [ $W/m^2$ ], on the surfaces of optical element #04, for case #02, at 16955 eV photon energy setting. . . . .	403
31.6 Temperature, $T$ [K], on the surfaces of optical element #04, for case #02, at 16955 eV photon energy setting. . . . .	403
31.7 Thermal conductivity, $\lambda$ [ $W/(m K)$ ], on the surfaces of optical element #04, for case #02, at 16955 eV photon energy setting. . . . .	404
31.8 Von Mises stress, $\sigma$ [Pa], on the surfaces of optical element #04, for case #02, at 16955 eV photon energy setting. . . . .	404
31.9 Thermoelastic deformation, $dz$ [m], on the surfaces of optical element #04, for case #02, at 16955 eV photon energy setting. . . . .	405
31.10Geometry [m] of optical element #04, for case #03, at 16955 eV photon energy setting. . . . .	405

31.11Elastic boundary conditions on the surfaces of optical element #04, for case #03, at 16955 eV photon energy setting. Color legend: Blue: Surface can move freely in all directions. Cyan: Tension free kinematic mounting. Minimalistic constraint for three points in surface. One point is fixed, the second can move in one direction, and the third in two, in a fashion that defines angular orientation without introducing stress if the surface expands. . . . .	406
31.12Thermal boundary conditions on the surfaces of optical element #04, for case #03, at 16955 eV photon energy setting. Color legend: Orange: No heat transfer at all. Blue: Heat transfer coefficient and temperature difference define heat current density, $j_q=h(T-T_{cool})$ . Red: Forced heat flux from e.g. absorbed X-rays. Cyan: Heat transfer coefficient and temperature difference define heat current density, $j_q=h^*\Delta T$ (only at inner surfaces). . . . .	407
31.13Heat transfer coefficient, $h$ [W/(m <sup>2</sup> K)], on the surfaces of optical element #04, for case #03, at 16955 eV photon energy setting. . . . .	407
31.14Absorbed irradiance, $p_{abs}$ [W/m <sup>2</sup> ], on the surfaces of optical element #04, for case #03, at 16955 eV photon energy setting. . . . .	408
31.15Temperature, $T$ [K], on the surfaces of optical element #04, for case #03, at 16955 eV photon energy setting. . . . .	408
31.16Thermal conductivity, $\lambda$ [W/(m K)], on the surfaces of optical element #04, for case #03, at 16955 eV photon energy setting. . . . .	409
31.17Von Mises stress, $\sigma$ [Pa], on the surfaces of optical element #04, for case #03, at 16955 eV photon energy setting. . . . .	409
31.18Thermoelastic deformation, $dz$ [m], on the surfaces of optical element #04, for case #03, at 16955 eV photon energy setting. . . . .	410
31.19Geometry [m] of optical element #04, for case #04, at 16955 eV photon energy setting. . . . .	410
31.20Elastic boundary conditions on the surfaces of optical element #04, for case #04, at 16955 eV photon energy setting. Color legend: Blue: Surface can move freely in all directions. Cyan: Tension free kinematic mounting. Minimalistic constraint for three points in surface. One point is fixed, the second can move in one direction, and the third in two, in a fashion that defines angular orientation without introducing stress if the surface expands. . . . .	411
31.21Thermal boundary conditions on the surfaces of optical element #04, for case #04, at 16955 eV photon energy setting. Color legend: Orange: No heat transfer at all. Blue: Heat transfer coefficient and temperature difference define heat current density, $j_q=h(T-T_{cool})$ . Red: Forced heat flux from e.g. absorbed X-rays. Cyan: Heat transfer coefficient and temperature difference define heat current density, $j_q=h^*\Delta T$ (only at inner surfaces). . . . .	412
31.22Heat transfer coefficient, $h$ [W/(m <sup>2</sup> K)], on the surfaces of optical element #04, for case #04, at 16955 eV photon energy setting. . . . .	412
31.23Absorbed irradiance, $p_{abs}$ [W/m <sup>2</sup> ], on the surfaces of optical element #04, for case #04, at 16955 eV photon energy setting. . . . .	413
31.24Temperature, $T$ [K], on the surfaces of optical element #04, for case #04, at 16955 eV photon energy setting. . . . .	413
31.25Thermal conductivity, $\lambda$ [W/(m K)], on the surfaces of optical element #04, for case #04, at 16955 eV photon energy setting. . . . .	414
31.26Von Mises stress, $\sigma$ [Pa], on the surfaces of optical element #04, for case #04, at 16955 eV photon energy setting. . . . .	414
31.27Thermoelastic deformation, $dz$ [m], on the surfaces of optical element #04, for case #04, at 16955 eV photon energy setting. . . . .	415

34.1	Incident peak irradiance of optical element #04 (BS). . . . .	421
34.2	Incident flux of optical element #04 (BS). . . . .	422
34.3	Absorbed peak irradiance of optical element #04 (BS). . . . .	422
34.4	Absorbed flux of optical element #04 (BS). . . . .	423
34.5	Peak temperature of optical element #04 (BS). . . . .	423
34.6	Peak mechanical stress (Von Mises stress) of optical element #04 (BS). . . . .	424
34.7	Peak deformation of optical element #04 (BS). . . . .	424
34.8	Sagittal footprint diameter (FWHM) of optical element #04 (BS). .	425
34.9	Sagittal footprint diameter (FWHM) of optical element #05 (DanMAX). . . . .	425
34.10	Meridional footprint diameter (FWHM) of optical element #04 (BS). .	426
34.11	Meridional footprint diameter (FWHM) of optical element #05 (DanMAX). . . . .	426
34.12	Incident photon flux on surface of optical element #04 (BS). . . .	427
34.13	Incident photon flux on surface of optical element #05 (DanMAX). .	427
34.14	Sagittal coordinate of footprint's centre of 'gravity' on surface of optical element #04 (BS). . . . .	428
34.15	Sagittal coordinate of footprint's centre of 'gravity' on surface of optical element #05 (DanMAX). . . . .	428
34.16	Meridional coordinate of footprint's centre of 'gravity' on surface of optical element #04 (BS). . . . .	429
34.17	Meridional coordinate of footprint's centre of 'gravity' on surface of optical element #05 (DanMAX). . . . .	429
34.18	Sagittal beam diameter (FWHM) of optical element #04 (BS). . .	430
34.19	Sagittal beam diameter (FWHM) of optical element #05 (DanMAX). .	430
34.20	Meridional beam diameter (FWHM) of optical element #04 (BS). .	431
34.21	Meridional beam diameter (FWHM) of optical element #05 (DanMAX). . . . .	431
34.22	Photon flux in beam cross section of optical element #04 (BS). . .	432
34.23	Photon flux in beam cross section of optical element #05 (DanMAX). .	432
34.24	Sagittal coordinate of beam's centre of 'gravity' in beam cross section of optical element #04 (BS). . . . .	433
34.25	Sagittal coordinate of beam's centre of 'gravity' in beam cross section of optical element #05 (DanMAX). . . . .	433
34.26	Meridional coordinate of beam's centre of 'gravity' in beam cross section of optical element #04 (BS). . . . .	434
34.27	Meridional coordinate of beam's centre of 'gravity' in beam cross section of optical element #05 (DanMAX). . . . .	434
34.28	Sagittal beam divergence (FWHM) of optical element #04 (BS). .	435
34.29	Sagittal beam divergence (FWHM) of optical element #05 (DanMAX). . . . .	435
34.30	Meridional beam divergence (FWHM) of optical element #04 (BS). .	436
34.31	Meridional beam divergence (FWHM) of optical element #05 (DanMAX). . . . .	436
34.32	Photon flux in beam cross section of optical element #04 (BS). . .	437
34.33	Photon flux in beam cross section of optical element #05 (DanMAX). .	437
34.34	Sagittal coordinate of beam's centre of 'gravity' in angle space of optical element #04 (BS). . . . .	438
34.35	Sagittal coordinate of beam's centre of 'gravity' in angle space of optical element #05 (DanMAX). . . . .	438
34.36	Meridional coordinate of beam's centre of 'gravity' in angle space of optical element #04 (BS). . . . .	439

34.37	Meridional coordinate of beam's centre of 'gravity' in angle space of optical element #05 (DanMAX) . . . . .	439
34.38	Bandwidth (FWHM) in beam cross section of optical element #04 (BS) . . . . .	440
34.39	Bandwidth (FWHM) in beam cross section of optical element #05 (DanMAX) . . . . .	440
34.40	Absorbed irradiance on surface of optical element #04 (BS) for case #2 for 16955.9 eV photon energy setting. . . . .	442
34.41	Absorbed irradiance on surface of optical element #04 (BS) for case #3 for 16955.9 eV photon energy setting. . . . .	443
34.42	Absorbed irradiance on surface of optical element #04 (BS) for case #4 for 16955.9 eV photon energy setting. . . . .	444
34.43	Incident spectral flux on surface of optical element #04 (BS) for case #2 for 16955.9 eV photon energy setting. . . . .	445
34.44	Incident spectral flux on surface of optical element #04 (BS) for case #3 for 16955.9 eV photon energy setting. . . . .	445
34.45	Incident spectral flux on surface of optical element #04 (BS) for case #4 for 16955.9 eV photon energy setting. . . . .	446
34.46	Temperature on surface of optical element #04 (BS) for case #2 for 16955.9 eV photon energy setting. . . . .	448
34.47	Temperature on surface of optical element #04 (BS) for case #3 for 16955.9 eV photon energy setting. . . . .	449
34.48	Temperature on surface of optical element #04 (BS) for case #4 for 16955.9 eV photon energy setting. . . . .	450
34.49	Mechanical stress (Von Mises stress) on surface of optical element #04 (BS) for case #2 for 16955.9 eV photon energy setting. . . . .	452
34.50	Mechanical stress (Von Mises stress) on surface of optical element #04 (BS) for case #3 for 16955.9 eV photon energy setting. . . . .	453
34.51	Mechanical stress (Von Mises stress) on surface of optical element #04 (BS) for case #4 for 16955.9 eV photon energy setting. . . . .	454
34.52	Surface slope error in meridional direction (y) of optical element #04 (BS) for case #2 for 16955.9 eV photon energy setting. . . . .	456
34.53	Surface slope error in meridional direction (y) of optical element #04 (BS) for case #3 for 16955.9 eV photon energy setting. . . . .	457
34.54	Surface slope error in meridional direction (y) of optical element #04 (BS) for case #4 for 16955.9 eV photon energy setting. . . . .	458
34.55	Incident photon irradiance on surface of optical element #04 (BS) for case #1 for 16955.9 eV photon energy setting. . . . .	460
34.56	Incident photon irradiance on surface of optical element #04 (BS) for case #2 for 16955.9 eV photon energy setting. . . . .	461
34.57	Incident photon irradiance on surface of optical element #04 (BS) for case #3 for 16955.9 eV photon energy setting. . . . .	462
34.58	Incident photon irradiance on surface of optical element #04 (BS) for case #4 for 16955.9 eV photon energy setting. . . . .	463
34.59	Incident photon irradiance on surface of optical element #05 (DanMAX) for case #1 for 16955.9 eV photon energy setting. . . . .	464
34.60	Incident photon irradiance on surface of optical element #05 (DanMAX) for case #2 for 16955.9 eV photon energy setting. . . . .	465
34.61	Incident photon irradiance on surface of optical element #05 (DanMAX) for case #3 for 16955.9 eV photon energy setting. . . . .	466
34.62	Incident photon irradiance on surface of optical element #05 (DanMAX) for case #4 for 16955.9 eV photon energy setting. . . . .	467
34.63	Photon irradiance in beam cross section of optical element #04 (BS) for case #1 for 16955.9 eV photon energy setting. . . . .	469

34.64	Photon irradiance in beam cross section of optical element #04 (BS) for case #2 for 16955.9 eV photon energy setting.	470
34.65	Photon irradiance in beam cross section of optical element #04 (BS) for case #3 for 16955.9 eV photon energy setting.	471
34.66	Photon irradiance in beam cross section of optical element #04 (BS) for case #4 for 16955.9 eV photon energy setting.	472
34.67	Photon irradiance in beam cross section of optical element #05 (Dan- MAX) for case #1 for 16955.9 eV photon energy setting.	473
34.68	Photon irradiance in beam cross section of optical element #05 (Dan- MAX) for case #2 for 16955.9 eV photon energy setting.	474
34.69	Photon irradiance in beam cross section of optical element #05 (Dan- MAX) for case #3 for 16955.9 eV photon energy setting.	475
34.70	Photon irradiance in beam cross section of optical element #05 (Dan- MAX) for case #4 for 16955.9 eV photon energy setting.	476
34.71	Spectral photon flux in beam cross section of optical element #04 (BS) for case #1 for 16955.9 eV photon energy setting.	477
34.72	Spectral photon flux in beam cross section of optical element #04 (BS) for case #2 for 16955.9 eV photon energy setting.	477
34.73	Spectral photon flux in beam cross section of optical element #04 (BS) for case #3 for 16955.9 eV photon energy setting.	478
34.74	Spectral photon flux in beam cross section of optical element #04 (BS) for case #4 for 16955.9 eV photon energy setting.	478
34.75	Spectral photon flux in beam cross section of optical element #05 (DanMAX) for case #1 for 16955.9 eV photon energy setting.	479
34.76	Spectral photon flux in beam cross section of optical element #05 (DanMAX) for case #2 for 16955.9 eV photon energy setting.	479
34.77	Spectral photon flux in beam cross section of optical element #05 (DanMAX) for case #3 for 16955.9 eV photon energy setting.	480
34.78	Spectral photon flux in beam cross section of optical element #05 (DanMAX) for case #4 for 16955.9 eV photon energy setting.	480
36.1	Schematic of optical setup	485
39.1	Incident peak irradiance of optical element #03 (BS).	500
39.2	Incident flux of optical element #03 (BS).	501
39.3	Absorbed peak irradiance of optical element #03 (BS).	501
39.4	Absorbed flux of optical element #03 (BS).	502
39.5	Peak temperature of optical element #03 (BS).	502
39.6	Peak mechanical stress (Von Mises stress) of optical element #03 (BS).	503
39.7	Peak deformation of optical element #03 (BS).	503
39.8	Sagittal footprint diameter (FWHM) of optical element #04 (CM2).	504
39.9	Sagittal footprint diameter (FWHM) of optical element #09 (sam- ple).	504
39.10	Meridional footprint diameter (FWHM) of optical element #04 (CM2).	505
39.11	Meridional footprint diameter (FWHM) of optical element #09 (sam- ple).	505
39.12	Incident photon flux on surface of optical element #04 (CM2).	506
39.13	Incident photon flux on surface of optical element #09 (sample).	506
39.14	Sagittal coordinate of footprint's centre of 'gravity' on surface of op- tical element #04 (CM2).	507
39.15	Sagittal coordinate of footprint's centre of 'gravity' on surface of op- tical element #09 (sample).	507

39.16	Meridional coordinate of footprint's centre of 'gravity' on surface of optical element #04 (CM2). . . . .	508
39.17	Meridional coordinate of footprint's centre of 'gravity' on surface of optical element #09 (sample). . . . .	508
39.18	Sagittal beam diameter (FWHM) of optical element #04 (CM2). . . . .	509
39.19	Sagittal beam diameter (FWHM) of optical element #09 (sample). . . . .	509
39.20	Meridional beam diameter (FWHM) of optical element #04 (CM2). . . . .	510
39.21	Meridional beam diameter (FWHM) of optical element #09 (sample). . . . .	510
39.22	Photon flux in beam cross section of optical element #04 (CM2). . . . .	511
39.23	Photon flux in beam cross section of optical element #09 (sample). . . . .	511
39.24	Sagittal coordinate of beam's centre of 'gravity' in beam cross section of optical element #04 (CM2). . . . .	512
39.25	Sagittal coordinate of beam's centre of 'gravity' in beam cross section of optical element #09 (sample). . . . .	512
39.26	Meridional coordinate of beam's centre of 'gravity' in beam cross section of optical element #04 (CM2). . . . .	513
39.27	Meridional coordinate of beam's centre of 'gravity' in beam cross section of optical element #09 (sample). . . . .	513
39.28	Sagittal beam divergence (FWHM) of optical element #04 (CM2). . . . .	514
39.29	Sagittal beam divergence (FWHM) of optical element #09 (sample). . . . .	514
39.30	Meridional beam divergence (FWHM) of optical element #04 (CM2). . . . .	515
39.31	Meridional beam divergence (FWHM) of optical element #09 (sample). . . . .	515
39.32	Photon flux in beam cross section of optical element #04 (CM2). . . . .	516
39.33	Photon flux in beam cross section of optical element #09 (sample). . . . .	516
39.34	Sagittal coordinate of beam's centre of 'gravity' in angle space of optical element #04 (CM2). . . . .	517
39.35	Sagittal coordinate of beam's centre of 'gravity' in angle space of optical element #09 (sample). . . . .	517
39.36	Meridional coordinate of beam's centre of 'gravity' in angle space of optical element #04 (CM2). . . . .	518
39.37	Meridional coordinate of beam's centre of 'gravity' in angle space of optical element #09 (sample). . . . .	518
39.38	Bandwidth (FWHM) in beam cross section of optical element #04 (CM2). . . . .	519
39.39	Bandwidth (FWHM) in beam cross section of optical element #09 (sample). . . . .	519
39.40	Absorbed irradiance on surface of optical element #03 (BS) for case #29 for 21800 eV photon energy setting. . . . .	520
39.41	Incident spectral flux on surface of optical element #03 (BS) for case #29 for 21800 eV photon energy setting. . . . .	521
39.42	Temperature on surface of optical element #03 (BS) for case #29 for 21800 eV photon energy setting. . . . .	522
39.43	Mechanical stress (Von Mises stress) on surface of optical element #03 (BS) for case #29 for 21800 eV photon energy setting. . . . .	523
39.44	Surface slope error in meridional direction (y) of optical element #03 (BS) for case #29 for 21800 eV photon energy setting. . . . .	524
39.45	Incident photon irradiance on surface of optical element #04 (CM2) for case #5 for 21800 eV photon energy setting. . . . .	526
39.46	Incident photon irradiance on surface of optical element #04 (CM2) for case #29 for 21800 eV photon energy setting. . . . .	527
39.47	Incident photon irradiance on surface of optical element #09 (sample) for case #5 for 21800 eV photon energy setting. . . . .	528

39.48	Incident photon irradiance on surface of optical element #09 (sample) for case #29 for 21800 eV photon energy setting.	528
39.49	Photon irradiance in beam cross section of optical element #04 (CM2) for case #5 for 21800 eV photon energy setting.	530
39.50	Photon irradiance in beam cross section of optical element #04 (CM2) for case #29 for 21800 eV photon energy setting.	531
39.51	Photon irradiance in beam cross section of optical element #09 (sample) for case #5 for 21800 eV photon energy setting.	532
39.52	Photon irradiance in beam cross section of optical element #09 (sample) for case #29 for 21800 eV photon energy setting.	532
39.53	Spectral photon flux in beam cross section of optical element #04 (CM2) for case #5 for 21800 eV photon energy setting.	532
39.54	Spectral photon flux in beam cross section of optical element #04 (CM2) for case #29 for 21800 eV photon energy setting.	533
39.55	Spectral photon flux in beam cross section of optical element #09 (sample) for case #5 for 21800 eV photon energy setting.	533
39.56	Spectral photon flux in beam cross section of optical element #09 (sample) for case #29 for 21800 eV photon energy setting.	534
40.1	Schematic of optical setup	536
43.1	Incident peak irradiance of optical element #03 (BS).	551
43.2	Incident flux of optical element #03 (BS).	552
43.3	Absorbed peak irradiance of optical element #03 (BS).	552
43.4	Absorbed flux of optical element #03 (BS).	553
43.5	Peak temperature of optical element #03 (BS).	553
43.6	Peak mechanical stress (Von Mises stress) of optical element #03 (BS).	554
43.7	Peak deformation of optical element #03 (BS).	554
43.8	Sagittal footprint diameter (FWHM) of optical element #04 (CM2).	555
43.9	Sagittal footprint diameter (FWHM) of optical element #09 (sample).	555
43.10	Meridional footprint diameter (FWHM) of optical element #04 (CM2).	556
43.11	Meridional footprint diameter (FWHM) of optical element #09 (sample).	556
43.12	Incident photon flux on surface of optical element #04 (CM2).	557
43.13	Incident photon flux on surface of optical element #09 (sample).	557
43.14	Sagittal coordinate of footprint's centre of 'gravity' on surface of op- tical element #04 (CM2).	558
43.15	Sagittal coordinate of footprint's centre of 'gravity' on surface of op- tical element #09 (sample).	558
43.16	Meridional coordinate of footprint's centre of 'gravity' on surface of optical element #04 (CM2).	559
43.17	Meridional coordinate of footprint's centre of 'gravity' on surface of optical element #09 (sample).	559
43.18	Sagittal beam diameter (FWHM) of optical element #04 (CM2).	560
43.19	Sagittal beam diameter (FWHM) of optical element #09 (sample).	560
43.20	Meridional beam diameter (FWHM) of optical element #04 (CM2).	561
43.21	Meridional beam diameter (FWHM) of optical element #09 (sam- ple).	561
43.22	Photon flux in beam cross section of optical element #04 (CM2).	562
43.23	Photon flux in beam cross section of optical element #09 (sample).	562

43.24 Sagittal coordinate of beam's centre of 'gravity' in beam cross section of optical element #04 (CM2). . . . .	563
43.25 Sagittal coordinate of beam's centre of 'gravity' in beam cross section of optical element #09 (sample). . . . .	563
43.26 Meridional coordinate of beam's centre of 'gravity' in beam cross section of optical element #04 (CM2). . . . .	564
43.27 Meridional coordinate of beam's centre of 'gravity' in beam cross section of optical element #09 (sample). . . . .	564
43.28 Sagittal beam divergence (FWHM) of optical element #04 (CM2). . . . .	565
43.29 Sagittal beam divergence (FWHM) of optical element #09 (sample). . . . .	565
43.30 Meridional beam divergence (FWHM) of optical element #04 (CM2). . . . .	566
43.31 Meridional beam divergence (FWHM) of optical element #09 (sam- ple). . . . .	566
43.32 Photon flux in beam cross section of optical element #04 (CM2). . . . .	567
43.33 Photon flux in beam cross section of optical element #09 (sample). . . . .	567
43.34 Sagittal coordinate of beam's centre of 'gravity' in angle space of optical element #04 (CM2). . . . .	568
43.35 Sagittal coordinate of beam's centre of 'gravity' in angle space of optical element #09 (sample). . . . .	568
43.36 Meridional coordinate of beam's centre of 'gravity' in angle space of optical element #04 (CM2). . . . .	569
43.37 Meridional coordinate of beam's centre of 'gravity' in angle space of optical element #09 (sample). . . . .	569
43.38 Bandwidth (FWHM) in beam cross section of optical element #04 (CM2). . . . .	570
43.39 Bandwidth (FWHM) in beam cross section of optical element #09 (sample). . . . .	570
43.40 Absorbed irradiance on surface of optical element #03 (BS) for case #29 for 21800 eV photon energy setting. . . . .	572
43.41 Incident spectral flux on surface of optical element #03 (BS) for case #29 for 21800 eV photon energy setting. . . . .	573
43.42 Temperature on surface of optical element #03 (BS) for case #29 for 21800 eV photon energy setting. . . . .	575
43.43 Mechanical stress (Von Mises stress) on surface of optical element #03 (BS) for case #29 for 21800 eV photon energy setting. . . . .	577
43.44 Surface slope error in meridional direction (y) of optical element #03 (BS) for case #29 for 21800 eV photon energy setting. . . . .	579
43.45 Incident photon irradiance on surface of optical element #04 (CM2) for case #5 for 21800 eV photon energy setting. . . . .	581
43.46 Incident photon irradiance on surface of optical element #04 (CM2) for case #29 for 21800 eV photon energy setting. . . . .	582
43.47 Incident photon irradiance on surface of optical element #09 (sample) for case #5 for 21800 eV photon energy setting. . . . .	583
43.48 Incident photon irradiance on surface of optical element #09 (sample) for case #29 for 21800 eV photon energy setting. . . . .	583
43.49 Photon irradiance in beam cross section of optical element #04 (CM2) for case #5 for 21800 eV photon energy setting. . . . .	583
43.50 Photon irradiance in beam cross section of optical element #04 (CM2) for case #29 for 21800 eV photon energy setting. . . . .	584
43.51 Photon irradiance in beam cross section of optical element #09 (sam- ple) for case #5 for 21800 eV photon energy setting. . . . .	584
43.52 Photon irradiance in beam cross section of optical element #09 (sam- ple) for case #29 for 21800 eV photon energy setting. . . . .	584

43.53	Spectral photon flux in beam cross section of optical element #04 (CM2) for case #5 for 21800 eV photon energy setting. . . . .	585
43.54	Spectral photon flux in beam cross section of optical element #04 (CM2) for case #29 for 21800 eV photon energy setting. . . . .	585
43.55	Spectral photon flux in beam cross section of optical element #09 (sample) for case #5 for 21800 eV photon energy setting. . . . .	586
43.56	Spectral photon flux in beam cross section of optical element #09 (sample) for case #29 for 21800 eV photon energy setting. . . . .	586
45.1	Schematic of optical setup . . . . .	590
48.1	Sagittal footprint diameter (FWHM) of optical element #09 (sample). . . . .	606
48.2	Meridional footprint diameter (FWHM) of optical element #09 (sample). . . . .	607
48.3	Incident photon flux on surface of optical element #09 (sample). . . . .	607
48.4	Sagittal coordinate of footprint's centre of 'gravity' on surface of optical element #09 (sample). . . . .	608
48.5	Meridional coordinate of footprint's centre of 'gravity' on surface of optical element #09 (sample). . . . .	608
48.6	Sagittal beam diameter (FWHM) of optical element #09 (sample). . . . .	609
48.7	Meridional beam diameter (FWHM) of optical element #09 (sample). . . . .	609
48.8	Photon flux in beam cross section of optical element #09 (sample). . . . .	610
48.9	Sagittal coordinate of beam's centre of 'gravity' in beam cross section of optical element #09 (sample). . . . .	610
48.10	Meridional coordinate of beam's centre of 'gravity' in beam cross section of optical element #09 (sample). . . . .	611
48.11	Sagittal beam divergence (FWHM) of optical element #09 (sample). . . . .	611
48.12	Meridional beam divergence (FWHM) of optical element #09 (sample). . . . .	612
48.13	Photon flux in beam cross section of optical element #09 (sample). . . . .	612
48.14	Sagittal coordinate of beam's centre of 'gravity' in angle space of optical element #09 (sample). . . . .	613
48.15	Meridional coordinate of beam's centre of 'gravity' in angle space of optical element #09 (sample). . . . .	613
48.16	Bandwidth (FWHM) in beam cross section of optical element #09 (sample). . . . .	614
48.17	Incident photon irradiance on surface of optical element #09 (sample) for case #1 for 21800 eV photon energy setting. . . . .	614
48.18	Incident photon irradiance on surface of optical element #09 (sample) for case #2 for 21800 eV photon energy setting. . . . .	614
48.19	Incident photon irradiance on surface of optical element #09 (sample) for case #3 for 21800 eV photon energy setting. . . . .	614
48.20	Incident photon irradiance on surface of optical element #09 (sample) for case #4 for 21800 eV photon energy setting. . . . .	615
48.21	Incident photon irradiance on surface of optical element #09 (sample) for case #5 for 21800 eV photon energy setting. . . . .	615
48.22	Photon irradiance in beam cross section of optical element #09 (sample) for case #1 for 21800 eV photon energy setting. . . . .	616
48.23	Photon irradiance in beam cross section of optical element #09 (sample) for case #2 for 21800 eV photon energy setting. . . . .	617
48.24	Photon irradiance in beam cross section of optical element #09 (sample) for case #3 for 21800 eV photon energy setting. . . . .	618

48.25	Photon irradiance in beam cross section of optical element #09 (sample) for case #4 for 21800 eV photon energy setting. . . . .	618
48.26	Photon irradiance in beam cross section of optical element #09 (sample) for case #5 for 21800 eV photon energy setting. . . . .	619
48.27	Spectral photon flux in beam cross section of optical element #09 (sample) for case #1 for 21800 eV photon energy setting. . . . .	619
48.28	Spectral photon flux in beam cross section of optical element #09 (sample) for case #2 for 21800 eV photon energy setting. . . . .	620
48.29	Spectral photon flux in beam cross section of optical element #09 (sample) for case #3 for 21800 eV photon energy setting. . . . .	620
48.30	Spectral photon flux in beam cross section of optical element #09 (sample) for case #4 for 21800 eV photon energy setting. . . . .	621
48.31	Spectral photon flux in beam cross section of optical element #09 (sample) for case #5 for 21800 eV photon energy setting. . . . .	621
49.1	Schematic of optical setup . . . . .	623
52.1	Sagittal footprint diameter (FWHM) of optical element #09 (sample). . . . .	639
52.2	Meridional footprint diameter (FWHM) of optical element #09 (sample). . . . .	640
52.3	Incident photon flux on surface of optical element #09 (sample). . . . .	640
52.4	Sagittal coordinate of footprint's centre of 'gravity' on surface of optical element #09 (sample). . . . .	641
52.5	Meridional coordinate of footprint's centre of 'gravity' on surface of optical element #09 (sample). . . . .	641
52.6	Sagittal beam diameter (FWHM) of optical element #09 (sample). . . . .	642
52.7	Meridional beam diameter (FWHM) of optical element #09 (sample). . . . .	642
52.8	Photon flux in beam cross section of optical element #09 (sample). . . . .	643
52.9	Sagittal coordinate of beam's centre of 'gravity' in beam cross section of optical element #09 (sample). . . . .	643
52.10	Meridional coordinate of beam's centre of 'gravity' in beam cross section of optical element #09 (sample). . . . .	644
52.11	Sagittal beam divergence (FWHM) of optical element #09 (sample). . . . .	644
52.12	Meridional beam divergence (FWHM) of optical element #09 (sample). . . . .	645
52.13	Photon flux in beam cross section of optical element #09 (sample). . . . .	645
52.14	Sagittal coordinate of beam's centre of 'gravity' in angle space of optical element #09 (sample). . . . .	646
52.15	Meridional coordinate of beam's centre of 'gravity' in angle space of optical element #09 (sample). . . . .	646
52.16	Bandwidth (FWHM) in beam cross section of optical element #09 (sample). . . . .	647
52.17	Incident photon irradiance on surface of optical element #09 (sample) for case #1 for 21800 eV photon energy setting. . . . .	647
52.18	Incident photon irradiance on surface of optical element #09 (sample) for case #2 for 21800 eV photon energy setting. . . . .	647
52.19	Incident photon irradiance on surface of optical element #09 (sample) for case #3 for 21800 eV photon energy setting. . . . .	648
52.20	Incident photon irradiance on surface of optical element #09 (sample) for case #4 for 21800 eV photon energy setting. . . . .	649
52.21	Incident photon irradiance on surface of optical element #09 (sample) for case #5 for 21800 eV photon energy setting. . . . .	650

52.22	Photon irradiance in beam cross section of optical element #09 (sample) for case #1 for 21800 eV photon energy setting.	651
52.23	Photon irradiance in beam cross section of optical element #09 (sample) for case #2 for 21800 eV photon energy setting.	651
52.24	Photon irradiance in beam cross section of optical element #09 (sample) for case #3 for 21800 eV photon energy setting.	652
52.25	Photon irradiance in beam cross section of optical element #09 (sample) for case #4 for 21800 eV photon energy setting.	652
52.26	Photon irradiance in beam cross section of optical element #09 (sample) for case #5 for 21800 eV photon energy setting.	653
52.27	Spectral photon flux in beam cross section of optical element #09 (sample) for case #1 for 21800 eV photon energy setting.	653
52.28	Spectral photon flux in beam cross section of optical element #09 (sample) for case #2 for 21800 eV photon energy setting.	654
52.29	Spectral photon flux in beam cross section of optical element #09 (sample) for case #3 for 21800 eV photon energy setting.	654
52.30	Spectral photon flux in beam cross section of optical element #09 (sample) for case #4 for 21800 eV photon energy setting.	655
52.31	Spectral photon flux in beam cross section of optical element #09 (sample) for case #5 for 21800 eV photon energy setting.	655
54.1	Schematic of optical setup	659
57.1	Photon flux in beam cross section of optical element #09 (sample). Case #1 represents the useful signal from the undulator's 9th harmonic. Case #2 is the higher harmonic contamination that would occur naturally, whilst case #3 is harmonic contamination artificially increased by tweaking the pitch of the second diamond 111 crystal. The latter merely serves as an explanation for the unexpectedly low high harmonic throughput in Laue geometry. More about this in the text. The photon energy in the abscissa of the higher harmonic curves has been divided by three to match that of the useful signal from the 9th undulator harmonic.	671
58.1	Schematic of optical setup	673
61.1	Photon flux in beam cross section of optical element #09 (sample). Case #1 represents the useful signal from the undulator's 9th harmonic. Case #2 and #3 are the higher harmonic contaminations with perfect alignment and with a relative misalignment by one microradian respectively. The photon energy in the abscissa of the higher harmonic curve has been divided by three to match that of the useful signal from the 9th undulator harmonic.	685

# **Chapter 1**

## **Introduction**

SinCrys is a prospect single crystal X-ray diffraction side-station of the DanMAX beamline situated at the MAX IV synchrotron radiation facility in Lund. With help of a beam splitter, a small fraction of the synchrotron radiation from the DanMAX source will be diverted to the SinCrys side-station. The beam splitter must not affect the main beam by either diverting a too large fraction of the radiation, by absorption, or by distorting it. Both the main- and the side-station must be operable in parallel. To facilitate this, a minimum distance of one metre between diverted and undiverted beam is required.

# Chapter 2

## Models used in the simulations

### 2.1 Shadow heat flux

Shadow allows for only up to 51 sampling points for the photon energy. This is insufficient for the modelling of sources with many spectral features, as for example the entire spectrum of an undulator. In most cases this is not a serious limitation, since one is anyway interested in a narrow spectral window only. Somewhere in the optical path there is usually a monochromator, that filters out the unwanted parts of the spectrum, and it would be computationally inefficient to generate rays in these spectral regimes in the first place. However, this becomes a problem, if one is interested in the heat load on optical elements before the monochromator. Photons from all spectral regimes contribute and one does not get around to model the entire spectrum. The trick is to split up the spectrum in narrow slots, each sufficiently poor in features to be accurately sampled with only 51 points. Then, ray-tracing is done for each slot separately. The reassembly happens when histograms are calculated:<sup>1</sup> the bins accumulate the rays from all slots, i.e. they are not “emptied” in between. A prerequisite is of course to keep bin sizes and positions constant. For performance reasons one matches the number of rays to the power in the respective slot, such that the power in rays from different slots is about the same. In fact MASH chooses slot widths and number of rays, such that all rays represent approximately the same power. This reduces computational costs in the adding of rays, since the rays do not require an extra weight for photon energy. In Shadow, photon energy is not one of the fundamental ray-parameters but has to be calculated from wavenumber instead.

### 2.2 Undulator scanning

At a beamline with an undulator source the undulator gap, i.e. the distance between the magnetic arrays, is usually scanned with photon energy, in order to maximise photon flux and to keep a regular beam profile.<sup>2</sup> In order to reach high photon energies, one might even have to switch to higher harmonics. To allow for the simulation of e.g. photon flux as function of photon energy one therefore needs to implement a fully automatic undulator gap scanning algorithm. The basis for this

---

<sup>1</sup> power distribution in e.g. real or energy space

<sup>2</sup>not e.g. doughnut shaped

algorithm is the following expression for the wavelength of the  $n$ th harmonic [10]

$$\lambda_n = \frac{\lambda_0}{2n\gamma^2} \left( 1 + \frac{K^2}{2} + \gamma^2 \theta^2 \right) , \quad (2.1)$$

where  $\lambda_0$  is the magnetic period,  $\gamma \stackrel{\text{def}}{=} E_e/(mc^2)$  the electrons' relativistic factor, and  $\theta$  the angle of observation with respect to the central axis of the undulator. The undulator's *deflection parameter*  $K = eB_0\lambda_0/(2\pi m_e c)$  is what changes when scanning the undulator gap, via the involved change of peak magnetic field  $B_0$ . Expression (2.1) for  $K = 0$  and  $\theta = 0$  defines the smallest on-axis wavelength, i.e. top photon energy, that can be reached with a given harmonic. For a given wavelength  $\lambda > \lambda_n(K=0, \theta=0)$  it defines the minimum odd harmonic  $n$  required to reach this wavelength,  $n_{\min} > \lambda_0/(2\lambda\gamma^2)$ . This is where the algorithm starts. It then checks the flux for increasing  $n$  with  $K$  tuned in a specific way, which is described later, until the flux starts to decline. The harmonic with the highest flux is selected. MASH offers different ways to tune  $K$  with wavelength:

**Maximum on axis:** Extracting  $K$  directly from expression (2.1) with  $\lambda_n(K) = \lambda$  provides peak intensity on axis for the given wavelength  $\lambda$ .

**Maximum flux in aperture:** Extracting  $K$  from the following modification of expression (2.1),  $\lambda_n(K)(1 + 1/(nN)) = \lambda$ , where  $N$  stands for the number of magnetic poles, provides maximum flux through an aperture [13]. The beam though might have a "doughnut" profile.

**Arbitrary offset:** Adding a free dimensionless parameter  $r_{\text{off}}$  to the previous modification of expression (2.1), i.e.  $\lambda_n(K)(1+1/(nN)+r_{\text{off}}) = \lambda$ , allows to choose any part of the undulator spectrum.

## 2.3 Thermoelastic model

Comsol [3] was employed for these simulations, or more specifically, Comsol's (stationary) Thermal Stress module in the Structural Mechanics section. The module combines solid mechanics with heat transfer in solids. The coupling occurs, where the temperature from heat transfer creates thermal expansion which in turn leads to mechanical stress. A Heat Transfer in Solids model is active by default on all domains. All functionality for including other domain types, such as a fluid domain, is also available. The temperature equation defined in solid domains corresponds to the differential form of Fourier's law [14] that may contain additional contributions like heat sources:

$$-\nabla \cdot (\lambda \nabla T) = Q_{\text{src}} \quad (2.2)$$

Here,  $\lambda$  stands for the thermal conductivity and  $Q_{\text{src}}$  for heat production per unit volume. The latter is due to the absorption of synchrotron radiation. Let  $dy_{\text{abs}}$  be the absorption depth. For simplicity we assume that the radiation beam has a Gaussian profile. Altogether, this leads to the following expression:

$$Q_{\text{src}} = p_0 \times \exp(-y/dy_{\text{abs}}) \times \exp(-(x/dx_{\text{Gauss}})^2) \times \exp(-(z/dz_{\text{Gauss}})^2) . \quad (2.3)$$

Mechanical stress,  $\sigma$  and strain,  $\eta$ , for a given temperature increase,  $\Delta T$ , follow from minimising elastic energy [12]

$$W_{\text{elast}} = \frac{1}{2}(\eta - \beta \Delta T) \cdot \sigma . \quad (2.4)$$

Here,  $\beta$  stands for the thermal expansion coefficient. For a linear elastic material stress and strain are related via Hook's law [12]

$$\sigma = \mathbf{c}(\eta - \beta\Delta T) \quad , \quad (2.5)$$

where  $\mathbf{c}$  stands for the  $6 \times 6$  elastic constant matrix.

In fluid domains one more term, representing heat transfer by material transport, enters into the equation

$$\rho c_p \mathbf{u} \cdot \nabla T - \nabla \cdot (\lambda \nabla T) = Q_{\text{src}} \quad , \quad (2.6)$$

where  $\rho$  stands for the fluids mass density,  $c_p$  for its specific heat capacity at constant pressure, and finally  $\mathbf{u}$  for its velocity field.

A criteria for whether a flow is turbulent or laminar is the Reynolds number [5]:

$$\text{Re} = \frac{\rho u D}{\eta} \quad , \quad (2.7)$$

where  $D$  stands for a characteristic length of the flow cross-section and  $\eta$  for the dynamic viscosity. For shapes such as squares, rectangular or annular ducts where the height and width are comparable, the characteristic length for internal flow situations is taken to be the hydraulic diameter [5],  $D_H$  defined as:

$$D_H = \frac{4A}{P} \quad , \quad (2.8)$$

where  $A$  is the cross-sectional area and  $P$  is the wetted perimeter. The wetted perimeter for a channel is the total perimeter of all channel walls that are in contact with the flow. For an entirely filled rectangular cross-section with width  $w$  and height  $h$  this becomes:

$$D_H = \left( \frac{1}{2w} + \frac{1}{2h} \right)^{-1} \quad . \quad (2.9)$$

The critical Reynolds number  $\text{Re}_{\text{crit}} = 1000 \dots 2500$  is the boundary above which turbulent flow can be expected.

Modelling heat transfer with turbulent flow is difficult and computationally expensive. The field is called Conjugate Heat Transfer (CHT). CHT solves the problem by determining the velocity field  $\mathbf{u}_{\text{turb}}(\mathbf{r}, t)$ , which in turn allows to solve the heat transfer equation 2.6. Alternatively, one can assume a stationary average velocity field  $\mathbf{u}(\mathbf{r})$  and take account of the heat transfer by turbulent eddies via an enhanced effective thermal conductivity. The problem now lies in determining this effective turbulent heat conductivity  $\lambda_{\text{eff}}$  also known as eddy conductivity [18]. Fortunately, the 'flow in a small cross-section' problem does not depend very much on the specific value of  $\lambda_{\text{eff}}$ , unless the heat transfer is so low, that there is a relevant temperature gradient over the cross-section area. So, the trick is to increase thermal conductivity, until there is only a minor temperature gradient across the cooling channel left, and to define an average velocity field manually.

## 2.4 Boundary conditions

### 2.4.1 Wet wall

At the cooling channel wall there is usually a thin laminar layer, [11] with reduced thermal conductivity. This thin layer can be taken account for by its thermal resistance, or what is equivalent, by a heat transfer coefficient  $h_{\text{ww}}$ . Then, the

thermal flow across a surface element in the channel wall with surface normal  $\mathbf{n}$  is given by

$$-\mathbf{n} \cdot (\lambda \nabla T) = h_{\text{ww}} (T_{\text{wall}} - T_{\text{water}}) . \quad (2.10)$$

For turbulent flow the heat transfer coefficient,  $h_{\text{ww}}$ , can be estimated with help of the Dittus-Boelter relation [6]. For laminar flow there is an equivalent relation [6]. If water flow, temperature or pressure are not specified, one can use a typical value for laminar flow instead – as sort of a worst case scenario –  $h_{\text{ww}} = 3000 \text{ W}/(\text{m}^2\text{K})$ . A typical value for turbulent flow would have been  $10000 \text{ W}/(\text{m}^2\text{K})$ .

### 2.4.2 Solid-solid interface

Heat transfer across solid / solid interfaces, either clamped brazed or welded are described best by a heat transfer coefficient,  $h_{\text{ss}}$

$$-\mathbf{n} \cdot (\lambda \nabla T) = h_{\text{ss}} \Delta T . \quad (2.11)$$

In this case one usually refers to  $h$  as thermal *contact conductance coefficient (TCCC)*, if the solids are just clamped together, or as *thermal boundary conductance coefficient (TBCC)* if there are no voids due to surface roughness or waviness, which is e.g. the case for an epitaxial interface. Typical values for TCCCs lie between 2000 and  $200000 \text{ W}/(\text{m}^2\text{K})$ . Typical values for TBCCs are in the order of  $\text{MW}/(\text{m}^2\text{K})$ . A brazed interface probably lies between those regimes. A conservative estimate is  $h_{\text{brz}} = 100000$ .

### 2.4.3 Free air convection

Flow due to free air convection can be described by a heat transfer coefficient,  $h_{\text{free}}$ . There are expressions for heat transfer coefficients in various geometries. The heat transfer coefficient for free convection at a vertical wall for example is actually a function of temperature  $h(T)$ . A typical estimate is  $h_{\text{free}} \approx 5 \text{ W}/(\text{m}^2\text{K})$ .

### 2.4.4 Surface to ambient radiation

The radiated power per surface area is according to the Stefan-Boltzmann law,  $P/A = \epsilon \sigma T^4$ , and hence the boundary condition on all surfaces is

$$-\mathbf{n} \cdot (\lambda \nabla T) = -\epsilon \sigma (T^4 - T_{\text{amb}}^4) , \quad (2.12)$$

where  $\mathbf{n}$  stands for the surface normal,  $\epsilon$  for the surface emissivity ( $\epsilon = 1$  for a black body), and  $\sigma$  for the Stefan-Boltzmann constant.

### 2.4.5 Absorption of radiation

Absorption of synchrotron radiation on a surface enforces a certain heat flux distribution there. In Comsol so called Interpolation Functions provide the means to introduce that into the model. These are functions of one or more variables, e.g.  $f(x, y, z)$ , defined by a set of values  $f_{ijk}$  at discrete points  $(x_i, y_j, z_k)$ , which do not have to be equidistant. In-between points, Comsol interpolates.

Let  $p_{\text{plan}}(x, z)$  be the power per unit area of radiation impinging perpendicularly onto the  $xz$ -plane, i.e. going parallel to the  $y$ -axis. It can be given as an interpolation function, directly defined by data as provided by e.g. SPECTRA [19]. Then, the power per unit area on a surface element with surface normal vector  $n = (n_x, n_y, n_z)$  is given by

$$p(x, y, z) = p_{\text{plan}}(x, z) |n_y(x, y, z)| \theta(-n_y(x, y, z)) . \quad (2.13)$$

where  $\theta(x)$  is the Heaviside step function with  $\theta(x < 0) = 0$  and  $\theta(x \geq 0) = 1$ . The step function is required to prevent absorption of radiation on averted surfaces, i.e. those lying in the radiation shadow ( $n_y > 0$  for radiation parallel to the  $y$ -axis). The absolute value,  $|n_y|$ , prevents negative heat loads on surfaces facing the radiation source ( $n_y < 0$  for radiation parallel to  $y$ -axis).

## 2.5 Asymmetric diffraction focusing

A symmetrically (Bragg-)reflecting crystal, i.e. a crystal where the diffracting planes are parallel to the crystal surface, acts like a mirror. That is, it does not alter the divergence or convergence of a beam, and thus is neutral in an imaging setup, where in the most common case, with a real source and a real image, a divergent beam needs to be turned into a convergent one.

As soon as the diffracting planes are at an angle to the crystal surface,  $\phi_a \neq 0$ , this flat-mirror neutrality is lost. This is somewhat counter intuitive, as all the asymmetry is doing is to rotate each ray in the beam by the same angle, namely  $2\phi_a$ . So how should this alter divergence? The crucial point is that each ray is turned around a different turning point, and it is the relation between turning point and direction that is different in the asymmetric case. This is shown in Fig. 2.1 and explained in more detail below.

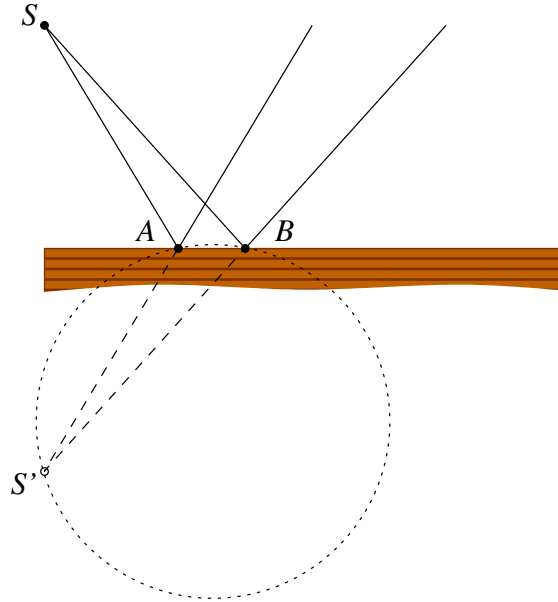


Figure 2.1: Point  $S$  is a source point, points  $A$  and  $B$  are the points, where two rays originating from  $S$  are reflected.  $S'$  is the point where the symmetrically reflected rays appear to come from, i.e. a virtual source point.

Virtual source points for asymmetrically reflected beams lie on a circle encompassing points  $S'$ ,  $A$  and  $B$ . This follows from the *inscribed angle theorem* [2], of which Thales' theorem is a special case. The inscribed angle theorem says, that the intersection point of two lines going through two fixed non-coinciding points,  $A$  and  $B$ , cutting each other at a constant angle are lying on a circle encompassing both points  $A$  and  $B$ .

Hence, drawing a circle through points  $A$ ,  $B$  and  $S'$  shows where the virtual source points are for arbitrary angle of asymmetry  $\phi_a$ . From that it is obvious that

in any asymmetric reflection,  $\phi_a \neq 0$ , the effective source distance changes. Hence, an asymmetric crystal acts as a focusing / defocusing optical element.

In this respect, diffraction in Laue geometry, as shown in Fig. 2.2, is never neutral and always has a focusing / defocusing effect.

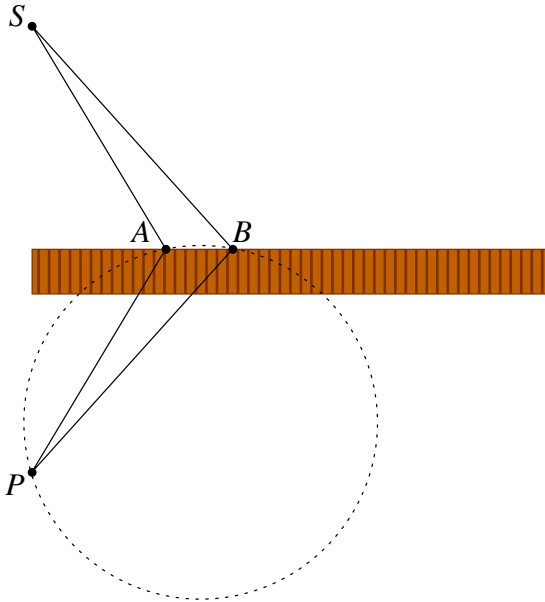


Figure 2.2: Diffraction in Laue geometry from lattice planes perpendicular to the surface, which is strongly focusing. Diffraction in Laue geometry from lattice planes parallel to the surface is not possible, and hence always counts as asymmetric in a focusing context.

In the pictured case with an angle of asymmetry of 90 degrees, often referred to as the symmetric Laue case, the focusing effect is quite pronounced, and the real image point  $P$  is at the source position mirrored at the plane of the crystal slab.

The imaging by an asymmetric crystal, whether in Bragg or in Laue geometry, is imperfect, i.e. shows aberrations. If one chooses two points  $A'$  and  $B'$  in Fig. 2.2 that are further off-axis and repeats the inscribed angle construction it will result in different focal positions. This obviously leads to an aberration that scales with aperture size, like with spherical aberration.

## 2.6 Autofocusing

In practice the deformation of optical components from their designed shape due to e.g. heat load, gravitation or low frequency random slope errors is to a large part compensated for by refocusing, i.e. by moving or rebending a mirror for example. If one wants to include such deviations from perfect shape in a simulation one should do the same. Otherwise, one would grossly overestimate their effect on the overall optical performance. Of course refocusing should be done automatically, since the deformation often varies from case to case.

In the case of non-dispersive focusing optics like mirrors, autofocusing is a useful feature to counteract second order effects, i.e. deviations from ideal imaging conditions. In the case of dispersive optical elements such as compound refractive lenses (CRL), autofocusing is a fundamental prerequisite even under ideal conditions. Merely a small change in photon energy can dramatically change imaging

conditions, speak focal length. This has to be compensated for by adding or removing lens elements and / or by moving the CRL forward or backward, which is if automated nothing else but auto-focusing.

A fundamental prerequisite for autofocusing is the determination of the focal point position. What might come into mind first, is to choose minimum beam diameter at the focal plane as a criterion for best focus. Though, this is most likely not the best choice. X-ray beams from synchrotron light sources tend to have very small opening angles. Hence, the beam diameter does not vary much, when tweaking the focusing conditions. Even worse, for beams with small divergence best focus sometimes does not even coincide with smallest beam waist [17]. Above that, the focal spot size does not tell you how far off you might be, and whether you are behind or before best focus.

A better choice is, to consider the slope of the point cloud in a *beam phase diagram* (BPD), i.e. a diagram where you plot ray position  $x$  as function of ray direction<sup>3</sup>  $x'$  for each ray in the beam (see Fig. 2.3).

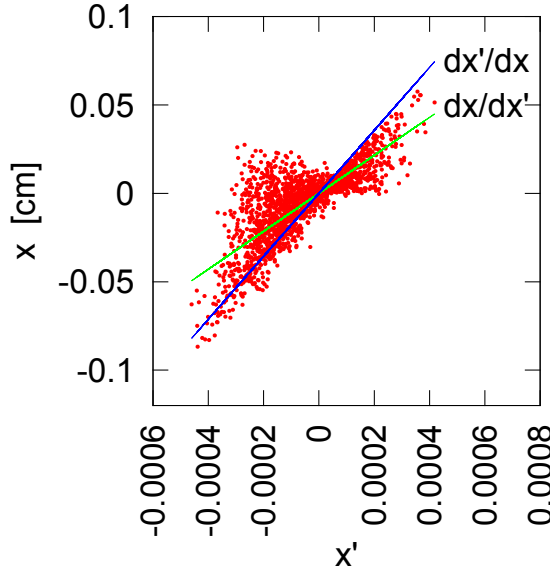


Figure 2.3: Beam phase diagram for a divergent beam, i.e. behind best focus.

The slope  $dx/dx'$  provides directly the distance from best focus

$$\Delta l = \frac{dx}{dx'} , \quad (2.14)$$

and hence autofocusing can be done in a single step rather than iteratively. One does not even need to be in the focal plane. Instead of minimising  $dx/dx'$  in the focal plane itself, one could minimise  $dx/dx' - l_0$ , where  $l_0$  stands for the distance of the cross section to the focal plane. The BPD can be also used to regain collimation: therefore the inverse slope  $dx'/dx$  needs to be minimised.

The method of choice to determine the slope of the point cloud in the BPD is linear regression:

$$\frac{dx}{dx'} = \frac{s_{xx'} - s_x s_{x'}/s}{s_{x'x'} - s_{x'}^2/s} , \quad \frac{dx'}{dx} = \frac{s_{xx'} - s_x s_{x'}/s}{s_{xx} - s_x^2/s} , \quad r_{xx'} = \frac{s_{xx'} - s_x s_{x'}/s}{\sqrt{s_{xx} - s_x^2/s} \sqrt{s_{x'x'} - s_{x'}^2/s}} , \quad (2.15)$$

---

<sup>3</sup>projection of the normalised direction vector, here onto  $x$ -axis

where  $s$ ,  $s_x$ , and  $s_{xx'}$  stand for

$$s \stackrel{\text{def}}{=} \sum_i w_i \quad , \quad s_x \stackrel{\text{def}}{=} \sum_i w_i x_i \quad , \quad s_{xx'} \stackrel{\text{def}}{=} \sum_i w_i x_i x'_i \quad , \quad (2.16)$$

and  $w_i$ ,  $x_i$ ,  $x'_i$  for the weight, the position and the direction of the  $i$ th ray respectively. A criterion for how well a slope is actually defined is the *empirical correlation coefficient*  $r_{xx'}$ , which is 0 if there is no correlation between  $x_i$  and  $x'_i$  and near 1 if the correlation is very strong.

## 2.7 Lens design

*Compound refractive lenses* (CRL) are highly dispersive, i.e. their imaging properties change considerably with photon energy. Therefore MASH supports an auto-tuning of CRLs similar to Shadow3's auto-tuning of Bragg angles for crystals. Details of the auto-tuning (auto-focusing) algorithm are described in a different section. The basis for this auto-tuning algorithm is the *lens makers equation* [4]

$$f = \frac{R}{2N\delta} \quad , \quad (2.17)$$

for a (thin) CRL with  $N$  symmetric biconcave lens elements, where  $f$  stands for the focal length,  $\delta$  for the refraction index decrement,  $n = 1 - \delta + i\beta$ ,  $\beta$  for the absorption index, and  $R$  for the radius of curvature. Since the refraction index decrement is very small,<sup>4</sup> the radius of curvature has to be small and the number of lens elements large, in order to achieve a reasonably short focal length. Small lens radii in turn mean large spherical aberration. Hence, in order to achieve good imaging quality, parabolic lens profiles are indispensable. In this case, the radius  $R$  in the lens makers equation (2.17) has to be interpreted as the radius of curvature in the vertex of the parabola,<sup>5</sup> i.e. if the parabola is given by,  $y = ax^2$ , this is

$$R = \frac{1}{2a} \quad . \quad (2.18)$$

---

<sup>4</sup>of the order  $\delta \approx 10^{-5}$  for beryllium at around 5 keV

<sup>5</sup>see Fig. 2.4

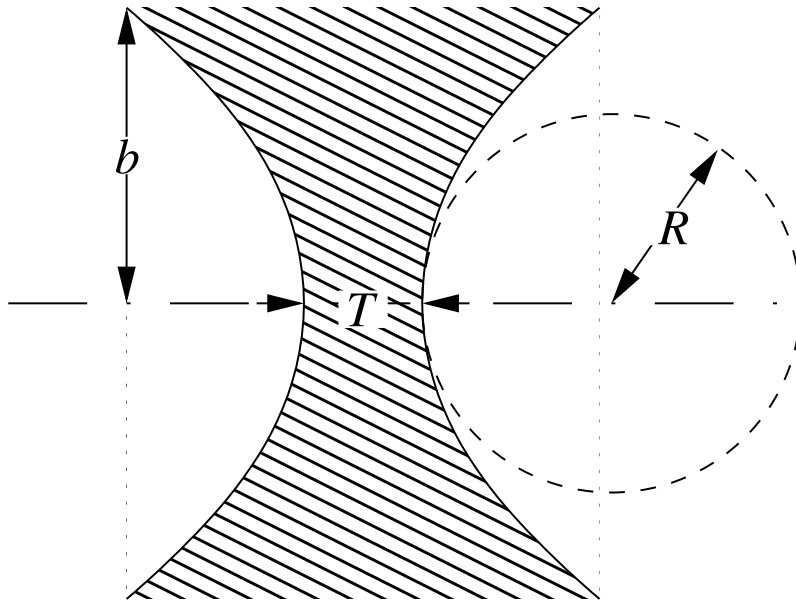


Figure 2.4: Parabolic bi-concave lens element in CRL

One of the most critical parameters for the design of an X-ray CRL is the throughput, i.e. the ratio between incident and transmitted power. Absorption is generally strong compared to e.g. visible light, and large number of lens elements with short radii of curvature lead to large thicknesses, that have to be penetrated.

The throughput can be estimated with the following analytical expressions for a bi-concave parabolic CRL with either a one-dimensionally curved (“cylindrical”) profile [4] or a rotationally symmetric profile [7]<sup>6</sup>

$$\frac{P_{\text{cyl}}}{P_0} = \frac{\sigma}{\sigma_0} \exp\left(\frac{-RT}{2\Sigma^2}\right) \operatorname{erf}\left(\frac{b}{\sqrt{2}\sigma}\right) , \quad \frac{P_{\text{rot}}}{P_0} = \frac{\sigma^2}{\sigma_0^2} \exp\left(\frac{-RT}{2\Sigma^2}\right) \left(1 - \exp\left(\frac{b^2}{2\sigma^2}\right)\right) . \quad (2.19)$$

Here  $\sigma_0$  stands for the RMS width of the incident X-ray beam, which is assumed to be Gaussian,  $b$  for the half width / radius of the lens aperture, and  $T$  for the lens thickness, i.e. the distance between the vertices of the parabolas. A key parameter is the *RMS lens aperture*

$$\Sigma = \sqrt{f\Lambda\delta} , \quad (2.20)$$

where  $\Lambda$  stands for the total attenuation length. There are two effects attenuating the X-ray beam: one is absorption, the other is Compton scattering [4]:

$$\frac{1}{\Lambda} = \frac{1}{l_{\text{abs}}} + \frac{1}{l_{\text{scatt}}} = \frac{4\pi\beta}{\lambda} + \left(\frac{4\pi}{\lambda}\right)^2 \frac{r_e\delta}{3} , \quad (2.21)$$

Here,  $\lambda$  stands for the X-ray wavelength and  $r_e$  for the classical electron radius. Finally  $\sigma$  is defined by

$$\frac{1}{\sigma^2} = \frac{1}{\sigma_0^2} + \frac{1}{\Sigma^2} , \quad (2.22)$$

and can be interpreted as the effective RMS beam size after passing through the CRL. The expressions in equation (2.19) have been derived within the ray optics approximation, assuming that the rays are parallel.

From expression (2.19) for throughput of a CRL, the following *design principles* can be derived:

---

<sup>6</sup>Equation (48) there is consistent with the expression in equation (2.19) here, but calculated for a homogeneous beam instead,  $\sigma_0 \rightarrow \infty$ .

- Lens thickness  $T$  should be reduced to the technological limit.
- Radius of curvature  $R$  should be chosen as short as possible. Shorter radius lens elements become thicker more quickly as one moves off centre, which increases absorption per lens element. Though, this is overcompensated for by the need for fewer elements to achieve the same focal length. By the manufacturing process the radius of curvature usually is closely correlated with element size, i.e. the radius  $r$  where the parabolic profile ends. If the beam is clipped by the lens the elements with shortest  $R$  might then be not optimal. In this case one has to find the combination of bending radius and size that provides maximum throughput. Ray-tracing or specialised codes for CRL throughput are usually required for this. The optimum defines the *fundamental* element type, which makes out the majority of elements in a CRL.
- The fundamental elements can be supplemented with a few elements of longer radius  $R$ , in order to reduce the step size when adding or removing a lens element. Ideally these supplemental elements come as a series of 2, 4, 8, ... times the radius of the fundamental lenses. Then, only one of each kind is required, each effectively halving the step size of the whole CRL.

## 2.8 Transfocator

A compound refractive lens (CRL) for X-rays consists of a collinear stack of lens elements. Each element is usually a biconcave lens. Concave, because of the refraction index for X-rays is usually smaller than one, and thus a concave lens is a positive lens.<sup>7</sup> Biconcave, since usually many refracting surfaces are required, and a biconcave lens has twice as many as a planoconcave.

The most popular material up to about 40 keV is beryllium, as it offers most refraction for least absorption in this regime. At higher photon energies aluminium and nickel are more appropriate.

CRLs for X-rays have a large chromatic error, i.e. their focal length is highly dependant on photon energy. In order to keep imaging properties constant, the number of elements must be adjusted. A device which does this automatically is called a *transfocator*. This is usually only possible in small steps of course, unless one has an infinite variety of lenses. Therefore, a small adjustment of the CRL's position is most frequently required, too. To keep this adjustment small, it is therefore most favourable to use weak lenses, such that the step from adding a lens or taking one away is small.

On the other hand, for maximum transmission lens elements should be as strong as possible, minimising the number of elements required. These two apparently conflicting goals can be achieved simultaneously, by combining lens elements with different radii of curvature.

### 2.8.1 Numbers of lens elements in thin lens approximation

In the thin lens approximation the focal length  $f$  of  $N$  identical lenses is given by

$$\frac{1}{f} = \frac{2\delta N}{R} , \quad (2.23)$$

where  $R$  stands for the radius of curvature in the vertex of the lens. Obviously, in thin lens approximation the inverse of the focal length of multiple lenses just

---

<sup>7</sup>Thus, a convex lens would be a negative lens. It would not be very useful though in general, as it is thickest in the middle, where the beam usually is most intense.

adds up, and one can write down the following expression for the focal length of a combination of different lenses:

$$\frac{1}{f} = \sum_{j=1}^J \frac{N_j}{f_j} = \frac{2\delta}{R_{\min}} \sum_{j=1}^J \frac{N_j}{r_j} , \quad (2.24)$$

where  $r_j$  is the ratio  $R_j/R_{\min}$ , i.e. the radius  $R_j$  given in multiples of the shortest available radius. This expression is used to determine the optimum combination of lens elements in order to build a CRL with a given focal length  $f$ . One starts with the strongest lens elements, i.e. those with smallest radius of curvature, which get the index number 1. Their number is simply given by a whole number division

$$N_1 = \left[ \frac{f^{-1}}{f_1^{-1}} \right] = \left[ \frac{R_{\min}}{2\delta f} \right] . \quad (2.25)$$

We refer to these elements as the *main elements* and all elements with larger radius as the *supplemental elements*. The number of lenses with the next smallest radius of curvature  $R_2$  is obtained by multiplying the remainder of the whole number division above by  $f_1^{-1}$  to obtain the remaining inverse focal length and by dividing the result by  $f_2^{-1}$ :

$$N_2 = \left[ \frac{f_1^{-1} \left( \frac{f^{-1}}{f_1^{-1}} - N_1 \right)}{f_2^{-1}} \right] = \left[ r_2 \left( \frac{R_{\min}}{2\delta f} - \frac{N_1}{r_1} \right) \right] . \quad (2.26)$$

Continuing this procedure provides the general expression

$$N_{j+1} = \left[ r_{j+1} \left( \frac{R_{\min}}{2\delta f} - \frac{N_1}{r_1} - \dots - \frac{N_j}{r_j} \right) \right] . \quad (2.27)$$

For the last set of lenses, those with largest radius of curvature, the whole number division is better replaced by rounding, which can provide a somewhat more accurate overall focal length. In this case it might be slightly shorter than required, but closer.

Often lens elements are provided in a series with radii doubling from one type to the next. The doubling might be only approximate, such as for example in a 1, 2, 5 rather than 1, 2, 4 series. In any case, each lens type with double radius halves the step size in the approach to the desired focal length. As the remainder of a whole number division is always smaller than one, usually only one of each half step elements is required, as two elements would provide the same step as the previous type. Only in case of the type with largest radius it could be two if rounding up. Alternatively, one could include the other element types in the rounding process. In case a combination of elements where two of the largest radius elements would provide best match, one could use instead one element with half the radius. Of course this might be already in use, if there is only one. In this case, one has to go to the element types with even shorter radius, and replace both the two lenses with largest radius and the one with half their radius. In the worst case one has to go back all the way to the elements with shortest radius, of which there are usually plenty of.

$$\frac{1}{f} = \frac{2\delta}{R_{\min}} \left( N_1 + \frac{1}{2} + 2\frac{1}{4} \right) = \frac{2\delta}{R_{\min}} \left( N_1 + 2\frac{1}{2} + 0\frac{1}{4} \right) = \frac{2\delta}{R_{\min}} \left( N_1 + 1 + 0\frac{1}{2} + 0\frac{1}{4} \right) . \quad (2.28)$$

This is a somewhat more elaborate scheme, but it pays off by requiring only one element of each half step type. Apart from one less element, this is also one less lens stack and one less actuator with associated motion controller.

## 2.8.2 Transfocator as a thick lens

At higher photon energies, required element numbers can go into the dozens. Above that, the most numerous main lens elements are usually divided into stacks of 1, 2, 4, ... elements to allow the variation of total element number with a minimum number of actuators. This setup allows for a binary encoding of a given number of elements, e.g.

$$21 = 1 \times 16 + 0 \times 8 + 1 \times 4 + 0 \times 2 + 1 \times 1$$

simply by moving stacks in and out. Consequently, the lenses are spread over a considerable range. This makes the use of thin lens approximation questionable. Even if the thin lens approximation should apply, one still has to determine the position of the principal plane in some kind of centre of mass calculation. If it has to be dealt with as a thick lens, one has to determine overall focal length and the positions of two principal planes. In any case, one has to dive somewhat into the theory of thick lenses and lens combinations.

### System matrix of an optical system

A system of multiple optical elements can be described by six *cardinal points*: the focal points, the surface vertices and the principal points. The *surface vertices* are the points where the first and the last optical surface respectively intersect with the optical axis. Of course, there is such a vertex for every optical surface in the system, but only the first and the last remain relevant in the optical description of the system as a whole. The principal points are the intersection of the principal planes with the optical axis. The principal planes in turn, are the planes where the rays are kinked.

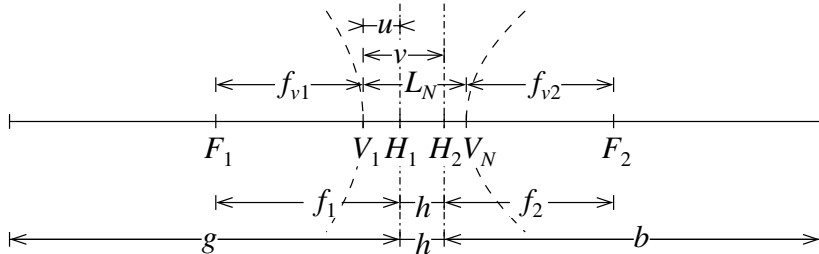


Figure 2.5: Cardinal points of an optical system with  $N$  optical planes.

Figure 2.5 marks the cardinal points of an optical system: focal points,  $F_{1|2}$ , principal points  $H_{1|2}$  and first and last surface vertices,  $V_{1|N}$ . There are  $N - 2$  other surface vertices, that define the optical system. They are no longer needed, once the cardinal points are calculated. The principal points are defined by their distances,  $u$  and  $v$ , to the first surface vertex (the position of the very first optical surface). Other distances such as focal length in object and image space,  $f_{1|2}$ , source and image distance,  $g$  and  $b$ , are measured relatively to the principal planes. The distance,  $h$ , between principal planes might well be negative.

The cardinal points of a non-trivial optical system are usually calculated using  $2 \times 2$  ray transfer matrices. A system matrix, i.e. the ray transfer matrix of the system as a whole, is obtained by matrix multiplication of the ray transfer matrices of each optical surface and the space in between, in the order in which they occur. Unfortunately there is a variety of different definitions of these matrices around. We use the definition according to Meyer-Arendt [9]. A short description can be found online [1]. In this definition rays are described by the two dimensional vector  $(n\gamma, r)$ , where  $\gamma$  stands for the rays' angle to the optical axis and  $r$  for their distance

to the optical axis at the principal planes. The ray transfer matrix  $M$  then describes the kink that the rays get at the principal planes:

$$\begin{pmatrix} M_{11} & M_{12} \\ M_{21} & M_{22} \end{pmatrix} \begin{pmatrix} n_1\gamma \\ r_1 \end{pmatrix} = \begin{pmatrix} n_2\gamma' \\ r_2 \end{pmatrix}$$

The elements of the ray transfer matrix are related to the cardinal points via the following expressions:

Focal length in object and image space

$$f_1 \stackrel{\text{def}}{=} \overline{H_1 F_1} = -\frac{n_1}{M_{12}}, \quad (2.29)$$

$$f_2 \stackrel{\text{def}}{=} \overline{H_2 F_2} = \frac{n_2}{M_{12}}, \quad (2.30)$$

position of the first principal plane relative to the first surface vertex

$$u = \overline{V_1 H_1} = \frac{n_1(1 - M_{11})}{M_{12}}, \quad (2.31)$$

and finally position of the second principal plane relative to the last surface vertex

$$L_N - v = -\overline{V_N H_2} = \frac{n_2(1 - M_{22})}{M_{12}}, \quad (2.32)$$

where  $L_N$  is the distance of the  $N$ th vertex from the very first. Subtracting the distance of the principal plane to the respective surface vertex from the respective focal length provides expressions for the *front vertex focal length*

$$f_{v1} = \overline{V_1 F_1} = \frac{-n_1 M_{11}}{M_{12}}, \quad (2.33)$$

and the *back vertex focal length*:

$$f_{v2} = \overline{V_2 F_2} = \frac{n_2 M_{22}}{M_{12}}. \quad (2.34)$$

The ray transfer matrix for a single refracting surface, the *refraction matrix*, is given by

$$M_R = \begin{pmatrix} 1 & P_s \\ 0 & 1 \end{pmatrix} \quad (2.35)$$

where  $P_s$  stands for the *surface power*

$$P_s \stackrel{\text{def}}{=} \frac{n_2 - n_1}{R} = \frac{\delta_1 - \delta_2}{R}, \quad (2.36)$$

$n_{1|2}$  for the refractive indices in object and image space respectively,  $\delta_{1|2}$  for the corresponding refraction index decrements ( $n = 1 - \delta$ ), and  $R$  for the central *radius of curvature*. The form of above expression is based on the following sign convention:  $R$  is positive if the radius drawn from surface to centre is going into the same direction as the light (convex) and negative otherwise (concave). This convention is designed for normal optics, where positive lenses have positive  $R$ . For X-rays, with refraction indices usually smaller than one, its unfortunately the other way round. Of course, the surface powers of the front and the back surface of a concave (positive) X-ray lens are both positive and  $P_s = +\delta/R$ .

The ray transfer matrix for the space between two optical surfaces, the *translation matrix*, is given by

$$M_T = \begin{pmatrix} 1 & 0 \\ -L/n & 1 \end{pmatrix}, \quad (2.37)$$

where  $L$  is the thickness and  $n$  the refraction index of the slab.

The ray transfer matrix for a parabolic lens surface with adjacent space (downstream) of length  $L$  and refraction index  $n$ , is given by the matrix product

$$M_S = M_T M_R = \begin{pmatrix} 1 & P \\ -L/n & 1 - PL/n \end{pmatrix}, \quad (2.38)$$

Due to the smallness of the refractive index decrement,  $\delta$ , for X-rays, the refractive surface power  $P = \delta/R$  is small and  $L/n = L/(1 - \delta) \approx L(1 + \delta)$ . The product  $PL/n$  on the other hand is  $PL + (\delta^2)$  and hence can be approximated more radically by  $PL$ :

$$M_S = \begin{pmatrix} 1 & P \\ -L(1 + \delta) & 1 - PL \end{pmatrix}. \quad (2.39)$$

The system matrix of a compound refractive lens with  $N$  elements constitutes of the product of  $2N$  such matrices with alternating materials. One of these “materials” most commonly is vacuum,  $\delta = 0$ .

### 2.8.3 An algorithm for design and optimization of transfocators

Transfocators are unique in a sense that they consist of a large and varying number of optical elements. Therefore, it is not straight forward to determine its configuration from the required imaging geometry. Thin lens approximation does not apply for the system of lens elements as a whole, as the distances between the elements are too large. On the other hand, the inverse process, i.e. the calculation of overall focal length and principal points for a given configuration of lens elements is straight forward. For example, the ray transfer matrix method can be used. Hence, the way to go is to calculate the positions of the transfocator to fulfill the imaging equation for all configurations and to pick the configuration with the transfocator closest to a default position defined by required (de)magnification or similar constraints.

Before, the lens elements with the highest throughput must be found. If the beamsize is generally small compared to the opening diameter of the lens elements, this would be the elements with the steepest profile. Under this condition they provide most focussing power per absorption. Opening diameters of lens elements are usually very small and very often clip the periphery of the beam. Therefore elements with shallower profile but larger opening diameters often have higher throughput. The elements with the highest throughput are chosen as the main elements, that make out the majority of elements in a CRL. This throughput optimization can be safely done in thin lens approximation, as the exact position of the lens or the focus are not critical.

Figure 2.6 shows a flowchart of the design and optimisation process for transfocators including throughput optimisation and configuration design.

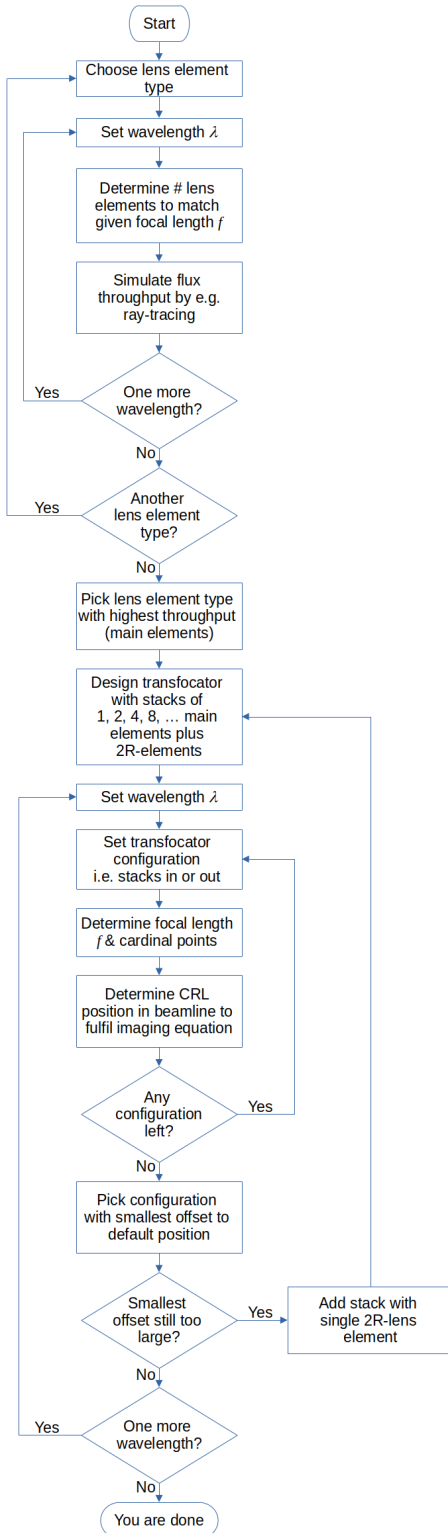


Figure 2.6: Simplified flowchart of the transfocator design and optimisation algorithm.

# Part I

## Choice of beam splitter

## Chapter 3

# Setup with Si333 beam splitter

A thin silicon crystal is employed as a diffractive beam splitter, using the Si333 reflection in Laue geometry. The Si333 reflection diverts radiation within a narrow bandwidth of

$$\delta E/E = \delta\theta/\tan\theta$$

to the SinCrys side branch. The thickness of the crystal slab has to be optimised in order to maximise diffraction efficiency under the constraint of keeping absorption of the transmitted main beam low. A natural choice is a maximum of the pendel-solution, i.e. the reflectivity oscillating with crystal thickness as predicted by the theory of dynamic diffraction from nearly perfect crystals.

Subsequent reflection from a second crystal with equal inter-planar spacing and diffracting planes parallel to the first is the golden standard in crystal monochromator design. This returns the twice diffracted beam parallel to the direction of the incident, with an adjustable spatial offset, such that downstream optical components and the sample do not have to follow the Bragg angle changes with selected photon energy. Si333 in Bragg geometry is chosen for the second crystal. Putting the second crystal at a distance of around 1.91 metres behind the first provides the required offset of more than one metre between the twice deflected beam and the main beam.

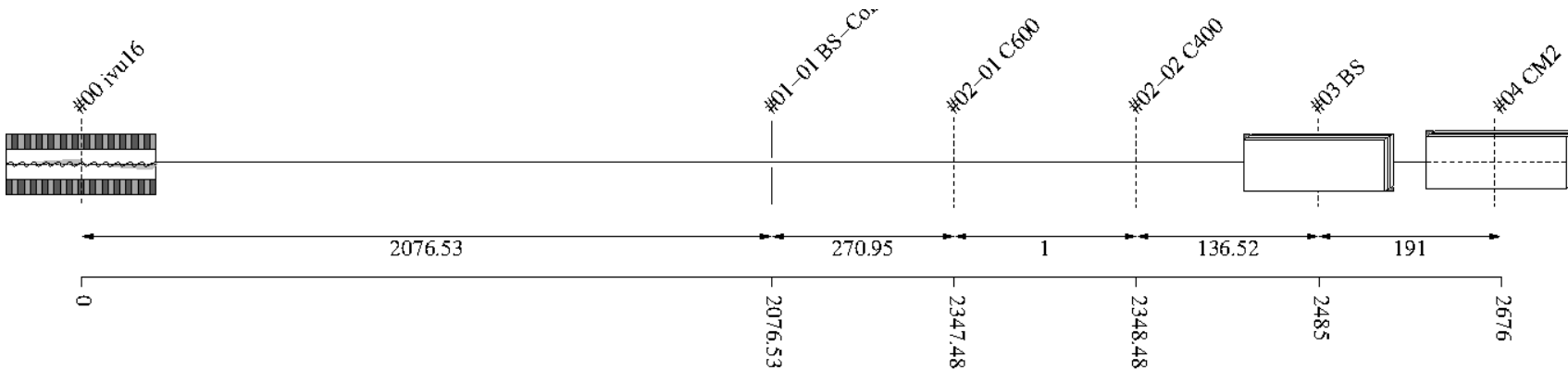


Figure 3.1: Schematic of optical setup

#	Name	Pathlen. cm	Descript.	Shape	Pitch* deg	Roll deg	Yaw deg	x_min cm	x_max cm	y_min cm	y_max cm	Thick. cm	Surface
0	ivu16	0	undulator	auto	0	0	0	-0.0027	0.0027	-0.0002	0.0002	auto	
1		2076.53	none	plane	0	0	0	-inf	inf	-inf	inf		perfect
1-1	BS-Collim	2076.53	aperture	rectangle	0	0	0	-0.035	0.035	-0.035	0.035		
2	Filter	2347.48	none	plane	0	0	0	-inf	inf	-inf	inf		perfect
2-1	C600	2347.48	C-filter	rectangle	0	0	0	-inf	inf	-inf	inf	0.06	
2-2	C400	2348.48	C-filter	rectangle	0	0	0	-inf	inf	-inf	inf	0.04	
3	BS	2485	Si(3,3,3)-crystal	plane	105.788	90	0	-0.15	0.15	-0.15	0.15		heat bump
4	CM2	2676	Si(3,3,3)-crystal	plane	15.7878	180	0	-inf	inf	-inf	inf		perfect

Table 3.1: Setup parameters common to all components. (\*Glancing angle for mirrors, multilayers and crystals. Angle to surface normal otherwise.)

**Rays:** Polar type = total

Polar phase = 0 deg

Polar degree = 0

Is coherent = no

**Spectrum:** E min = 500 eV

E max = 40000 eV

Relative linewidth = 1

**Band:** Bandwidth = 0.0001

**Insertion Device:** lambda period = 1.6 cm

n period = 187

I electron = 0.5 A

E electron = 3 GeV

y horizontal waist = 0 cm

y vertical waist = 0 cm

epsilon x = 3.2E-08 cm rad

epsilon z = 8E-10 cm rad

K y = 1.66

K ymax = 1.7

Divergence limit = 5E-05 rad

**Undulator:** n harmonic max = 99

Tuning type = fixed gap

l aperture = 2076.53 cm

dx aperture = 0.07 cm

dz aperture = 0.07 cm

#1

**Screen:** Is absorbing[1] = no

**Shape:** Thickness = 0 cm

#2 Filter

**Screen:** Is absorbing[1] = yes

Is absorbing[2] = yes

Molecular formula[1] = C

Molecular formula[2] = C

Mass density[1] = 3.5 g/cm^3

Mass density[2] = 3.5 g/cm^3

Thickness[1] = 0.06 cm

Thickness[2] = 0.04 cm

**Shape:** Thickness = 0 cm

### #3 BS

**Grating:** n order = 1

**Crystal:** Structure type = zincblende

Lattice constant[1] = 5.43094 Angstrom

Lattice constant[2] = 5.43094 Angstrom

Lattice constant[3] = 5.43094 Angstrom

Debye Waller factor = 1

Is absorbing = yes

Is asymmetric = yes

Angle asymmetry = 90 deg

Is inclined = no

Is Johansson geometry = no

Is mosaic = no

**Tune:** z rotation axis = 0 cm

**Geometry:** Is thin = yes

Tune automatic = yes

**Shape:** Thickness = 0.0039 cm

**Boundary:** Type = rectangle

x rim = 0.5 cm

y rim = 0.5 cm

**Surface:** Is rough = no

**FEA:** Design type = type specific

Crystal design = laue with cooling loop

Is isotropic = no

Angle x = 45 deg

Angle y = 35.2644 deg

Angle z = 0 deg

Mass density = 2.329 g/cm<sup>3</sup>

**Heat:** Heat transfer type[1] = insulated

Heat transfer type[2] = heat transfer

Heat transfer type[3] = insulated

Heat transfer type[4] = insulated

Heat transfer type[5] = heat transfer

Heat transfer type[6] = flux

Heat transfer type[7] = insulated

Heat transfer type[8] = heat transfer

Heat transfer type[9] = heat sink

Heat transfer coefficient = 1 W/(cm<sup>2</sup>K)

Heat sink coefficient = 10 W/(cm<sup>2</sup>K)

T reference = 77 K  
 T cooling = 77 K  
 Heat capacity = 0.2 J/(gK)  
 Thermal conductivity[1] = 68.908 W/(cmK^n)  
 Thermal conductivity[2] = -1.2807 W/(cmK^n)  
 Thermal conductivity[3] = 0.01038 W/(cmK^n)  
 Thermal conductivity[4] = -4.46212E-05 W/(cmK^n)  
 Thermal conductivity[5] = 1.0589E-07 W/(cmK^n)  
 Thermal conductivity[6] = -1.3103E-10 W/(cmK^n)  
 Thermal conductivity[7] = 6.6033E-14 W/(cmK^n)

**Stress and strain:** Constraint[1] = free

Constraint[2] = kinematic  
 Constraint[3] = free  
 Constraint[4] = free  
 Constraint[5] = free  
 Constraint[6] = free  
 Constraint[7] = free  
 Constraint[8] = free  
 Constraint[9] = free  
 Thermal expansion[1] = 2.5458E-06 1/K^n  
 Thermal expansion[2] = -9.28E-08 1/K^n  
 Thermal expansion[3] = 9.0015E-10 1/K^n  
 Thermal expansion[4] = -3.0037E-12 1/K^n  
 Thermal expansion[5] = 3.4632E-15 1/K^n  
 Stiffness tensor(1)(1) = 1.6772E+11 Pa  
 Stiffness tensor(2)[1] = 6.498E+10 Pa  
 Stiffness tensor(2)[2] = 1.6772E+11 Pa  
 Stiffness tensor(3)[1] = 6.498E+10 Pa  
 Stiffness tensor(3)[2] = 6.498E+10 Pa  
 Stiffness tensor(3)[3] = 1.6772E+11 Pa  
 Stiffness tensor(4)[1] = 0 Pa  
 Stiffness tensor(4)[2] = 0 Pa  
 Stiffness tensor(4)[3] = 0 Pa  
 Stiffness tensor(4)[4] = 8.036E+10 Pa  
 Stiffness tensor(5)[1] = 0 Pa  
 Stiffness tensor(5)[2] = 0 Pa  
 Stiffness tensor(5)[3] = 0 Pa  
 Stiffness tensor(5)[4] = 0 Pa  
 Stiffness tensor(5)[5] = 8.036E+10 Pa  
 Stiffness tensor(6)[1] = 0 Pa  
 Stiffness tensor(6)[2] = 0 Pa  
 Stiffness tensor(6)[3] = 0 Pa  
 Stiffness tensor(6)[4] = 0 Pa  
 Stiffness tensor(6)[5] = 0 Pa  
 Stiffness tensor(6)[6] = 8.036E+10 Pa

#### #4 CM2

**Crystal:** Structure type = zincblende

Lattice constant[1] = 5.43094 Angstrom  
 Lattice constant[2] = 5.43094 Angstrom  
 Lattice constant[3] = 5.43094 Angstrom

Debye Waller factor = 1  
Is absorbing = yes  
Is asymmetric = no  
Is inclined = no  
Is Johansson geometry = no  
Is mosaic = no

**Tune:** Type = constant pathlength  
Are downstream elements fixed = no

**Geometry:** Is thin = no  
Tune automatic = yes

**Boundary:** Type = none

**Surface:** Is rough = no

## Chapter 4

# Finite element analysis (FEA)

The cooling design of the diffractive beam splitter, that simultaneously serves as the first monochromator crystal, is very similar to that of a thin filter. The thin crystal slab is mounted on a thick OFC-copper plate that has a hole in the middle for the beam to pass. The hole should be of minimum size to keep cooling pathways short and thus the peak temperature low. Despite of the high thermal conductivity, heat transport across the crystal slab is not very efficient due to its thinness. The crystal slab is clamped in place by a small copper frame ensuring good thermal contact to the copper plate. A copper pipe loop for cooling is brazed onto the copper plate keeping roughly the same distance to the hole in three out of four directions. The distance to the hole is not very critical here thanks to the good heat transport in the thick copper plate. It has to be checked whether cooling with water is sufficient or whether cryo-cooling is required.

In the finite element analysis (FEA) of the heat transfer, heat removal by the cooling agent is simplified by assuming a constant heat transfer coefficient of  $1 \text{ W}/(\text{K cm}^2)$  to a cooling agent reservoir of constant temperature. The chosen heat transfer coefficient is typical for turbulent flow.

## 4.1 Room temperature

"fig/BS\_choice\_Si333/fea\_plot\_geom\_c16\_21800eV\_03.png" Lbl.:BS\_choice\_Si333\_Surface\_plot\_fea\_plot\_geom\_c16\_21800eV\_03

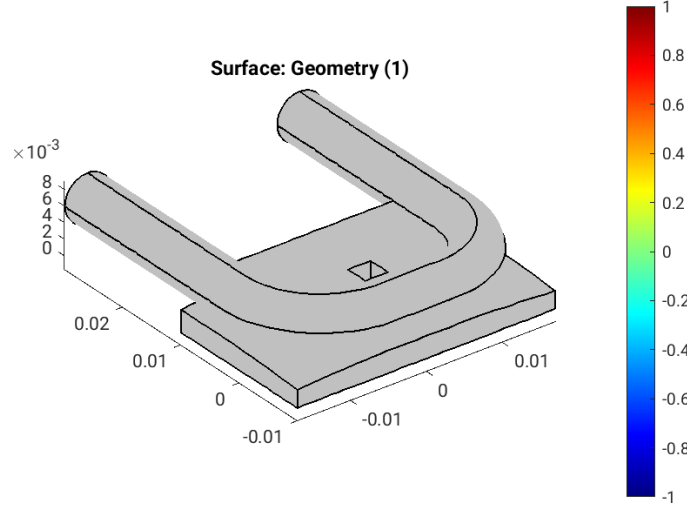


Figure 4.1: Geometry [m] of optical element #03, for case #16, at 21800 eV photon energy setting.

"fig/BS\_choice\_Si333/fea\_plot\_cnstr\_c16\_21800eV\_03.png" Lbl.:BS\_choice\_Si333\_Surface\_plot\_fea\_plot\_cnstr\_c16\_21800eV\_03

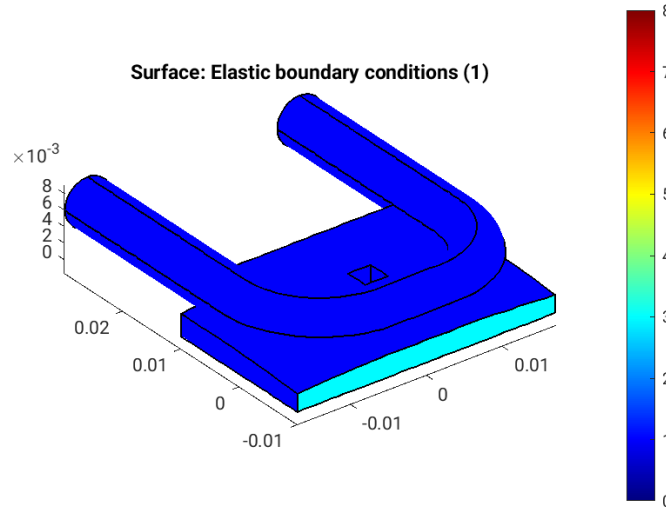


Figure 4.2: Elastic boundary conditions on the surfaces of optical element #03, for case #16, at 21800 eV photon energy setting. Color legend: Blue: Surface can move freely in all directions. Cyan: Tension free kinematic mounting. Minimalistic constraint for three points in surface. One point is fixed, the second can move in one direction, and the third in two, in a fashion that defines angular orientation without introducing stress if the surface expands.

"fig/BS\_choice\_Si333/fea\_plot\_trans\_c16\_21800eV\_03.png" Lbl.:BS\_choice\_Si333\_Surface\_plot\_fea\_plot\_trans\_c16\_21800eV\_03

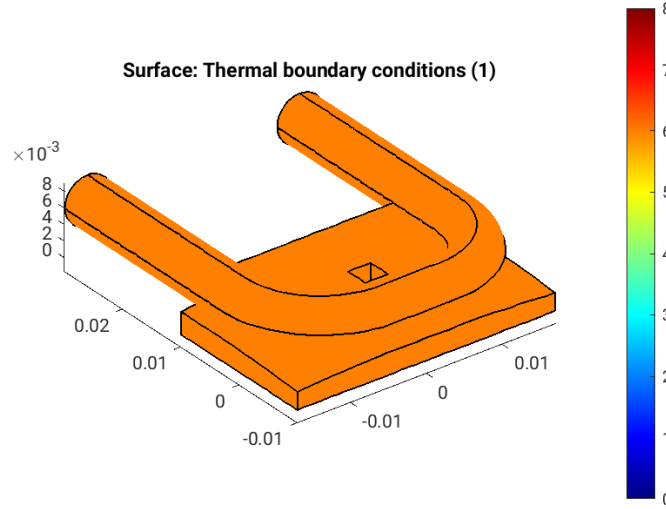


Figure 4.3: Thermal boundary conditions on the surfaces of optical element #03, for case #16, at 21800 eV photon energy setting. Color legend: Orange: No heat transfer at all. Blue: Heat transfer coefficient and temperature difference define heat current density,  $j_q = h(T - T_{cool})$ . Red: Forced heat flux from e.g. absorbed X-rays. Cyan: Heat transfer coefficient and temperature difference define heat current density,  $j_q = h^* \Delta T$  (only at inner surfaces).

"fig/BS\_choice\_Si333/fea\_plot\_heattrans\_c16\_21800eV\_03.png" Lbl.:BS\_choice\_Si333\_Surface\_plot\_fea\_plot\_heattrans\_c16\_21800eV\_03

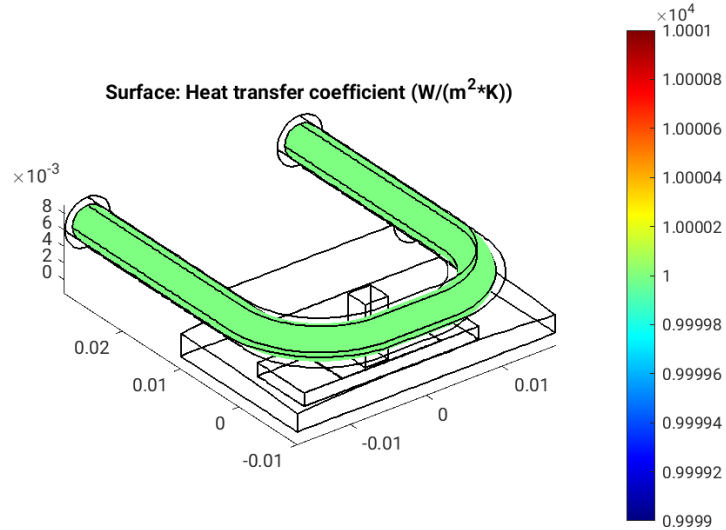


Figure 4.4: Heat transfer coefficient,  $h$  [ $W/(m^2 K)$ ], on the surfaces of optical element #03, for case #16, at 21800 eV photon energy setting.

"fig/BS\_choice\_Si333/fea\_plot\_heatflux\_c16\_21800eV\_03.png" Lbl.:BS\_choice\_Si333\_Surface\_plot\_fea\_plot\_heatflux\_c16\_21800eV\_03

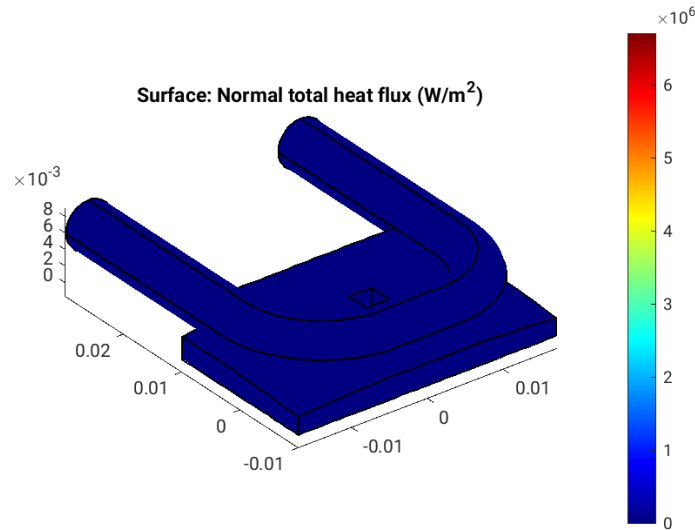


Figure 4.5: Absorbed irradiance,  $p_{\text{abs}}$  [W/m<sup>2</sup>], on the surfaces of optical element #03, for case #16, at 21800 eV photon energy setting.

"fig/BS\_choice\_Si333/fea\_plot\_temp\_c16\_21800eV\_03.png" Lbl.:BS\_choice\_Si333\_Surface\_plot\_fea\_plot\_temp\_c16\_21800eV\_03

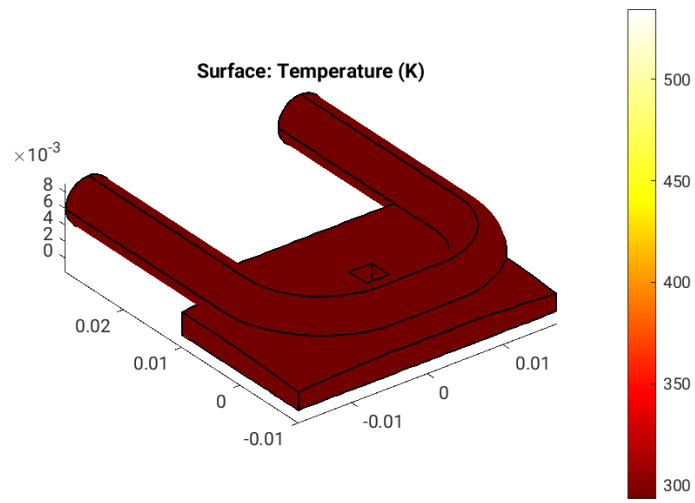


Figure 4.6: Temperature,  $T$  [K], on the surfaces of optical element #03, for case #16, at 21800 eV photon energy setting.

"fig/BS\_choice\_Si333/fea\_plot\_thermcond\_c16\_21800eV\_03.png" Lbl.:BS\_choice\_Si333\_Surface\_plot\_fea\_plot\_thermcond\_c16\_21800eV\_03

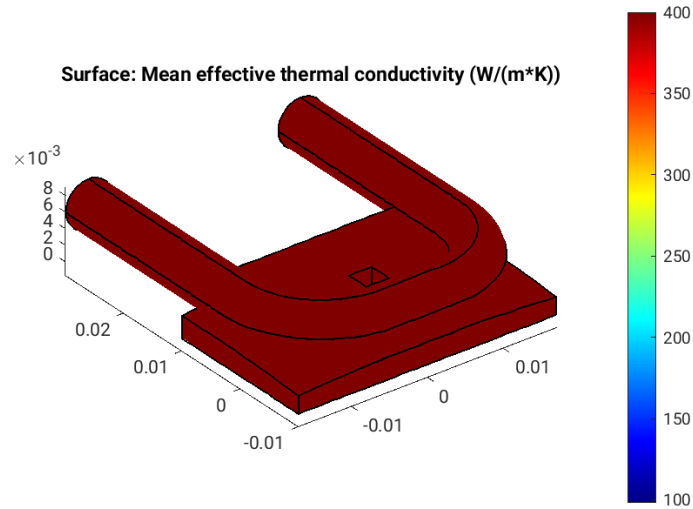


Figure 4.7: Thermal conductivity, lambda [W/(m K)], on the surfaces of optical element #03, for case #16, at 21800 eV photon energy setting.

"fig/BS\_choice\_Si333/fea\_plot\_stress\_c16\_21800eV\_03.png" Lbl.:BS\_choice\_Si333\_Surface\_plot\_fea\_plot\_stress\_c16\_21800eV\_03

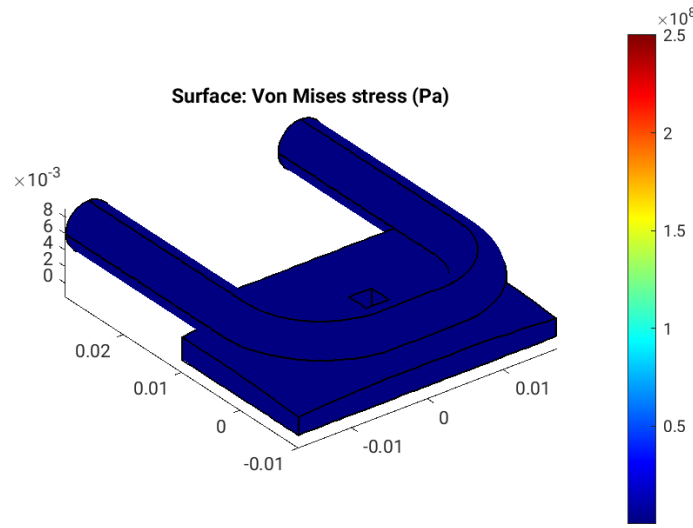


Figure 4.8: Von Mises stress, sigma [Pa], on the surfaces of optical element #03, for case #16, at 21800 eV photon energy setting.

```
"fig/BS_choice_Si333/fea_plot_deform_c16_21800eV_03.png" Lbl.:BS_choice_Si333_Surface_plot_fea_plot_deform_c16_21800eV_03
```

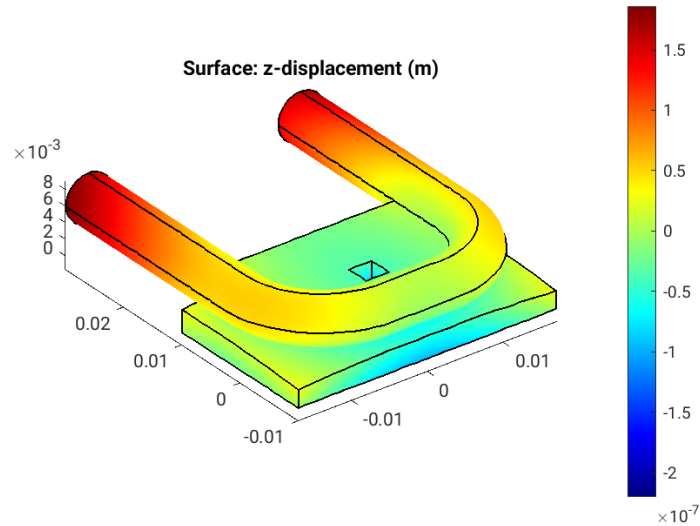


Figure 4.9: Thermoelastic deformation,  $dz$  [m], on the surfaces of optical element #03, for case #16, at 21800 eV photon energy setting.

## 4.2 Cryogenic temperature

```
"fig/BS_choice_Si333/fea_plot_geom_c26_21800eV_03.png" Lbl.:BS_choice_Si333_Surface_plot_fea_plot_geom_c26_21800eV_03
```

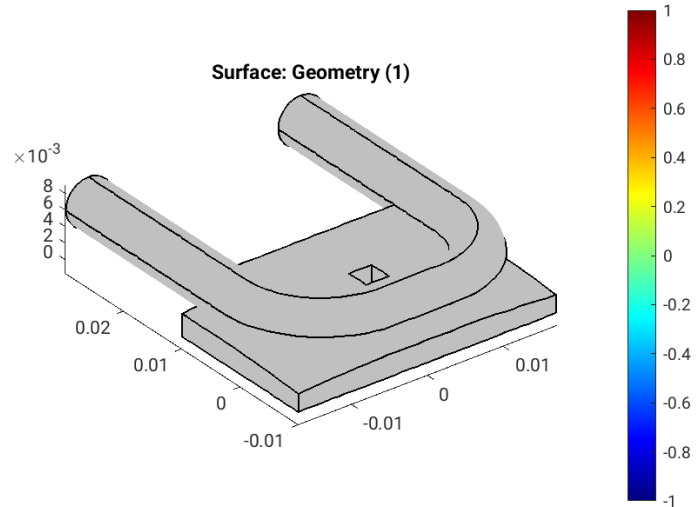


Figure 4.10: Geometry [m] of optical element #03, for case #26, at 21800 eV photon energy setting.

"fig/BS\_choice\_Si333/fea\_plot\_cnstr\_c26\_21800eV\_03.png" Lbl.:BS\_choice\_Si333\_Surface\_plot\_fea\_plot\_cnstr\_c26\_21800eV\_03

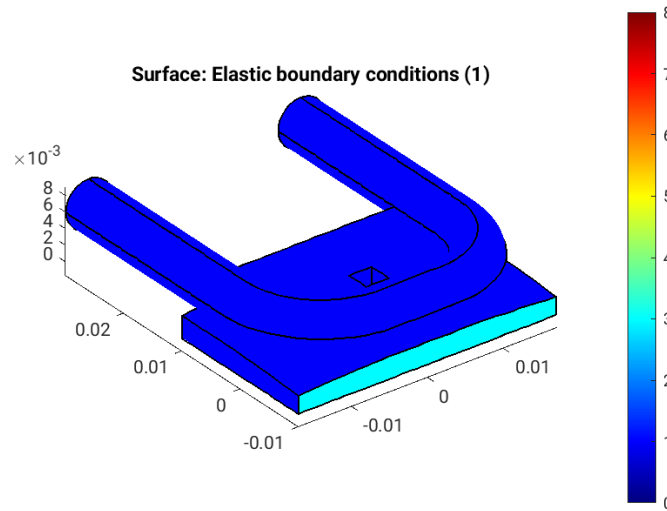


Figure 4.11: Elastic boundary conditions on the surfaces of optical element #03, for case #26, at 21800 eV photon energy setting. Color legend: Blue: Surface can move freely in all directions. Cyan: Tension free kinematic mounting. Minimalistic constraint for three points in surface. One point is fixed, the second can move in one direction, and the third in two, in a fashion that defines angular orientation without introducing stress if the surface expands.

"fig/BS\_choice\_Si333/fea\_plot\_trans\_c26\_21800eV\_03.png" Lbl.:BS\_choice\_Si333\_Surface\_plot\_fea\_plot\_trans\_c26\_21800eV\_03

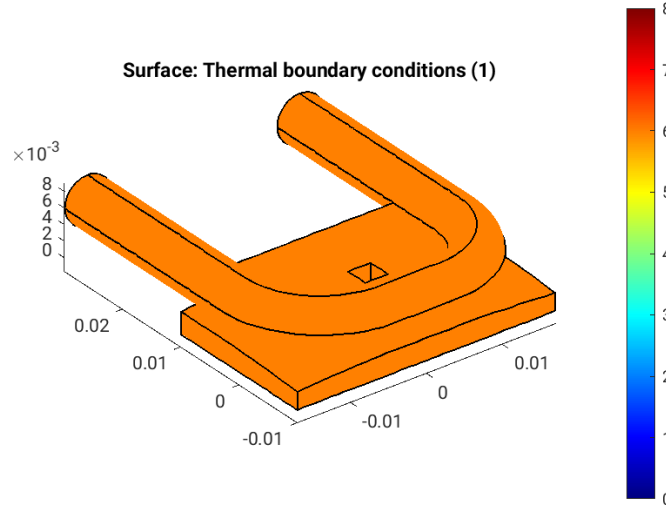


Figure 4.12: Thermal boundary conditions on the surfaces of optical element #03, for case #26, at 21800 eV photon energy setting. Color legend: Orange: No heat transfer at all. Blue: Heat transfer coefficient and temperature difference define heat current density,  $j_q = h(T - T_{cool})$ . Red: Forced heat flux from e.g. absorbed X-rays. Cyan: Heat transfer coefficient and temperature difference define heat current density,  $j_q = h^* \Delta T$  (only at inner surfaces).

"fig/BS\_choice\_Si333/fea\_plot\_heattrans\_c26\_21800eV\_03.png" Lbl.:BS\_choice\_Si333\_Surface\_plot\_fea\_plot\_heattrans\_c26\_21800eV\_03

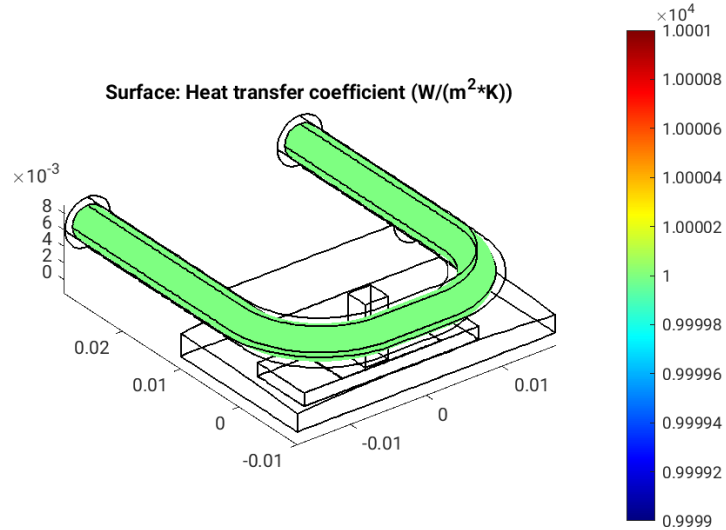


Figure 4.13: Heat transfer coefficient,  $h$  [ $\text{W}/(\text{m}^2 \text{ K})$ ], on the surfaces of optical element #03, for case #26, at 21800 eV photon energy setting.

"fig/BS\_choice\_Si333/fea\_plot\_heatflux\_c26\_21800eV\_03.png" Lbl.:BS\_choice\_Si333\_Surface\_plot\_fea\_plot\_heatflux\_c26\_21800eV\_03

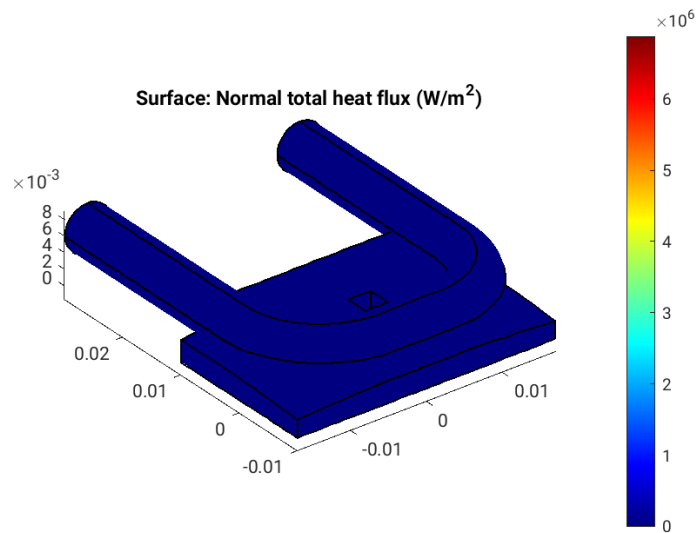


Figure 4.14: Absorbed irradiance,  $p_{\text{abs}}$  [W/m<sup>2</sup>], on the surfaces of optical element #03, for case #26, at 21800 eV photon energy setting.

"fig/BS\_choice\_Si333/fea\_plot\_temp\_c26\_21800eV\_03.png" Lbl.:BS\_choice\_Si333\_Surface\_plot\_fea\_plot\_temp\_c26\_21800eV\_03

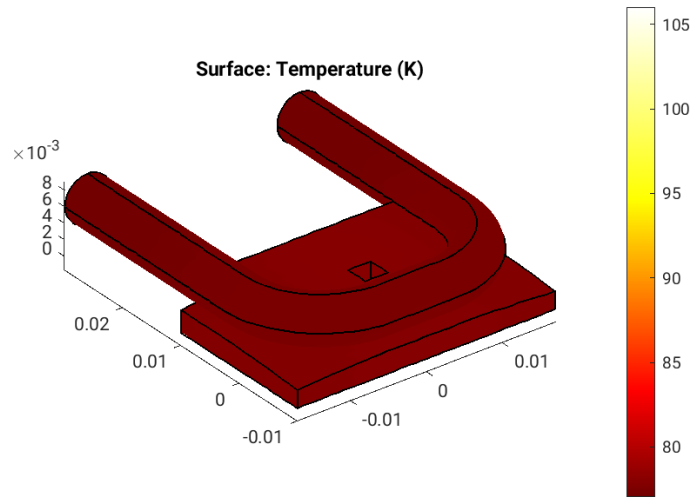


Figure 4.15: Temperature, T [K], on the surfaces of optical element #03, for case #26, at 21800 eV photon energy setting.

"fig/BS\_choice\_Si333/fea\_plot\_thermcond\_c26\_21800eV\_03.png" Lbl.:BS\_choice\_Si333\_Surface\_plot\_fea\_plot\_thermcond\_c26\_21800eV\_03

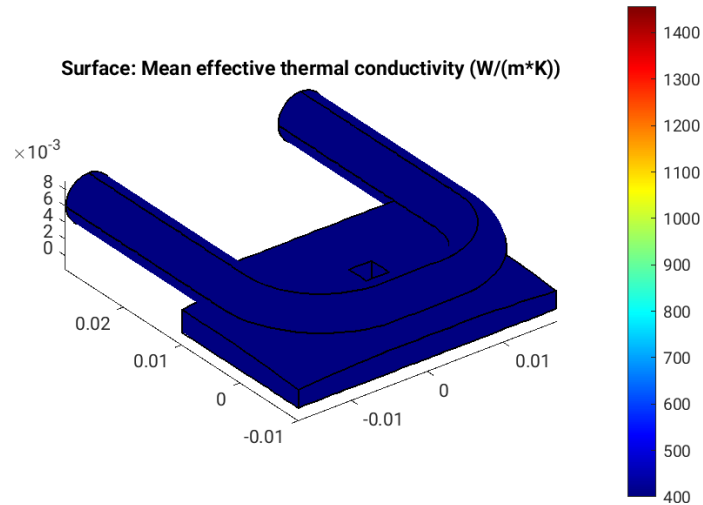


Figure 4.16: Thermal conductivity, lambda [W/(m K)], on the surfaces of optical element #03, for case #26, at 21800 eV photon energy setting.

"fig/BS\_choice\_Si333/fea\_plot\_stress\_c26\_21800eV\_03.png" Lbl.:BS\_choice\_Si333\_Surface\_plot\_fea\_plot\_stress\_c26\_21800eV\_03

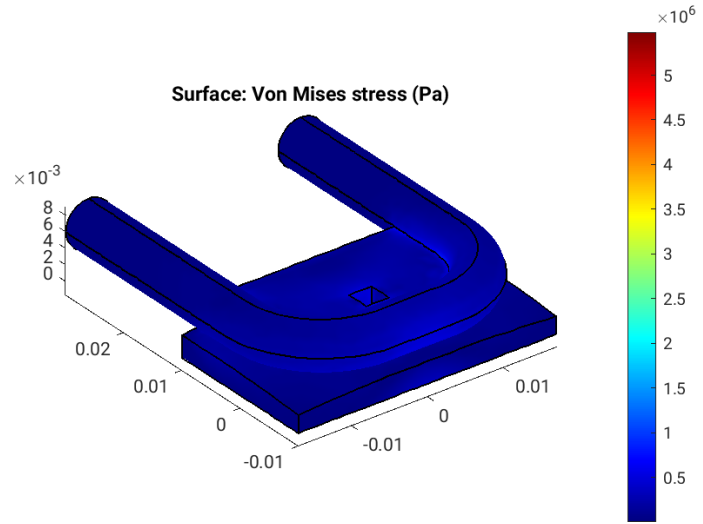


Figure 4.17: Von Mises stress, sigma [Pa], on the surfaces of optical element #03, for case #26, at 21800 eV photon energy setting.

"fig/BS\_choice\_Si333/fea\_plot\_deform\_c26\_21800eV\_03.png" Lbl.:BS\_choice\_Si333\_Surface\_plot\_fea\_plot\_deform\_c26\_21800eV\_03

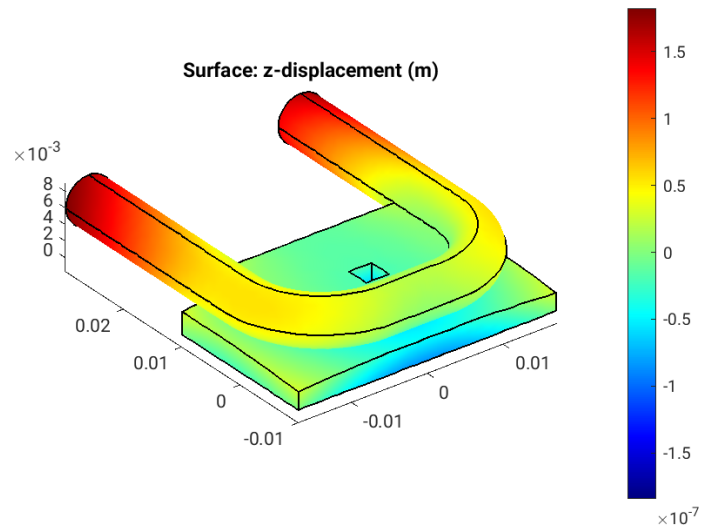


Figure 4.18: Thermoelastic deformation,  $dz$  [m], on the surfaces of optical element #03, for case #26, at 21800 eV photon energy setting.

# Chapter 5

## Parameter scan cases

There are thirty cases in total, which fall into three groups á ten cases. The first group, is for the perfect crystal case without deformation of the beam splitter under heat load due to X-ray absorption. Second and third group are for the beam splitter deformed under heat load at room temperature and at cryogenic temperature (77 K) respectively. Within the ten cases of every group the thickness of the beam splitter is varied in order to optimize reflectivity that varies periodically with this thickness (so called pendellösung). Due to the periodic character there are several thicknesses with a reflectivity close to 100%. On one hand, the first reflectivity maximum, i.e. that for smallest thickness, offers the highest transparency for the transmitted main beam. On the other hand, manufacturing, mounting and stability under heat load are more challenging the thinner the beam splitter is. As silicon has an absorption problem, as will be seen later, we went for the thinnest option anyway, quasi as the best case scenario. If it is still worse than other set ups, one can safely disregard Si333 beam splitters.

Case	T_cooling_03 K	heat_capacity_03 J/(gK)	Has_slope_error_03	Skip_heatload	Thickness_03 cm
1	293.15	0.7	no	yes	0.0005
2	293.15	0.7	no	yes	0.001
3	293.15	0.7	no	yes	0.0015
4	293.15	0.7	no	yes	0.002
5	293.15	0.7	no	yes	0.0025
6	293.15	0.7	no	yes	0.003
7	293.15	0.7	no	yes	0.0035
8	293.15	0.7	no	yes	0.004
9	293.15	0.7	no	yes	0.0045
10	293.15	0.7	no	yes	0.005
11	293.15	0.7	yes	no	0.0005
12	293.15	0.7	yes	no	0.001
13	293.15	0.7	yes	no	0.0015
14	293.15	0.7	yes	no	0.002
15	293.15	0.7	yes	no	0.0025
16	293.15	0.7	yes	no	0.003
17	293.15	0.7	yes	no	0.0035
18	293.15	0.7	yes	no	0.004
19	293.15	0.7	yes	no	0.0045
20	293.15	0.7	yes	no	0.005
21	77	0.2	yes	no	0.0005
22	77	0.2	yes	no	0.001
23	77	0.2	yes	no	0.0015
24	77	0.2	yes	no	0.002
25	77	0.2	yes	no	0.0025
26	77	0.2	yes	no	0.003
27	77	0.2	yes	no	0.0035
28	77	0.2	yes	no	0.004
29	77	0.2	yes	no	0.0045
30	77	0.2	yes	no	0.005

Table 5.1: Parameter values for different cases in parameter scan

### Legend

**Case:** Case number in parameter scan

**T\_cooling\_03:** Optical\_element\_#3.FEA.Heat.T\_cooling (Cooling temperature.)

**heat\_capacity\_03:** Optical\_element\_#3.FEA.Heat.heat\_capacity (Specific heat capacity.)

**Has\_slope\_error\_03:** Optical\_element\_#3.Surface.Has\_slope\_error (Has surface slope error?)

**Skip\_heatload:** Session.Skip\_heatload (Skip heat load calculation for all optical elements? (heat load parameters are kept))

**Thickness\_03:** Optical\_element\_#3.Shape.Thickness (Optical element's thickness or thickness of optically active layer.)

## Chapter 6

# Photon energy scan

As SinCrys basically runs in “parasitic” mode to DanMAX’s main branch, the undulator will be set up for the needs of the latter. The automatic undulator scanning routine in MASH on the other hand is designed to adjust the undulator gap for the energy range defined in the simulation parameters, i.e. the range required by SinCrys. Hence, it does not work here.

The  $K_y$ -values in the table below are those for optimised output between 15.6 and 18.3 keV – the whole range being covered by the 7th harmonic that is brightest there – used by DanMAX’ main branch. SinCrys, foreseen to be working at a higher photon energy range, is then going to use the 9th harmonic that is not necessarily brightest there.

E eV	K_y	n_harm/step	P_sum W	theta_B03 deg	theta_B04 deg
20000	1.67551	9	0	17.251274	17.251274
20100	1.66836	9	0	17.162777	17.162777
20200	1.66125	9	0	17.075199	17.075199
20300	1.65418	9	0	16.988522	16.988522
20400	1.64714	9	0	16.902735	16.902735
20500	1.64015	9	0	16.817823	16.817823
20600	1.63319	9	0	16.733774	16.733774
20700	1.62628	9	0	16.650574	16.650574
20800	1.6194	9	0	16.568207	16.568207
20900	1.61255	9	0	16.486664	16.486664
21000	1.60575	9	0	16.405933	16.405933
21100	1.59898	9	0	16.325998	16.325998
21200	1.59224	9	0	16.246851	16.246851
21300	1.58554	9	0	16.168478	16.168478
21400	1.57887	9	0	16.090868	16.090868
21500	1.57224	9	0	16.014009	16.014009
21600	1.56564	9	0	15.937893	15.937893
21700	1.55908	9	0	15.862506	15.862506
21800	1.55255	9	0	15.787838	15.787838
21900	1.54605	9	0	15.713879	15.713879
22000	1.53958	9	0	15.640618	15.640618
22100	1.53315	9	0	15.568048	15.568048
22200	1.52674	9	0	15.496156	15.496156
22300	1.52037	9	0	15.424932	15.424932
22400	1.51402	9	0	15.35437	15.35437
22500	1.50771	9	0	15.284458	15.284458
22600	1.50143	9	0	15.215188	15.215188
22700	1.49517	9	0	15.146551	15.146551
22800	1.48895	9	0	15.078537	15.078537
22900	1.48275	9	0	15.011114	15.011114
23000	1.47658	9	0	14.944348	14.944348
23100	1.47044	9	0	14.878157	14.878157
23200	1.46433	9	0	14.812555	14.812555
23300	1.45824	9	0	14.747537	14.747537
23400	1.45218	9	0	14.683092	14.683092
23500	1.44615	9	0	14.619216	14.619216

Table 6.1: Scan values for different photon energies in energy scan

### Legend

**E:** photon energy

**K\_y:** deflection parameter for vertical field component of insertion device

**n\_harm/step:** number of undulator harmonic or number of energy slot for continuous source (e.g. wiggler)

**P\_sum:** sum of power in harmonics / energy intervals,  $P_{\text{sum}} = P_{\text{src}}$

**theta\_B03:** Bragg angle, i.e. glancing angle of incident and reflected beam w.r.t. the set of diffracting planes of optical element 03

**theta\_B04:** Bragg angle, i.e. glancing angle of incident and reflected beam w.r.t. the set of diffracting planes of optical element 04

# Chapter 7

## Plots

### 7.1 Statistics of incident irradiance

```
"fig/BS_choice_Si333/plot001.png" Lbl.:BS_choice_Si333_2d_plot_I_peak_incstat_oe0101
```

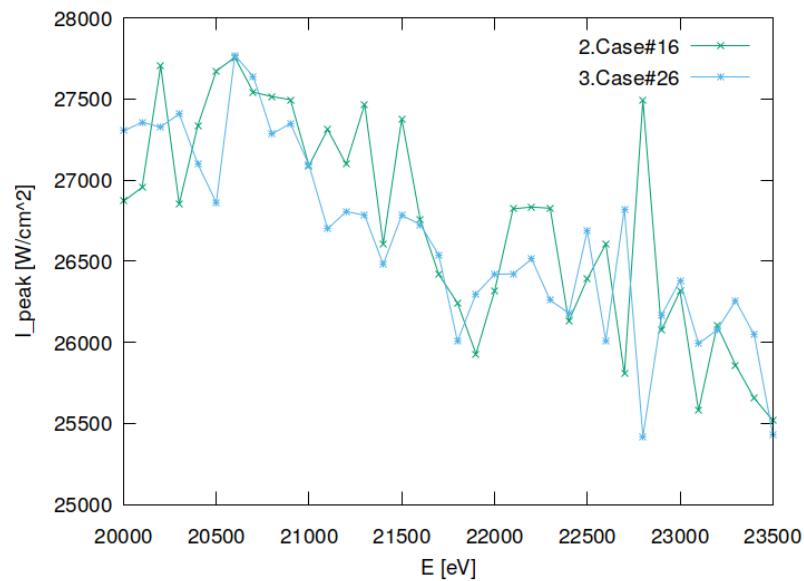


Figure 7.1: Incident peak irradiance of screen #01 belonging to optical element #01.

```
"fig/BS_choice_Si333/plot002.png" Lbl.:BS_choice_Si333_2d_plot_I_peak_incstat_oe0201
```

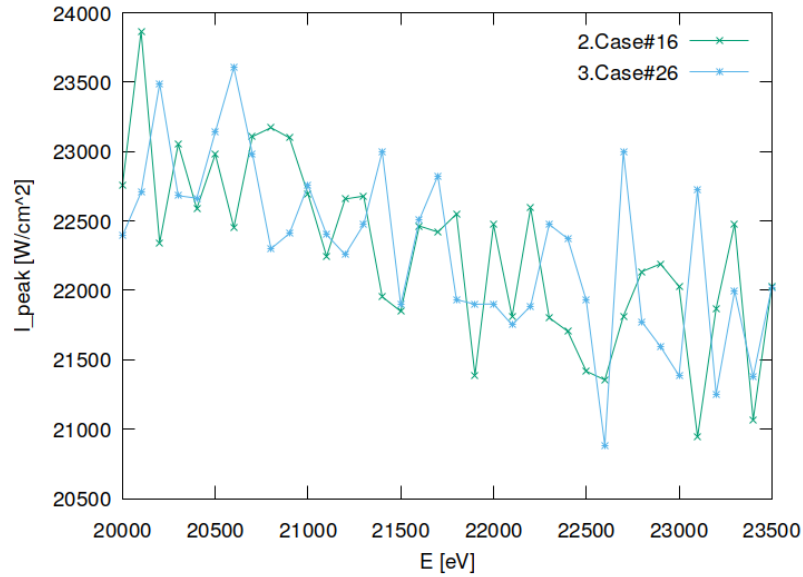


Figure 7.2: Incident peak irradiance of screen #01 belonging to optical element #02 (Filter).

```
"fig/BS_choice_Si333/plot003.png" Lbl.:BS_choice_Si333_2d_plot_I_peak_incstat_oe0202
```

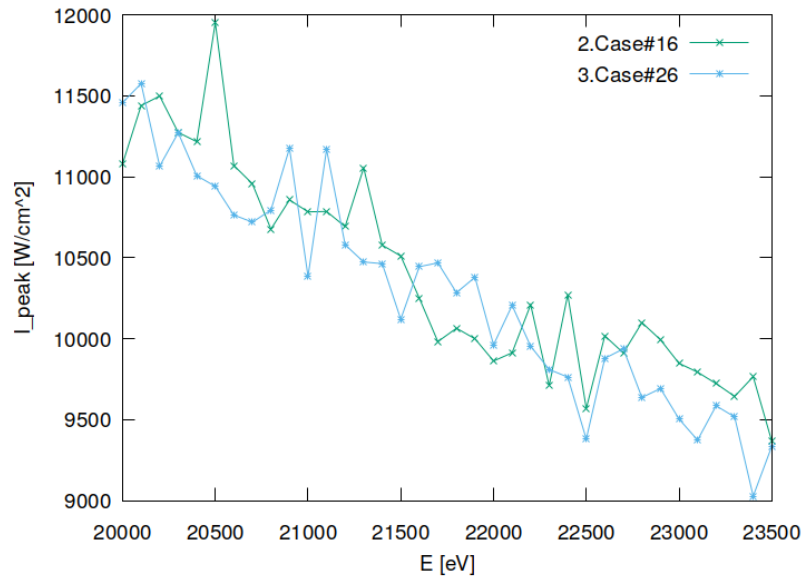


Figure 7.3: Incident peak irradiance of screen #02 belonging to optical element #02 (Filter).

```
"fig/BS_choice_Si333/plot004.png" Lbl.:BS_choice_Si333_2d_plot_I_peak_incstat_oe03
```

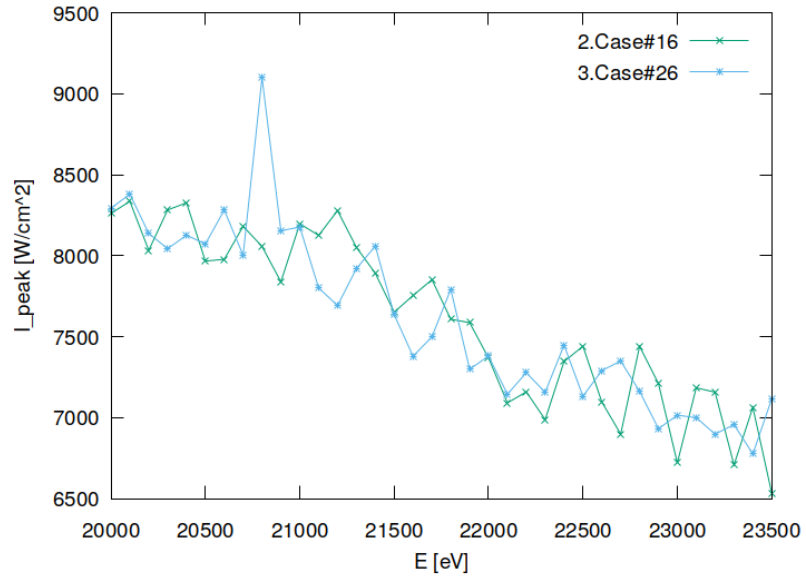


Figure 7.4: Incident peak irradiance of optical element #03 (BS).

```
"fig/BS_choice_Si333/plot005.png" Lbl.:BS_choice_Si333_2d_plot_I_int_incstat_oe0101
```

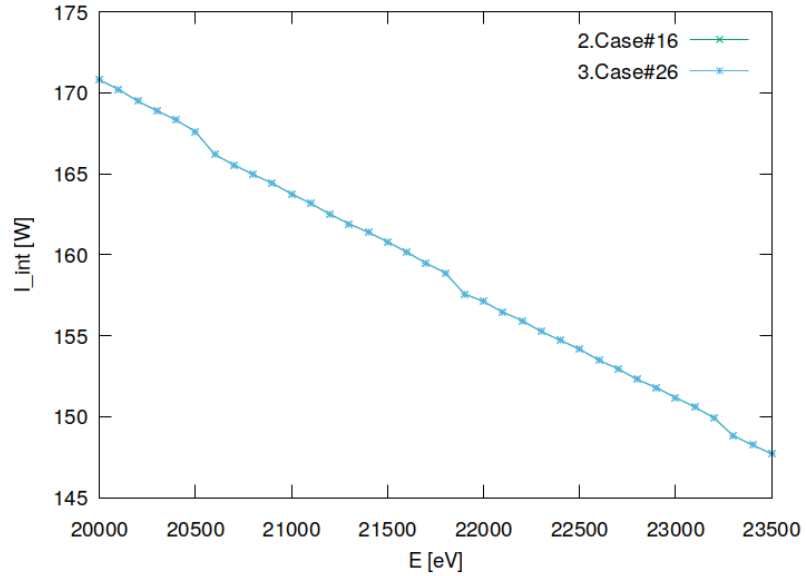


Figure 7.5: Incident flux of screen #01 belonging to optical element #01.

"fig/BS\_choice\_Si333/plot006.png" Lbl.:BS\_choice\_Si333\_2d\_plot\_I\_int\_incstat\_oe0201

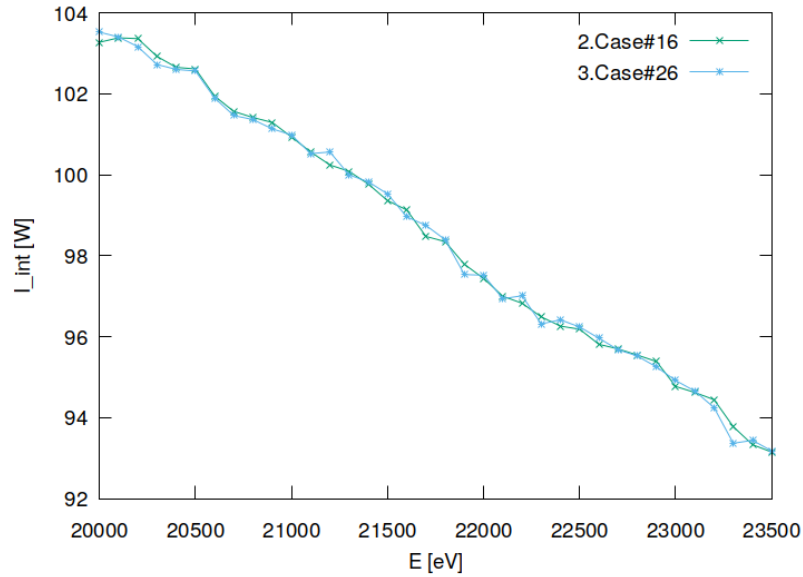


Figure 7.6: Incident flux of screen #01 belonging to optical element #02 (Filter).

"fig/BS\_choice\_Si333/plot007.png" Lbl.:BS\_choice\_Si333\_2d\_plot\_I\_int\_incstat\_oe0202

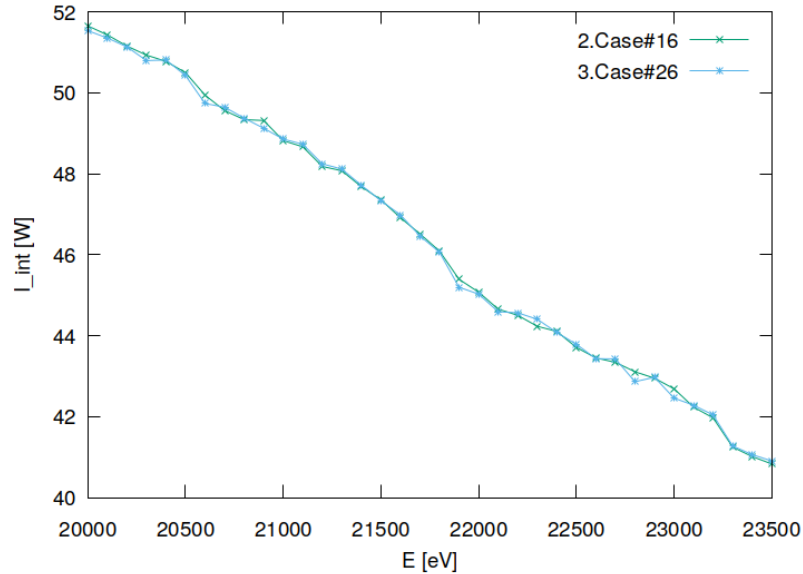


Figure 7.7: Incident flux of screen #02 belonging to optical element #02 (Filter).

```
"fig/BS_choice_Si333/plot008.png" Lbl.:BS_choice_Si333_2d_plot_I_int_incstat_oe03
```

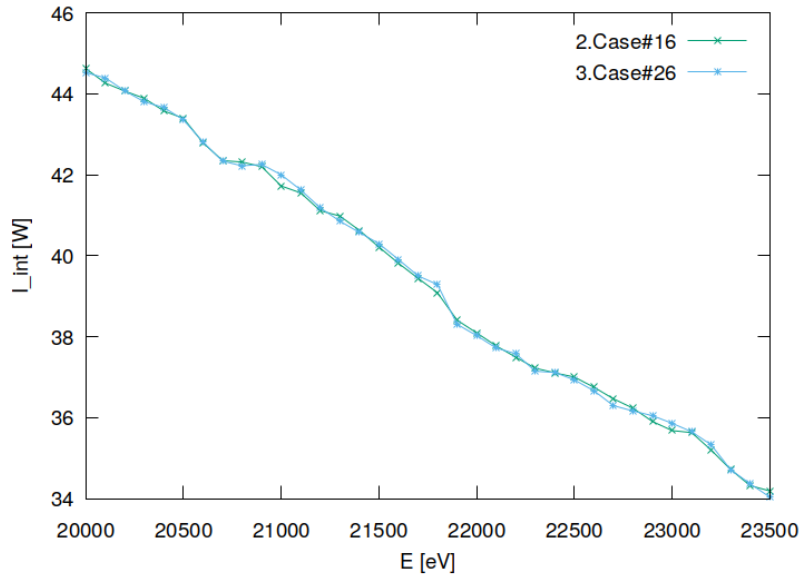


Figure 7.8: Incident flux of optical element #03 (BS).

## 7.2 Statistics of absorbed irradiance

```
"fig/BS_choice_Si333/plot009.png" Lbl.:BS_choice_Si333_2d_plot_I_peak_absstat_oe0101
```

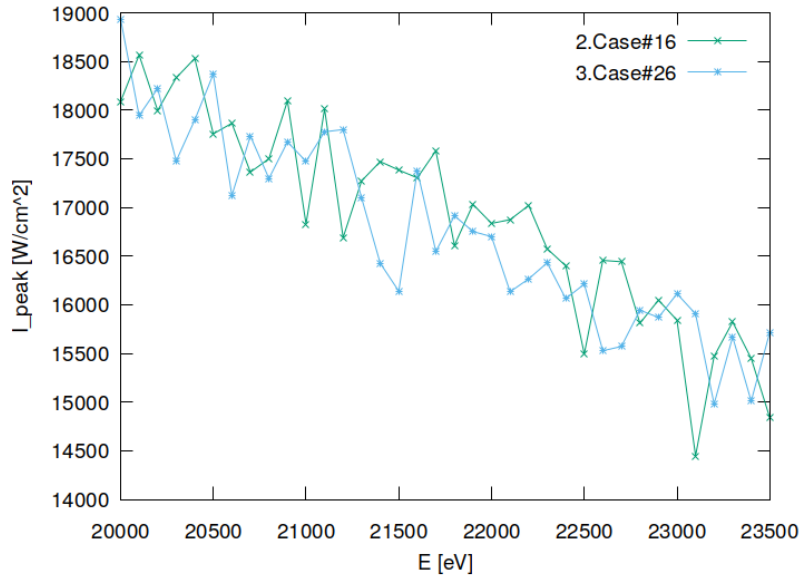


Figure 7.9: Absorbed peak irradiance of screen #01 belonging to optical element #01.

```
"fig/BS_choice_Si333/plot010.png" Lbl.:BS_choice_Si333_2d_plot_I_peak_absstat_oe0201
```

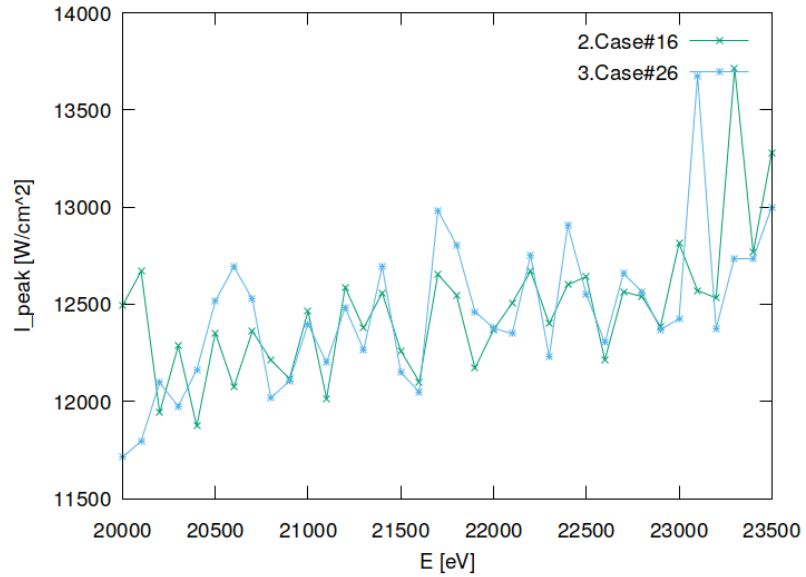


Figure 7.10: Absorbed peak irradiance of screen #01 belonging to optical element #02 (Filter).

```
"fig/BS_choice_Si333/plot011.png" Lbl.:BS_choice_Si333_2d_plot_I_peak_absstat_oe0202
```

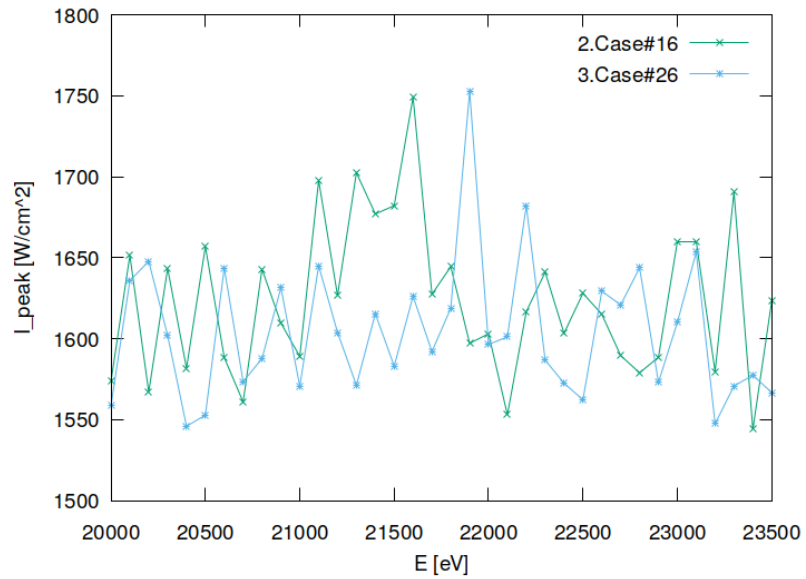


Figure 7.11: Absorbed peak irradiance of screen #02 belonging to optical element #02 (Filter).

```
"fig/BS_choice_Si333/plot012.png" Lbl.:BS_choice_Si333_2d_plot_I_peak_absstat_oe03
```

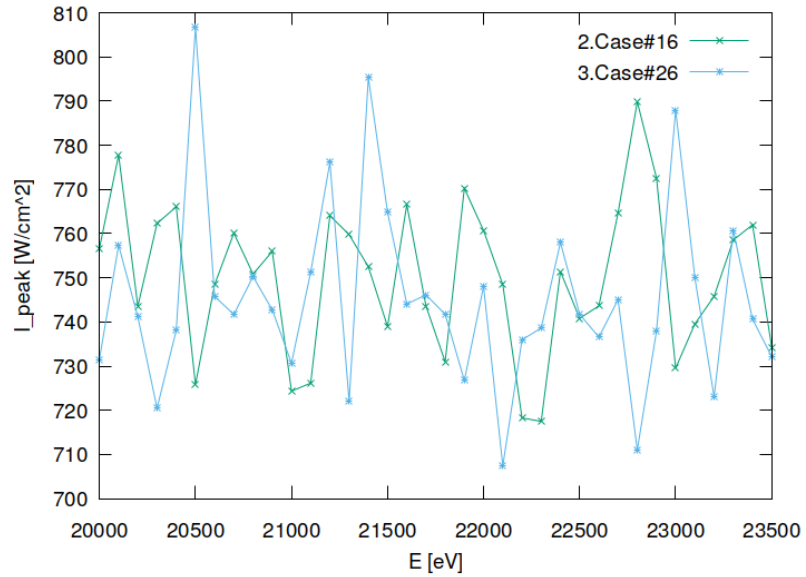


Figure 7.12: Absorbed peak irradiance of optical element #03 (BS).

```
"fig/BS_choice_Si333/plot013.png" Lbl.:BS_choice_Si333_2d_plot_I_int_absstat_oe0101
```

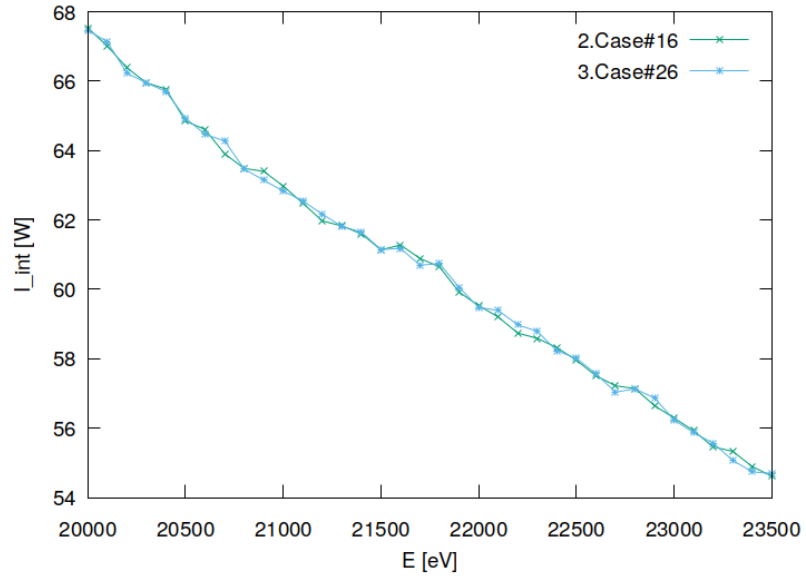


Figure 7.13: Absorbed flux of screen #01 belonging to optical element #01.

"fig/BS\_choice\_Si333/plot014.png" Lbl.:BS\_choice\_Si333\_2d\_plot\_I\_int\_absstat\_oe0201

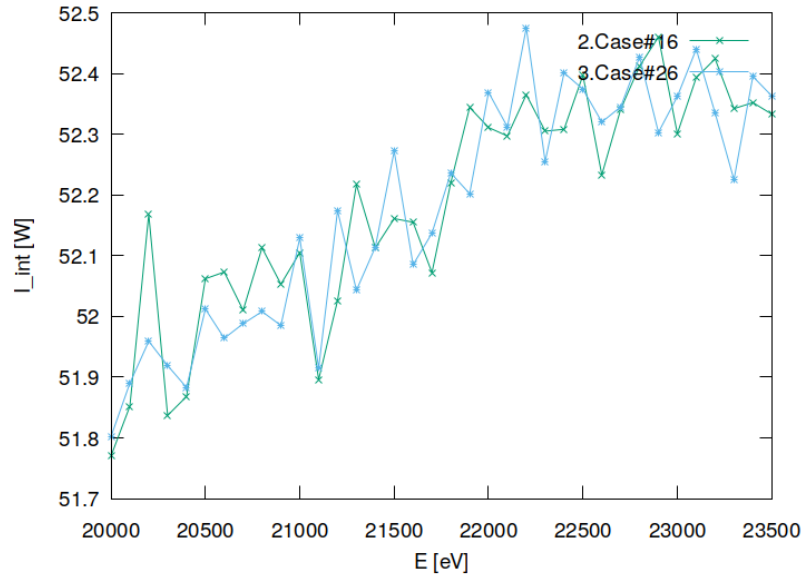


Figure 7.14: Absorbed flux of screen #01 belonging to optical element #02 (Filter).

"fig/BS\_choice\_Si333/plot015.png" Lbl.:BS\_choice\_Si333\_2d\_plot\_I\_int\_absstat\_oe0202

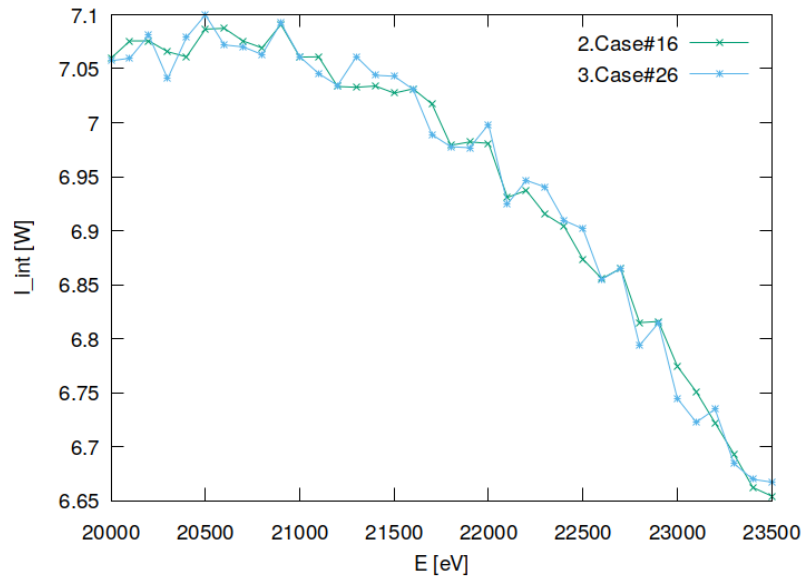


Figure 7.15: Absorbed flux of screen #02 belonging to optical element #02 (Filter).

```
"fig/BS_choice_Si333/plot016.png" Lbl.:BS_choice_Si333_2d_plot_I_int_absstat_oe03
```

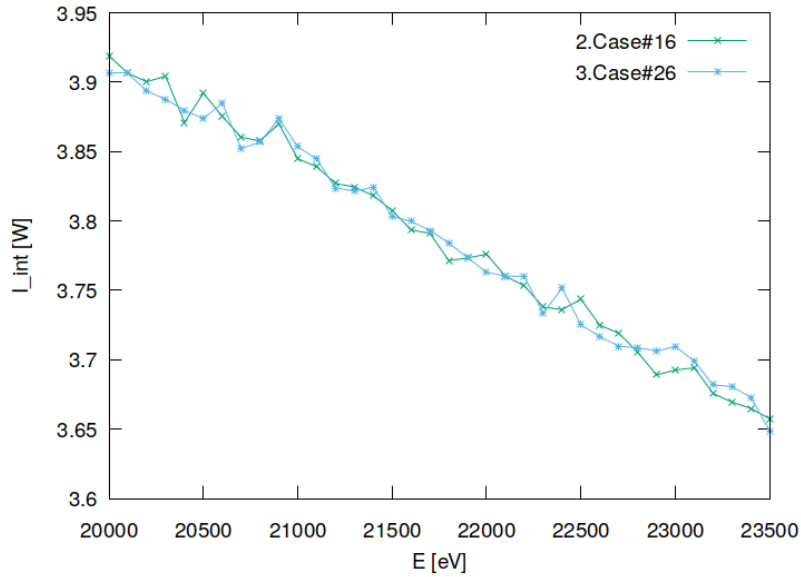


Figure 7.16: Absorbed flux of optical element #03 (BS).

### 7.3 Statistics of temperature

```
"fig/BS_choice_Si333/plot017.png" Lbl.:BS_choice_Si333_2d_plot_T_peak_stat_oe03
```

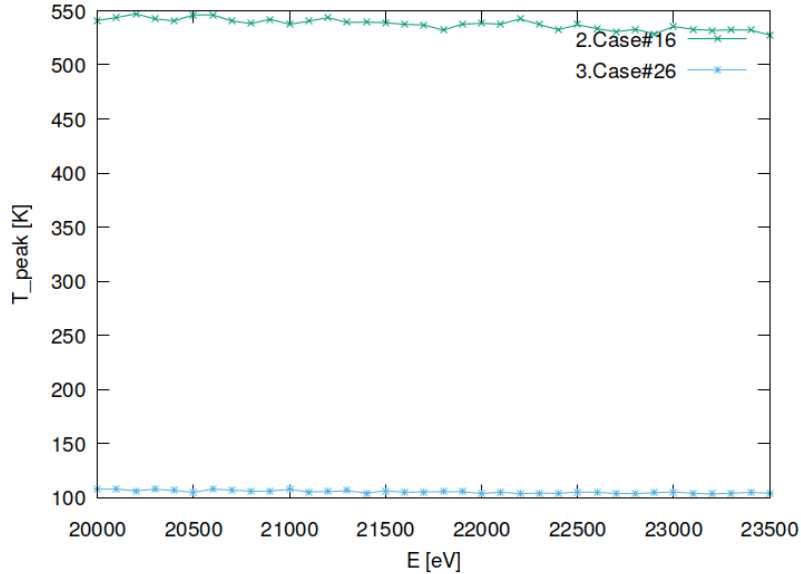


Figure 7.17: Peak temperature of optical element #03 (BS).

## 7.4 Statistics of mechanical stress (von Mises stress)

```
"fig/BS_choice_Si333/plot018.png" Lbl.:BS_choice_Si333_2d_plot_sigma_peak_stat_oe03
```

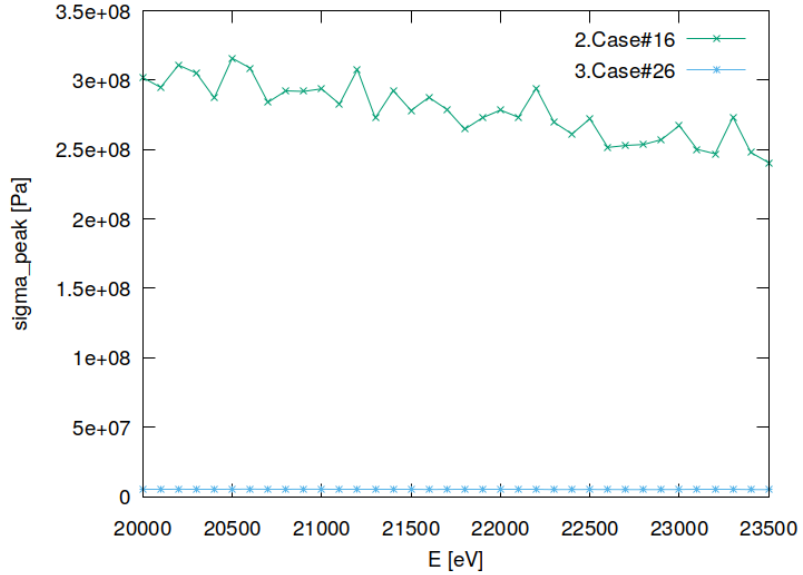


Figure 7.18: Peak mechanical stress (Von Mises stress) of optical element #03 (BS).

## 7.5 Statistics of optical surface deformation

```
"fig/BS_choice_Si333/plot019.png" Lbl.:BS_choice_Si333_2d_plot_dz_peak_stat_oe03
```

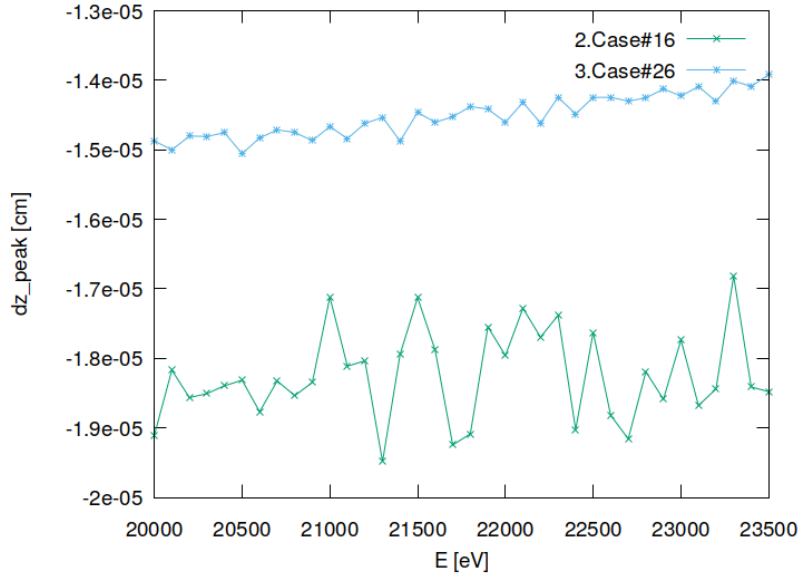


Figure 7.19: Peak deformation of optical element #03 (BS).

## 7.6 Statistics of photon irradiance on optical surface

```
"fig/BS_choice_Si333/plot020.png" Lbl.:BS_choice_Si333_2d_plot_dx_fwhm_inc_footstat_oe04
```

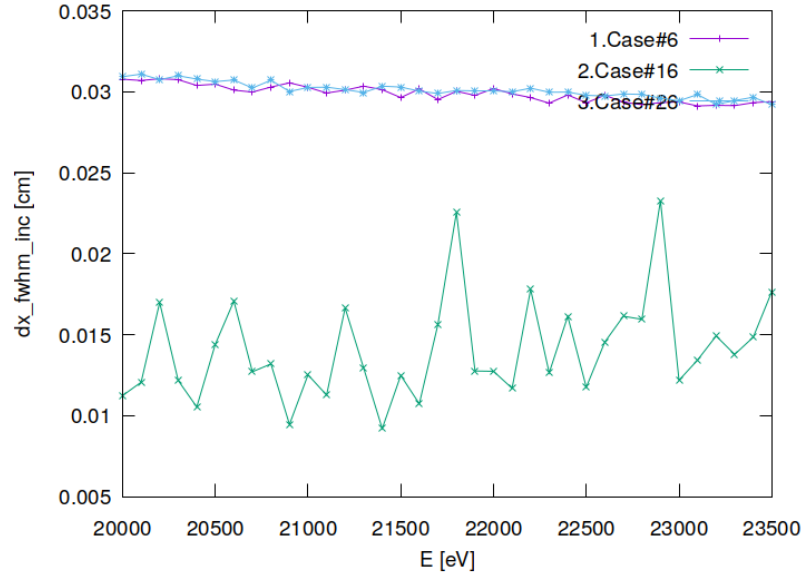


Figure 7.20: Sagittal footprint diameter (FWHM) of optical element #04 (CM2).

```
"fig/BS_choice_Si333/plot021.png" Lbl.:BS_choice_Si333_2d_plot_dy_fwhm_inc_footstat_oe04
```

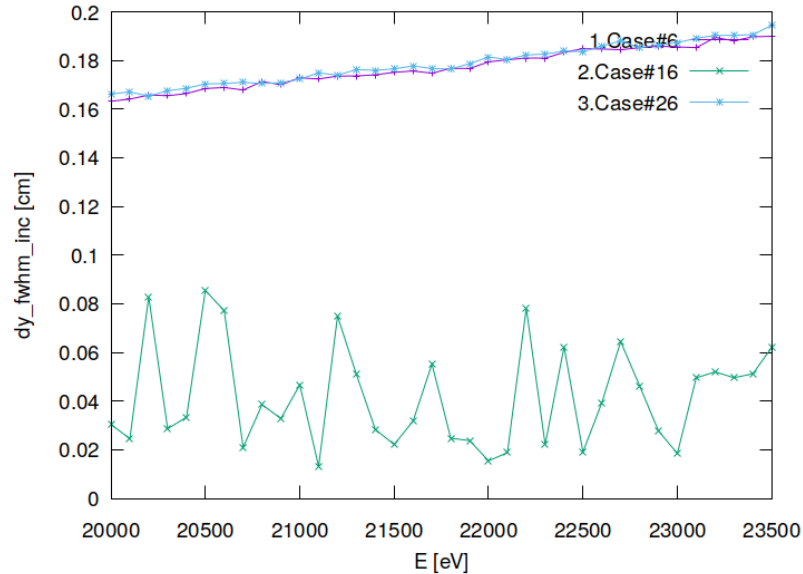


Figure 7.21: Meridional footprint diameter (FWHM) of optical element #04 (CM2).

```
"fig/BS_choice_Si333/plot022.png" Lbl.:BS_choice_Si333_2d_plot_I_inc_int_footstat_oe04
```

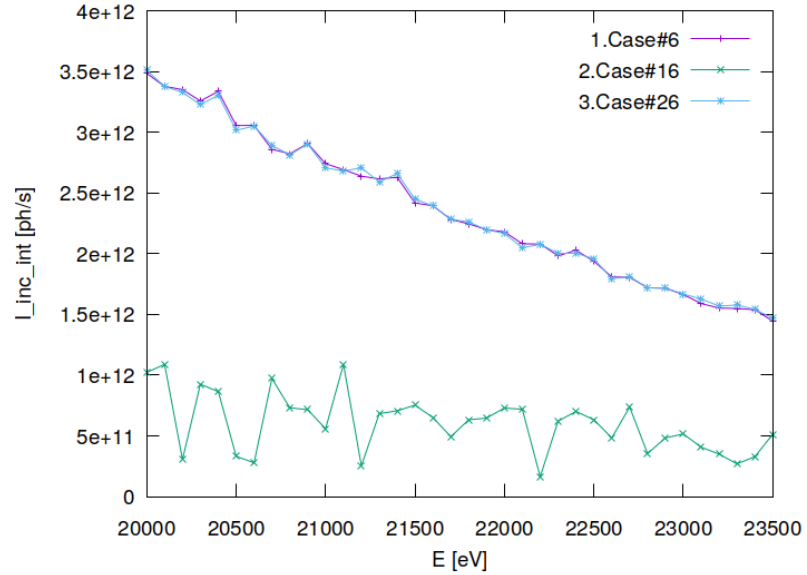


Figure 7.22: Incident photon flux on surface of optical element #04 (CM2).

```
"fig/BS_choice_Si333/plot023.png" Lbl.:BS_choice_Si333_2d_plot_x_cen_inc_footstat_oe04
```

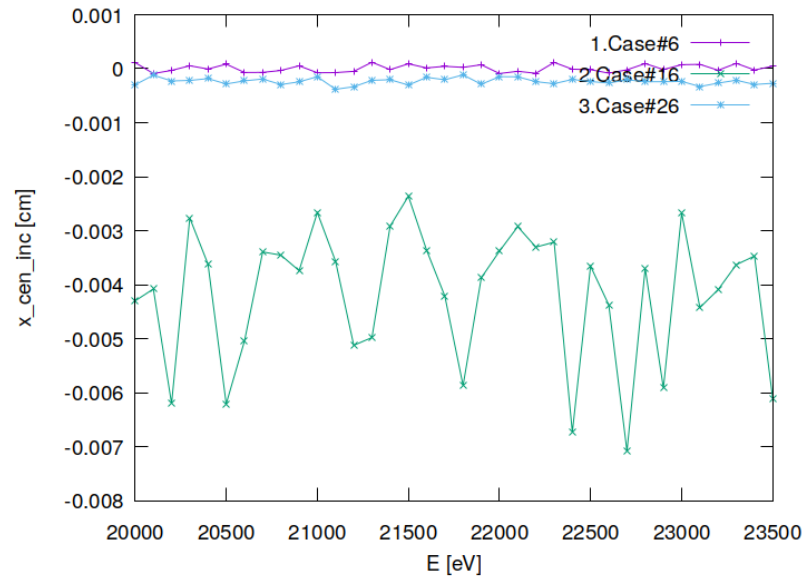


Figure 7.23: Sagittal coordinate of footprint's centre of 'gravity' on surface of optical element #04 (CM2).

```
"fig/BS_choice_Si333/plot024.png" Lbl.:BS_choice_Si333_2d_plot_y_cen_inc_footstat_oe04
```

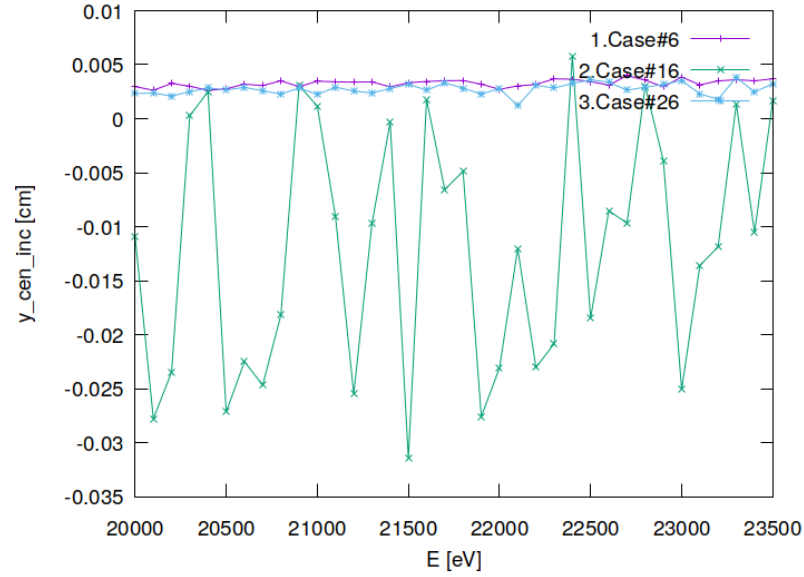


Figure 7.24: Meridional coordinate of footprint's centre of 'gravity' on surface of optical element #04 (CM2).

## 7.7 Statistics of photon irradiance in beam cross section

```
"fig/BS_choice_Si333/plot025.png" Lbl.:BS_choice_Si333_2d_plot_dx_fwhm_focstatavg_oe04
```

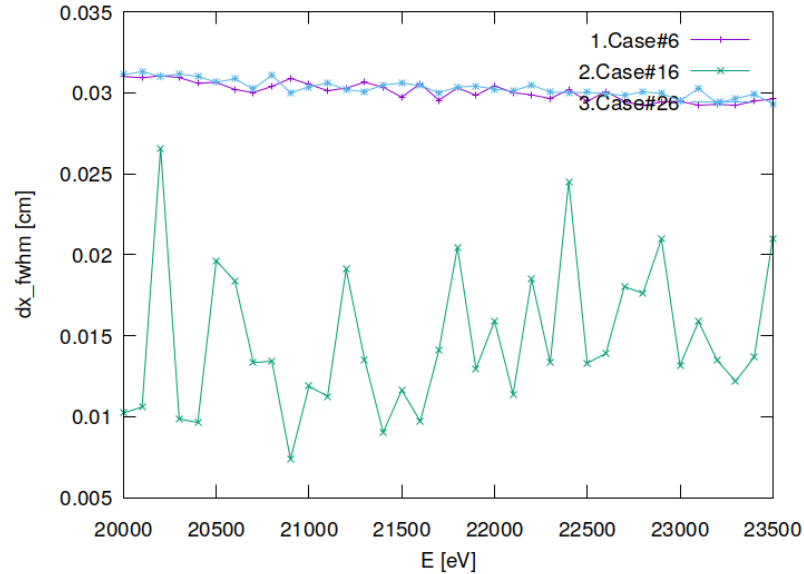


Figure 7.25: Sagittal beam diameter (FWHM) of optical element #04 (CM2).

```
"fig/BS_choice_Si333/plot026.png" Lbl.:BS_choice_Si333_2d_plot_dz_fwhm_focstatavg_oe04
```

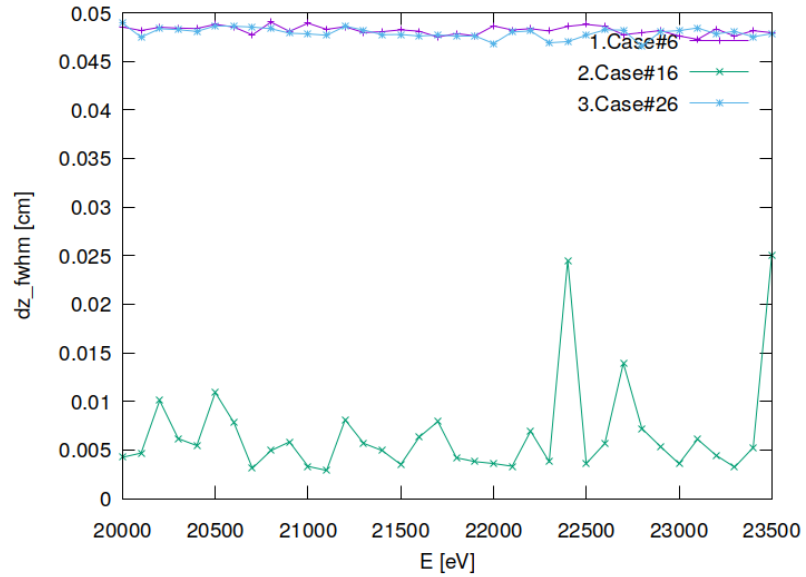


Figure 7.26: Meridional beam diameter (FWHM) of optical element #04 (CM2).

```
"fig/BS_choice_Si333/plot027.png" Lbl.:BS_choice_Si333_2d_plot_I_int_focstatavg_oe04
```

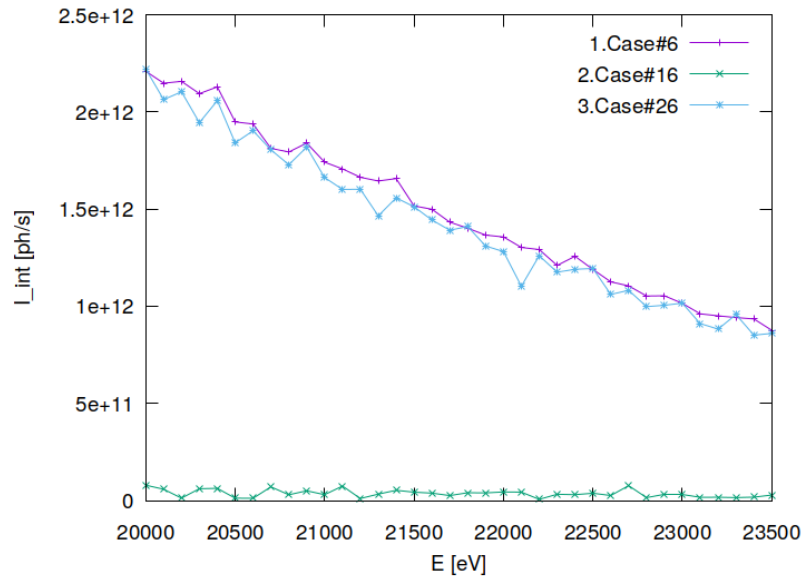


Figure 7.27: Photon flux in beam cross section of optical element #04 (CM2).

```
"fig/BS_choice_Si333/plot028.png" Lbl.:BS_choice_Si333_2d_plot_x_cen_focstatavg_oe04
```

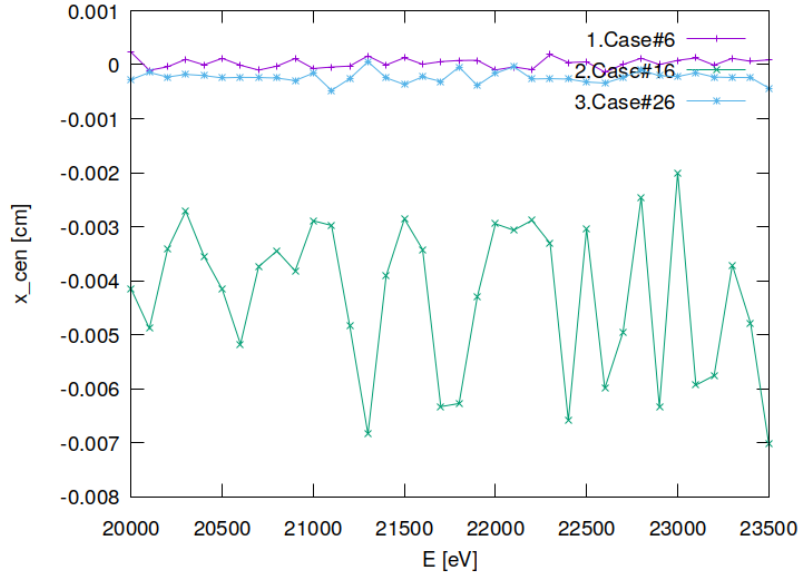


Figure 7.28: Sagittal coordinate of beam's centre of 'gravity' in beam cross section of optical element #04 (CM2).

```
"fig/BS_choice_Si333/plot029.png" Lbl.:BS_choice_Si333_2d_plot_z_cen_focstatavg_oe04
```

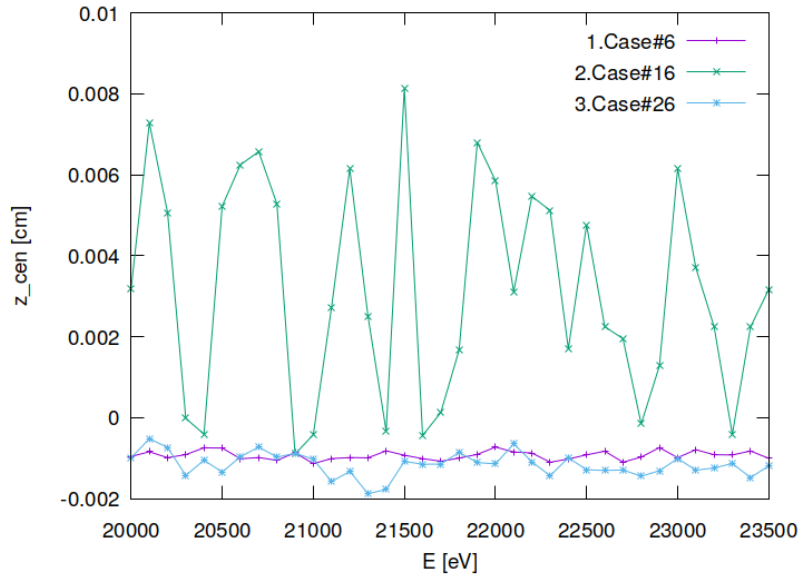


Figure 7.29: Meridional coordinate of beam's centre of 'gravity' in beam cross section of optical element #04 (CM2).

```
"fig/BS_choice_Si333/plot030.png" Lbl.:BS_choice_Si333_2d_plot_dxp_fwhm_focstatavg_oe04
```

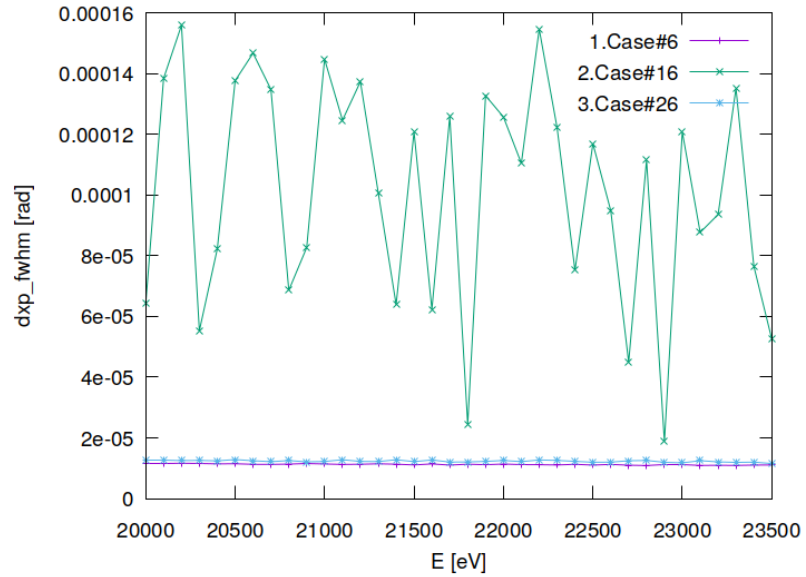


Figure 7.30: Sagittal beam divergence (FWHM) of optical element #04 (CM2).

```
"fig/BS_choice_Si333/plot031.png" Lbl.:BS_choice_Si333_2d_plot_dzp_fwhm_focstatavg_oe04
```

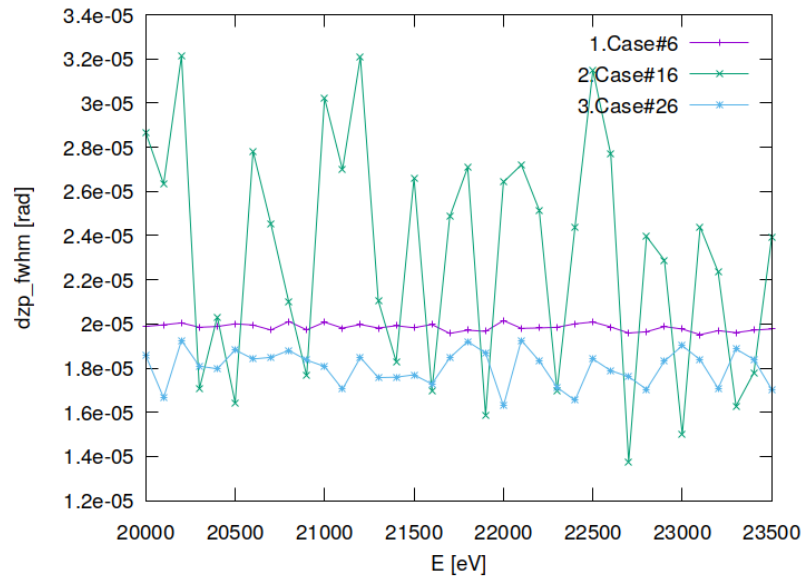


Figure 7.31: Meridional beam divergence (FWHM) of optical element #04 (CM2).

```
"fig/BS_choice_Si333/plot032.png" Lbl.:BS_choice_Si333_2d_plot_I_int_focstatavg_oe04
```

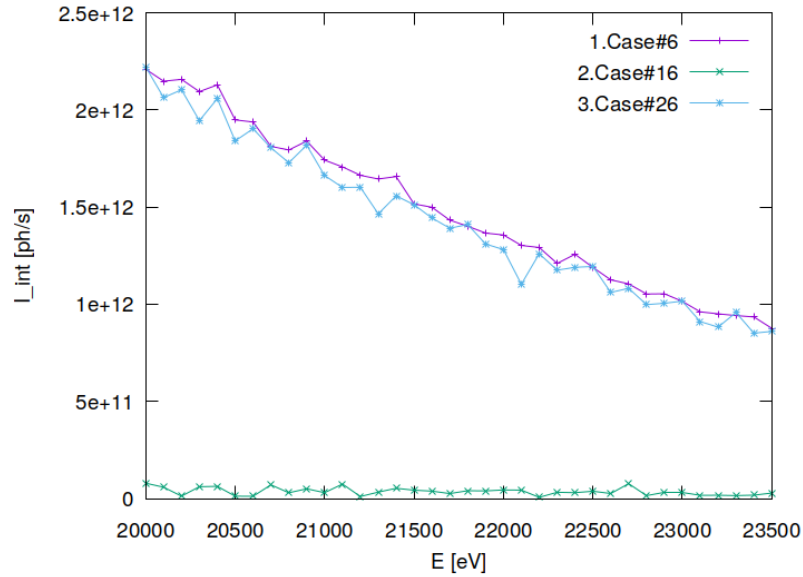


Figure 7.32: Photon flux in beam cross section of optical element #04 (CM2).

```
"fig/BS_choice_Si333/plot033.png" Lbl.:BS_choice_Si333_2d_plot_xp_cen_focstatavg_oe04
```

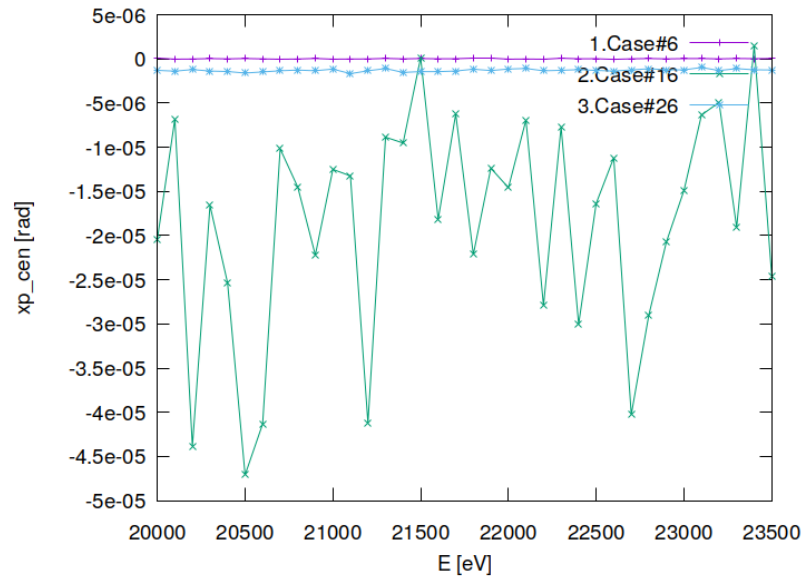


Figure 7.33: Sagittal coordinate of beam's centre of 'gravity' in angle space of optical element #04 (CM2).

```
"fig/BS_choice_Si333/plot034.png" Lbl.:BS_choice_Si333_2d_plot_zp_cen_focstatavg_oe04
```

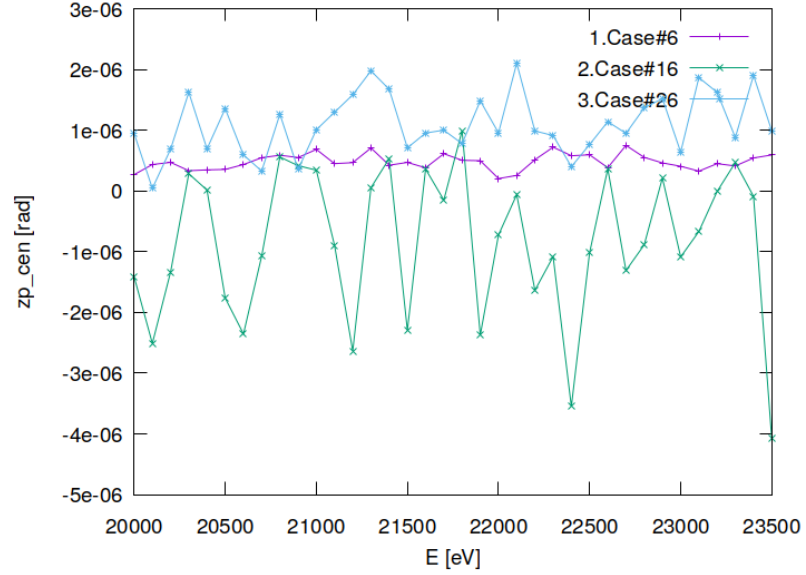


Figure 7.34: Meridional coordinate of beam's centre of 'gravity' in angle space of optical element #04 (CM2).

```
"fig/BS_choice_Si333/plot035.png" Lbl.:BS_choice_Si333_2d_plot_dE_fwhm_focstatavg_oe04
```

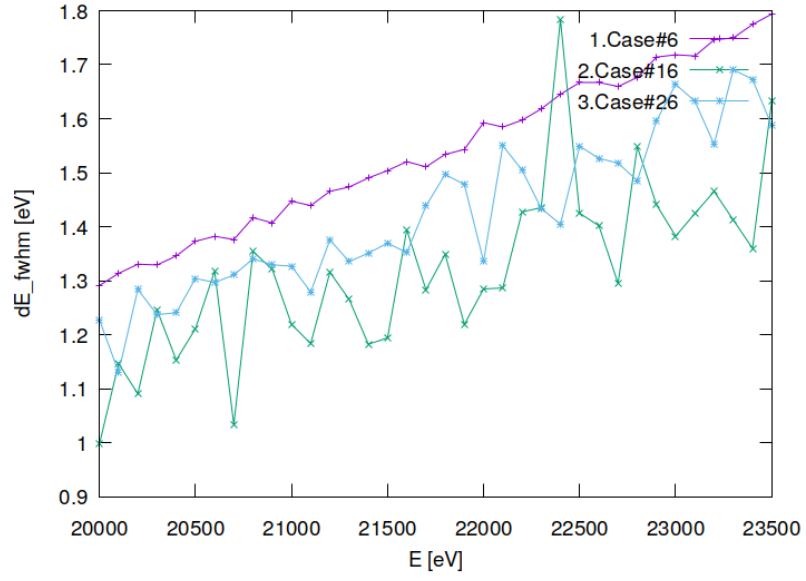


Figure 7.35: Bandwidth (FWHM) in beam cross section of optical element #04 (CM2).

## 7.8 Absorbed irradiance on surface

"fig/BS\_choice\_Si333/plot036.png" Lbl.:BS\_choice\_Si333\_false\_colour\_plot\_p\_abs\_foot\_oe0101\_c16\_21800eV

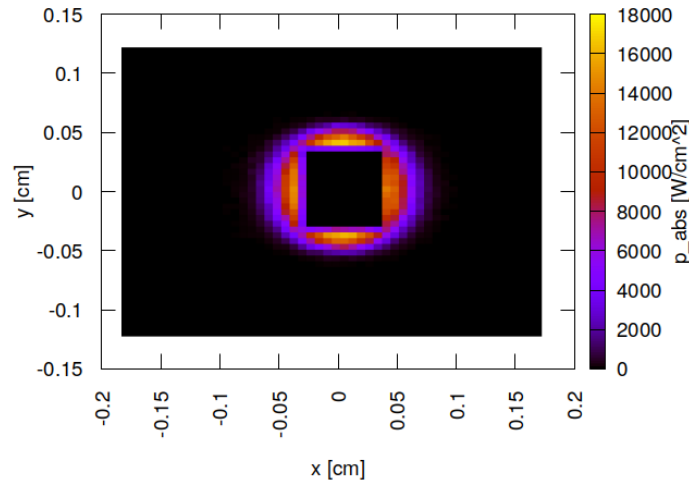


Figure 7.36: Absorbed irradiance on surface of screen #01 belonging to optical element #01 for case #16 for 21800 eV photon energy setting.

"fig/BS\_choice\_Si333/plot037.png" Lbl.:BS\_choice\_Si333\_false\_colour\_plot\_p\_abs\_foot\_oe0101\_c26\_21800eV

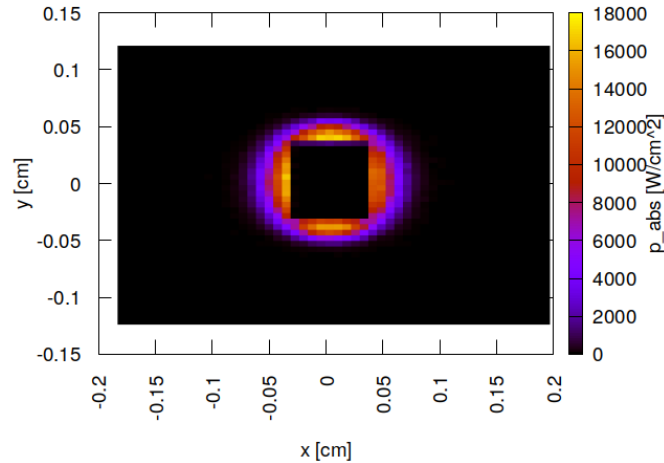


Figure 7.37: Absorbed irradiance on surface of screen #01 belonging to optical element #01 for case #26 for 21800 eV photon energy setting.

"fig/BS\_choice\_Si333/plot038.png" Lbl.:BS\_choice\_Si333\_false\_colour\_plot\_p\_abs\_foot\_oe0201\_c16\_21800eV

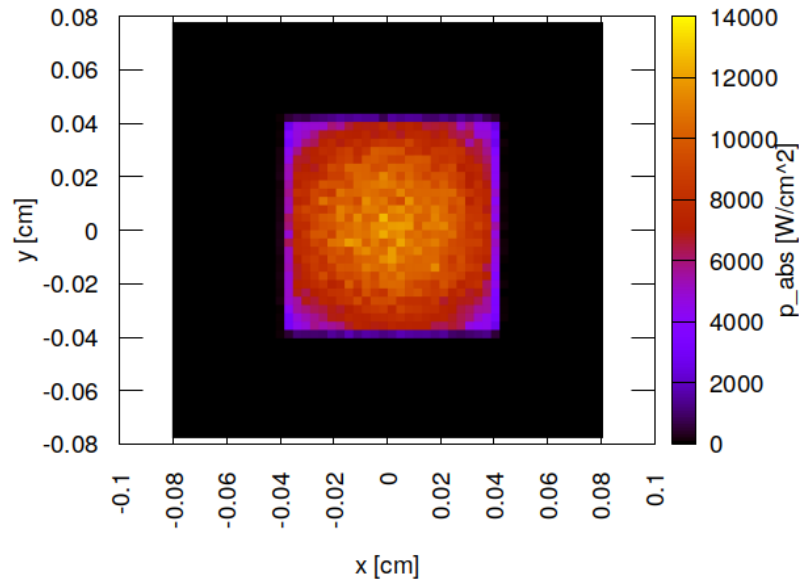


Figure 7.38: Absorbed irradiance on surface of screen #01 belonging to optical element #02 (Filter) for case #16 for 21800 eV photon energy setting.

"fig/BS\_choice\_Si333/plot039.png" Lbl.:BS\_choice\_Si333\_false\_colour\_plot\_p\_abs\_foot\_oe0201\_c26\_21800eV

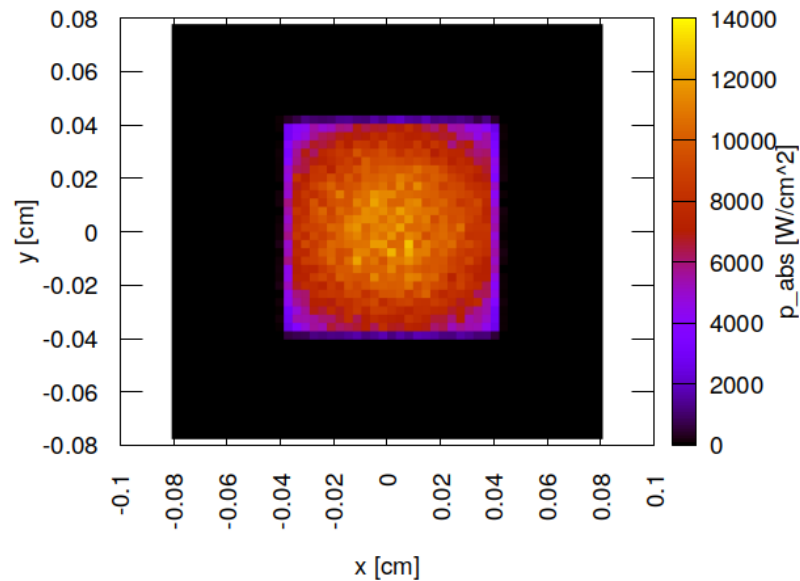


Figure 7.39: Absorbed irradiance on surface of screen #01 belonging to optical element #02 (Filter) for case #26 for 21800 eV photon energy setting.

"fig/BS\_choice\_Si333/plot040.png" Lbl.:BS\_choice\_Si333\_false\_colour\_plot\_p\_abs\_foot\_oe0202\_c16\_21800eV

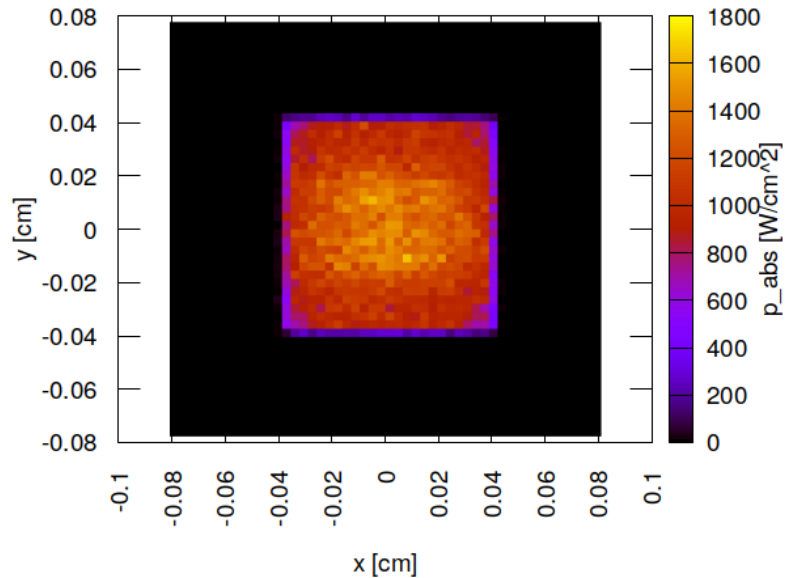


Figure 7.40: Absorbed irradiance on surface of screen #02 belonging to optical element #02 (Filter) for case #16 for 21800 eV photon energy setting.

"fig/BS\_choice\_Si333/plot041.png" Lbl.:BS\_choice\_Si333\_false\_colour\_plot\_p\_abs\_foot\_oe0202\_c26\_21800eV

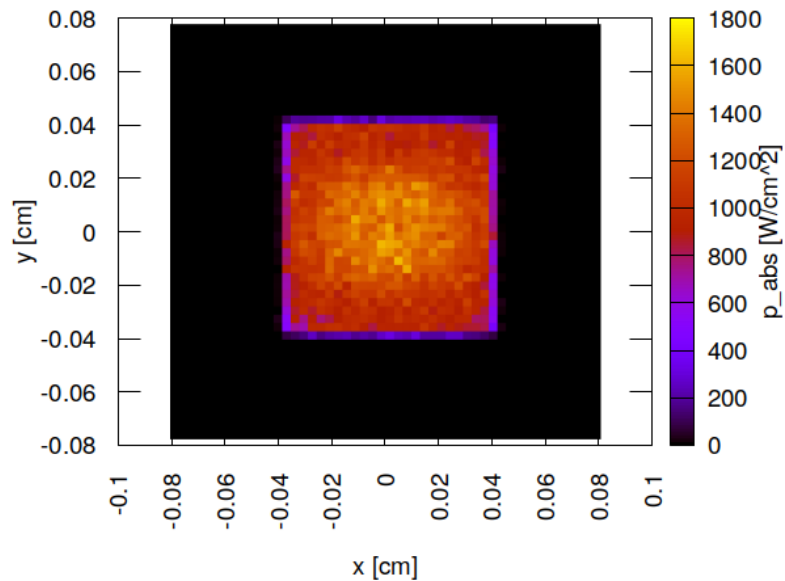


Figure 7.41: Absorbed irradiance on surface of screen #02 belonging to optical element #02 (Filter) for case #26 for 21800 eV photon energy setting.

"fig/BS\_choice\_Si333/plot042.png" Lbl.:BS\_choice\_Si333\_false\_colour\_plot\_p\_abs\_foot\_oe03\_c16\_21800eV

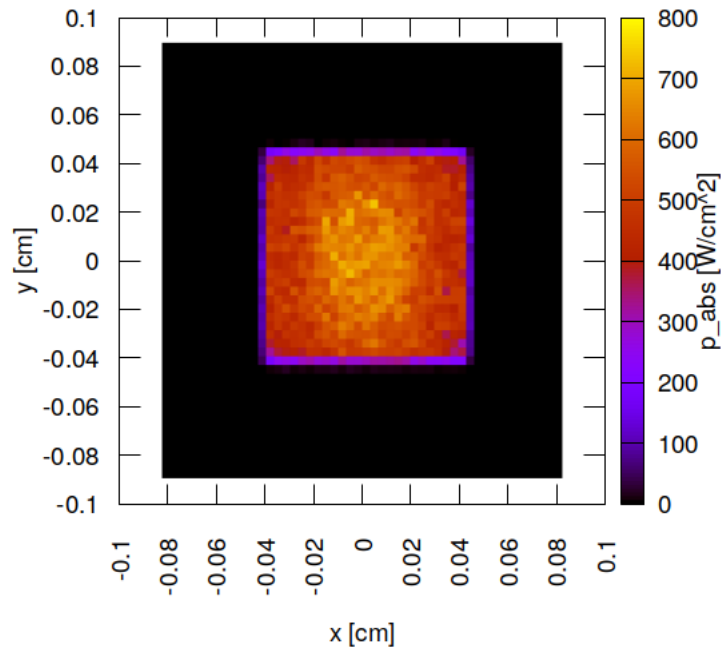


Figure 7.42: Absorbed irradiance on surface of optical element #03 (BS) for case #16 for 21800 eV photon energy setting.

"fig/BS\_choice\_Si333/plot043.png" Lbl.:BS\_choice\_Si333\_false\_colour\_plot\_p\_abs\_foot\_oe03\_c26\_21800eV

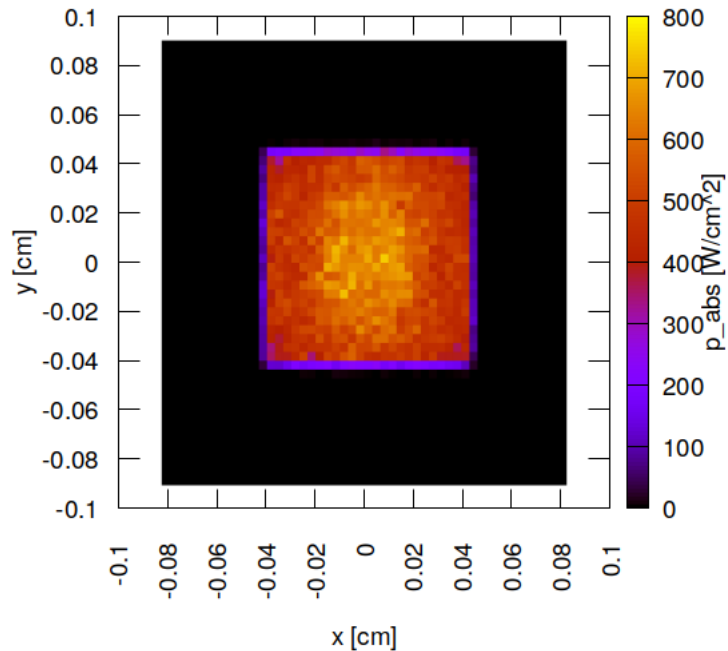


Figure 7.43: Absorbed irradiance on surface of optical element #03 (BS) for case #26 for 21800 eV photon energy setting.

## 7.9 Incident spectral flux on surface

"fig/BS\_choice\_Si333/plot044.png" Lbl.:BS\_choice\_Si333\_2d\_plot\_P\_spec\_spec\_oe0101\_c16\_21800eV

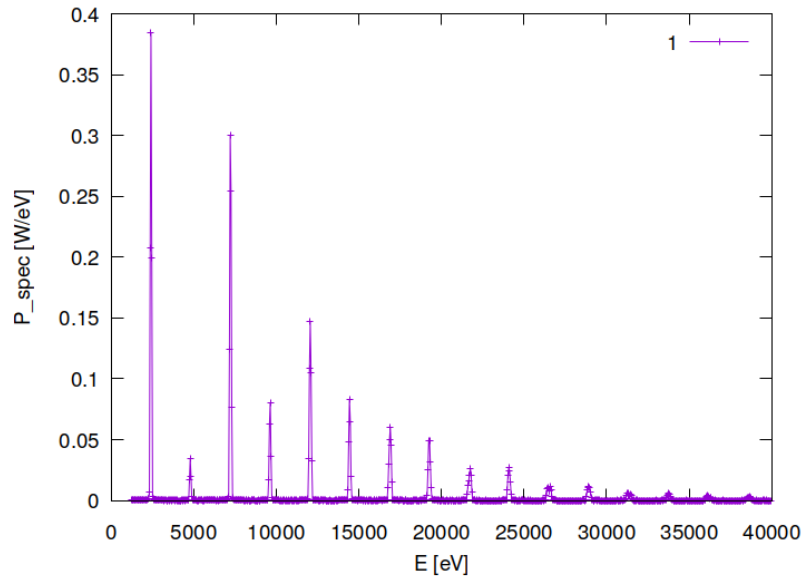


Figure 7.44: Incident spectral flux on surface of screen #01 belonging to optical element #01 for case #16 for 21800 eV photon energy setting.

"fig/BS\_choice\_Si333/plot045.png" Lbl.:BS\_choice\_Si333\_2d\_plot\_P\_spec\_spec\_oe0101\_c26\_21800eV

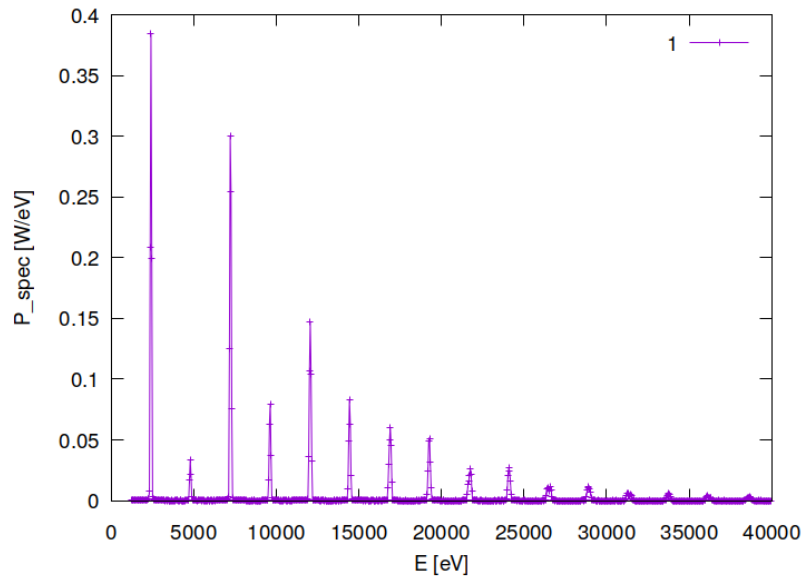


Figure 7.45: Incident spectral flux on surface of screen #01 belonging to optical element #01 for case #26 for 21800 eV photon energy setting.

"fig/BS\_choice\_Si333/plot046.png" Lbl.:BS\_choice\_Si333\_2d\_plot\_P\_spec\_spec\_oe0201\_c16\_21800eV

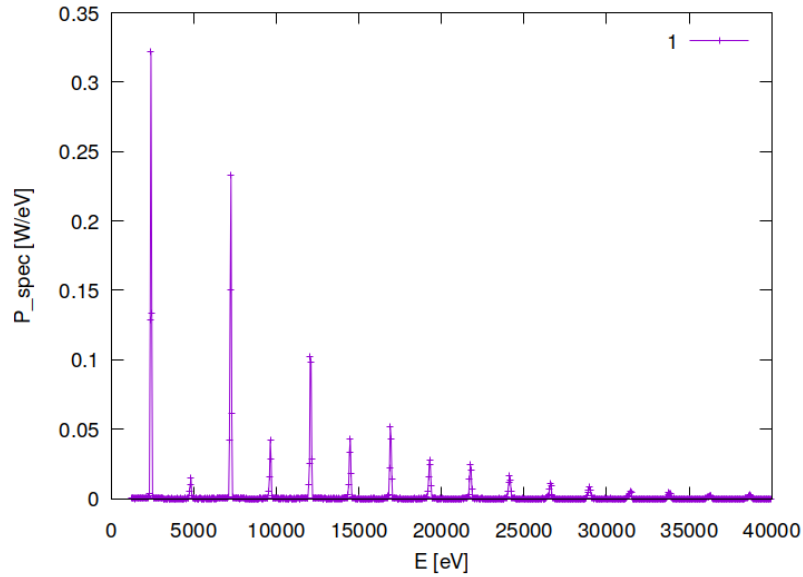


Figure 7.46: Incident spectral flux on surface of screen #01 belonging to optical element #02 (Filter) for case #16 for 21800 eV photon energy setting.

"fig/BS\_choice\_Si333/plot047.png" Lbl.:BS\_choice\_Si333\_2d\_plot\_P\_spec\_spec\_oe0201\_c26\_21800eV

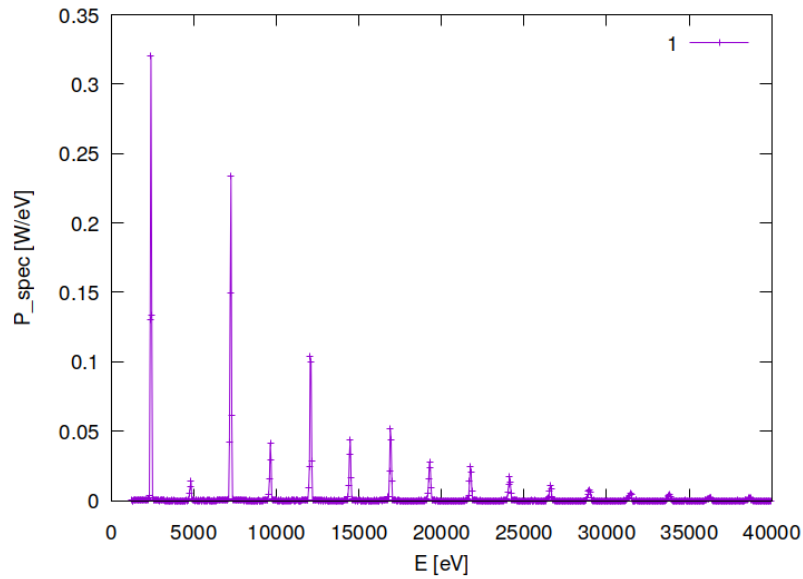


Figure 7.47: Incident spectral flux on surface of screen #01 belonging to optical element #02 (Filter) for case #26 for 21800 eV photon energy setting.

"fig/BS\_choice\_Si333/plot048.png" Lbl.:BS\_choice\_Si333\_2d\_plot\_P\_spec\_spec\_oe0202\_c16\_21800eV

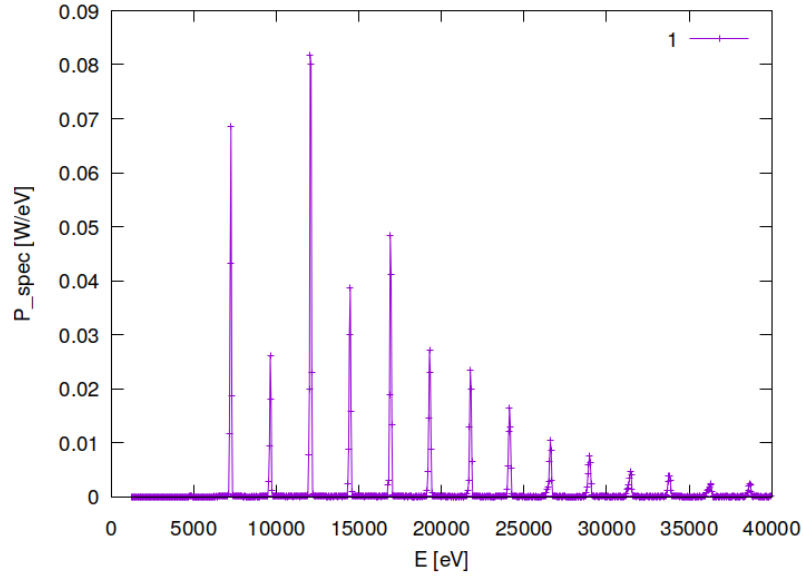


Figure 7.48: Incident spectral flux on surface of screen #02 belonging to optical element #02 (Filter) for case #16 for 21800 eV photon energy setting.

"fig/BS\_choice\_Si333/plot049.png" Lbl.:BS\_choice\_Si333\_2d\_plot\_P\_spec\_spec\_oe0202\_c26\_21800eV

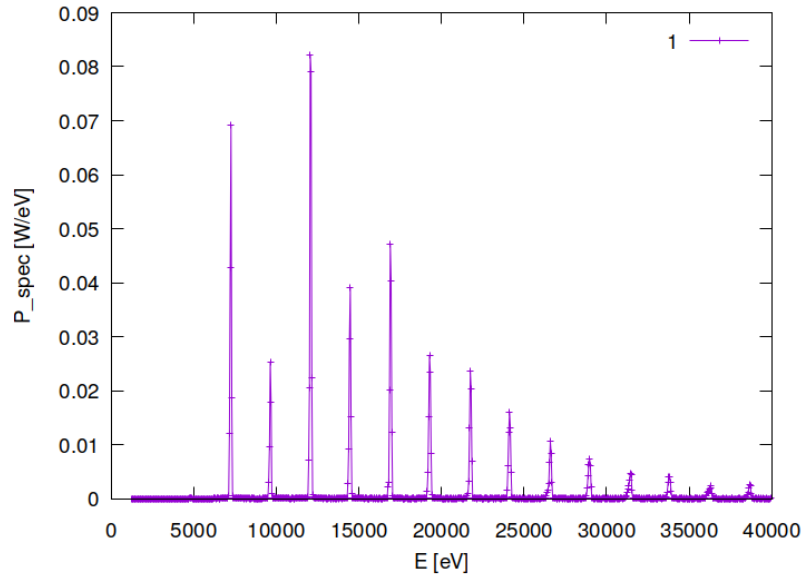


Figure 7.49: Incident spectral flux on surface of screen #02 belonging to optical element #02 (Filter) for case #26 for 21800 eV photon energy setting.

```
"fig/BS_choice_Si333/plot050.png" Lbl.:BS_choice_Si333_2d_plot_P_spec_spec_oe03_c16_21800eV
```

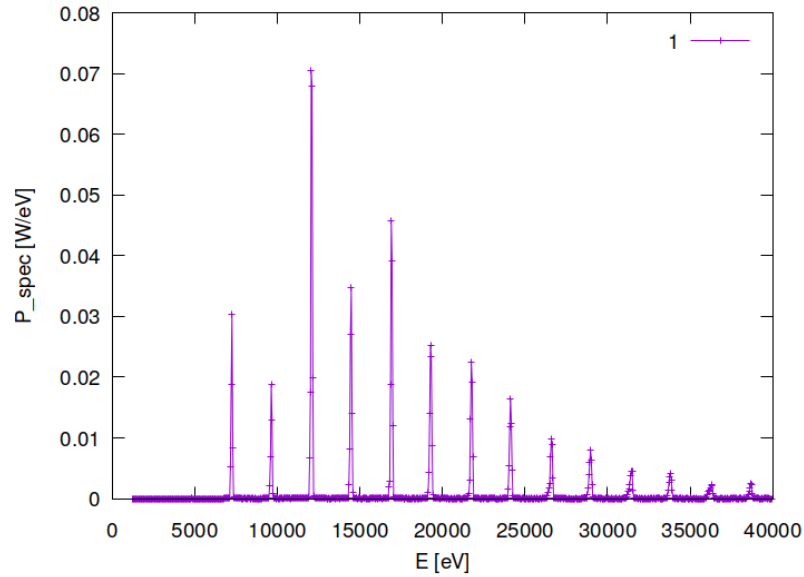


Figure 7.50: Incident spectral flux on surface of optical element #03 (BS) for case #16 for 21800 eV photon energy setting.

```
"fig/BS_choice_Si333/plot051.png" Lbl.:BS_choice_Si333_2d_plot_P_spec_spec_oe03_c26_21800eV
```

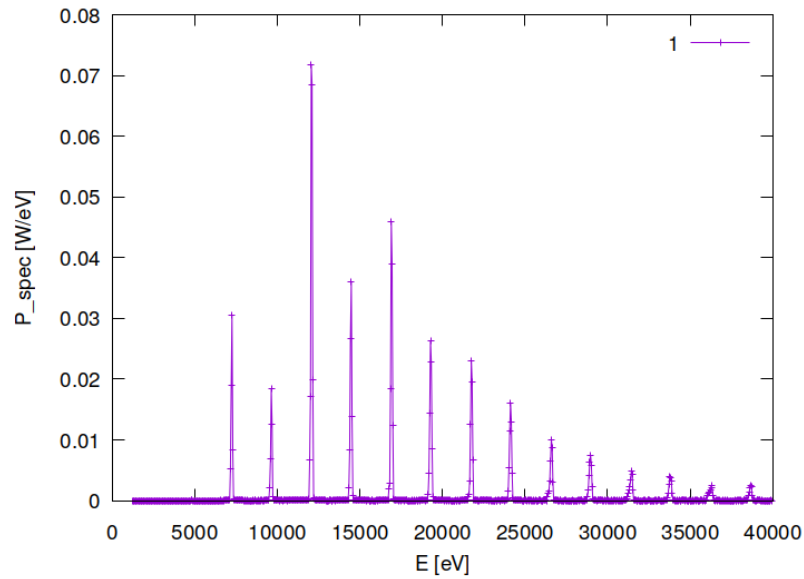


Figure 7.51: Incident spectral flux on surface of optical element #03 (BS) for case #26 for 21800 eV photon energy setting.

## 7.10 Temperature on surface

"fig/BS\_choice\_Si333/plot052.png" Lbl.:BS\_choice\_Si333\_false\_colour\_plot\_T\_oe03\_c16\_21800eV

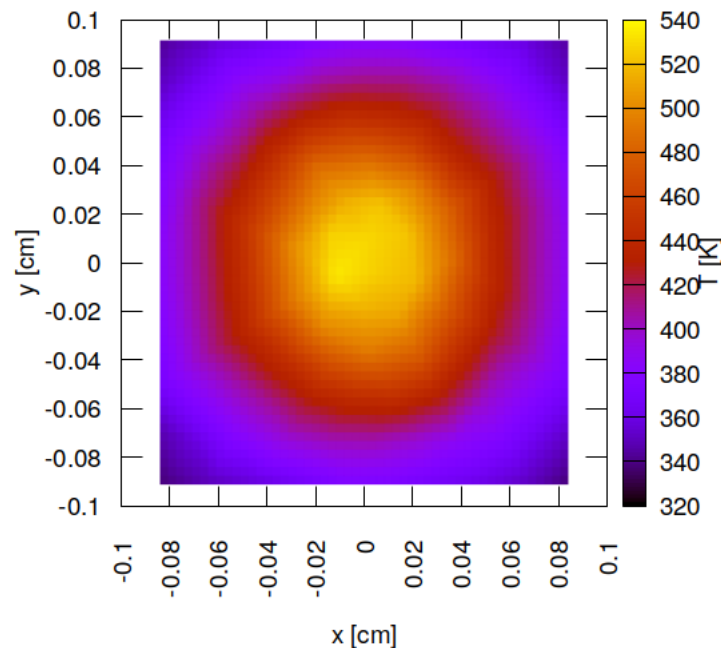


Figure 7.52: Temperature on surface of optical element #03 (BS) for case #16 for 21800 eV photon energy setting.

"fig/BS\_choice\_Si333/plot053.png" Lbl.:BS\_choice\_Si333\_false\_colour\_plot\_T\_oe03\_c26\_21800eV

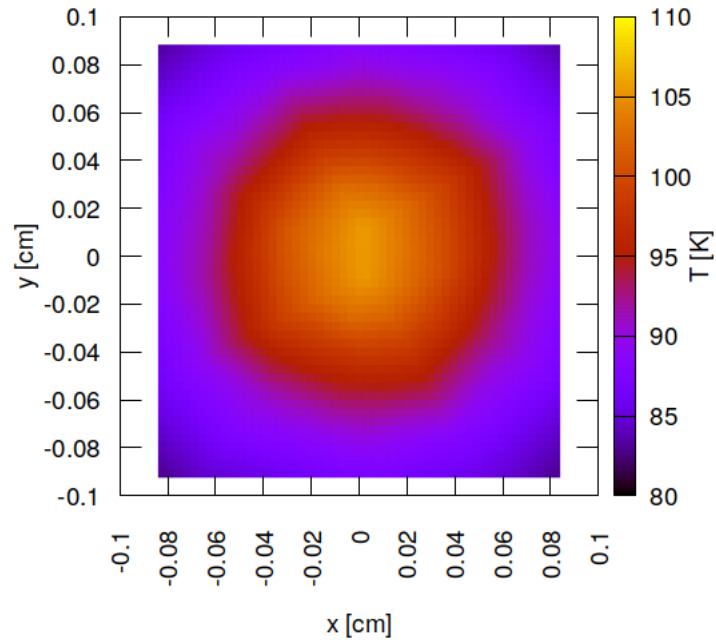


Figure 7.53: Temperature on surface of optical element #03 (BS) for case #26 for 21800 eV photon energy setting.

## 7.11 Mechanical stress (Von Mises stress) on surface

"fig/BS\_choice\_Si333/plot054.png" Lbl.:BS\_choice\_Si333\_false\_colour\_plot\_sigma\_oe03\_c16\_21800eV

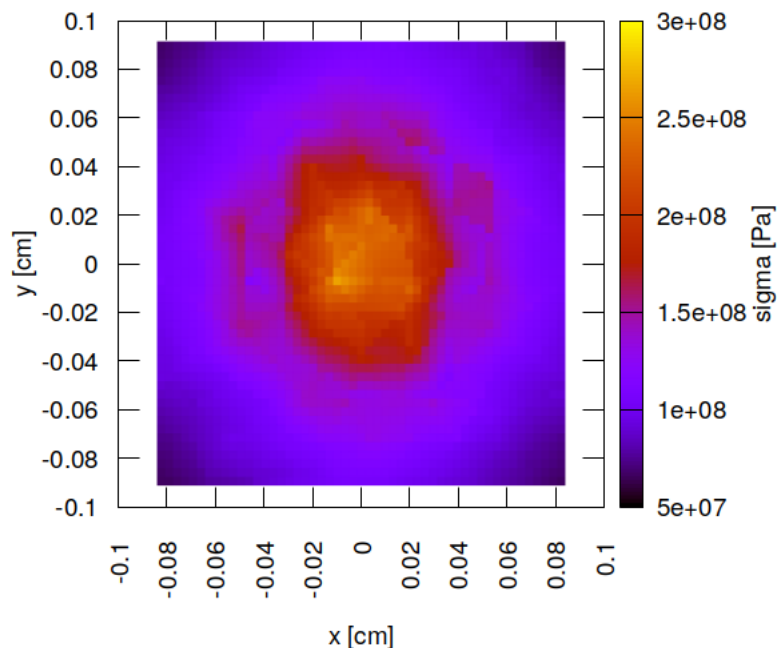


Figure 7.54: Mechanical stress (Von Mises stress) on surface of optical element #03 (BS) for case #16 for 21800 eV photon energy setting.

"fig/BS\_choice\_Si333/plot055.png" Lbl.:BS\_choice\_Si333\_false\_colour\_plot\_sigma\_oe03\_c26\_21800eV

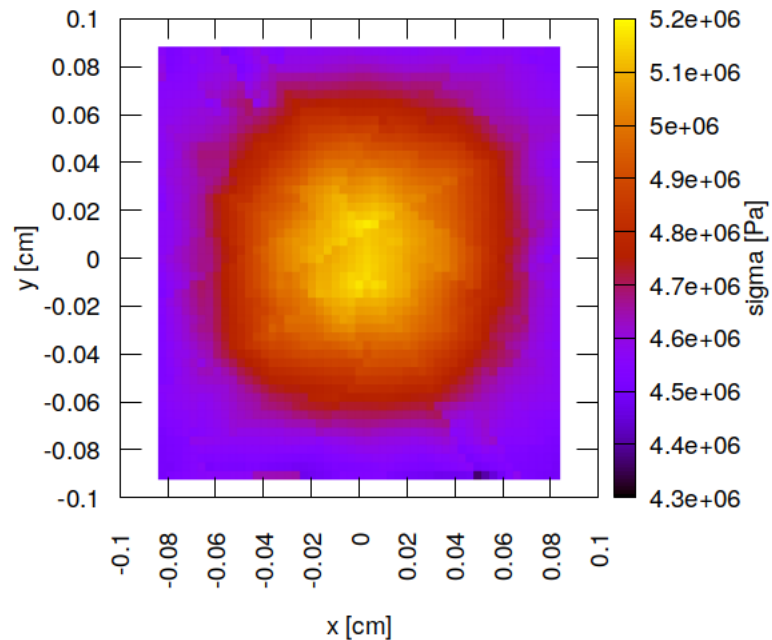


Figure 7.55: Mechanical stress (Von Mises stress) on surface of optical element #03 (BS) for case #26 for 21800 eV photon energy setting.

## 7.12 Surface slope error in meridional direction (y)

"fig/BS\_choice\_Si333/plot056.png" Lbl.:BS\_choice\_Si333\_false\_colour\_plot\_phi\_y\_oe03\_c16\_21800eV

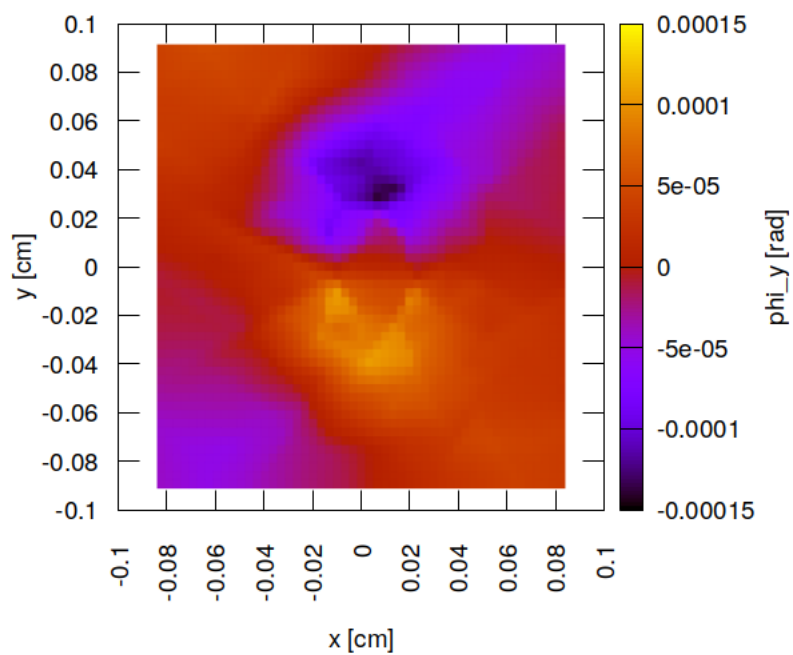


Figure 7.56: Surface slope error in meridional direction (y) of optical element #03 (BS) for case #16 for 21800 eV photon energy setting.

"fig/BS\_choice\_Si333/plot057.png" Lbl.:BS\_choice\_Si333\_false\_colour\_plot\_phi\_y\_oe03\_c26\_21800eV

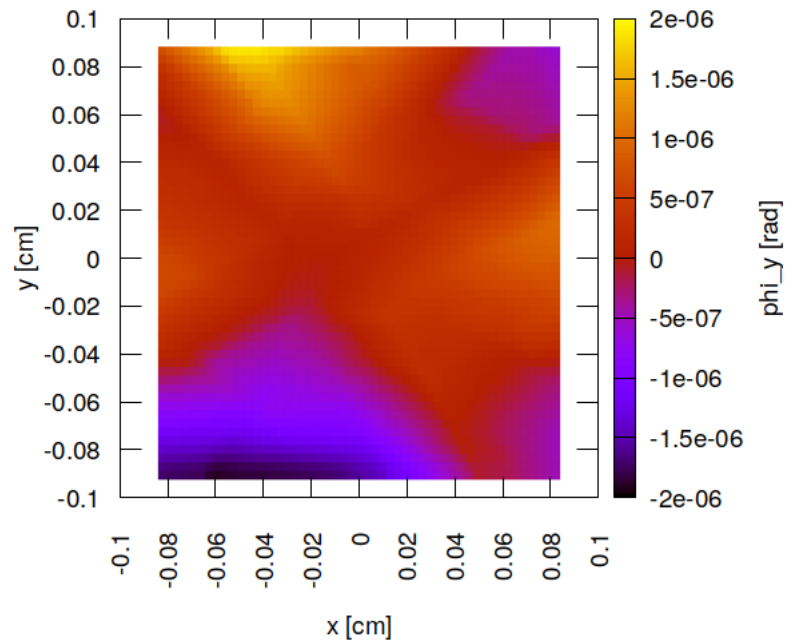


Figure 7.57: Surface slope error in meridional direction (y) of optical element #03 (BS) for case #26 for 21800 eV photon energy setting.



## 7.13 Incident photon irradiance on surface

"fig/BS\_choice\_Si333/plot058.png" Lbl.:BS\_choice\_Si333\_false\_colour\_plot\_I\_inc\_foot\_oe04\_c6\_21800eV

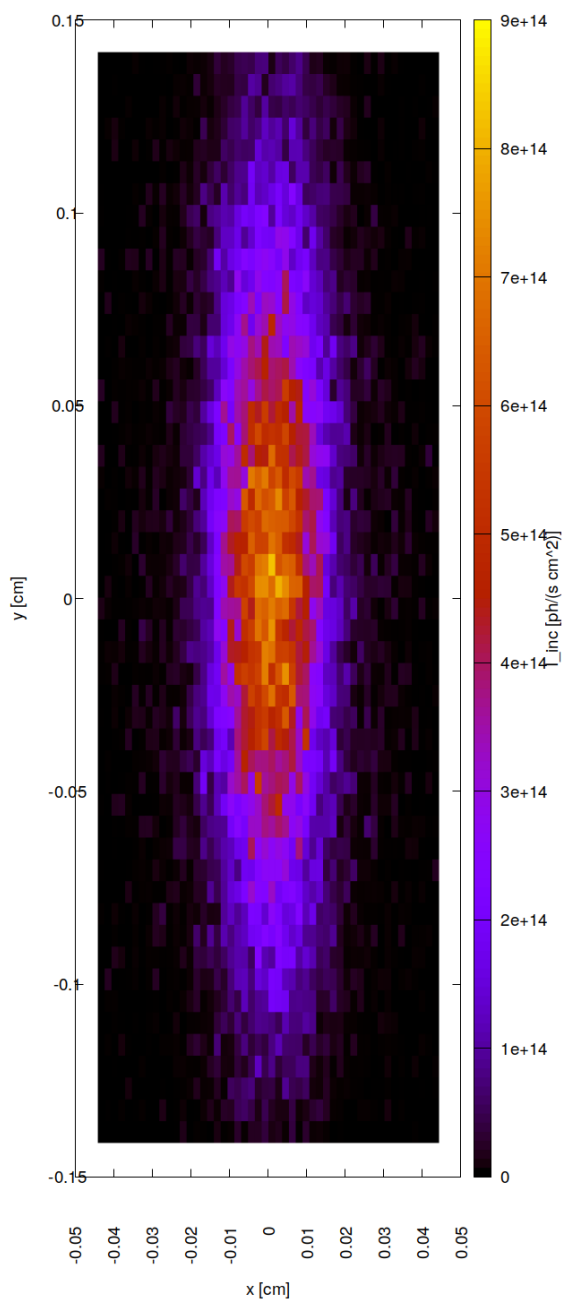


Figure 7.58: Incident photon irradiance on surface of optical element #04 (CM2) for case #6 for 21800 eV photon energy setting.

"fig/BS\_choice\_Si333/plot059.png" Lbl.:BS\_choice\_Si333\_false\_colour\_plot\_I\_inc\_foot\_oe04\_c16\_21800eV

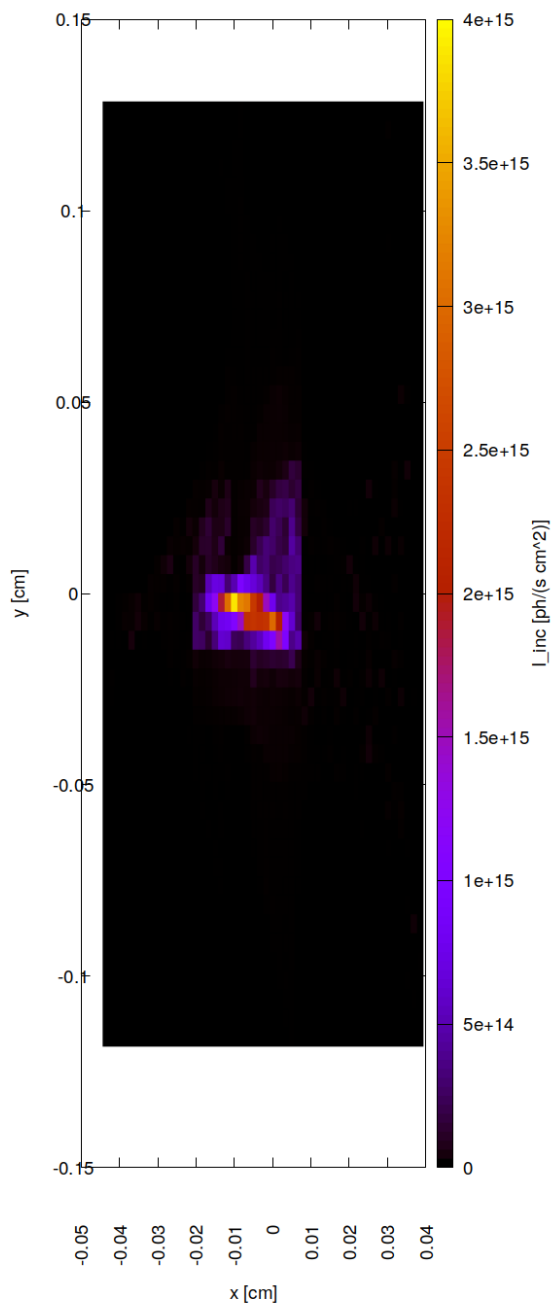


Figure 7.59: Incident photon irradiance on surface of optical element #04 (CM2) for case #16 for 21800 eV photon energy setting.

```
"fig/BS_choice_Si333/plot060.png" Lbl.:BS_choice_Si333_false_colour_plot_I_inc_foot_oe04_c26_21800eV
```

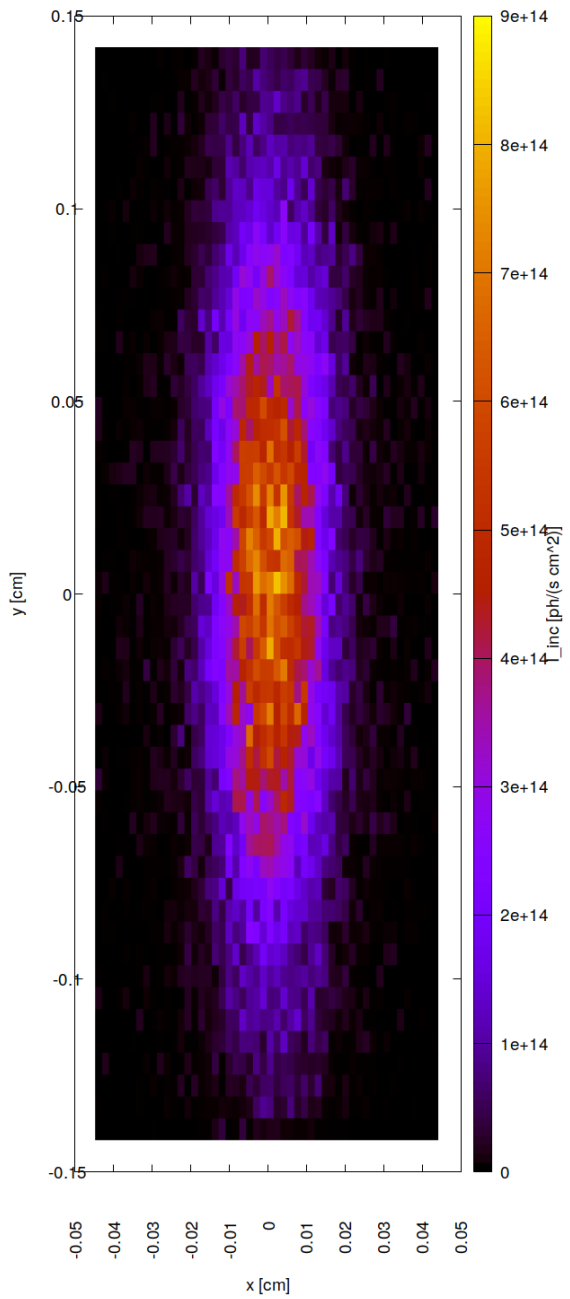


Figure 7.60: Incident photon irradiance on surface of optical element #04 (CM2) for case #26 for 21800 eV photon energy setting.

## 7.14 Photon irradiance in beam cross section

"fig/BS\_choice\_Si333/plot061.png" Lbl.:BS\_choice\_Si333\_false\_colour\_plot\_I\_foc\_oe04\_c6\_21800eV

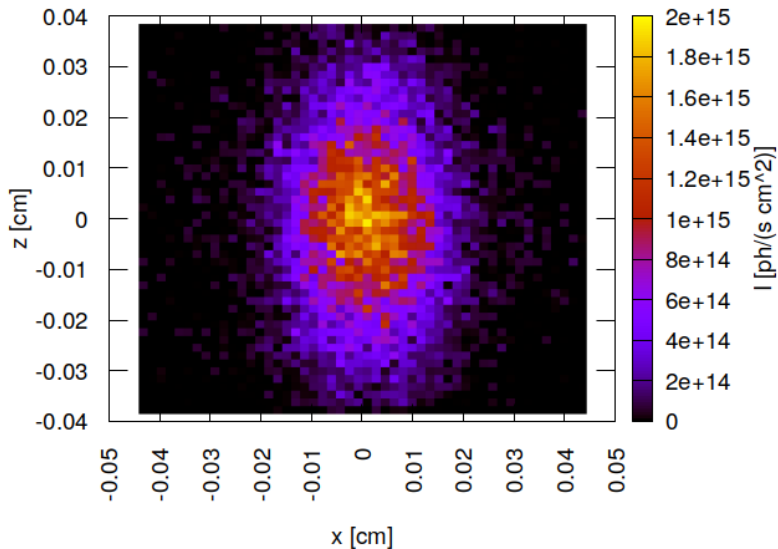


Figure 7.61: Photon irradiance in beam cross section of optical element #04 (CM2) for case #6 for 21800 eV photon energy setting.

"fig/BS\_choice\_Si333/plot062.png" Lbl.:BS\_choice\_Si333\_false\_colour\_plot\_I\_foc\_oe04\_c16\_21800eV

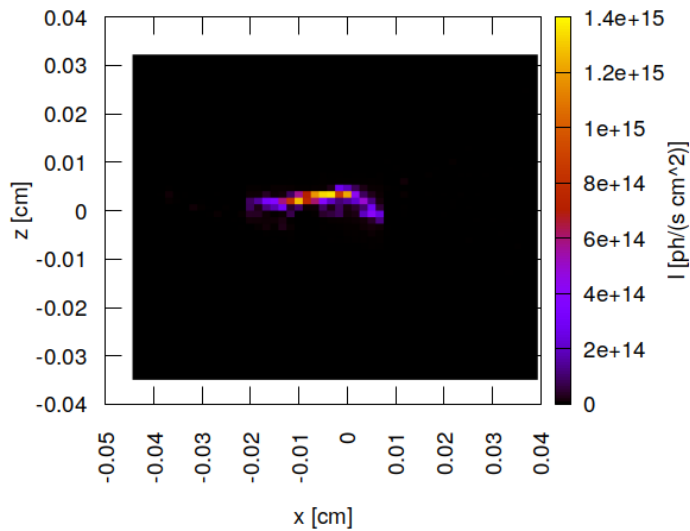


Figure 7.62: Photon irradiance in beam cross section of optical element #04 (CM2) for case #16 for 21800 eV photon energy setting.

"fig/BS\_choice\_Si333/plot063.png" Lbl.:BS\_choice\_Si333\_false\_colour\_plot\_I\_foc\_oe04\_c26\_21800eV

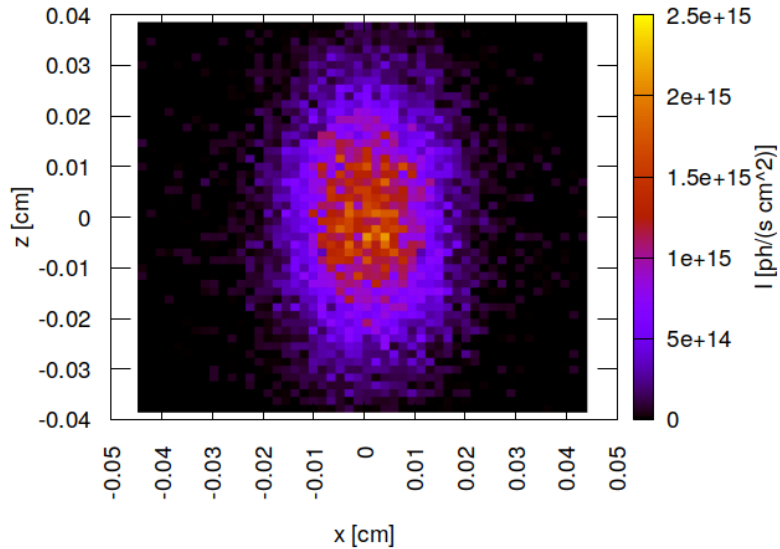


Figure 7.63: Photon irradiance in beam cross section of optical element #04 (CM2) for case #26 for 21800 eV photon energy setting.

## 7.15 Spectral photon flux in beam cross section

"fig/BS\_choice\_Si333/plot064.png" Lbl.:BS\_choice\_Si333\_2d\_plot\_I\_bandfoc\_oe04\_c6\_21800eV

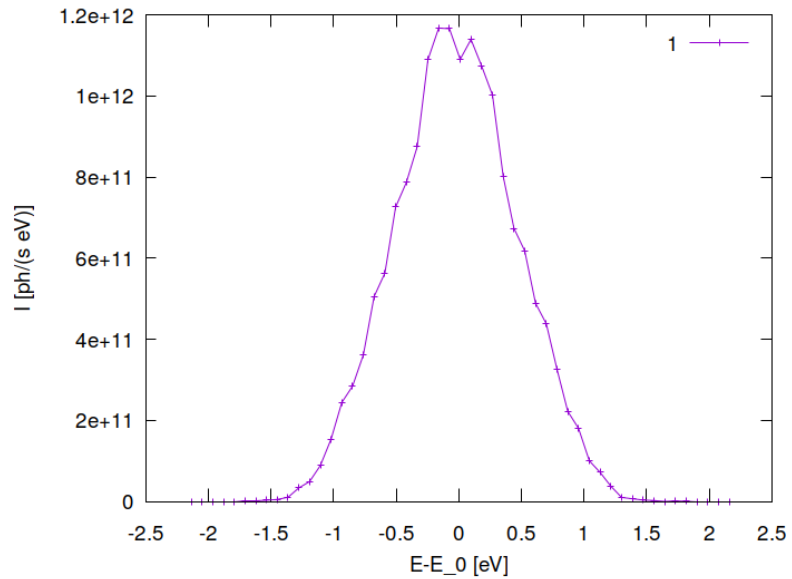


Figure 7.64: Spectral photon flux in beam cross section of optical element #04 (CM2) for case #6 for 21800 eV photon energy setting.

```
"fig/BS_choice_Si333/plot065.png" Lbl.:BS_choice_Si333_2d_plot_I_bandfoc_oe04_c16_21800eV
```

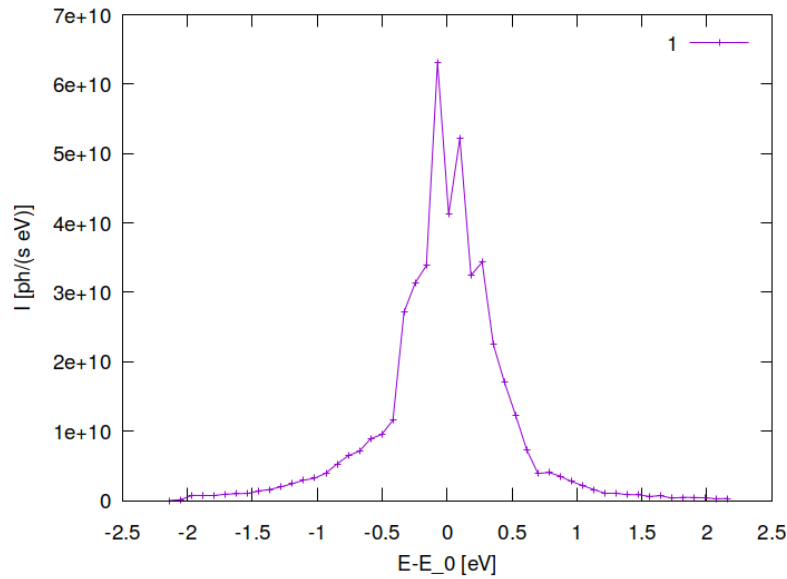


Figure 7.65: Spectral photon flux in beam cross section of optical element #04 (CM2) for case #16 for 21800 eV photon energy setting.

```
"fig/BS_choice_Si333/plot066.png" Lbl.:BS_choice_Si333_2d_plot_I_bandfoc_oe04_c26_21800eV
```

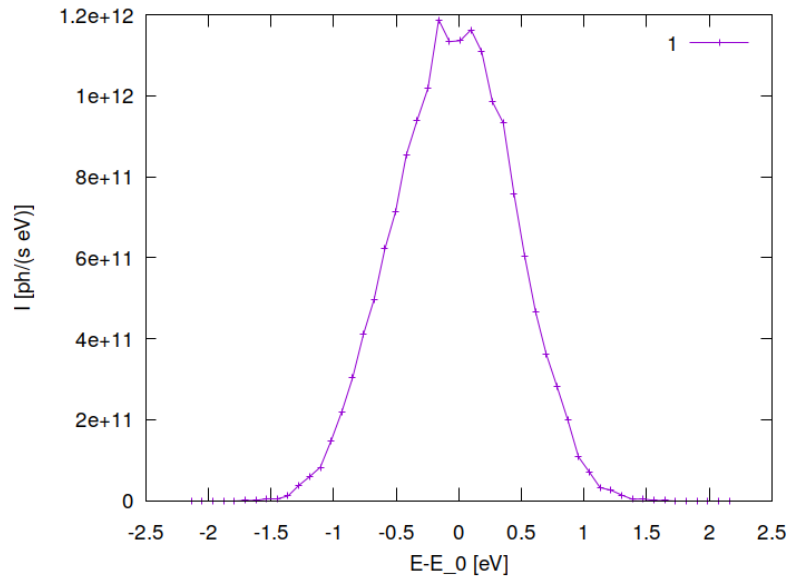


Figure 7.66: Spectral photon flux in beam cross section of optical element #04 (CM2) for case #26 for 21800 eV photon energy setting.

## Chapter 8

# Setup with Si111 beam splitter

A thin silicon crystal is employed as a diffractive beam splitter, using the Si111 reflection in Laue geometry. The Si111 reflection diverts radiation within a narrow bandwidth of

$$\delta E/E = \delta\theta/\tan\theta$$

to the SinCrys side branch. The thickness of the crystal slab has to be optimised in order to maximise diffraction efficiency under the constraint of keeping absorption of the transmitted main beam low. A natural choice is a maximum of the pendel-solution, i.e. the reflectivity oscillating with crystal thickness as predicted by the theory of dynamic diffraction from nearly perfect crystals.

Subsequent reflection from a second crystal with equal inter-planar spacing and diffracting planes parallel to the first is the golden standard in crystal monochromator design, which is followed here. This returns the twice diffracted beam parallel to the direction of the incident, with an adjustable offset, such that downstream optical components and the sample do not have to follow the Bragg angle changes with selected photon energy. Si111 in Bragg geometry is chosen for the second crystal. Putting the second crystal at a distance of around 5.54 metres behind the first provides the required offset of more than one metre between the twice deflected beam and the main beam.

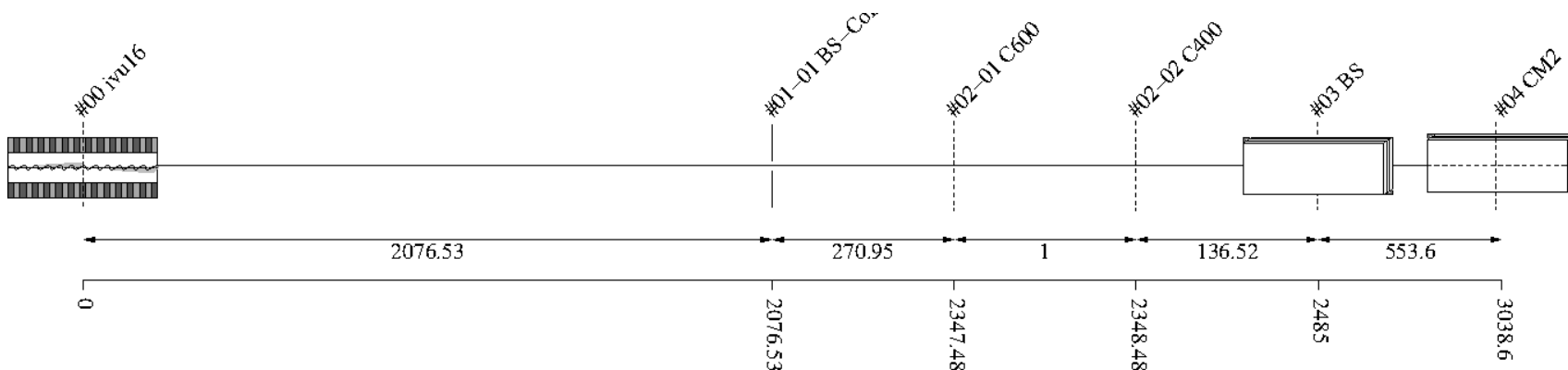


Figure 8.1: Schematic of optical setup

#	Name	Pathlen. cm	Descript.	Shape	Pitch* deg	Roll deg	Yaw deg	x_min cm	x_max cm	y_min cm	y_max cm	Thick. cm	Surface
0	ivu16	0	undulator	auto	0	0	0	-0.0027	0.0027	-0.0002	0.0002	auto	
1		2076.53	none	plane	0	0	0	-inf	inf	-inf	inf		perfect
1-1	BS-Collim	2076.53	aperture	rectangle	0	0	0	-0.035	0.035	-0.035	0.035		
2	Filter	2347.48	none	plane	0	0	0	-inf	inf	-inf	inf		perfect
2-1	C600	2347.48	C-filter	rectangle	0	0	0	-inf	inf	-inf	inf	0.06	
2-2	C400	2348.48	C-filter	rectangle	0	0	0	-inf	inf	-inf	inf	0.04	
3	BS	2485	Si(1,1,1)-crystal	plane	95.2034	90	0	-0.15	0.15	-0.15	0.15		heat bump
4	CM2	3038.6	Si(1,1,1)-crystal	plane	5.20342	180	0	-inf	inf	-inf	inf		perfect

Table 8.1: Setup parameters common to all components. (\*Glancing angle for mirrors, multilayers and crystals. Angle to surface normal otherwise.)

**Rays:** Polar type = total

Polar phase = 0 deg

Polar degree = 0

Is coherent = no

**Spectrum:** E min = 500 eV

E max = 40000 eV

Relative linewidth = 1

**Band:** Bandwidth = 0.0001

**Insertion Device:** lambda period = 1.6 cm

n period = 187

I electron = 0.5 A

E electron = 3 GeV

y horizontal waist = 0 cm

y vertical waist = 0 cm

epsilon x = 3.2E-08 cm rad

epsilon z = 8E-10 cm rad

K y = 1.66

K ymax = 1.7

Divergence limit = 5E-05 rad

**Undulator:** n harmonic max = 99

Tuning type = fixed gap

l aperture = 2076.53 cm

dx aperture = 0.07 cm

dz aperture = 0.07 cm

#1

**Screen:** Is absorbing[1] = no

**Shape:** Thickness = 0 cm

#2 Filter

**Screen:** Is absorbing[1] = yes

Is absorbing[2] = yes

Molecular formula[1] = C

Molecular formula[2] = C

Mass density[1] = 3.5 g/cm^3

Mass density[2] = 3.5 g/cm^3

Thickness[1] = 0.06 cm

Thickness[2] = 0.04 cm

**Shape:** Thickness = 0 cm

### #3 BS

**Grating:** n order = 1

**Crystal:** Structure type = zincblende

Lattice constant[1] = 5.43094 Angstrom

Lattice constant[2] = 5.43094 Angstrom

Lattice constant[3] = 5.43094 Angstrom

Debye Waller factor = 1

Is absorbing = yes

Is asymmetric = yes

Angle asymmetry = 90 deg

Is inclined = no

Is Johansson geometry = no

Is mosaic = no

**Tune:** z rotation axis = 0 cm

**Geometry:** Is thin = yes

Tune automatic = yes

**Shape:** Thickness = 0.0039 cm

**Boundary:** Type = rectangle

x rim = 0.5 cm

y rim = 0.5 cm

**Surface:** Is rough = no

**FEA:** Design type = type specific

Crystal design = laue with cooling loop

Is isotropic = no

Angle x = 45 deg

Angle y = 35.2644 deg

Angle z = 0 deg

Mass density = 2.329 g/cm<sup>3</sup>

**Heat:** Heat transfer type[1] = insulated

Heat transfer type[2] = heat transfer

Heat transfer type[3] = insulated

Heat transfer type[4] = insulated

Heat transfer type[5] = heat transfer

Heat transfer type[6] = flux

Heat transfer type[7] = insulated

Heat transfer type[8] = heat transfer

Heat transfer type[9] = heat sink

Heat transfer coefficient = 1 W/(cm<sup>2</sup>K)

Heat sink coefficient = 10 W/(cm<sup>2</sup>K)

T reference = 77 K  
 T cooling = 77 K  
 Heat capacity = 0.2 J/(gK)  
 Thermal conductivity[1] = 68.908 W/(cmK^n)  
 Thermal conductivity[2] = -1.2807 W/(cmK^n)  
 Thermal conductivity[3] = 0.01038 W/(cmK^n)  
 Thermal conductivity[4] = -4.46212E-05 W/(cmK^n)  
 Thermal conductivity[5] = 1.0589E-07 W/(cmK^n)  
 Thermal conductivity[6] = -1.3103E-10 W/(cmK^n)  
 Thermal conductivity[7] = 6.6033E-14 W/(cmK^n)

**Stress and strain:** Constraint[1] = free

Constraint[2] = kinematic  
 Constraint[3] = free  
 Constraint[4] = free  
 Constraint[5] = free  
 Constraint[6] = free  
 Constraint[7] = free  
 Constraint[8] = free  
 Constraint[9] = free  
 Thermal expansion[1] = 2.5458E-06 1/K^n  
 Thermal expansion[2] = -9.28E-08 1/K^n  
 Thermal expansion[3] = 9.0015E-10 1/K^n  
 Thermal expansion[4] = -3.0037E-12 1/K^n  
 Thermal expansion[5] = 3.4632E-15 1/K^n  
 Stiffness tensor(1)(1) = 1.6772E+11 Pa  
 Stiffness tensor(2)[1] = 6.498E+10 Pa  
 Stiffness tensor(2)[2] = 1.6772E+11 Pa  
 Stiffness tensor(3)[1] = 6.498E+10 Pa  
 Stiffness tensor(3)[2] = 6.498E+10 Pa  
 Stiffness tensor(3)[3] = 1.6772E+11 Pa  
 Stiffness tensor(4)[1] = 0 Pa  
 Stiffness tensor(4)[2] = 0 Pa  
 Stiffness tensor(4)[3] = 0 Pa  
 Stiffness tensor(4)[4] = 8.036E+10 Pa  
 Stiffness tensor(5)[1] = 0 Pa  
 Stiffness tensor(5)[2] = 0 Pa  
 Stiffness tensor(5)[3] = 0 Pa  
 Stiffness tensor(5)[4] = 0 Pa  
 Stiffness tensor(5)[5] = 8.036E+10 Pa  
 Stiffness tensor(6)[1] = 0 Pa  
 Stiffness tensor(6)[2] = 0 Pa  
 Stiffness tensor(6)[3] = 0 Pa  
 Stiffness tensor(6)[4] = 0 Pa  
 Stiffness tensor(6)[5] = 0 Pa  
 Stiffness tensor(6)[6] = 8.036E+10 Pa

#### #4 CM2

**Crystal:** Structure type = zincblende

Lattice constant[1] = 5.43094 Angstrom  
 Lattice constant[2] = 5.43094 Angstrom  
 Lattice constant[3] = 5.43094 Angstrom

Debye Waller factor = 1  
Is absorbing = yes  
Is asymmetric = no  
Is inclined = no  
Is Johansson geometry = no  
Is mosaic = no

**Tune:** Type = constant pathlength  
Are downstream elements fixed = no

**Geometry:** Is thin = no  
Tune automatic = yes

**Boundary:** Type = none

**Surface:** Is rough = no

# Chapter 9

## Finite element analysis (FEA)

A description of the FEA model can be found in section 4

### 9.1 Room temperature

"fig/BS\_choice\_Si111/fea\_plot\_geom\_c14\_21800eV\_03.png" Lbl.:BS\_choice\_Si111\_Surface\_plot\_fea\_plot\_geom\_c14\_21800eV\_03

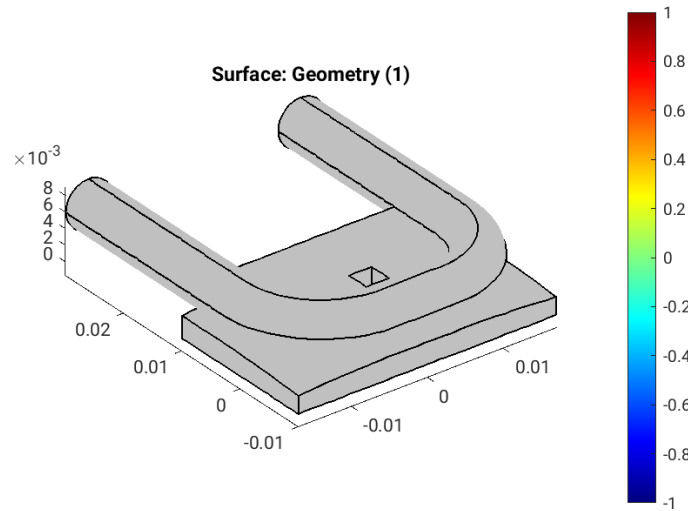


Figure 9.1: Geometry [m] of optical element #03, for case #14, at 21800 eV photon energy setting.

"fig/BS\_choice\_Si111/fea\_plot\_cnstr\_c14\_21800eV\_03.png" Lbl.:BS\_choice\_Si111\_Surface\_plot\_fea\_plot\_cnstr\_c14\_21800eV\_03

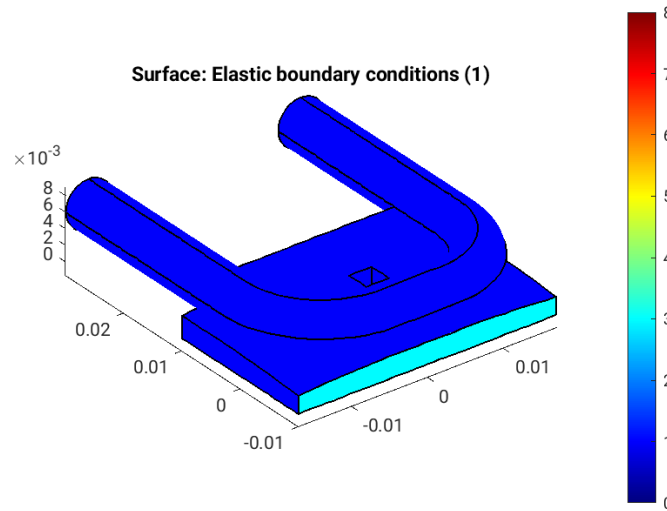


Figure 9.2: Elastic boundary conditions on the surfaces of optical element #03, for case #14, at 21800 eV photon energy setting. Color legend: Blue: Surface can move freely in all directions. Cyan: Tension free kinematic mounting. Minimalistic constraint for three points in surface. One point is fixed, the second can move in one direction, and the third in two, in a fashion that defines angular orientation without introducing stress if the surface expands.

"fig/BS\_choice\_Si111/fea\_plot\_trans\_c14\_21800eV\_03.png" Lbl.:BS\_choice\_Si111\_Surface\_plot\_fea\_plot\_trans\_c14\_21800eV\_03

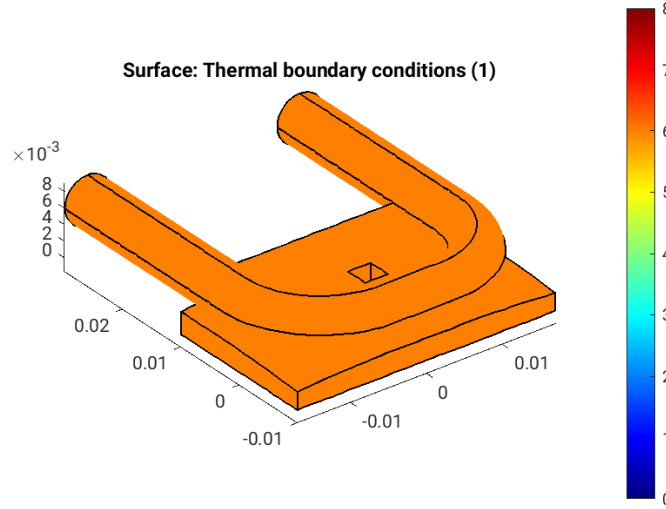


Figure 9.3: Thermal boundary conditions on the surfaces of optical element #03, for case #14, at 21800 eV photon energy setting. Color legend: Orange: No heat transfer at all. Blue: Heat transfer coefficient and temperature difference define heat current density,  $j_q = h(T - T_{cool})$ . Red: Forced heat flux from e.g. absorbed X-rays. Cyan: Heat transfer coefficient and temperature difference define heat current density,  $j_q = h^* \Delta T$  (only at inner surfaces).

"fig/BS\_choice\_Si111/fea\_plot\_heattrans\_c14\_21800eV\_03.png" Lbl.:BS\_choice\_Si111\_Surface\_plot\_fea\_plot\_heattrans\_c14\_21800eV\_03

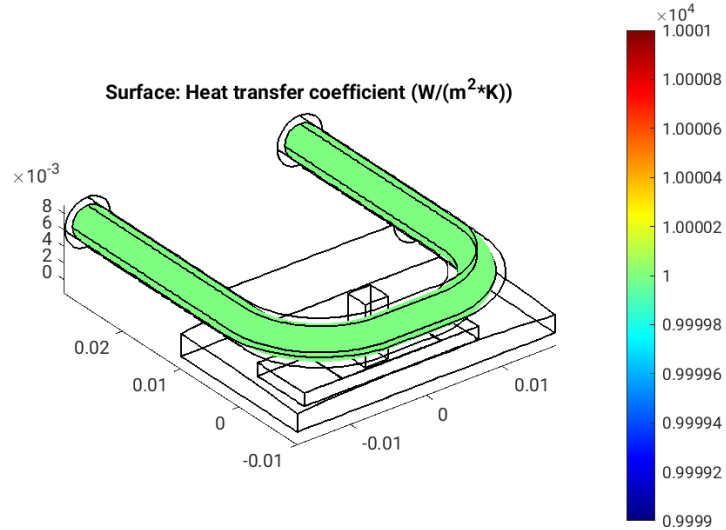


Figure 9.4: Heat transfer coefficient,  $h$  [ $W/(m^2 \cdot K)$ ], on the surfaces of optical element #03, for case #14, at 21800 eV photon energy setting.

"fig/BS\_choice\_Si111/fea\_plot\_heatflux\_c14\_21800eV\_03.png" Lbl.:BS\_choice\_Si111\_Surface\_plot\_fea\_plot\_heatflux\_c14\_21800eV\_03

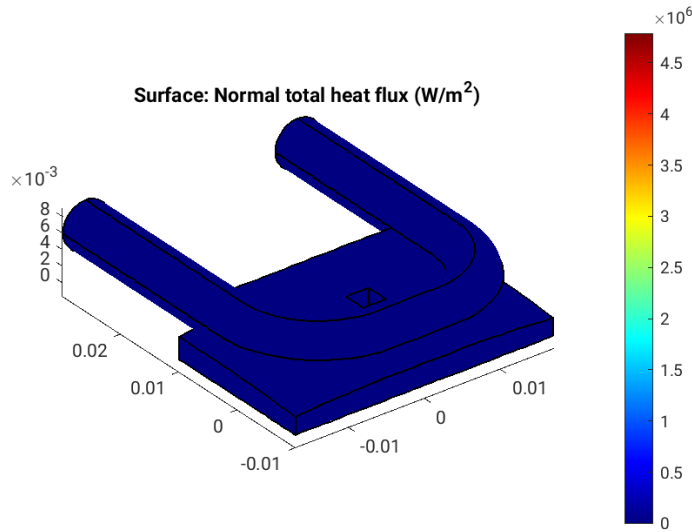


Figure 9.5: Absorbed irradiance,  $p_{\text{abs}}$  [W/m<sup>2</sup>], on the surfaces of optical element #03, for case #14, at 21800 eV photon energy setting.

"fig/BS\_choice\_Si111/fea\_plot\_temp\_c14\_21800eV\_03.png" Lbl.:BS\_choice\_Si111\_Surface\_plot\_fea\_plot\_temp\_c14\_21800eV\_03

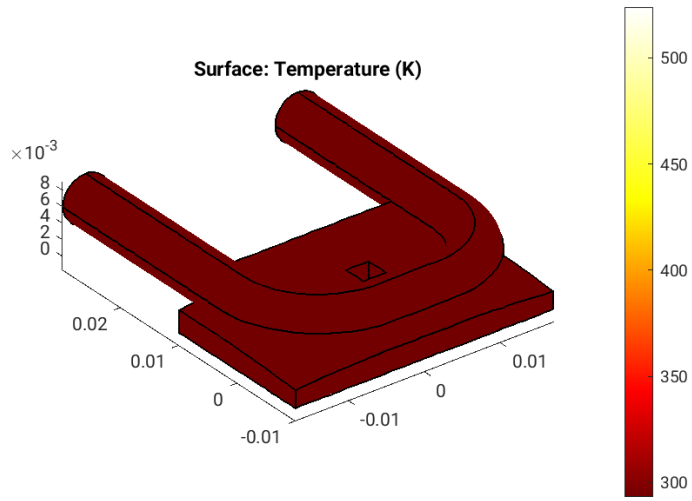


Figure 9.6: Temperature, T [K], on the surfaces of optical element #03, for case #14, at 21800 eV photon energy setting.

"fig/BS\_choice\_Si111/fea\_plot\_thermcond\_c14\_21800eV\_03.png" Lbl.:BS\_choice\_Si111\_Surface\_plot\_fea\_plot\_thermcond\_c14\_21800eV\_03

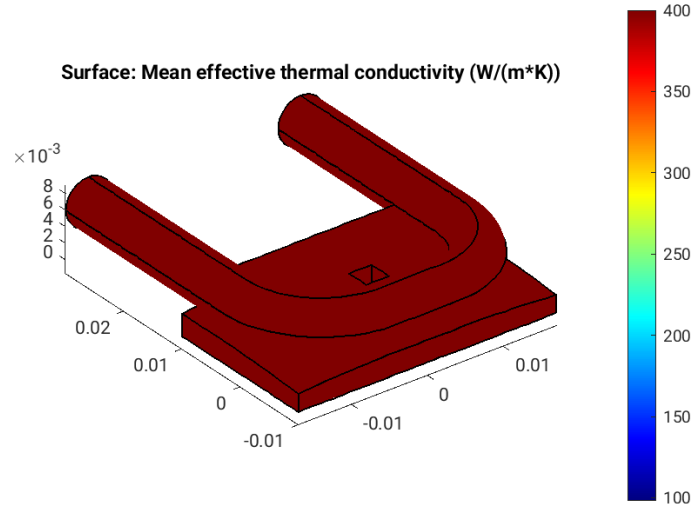


Figure 9.7: Thermal conductivity, lambda [W/(m K)], on the surfaces of optical element #03, for case #14, at 21800 eV photon energy setting.

"fig/BS\_choice\_Si111/fea\_plot\_stress\_c14\_21800eV\_03.png" Lbl.:BS\_choice\_Si111\_Surface\_plot\_fea\_plot\_stress\_c14\_21800eV\_03

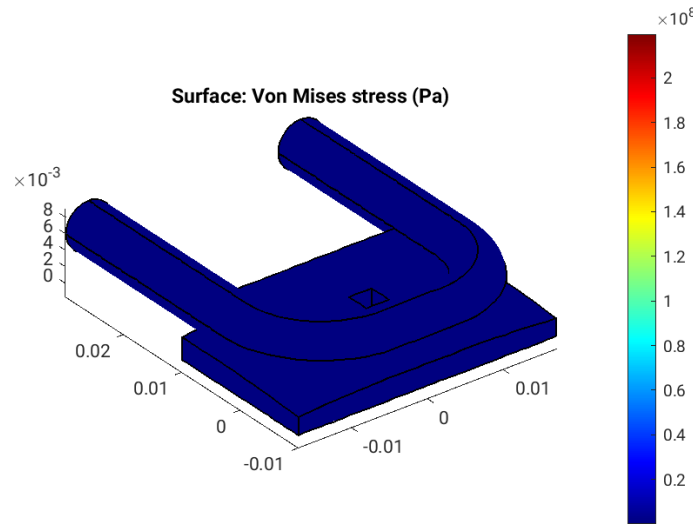


Figure 9.8: Von Mises stress, sigma [Pa], on the surfaces of optical element #03, for case #14, at 21800 eV photon energy setting.

```
"fig/BS_choice_Si111/fea_plot_deform_c14_21800eV_03.png" Lbl.:BS_choice_Si111_Surface_plot_fea_plot_deform_c14_21800eV_03
```

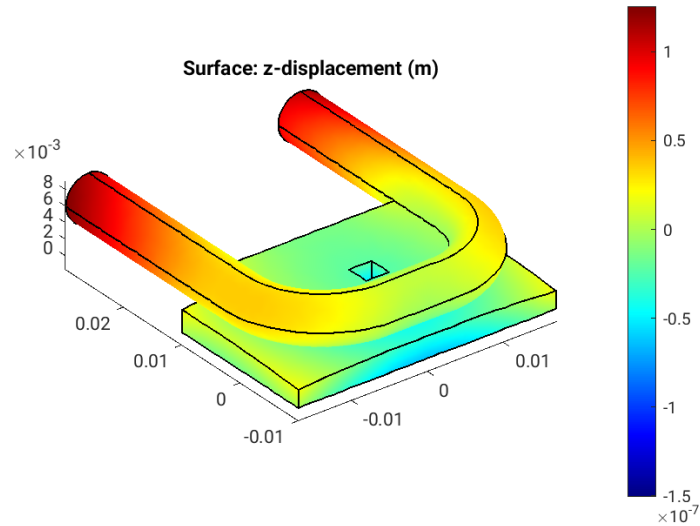


Figure 9.9: Thermoelastic deformation,  $dz$  [m], on the surfaces of optical element #03, for case #14, at 21800 eV photon energy setting.

## 9.2 Cryogenic temperature

```
"fig/BS_choice_Si111/fea_plot_geom_c24_21800eV_03.png" Lbl.:BS_choice_Si111_Surface_plot_fea_plot_geom_c24_21800eV_03
```

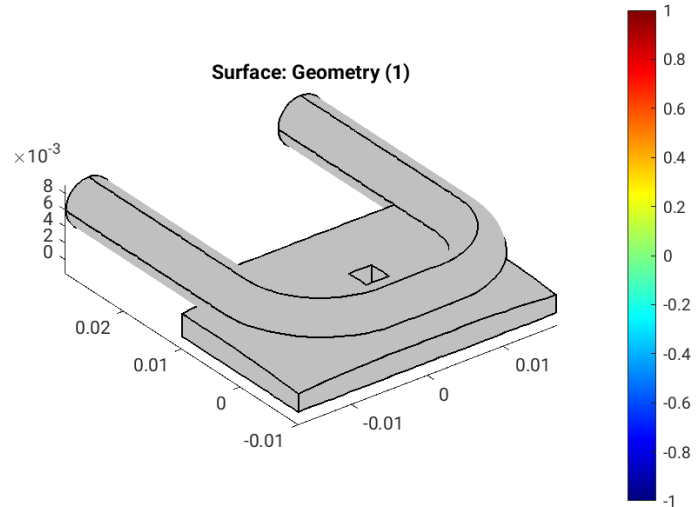


Figure 9.10: Geometry [m] of optical element #03, for case #24, at 21800 eV photon energy setting.

"fig/BS\_choice\_Si111/fea\_plot\_cnstr\_c24\_21800eV\_03.png" Lbl.:BS\_choice\_Si111\_Surface\_plot\_fea\_plot\_cnstr\_c24\_21800eV\_03

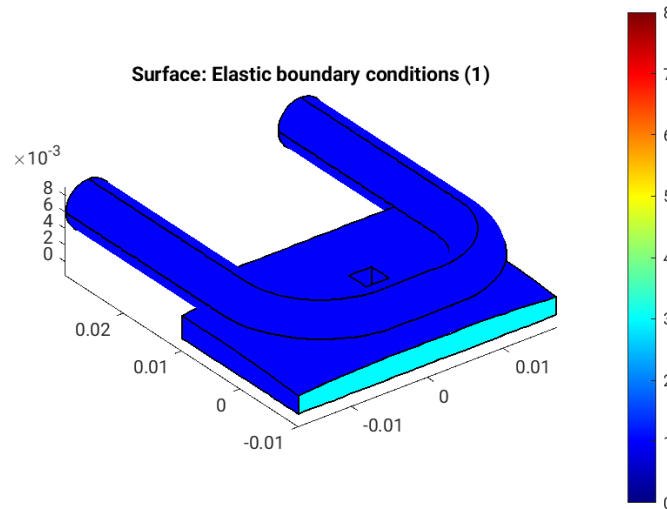


Figure 9.11: Elastic boundary conditions on the surfaces of optical element #03, for case #24, at 21800 eV photon energy setting. Color legend: Blue: Surface can move freely in all directions. Cyan: Tension free kinematic mounting. Minimalistic constraint for three points in surface. One point is fixed, the second can move in one direction, and the third in two, in a fashion that defines angular orientation without introducing stress if the surface expands.

"fig/BS\_choice\_Si111/fea\_plot\_trans\_c24\_21800eV\_03.png" Lbl.:BS\_choice\_Si111\_Surface\_plot\_fea\_plot\_trans\_c24\_21800eV\_03

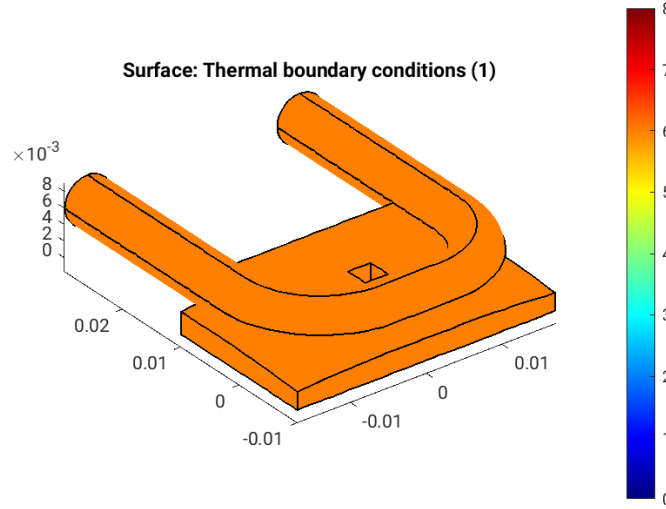


Figure 9.12: Thermal boundary conditions on the surfaces of optical element #03, for case #24, at 21800 eV photon energy setting. Color legend: Orange: No heat transfer at all. Blue: Heat transfer coefficient and temperature difference define heat current density,  $j_q = h(T - T_{cool})$ . Red: Forced heat flux from e.g. absorbed X-rays. Cyan: Heat transfer coefficient and temperature difference define heat current density,  $j_q = h^* \Delta T$  (only at inner surfaces).

"fig/BS\_choice\_Si111/fea\_plot\_heattrans\_c24\_21800eV\_03.png" Lbl.:BS\_choice\_Si111\_Surface\_plot\_fea\_plot\_heattrans\_c24\_21800eV\_03

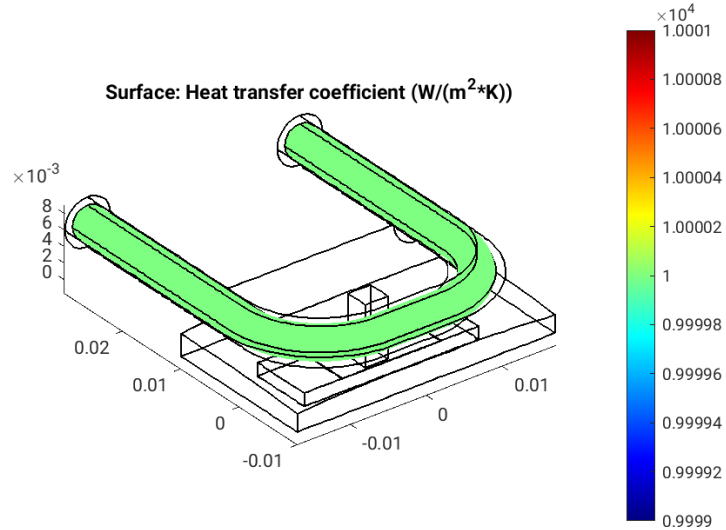


Figure 9.13: Heat transfer coefficient,  $h$  [W/(m<sup>2</sup> K)], on the surfaces of optical element #03, for case #24, at 21800 eV photon energy setting.

"fig/BS\_choice\_Si111/fea\_plot\_heatflux\_c24\_21800eV\_03.png" Lbl.:BS\_choice\_Si111\_Surface\_plot\_fea\_plot\_heatflux\_c24\_21800eV\_03

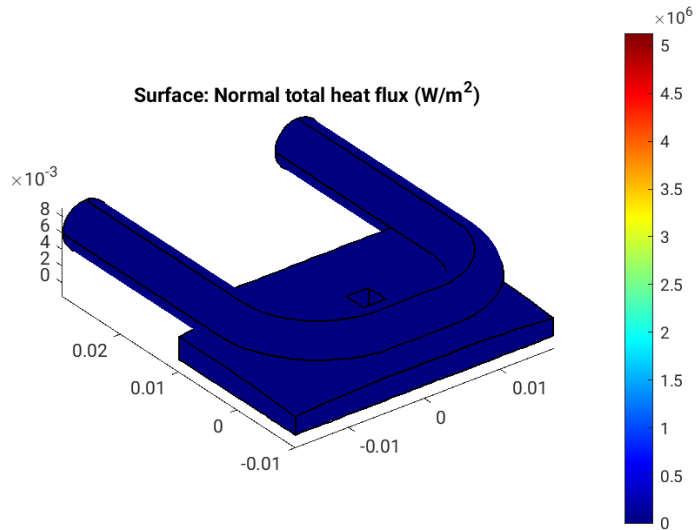


Figure 9.14: Absorbed irradiance,  $p_{\text{abs}}$  [W/m<sup>2</sup>], on the surfaces of optical element #03, for case #24, at 21800 eV photon energy setting.

"fig/BS\_choice\_Si111/fea\_plot\_temp\_c24\_21800eV\_03.png" Lbl.:BS\_choice\_Si111\_Surface\_plot\_fea\_plot\_temp\_c24\_21800eV\_03

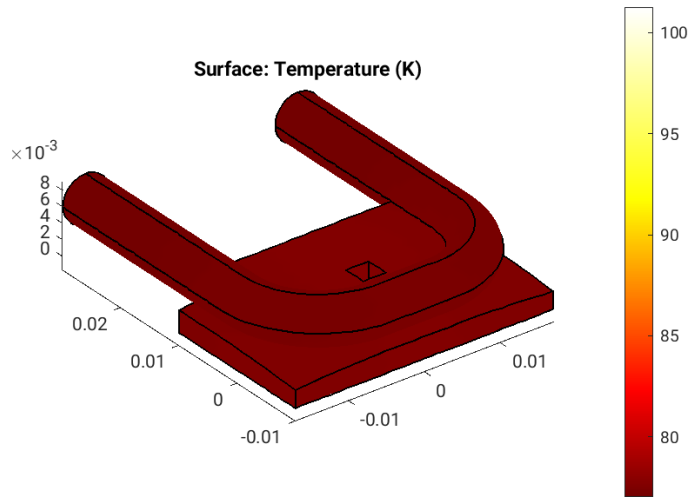


Figure 9.15: Temperature, T [K], on the surfaces of optical element #03, for case #24, at 21800 eV photon energy setting.

"fig/BS\_choice\_Si111/fea\_plot\_thermcond\_c24\_21800eV\_03.png" Lbl.:BS\_choice\_Si111\_Surface\_plot\_fea\_plot\_thermcond\_c24\_21800eV\_03

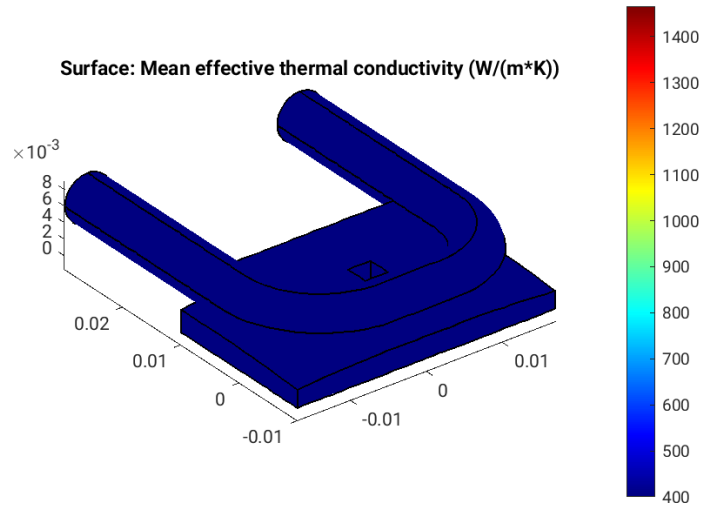


Figure 9.16: Thermal conductivity, lambda [W/(m K)], on the surfaces of optical element #03, for case #24, at 21800 eV photon energy setting.

"fig/BS\_choice\_Si111/fea\_plot\_stress\_c24\_21800eV\_03.png" Lbl.:BS\_choice\_Si111\_Surface\_plot\_fea\_plot\_stress\_c24\_21800eV\_03

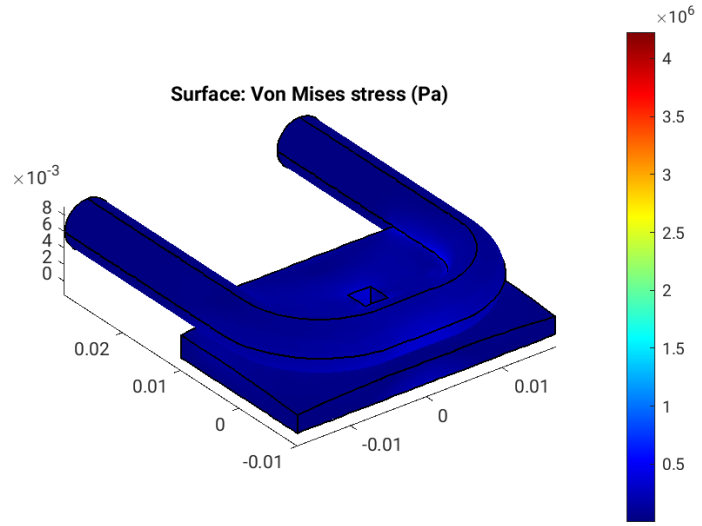


Figure 9.17: Von Mises stress, sigma [Pa], on the surfaces of optical element #03, for case #24, at 21800 eV photon energy setting.

"fig/BS\_choice\_Si111/fea\_plot\_deform\_c24\_21800eV\_03.png" Lbl.:BS\_choice\_Si111\_Surface\_plot\_fea\_plot\_deform\_c24\_21800eV\_03

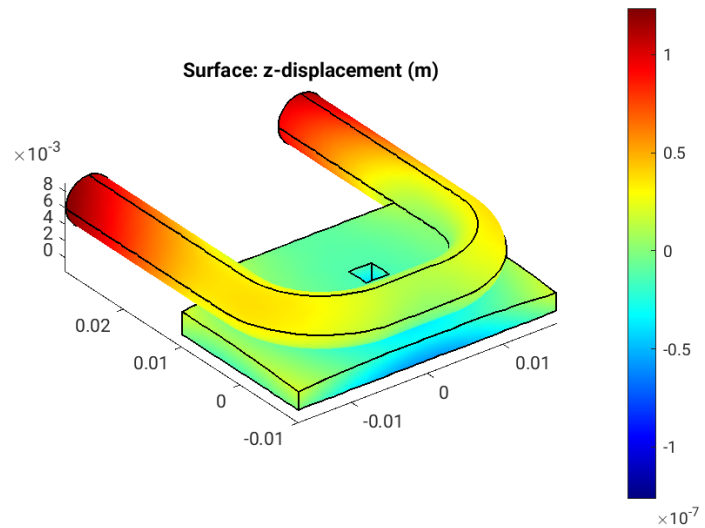


Figure 9.18: Thermoelastic deformation,  $dz$  [m], on the surfaces of optical element #03, for case #24, at 21800 eV photon energy setting.

# Chapter 10

## Parameter scan cases

There are thirty cases in total, which fall into three groups á ten cases. The first group, is for the perfect crystal case without deformation of the beam splitter under heat load due to X-ray absorption. Second and third group are for the beam splitter deformed under heat load at room temperature and at cryogenic temperature (77 K) respectively. Within the ten cases of every group the thickness of the beam splitter is varied in order to optimize reflectivity that varies periodically with this thickness (so called pendellösung).

Due to the periodic character there are several thicknesses with a reflectivity close to 100%. On one hand, the first reflectivity maximum, i.e. that for smallest thickness, offers the highest transparency for the transmitted main beam. On the other hand, manufacturing, mounting and stability under heat load are more challenging the thinner the beam splitter is. As silicon has an absorption problem, as will be seen later, we went for the thinnest option anyway, quasi as the best case scenario. If it is still worse than other set ups, one can safely disregard Si333 beam splitters.

Case	T_cooling_03 K	heat_capacity_03 J/(gK)	Has_slope_error_03	Skip_heatload	Thickness_03 cm
1	293.15	0.7	no	yes	0.0005
2	293.15	0.7	no	yes	0.001
3	293.15	0.7	no	yes	0.0015
4	293.15	0.7	no	yes	0.002
5	293.15	0.7	no	yes	0.0025
6	293.15	0.7	no	yes	0.003
7	293.15	0.7	no	yes	0.0035
8	293.15	0.7	no	yes	0.004
9	293.15	0.7	no	yes	0.0045
10	293.15	0.7	no	yes	0.005
11	293.15	0.7	yes	no	0.0005
12	293.15	0.7	yes	no	0.001
13	293.15	0.7	yes	no	0.0015
14	293.15	0.7	yes	no	0.002
15	293.15	0.7	yes	no	0.0025
16	293.15	0.7	yes	no	0.003
17	293.15	0.7	yes	no	0.0035
18	293.15	0.7	yes	no	0.004
19	293.15	0.7	yes	no	0.0045
20	293.15	0.7	yes	no	0.005
21	77	0.2	yes	no	0.0005
22	77	0.2	yes	no	0.001
23	77	0.2	yes	no	0.0015
24	77	0.2	yes	no	0.002
25	77	0.2	yes	no	0.0025
26	77	0.2	yes	no	0.003
27	77	0.2	yes	no	0.0035
28	77	0.2	yes	no	0.004
29	77	0.2	yes	no	0.0045
30	77	0.2	yes	no	0.005

Table 10.1: Parameter values for different cases in parameter scan

### Legend

**Case:** Case number in parameter scan

**T\_cooling\_03:** Optical\_element\_#3.FEA.Heat.T\_cooling (Cooling temperature.)

**heat\_capacity\_03:** Optical\_element\_#3.FEA.Heat.heat\_capacity (Specific heat capacity.)

**Has\_slope\_error\_03:** Optical\_element\_#3.Surface.Has\_slope\_error (Has surface slope error?)

**Skip\_heatload:** Session.Skip\_heatload (Skip heat load calculation for all optical elements? (heat load parameters are kept))

**Thickness\_03:** Optical\_element\_#3.Shape.Thickness (Optical element's thickness or thickness of optically active layer.)

## Chapter 11

# Photon energy scan

The  $K_y$ -values in the table below are those for optimised output between 15.6 and 18.3 keV – the whole range being covered by the 7th harmonic that is brightest there – used by DanMAX’ main branch. SinCrys, foreseen to be working at a higher photon energy range, is then going to use the 9th harmonic that is not necessarily the brightest there.

E eV	K_y	n_harm/step	P_sum W	theta_B03 deg	theta_B04 deg
<b>20000</b>	1.67551	9	170.798	5.6731987	5.6731987
<b>20100</b>	1.66836	9	170.209	5.6448817	5.6448817
<b>20200</b>	1.66125	9	169.47	5.6168466	5.6168466
<b>20300</b>	1.65418	9	168.879	5.5890894	5.5890894
<b>20400</b>	1.64714	9	168.315	5.561605	5.561605
<b>20500</b>	1.64015	9	167.588	5.5343904	5.5343904
<b>20600</b>	1.63319	9	166.189	5.507441	5.507441
<b>20700</b>	1.62628	9	165.542	5.4807534	5.4807534
<b>20800</b>	1.6194	9	164.949	5.4543238	5.4543238
<b>20900</b>	1.61255	9	164.413	5.4281478	5.4281478
<b>21000</b>	1.60575	9	163.752	5.4022226	5.4022226
<b>21100</b>	1.59898	9	163.16	5.376544	5.376544
<b>21200</b>	1.59224	9	162.507	5.351109	5.351109
<b>21300</b>	1.58554	9	161.904	5.3259134	5.3259134
<b>21400</b>	1.57887	9	161.386	5.3009543	5.3009543
<b>21500</b>	1.57224	9	160.797	5.2762289	5.2762289
<b>21600</b>	1.56564	9	160.163	5.2517333	5.2517333
<b>21700</b>	1.55908	9	159.473	5.2274642	5.2274642
<b>21800</b>	1.55255	9	158.884	5.2034187	5.2034187
<b>21900</b>	1.54605	9	157.585	5.1795936	5.1795936
<b>22000</b>	1.53958	9	157.101	5.1559858	5.1559858
<b>22100</b>	1.53315	9	156.451	5.1325932	5.1325932
<b>22200</b>	1.52674	9	155.93	5.1094117	5.1094117
<b>22300</b>	1.52037	9	155.254	5.0864391	5.0864391
<b>22400</b>	1.51402	9	154.716	5.0636721	5.0636721
<b>22500</b>	1.50771	9	154.16	5.0411086	5.0411086
<b>22600</b>	1.50143	9	153.484	5.0187454	5.0187454
<b>22700</b>	1.49517	9	152.951	4.9965801	4.9965801
<b>22800</b>	1.48895	9	152.294	4.9746099	4.9746099
<b>22900</b>	1.48275	9	151.786	4.9528322	4.9528322
<b>23000</b>	1.47658	9	151.176	4.9312449	4.9312449
<b>23100</b>	1.47044	9	150.589	4.9098449	4.9098449
<b>23200</b>	1.46433	9	149.911	4.8886304	4.8886304
<b>23300</b>	1.45824	9	148.827	4.8675981	4.8675981
<b>23400</b>	1.45218	9	148.246	4.8467464	4.8467464
<b>23500</b>	1.44615	9	147.698	4.8260732	4.8260732

Table 11.1: Scan values for different photon energies in energy scan

### Legend

**E:** photon energy

**K\_y:** deflection parameter for vertical field component of insertion device

**n\_harm/step:** number of undulator harmonic or number of energy slot for continuous source (e.g. wiggler)

**P\_sum:** sum of power in harmonics / energy intervals, P\_sum = P\_src

**theta\_B03:** Bragg angle, i.e. glancing angle of incident and reflected beam w.r.t. the set of diffracting planes of optical element 03

**theta\_B04:** Bragg angle, i.e. glancing angle of incident and reflected beam w.r.t. the set of diffracting planes of optical element 04

# Chapter 12

## Plots

### 12.1 Statistics of incident irradiance

```
"fig/BS_choice_Si111/plot001.png" Lbl.:BS_choice_Si111_2d_plot_I_peak_incstat_oe03
```

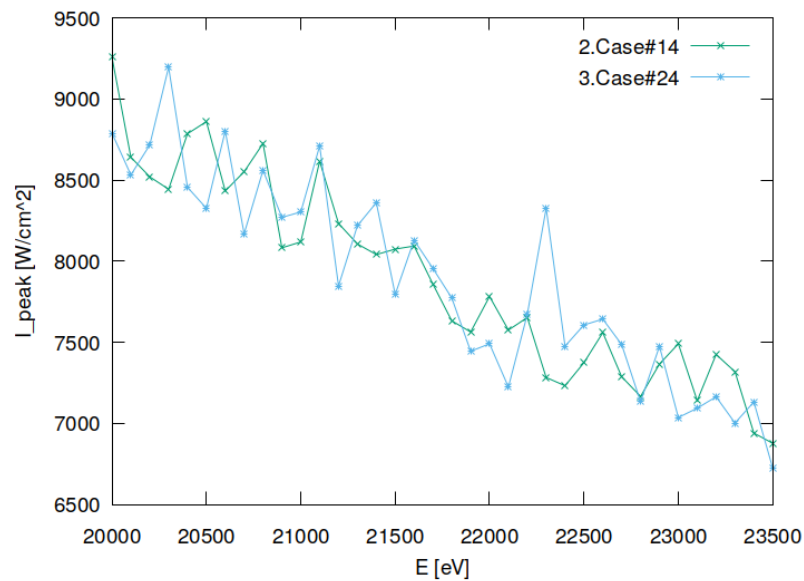


Figure 12.1: Incident peak irradiance of optical element #03 (BS).

```
"fig/BS_choice_Si111/plot002.png" Lbl.:BS_choice_Si111_2d_plot_I_int_incstat_oe03
```

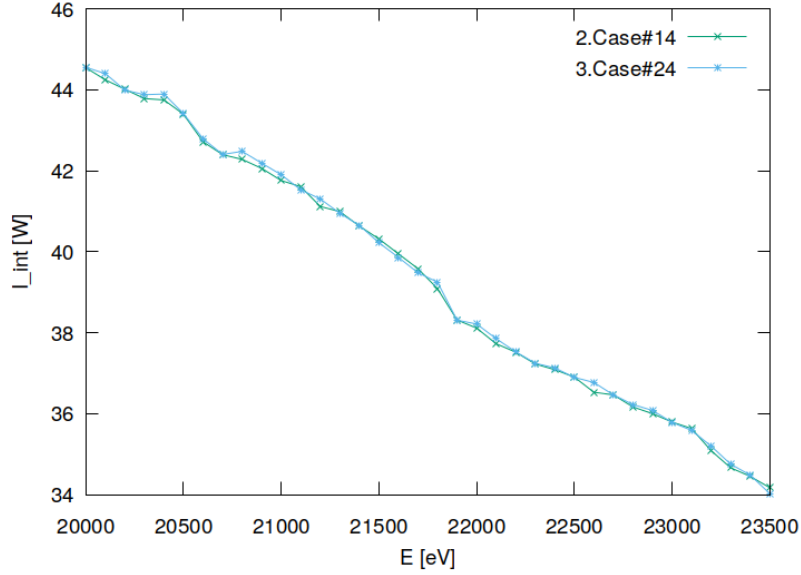


Figure 12.2: Incident flux of optical element #03 (BS).

## 12.2 Statistics of absorbed irradiance

```
"fig/BS_choice_Si111/plot003.png" Lbl.:BS_choice_Si111_2d_plot_I_peak_absstat_oe03
```

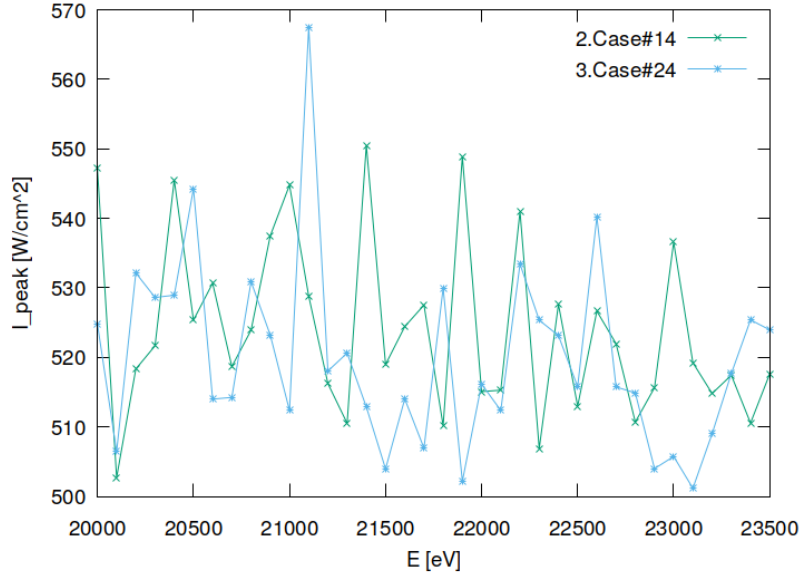


Figure 12.3: Absorbed peak irradiance of optical element #03 (BS).

```
"fig/BS_choice_Si111/plot004.png" Lbl.:BS_choice_Si111_2d_plot_I_int_absstat_oe03
```

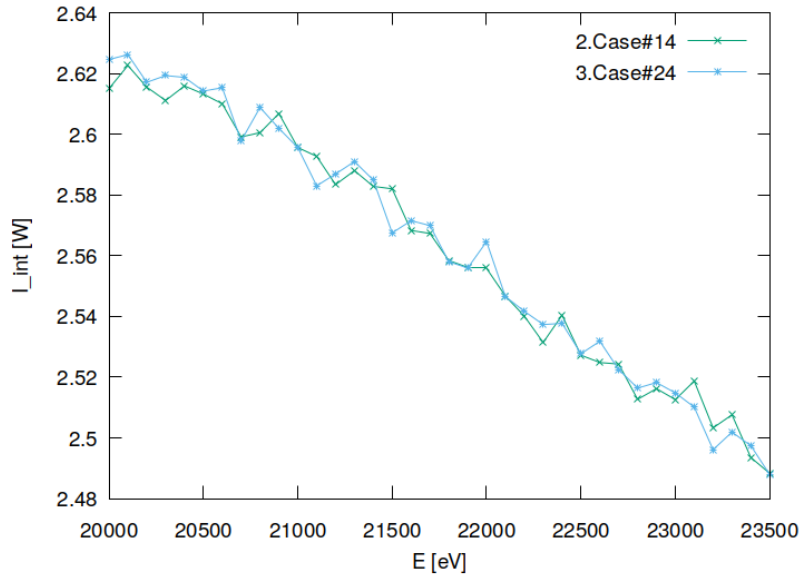


Figure 12.4: Absorbed flux of optical element #03 (BS).

### 12.3 Statistics of temperature

```
"fig/BS_choice_Si111/plot005.png" Lbl.:BS_choice_Si111_2d_plot_T_peak_stat_oe03
```

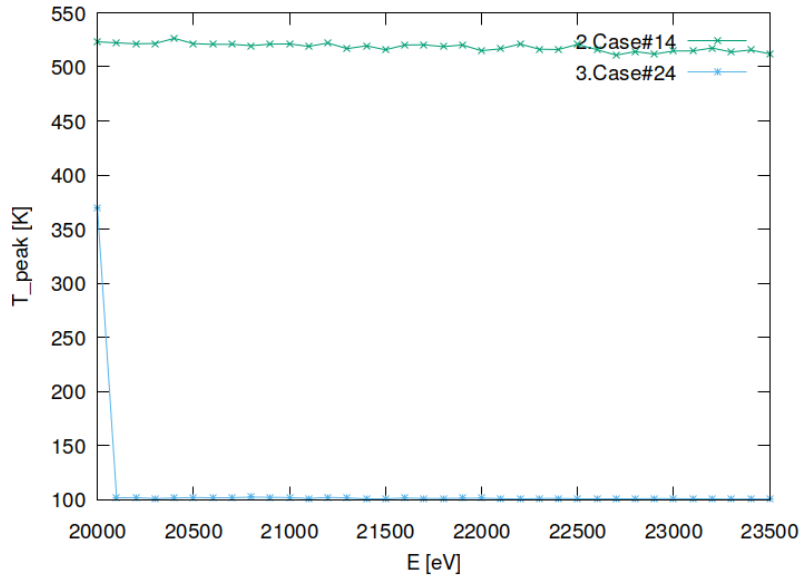


Figure 12.5: Peak temperature of optical element #03 (BS).

## 12.4 Statistics of mechanical stress (von Mises stress)

"fig/BS\_choice\_Si111/plot006.png" Lbl.:BS\_choice\_Si111\_2d\_plot\_sigma\_peak\_stat\_oe03

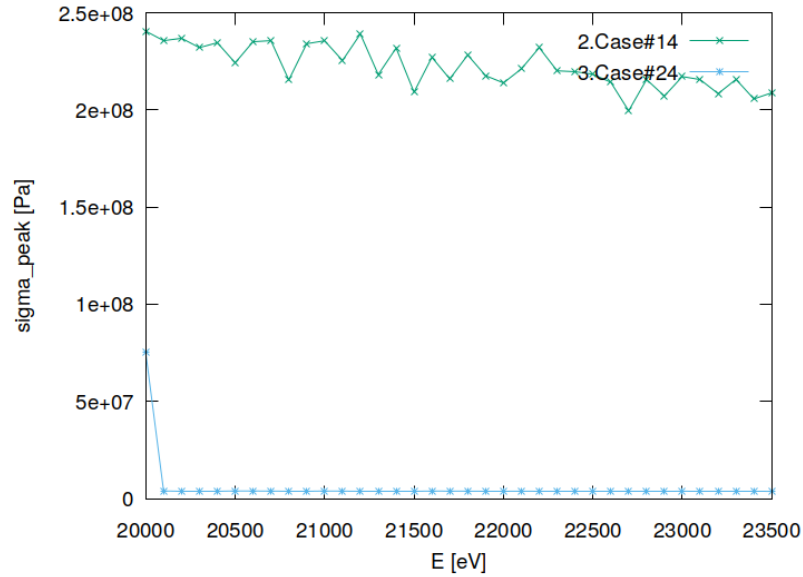


Figure 12.6: Peak mechanical stress (Von Mises stress) of optical element #03 (BS).

## 12.5 Statistics of optical surface deformation

"fig/BS\_choice\_Si111/plot007.png" Lbl.:BS\_choice\_Si111\_2d\_plot\_dz\_peak\_stat\_oe03

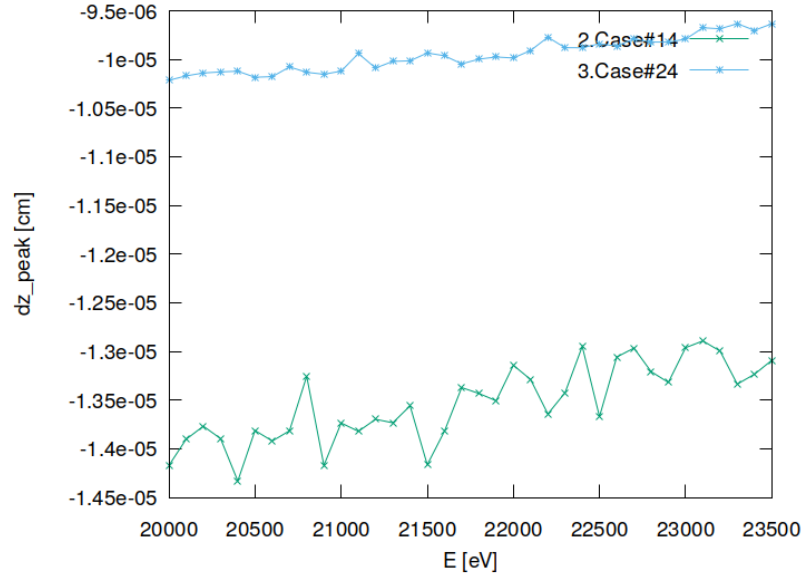


Figure 12.7: Peak deformation of optical element #03 (BS).

## 12.6 Statistics of photon irradiance on optical surface

"fig/BS\_choice\_Si111/plot008.png" Lbl.:BS\_choice\_Si111\_2d\_plot\_dx\_fwhm\_inc\_footstat\_oe04

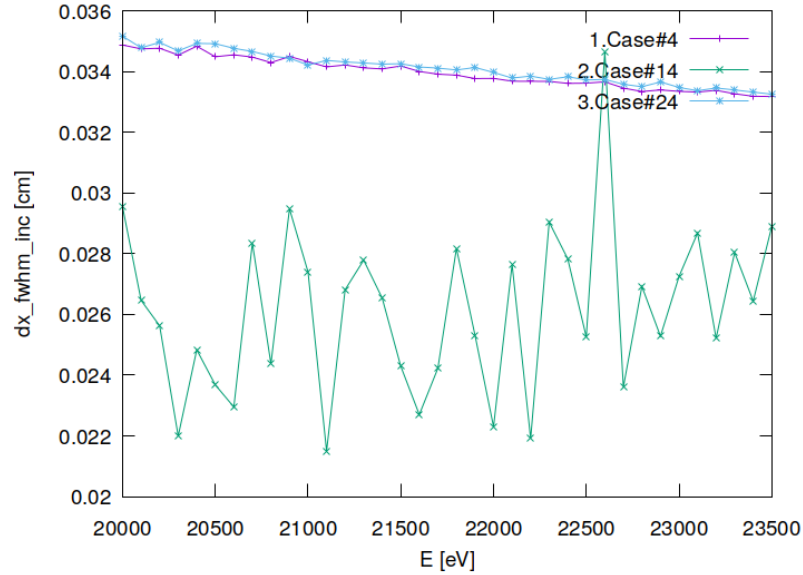


Figure 12.8: Sagittal footprint diameter (FWHM) of optical element #04 (CM2).

"fig/BS\_choice\_Si111/plot009.png" Lbl.:BS\_choice\_Si111\_2d\_plot\_dy\_fwhm\_inc\_footstat\_oe04

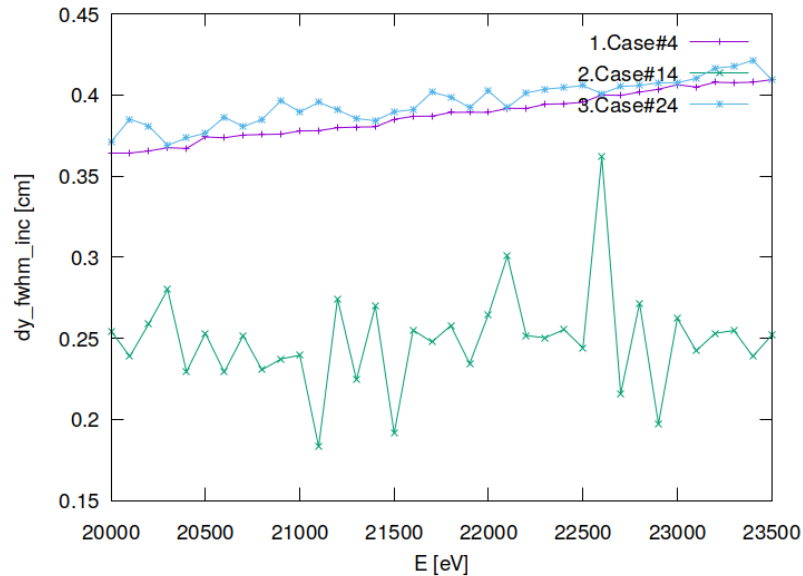


Figure 12.9: Meridional footprint diameter (FWHM) of optical element #04 (CM2).

```
"fig/BS_choice_Si111/plot010.png" Lbl.:BS_choice_Si111_2d_plot_I_inc_int_footstat_oe04
```

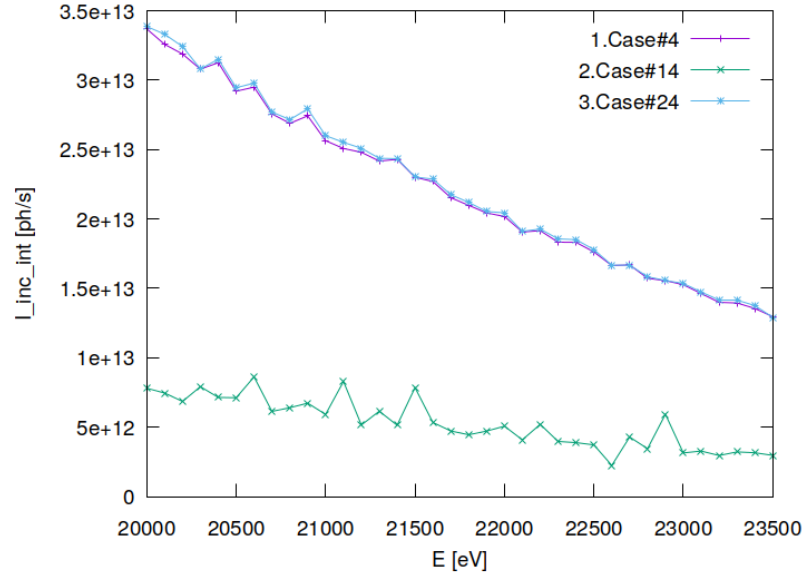


Figure 12.10: Incident photon flux on surface of optical element #04 (CM2).

```
"fig/BS_choice_Si111/plot011.png" Lbl.:BS_choice_Si111_2d_plot_x_cen_inc_footstat_oe04
```

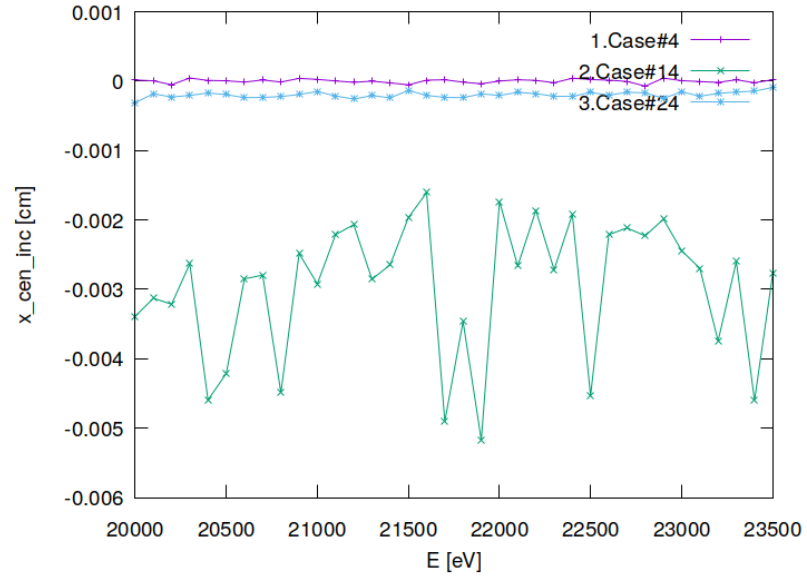


Figure 12.11: Sagittal coordinate of footprint's centre of 'gravity' on surface of optical element #04 (CM2).

```
"fig/BS_choice_Si111/plot012.png" Lbl.:BS_choice_Si111_2d_plot_y_cen_inc_footstat_oe04
```

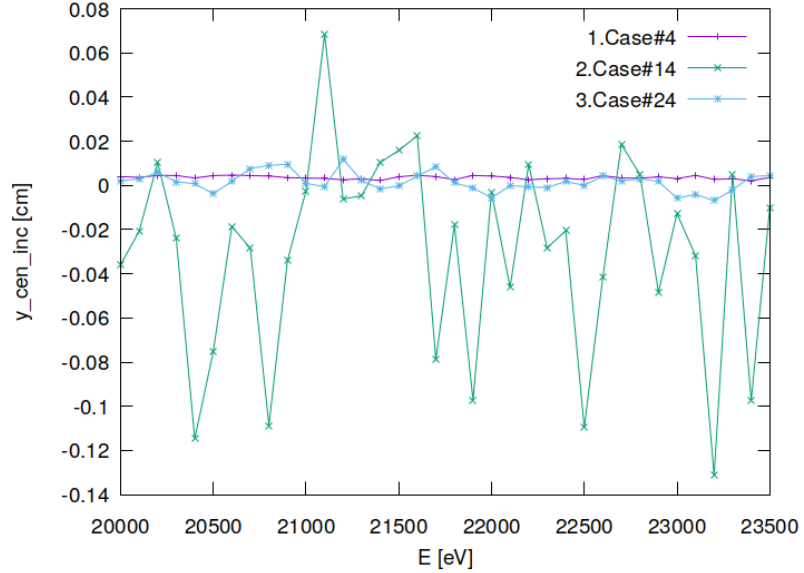


Figure 12.12: Meridional coordinate of footprint's centre of 'gravity' on surface of optical element #04 (CM2).

## 12.7 Statistics of photon irradiance in beam cross section

```
"fig/BS_choice_Si111/plot013.png" Lbl.:BS_choice_Si111_2d_plot_dx_fwhm_focstatavg_oe04
```

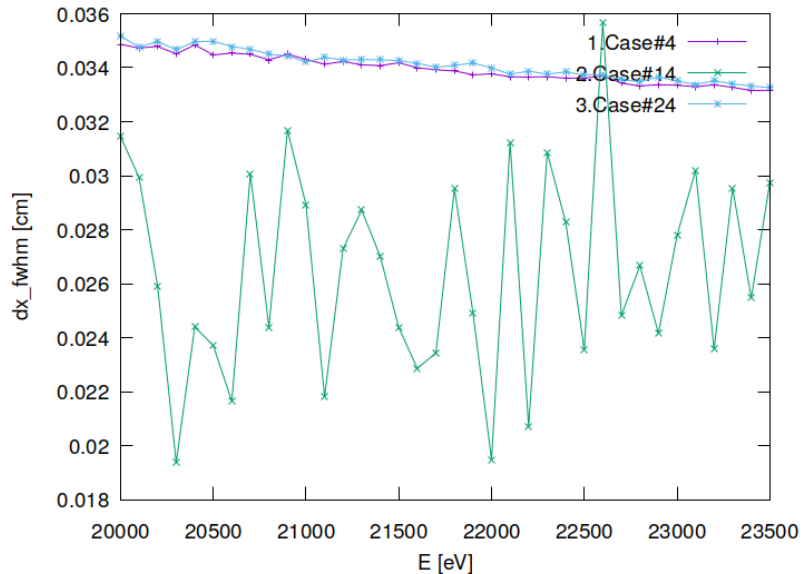


Figure 12.13: Sagittal beam diameter (FWHM) of optical element #04 (CM2).

```
"fig/BS_choice_Si111/plot014.png" Lbl.:BS_choice_Si111_2d_plot_dz_fwhm_focstatavg_oe04
```

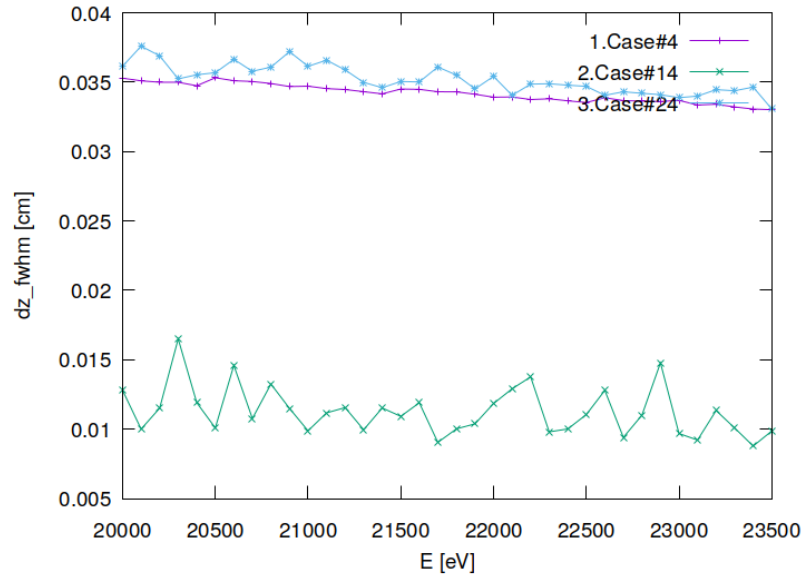


Figure 12.14: Meridional beam diameter (FWHM) of optical element #04 (CM2).

```
"fig/BS_choice_Si111/plot015.png" Lbl.:BS_choice_Si111_2d_plot_I_int_focstatavg_oe04
```

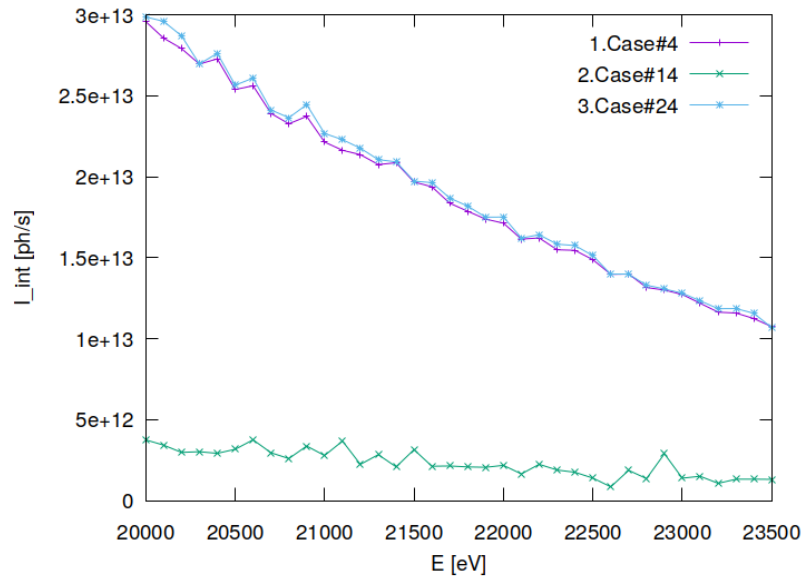


Figure 12.15: Photon flux in beam cross section of optical element #04 (CM2).

"fig/BS\_choice\_Si111/plot016.png" Lbl.:BS\_choice\_Si111\_2d\_plot\_x\_cen\_focstatavg\_oe04

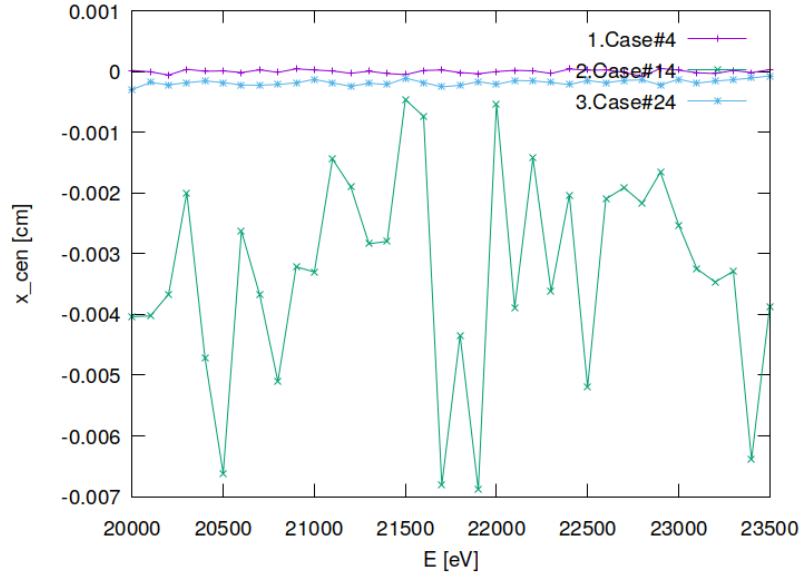


Figure 12.16: Sagittal coordinate of beam's centre of 'gravity' in beam cross section of optical element #04 (CM2).

"fig/BS\_choice\_Si111/plot017.png" Lbl.:BS\_choice\_Si111\_2d\_plot\_z\_cen\_focstatavg\_oe04

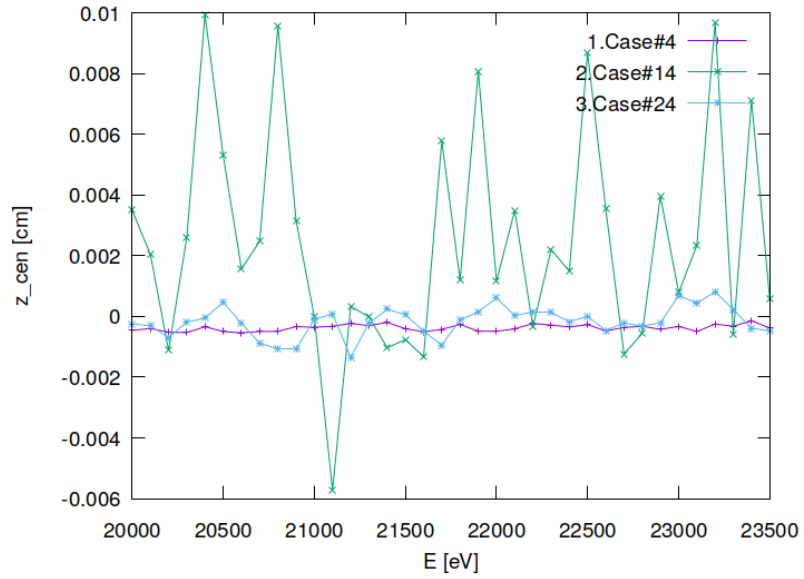


Figure 12.17: Meridional coordinate of beam's centre of 'gravity' in beam cross section of optical element #04 (CM2).

```
"fig/BS_choice_Si111/plot018.png" Lbl.:BS_choice_Si111_2d_plot_dxp_fwhm_focstatavg_oe04
```

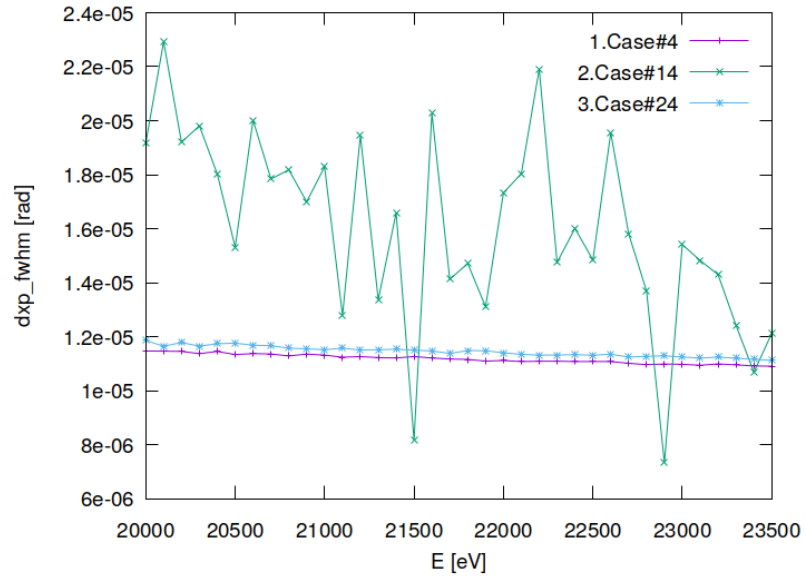


Figure 12.18: Sagittal beam divergence (FWHM) of optical element #04 (CM2).

```
"fig/BS_choice_Si111/plot019.png" Lbl.:BS_choice_Si111_2d_plot_dzp_fwhm_focstatavg_oe04
```

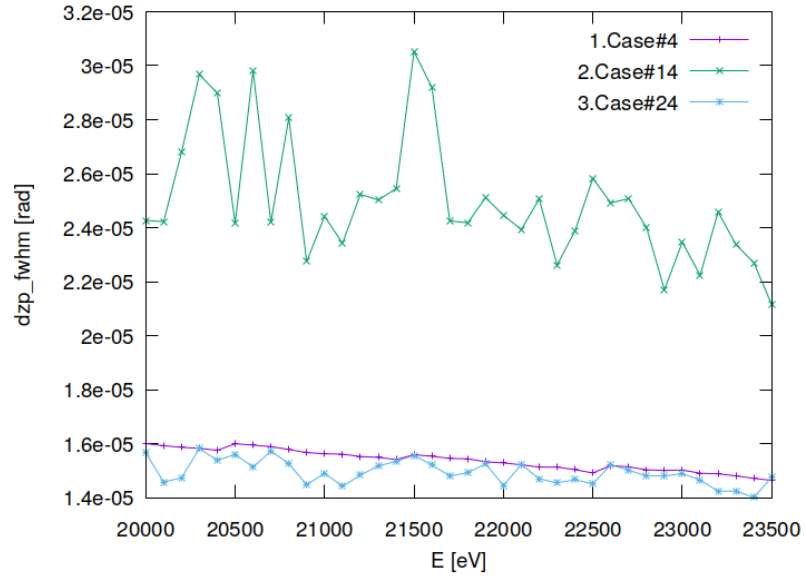


Figure 12.19: Meridional beam divergence (FWHM) of optical element #04 (CM2).

```
"fig/BS_choice_Si111/plot020.png" Lbl.:BS_choice_Si111_2d_plot_I_int_focstatavg_oe04
```

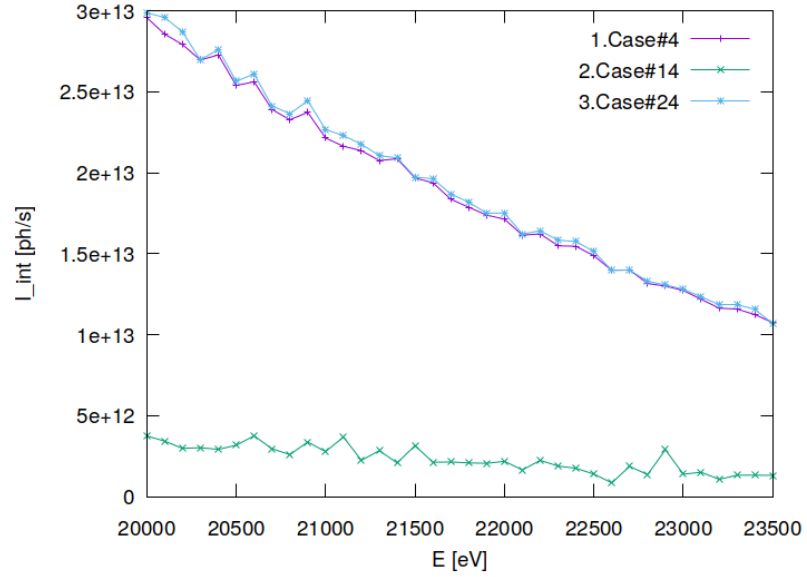


Figure 12.20: Photon flux in beam cross section of optical element #04 (CM2).

```
"fig/BS_choice_Si111/plot021.png" Lbl.:BS_choice_Si111_2d_plot_xp_cen_focstatavg_oe04
```

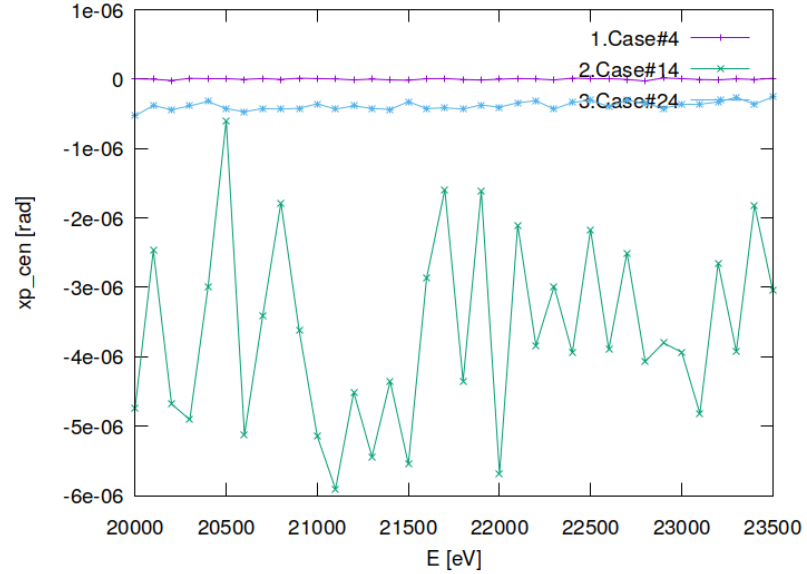


Figure 12.21: Sagittal coordinate of beam's centre of 'gravity' in angle space of optical element #04 (CM2).

```
"fig/BS_choice_Si111/plot022.png" Lbl.:BS_choice_Si111_2d_plot_zp_cen_focstatavg_oe04
```

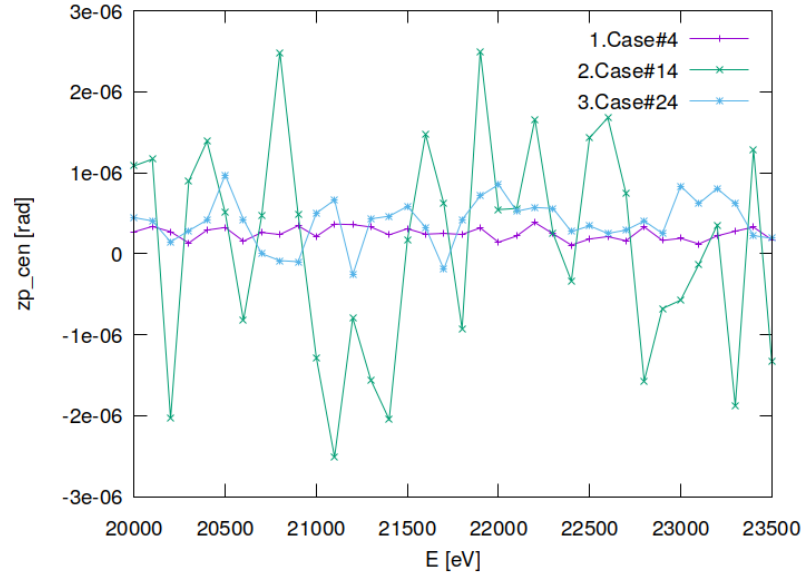


Figure 12.22: Meridional coordinate of beam's centre of 'gravity' in angle space of optical element #04 (CM2).

```
"fig/BS_choice_Si111/plot023.png" Lbl.:BS_choice_Si111_2d_plot_dE_fwhm_focstatavg_oe04
```

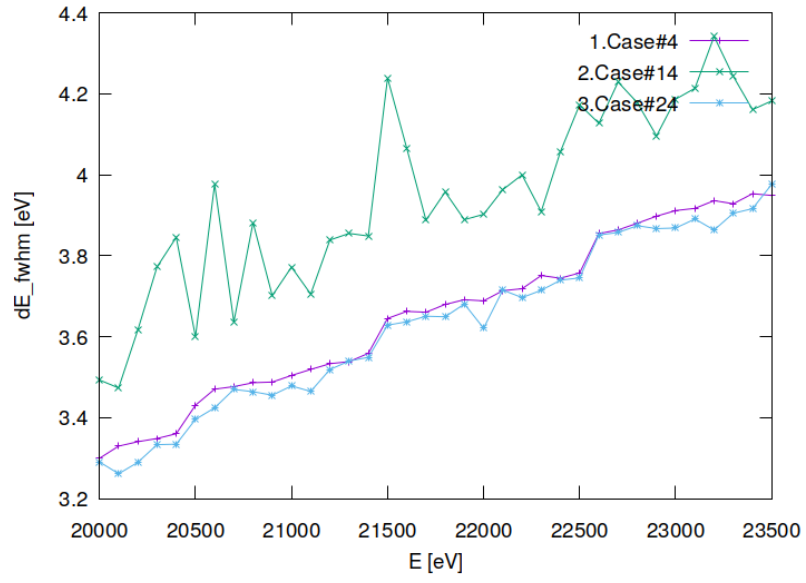


Figure 12.23: Bandwidth (FWHM) in beam cross section of optical element #04 (CM2).

## 12.8 Absorbed irradiance on surface

"fig/BS\_choice\_Si111/plot024.png" Lbl.:BS\_choice\_Si111\_false\_colour\_plot\_p\_abs\_foot\_oe03\_c14\_21800eV

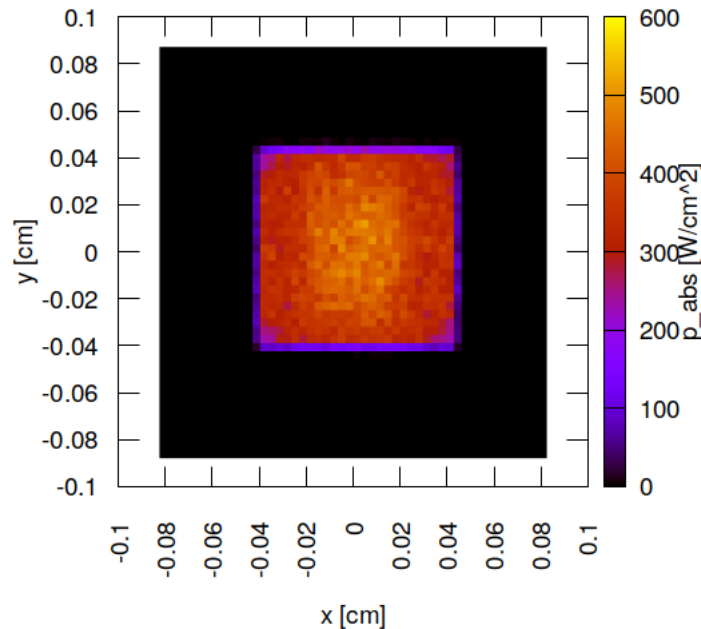


Figure 12.24: Absorbed irradiance on surface of optical element #03 (BS) for case #14 for 21800 eV photon energy setting.

"fig/BS\_choice\_Si111/plot025.png" Lbl.:BS\_choice\_Si111\_false\_colour\_plot\_p\_abs\_foot\_oe03\_c24\_21800eV

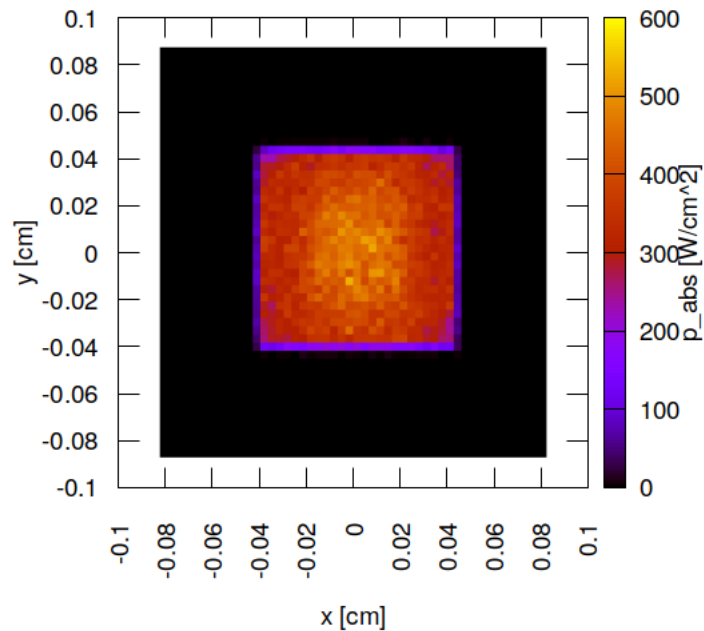


Figure 12.25: Absorbed irradiance on surface of optical element #03 (BS) for case #24 for 21800 eV photon energy setting.

## 12.9 Incident spectral flux on surface

"fig/BS\_choice\_Si111/plot026.png" Lbl.:BS\_choice\_Si111\_2d\_plot\_P\_spec\_spec\_oe03\_c14\_21800eV

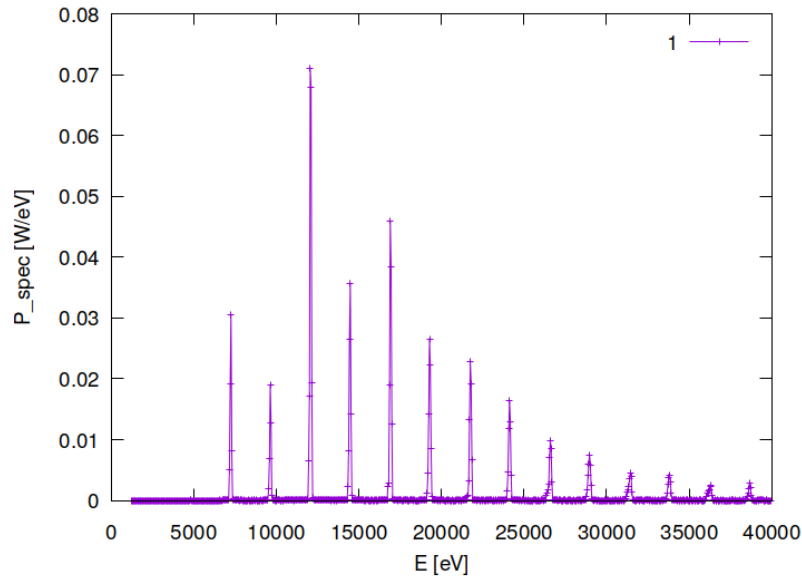


Figure 12.26: Incident spectral flux on surface of optical element #03 (BS) for case #14 for 21800 eV photon energy setting.

"fig/BS\_choice\_Si111/plot027.png" Lbl.:BS\_choice\_Si111\_2d\_plot\_P\_spec\_spec\_oe03\_c24\_21800eV

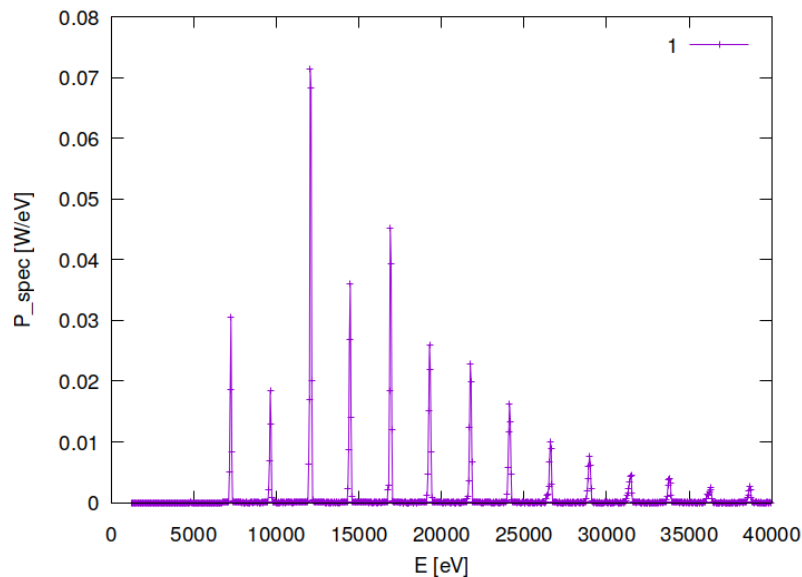


Figure 12.27: Incident spectral flux on surface of optical element #03 (BS) for case #24 for 21800 eV photon energy setting.

## 12.10 Temperature on surface

"fig/BS\_choice\_Si111/plot028.png" Lbl.:BS\_choice\_Si111\_false\_colour\_plot\_T\_oe03\_c14\_21800eV

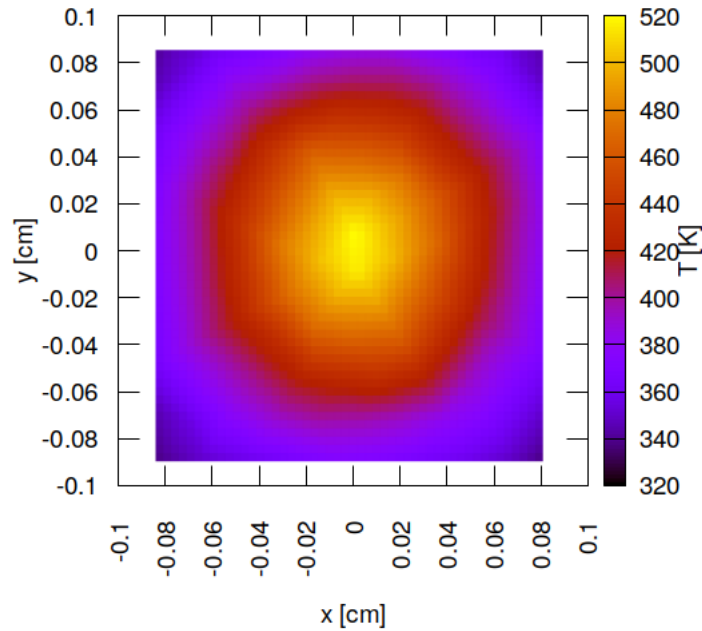


Figure 12.28: Temperature on surface of optical element #03 (BS) for case #14 for 21800 eV photon energy setting.

"fig/BS\_choice\_Si111/plot029.png" Lbl.:BS\_choice\_Si111\_false\_colour\_plot\_T\_oe03\_c24\_21800eV

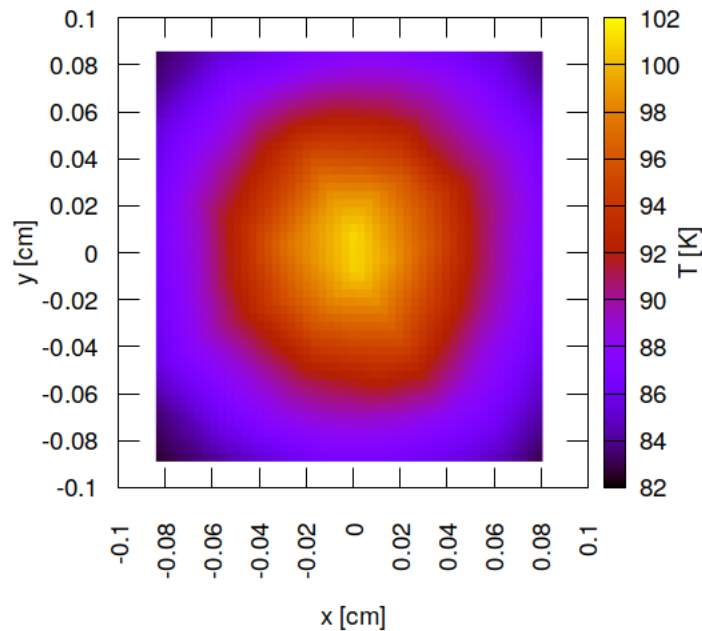


Figure 12.29: Temperature on surface of optical element #03 (BS) for case #24 for 21800 eV photon energy setting.

## 12.11 Mechanical stress (Von Mises stress) on surface

"fig/BS\_choice\_Si111/plot030.png" Lbl.:BS\_choice\_Si111\_false\_colour\_plot\_sigma\_oe03\_c14\_21800eV

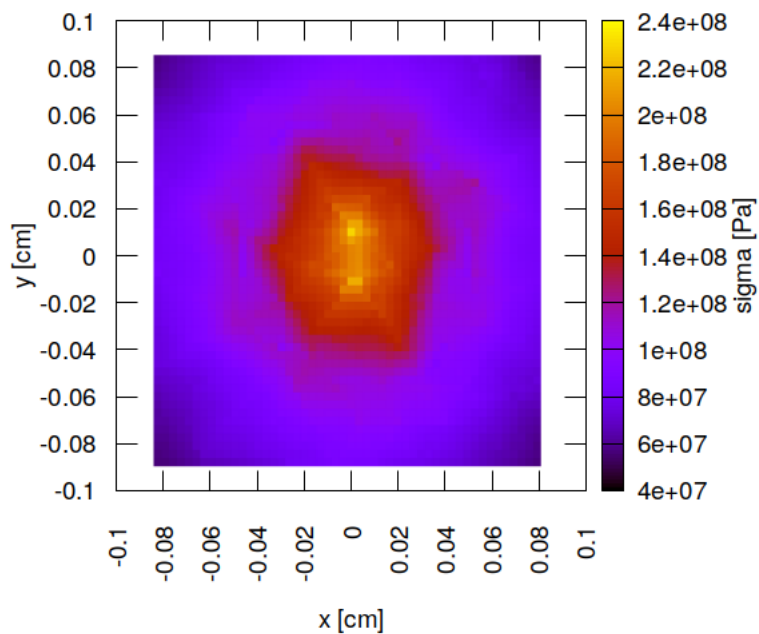


Figure 12.30: Mechanical stress (Von Mises stress) on surface of optical element #03 (BS) for case #14 for 21800 eV photon energy setting.

"fig/BS\_choice\_Si111/plot031.png" Lbl.:BS\_choice\_Si111\_false\_colour\_plot\_sigma\_oe03\_c24\_21800eV

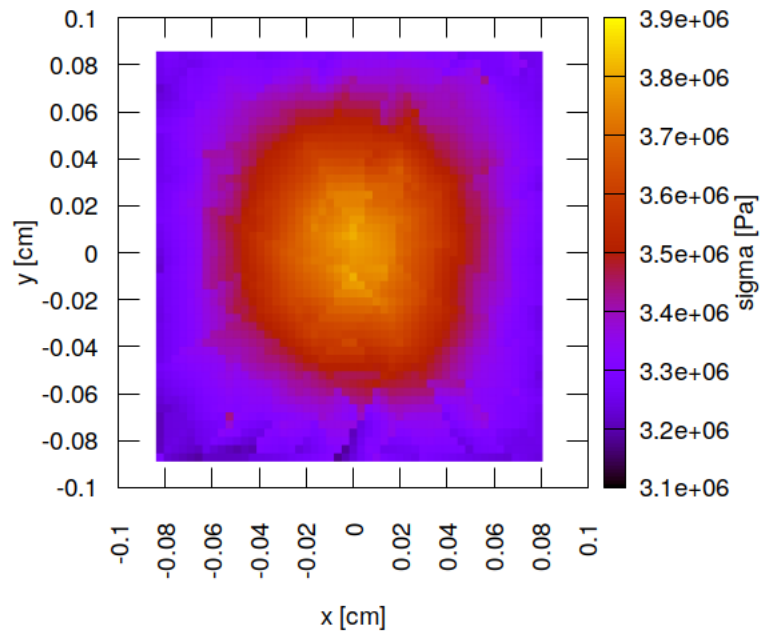


Figure 12.31: Mechanical stress (Von Mises stress) on surface of optical element #03 (BS) for case #24 for 21800 eV photon energy setting.

## 12.12 Surface slope error in meridional direction (y)

"fig/BS\_choice\_Si111/plot032.png" Lbl.:BS\_choice\_Si111\_false\_colour\_plot\_phi\_y\_oe03\_c14\_21800eV

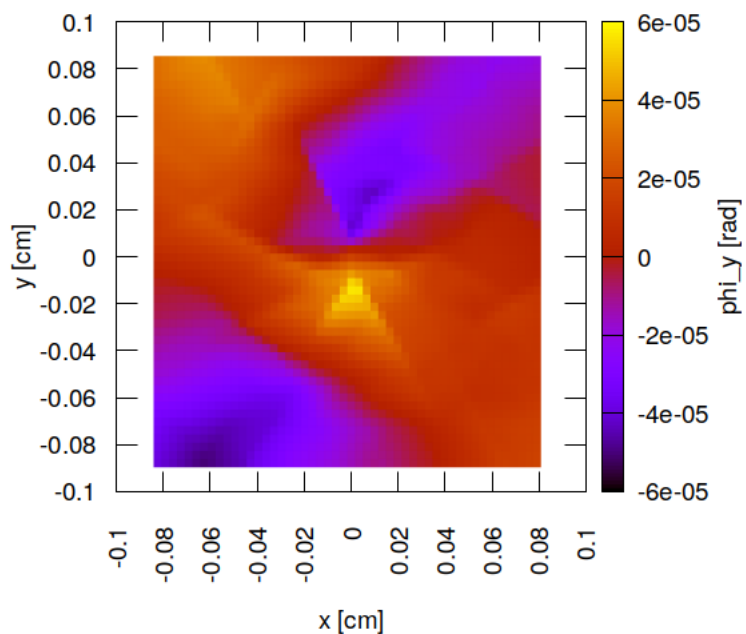


Figure 12.32: Surface slope error in meridional direction (y) of optical element #03 (BS) for case #14 for 21800 eV photon energy setting.

"fig/BS\_choice\_Si111/plot033.png" Lbl.:BS\_choice\_Si111\_false\_colour\_plot\_phi\_y\_oe03\_c24\_21800eV

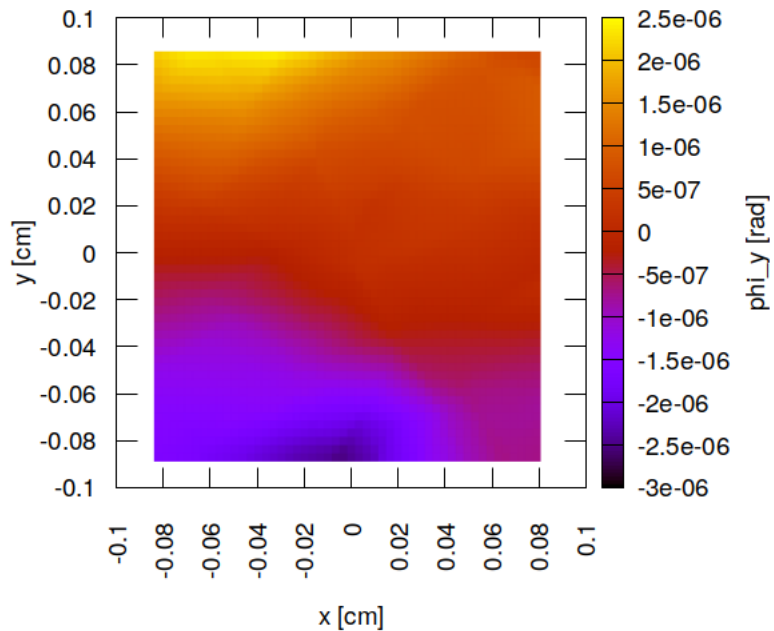


Figure 12.33: Surface slope error in meridional direction (y) of optical element #03 (BS) for case #24 for 21800 eV photon energy setting.



## 12.13 Incident photon irradiance on surface

"fig/BS\_choice\_Si111/plot034.png" Lbl.:BS\_choice\_Si111\_false\_colour\_plot\_I\_inc\_foot\_oe04\_c4\_21800eV

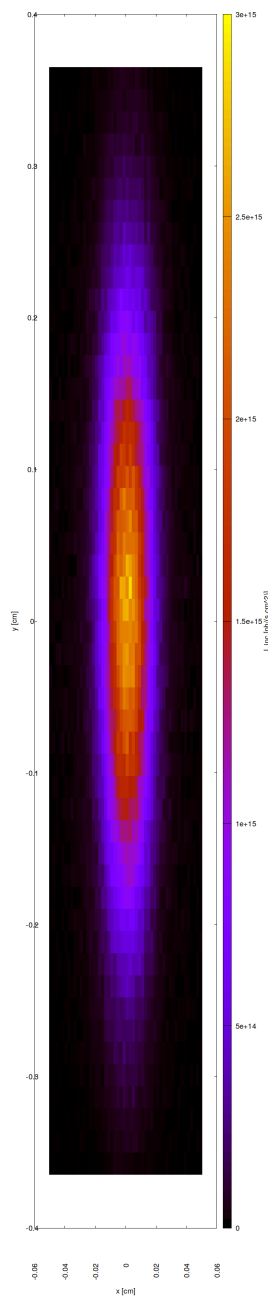


Figure 12.34: Incident photon irradiance on surface of optical element #04 (CM2) for case #4 for 21800 eV photon energy setting.

```
"fig/BS_choice_Si111/plot035.png" Lbl.:BS_choice_Si111_false_colour_plot_I_inc_foot_oe04_c14_21800eV
```

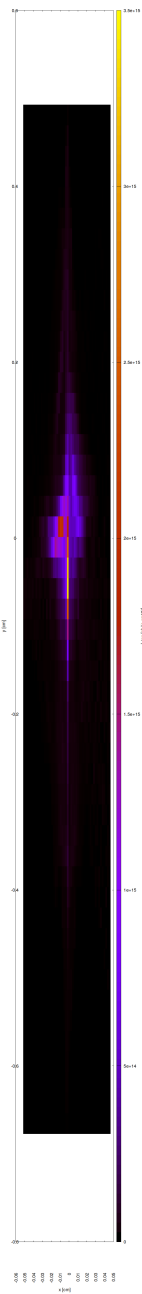


Figure 12.35: Incident photon irradiance on surface of optical element #04 (CM2) for case #14 for 21800 eV photon energy setting.

```
"fig/BS_choice_Si111/plot036.png" Lbl.:BS_choice_Si111_false_colour_plot_I_inc_foot_oe04_c24_21800eV
```

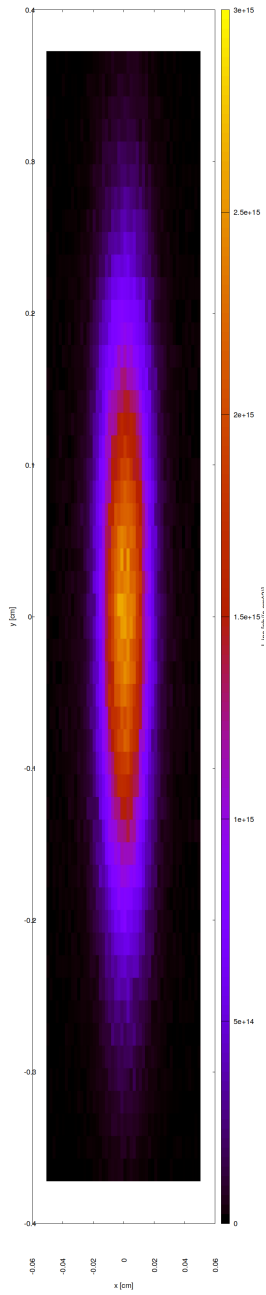


Figure 12.36: Incident photon irradiance on surface of optical element #04 (CM2) for case #24 for 21800 eV photon energy setting.

## 12.14 Photon irradiance in beam cross section

"fig/BS\_choice\_Si111/plot037.png" Lbl.:BS\_choice\_Si111\_false\_colour\_plot\_I\_foc\_oe04\_c4\_21800eV

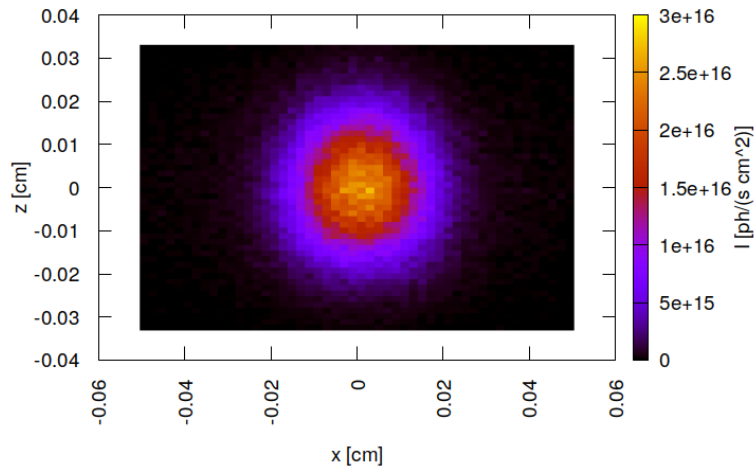


Figure 12.37: Photon irradiance in beam cross section of optical element #04 (CM2) for case #4 for 21800 eV photon energy setting.

"fig/BS\_choice\_Si111/plot038.png" Lbl.:BS\_choice\_Si111\_false\_colour\_plot\_I\_foc\_oe04\_c14\_21800eV

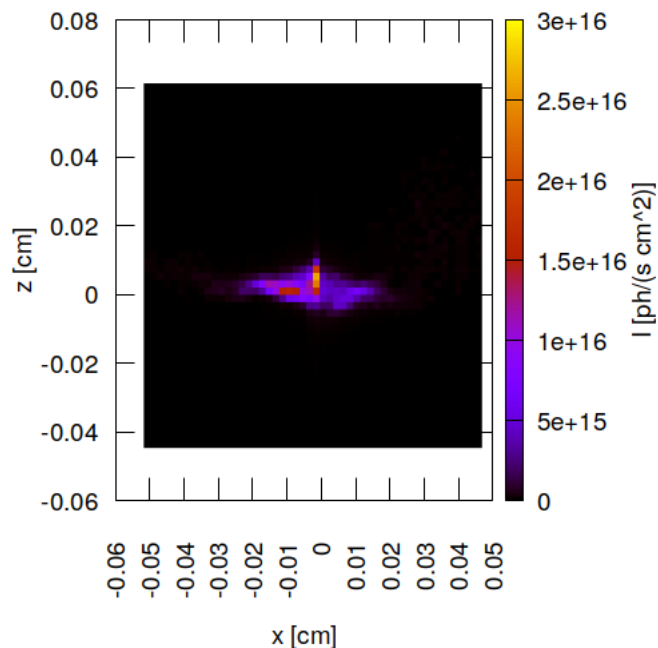


Figure 12.38: Photon irradiance in beam cross section of optical element #04 (CM2) for case #14 for 21800 eV photon energy setting.

"fig/BS\_choice\_Si111/plot039.png" Lbl.:BS\_choice\_Si111\_false\_colour\_plot\_I\_foc\_oe04\_c24\_21800eV

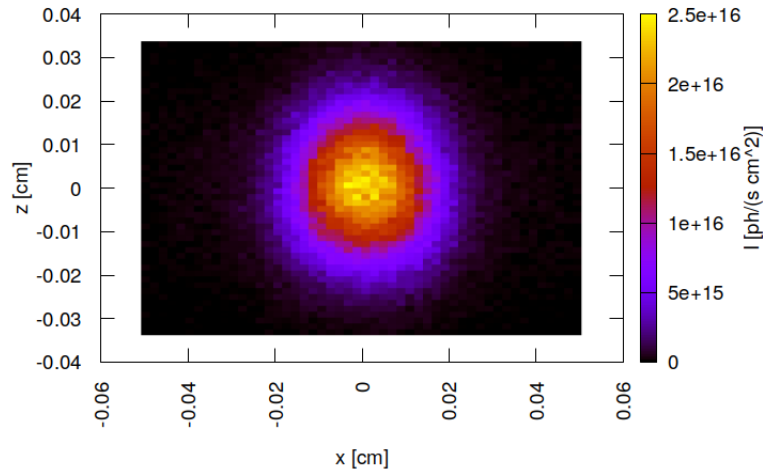


Figure 12.39: Photon irradiance in beam cross section of optical element #04 (CM2) for case #24 for 21800 eV photon energy setting.

## 12.15 Spectral photon flux in beam cross section

"fig/BS\_choice\_Si111/plot040.png" Lbl.:BS\_choice\_Si111\_2d\_plot\_I\_bandfoc\_oe04\_c4\_21800eV

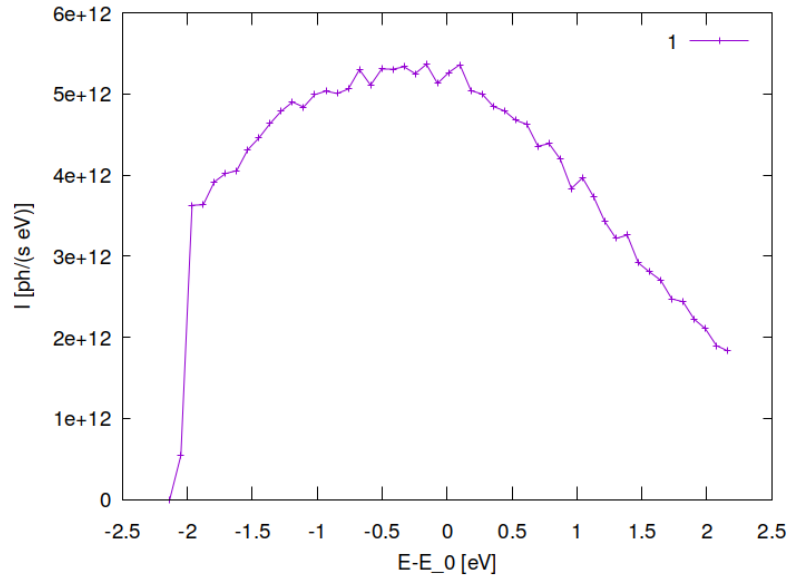


Figure 12.40: Spectral photon flux in beam cross section of optical element #04 (CM2) for case #4 for 21800 eV photon energy setting.

```
"fig/BS_choice_Si111/plot041.png" Lbl.:BS_choice_Si111_2d_plot_I_bandfoc_oe04_c14_21800eV
```

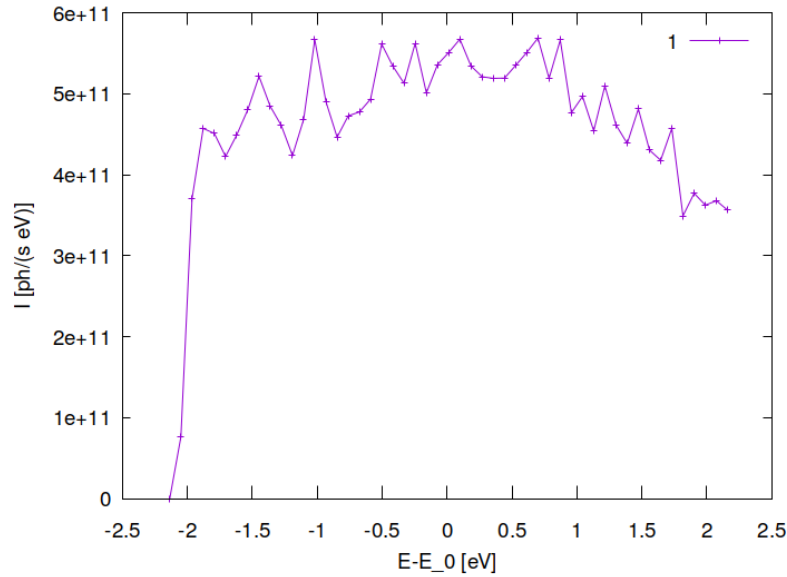


Figure 12.41: Spectral photon flux in beam cross section of optical element #04 (CM2) for case #14 for 21800 eV photon energy setting.

```
"fig/BS_choice_Si111/plot042.png" Lbl.:BS_choice_Si111_2d_plot_I_bandfoc_oe04_c24_21800eV
```

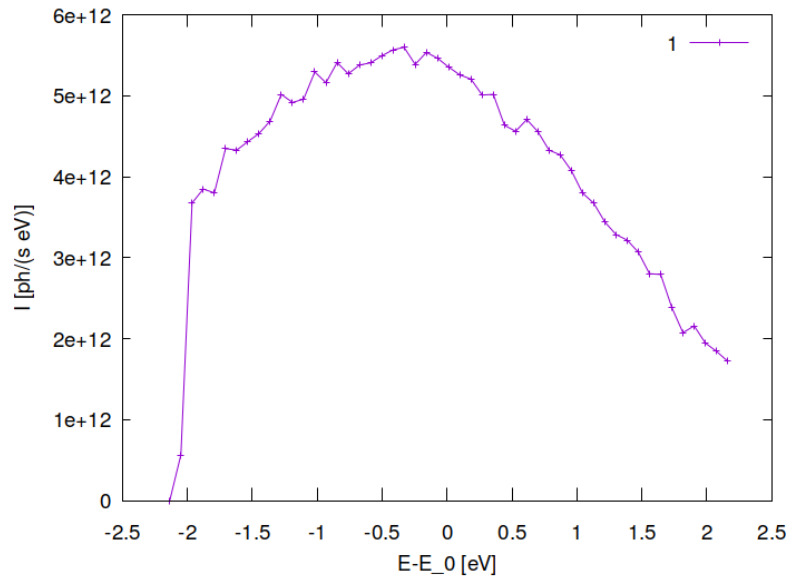


Figure 12.42: Spectral photon flux in beam cross section of optical element #04 (CM2) for case #24 for 21800 eV photon energy setting.

## Chapter 13

# Setup with diamond 111 beam splitter in Laue geometry

A thin CVD diamond crystal is employed as a diffractive beam splitter, using the 111 reflection in Laue geometry. Consisting of low-Z element carbon, diamond exhibits generally low absorption. Above that, diamond provides the highest thermal conductivity of all natural materials and therefore is likely to withstand the heat load from absorption. Such a diamond beamsplitter has shown its practicality for example at the macromolecular crystallography (MMC) beamline ID-14 in Grenoble (ESRF) [20] and at the MMC beamline Cassiopeia [8] at the now defunct MAX-lab.

The C111 reflection diverts radiation within a narrow bandwidth of

$$\delta E/E = \delta\theta/\tan\theta$$

to the SinCrys side branch. The thickness of the crystal slab has to be optimised in order to maximise diffraction efficiency under the constraint of keeping absorption of the transmitted main beam low. A natural choice is a maximum of the pendel-solution, i.e. the reflectivity oscillating with crystal thickness as predicted by the theory of dynamic diffraction from nearly perfect crystals.

Subsequent reflection from a second crystal with equal inter-planar spacing and diffracting planes parallel to the first is the golden standard in crystal monochromator design, which is followed here. This has the advantage to return the twice diffracted beam parallel to the direction of the incident, with an adjustable offset, such that downstream optical components and the sample do not have to follow the Bragg angle changes with selected photon energy.

Germanium 220 has an inter-planar spacing very close to that of diamond 111. It differs by only 3%. As germanium is cheaper, readily available in better quality and actually more efficient than diamond for the reflections in question (larger structure factor), Ge220 in Bragg geometry is chosen for the second crystal. Putting the second crystal at a distance of around 3.66 metres behind the first provides the required offset of more than one metre between the twice deflected beam and the main beam.

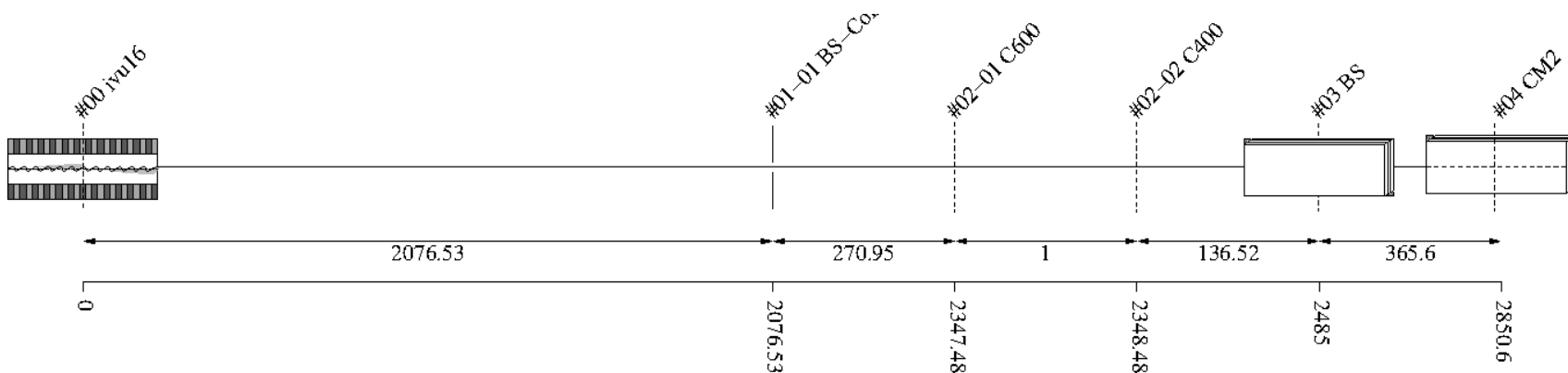


Figure 13.1: Schematic of optical setup

#	Name	Pathlen. cm	Descript.	Shape	Pitch* deg	Roll deg	Yaw deg	x_min cm	x_max cm	y_min cm	y_max cm	Thick. cm	Surface
0	ivu16	0	undulator	auto	0	0	0	-0.0027	0.0027	-0.0002	0.0002	0.0002	auto
1		2076.53	none	plane	0	0	0	-inf	inf	-inf	inf		perfect
1-1	BS-Collim	2076.53	aperture	rectangle	0	0	0	-0.035	0.035	-0.035	0.035	0.035	
2	Filter	2347.48	none	plane	0	0	0	-inf	inf	-inf	inf		perfect
2-1	C600	2347.48	C-filter	rectangle	0	0	0	-inf	inf	-inf	inf	0.06	
2-2	C400	2348.48	C-filter	rectangle	0	0	0	-inf	inf	-inf	inf	0.04	
3	BS	2485	C(1,1,1)-crystal	plane	133.197	90	0	-0.15	0.15	-0.15	0.15		heat bump
4	CM2	2850.6	Ge(2,2,0)-crystal	plane	8.17292	180	0	-inf	inf	-inf	inf		perfect

Table 13.1: Setup parameters common to all components. (\*Glancing angle for mirrors, multilayers and crystals. Angle to surface normal otherwise.)

**Rays:** Polar type = total

Polar phase = 0 deg

Polar degree = 0

Is coherent = no

**Spectrum:** E min = 500 eV

E max = 40000 eV

Relative linewidth = 1

**Band:** Bandwidth = 0.0005

**Insertion Device:** lambda period = 1.6 cm

n period = 187

I electron = 0.5 A

E electron = 3 GeV

y horizontal waist = 0 cm

y vertical waist = 0 cm

epsilon x = 3.2E-08 cm rad

epsilon z = 8E-10 cm rad

K y = 1.66

K ymax = 1.7

Divergence limit = 5E-05 rad

**Undulator:** n harmonic max = 99

Tuning type = fixed gap

l aperture = 2076.53 cm

dx aperture = 0.07 cm

dz aperture = 0.07 cm

#1

**Screen:** Is absorbing[1] = no

**Shape:** Thickness = 0 cm

#2 Filter

**Screen:** Is absorbing[1] = yes

Is absorbing[2] = yes

Molecular formula[1] = C

Molecular formula[2] = C

Mass density[1] = 3.5 g/cm^3

Mass density[2] = 3.5 g/cm^3

Thickness[1] = 0.06 cm

Thickness[2] = 0.04 cm

**Shape:** Thickness = 0 cm

### #3 BS

**Grating:** n order = -1

**Crystal:** Structure type = zincblende

Lattice constant[1] = 3.567 Angstrom

Lattice constant[2] = 3.567 Angstrom

Lattice constant[3] = 3.567 Angstrom

Debye Waller factor = 1

Is absorbing = yes

Is asymmetric = yes

Angle asymmetry = 125.26 deg

Is inclined = no

Is Johansson geometry = no

Is mosaic = no

**Tune:** z rotation axis = 0 cm

**Geometry:** Is thin = yes

Tune automatic = yes

**Shape:** Thickness = 0.01 cm

**Boundary:** Type = rectangle

x rim = 0.5 cm

y rim = 0.5 cm

**Surface:** Is rough = no

**FEA:** Design type = type specific

Crystal design = laue with cooling loop

Is isotropic = no

Angle x = 45 deg

Angle y = 35.2644 deg

Angle z = 0 deg

Mass density = 3.516 g/cm<sup>3</sup>

**Heat:** Heat transfer type[1] = insulated

Heat transfer type[2] = heat transfer

Heat transfer type[3] = insulated

Heat transfer type[4] = insulated

Heat transfer type[5] = heat transfer

Heat transfer type[6] = flux

Heat transfer type[7] = insulated

Heat transfer type[8] = heat transfer

Heat transfer type[9] = heat sink

Heat transfer coefficient = 1 W/(cm<sup>2</sup>K)

Heat sink coefficient = 10 W/(cm<sup>2</sup>K)

T reference = 293.15 K  
T cooling = 293.15 K  
Heat capacity = 0.54 J/(gK)  
Thermal conductivity[1] = 25 W/(cmK^n)

**Stress and strain:** Constraint[1] = free  
Constraint[2] = kinematic  
Constraint[3] = free  
Constraint[4] = free  
Constraint[5] = free  
Constraint[6] = free  
Constraint[7] = free  
Constraint[8] = free  
Constraint[9] = free  
Thermal expansion tensor[1] = 1.1E-06 1/K  
Thermal expansion tensor[2] = 1.1E-06 1/K  
Thermal expansion tensor[3] = 1.1E-06 1/K  
Thermal expansion tensor[4] = 0 1/K  
Thermal expansion tensor[5] = 0 1/K  
Thermal expansion tensor[6] = 0 1/K  
Stiffness tensor(1)(1) = 1.07861E+12 Pa  
Stiffness tensor(2)[1] = 1.2663E+11 Pa  
Stiffness tensor(2)[2] = 1.07861E+12 Pa  
Stiffness tensor(3)[1] = 1.2663E+11 Pa  
Stiffness tensor(3)[2] = 1.2663E+11 Pa  
Stiffness tensor(3)[3] = 1.07861E+12 Pa  
Stiffness tensor(4)[1] = 0 Pa  
Stiffness tensor(4)[2] = 0 Pa  
Stiffness tensor(4)[3] = 0 Pa  
Stiffness tensor(4)[4] = 5.7756E+11 Pa  
Stiffness tensor(5)[1] = 0 Pa  
Stiffness tensor(5)[2] = 0 Pa  
Stiffness tensor(5)[3] = 0 Pa  
Stiffness tensor(5)[4] = 0 Pa  
Stiffness tensor(5)[5] = 5.7756E+11 Pa  
Stiffness tensor(6)[1] = 0 Pa  
Stiffness tensor(6)[2] = 0 Pa  
Stiffness tensor(6)[3] = 0 Pa  
Stiffness tensor(6)[4] = 0 Pa  
Stiffness tensor(6)[5] = 0 Pa  
Stiffness tensor(6)[6] = 5.7756E+11 Pa

#### #4 CM2

**Crystal:** Structure type = zinblende  
Lattice constant[1] = 5.6578 Angstrom  
Lattice constant[2] = 5.6578 Angstrom  
Lattice constant[3] = 5.6578 Angstrom  
Debye Waller factor = 1  
Is absorbing = yes  
Is asymmetric = no  
Is inclined = no  
Is Johansson geometry = no

Is mosaic = no

**Tune:** Type = constant pathlength  
Are downstream elements fixed = no

**Geometry:** Is thin = no  
Tune automatic = yes

**Boundary:** Type = none

**Surface:** Is rough = no

## Chapter 14

# Finite element analysis (FEA)

A description of the FEA model can be found in section 4.

There are three different heat load settings in this model. The first is with both diamond filters – 400 and 600 microns thick – in the beam path. This is presently the standard setting at DanMAX which provides the lowest heat load on the beam splitter.

The second setting is with the 600 micron diamond filter moved out. This is in order to compensate for the extra absorption in the beam splitter, to keep flux in the DanMAX main branch the same.

Finally the third setting is with all diamond filter out, which represents the worst case scenario for the beam splitter in terms of heat load.

## 14.1 FEA with both 600 and 400 micron diamond filters in

"fig/BS\_choice\_C111\_Laue/fea\_plot\_geom\_c16\_21800eV\_03.png" Lbl.:BS\_choice\_C111\_Laue\_Surface\_plot\_fea\_plot\_geom\_c16\_21800eV\_03

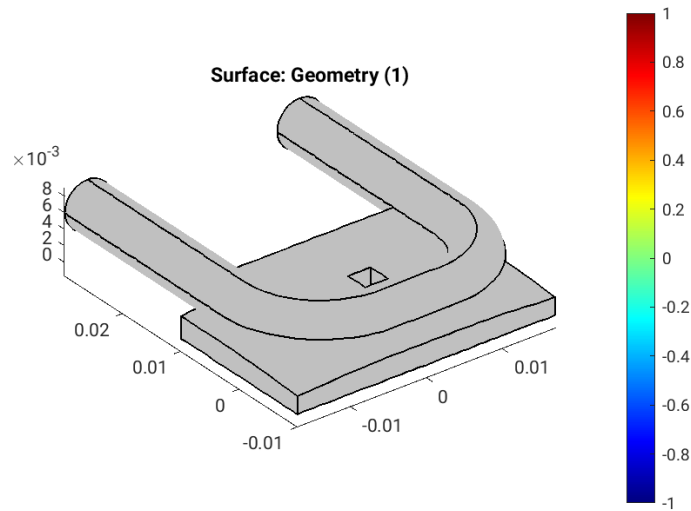


Figure 14.1: Geometry [m] of optical element #03, for case #16, at 21800 eV photon energy setting.

```
"fig/BS_choice_C111_Laue/fea_plot_cnstr_c16_21800eV_03.png" Lbl.:BS_choice_C111_Laue_Surface_plot_fea_plot_cnstr_c16_21800eV_03
```

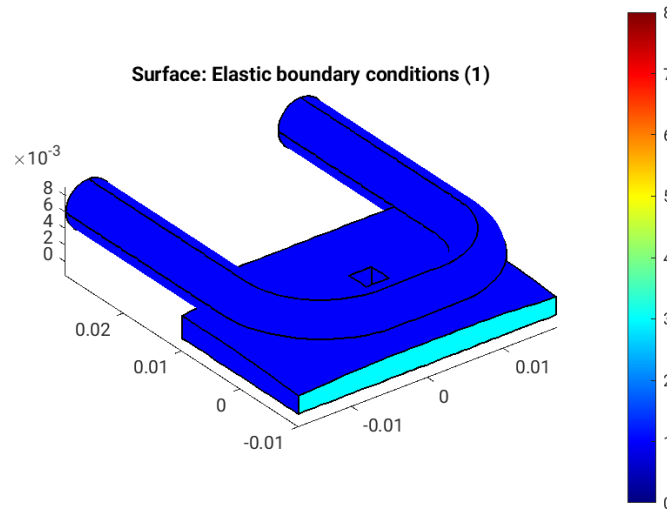


Figure 14.2: Elastic boundary conditions on the surfaces of optical element #03, for case #16, at 21800 eV photon energy setting. Color legend: Blue: Surface can move freely in all directions. Cyan: Tension free kinematic mounting. Minimalistic constraint for three points in surface. One point is fixed, the second can move in one direction, and the third in two, in a fashion that defines angular orientation without introducing stress if the surface expands.

```
"fig/BS_choice_C111_Laue/fea_plot_trans_c16_21800eV_03.png" Lbl.:BS_choice_C111_Laue_Surface_plot_fea_plot_trans_c16_21800eV_03
```

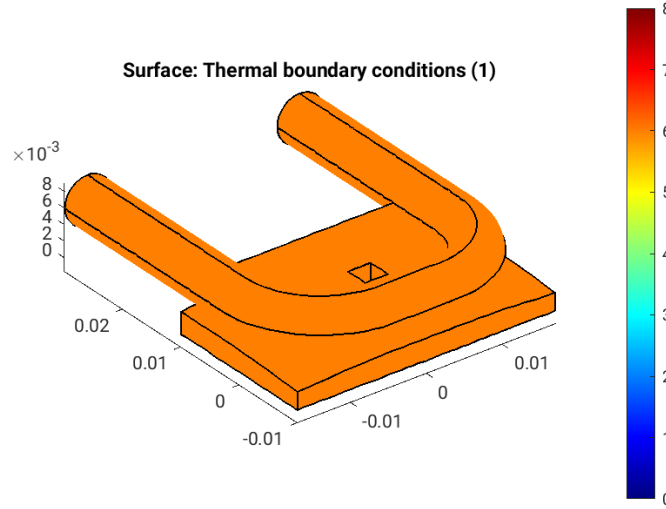


Figure 14.3: Thermal boundary conditions on the surfaces of optical element #03, for case #16, at 21800 eV photon energy setting. Color legend: Orange: No heat transfer at all. Blue: Heat transfer coefficient and temperature difference define heat current density,  $j_q = h(T - T_{cool})$ . Red: Forced heat flux from e.g. absorbed X-rays. Cyan: Heat transfer coefficient and temperature difference define heat current density,  $j_q = h^* \Delta T$  (only at inner surfaces).

```
"fig/BS_choice_C111_Laue/fea_plot_heattrans_c16_21800eV_03.png" Lbl.:BS_choice_C111_Laue_Surface_plot_fea_plot_heattrans_c16_21800eV_03
```

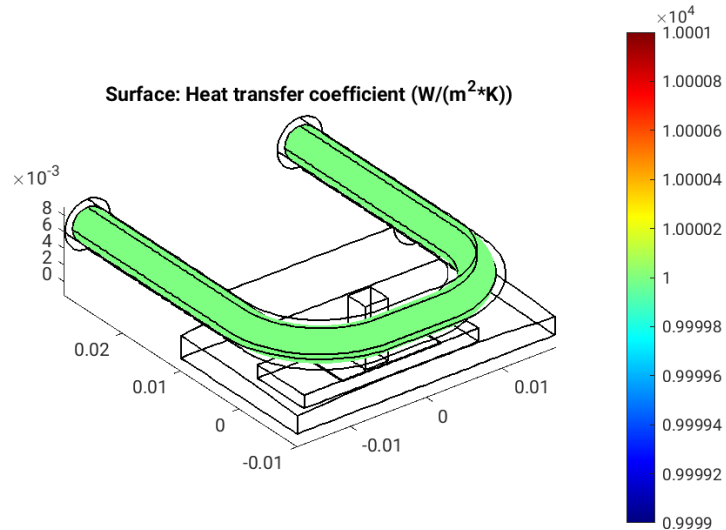


Figure 14.4: Heat transfer coefficient,  $h$  [W/(m<sup>2</sup> K)], on the surfaces of optical element #03, for case #16, at 21800 eV photon energy setting.

"fig/BS\_choice\_C111\_Laue/fea\_plot\_heatflux\_c16\_21800eV\_03.png" Lbl.:BS\_choice\_C111\_Laue\_Surface\_plot\_fea\_plot\_heatflux\_c16\_21800eV\_03

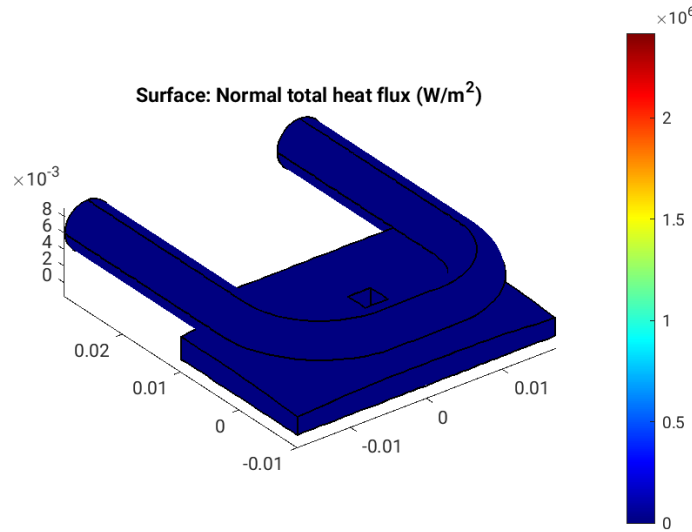


Figure 14.5: Absorbed irradiance,  $p_{\text{abs}}$  [W/m<sup>2</sup>], on the surfaces of optical element #03, for case #16, at 21800 eV photon energy setting.

"fig/BS\_choice\_C111\_Laue/fea\_plot\_temp\_c16\_21800eV\_03.png" Lbl.:BS\_choice\_C111\_Laue\_Surface\_plot\_fea\_plot\_temp\_c16\_21800eV\_03

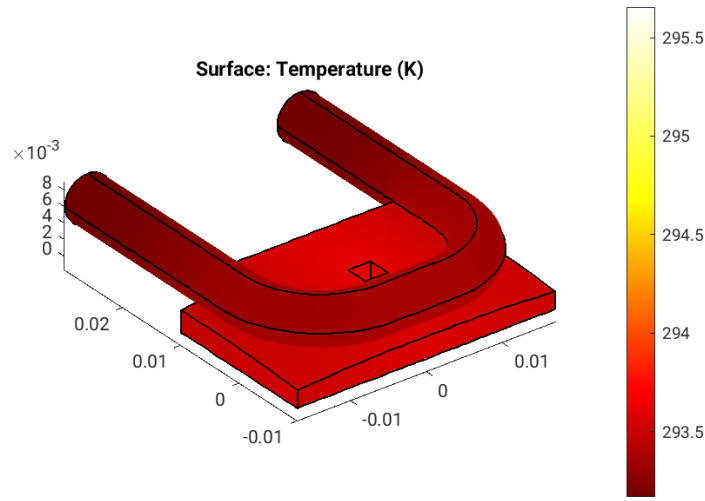


Figure 14.6: Temperature, T [K], on the surfaces of optical element #03, for case #16, at 21800 eV photon energy setting.

"fig/BS\_choice\_C111\_Laue/fea\_plot\_thermcond\_c16\_21800eV\_03.png" Lbl.:BS\_choice\_C111\_Laue\_Surface\_plot\_fea\_plot\_thermcond\_c16\_21800eV\_03

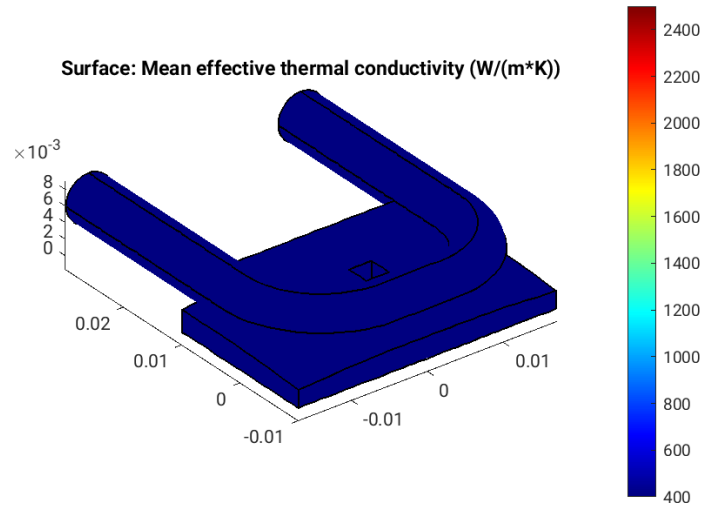


Figure 14.7: Thermal conductivity, lambda [W/(m K)], on the surfaces of optical element #03, for case #16, at 21800 eV photon energy setting.

"fig/BS\_choice\_C111\_Laue/fea\_plot\_stress\_c16\_21800eV\_03.png" Lbl.:BS\_choice\_C111\_Laue\_Surface\_plot\_fea\_plot\_stress\_c16\_21800eV\_03

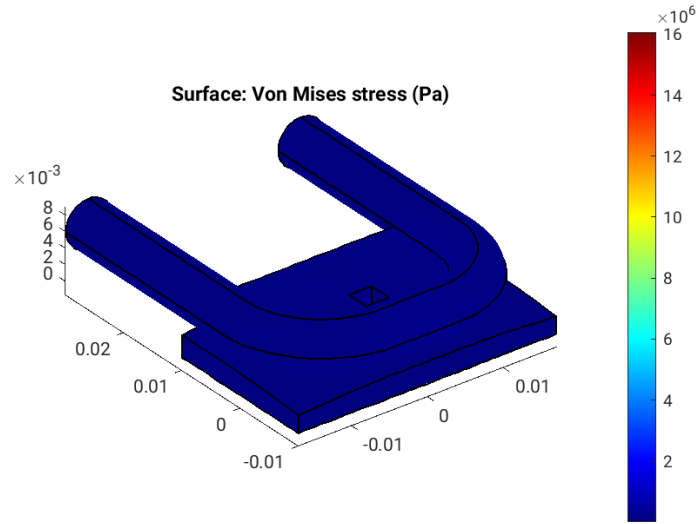


Figure 14.8: Von Mises stress, sigma [Pa], on the surfaces of optical element #03, for case #16, at 21800 eV photon energy setting.

```
"fig/BS_choice_C111_Laue/fea_plot_deform_c16_21800eV_03.png" Lbl.:BS_choice_C111_Laue_Surface_plot_fea_plot_deform_c16_21800eV_03
```

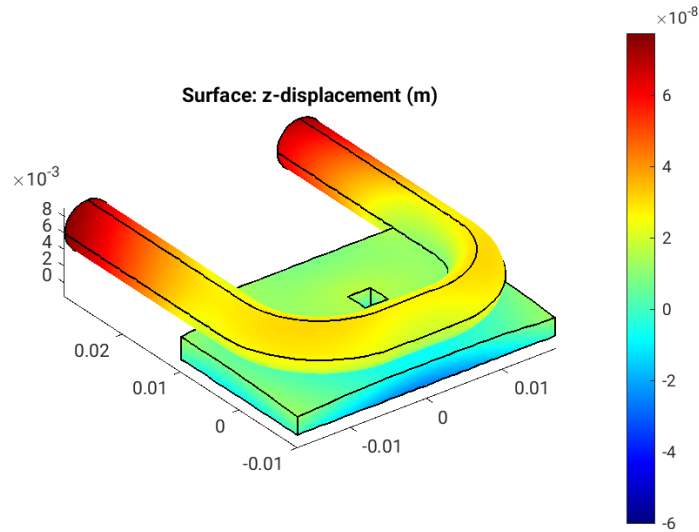


Figure 14.9: Thermoelastic deformation,  $dz$  [m], on the surfaces of optical element #03, for case #16, at 21800 eV photon energy setting.

## 14.2 FEA with only 400 micron diamond filter in

```
"fig/BS_choice_C111_Laue/fea_plot_geom_c26_21800eV_03.png" Lbl.:BS_choice_C111_Laue_Surface_plot_fea_plot_geom_c26_21800eV_03
```

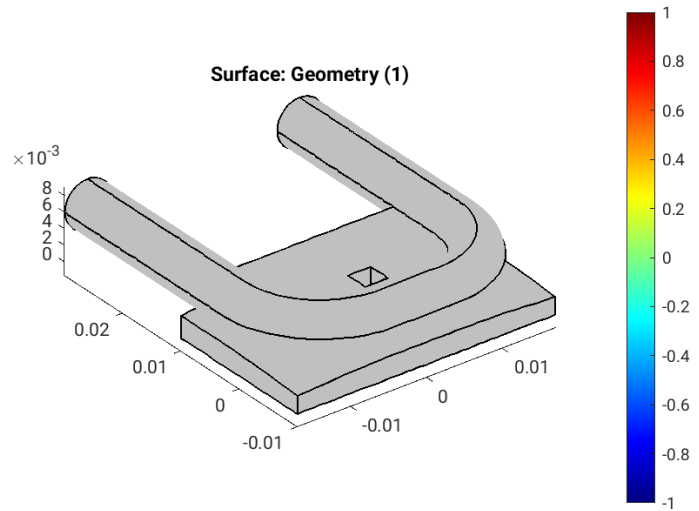


Figure 14.10: Geometry [m] of optical element #03, for case #26, at 21800 eV photon energy setting.

```
"fig/BS_choice_C111_Laue/fea_plot_cnstr_c26_21800eV_03.png" Lbl.:BS_choice_C111_Laue_Surface_plot_fea_plot_cnstr_c26_21800eV_03
```

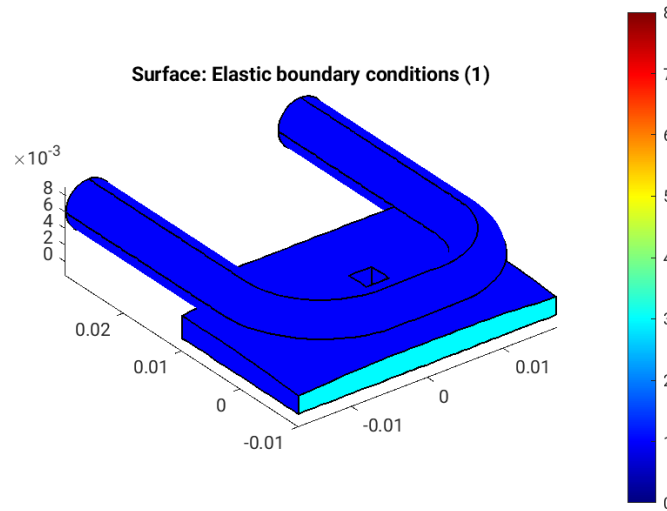


Figure 14.11: Elastic boundary conditions on the surfaces of optical element #03, for case #26, at 21800 eV photon energy setting. Color legend: Blue: Surface can move freely in all directions. Cyan: Tension free kinematic mounting. Minimalistic constraint for three points in surface. One point is fixed, the second can move in one direction, and the third in two, in a fashion that defines angular orientation without introducing stress if the surface expands.

```
"fig/BS_choice_C111_Laue/fea_plot_trans_c26_21800eV_03.png" Lbl.:BS_choice_C111_Laue_Surface_plot_fea_plot_trans_c26_21800eV_03
```

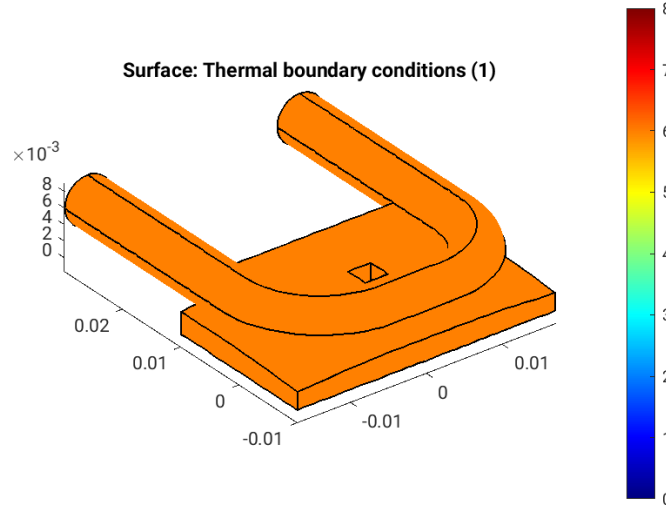


Figure 14.12: Thermal boundary conditions on the surfaces of optical element #03, for case #26, at 21800 eV photon energy setting. Color legend: Orange: No heat transfer at all. Blue: Heat transfer coefficient and temperature difference define heat current density,  $j_q = h(T - T_{cool})$ . Red: Forced heat flux from e.g. absorbed X-rays. Cyan: Heat transfer coefficient and temperature difference define heat current density,  $j_q = h^* \Delta T$  (only at inner surfaces).

```
"fig/BS_choice_C111_Laue/fea_plot_heattrans_c26_21800eV_03.png" Lbl.:BS_choice_C111_Laue_Surface_plot_fea_plot_heattrans_c26_21800eV_03
```

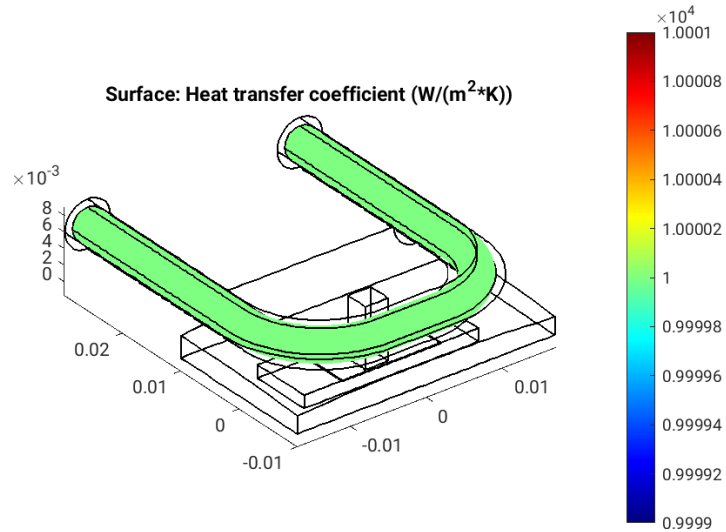


Figure 14.13: Heat transfer coefficient,  $h$  [W/(m<sup>2</sup> K)], on the surfaces of optical element #03, for case #26, at 21800 eV photon energy setting.

```
"fig/BS_choice_C111_Laue/fea_plot_heatflux_c26_21800eV_03.png" Lbl.:BS_choice_C111_Laue_Surface_plot_fea_plot_heatflux_c26_21800eV_03
```

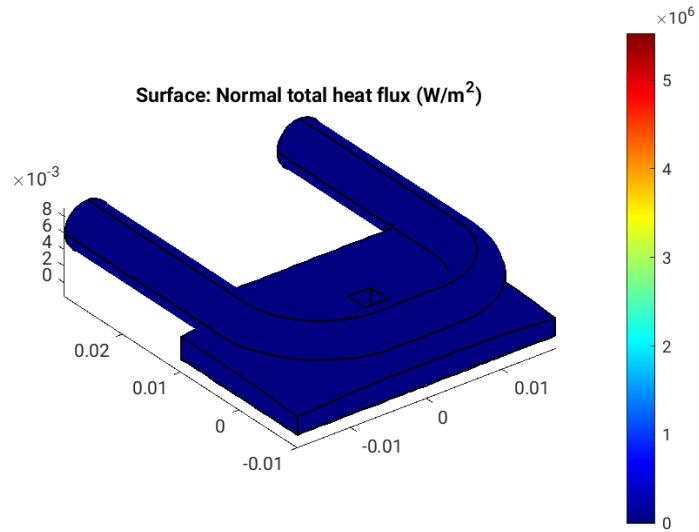


Figure 14.14: Absorbed irradiance,  $p_{\text{abs}}$  [W/m<sup>2</sup>], on the surfaces of optical element #03, for case #26, at 21800 eV photon energy setting.

```
"fig/BS_choice_C111_Laue/fea_plot_temp_c26_21800eV_03.png" Lbl.:BS_choice_C111_Laue_Surface_plot_fea_plot_temp_c26_21800eV_03
```

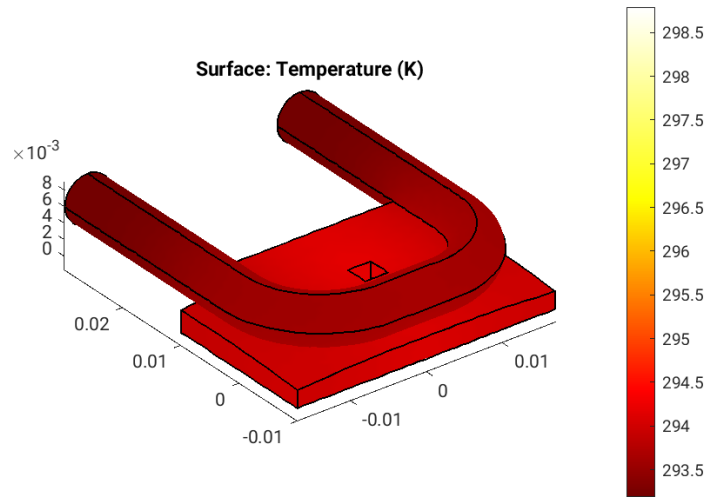


Figure 14.15: Temperature, T [K], on the surfaces of optical element #03, for case #26, at 21800 eV photon energy setting.

"fig/BS\_choice\_C111\_Laue/fea\_plot\_thermcond\_c26\_21800eV\_03.png" Lbl.:BS\_choice\_C111\_Laue\_Surface\_plot\_fea\_plot\_thermcond\_c26\_21800eV\_03

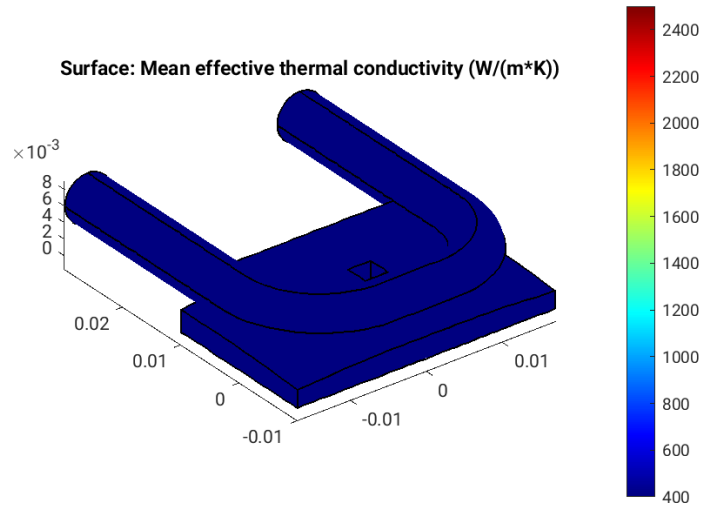


Figure 14.16: Thermal conductivity, lambda [W/(m K)], on the surfaces of optical element #03, for case #26, at 21800 eV photon energy setting.

"fig/BS\_choice\_C111\_Laue/fea\_plot\_stress\_c26\_21800eV\_03.png" Lbl.:BS\_choice\_C111\_Laue\_Surface\_plot\_fea\_plot\_stress\_c26\_21800eV\_03

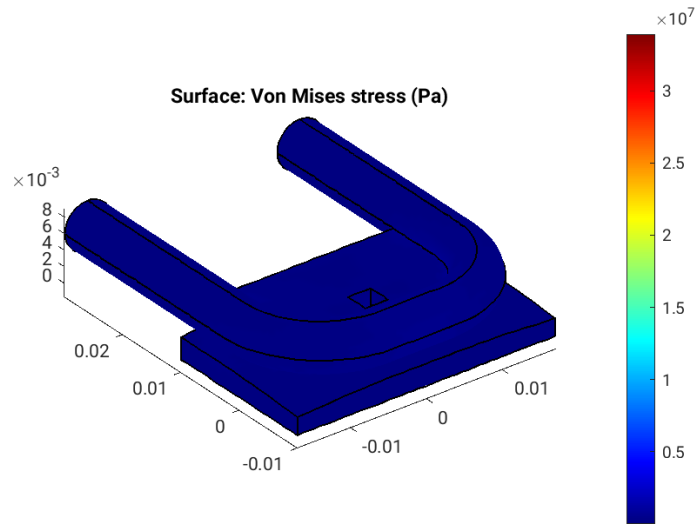


Figure 14.17: Von Mises stress, sigma [Pa], on the surfaces of optical element #03, for case #26, at 21800 eV photon energy setting.

```
"fig/BS_choice_C111_Laue/fea_plot_deform_c26_21800eV_03.png" Lbl.:BS_choice_C111_Laue_Surface_plot_fea_plot_deform_c26_21800eV_03
```

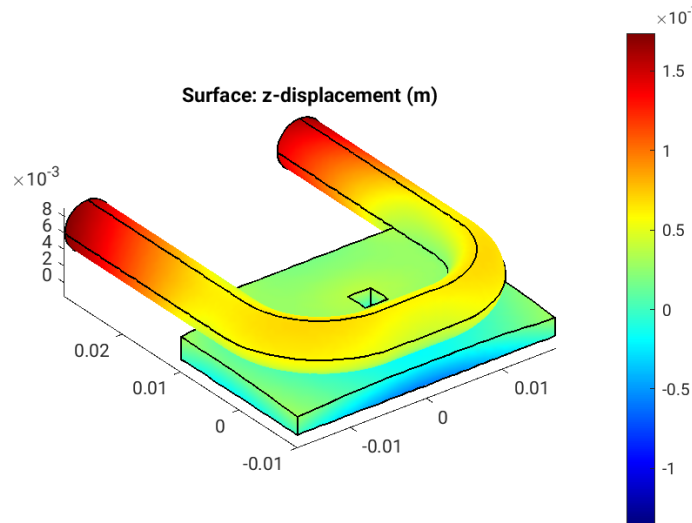


Figure 14.18: Thermoelastic deformation,  $dz$  [m], on the surfaces of optical element #03, for case #26, at 21800 eV photon energy setting.

### 14.3 FEA with no diamond filters in

```
"fig/BS_choice_C111_Laue/fea_plot_geom_c36_21800eV_03.png" Lbl.:BS_choice_C111_Laue_Surface_plot_fea_plot_geom_c36_21800eV_03
```

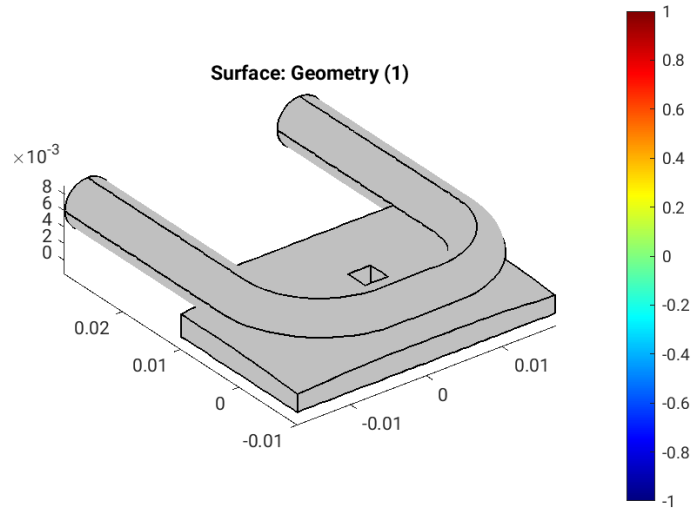


Figure 14.19: Geometry [m] of optical element #03, for case #36, at 21800 eV photon energy setting.

```
"fig/BS_choice_C111_Laue/fea_plot_cnstr_c36_21800eV_03.png" Lbl.:BS_choice_C111_Laue_Surface_plot_fea_plot_cnstr_c36_21800eV_03
```

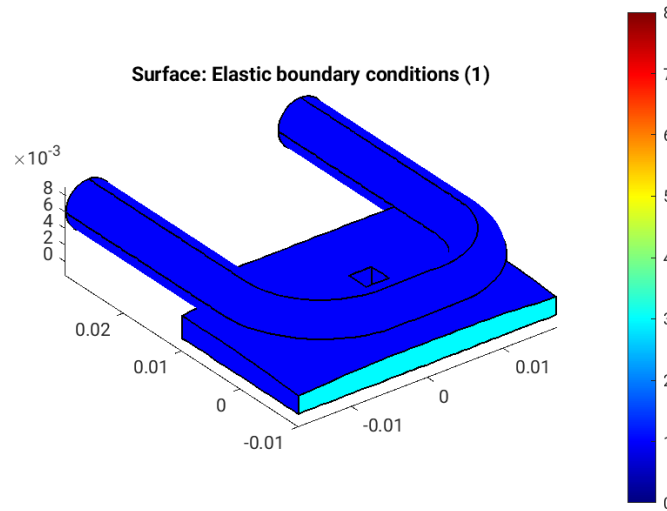


Figure 14.20: Elastic boundary conditions on the surfaces of optical element #03, for case #36, at 21800 eV photon energy setting. Color legend: Blue: Surface can move freely in all directions. Cyan: Tension free kinematic mounting. Minimalistic constraint for three points in surface. One point is fixed, the second can move in one direction, and the third in two, in a fashion that defines angular orientation without introducing stress if the surface expands.

```
"fig/BS_choice_C111_Laue/fea_plot_trans_c36_21800eV_03.png" Lbl.:BS_choice_C111_Laue_Surface_plot_fea_plot_trans_c36_21800eV_03
```

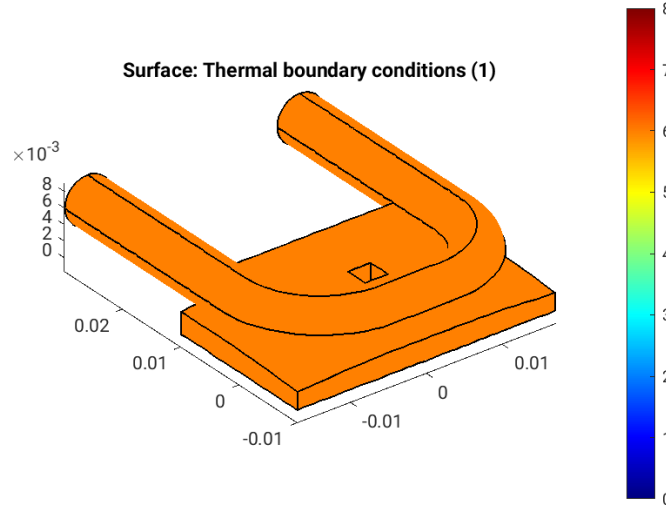


Figure 14.21: Thermal boundary conditions on the surfaces of optical element #03, for case #36, at 21800 eV photon energy setting. Color legend: Orange: No heat transfer at all. Blue: Heat transfer coefficient and temperature difference define heat current density,  $j_q = h(T - T_{cool})$ . Red: Forced heat flux from e.g. absorbed X-rays. Cyan: Heat transfer coefficient and temperature difference define heat current density,  $j_q = h^* \Delta T$  (only at inner surfaces).

```
"fig/BS_choice_C111_Laue/fea_plot_heattrans_c36_21800eV_03.png" Lbl.:BS_choice_C111_Laue_Surface_plot_fea_plot_heattrans_c36_21800eV_03
```

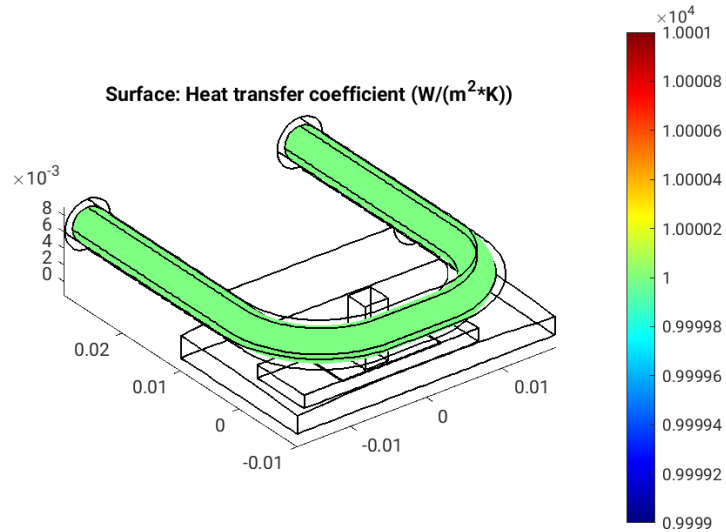


Figure 14.22: Heat transfer coefficient,  $h$  [W/(m<sup>2</sup> K)], on the surfaces of optical element #03, for case #36, at 21800 eV photon energy setting.

```
"fig/BS_choice_C111_Laue/fea_plot_heatflux_c36_21800eV_03.png" Lbl.:BS_choice_C111_Laue_Surface_plot_fea_plot_heatflux_c36_21800eV_03
```

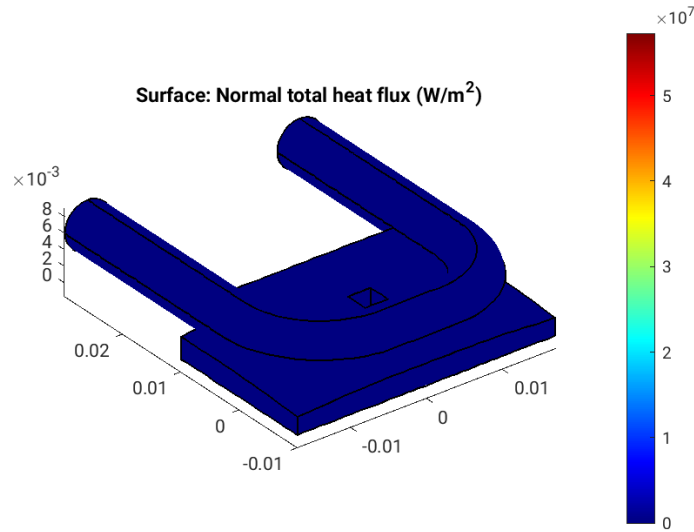


Figure 14.23: Absorbed irradiance,  $p_{\text{abs}}$  [W/m<sup>2</sup>], on the surfaces of optical element #03, for case #36, at 21800 eV photon energy setting.

```
"fig/BS_choice_C111_Laue/fea_plot_temp_c36_21800eV_03.png" Lbl.:BS_choice_C111_Laue_Surface_plot_fea_plot_temp_c36_21800eV_03
```

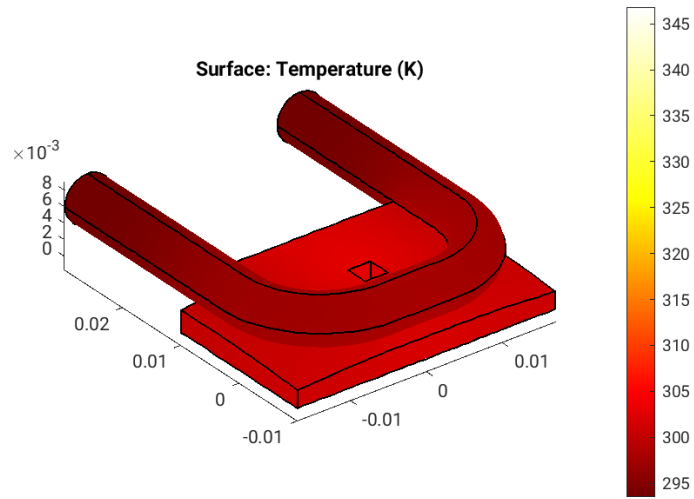


Figure 14.24: Temperature,  $T$  [K], on the surfaces of optical element #03, for case #36, at 21800 eV photon energy setting.

"fig/BS\_choice\_C111\_Laue/fea\_plot\_thermcond\_c36\_21800eV\_03.png" Lbl.:BS\_choice\_C111\_Laue\_Surface\_plot\_fea\_plot\_thermcond\_c36\_21800eV\_03

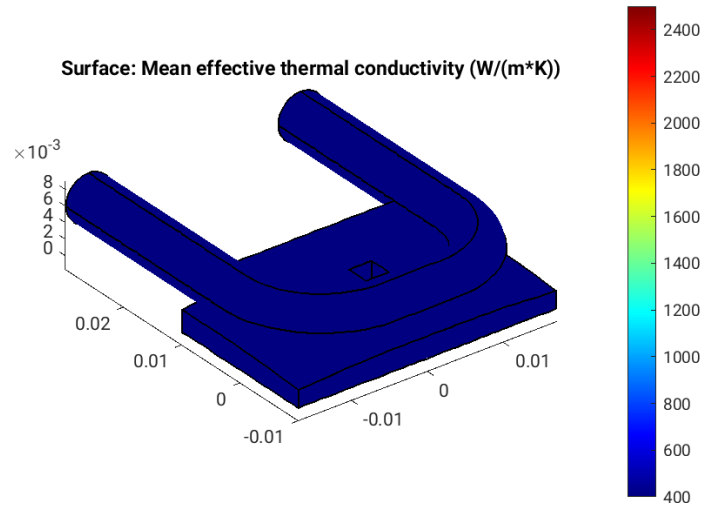


Figure 14.25: Thermal conductivity, lambda [W/(m K)], on the surfaces of optical element #03, for case #36, at 21800 eV photon energy setting.

"fig/BS\_choice\_C111\_Laue/fea\_plot\_stress\_c36\_21800eV\_03.png" Lbl.:BS\_choice\_C111\_Laue\_Surface\_plot\_fea\_plot\_stress\_c36\_21800eV\_03

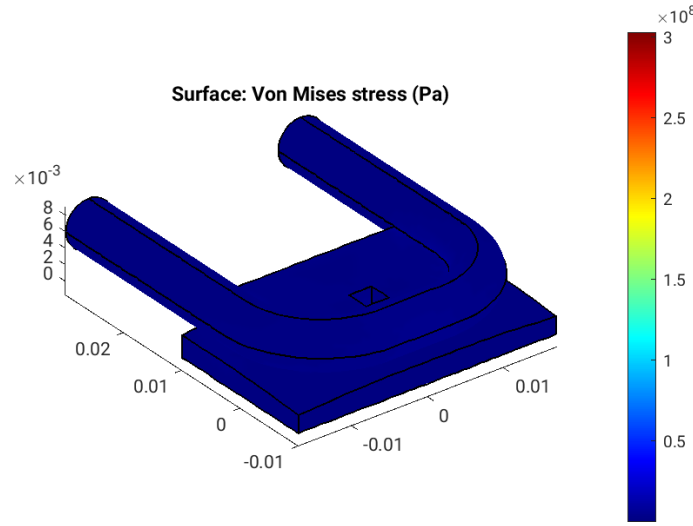


Figure 14.26: Von Mises stress, sigma [Pa], on the surfaces of optical element #03, for case #36, at 21800 eV photon energy setting.

```
"fig/BS_choice_C111_Laue/fea_plot_deform_c36_21800eV_03.png" Lbl.:BS_choice_C111_Laue_Surface_plot_fea_plot_deform_c36_21800eV_03
```

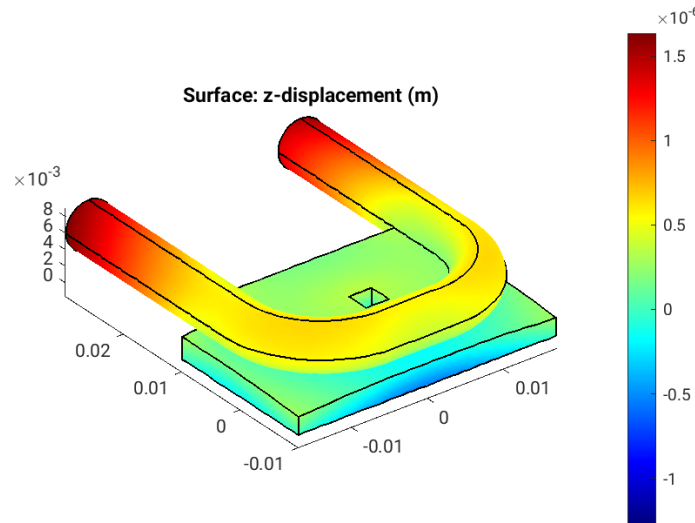


Figure 14.27: Thermoelastic deformation,  $dz$  [m], on the surfaces of optical element #03, for case #36, at 21800 eV photon energy setting.

# Chapter 15

## Parameter scan cases

There are forty cases in total, which fall into four groups of ten cases. The first group, is for the perfect crystal case without deformation of the beam splitter under heat load due to X-ray absorption. The second group is for the beam splitter at room temperature with both diamond filters – 600 and 400 micrometer in thickness – in the upstream beam path. The third group is with only the 400 micron thick filter in, whilst the fourth group is without filters.

Within the ten cases of every group the thickness of the beam splitter is varied in order to optimize reflectivity that varies periodically with this thickness (so called pendellösung).

Diamond 111 beam splitters have been successfully implemented at several beamlines at different facilities [20] [8]. The thicknesses of these beam splitters are in the order of hundreds of micrometres. In one study [16] beam splitter thicknesses below 100 microns led to stability problems. Therefore, we went for the first reflectivity maximum above a thickness of 100 microns. It turned out to be quite precisely at 100 microns.

Case	Thickness(1)_02 cm	Thickness(2)_02 cm	Has_slope_error_03	Skip_heatload	Thickness_03 cm
1	0.06	0.04	no	yes	0.0075
2	0.06	0.04	no	yes	0.008
3	0.06	0.04	no	yes	0.0085
4	0.06	0.04	no	yes	0.009
5	0.06	0.04	no	yes	0.0095
6	0.06	0.04	no	yes	0.01
7	0.06	0.04	no	yes	0.0105
8	0.06	0.04	no	yes	0.0110
9	0.06	0.04	no	yes	0.0115
10	0.06	0.04	no	yes	0.012
11	0.06	0.04	yes	no	0.0075
12	0.06	0.04	yes	no	0.008
13	0.06	0.04	yes	no	0.0085
14	0.06	0.04	yes	no	0.009
15	0.06	0.04	yes	no	0.0095
16	0.06	0.04	yes	no	0.01
17	0.06	0.04	yes	no	0.0105
18	0.06	0.04	yes	no	0.0110
19	0.06	0.04	yes	no	0.0115
20	0.06	0.04	yes	no	0.012
21	0.00001	0.04	yes	no	0.0075
22	0.00001	0.04	yes	no	0.008
23	0.00001	0.04	yes	no	0.0085
24	0.00001	0.04	yes	no	0.009
25	0.00001	0.04	yes	no	0.0095
26	0.00001	0.04	yes	no	0.01
27	0.00001	0.04	yes	no	0.0105
28	0.00001	0.04	yes	no	0.0110
29	0.00001	0.04	yes	no	0.0115
30	0.00001	0.04	yes	no	0.012
31	0.00001	0.00001	yes	no	0.0075
32	0.00001	0.00001	yes	no	0.008
33	0.00001	0.00001	yes	no	0.0085
34	0.00001	0.00001	yes	no	0.009
35	0.00001	0.00001	yes	no	0.0095
36	0.00001	0.00001	yes	no	0.01
37	0.00001	0.00001	yes	no	0.0105
38	0.00001	0.00001	yes	no	0.0110
39	0.00001	0.00001	yes	no	0.0115
40	0.00001	0.00001	yes	no	0.012

Table 15.1: Parameter values for different cases in parameter scan

### Legend

**Case:** Case number in parameter scan

**Thickness(1)\_02:** Optical\_element\_#2.Type.Screen.Thickness(1) (Optical thickness of resp. screen with absorption.)

**Thickness(2)\_02:** Optical\_element\_#2.Type.Screen.Thickness(2) (Optical thickness of resp. screen with absorption.)

**Has\_slope\_error\_03:** Optical\_element\_#3.Surface.Has\_slope\_error (Has surface slope error?)

**Skip\_heatload:** Session.Skip\_heatload (Skip heat load calculation for all optical elements? (heat load parameters are kept))

**Thickness\_03:** Optical\_element\_#3.Shape.Thickness (Optical element's thickness or thickness of optically active layer.)

## Chapter 16

# Photon energy scan

The  $K_y$ -values in the table below are those for optimised output between 15.6 and 18.3 keV – the whole range being covered by the 7th harmonic that is brightest there – used by DanMAX’ main branch. SinCrys, foreseen to be working at a higher photon energy range, is then going to use the 9th harmonic that is not necessarily the brightest there.

E eV	K_y	n_harm/step	theta_B03 deg	theta_B04 deg
<b>20000</b>	1.67551	9	8.6565237	8.9142208
<b>20100</b>	1.66836	9	8.6131277	8.8695126
<b>20200</b>	1.66125	9	8.5701675	8.8252525
<b>20300</b>	1.65418	9	8.5276346	8.7814341
<b>20400</b>	1.64714	9	8.4855232	8.7380495
<b>20500</b>	1.64015	9	8.4438276	8.6950941
<b>20600</b>	1.63319	9	8.4025402	8.6525602
<b>20700</b>	1.62628	9	8.3616571	8.6104422
<b>20800</b>	1.6194	9	8.3211708	8.5687342
<b>20900</b>	1.61255	9	8.2810764	8.5274286
<b>21000</b>	1.60575	9	8.2413683	8.4865217
<b>21100</b>	1.59898	9	8.2020397	8.4460068
<b>21200</b>	1.59224	9	8.1630869	8.4058781
<b>21300</b>	1.58554	9	8.1245022	8.3661299
<b>21400</b>	1.57887	9	8.0862827	8.3267574
<b>21500</b>	1.57224	9	8.0484219	8.287756
<b>21600</b>	1.56564	9	8.0109158	8.2491188
<b>21700</b>	1.55908	9	7.9737582	8.2108412
<b>21800</b>	1.55255	9	7.936945	8.1729183
<b>21900</b>	1.54605	9	7.9004712	8.1353455
<b>22000</b>	1.53958	9	7.8643322	8.0981178
<b>22100</b>	1.53315	9	7.8285236	8.0612307
<b>22200</b>	1.52674	9	7.7930403	8.0246792
<b>22300</b>	1.52037	9	7.7578783	7.9884586
<b>22400</b>	1.51402	9	7.7230334	7.9525642
<b>22500</b>	1.50771	9	7.6885004	7.9169927
<b>22600</b>	1.50143	9	7.6542764	7.8817382
<b>22700</b>	1.49517	9	7.6203566	7.8467979
<b>22800</b>	1.48895	9	7.5867367	7.8121667
<b>22900</b>	1.48275	9	7.5534129	7.7778411
<b>23000</b>	1.47658	9	7.5203819	7.7438164
<b>23100</b>	1.47044	9	7.487639	7.7100892
<b>23200</b>	1.46433	9	7.4551811	7.6766553
<b>23300</b>	1.45824	9	7.4230037	7.6435108
<b>23400</b>	1.45218	9	7.3911042	7.6106524
<b>23500</b>	1.44615	9	7.359478	7.5780759

Table 16.1: Scan values for different photon energies in energy scan

### Legend

**E:** photon energy

**K\_y:** deflection parameter for vertical field component of insertion device

**n\_harm/step:** number of undulator harmonic or number of energy slot for continuous source (e.g. wiggler)

**theta\_B03:** Bragg angle, i.e. glancing angle of incident and reflected beam w.r.t. the set of diffracting planes of optical element 03

**theta\_B04:** Bragg angle, i.e. glancing angle of incident and reflected beam w.r.t. the set of diffracting planes of optical element 04

E eV	P_sum W	P_abs02-01 W	P_abs02-02 W	P_abs03 W
<b>20000</b>	170.798	51.8133	7.07269	1.73407
<b>20100</b>	170.209	51.7819	7.07207	1.73345
<b>20200</b>	169.47	51.9401	7.0691	1.73587
<b>20300</b>	168.879	51.8032	7.06596	1.73384
<b>20400</b>	168.315	51.9832	7.06293	1.73147
<b>20500</b>	167.588	51.9606	7.07492	1.73206
<b>20600</b>	166.189	51.9253	7.07625	1.73277
<b>20700</b>	165.542	52.0049	7.08503	1.73251
<b>20800</b>	164.949	52.0113	7.058	1.72671
<b>20900</b>	164.413	52.0653	7.09147	1.73343
<b>21000</b>	163.752	52.0889	7.04593	1.72716
<b>21100</b>	163.16	52.0394	7.03478	1.727
<b>21200</b>	162.507	52.028	7.06834	1.71667
<b>21300</b>	161.904	52.0565	7.02809	1.71856
<b>21400</b>	161.386	52.1115	7.03604	1.72306
<b>21500</b>	160.797	52.1844	7.0246	1.71908
<b>21600</b>	160.163	51.8697	7.0074	1.71966
<b>21700</b>	159.473	52.1092	7.01325	1.7183
<b>21800</b>	158.884	52.1874	6.97463	1.70937
<b>21900</b>	157.585	52.2219	6.97824	1.71138
<b>22000</b>	157.101	52.2517	6.96569	1.70812
<b>22100</b>	156.451	52.3465	6.96309	1.70591
<b>22200</b>	155.93	52.4923	6.95436	1.70568
<b>22300</b>	155.254	52.3067	6.90514	1.6975
<b>22400</b>	154.716	52.3717	6.92106	1.70518
<b>22500</b>	154.16	52.6043	6.91683	1.69563
<b>22600</b>	153.484	52.3064	6.88702	1.69313
<b>22700</b>	152.951	52.4228	6.86291	1.69498
<b>22800</b>	152.294	52.3512	6.80748	1.67888
<b>22900</b>	151.786	52.3212	6.80744	1.68335
<b>23000</b>	151.176	52.3092	6.76081	1.68187
<b>23100</b>	150.589	52.427	6.73326	1.66915
<b>23200</b>	149.911	52.3354	6.73258	1.66779
<b>23300</b>	148.827	52.2867	6.68381	1.66228
<b>23400</b>	148.246	52.4106	6.67729	1.66254
<b>23500</b>	147.698	52.2413	6.64353	1.66246

Table 16.2: Scan values for different photon energies with diamond filters of 1000 micron total thickness in

E eV	P_sum W	P_abs02-01 W	P_abs02-02 W	P_abs03 W
<b>20000</b>	170.798	0.197799	46.0071	4.10295
<b>20100</b>	170.209	0.196853	46.0819	4.08723
<b>20200</b>	169.47	0.196284	46.2593	4.08928
<b>20300</b>	168.879	0.195183	46.2189	4.06927
<b>20400</b>	168.315	0.193669	46.2916	4.06606
<b>20500</b>	167.588	0.192335	46.3344	4.06224
<b>20600</b>	166.189	0.191052	46.1898	4.03706
<b>20700</b>	165.542	0.189426	46.2335	4.02371
<b>20800</b>	164.949	0.189853	46.4327	4.0155
<b>20900</b>	164.413	0.187099	46.4326	3.99076
<b>21000</b>	163.752	0.185575	46.5099	3.97255
<b>21100</b>	163.16	0.184607	46.3445	3.95312
<b>21200</b>	162.507	0.184416	46.63	3.93282
<b>21300</b>	161.904	0.182314	46.4654	3.92474
<b>21400</b>	161.386	0.180449	46.3921	3.91589
<b>21500</b>	160.797	0.180427	46.4892	3.892
<b>21600</b>	160.163	0.178663	46.5362	3.87423
<b>21700</b>	159.473	0.177994	46.751	3.86634
<b>21800</b>	158.884	0.177911	46.756	3.82791
<b>21900</b>	157.585	0.175668	46.8648	3.82563
<b>22000</b>	157.101	0.175403	46.9126	3.79792
<b>22100</b>	156.451	0.173519	46.8176	3.76662
<b>22200</b>	155.93	0.172613	47.0846	3.76113
<b>22300</b>	155.254	0.171453	46.9939	3.72428
<b>22400</b>	154.716	0.170831	47.0515	3.71867
<b>22500</b>	154.16	0.169527	47.1971	3.69182
<b>22600</b>	153.484	0.168309	47.0599	3.66698
<b>22700</b>	152.951	0.167418	47.1726	3.65202
<b>22800</b>	152.294	0.166427	47.1808	3.6171
<b>22900</b>	151.786	0.164702	47.0985	3.59895
<b>23000</b>	151.176	0.16373	47.1588	3.56981
<b>23100</b>	150.589	0.162879	47.1601	3.54475
<b>23200</b>	149.911	0.161912	47.365	3.50841
<b>23300</b>	148.827	0.16138	47.1729	3.48394
<b>23400</b>	148.246	0.160546	47.298	3.45685
<b>23500</b>	147.698	0.158949	47.3875	3.44147

Table 16.3: Scan values for different photon energies with upstream diamond filter of 400 micron thickness in

E eV	P_sum W	P_abs02-01 W	P_abs02-02 W	P_abs03 W
<b>20000</b>	170.798	0.198116	0.195664	34.1702
<b>20100</b>	170.209	0.196172	0.195659	34.2919
<b>20200</b>	169.47	0.196702	0.19458	34.4838
<b>20300</b>	168.879	0.194157	0.192298	34.4662
<b>20400</b>	168.315	0.193668	0.192054	34.6481
<b>20500</b>	167.588	0.191699	0.192175	34.7589
<b>20600</b>	166.189	0.190316	0.189839	34.7852
<b>20700</b>	165.542	0.189327	0.188461	34.9542
<b>20800</b>	164.949	0.188318	0.188505	35.186
<b>20900</b>	164.413	0.186978	0.186918	35.2887
<b>21000</b>	163.752	0.185835	0.185325	35.3718
<b>21100</b>	163.16	0.184585	0.183695	35.3134
<b>21200</b>	162.507	0.183762	0.183109	35.4756
<b>21300</b>	161.904	0.182078	0.181216	35.5773
<b>21400</b>	161.386	0.181411	0.180411	35.5414
<b>21500</b>	160.797	0.180321	0.179169	35.811
<b>21600</b>	160.163	0.178935	0.178083	35.883
<b>21700</b>	159.473	0.17793	0.176475	36.0056
<b>21800</b>	158.884	0.177374	0.176482	36.1861
<b>21900</b>	157.585	0.175339	0.174895	36.2613
<b>22000</b>	157.101	0.17495	0.173963	36.4202
<b>22100</b>	156.451	0.173725	0.173037	36.6442
<b>22200</b>	155.93	0.172804	0.172103	36.8069
<b>22300</b>	155.254	0.1716	0.170442	36.8083
<b>22400</b>	154.716	0.170368	0.169419	36.9776
<b>22500</b>	154.16	0.169782	0.168729	37.0686
<b>22600</b>	153.484	0.168287	0.167223	36.9871
<b>22700</b>	152.951	0.166959	0.165934	37.3409
<b>22800</b>	152.294	0.166287	0.165455	37.3409
<b>22900</b>	151.786	0.16514	0.164116	37.4176
<b>23000</b>	151.176	0.164013	0.163416	37.445
<b>23100</b>	150.589	0.162502	0.162407	37.6908
<b>23200</b>	149.911	0.161787	0.161046	37.793
<b>23300</b>	148.827	0.16055	0.160501	37.8112
<b>23400</b>	148.246	0.16046	0.159073	38.0249
<b>23500</b>	147.698	0.159196	0.157991	38.2185

Table 16.4: Scan values for different photon energies with no upstream filters

### Legend

**E:** photon energy

**P\_sum:** sum of power in harmonics / energy intervals, P\_sum = P\_src

**P\_abs02-01:** total power absorbed by optical element 02-01

**P\_abs02-02:** total power absorbed by optical element 02-02

**P\_abs03:** total power absorbed by optical element 03

# Chapter 17

## Plots

### 17.1 Statistics of incident irradiance

```
"fig/BS_choice_C111_Laue/plot001.png" Lbl.:BS_choice_C111_Laue_2d_plot_I_peak_incstat_oe03
```

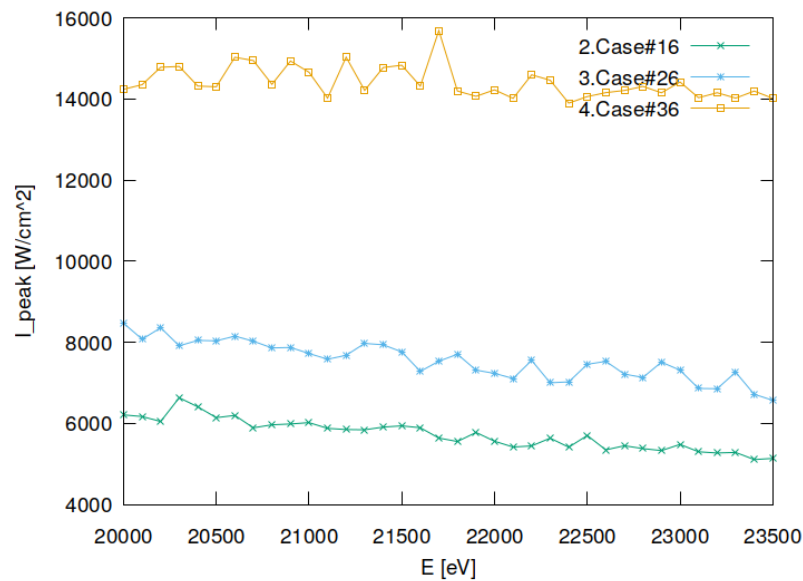


Figure 17.1: Incident peak irradiance of optical element #03 (BS).

```
"fig/BS_choice_C111_Laue/plot002.png" Lbl.:BS_choice_C111_Laue_2d_plot_I_int_incstat_oe03
```

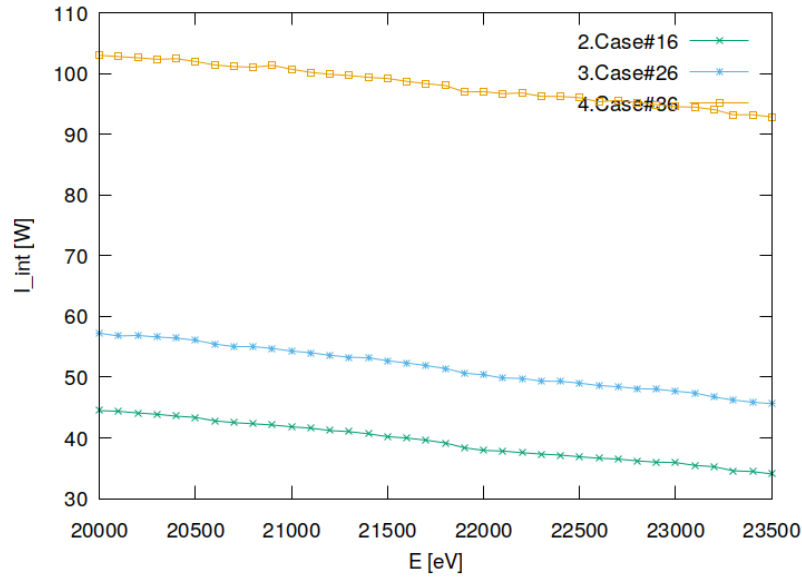


Figure 17.2: Incident flux of optical element #03 (BS).

## 17.2 Statistics of absorbed irradiance

```
"fig/BS_choice_C111_Laue/plot003.png" Lbl.:BS_choice_C111_Laue_2d_plot_I_peak_absstat_oe03
```

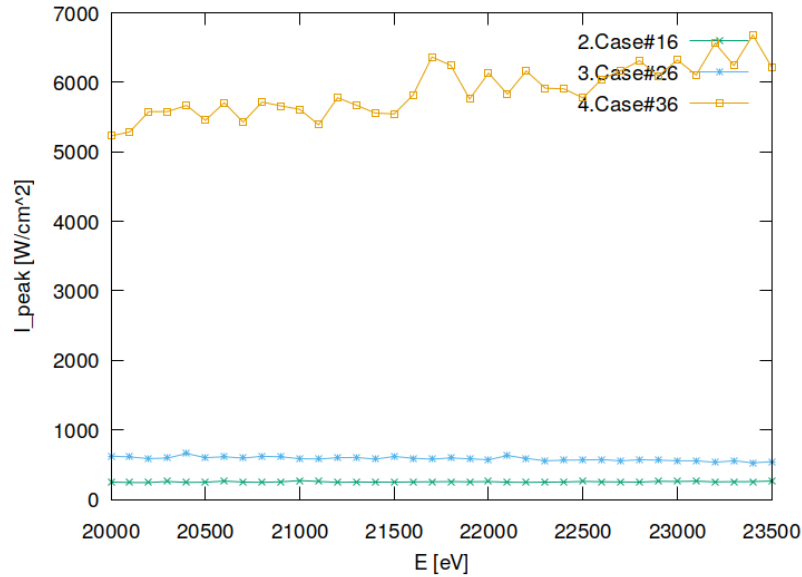


Figure 17.3: Absorbed peak irradiance of optical element #03 (BS).

```
"fig/BS_choice_C111_Laue/plot004.png" Lbl.:BS_choice_C111_Laue_2d_plot_I_int_absstat_oe03
```

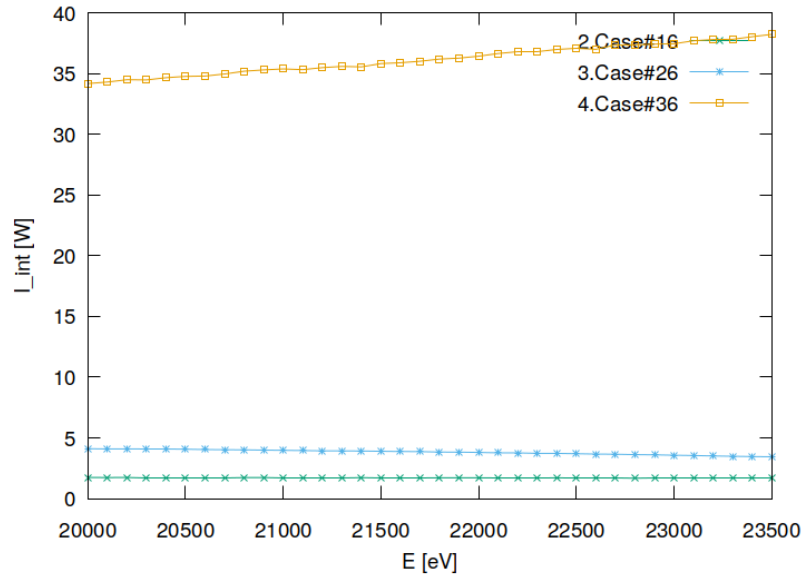


Figure 17.4: Absorbed flux of optical element #03 (BS).

### 17.3 Statistics of temperature

```
"fig/BS_choice_C111_Laue/plot005.png" Lbl.:BS_choice_C111_Laue_2d_plot_T_peak_stat_oe03
```

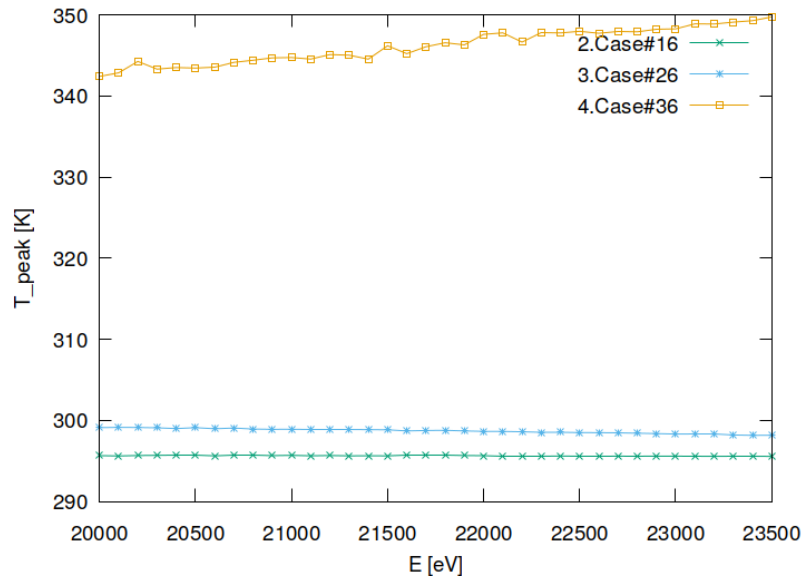


Figure 17.5: Peak temperature of optical element #03 (BS).

## 17.4 Statistics of mechanical stress (von Mises stress)

```
"fig/BS_choice_C111_Laue/plot006.png" Lbl.:BS_choice_C111_Laue_2d_plot_sigma_peak_stat_oe03
```

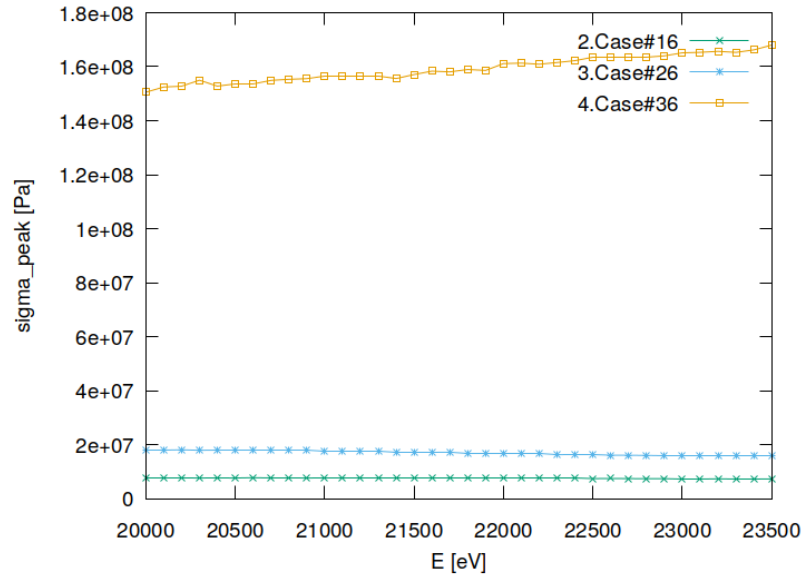


Figure 17.6: Peak mechanical stress (Von Mises stress) of optical element #03 (BS).

## 17.5 Statistics of optical surface deformation

```
"fig/BS_choice_C111_Laue/plot007.png" Lbl.:BS_choice_C111_Laue_2d_plot_dz_peak_stat_oe03
```

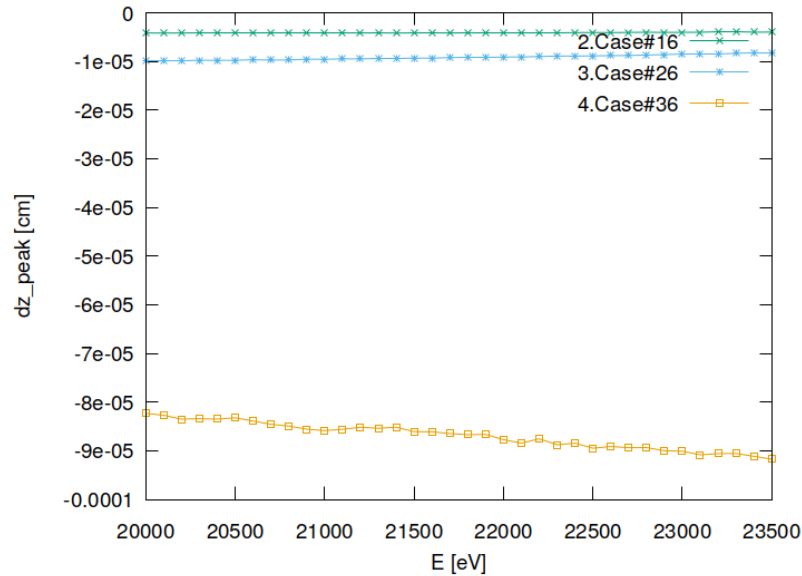


Figure 17.7: Peak deformation of optical element #03 (BS).

## 17.6 Statistics of photon irradiance on optical surface

"fig/BS\_choice\_C111\_Laue/plot008.png" Lbl.:BS\_choice\_C111\_Laue\_2d\_plot\_dx\_fwhm\_inc\_footstat\_oe04

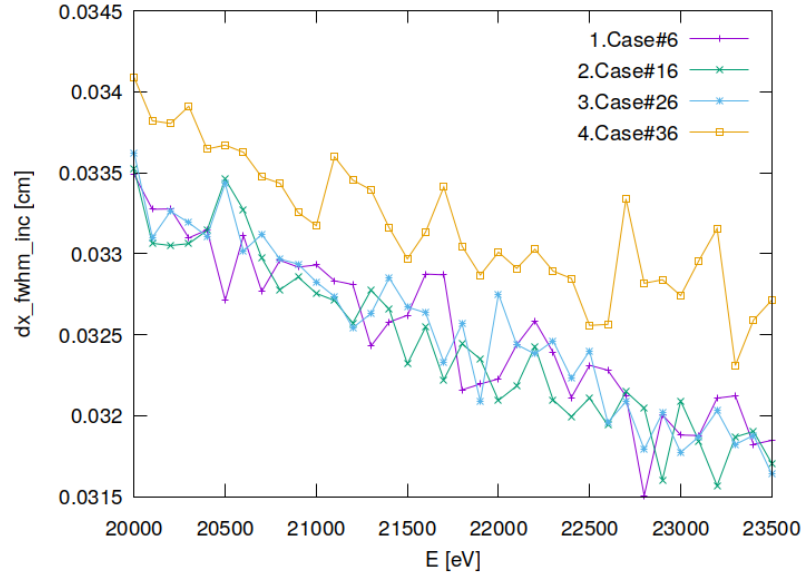


Figure 17.8: Sagittal footprint diameter (FWHM) of optical element #04 (CM2).

"fig/BS\_choice\_C111\_Laue/plot009.png" Lbl.:BS\_choice\_C111\_Laue\_2d\_plot\_dy\_fwhm\_inc\_footstat\_oe04

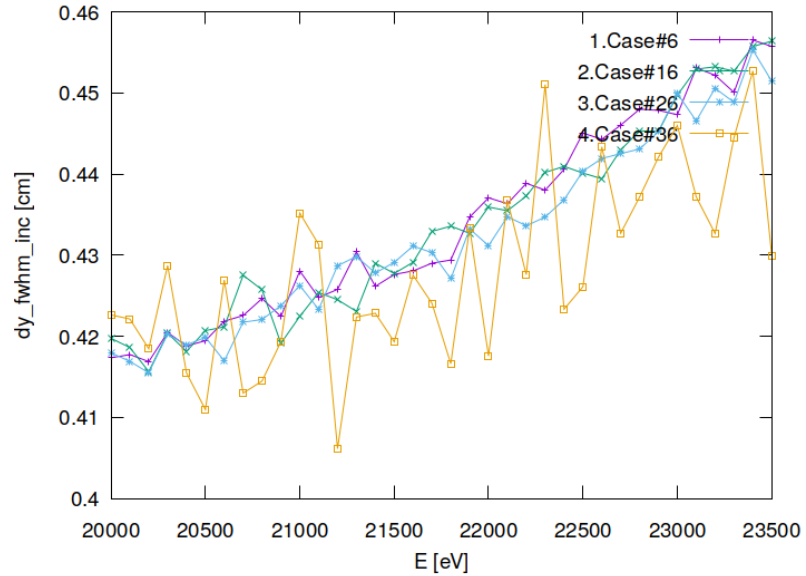


Figure 17.9: Meridional footprint diameter (FWHM) of optical element #04 (CM2).

"fig/BS\_choice\_C111\_Laue/plot010.png" Lbl.:BS\_choice\_C111\_Laue\_2d\_plot\_I\_inc\_int\_footstat\_oe04

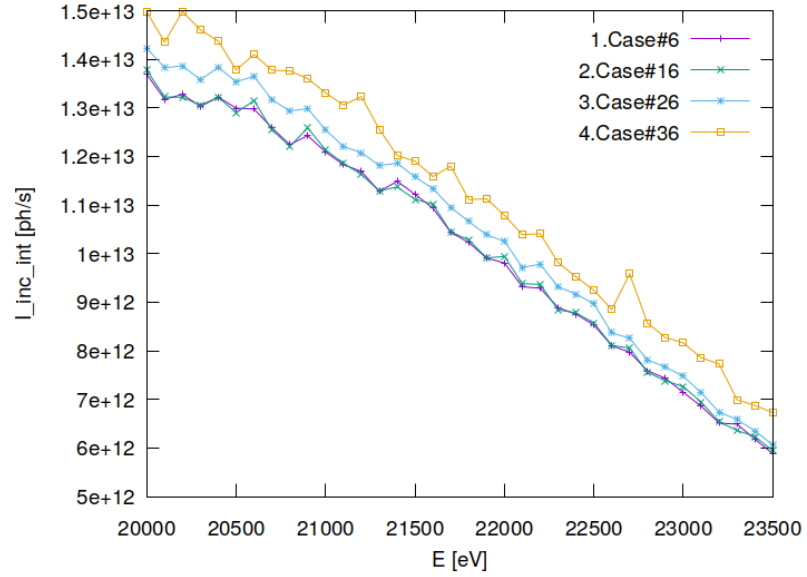


Figure 17.10: Incident photon flux on surface of optical element #04 (CM2).

"fig/BS\_choice\_C111\_Laue/plot011.png" Lbl.:BS\_choice\_C111\_Laue\_2d\_plot\_x\_cen\_inc\_footstat\_oe04

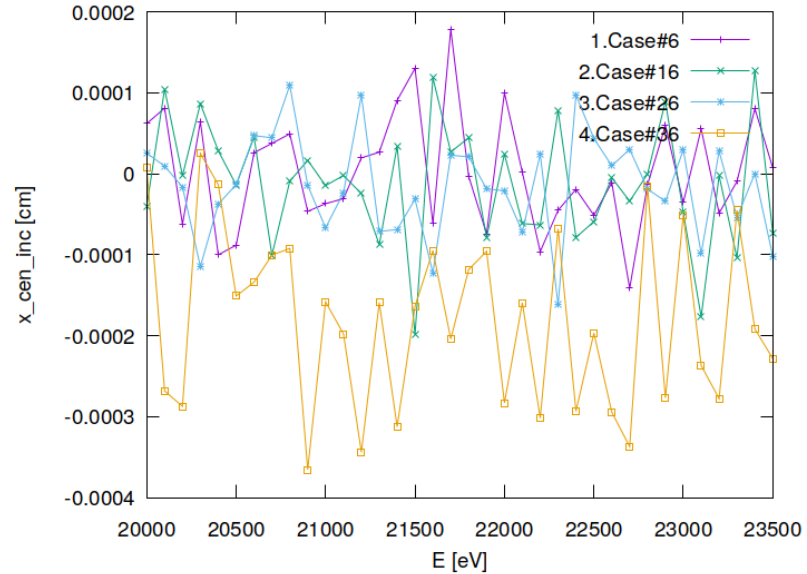


Figure 17.11: Sagittal coordinate of footprint's centre of 'gravity' on surface of optical element #04 (CM2).

```
"fig/BS_choice_C111_Laue/plot012.png" Lbl.:BS_choice_C111_Laue_2d_plot_y_cen_inc_footstat_oe04
```

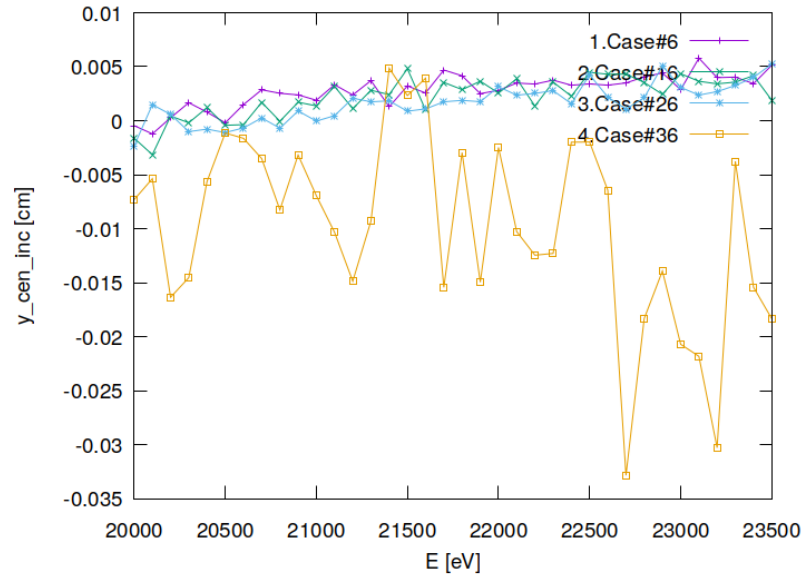


Figure 17.12: Meridional coordinate of footprint's centre of 'gravity' on surface of optical element #04 (CM2).

## 17.7 Statistics of photon irradiance in beam cross section

```
"fig/BS_choice_C111_Laue/plot013.png" Lbl.:BS_choice_C111_Laue_2d_plot_dx_fwhm_focstatavg_oe04
```

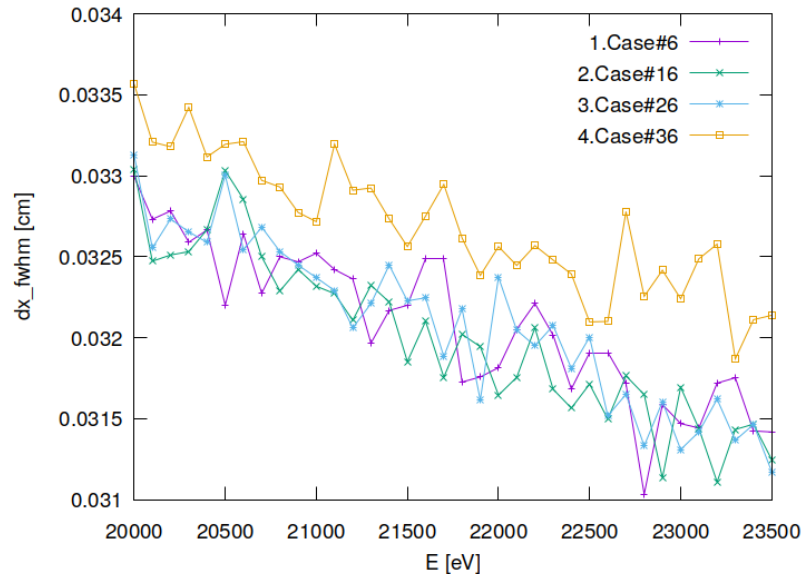


Figure 17.13: Sagittal beam diameter (FWHM) of optical element #04 (CM2).

"fig/BS\_choice\_C111\_Laue/plot014.png" Lbl.:BS\_choice\_C111\_Laue\_2d\_plot\_dz\_fwhm\_focstatavg\_oe04

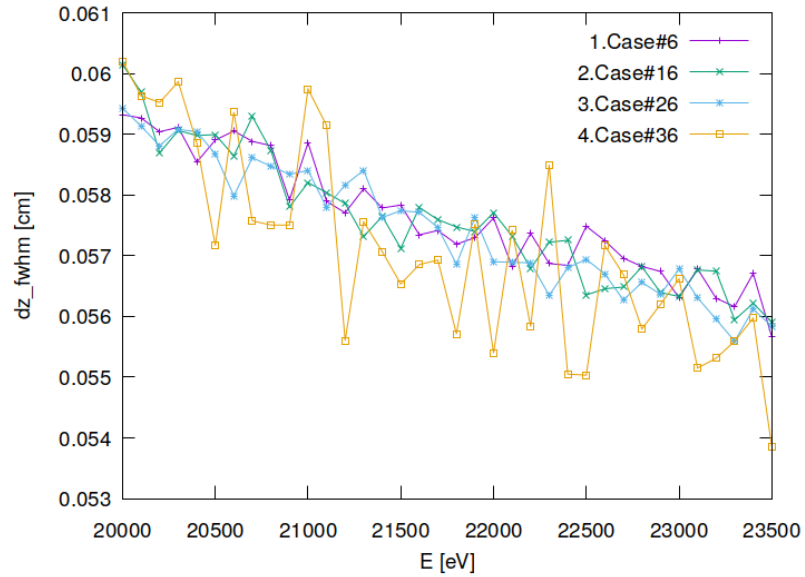


Figure 17.14: Meridional beam diameter (FWHM) of optical element #04 (CM2).

"fig/BS\_choice\_C111\_Laue/plot015.png" Lbl.:BS\_choice\_C111\_Laue\_2d\_plot\_I\_int\_focstatavg\_oe04

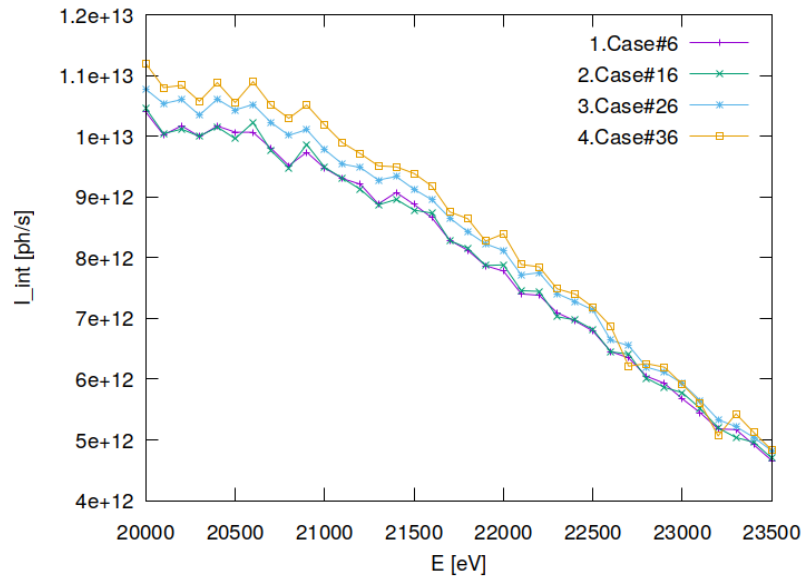


Figure 17.15: Photon flux in beam cross section of optical element #04 (CM2).

```
"fig/BS_choice_C111_Laue/plot016.png" Lbl.:BS_choice_C111_Laue_2d_plot_x_cen_focstatavg_oe04
```

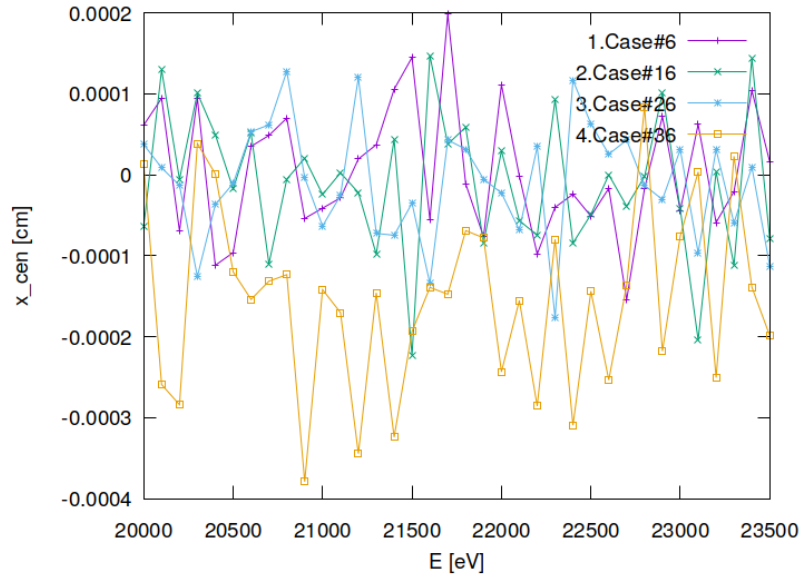


Figure 17.16: Sagittal coordinate of beam's centre of 'gravity' in beam cross section of optical element #04 (CM2).

```
"fig/BS_choice_C111_Laue/plot017.png" Lbl.:BS_choice_C111_Laue_2d_plot_z_cen_focstatavg_oe04
```

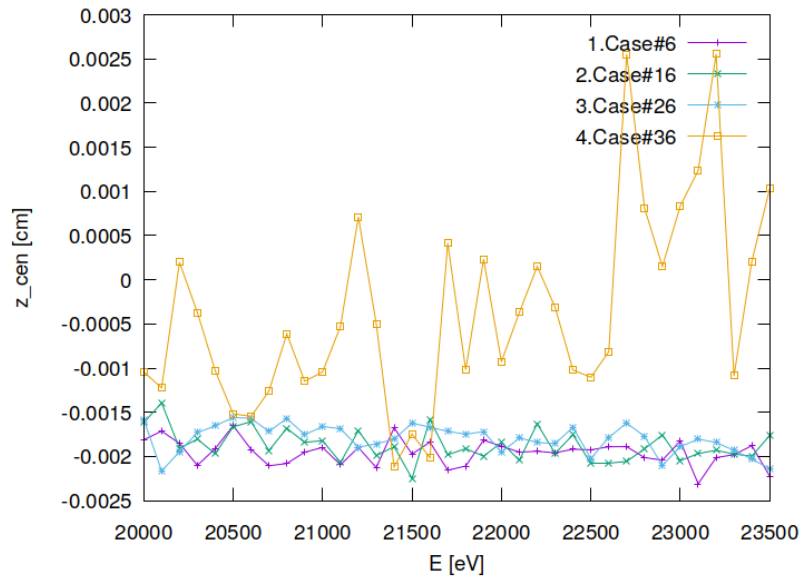


Figure 17.17: Meridional coordinate of beam's centre of 'gravity' in beam cross section of optical element #04 (CM2).

```
"fig/BS_choice_C111_Laue/plot018.png" Lbl.:BS_choice_C111_Laue_2d_plot_dxp_fwhm_focstatavg_oe04
```

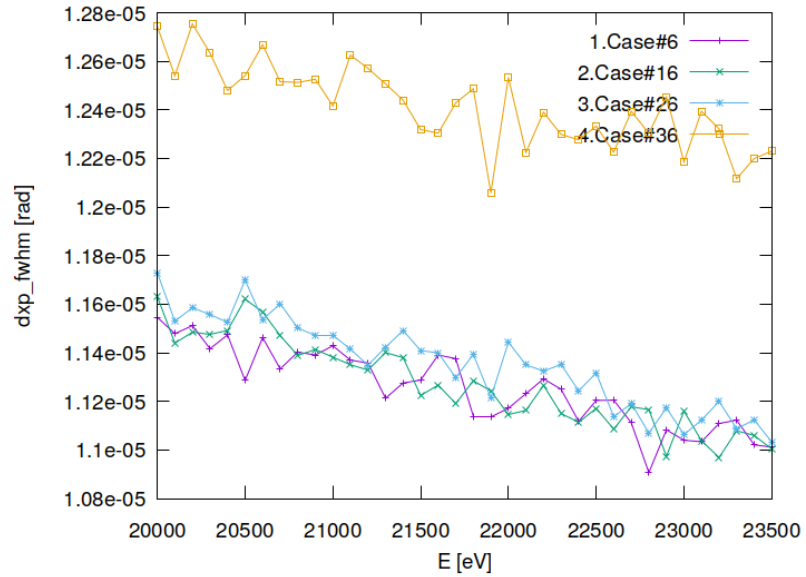


Figure 17.18: Sagittal beam divergence (FWHM) of optical element #04 (CM2).

```
"fig/BS_choice_C111_Laue/plot019.png" Lbl.:BS_choice_C111_Laue_2d_plot_dzp_fwhm_focstatavg_oe04
```

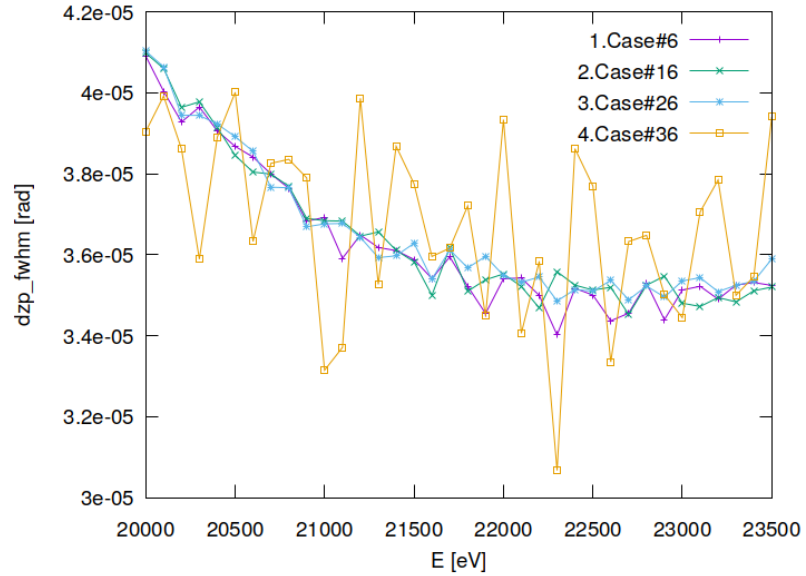


Figure 17.19: Meridional beam divergence (FWHM) of optical element #04 (CM2).

```
"fig/BS_choice_C111_Laue/plot020.png" Lbl.:BS_choice_C111_Laue_2d_plot_I_int_focstatavg_oe04
```

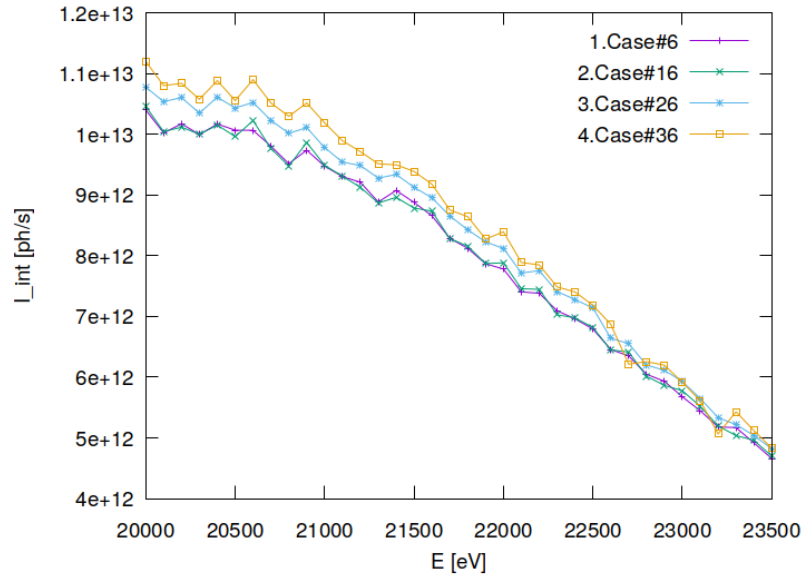


Figure 17.20: Photon flux in beam cross section of optical element #04 (CM2).

```
"fig/BS_choice_C111_Laue/plot021.png" Lbl.:BS_choice_C111_Laue_2d_plot_xp_cen_focstatavg_oe04
```

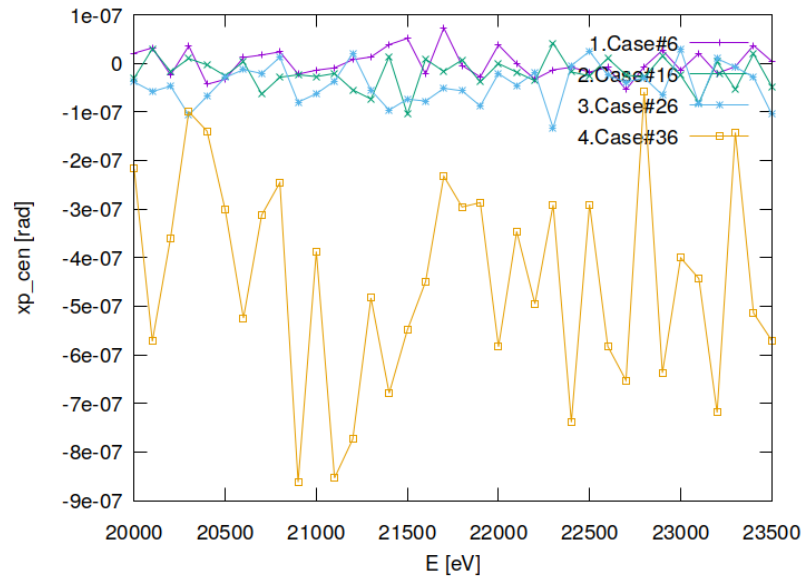


Figure 17.21: Sagittal coordinate of beam's centre of 'gravity' in angle space of optical element #04 (CM2).

```
"fig/BS_choice_C111_Laue/plot022.png" Lbl.:BS_choice_C111_Laue_2d_plot_zp_cen_focstatavg_oe04
```

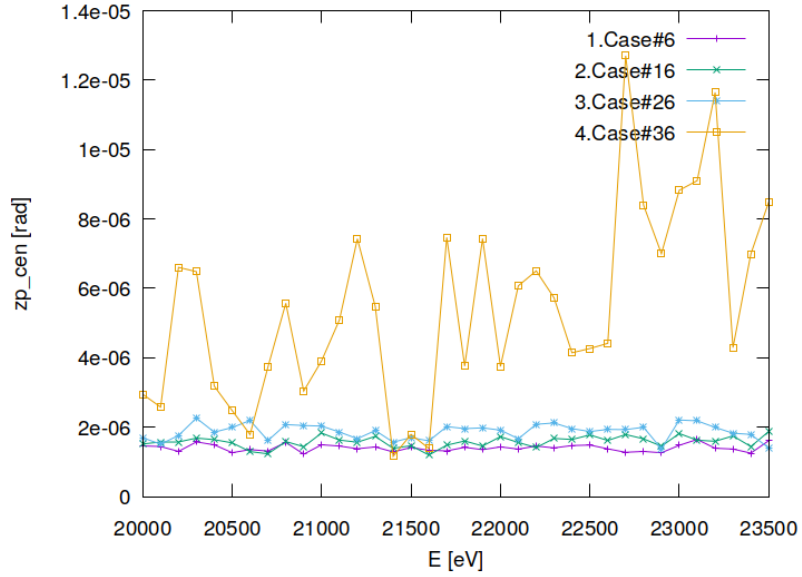


Figure 17.22: Meridional coordinate of beam's centre of 'gravity' in angle space of optical element #04 (CM2).

```
"fig/BS_choice_C111_Laue/plot023.png" Lbl.:BS_choice_C111_Laue_2d_plot_dE_fwhm_focstatavg_oe04
```

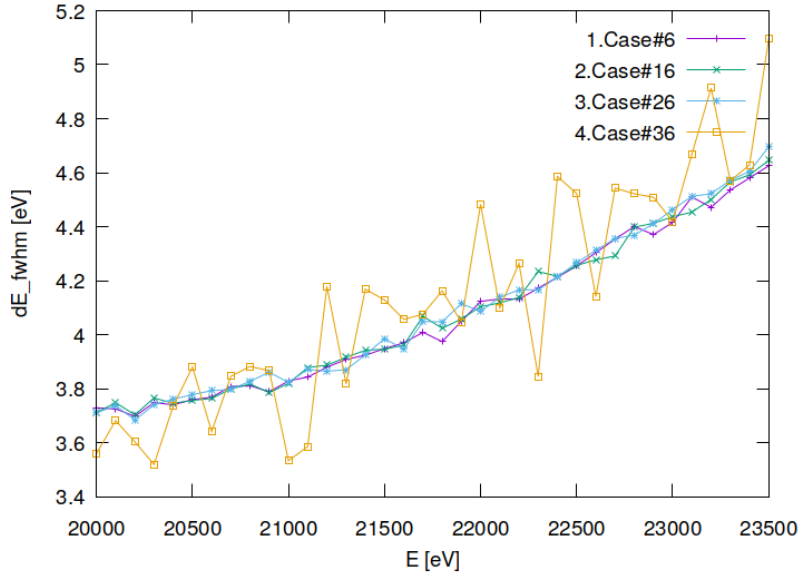


Figure 17.23: Bandwidth (FWHM) in beam cross section of optical element #04 (CM2).

## 17.8 Absorbed irradiance on surface

"fig/BS\_choice\_C111\_Laue/plot024.png" Lbl.:BS\_choice\_C111\_Laue\_false\_colour\_plot\_p\_abs\_foot\_oe03\_c16\_21800eV

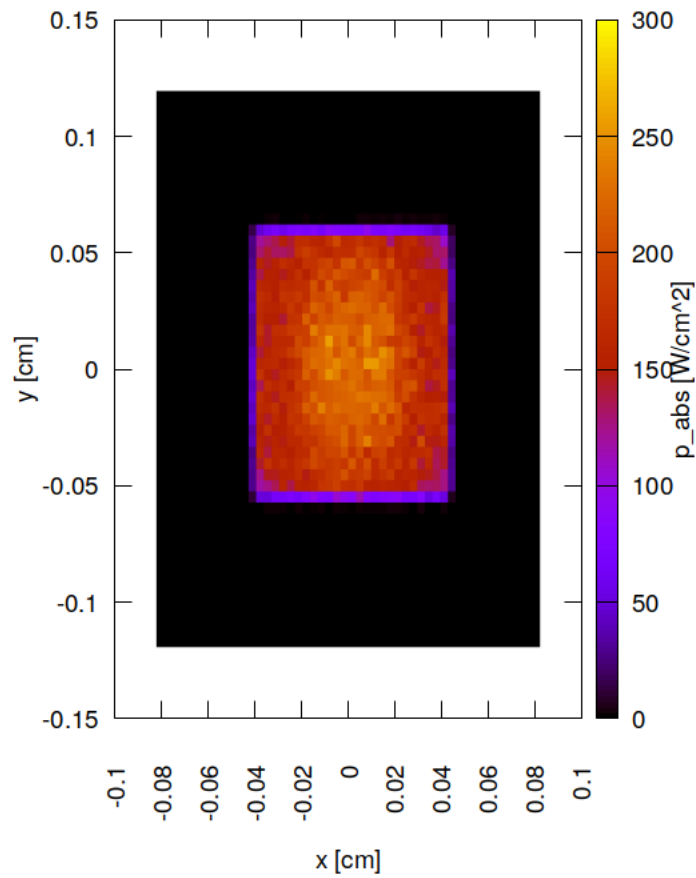


Figure 17.24: Absorbed irradiance on surface of optical element #03 (BS) for case #16 for 21800 eV photon energy setting.

"fig/BS\_choice\_C111\_Laue/plot025.png" Lbl.:BS\_choice\_C111\_Laue\_false\_colour\_plot\_p\_abs\_foot\_oe03\_c26\_21800eV

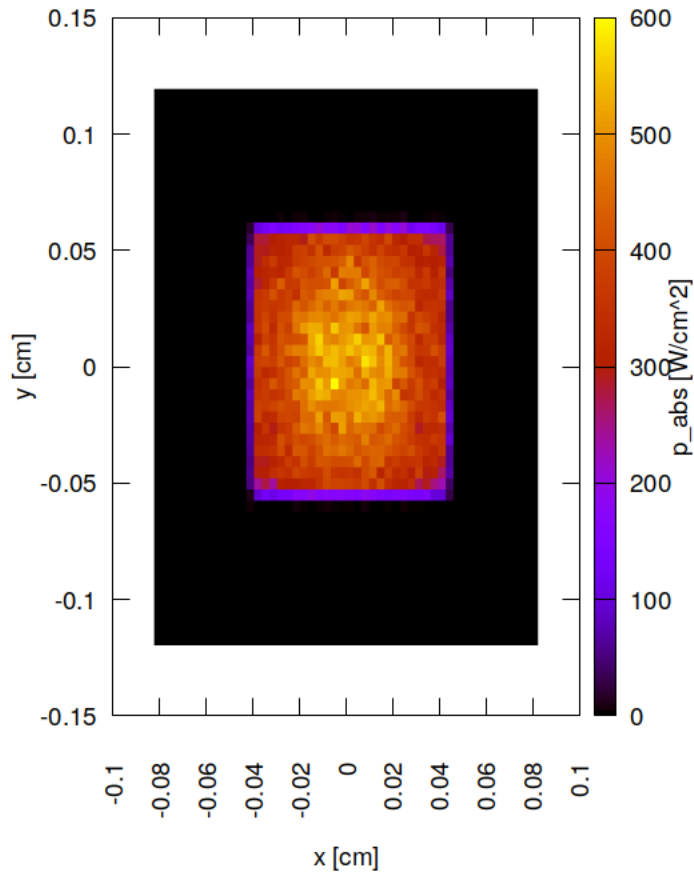


Figure 17.25: Absorbed irradiance on surface of optical element #03 (BS) for case #26 for 21800 eV photon energy setting.

"fig/BS\_choice\_C111\_Laue/plot026.png" Lbl.:BS\_choice\_C111\_Laue\_false\_colour\_plot\_p\_abs\_foot\_oe03\_c36\_21800eV

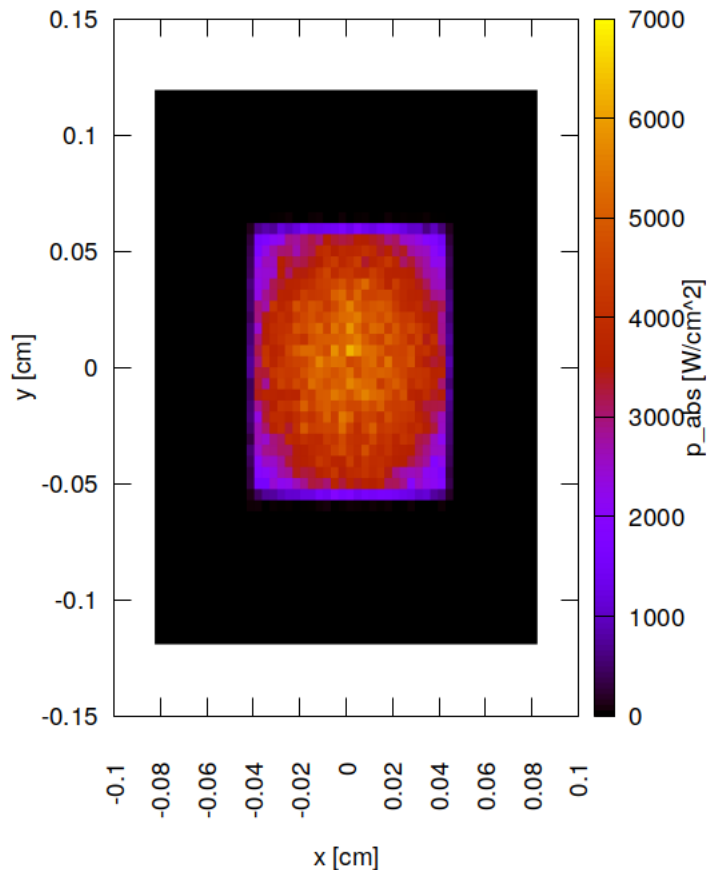


Figure 17.26: Absorbed irradiance on surface of optical element #03 (BS) for case #36 for 21800 eV photon energy setting.

## 17.9 Incident spectral flux on surface

"fig/BS\_choice\_C111\_Laue/plot027.png" Lbl.:BS\_choice\_C111\_Laue\_2d\_plot\_P\_spec\_spec\_oe03\_c16\_21800eV

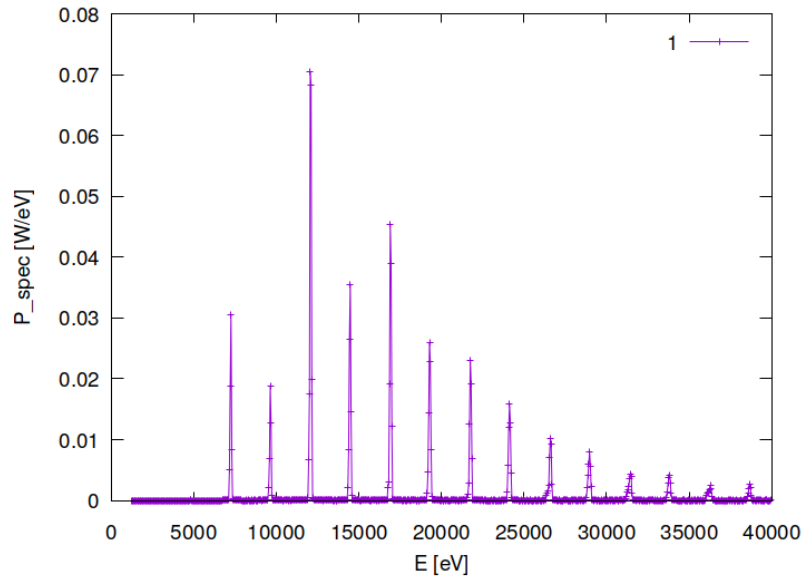


Figure 17.27: Incident spectral flux on surface of optical element #03 (BS) for case #16 for 21800 eV photon energy setting.

"fig/BS\_choice\_C111\_Laue/plot028.png" Lbl.:BS\_choice\_C111\_Laue\_2d\_plot\_P\_spec\_spec\_oe03\_c26\_21800eV

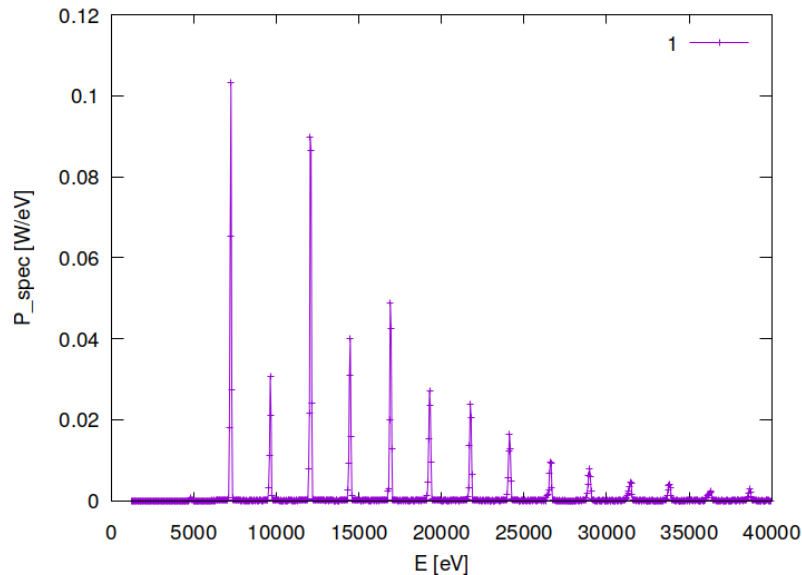


Figure 17.28: Incident spectral flux on surface of optical element #03 (BS) for case #26 for 21800 eV photon energy setting.

```
"fig/BS_choice_C111_Laue/plot029.png" Lbl.:BS_choice_C111_Laue_2d_plot_P_spec_spec_oe03_c36_21800eV
```

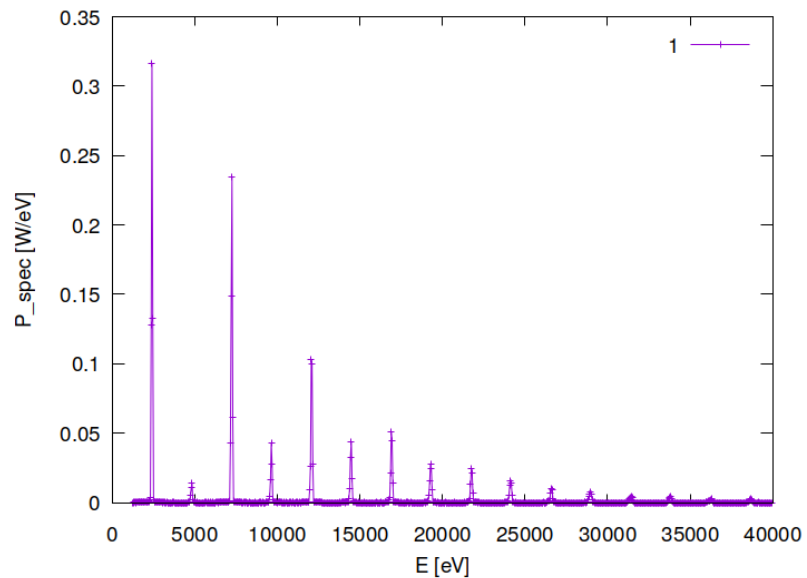


Figure 17.29: Incident spectral flux on surface of optical element #03 (BS) for case #36 for 21800 eV photon energy setting.

## 17.10 Temperature on surface

"fig/BS\_choice\_C111\_Laue/plot030.png" Lbl.:BS\_choice\_C111\_Laue\_false\_colour\_plot\_T\_oe03\_c16\_21800eV

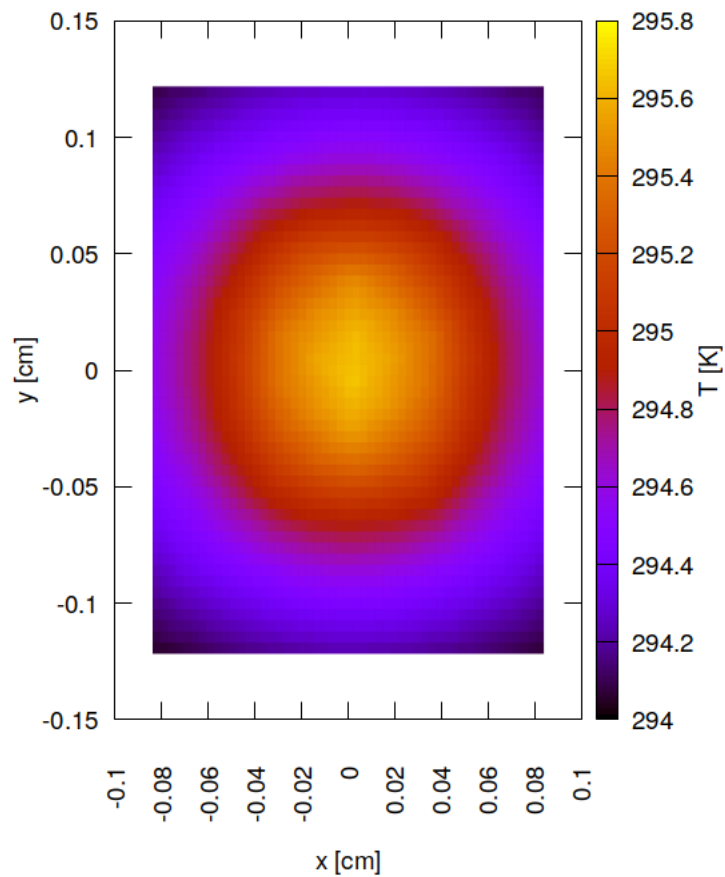


Figure 17.30: Temperature on surface of optical element #03 (BS) for case #16 for 21800 eV photon energy setting.

"fig/BS\_choice\_C111\_Laue/plot031.png" Lbl.:BS\_choice\_C111\_Laue\_false\_colour\_plot\_T\_oe03\_c26\_21800eV

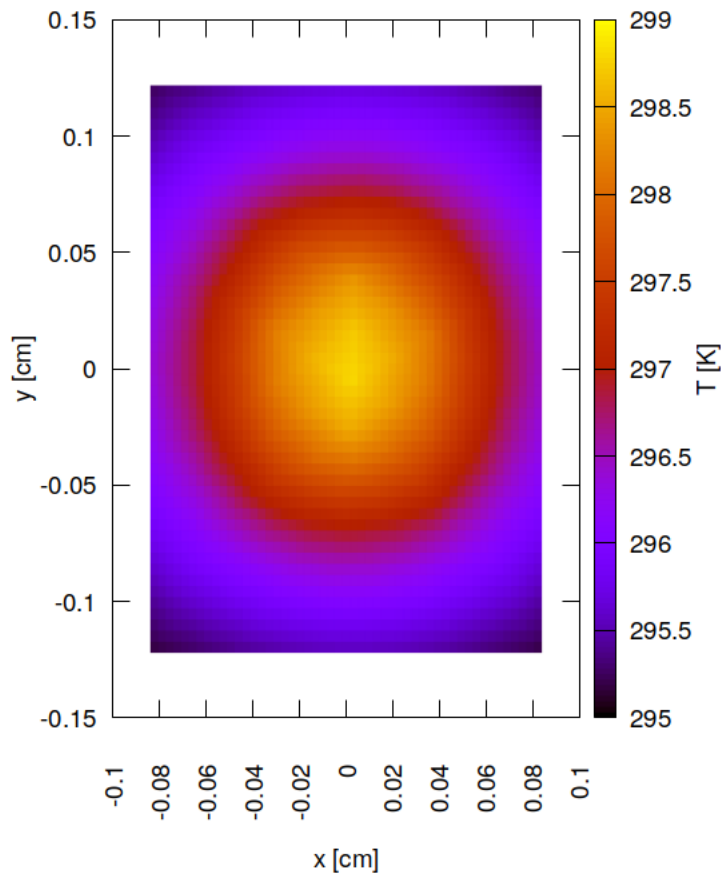


Figure 17.31: Temperature on surface of optical element #03 (BS) for case #26 for 21800 eV photon energy setting.

"fig/BS\_choice\_C111\_Laue/plot032.png" Lbl.:BS\_choice\_C111\_Laue\_false\_colour\_plot\_T\_oe03\_c36\_21800eV

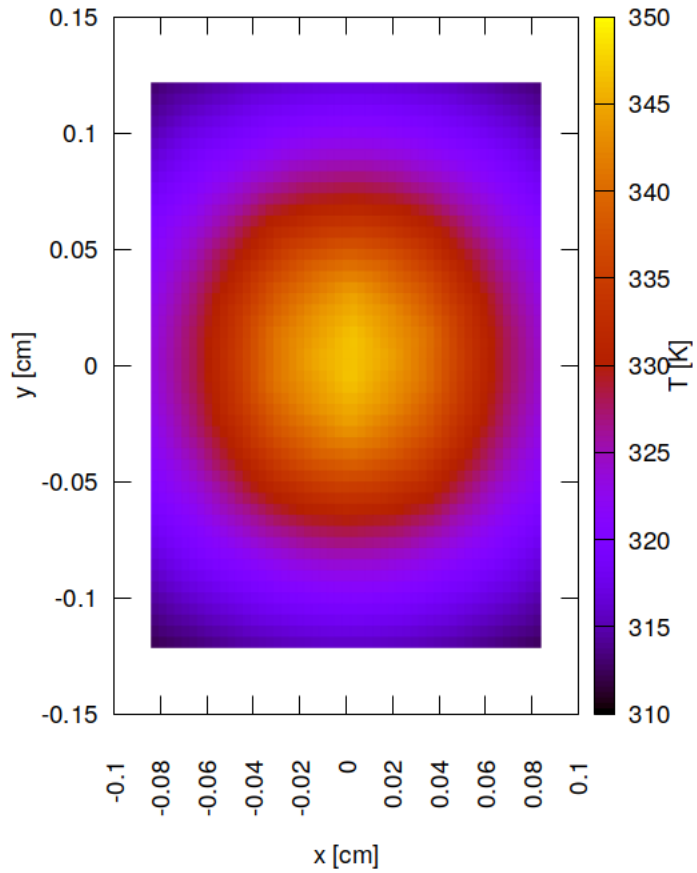


Figure 17.32: Temperature on surface of optical element #03 (BS) for case #36 for 21800 eV photon energy setting.

## 17.11 Mechanical stress (Von Mises stress) on surface

"fig/BS\_choice\_C111\_Laue/plot033.png" Lbl.:BS\_choice\_C111\_Laue\_false\_colour\_plot\_sigma\_oe03\_c16\_21800eV

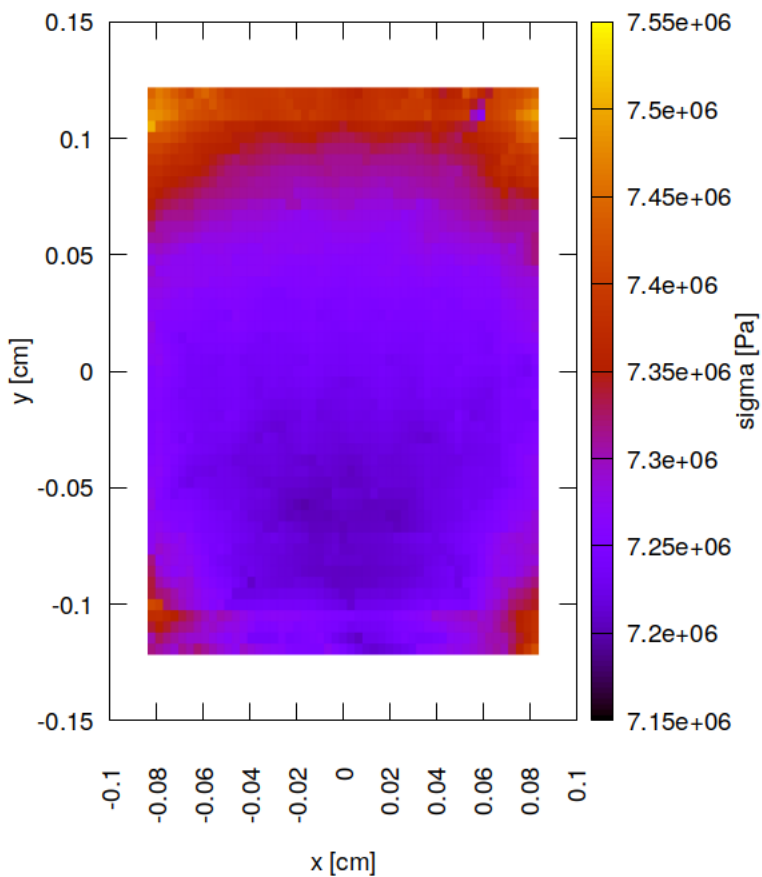


Figure 17.33: Mechanical stress (Von Mises stress) on surface of optical element #03 (BS) for case #16 for 21800 eV photon energy setting.

"fig/BS\_choice\_C111\_Laue/plot034.png" Lbl.:BS\_choice\_C111\_Laue\_false\_colour\_plot\_sigma\_oe03\_c26\_21800eV

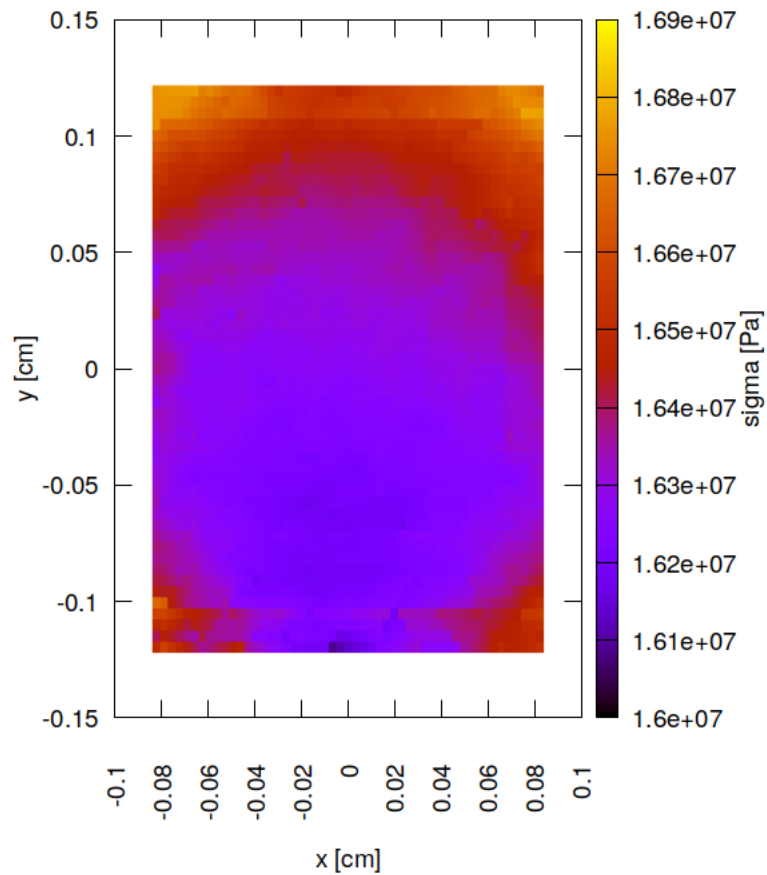


Figure 17.34: Mechanical stress (Von Mises stress) on surface of optical element #03 (BS) for case #26 for 21800 eV photon energy setting.

```
"fig/BS_choice_C111_Laue/plot035.png" Lbl.:BS_choice_C111_Laue_false_colour_plot_sigma_oe03_c36_21800eV
```

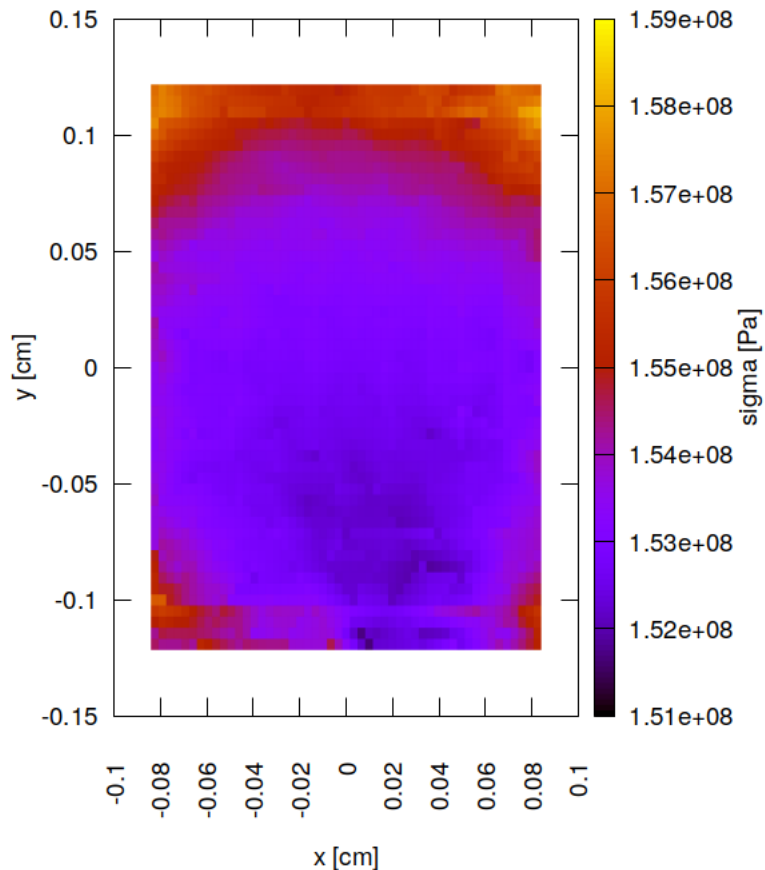


Figure 17.35: Mechanical stress (Von Mises stress) on surface of optical element #03 (BS) for case #36 for 21800 eV photon energy setting.

## 17.12 Surface slope error in meridional direction (y)

"fig/BS\_choice\_C111\_Laue/plot036.png" Lbl.:BS\_choice\_C111\_Laue\_false\_colour\_plot\_phi\_y\_oe03\_c16\_21800eV

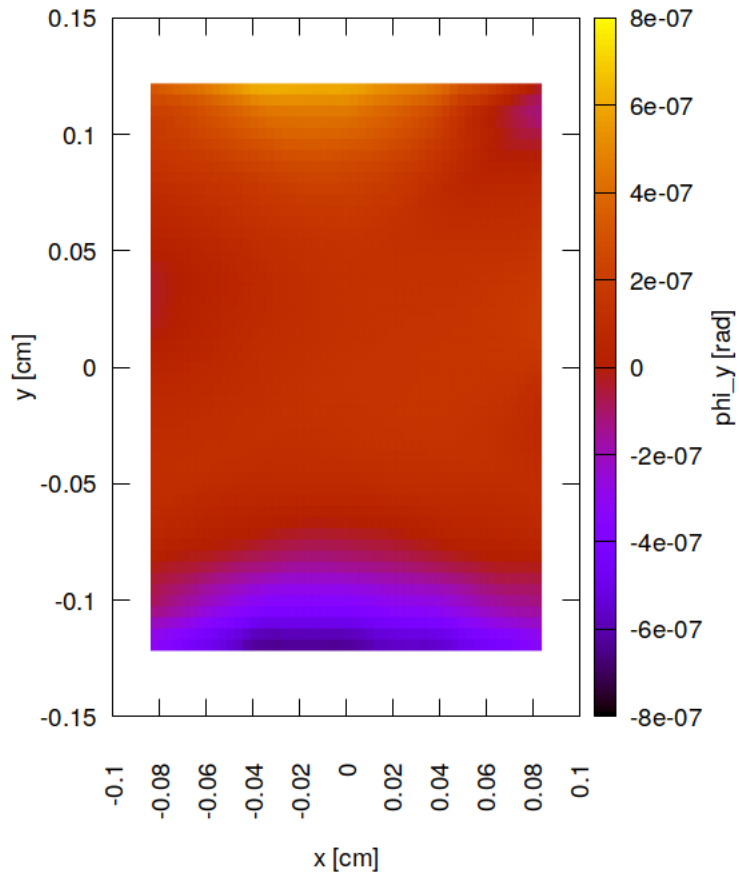


Figure 17.36: Surface slope error in meridional direction (y) of optical element #03 (BS) for case #16 for 21800 eV photon energy setting.

"fig/BS\_choice\_C111\_Laue/plot037.png" Lbl.:BS\_choice\_C111\_Laue\_false\_colour\_plot\_phi\_y\_oe03\_c26\_21800eV

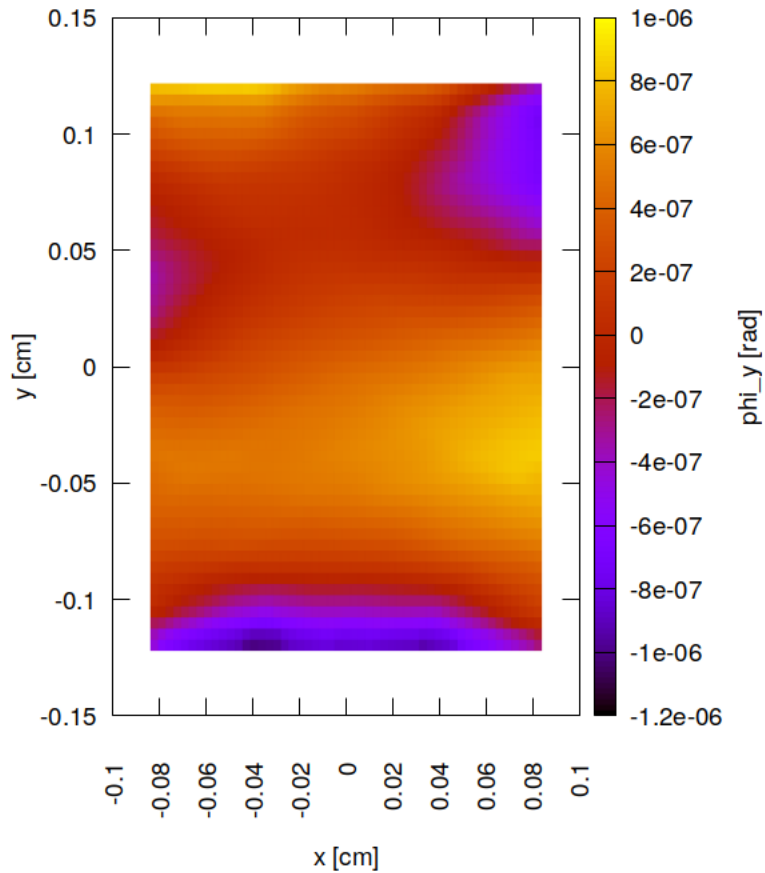


Figure 17.37: Surface slope error in meridional direction (y) of optical element #03 (BS) for case #26 for 21800 eV photon energy setting.

```
"fig/BS_choice_C111_Laue/plot038.png" Lbl.:BS_choice_C111_Laue_false_colour_plot_phi_y_oe03_c36_21800eV
```

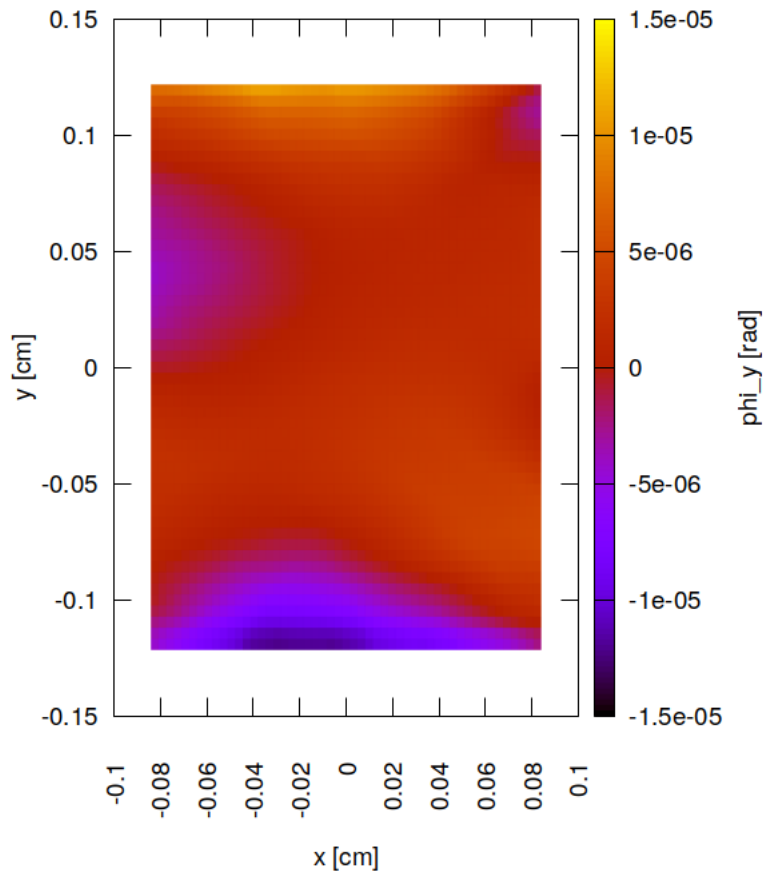


Figure 17.38: Surface slope error in meridional direction (y) of optical element #03 (BS) for case #36 for 21800 eV photon energy setting.



## 17.13 Incident photon irradiance on surface

"fig/BS\_choice\_C111\_Laue/plot039.png" Lbl.:BS\_choice\_C111\_Laue\_false\_colour\_plot\_I\_inc\_foot\_oe04\_c6\_21800eV

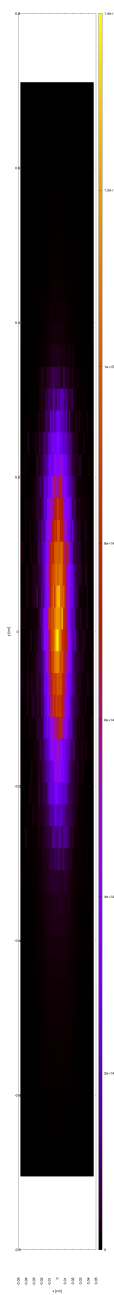


Figure 17.39: Incident photon irradiance on surface of optical element #04 (CM2) for case #6 for 21800 eV photon energy setting.

```
"fig/BS_choice_C111_Laue/plot040.png" Lbl.:BS_choice_C111_Laue_false_colour_plot_I_inc_foot_oe04_c16_21800eV
```

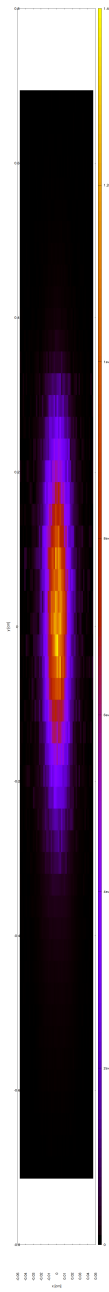


Figure 17.40: Incident photon irradiance on surface of optical element #04 (CM2) for case #16 for 21800 eV photon energy setting.

"fig/BS\_choice\_C111\_Laue/plot041.png" Lbl.:BS\_choice\_C111\_Laue\_false\_colour\_plot\_I\_inc\_foot\_oe04\_c26\_21800eV

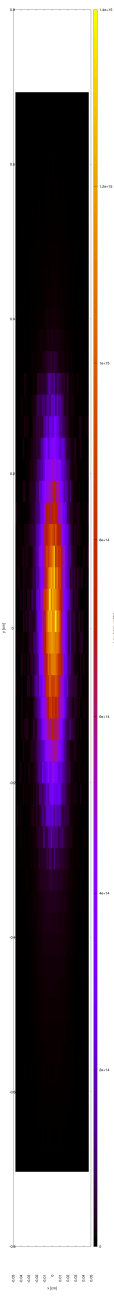


Figure 17.41: Incident photon irradiance on surface of optical element #04 (CM2) for case #26 for 21800 eV photon energy setting.

```
"fig/BS_choice_C111_Laue/plot042.png" Lbl.:BS_choice_C111_Laue_false_colour_plot_I_inc_foot_oe04_c36_21800eV
```

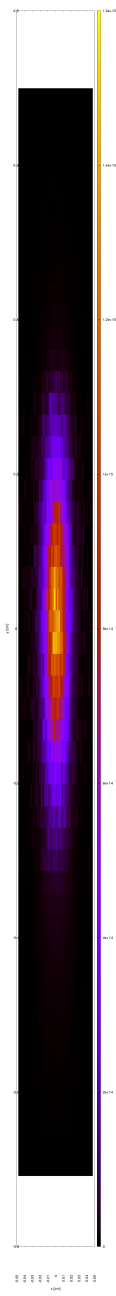


Figure 17.42: Incident photon irradiance on surface of optical element #04 (CM2) for case #36 for 21800 eV photon energy setting.



## 17.14 Photon irradiance in beam cross section

"fig/BS\_choice\_C111\_Laue/plot043.png" Lbl.:BS\_choice\_C111\_Laue\_false\_colour\_plot\_I\_foc\_oe04\_c6\_21800eV

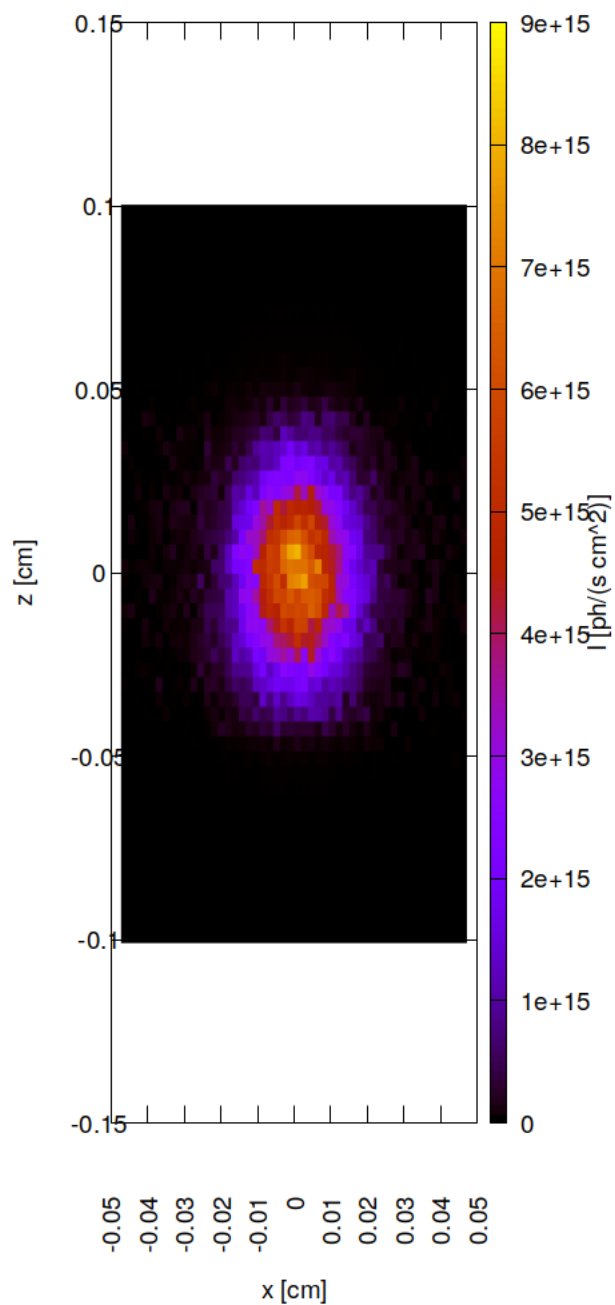


Figure 17.43: Photon irradiance in beam cross section of optical element #04 (CM2) for case #6 for 21800 eV photon energy setting.

"fig/BS\_choice\_C111\_Laue/plot044.png" Lbl.:BS\_choice\_C111\_Laue\_false\_colour\_plot\_I\_foc\_oe04\_c16\_21800eV

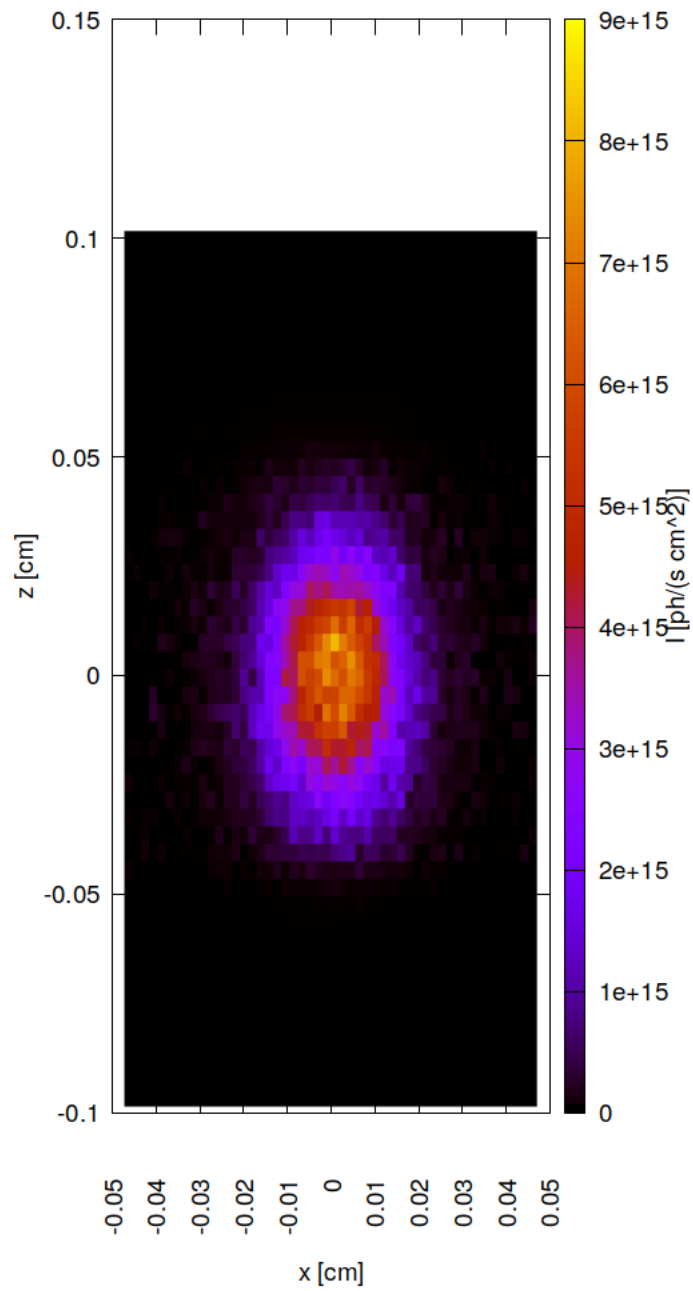


Figure 17.44: Photon irradiance in beam cross section of optical element #04 (CM2) for case #16 for 21800 eV photon energy setting.

"fig/BS\_choice\_C111\_Laue/plot045.png" Lbl.:BS\_choice\_C111\_Laue\_false\_colour\_plot\_I\_foc\_oe04\_c26\_21800eV

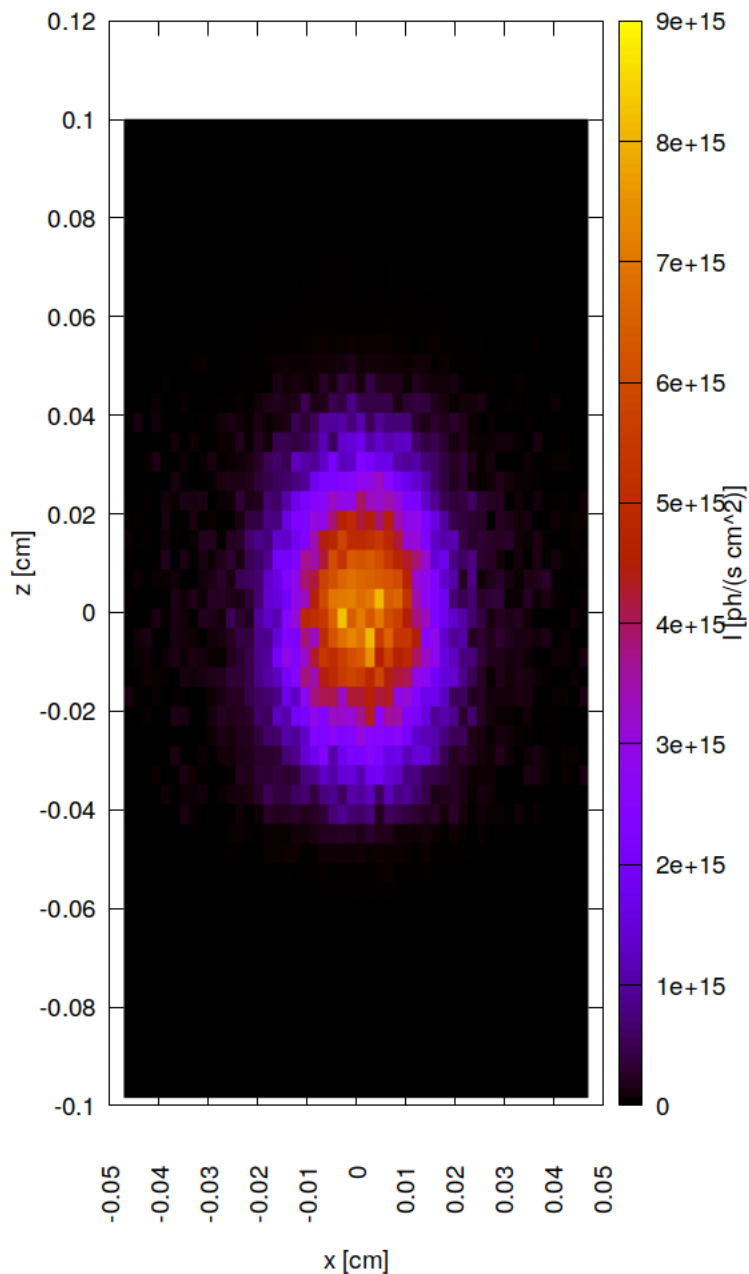


Figure 17.45: Photon irradiance in beam cross section of optical element #04 (CM2) for case #26 for 21800 eV photon energy setting.

```
"fig/BS_choice_C111_Laue/plot046.png" Lbl.:BS_choice_C111_Laue_false_colour_plot_I_foc_oe04_c36_21800eV
```

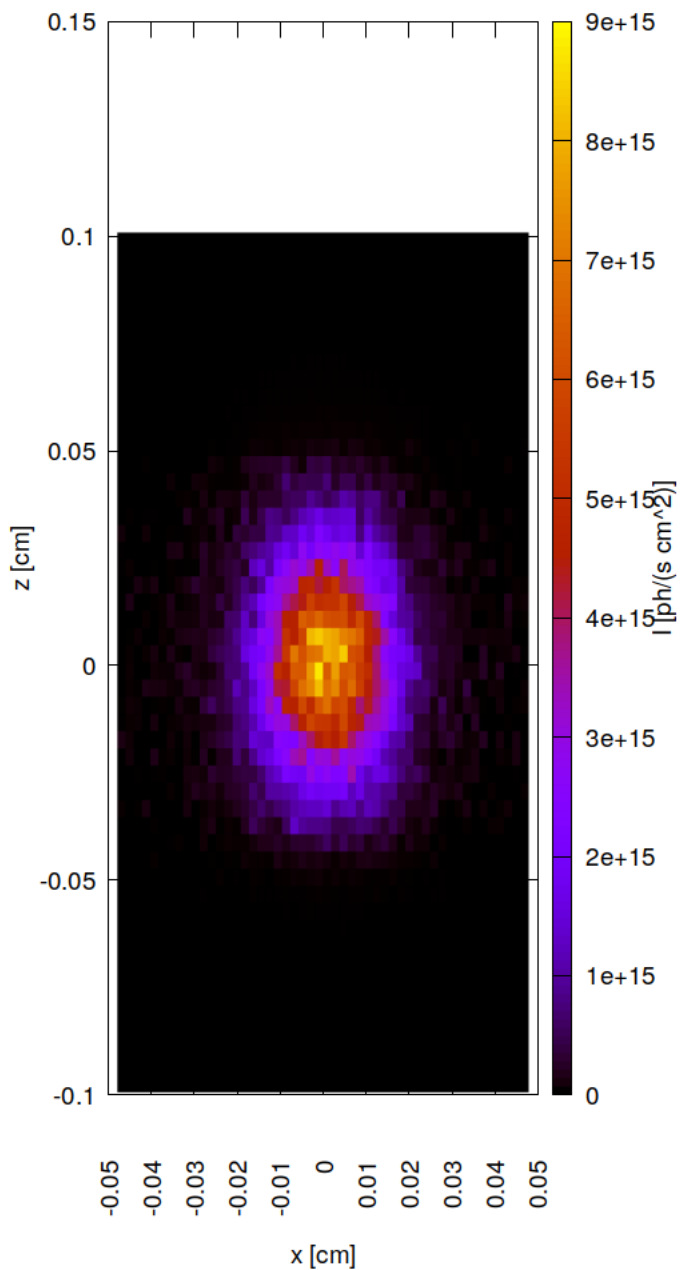


Figure 17.46: Photon irradiance in beam cross section of optical element #04 (CM2) for case #36 for 21800 eV photon energy setting.

## 17.15 Spectral photon flux in beam cross section

```
"fig/BS_choice_C111_Laue/plot047.png" Lbl.:BS_choice_C111_Laue_2d_plot_I_bandfoc_oe04_c6_21800eV
```

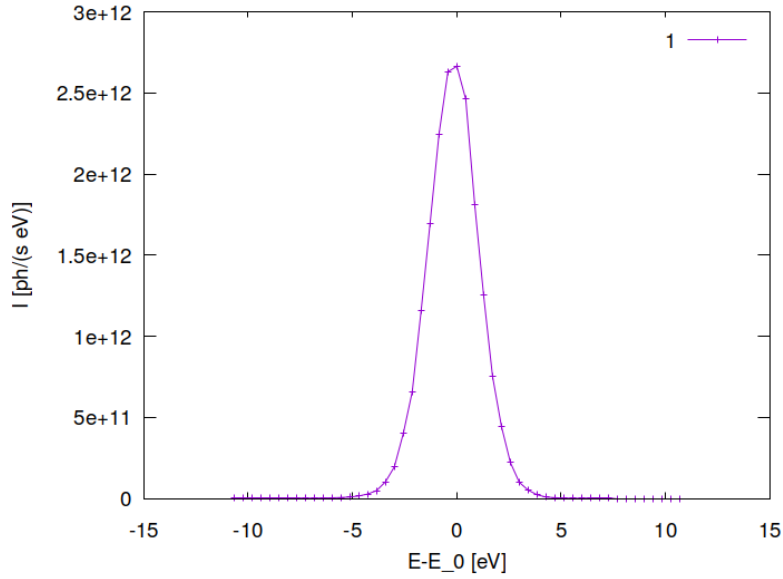


Figure 17.47: Spectral photon flux in beam cross section of optical element #04 (CM2) for case #6 for 21800 eV photon energy setting.

```
"fig/BS_choice_C111_Laue/plot048.png" Lbl.:BS_choice_C111_Laue_2d_plot_I_bandfoc_oe04_c16_21800eV
```

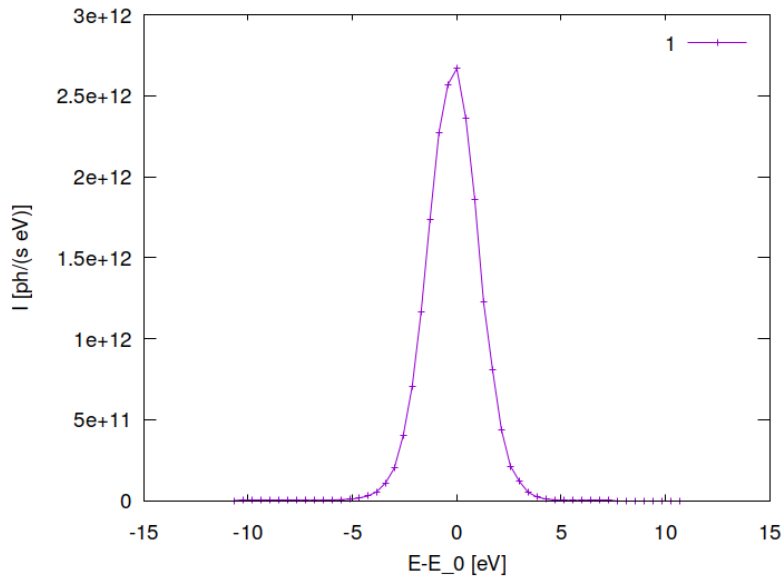


Figure 17.48: Spectral photon flux in beam cross section of optical element #04 (CM2) for case #16 for 21800 eV photon energy setting.

```
"fig/BS_choice_C111_Laue/plot049.png" Lbl.:BS_choice_C111_Laue_2d_plot_I_bandfoc_oe04_c26_21800eV
```

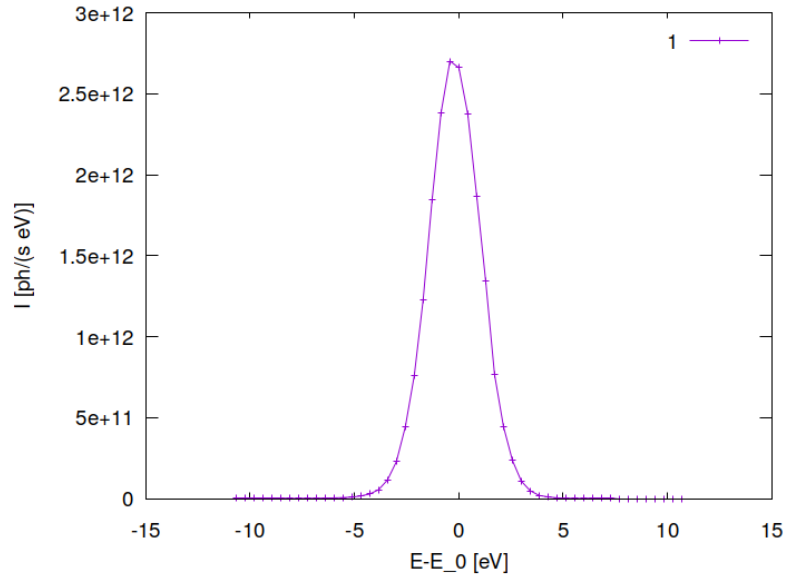


Figure 17.49: Spectral photon flux in beam cross section of optical element #04 (CM2) for case #26 for 21800 eV photon energy setting.

```
"fig/BS_choice_C111_Laue/plot050.png" Lbl.:BS_choice_C111_Laue_2d_plot_I_bandfoc_oe04_c36_21800eV
```

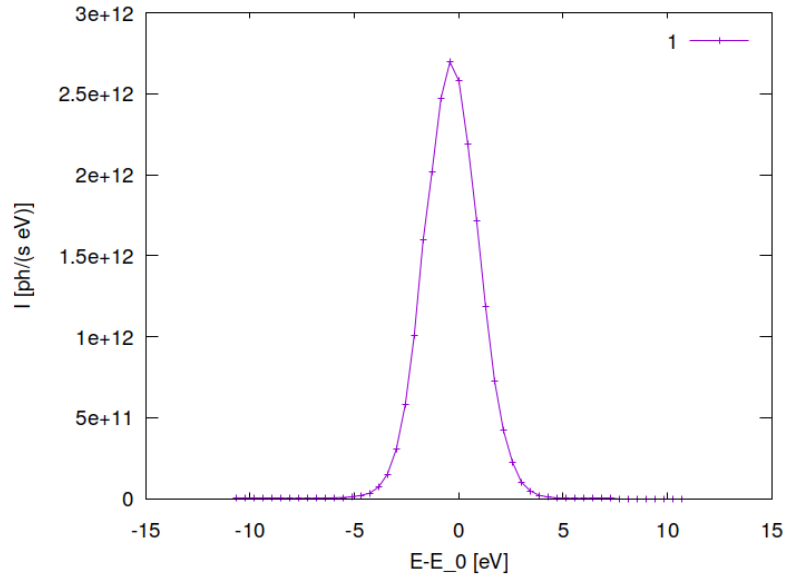


Figure 17.50: Spectral photon flux in beam cross section of optical element #04 (CM2) for case #36 for 21800 eV photon energy setting.

## Chapter 18

# Setup with diamond 111 beam splitter in Bragg geometry

A thin CVD diamond crystal is used as a diffractive beam splitter, using the 111 reflection in Bragg geometry. The diamond 111 reflection diverts radiation within a narrow bandwidth (RMS) of

$$\delta E/E = \delta\theta/\tan\theta$$

to the SinCrys side branch.

Subsequent reflection from a second crystal with equal inter-planar spacing and diffracting planes parallel to the first is the golden standard in crystal monochromator design, which is followed here.

Germanium 220 has an inter-planar spacing very close to that of diamond 111. It differs by only 3%. As germanium is cheaper, readily available in better quality and actually more efficient than diamond for the reflections in question (larger structure factor), Ge220 in Bragg geometry is chosen for the second crystal here.

Putting the second crystal at a distance of around 3.66 metres behind the first provides the required offset of more than one metre between the twice deflected beam and the main beam.

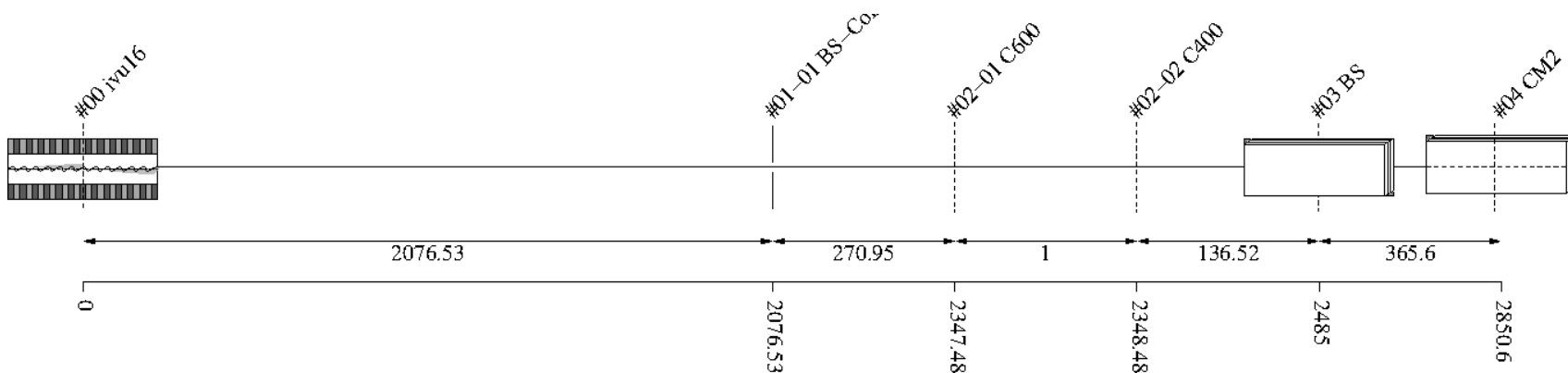


Figure 18.1: Schematic of optical setup

#	Name	Pathlen. cm	Descript.	Shape	Pitch* deg	Roll deg	Yaw deg	x_min cm	x_max cm	y_min cm	y_max cm	Thick. cm	Surface
0	ivu16	0	undulator	auto	0	0	0	-0.0027	0.0027	-0.0002	0.0002	0.0002	auto
1		2076.53	none	plane	0	0	0	-inf	inf	-inf	inf		perfect
1-1	BS-Collim	2076.53	aperture	rectangle	0	0	0	-0.035	0.035	-0.035	0.035	0.035	
2	Filter	2347.48	none	plane	0	0	0	-inf	inf	-inf	inf		perfect
2-1	C600	2347.48	C-filter	rectangle	0	0	0	-inf	inf	-inf	inf	0.06	
2-2	C400	2348.48	C-filter	rectangle	0	0	0	-inf	inf	-inf	inf	0.04	
3	BS	2485	C(1,1,1)-crystal	plane	7.93694	90	0	-0.15	0.15	-0.5	0.5		heat bump
4	CM2	2850.6	Ge(2,2,0)-crystal	plane	8.17292	180	0	-inf	inf	-inf	inf		perfect

Table 18.1: Setup parameters common to all components. (\*Glancing angle for mirrors, multilayers and crystals. Angle to surface normal otherwise.)

**Rays:** Polar type = total

Polar phase = 0 deg

Polar degree = 0

Is coherent = no

**Spectrum:** E min = 500 eV

E max = 40000 eV

Relative linewidth = 1

**Band:** Bandwidth = 0.0005

**Insertion Device:** lambda period = 1.6 cm

n period = 187

I electron = 0.5 A

E electron = 3 GeV

y horizontal waist = 0 cm

y vertical waist = 0 cm

epsilon x = 3.2E-08 cm rad

epsilon z = 8E-10 cm rad

K y = 1.66

K ymax = 1.7

Divergence limit = 5E-05 rad

**Undulator:** n harmonic max = 99

Tuning type = fixed gap

l aperture = 2076.53 cm

dx aperture = 0.07 cm

dz aperture = 0.07 cm

#1

**Screen:** Is absorbing[1] = no

**Shape:** Thickness = 0 cm

#2 Filter

**Screen:** Is absorbing[1] = yes

Is absorbing[2] = yes

Molecular formula[1] = C

Molecular formula[2] = C

Mass density[1] = 3.5 g/cm^3

Mass density[2] = 3.5 g/cm^3

Thickness[1] = 0.06 cm

Thickness[2] = 0.04 cm

**Shape:** Thickness = 0 cm

### #3 BS

**Crystal:** Structure type = zinblend

Lattice constant[1] = 3.567 Angstrom  
Lattice constant[2] = 3.567 Angstrom  
Lattice constant[3] = 3.567 Angstrom  
Debye Waller factor = 1  
Is absorbing = yes  
Is asymmetric = no  
Is inclined = no  
Is Johansson geometry = no  
Is mosaic = no

**Tune:** z rotation axis = 0 cm

**Geometry:** Is thin = yes

Tune automatic = yes

**Shape:** Thickness = 0.01 cm

**Boundary:** Type = rectangle

x rim = 0.5 cm  
y rim = 0.5 cm

**Surface:** Is rough = no

**FEA:** Design type = type specific

Crystal design = laue with cooling loop  
Is isotropic = no  
Angle x = 0 deg  
Angle y = 0 deg  
Angle z = 0 deg  
Mass density = 3.516 g/cm<sup>3</sup>

**Heat:** Heat transfer type[1] = insulated

Heat transfer type[2] = heat transfer  
Heat transfer type[3] = insulated  
Heat transfer type[4] = insulated  
Heat transfer type[5] = heat transfer  
Heat transfer type[6] = flux  
Heat transfer type[7] = insulated  
Heat transfer type[8] = heat transfer  
Heat transfer type[9] = heat sink  
Heat transfer coefficient = 1 W/(cm<sup>2</sup>K)  
Heat sink coefficient = 10 W/(cm<sup>2</sup>K)  
T reference = 293.15 K  
T cooling = 293.15 K  
Heat capacity = 0.54 J/(gK)  
Thermal conductivity[1] = 25 W/(cmK<sup>n</sup>)

**Stress and strain:** Constraint[1] = free  
 Constraint[2] = kinematic  
 Constraint[3] = free  
 Constraint[4] = free  
 Constraint[5] = free  
 Constraint[6] = free  
 Constraint[7] = free  
 Constraint[8] = free  
 Constraint[9] = free  
 Thermal expansion tensor[1] = 1.1E-06 1/K  
 Thermal expansion tensor[2] = 1.1E-06 1/K  
 Thermal expansion tensor[3] = 1.1E-06 1/K  
 Thermal expansion tensor[4] = 0 1/K  
 Thermal expansion tensor[5] = 0 1/K  
 Thermal expansion tensor[6] = 0 1/K  
 Stiffness tensor(1)(1) = 1.07861E+12 Pa  
 Stiffness tensor(2)[1] = 1.2663E+11 Pa  
 Stiffness tensor(2)[2] = 1.07861E+12 Pa  
 Stiffness tensor(3)[1] = 1.2663E+11 Pa  
 Stiffness tensor(3)[2] = 1.2663E+11 Pa  
 Stiffness tensor(3)[3] = 1.07861E+12 Pa  
 Stiffness tensor(4)[1] = 0 Pa  
 Stiffness tensor(4)[2] = 0 Pa  
 Stiffness tensor(4)[3] = 0 Pa  
 Stiffness tensor(4)[4] = 5.7756E+11 Pa  
 Stiffness tensor(5)[1] = 0 Pa  
 Stiffness tensor(5)[2] = 0 Pa  
 Stiffness tensor(5)[3] = 0 Pa  
 Stiffness tensor(5)[4] = 0 Pa  
 Stiffness tensor(5)[5] = 5.7756E+11 Pa  
 Stiffness tensor(6)[1] = 0 Pa  
 Stiffness tensor(6)[2] = 0 Pa  
 Stiffness tensor(6)[3] = 0 Pa  
 Stiffness tensor(6)[4] = 0 Pa  
 Stiffness tensor(6)[5] = 0 Pa  
 Stiffness tensor(6)[6] = 5.7756E+11 Pa

#### #4 CM2

**Crystal:** Structure type = zinblend  
 Lattice constant[1] = 5.6578 Angstrom  
 Lattice constant[2] = 5.6578 Angstrom  
 Lattice constant[3] = 5.6578 Angstrom  
 Debye Waller factor = 1  
 Is absorbing = yes  
 Is asymmetric = no  
 Is inclined = no  
 Is Johansson geometry = no  
 Is mosaic = no

**Tune:** Type = constant pathlength  
 Are downstream elements fixed = no

**Geometry:** Is thin = no  
Tune automatic = yes

**Boundary:** Type = none

**Surface:** Is rough = no

## Chapter 19

# Finite element analysis (FEA)

A description of the FEA model can be found in section 4

There are three different heat load settings in this model. The first is with both diamond filters – 400 and 600 microns thick – in the beam path. This is presently the standard setting at DanMAX which provides the lowest heat load on the beam splitter.

The second setting is with the 600 micron diamond filter moved out. This is in order to compensate for the extra absorption in the beam splitter, to keep flux in the DanMAX main branch the same. This is particularly important in Bragg geometry, since due to the small Bragg angles transmission occurs at a small glancing angle. This makes path lengths long with subsequently higher absorption. For the Bragg angles in question and a beam splitter thickness of 100 microns path length is around 700 microns, which matches quite well with the thicker of the diamond filters.

Finally the third setting is with all diamond filter out, which represents the worst case scenario for the beam splitter in terms of heat load.

## 19.1 FEA with both 600 and 400 micron diamond filters in

"fig/BS\_choice\_C111\_Bragg/fea\_plot\_geom\_c02\_21800eV\_03.png" Lbl.:BS\_choice\_C111\_Bragg\_Surface\_plotfea\_plot\_geom\_c02\_21800eV\_03

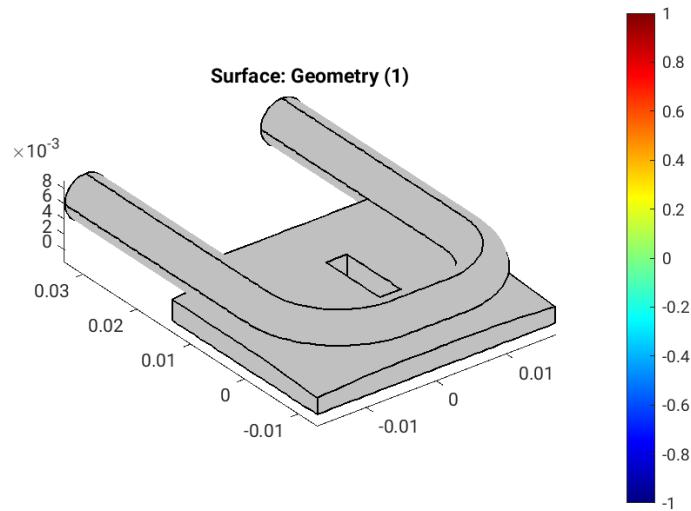


Figure 19.1: Geometry [m] of optical element #03, for case #02, at 21800 eV photon energy setting.

```
"fig/BS_choice_C111_Bragg/fea_plot_cnstr_c02_21800eV_03.png" Lbl.:BS_choice_C111_Bragg_Surface_plot_fea_plot_cnstr_c02_21800eV_03
```

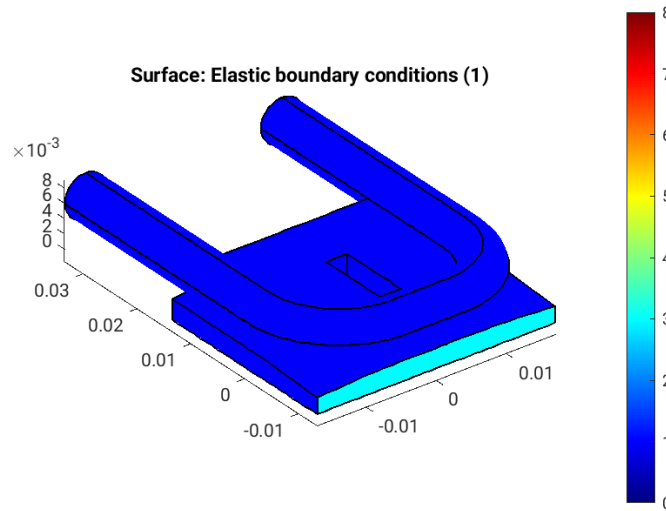


Figure 19.2: Elastic boundary conditions on the surfaces of optical element #03, for case #02, at 21800 eV photon energy setting. Color legend: Blue: Surface can move freely in all directions. Cyan: Tension free kinematic mounting. Minimalistic constraint for three points in surface. One point is fixed, the second can move in one direction, and the third in two, in a fashion that defines angular orientation without introducing stress if the surface expands.

```
"fig/BS_choice_C111_Bragg/fea_plot_trans_c02_21800eV_03.png" Lbl.:BS_choice_C111_Bragg_Surface_plot_fea_plot_trans_c02_21800eV_03
```

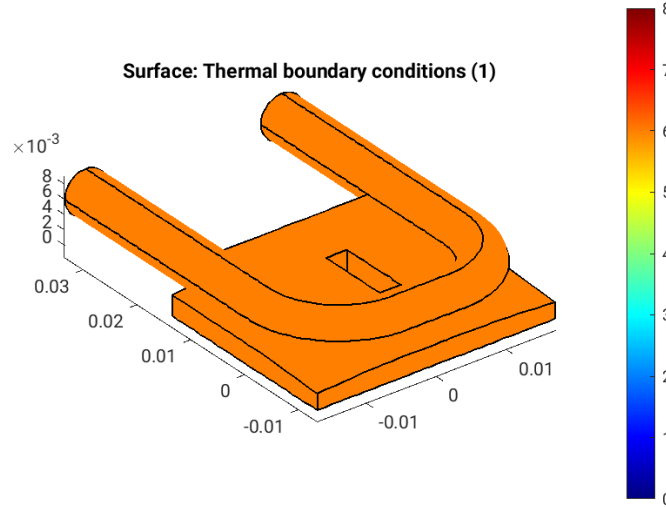


Figure 19.3: Thermal boundary conditions on the surfaces of optical element #03, for case #02, at 21800 eV photon energy setting. Color legend: Orange: No heat transfer at all. Blue: Heat transfer coefficient and temperature difference define heat current density,  $j_q = h(T - T_{cool})$ . Red: Forced heat flux from e.g. absorbed X-rays. Cyan: Heat transfer coefficient and temperature difference define heat current density,  $j_q = h^* \Delta T$  (only at inner surfaces).

```
"fig/BS_choice_C111_Bragg/fea_plot_heattrans_c02_21800eV_03.png" Lbl.:BS_choice_C111_Bragg_Surface_plot_fea_plot_heattrans_c02_21800eV_03
```

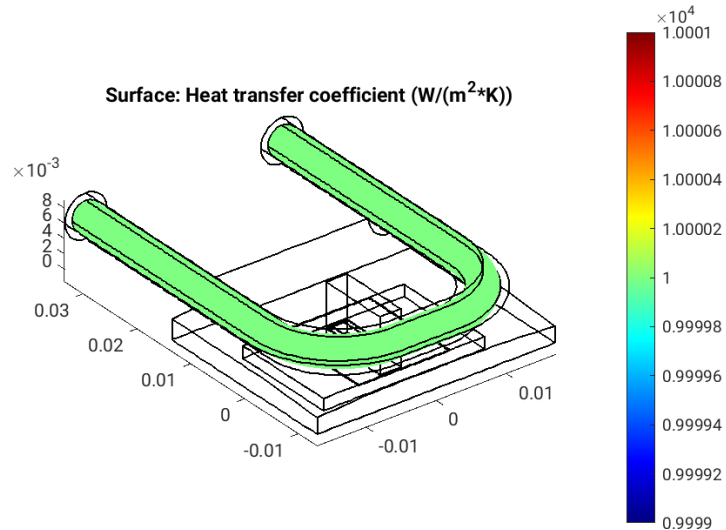


Figure 19.4: Heat transfer coefficient,  $h$  [ $W/(m^2 \cdot K)$ ], on the surfaces of optical element #03, for case #02, at 21800 eV photon energy setting.

```
"fig/BS_choice_C111_Bragg/fea_plot_heatflux_c02_21800eV_03.png" Lbl.:BS_choice_C111_Bragg_Surface_plotfea_plot_heatflux_c02_21800eV_03
```

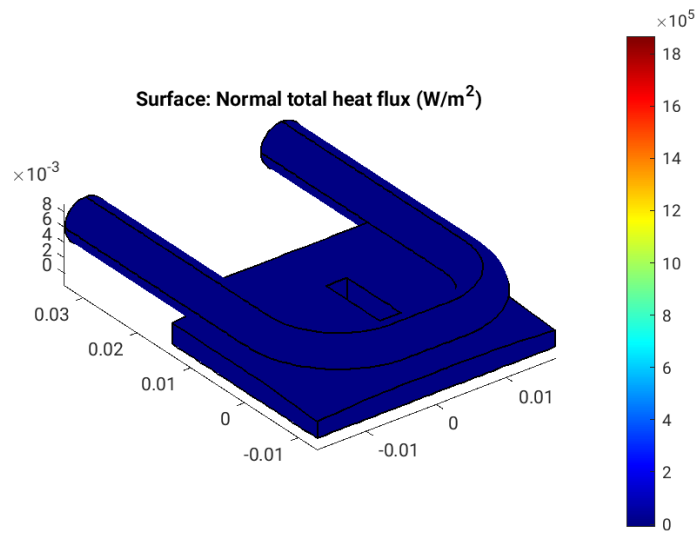


Figure 19.5: Absorbed irradiance,  $p_{\text{abs}}$  [W/m<sup>2</sup>], on the surfaces of optical element #03, for case #02, at 21800 eV photon energy setting.

```
"fig/BS_choice_C111_Bragg/fea_plot_temp_c02_21800eV_03.png" Lbl.:BS_choice_C111_Bragg_Surface_plotfea_plot_temp_c02_21800eV_03
```

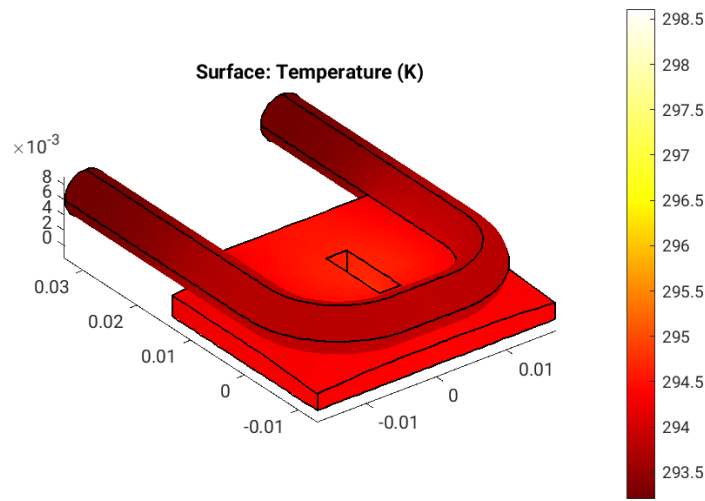


Figure 19.6: Temperature,  $T$  [K], on the surfaces of optical element #03, for case #02, at 21800 eV photon energy setting.

"fig/BS\_choice\_C111\_Bragg/fea\_plot\_thermcond\_c02\_21800eV\_03.png" Lbl.:BS\_choice\_C111\_Bragg\_Surface\_plot\_fea\_plot\_thermcond\_c02\_21800eV\_

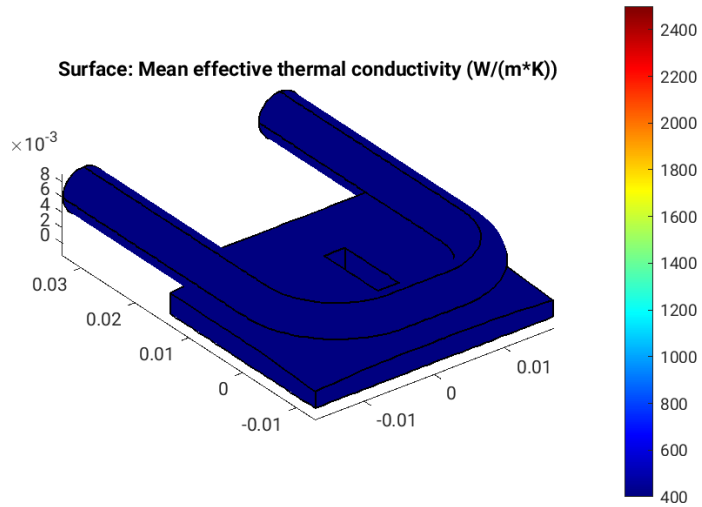


Figure 19.7: Thermal conductivity, lambda [W/(m K)], on the surfaces of optical element #03, for case #02, at 21800 eV photon energy setting.

"fig/BS\_choice\_C111\_Bragg/fea\_plot\_stress\_c02\_21800eV\_03.png" Lbl.:BS\_choice\_C111\_Bragg\_Surface\_plot\_fea\_plot\_stress\_c02\_21800eV\_03

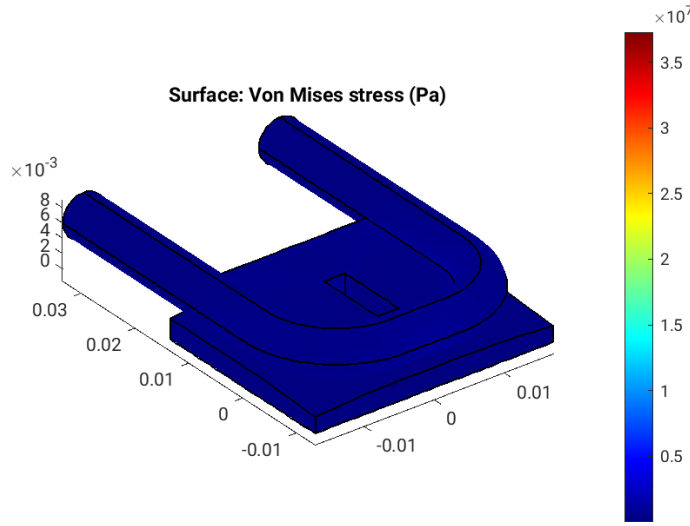


Figure 19.8: Von Mises stress, sigma [Pa], on the surfaces of optical element #03, for case #02, at 21800 eV photon energy setting.

```
"fig/BS_choice_C111_Bragg/fea_plot_deform_c02_21800eV_03.png" Lbl.:BS_choice_C111_Bragg_Surface_plot_fea_plot_deform_c02_21800eV_03
```

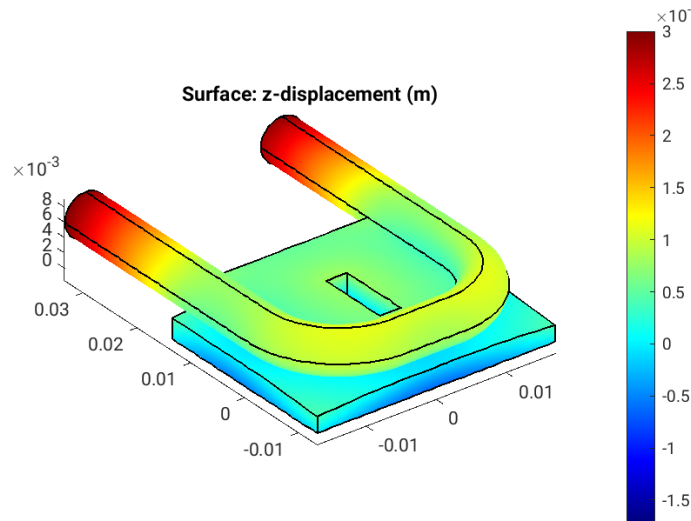


Figure 19.9: Thermoelastic deformation,  $dz$  [m], on the surfaces of optical element #03, for case #02, at 21800 eV photon energy setting.

## 19.2 FEA with only 400 micron diamond filter in

```
"fig/BS_choice_C111_Bragg/fea_plot_geom_c03_21800eV_03.png" Lbl.:BS_choice_C111_Bragg_Surface_plot_fea_plot_geom_c03_21800eV_03
```

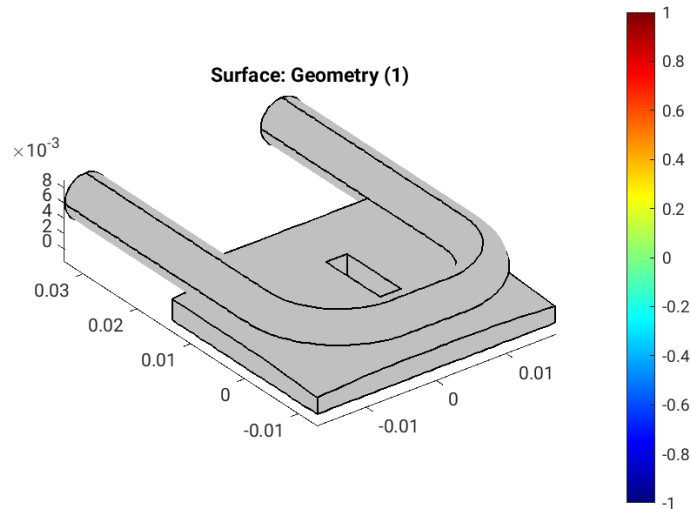


Figure 19.10: Geometry [m] of optical element #03, for case #03, at 21800 eV photon energy setting.

```
"fig/BS_choice_C111_Bragg/fea_plot_cnstr_c03_21800eV_03.png" Lbl.:BS_choice_C111_Bragg_Surface_plot_fea_plot_cnstr_c03_21800eV_03
```

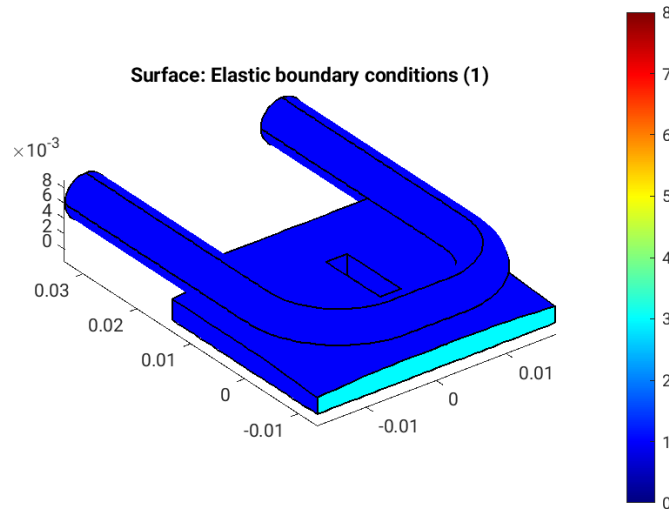


Figure 19.11: Elastic boundary conditions on the surfaces of optical element #03, for case #03, at 21800 eV photon energy setting. Color legend: Blue: Surface can move freely in all directions. Cyan: Tension free kinematic mounting. Minimalistic constraint for three points in surface. One point is fixed, the second can move in one direction, and the third in two, in a fashion that defines angular orientation without introducing stress if the surface expands.

```
"fig/BS_choice_C111_Bragg/fea_plot_trans_c03_21800eV_03.png" Lbl.:BS_choice_C111_Bragg_Surface_plot_fea_plot_trans_c03_21800eV_03
```

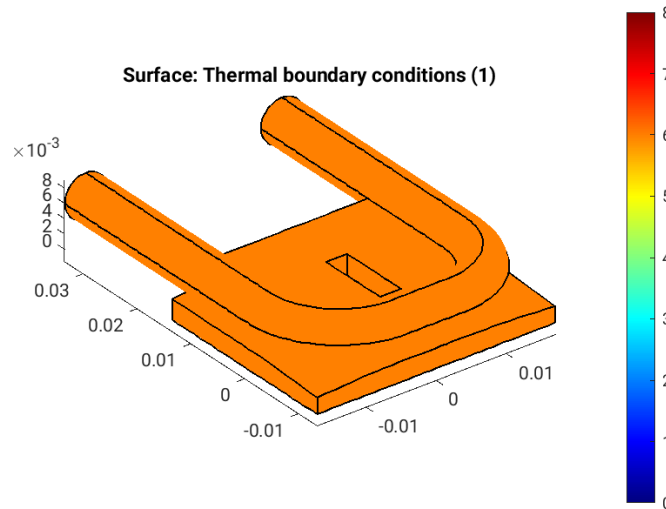


Figure 19.12: Thermal boundary conditions on the surfaces of optical element #03, for case #03, at 21800 eV photon energy setting. Color legend: Orange: No heat transfer at all. Blue: Heat transfer coefficient and temperature difference define heat current density,  $j_q = h(T - T_{cool})$ . Red: Forced heat flux from e.g. absorbed X-rays. Cyan: Heat transfer coefficient and temperature difference define heat current density,  $j_q = h^* \Delta T$  (only at inner surfaces).

```
"fig/BS_choice_C111_Bragg/fea_plot_heattrans_c03_21800eV_03.png" Lbl.:BS_choice_C111_Bragg_Surface_plot_fea_plot_heattrans_c03_21800eV_03
```

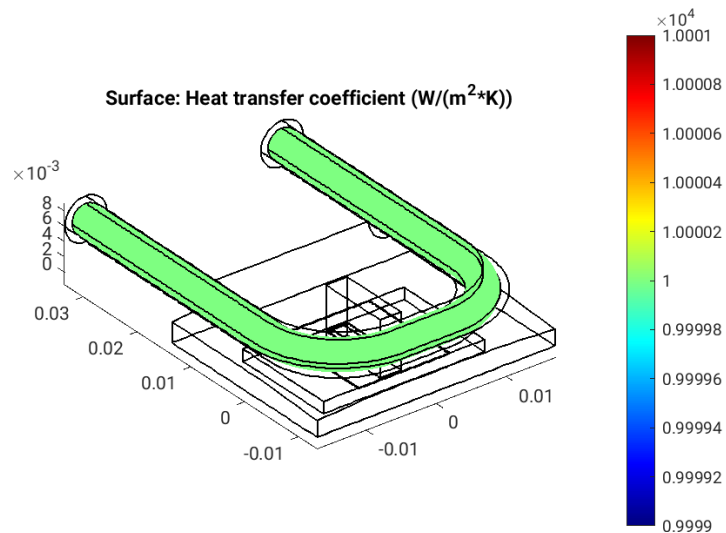


Figure 19.13: Heat transfer coefficient,  $h$  [ $W/(m^2 \cdot K)$ ], on the surfaces of optical element #03, for case #03, at 21800 eV photon energy setting.

```
"fig/BS_choice_C111_Bragg/fea_plot_heatflux_c03_21800eV_03.png" Lbl.:BS_choice_C111_Bragg_Surface_plotfea_plot_heatflux_c03_21800eV_03
```

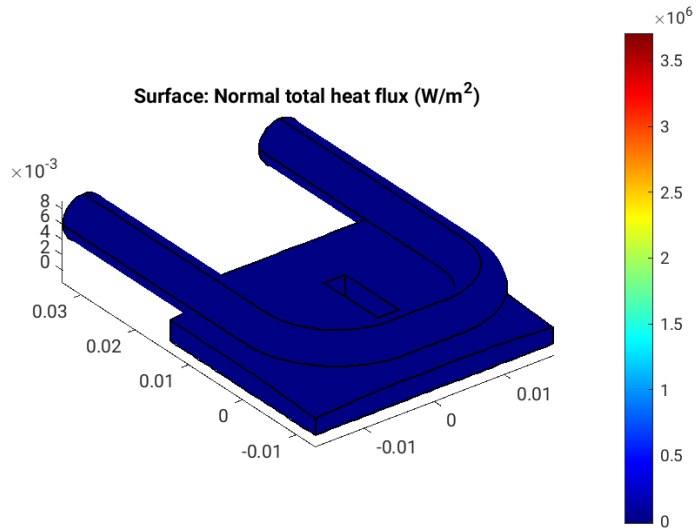


Figure 19.14: Absorbed irradiance,  $p_{\text{abs}}$  [W/m<sup>2</sup>], on the surfaces of optical element #03, for case #03, at 21800 eV photon energy setting.

```
"fig/BS_choice_C111_Bragg/fea_plot_temp_c03_21800eV_03.png" Lbl.:BS_choice_C111_Bragg_Surface_plotfea_plot_temp_c03_21800eV_03
```

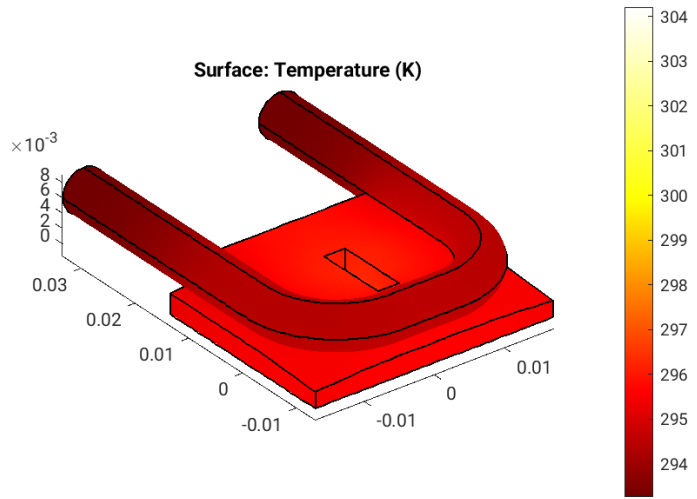


Figure 19.15: Temperature,  $T$  [K], on the surfaces of optical element #03, for case #03, at 21800 eV photon energy setting.

"fig/BS\_choice\_C111\_Bragg/fea\_plot\_thermcond\_c03\_21800eV\_03.png" Lbl.:BS\_choice\_C111\_Bragg\_Surface\_plot\_fea\_plot\_thermcond\_c03\_21800eV\_

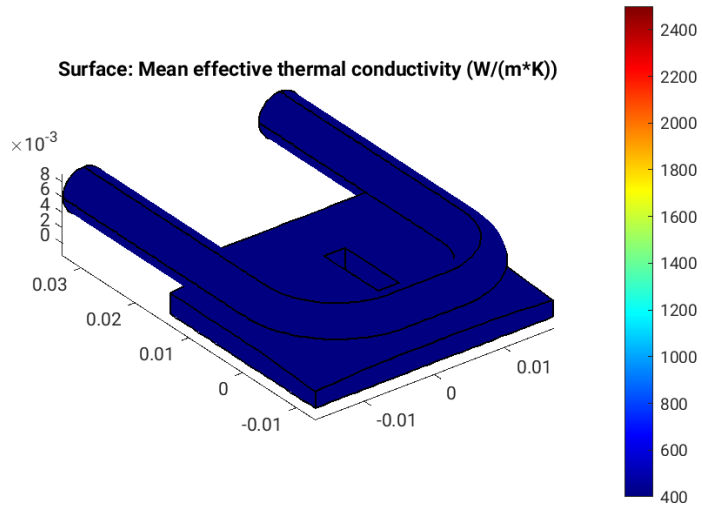


Figure 19.16: Thermal conductivity, lambda [W/(m K)], on the surfaces of optical element #03, for case #03, at 21800 eV photon energy setting.

"fig/BS\_choice\_C111\_Bragg/fea\_plot\_stress\_c03\_21800eV\_03.png" Lbl.:BS\_choice\_C111\_Bragg\_Surface\_plot\_fea\_plot\_stress\_c03\_21800eV\_03

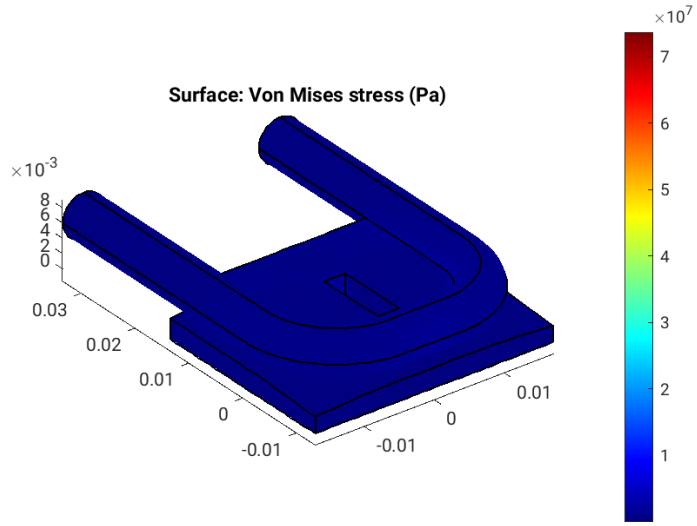


Figure 19.17: Von Mises stress, sigma [Pa], on the surfaces of optical element #03, for case #03, at 21800 eV photon energy setting.

"fig/BS\_choice\_C111\_Bragg/fea\_plot\_deform\_c03\_21800eV\_03.png" Lbl.:BS\_choice\_C111\_Bragg\_Surface\_plot\_fea\_plot\_deform\_c03\_21800eV\_03

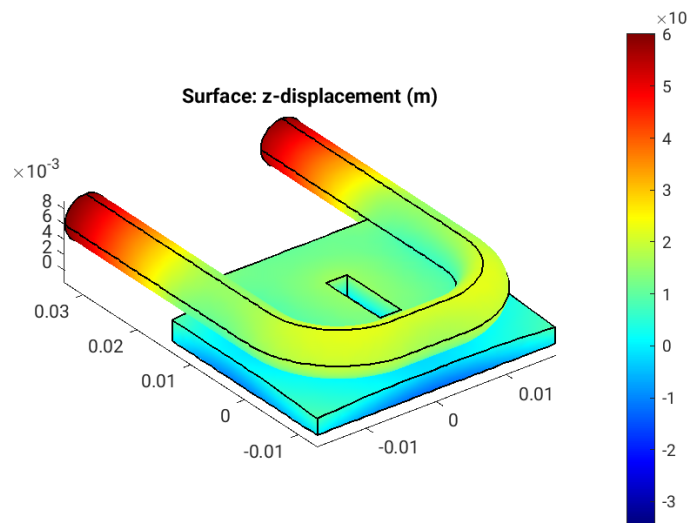


Figure 19.18: Thermoelastic deformation,  $dz$  [m], on the surfaces of optical element #03, for case #03, at 21800 eV photon energy setting.

### 19.3 FEA with no diamond filters in

"fig/BS\_choice\_C111\_Bragg/fea\_plot\_geom\_c04\_21800eV\_03.png" Lbl.:BS\_choice\_C111\_Bragg\_Surface\_plot\_fea\_plot\_geom\_c04\_21800eV\_03

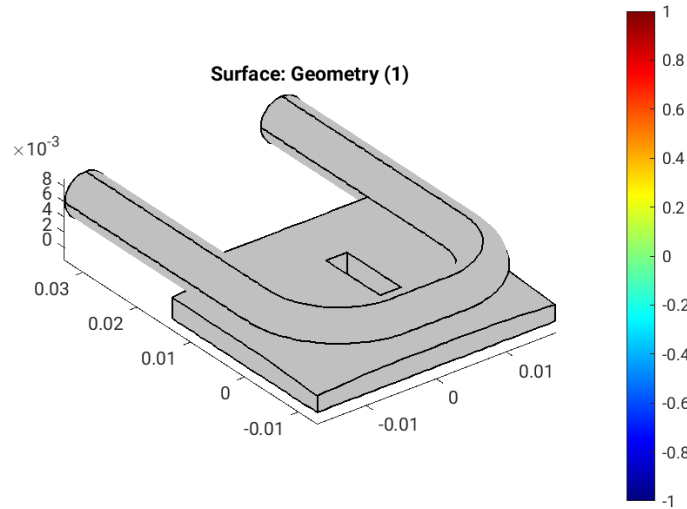


Figure 19.19: Geometry [m] of optical element #03, for case #04, at 21800 eV photon energy setting.

```
"fig/BS_choice_C111_Bragg/fea_plot_cnstr_c04_21800eV_03.png" Lbl.:BS_choice_C111_Bragg_Surface_plot_fea_plot_cnstr_c04_21800eV_03
```

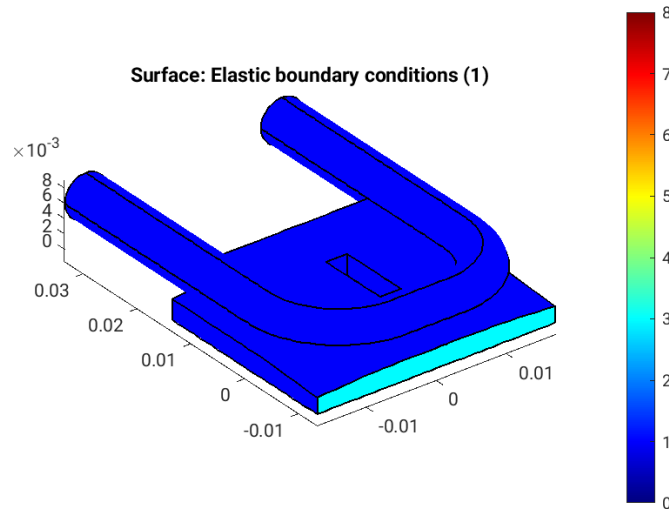


Figure 19.20: Elastic boundary conditions on the surfaces of optical element #03, for case #04, at 21800 eV photon energy setting. Color legend: Blue: Surface can move freely in all directions. Cyan: Tension free kinematic mounting. Minimalistic constraint for three points in surface. One point is fixed, the second can move in one direction, and the third in two, in a fashion that defines angular orientation without introducing stress if the surface expands.

```
"fig/BS_choice_C111_Bragg/fea_plot_trans_c04_21800eV_03.png" Lbl.:BS_choice_C111_Bragg_Surface_plot_fea_plot_trans_c04_21800eV_03
```

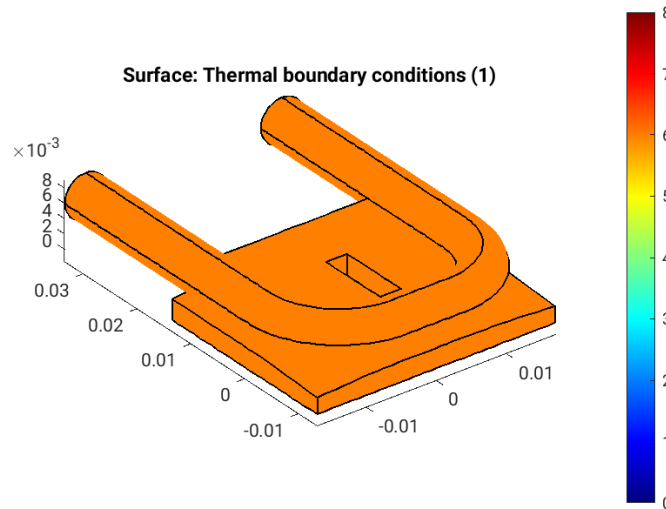


Figure 19.21: Thermal boundary conditions on the surfaces of optical element #03, for case #04, at 21800 eV photon energy setting. Color legend: Orange: No heat transfer at all. Blue: Heat transfer coefficient and temperature difference define heat current density,  $j_q = h(T - T_{cool})$ . Red: Forced heat flux from e.g. absorbed X-rays. Cyan: Heat transfer coefficient and temperature difference define heat current density,  $j_q = h^* \Delta T$  (only at inner surfaces).

```
"fig/BS_choice_C111_Bragg/fea_plot_heattrans_c04_21800eV_03.png" Lbl.:BS_choice_C111_Bragg_Surface_plot_fea_plot_heattrans_c04_21800eV_03
```

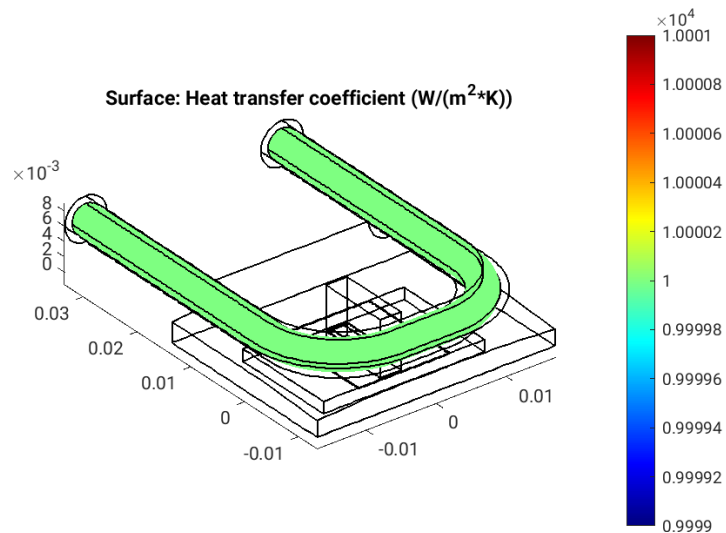


Figure 19.22: Heat transfer coefficient,  $h$  [ $W/(m^2 \cdot K)$ ], on the surfaces of optical element #03, for case #04, at 21800 eV photon energy setting.

```
"fig/BS_choice_C111_Bragg/fea_plot_heatflux_c04_21800eV_03.png" Lbl.:BS_choice_C111_Bragg_Surface_plotfea_plot_heatflux_c04_21800eV_03
```

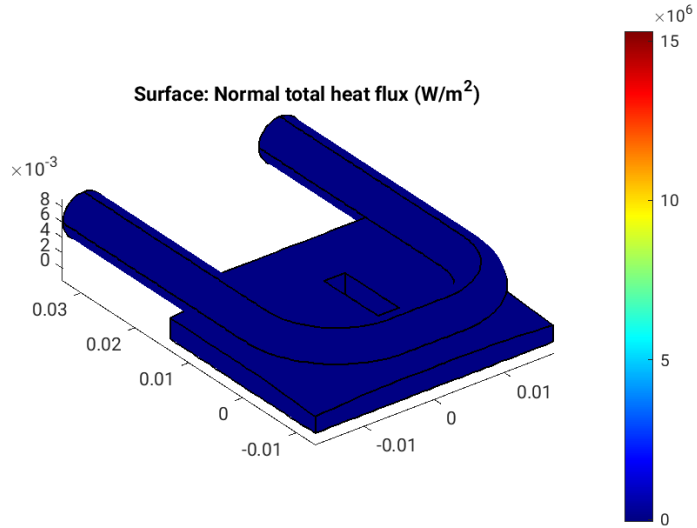


Figure 19.23: Absorbed irradiance,  $p_{\text{abs}}$  [W/m<sup>2</sup>], on the surfaces of optical element #03, for case #04, at 21800 eV photon energy setting.

```
"fig/BS_choice_C111_Bragg/fea_plot_temp_c04_21800eV_03.png" Lbl.:BS_choice_C111_Bragg_Surface_plotfea_plot_temp_c04_21800eV_03
```

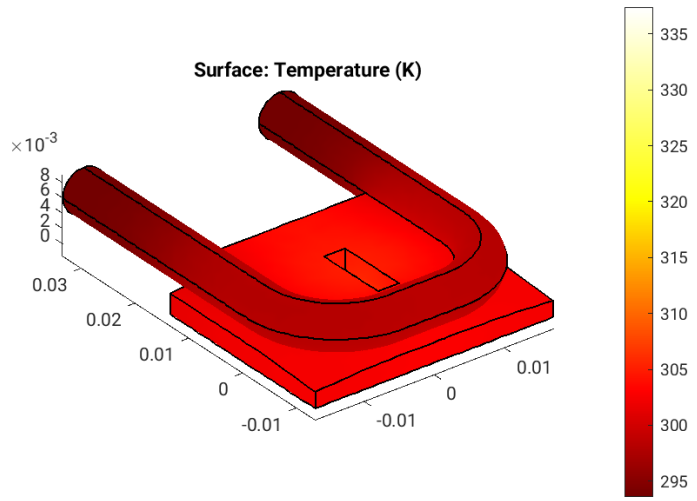


Figure 19.24: Temperature, T [K], on the surfaces of optical element #03, for case #04, at 21800 eV photon energy setting.

"fig/BS\_choice\_C111\_Bragg/fea\_plot\_thermcond\_c04\_21800eV\_03.png" Lbl.:BS\_choice\_C111\_Bragg\_Surface\_plot\_fea\_plot\_thermcond\_c04\_21800eV\_

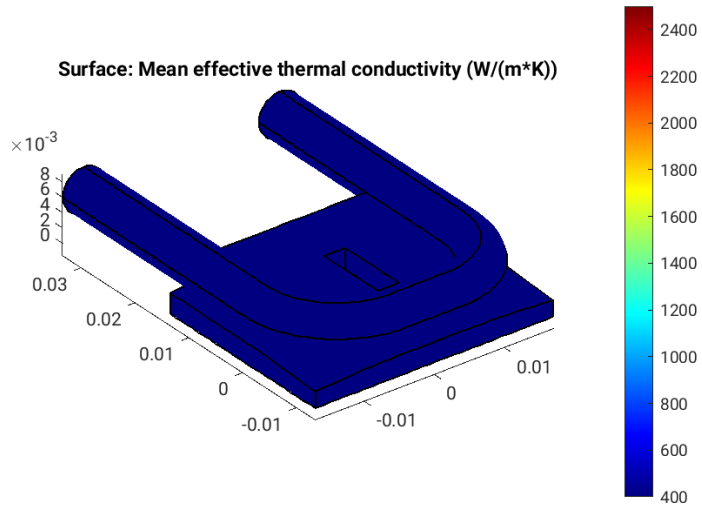


Figure 19.25: Thermal conductivity, lambda [W/(m K)], on the surfaces of optical element #03, for case #04, at 21800 eV photon energy setting.

"fig/BS\_choice\_C111\_Bragg/fea\_plot\_stress\_c04\_21800eV\_03.png" Lbl.:BS\_choice\_C111\_Bragg\_Surface\_plot\_fea\_plot\_stress\_c04\_21800eV\_03

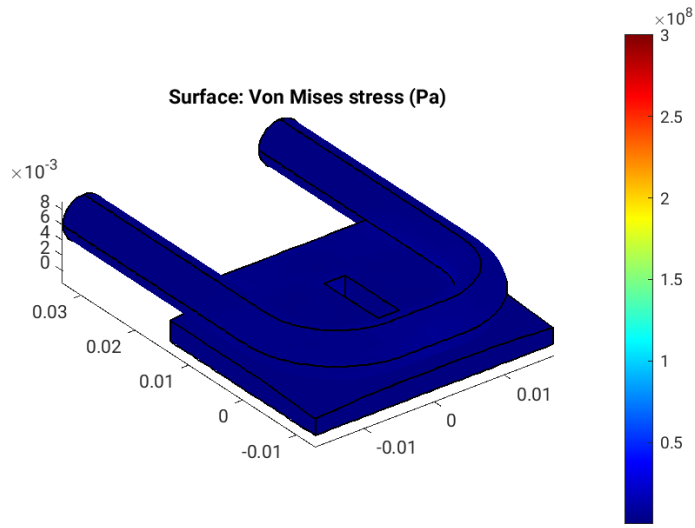


Figure 19.26: Von Mises stress, sigma [Pa], on the surfaces of optical element #03, for case #04, at 21800 eV photon energy setting.

"fig/BS\_choice\_C111\_Bragg/fea\_plot\_deform\_c04\_21800eV\_03.png" Lbl.:BS\_choice\_C111\_Bragg\_Surface\_plot\_fea\_plot\_deform\_c04\_21800eV\_03

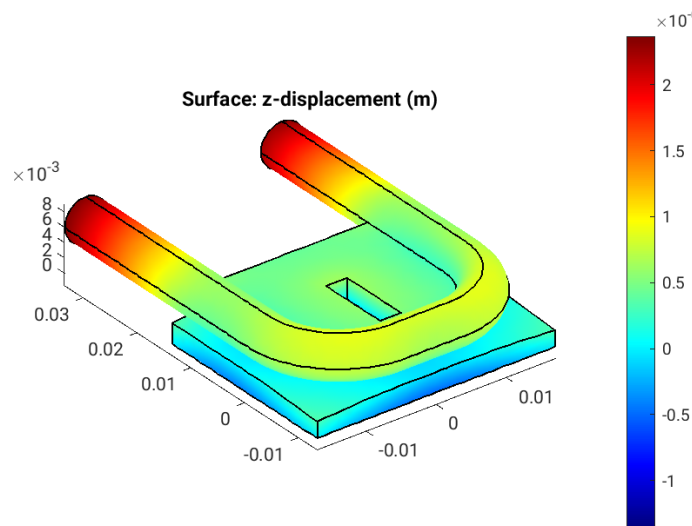


Figure 19.27: Thermoelastic deformation,  $dz$  [m], on the surfaces of optical element #03, for case #04, at 21800 eV photon energy setting.

# Chapter 20

## Parameter scan cases

The thickness of the diamond beam splitter is not very critical for its reflectivity – unless chosen unrealistically thin – due to the Bragg geometry. Hence, no thickness optimisation is required.

Therefore a parameter scan with only four cases is sufficient. Case #1 is the perfect crystal case with no heat load and consequently no deformation. Case #2 is with heat load and with both diamond filters – 600 and 400 micrometer in thickness – in the upstream beam path. Case #3 is with only the 400 micron thick filter in, and case #4 is without any filters.

Case	Thickness(1)_02 cm	Thickness(2)_02 cm	Has_slope_error_03	Skip_heatload
1	0.06	0.04	no	yes
2	0.06	0.04	yes	no
3	0.00001	0.04	yes	no
4	0.00001	0.00001	yes	no

Table 20.1: Parameter values for different cases in parameter scan

### Legend

**Case:** Case number in parameter scan

**Thickness(1)\_02:** Optical\_element\_#2.Type.Screen.Thickness(1) (Optical thickness of resp. screen with absorption.)

**Thickness(2)\_02:** Optical\_element\_#2.Type.Screen.Thickness(2) (Optical thickness of resp. screen with absorption.)

**Has\_slope\_error\_03:** Optical\_element\_#3.Surface.Has\_slope\_error (Has surface slope error?)

**Skip\_heatload:** Session.Skip\_heatload (Skip heat load calculation for all optical elements? (heat load parameters are kept))

## Chapter 21

# Photon energy scan

The  $K_y$ -values in the table below are those for optimised output between 15.6 and 18.3 keV – the whole range being covered by the 7th harmonic that is brightest there – used by DanMAX’ main branch. SinCrys, foreseen to be working at a higher photon energy range, is then going to use the 9th harmonic that is not necessarily the brightest there.

E eV	K_y	n_harm/step	theta_B03 deg	theta_B04 deg
20000	1.67551	9	8.6565237	8.9142208
20100	1.66836	9	8.6131277	8.8695126
20200	1.66125	9	8.5701675	8.8252525
20300	1.65418	9	8.5276346	8.7814341
20400	1.64714	9	8.4855232	8.7380495
20500	1.64015	9	8.4438276	8.6950941
20600	1.63319	9	8.4025402	8.6525602
20700	1.62628	9	8.3616571	8.6104422
20800	1.6194	9	8.3211708	8.5687342
20900	1.61255	9	8.2810764	8.5274286
21000	1.60575	9	8.2413683	8.4865217
21100	1.59898	9	8.2020397	8.4460068
21200	1.59224	9	8.1630869	8.4058781
21300	1.58554	9	8.1245022	8.3661299
21400	1.57887	9	8.0862827	8.3267574
21500	1.57224	9	8.0484219	8.287756
21600	1.56564	9	8.0109158	8.2491188
21700	1.55908	9	7.9737582	8.2108412
21800	1.55255	9	7.936945	8.1729183
21900	1.54605	9	7.9004712	8.1353455
22000	1.53958	9	7.8643322	8.0981178
22100	1.53315	9	7.8285236	8.0612307
22200	1.52674	9	7.7930403	8.0246792
22300	1.52037	9	7.7578783	7.9884586
22400	1.51402	9	7.7230334	7.9525642
22500	1.50771	9	7.6885004	7.9169927
22600	1.50143	9	7.6542764	7.8817382
22700	1.49517	9	7.6203566	7.8467979
22800	1.48895	9	7.5867367	7.8121667
22900	1.48275	9	7.5534129	7.7778411
23000	1.47658	9	7.5203819	7.7438164
23100	1.47044	9	7.487639	7.7100892
23200	1.46433	9	7.4551811	7.6766553
23300	1.45824	9	7.4230037	7.6435108
23400	1.45218	9	7.3911042	7.6106524
23500	1.44615	9	7.359478	7.5780759

Table 21.1: Scan values for different photon energies in energy scan

### Legend

**E:** photon energy

**K\_y:** deflection parameter for vertical field component of insertion device

**n\_harm/step:** number of undulator harmonic or number of energy slot for continuous source (e.g. wiggler)

**theta\_B03:** Bragg angle, i.e. glancing angle of incident and reflected beam w.r.t. the set of diffracting planes of optical element 03

**theta\_B04:** Bragg angle, i.e. glancing angle of incident and reflected beam w.r.t. the set of diffracting planes of optical element 04

E eV	P_sum W	P_abs02-01 W	P_abs02-02 W	P_abs03 W
<b>20000</b>	170.798	51.874	7.06359	6.6497
<b>20100</b>	170.209	51.7138	7.07388	6.66084
<b>20200</b>	169.47	51.8907	7.05492	6.68645
<b>20300</b>	168.879	51.9341	7.07103	6.68832
<b>20400</b>	168.315	51.8803	7.06715	6.71776
<b>20500</b>	167.588	51.99	7.07568	6.7185
<b>20600</b>	166.189	51.9873	7.09456	6.77676
<b>20700</b>	165.542	51.9229	7.09692	6.77069
<b>20800</b>	164.949	51.9763	7.07342	6.76198
<b>20900</b>	164.413	52.0863	7.08196	6.82583
<b>21000</b>	163.752	52.1423	7.05257	6.81984
<b>21100</b>	163.16	51.8659	7.04609	6.82055
<b>21200</b>	162.507	52.0891	7.04699	6.85203
<b>21300</b>	161.904	52.0602	7.05683	6.85535
<b>21400</b>	161.386	52.1829	7.04339	6.89613
<b>21500</b>	160.797	52.1456	7.03171	6.90083
<b>21600</b>	160.163	52.2462	7.03479	6.89757
<b>21700</b>	159.473	52.1952	7.00824	6.90468
<b>21800</b>	158.884	52.2113	6.9828	6.93794
<b>21900</b>	157.585	52.3614	6.9859	6.92445
<b>22000</b>	157.101	52.3552	7.00827	6.97071
<b>22100</b>	156.451	52.1865	6.93713	6.97683
<b>22200</b>	155.93	52.3722	6.94293	6.9755
<b>22300</b>	155.254	52.2295	6.92255	7.00193
<b>22400</b>	154.716	52.4291	6.90435	6.99927
<b>22500</b>	154.16	52.3949	6.87648	7.02798
<b>22600</b>	153.484	52.2823	6.86345	7.0288
<b>22700</b>	152.951	52.3549	6.8562	7.04282
<b>22800</b>	152.294	52.4449	6.7893	7.05786
<b>22900</b>	151.786	52.2665	6.77464	7.07385
<b>23000</b>	151.176	52.4135	6.75605	7.08386
<b>23100</b>	150.589	52.2865	6.74133	7.11261
<b>23200</b>	149.911	52.4011	6.72227	7.12372
<b>23300</b>	148.827	52.3082	6.70448	7.11072
<b>23400</b>	148.246	52.3477	6.68226	7.12107
<b>23500</b>	147.698	52.358	6.66284	7.13975

Table 21.2: Scan values for different photon energies with diamond filters of 1000 micron total thickness in

E eV	P_sum W	P_abs02-01 W	P_abs02-02 W	P_abs03 W
<b>20000</b>	170.798	0.198055	46.0113	13.5335
<b>20100</b>	170.209	0.197629	45.9742	13.5913
<b>20200</b>	169.47	0.196506	46.1677	13.5935
<b>20300</b>	168.879	0.194879	46.1353	13.6497
<b>20400</b>	168.315	0.193946	46.1259	13.7112
<b>20500</b>	167.588	0.192274	46.3158	13.7015
<b>20600</b>	166.189	0.190542	46.313	13.7214
<b>20700</b>	165.542	0.189817	46.3158	13.7426
<b>20800</b>	164.949	0.188986	46.4234	13.7515
<b>20900</b>	164.413	0.18724	46.3354	13.8247
<b>21000</b>	163.752	0.186197	46.4182	13.8188
<b>21100</b>	163.16	0.185241	46.4087	13.7989
<b>21200</b>	162.507	0.184341	46.6186	13.8019
<b>21300</b>	161.904	0.181944	46.3129	13.8355
<b>21400</b>	161.386	0.180953	46.555	13.9025
<b>21500</b>	160.797	0.180372	46.6006	13.871
<b>21600</b>	160.163	0.179201	46.6817	13.879
<b>21700</b>	159.473	0.177629	46.568	13.916
<b>21800</b>	158.884	0.17726	46.8348	13.8778
<b>21900</b>	157.585	0.175904	46.7849	13.8791
<b>22000</b>	157.101	0.17481	46.8261	13.9462
<b>22100</b>	156.451	0.17424	46.8755	13.8842
<b>22200</b>	155.93	0.172873	47.0673	13.9123
<b>22300</b>	155.254	0.171198	46.8425	13.8715
<b>22400</b>	154.716	0.169847	47.0578	13.9148
<b>22500</b>	154.16	0.169276	47.1721	13.8493
<b>22600</b>	153.484	0.168842	47.0858	13.862
<b>22700</b>	152.951	0.166879	47.0559	13.8472
<b>22800</b>	152.294	0.166709	47.1059	13.8639
<b>22900</b>	151.786	0.165572	47.1084	13.8036
<b>23000</b>	151.176	0.163779	47.2085	13.8231
<b>23100</b>	150.589	0.163243	47.1185	13.7439
<b>23200</b>	149.911	0.161974	47.2677	13.713
<b>23300</b>	148.827	0.160776	47.2638	13.6639
<b>23400</b>	148.246	0.15968	47.3604	13.7235
<b>23500</b>	147.698	0.159465	47.2555	13.6444

Table 21.3: Scan values for different photon energies with upstream diamond filter of 400 micron thickness in

E eV	P_sum W	P_abs02-01 W	P_abs02-02 W	P_abs03 W
<b>20000</b>	170.798	0.197774	0.19626	52.8558
<b>20100</b>	170.209	0.196606	0.19551	53.0777
<b>20200</b>	169.47	0.195501	0.195016	53.1716
<b>20300</b>	168.879	0.19425	0.19326	53.284
<b>20400</b>	168.315	0.193282	0.191084	53.2174
<b>20500</b>	167.588	0.191768	0.19132	53.5649
<b>20600</b>	166.189	0.190295	0.190091	53.5894
<b>20700</b>	165.542	0.189692	0.188357	53.4754
<b>20800</b>	164.949	0.188707	0.187854	53.6958
<b>20900</b>	164.413	0.186743	0.186948	53.7278
<b>21000</b>	163.752	0.185092	0.185511	53.8866
<b>21100</b>	163.16	0.185021	0.183774	53.9009
<b>21200</b>	162.507	0.183819	0.183075	54.1761
<b>21300</b>	161.904	0.1823	0.181226	54.0589
<b>21400</b>	161.386	0.180941	0.180058	54.1723
<b>21500</b>	160.797	0.180114	0.179592	54.2898
<b>21600</b>	160.163	0.179017	0.177646	54.1765
<b>21700</b>	159.473	0.177552	0.176516	54.3988
<b>21800</b>	158.884	0.177215	0.17709	54.4967
<b>21900</b>	157.585	0.175573	0.174883	54.5671
<b>22000</b>	157.101	0.174235	0.173412	54.6979
<b>22100</b>	156.451	0.17387	0.173636	54.9072
<b>22200</b>	155.93	0.172905	0.172689	54.9171
<b>22300</b>	155.254	0.172263	0.171257	54.8381
<b>22400</b>	154.716	0.170654	0.169504	54.9981
<b>22500</b>	154.16	0.169681	0.16916	55.1409
<b>22600</b>	153.484	0.167499	0.167246	55.082
<b>22700</b>	152.951	0.16775	0.166365	55.2783
<b>22800</b>	152.294	0.16578	0.165729	55.176
<b>22900</b>	151.786	0.164841	0.16439	55.2084
<b>23000</b>	151.176	0.164471	0.163381	55.3314
<b>23100</b>	150.589	0.163507	0.162883	55.2946
<b>23200</b>	149.911	0.161968	0.16138	55.3906
<b>23300</b>	148.827	0.16096	0.160384	55.342
<b>23400</b>	148.246	0.159552	0.15941	55.4351
<b>23500</b>	147.698	0.158804	0.158358	55.4383

Table 21.4: Scan values for different photon energies with no upstream filters

### Legend

**E:** photon energy

**P\_sum:** sum of power in harmonics / energy intervals, P\_sum = P\_src

**P\_abs02-01:** total power absorbed by optical element 02-01

**P\_abs02-02:** total power absorbed by optical element 02-02

**P\_abs03:** total power absorbed by optical element 03

# Chapter 22

## Plots

### 22.1 Statistics of incident irradiance

```
"fig/BS_choice_C111_Bragg/plot001.png" Lbl.:BS_choice_C111_Bragg_2d_plot_I_peak_incstat_oe03
```

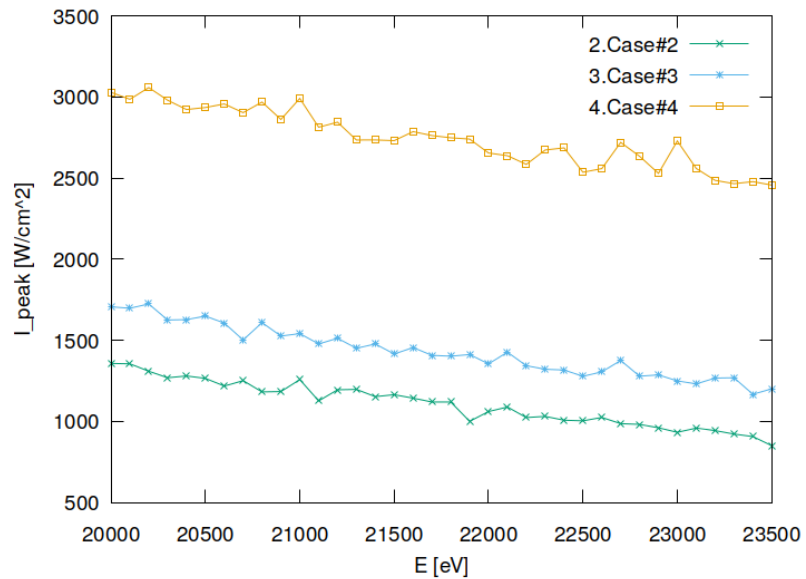


Figure 22.1: Incident peak irradiance of optical element #03 (BS).

```
"fig/BS_choice_C111_Bragg/plot002.png" Lbl.:BS_choice_C111_Bragg_2d_plot_I_int_incstat_oe03
```

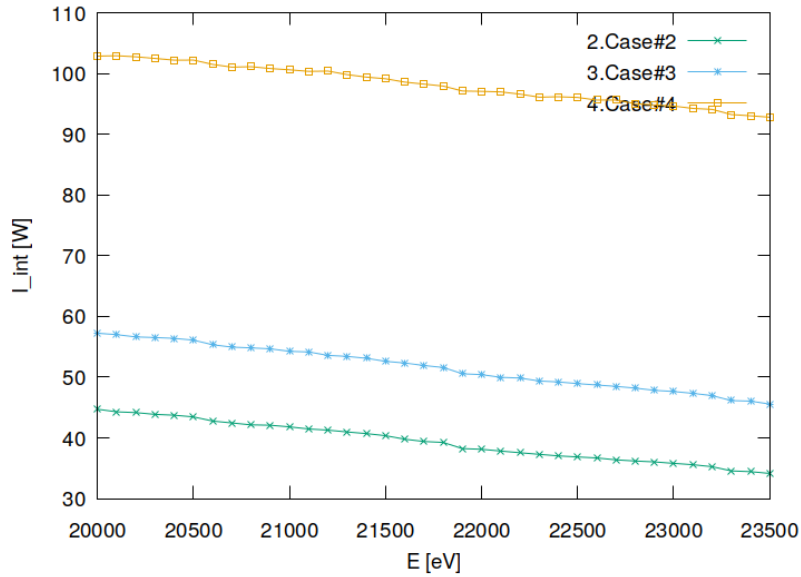


Figure 22.2: Incident flux of optical element #03 (BS).

## 22.2 Statistics of absorbed irradiance

```
"fig/BS_choice_C111_Bragg/plot003.png" Lbl.:BS_choice_C111_Bragg_2d_plot_I_peak_absstat_oe03
```

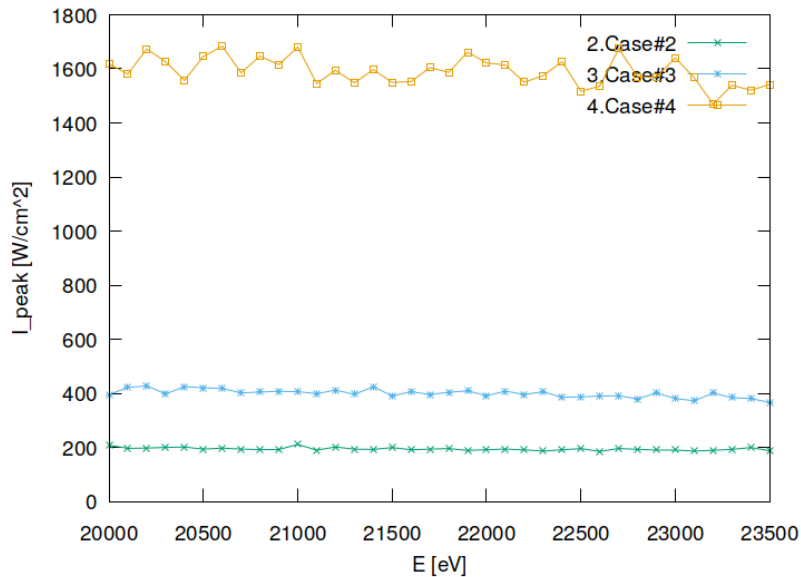


Figure 22.3: Absorbed peak irradiance of optical element #03 (BS).

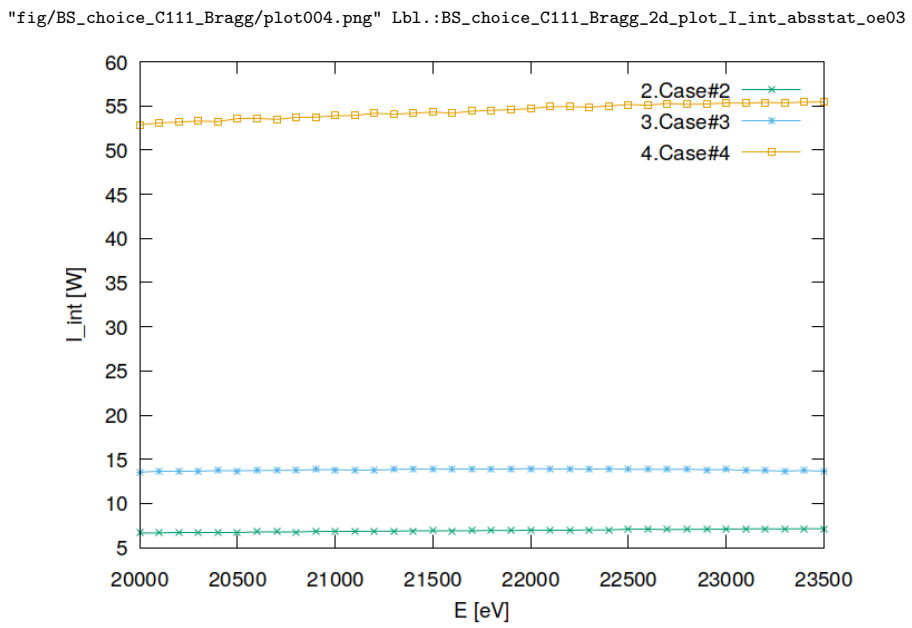


Figure 22.4: Absorbed flux of optical element #03 (BS).

## 22.3 Statistics of temperature

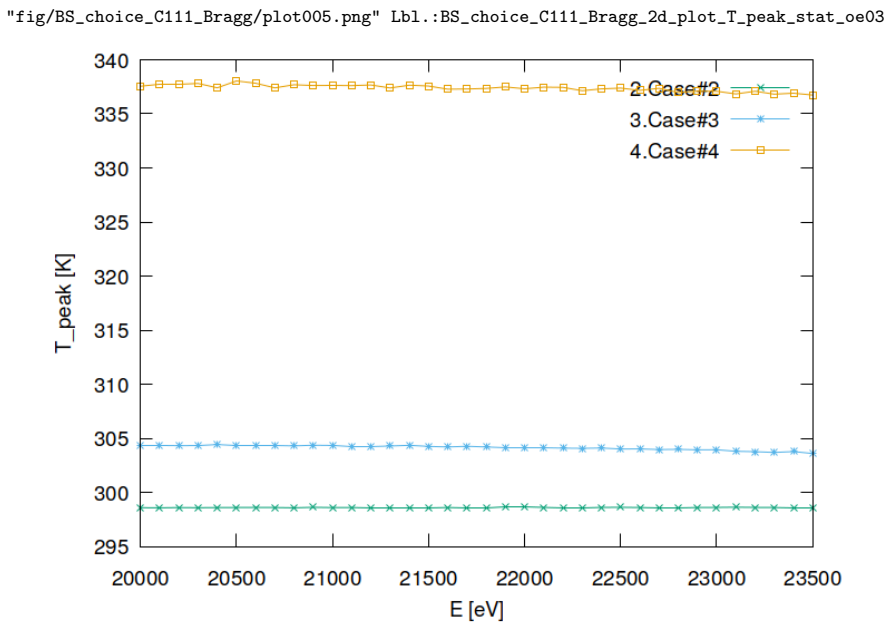


Figure 22.5: Peak temperature of optical element #03 (BS).

## 22.4 Statistics of mechanical stress (von Mises stress)

```
"fig/BS_choice_C111_Bragg/plot006.png" Lbl.:BS_choice_C111_Bragg_2d_plot_sigma_peak_stat_oe03
```

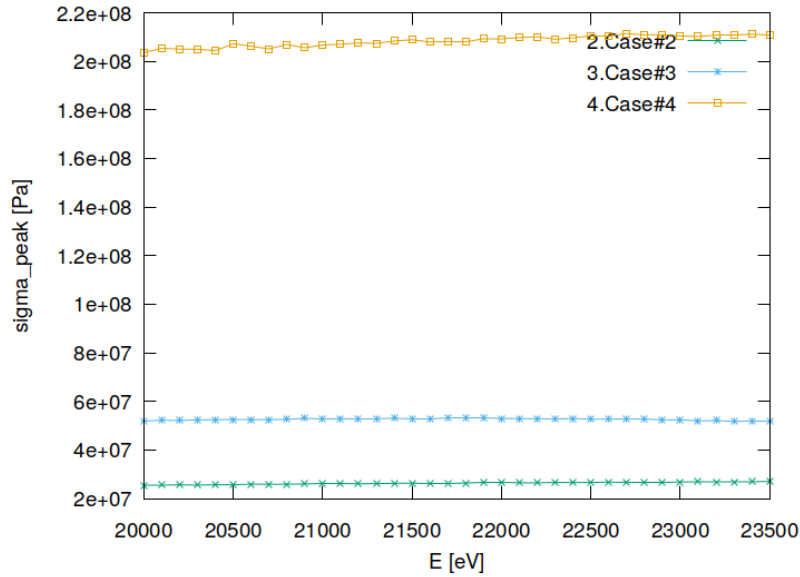


Figure 22.6: Peak mechanical stress (Von Mises stress) of optical element #03 (BS).

## 22.5 Statistics of optical surface deformation

```
"fig/BS_choice_C111_Bragg/plot007.png" Lbl.:BS_choice_C111_Bragg_2d_plot_dz_peak_stat_oe03
```

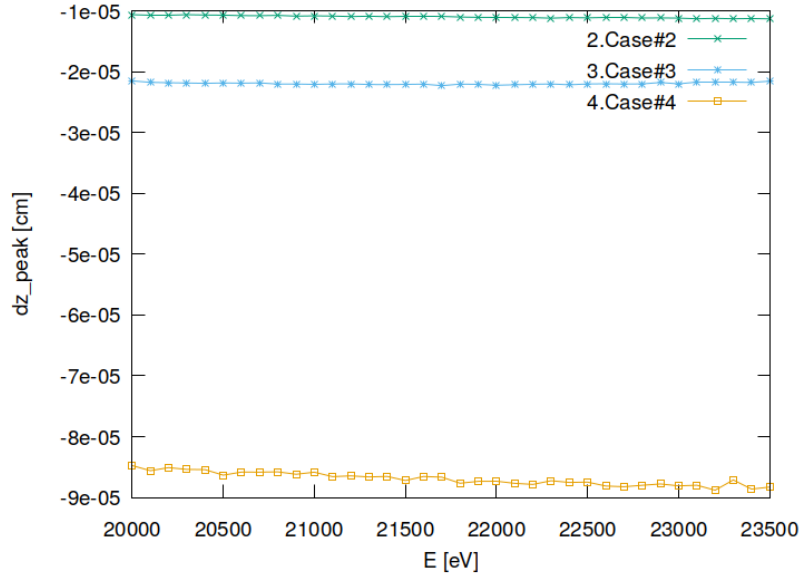


Figure 22.7: Peak deformation of optical element #03 (BS).

## 22.6 Statistics of photon irradiance on optical surface

"fig/BS\_choice\_C111\_Bragg/plot008.png" Lbl.:BS\_choice\_C111\_Bragg\_2d\_plot\_dx\_fwhm\_inc\_footstat\_oe04

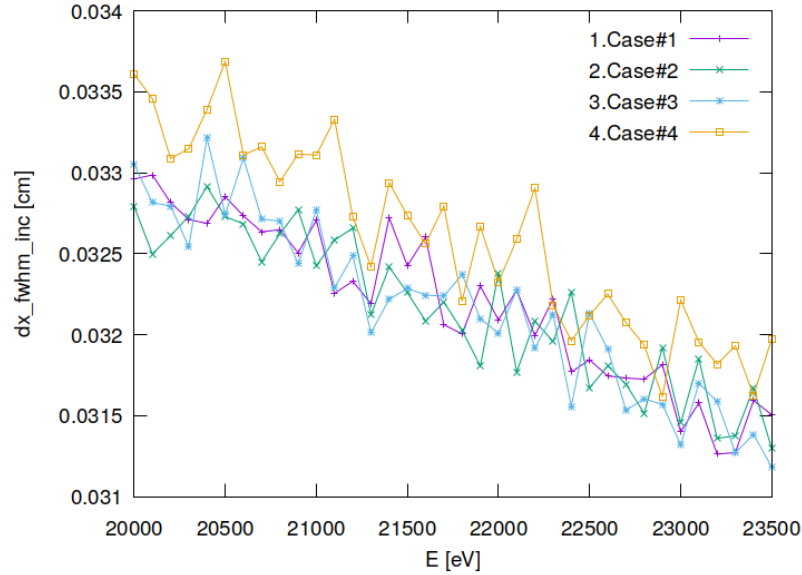


Figure 22.8: Sagittal footprint diameter (FWHM) of optical element #04 (CM2).

"fig/BS\_choice\_C111\_Bragg/plot009.png" Lbl.:BS\_choice\_C111\_Bragg\_2d\_plot\_dy\_fwhm\_inc\_footstat\_oe04

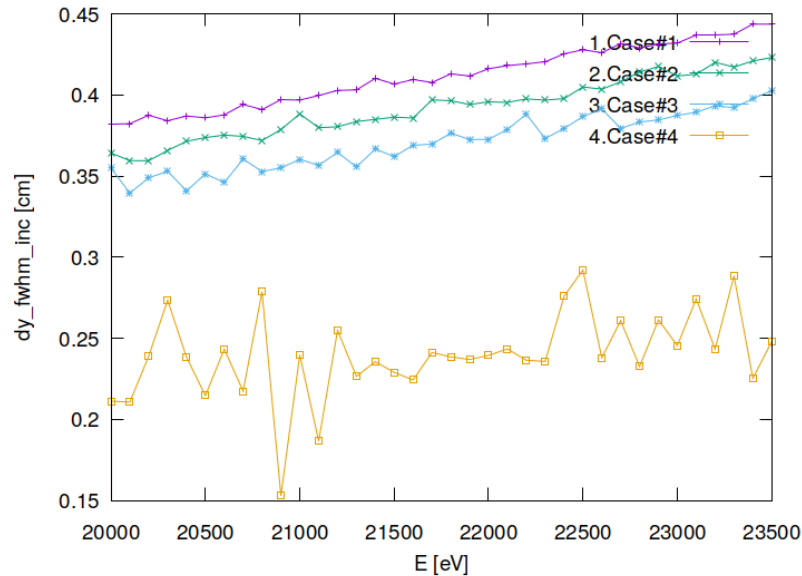


Figure 22.9: Meridional footprint diameter (FWHM) of optical element #04 (CM2).

```
"fig/BS_choice_C111_Bragg/plot010.png" Lbl.:BS_choice_C111_Bragg_2d_plot_I_inc_int_footstat_oe04
```

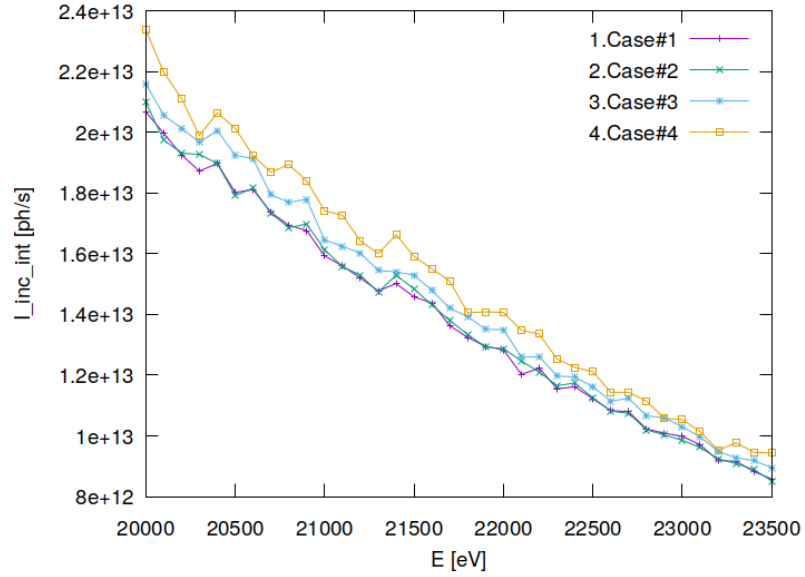


Figure 22.10: Incident photon flux on surface of optical element #04 (CM2).

```
"fig/BS_choice_C111_Bragg/plot011.png" Lbl.:BS_choice_C111_Bragg_2d_plot_x_cen_inc_footstat_oe04
```

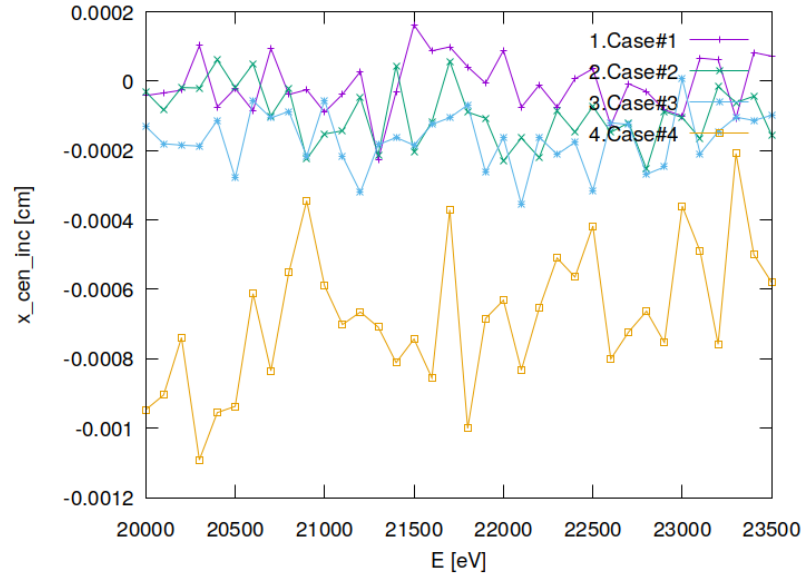


Figure 22.11: Sagittal coordinate of footprint's centre of 'gravity' on surface of optical element #04 (CM2).

"fig/BS\_choice\_C111\_Bragg/plot012.png" Lbl.:BS\_choice\_C111\_Bragg\_2d\_plot\_y\_cen\_inc\_footstat\_oe04

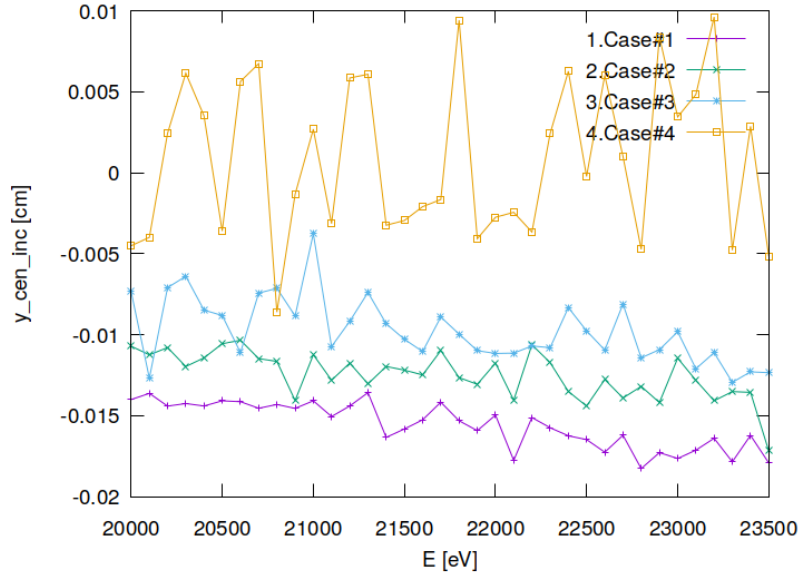


Figure 22.12: Meridional coordinate of footprint's centre of 'gravity' on surface of optical element #04 (CM2).

## 22.7 Statistics of photon irradiance in beam cross section

"fig/BS\_choice\_C111\_Bragg/plot013.png" Lbl.:BS\_choice\_C111\_Bragg\_2d\_plot\_dx\_fwhm\_focstatavg\_oe04

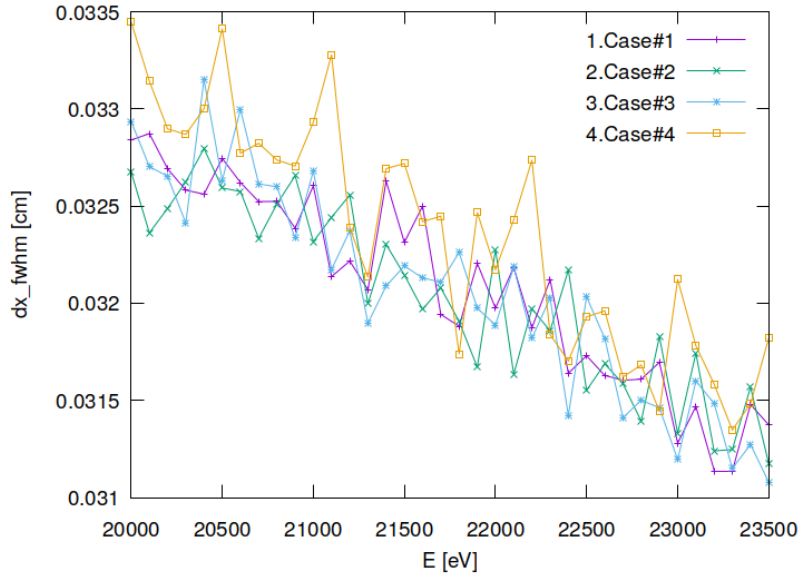


Figure 22.13: Sagittal beam diameter (FWHM) of optical element #04 (CM2).

```
"fig/BS_choice_C111_Bragg/plot014.png" Lbl.:BS_choice_C111_Bragg_2d_plot_dz_fwhm_focstatavg_oe04
```

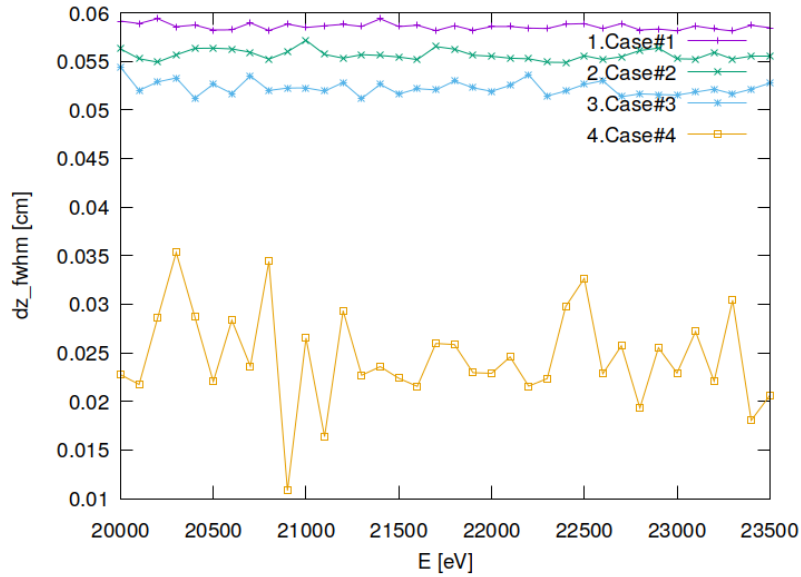


Figure 22.14: Meridional beam diameter (FWHM) of optical element #04 (CM2).

```
"fig/BS_choice_C111_Bragg/plot015.png" Lbl.:BS_choice_C111_Bragg_2d_plot_I_int_focstatavg_oe04
```

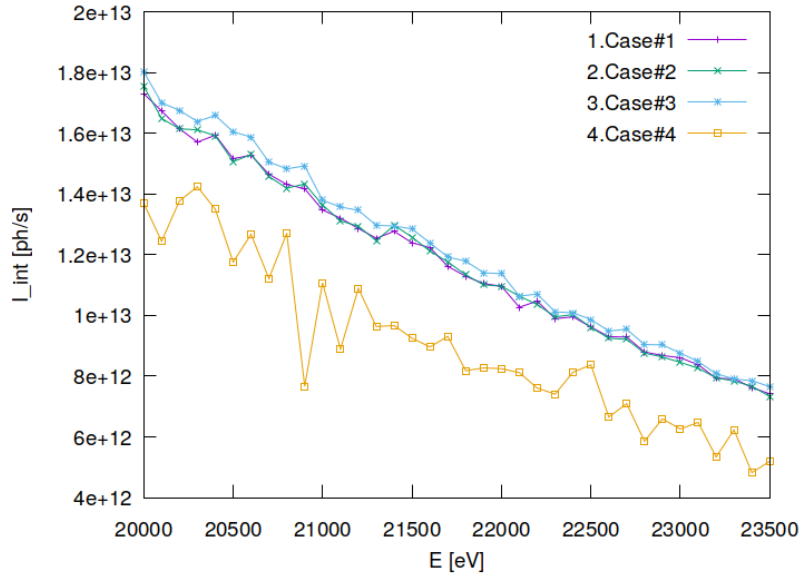


Figure 22.15: Photon flux in beam cross section of optical element #04 (CM2).

"fig/BS\_choice\_C111\_Bragg/plot016.png" Lbl.:BS\_choice\_C111\_Bragg\_2d\_plot\_x\_cen\_focstatavg\_oe04

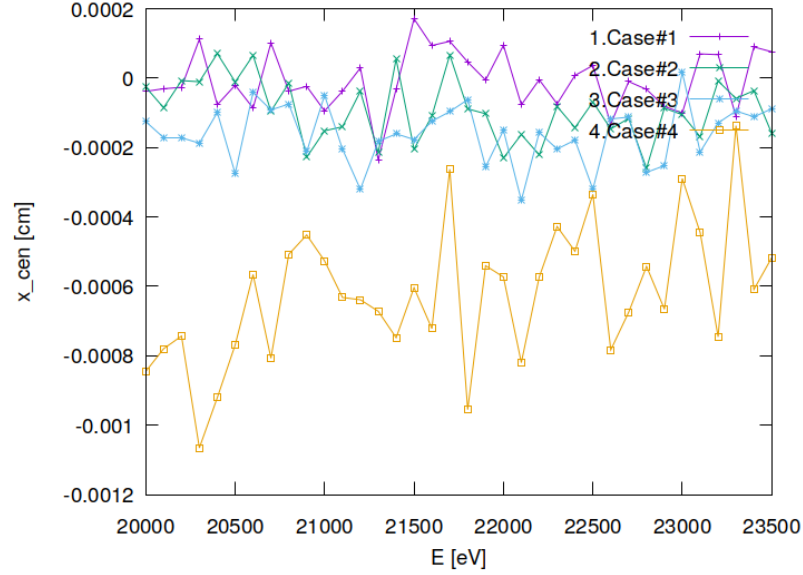


Figure 22.16: Sagittal coordinate of beam's centre of 'gravity' in beam cross section of optical element #04 (CM2).

"fig/BS\_choice\_C111\_Bragg/plot017.png" Lbl.:BS\_choice\_C111\_Bragg\_2d\_plot\_z\_cen\_focstatavg\_oe04

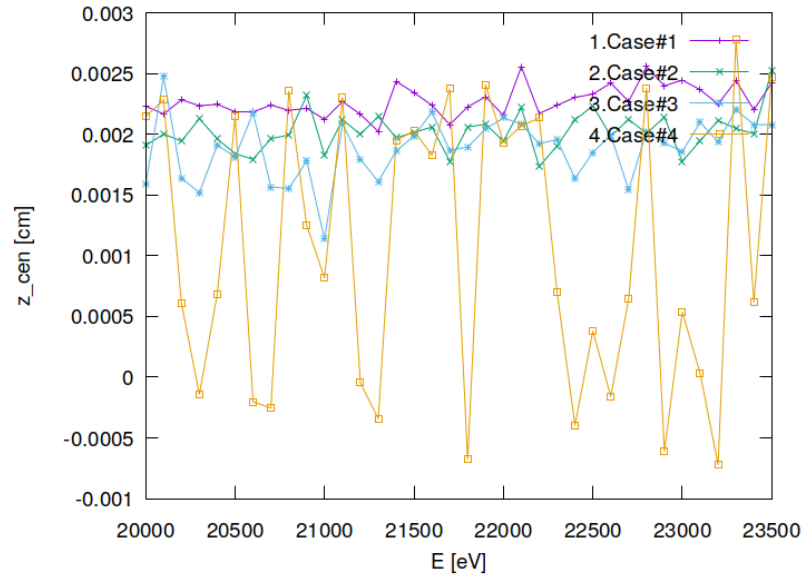


Figure 22.17: Meridional coordinate of beam's centre of 'gravity' in beam cross section of optical element #04 (CM2).

```
"fig/BS_choice_C111_Bragg/plot018.png" Lbl.:BS_choice_C111_Bragg_2d_plot_dxp_fwhm_focstatavg_oe04
```

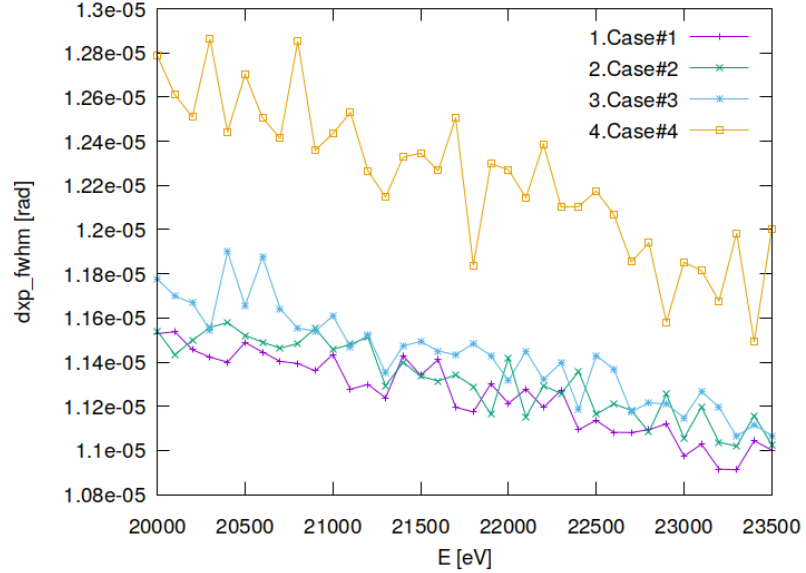


Figure 22.18: Sagittal beam divergence (FWHM) of optical element #04 (CM2).

```
"fig/BS_choice_C111_Bragg/plot019.png" Lbl.:BS_choice_C111_Bragg_2d_plot_dzp_fwhm_focstatavg_oe04
```

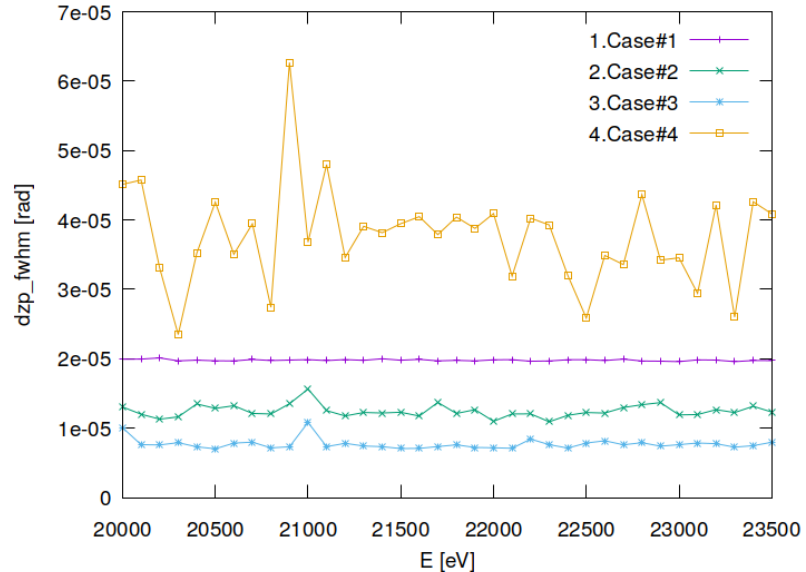


Figure 22.19: Meridional beam divergence (FWHM) of optical element #04 (CM2).

"fig/BS\_choice\_C111\_Bragg/plot020.png" Lbl.:BS\_choice\_C111\_Bragg\_2d\_plot\_I\_int\_focstatavg\_oe04

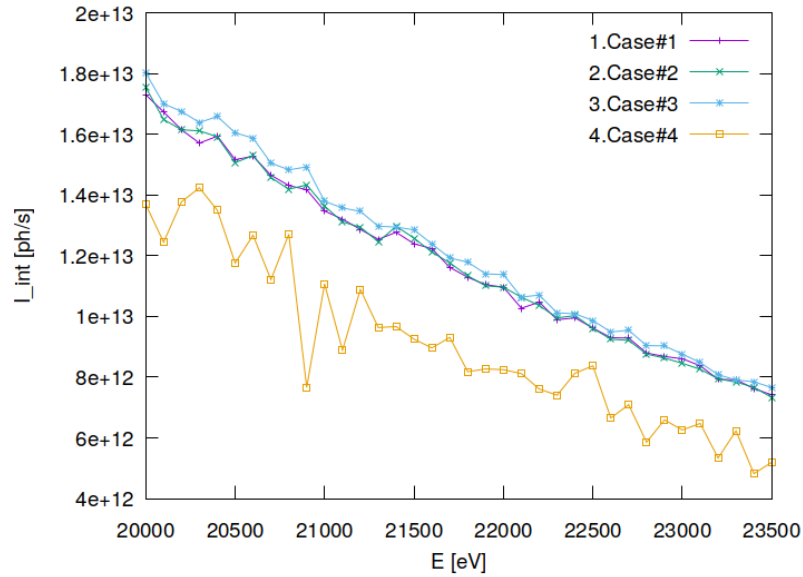


Figure 22.20: Photon flux in beam cross section of optical element #04 (CM2).

"fig/BS\_choice\_C111\_Bragg/plot021.png" Lbl.:BS\_choice\_C111\_Bragg\_2d\_plot\_xp\_cen\_focstatavg\_oe04

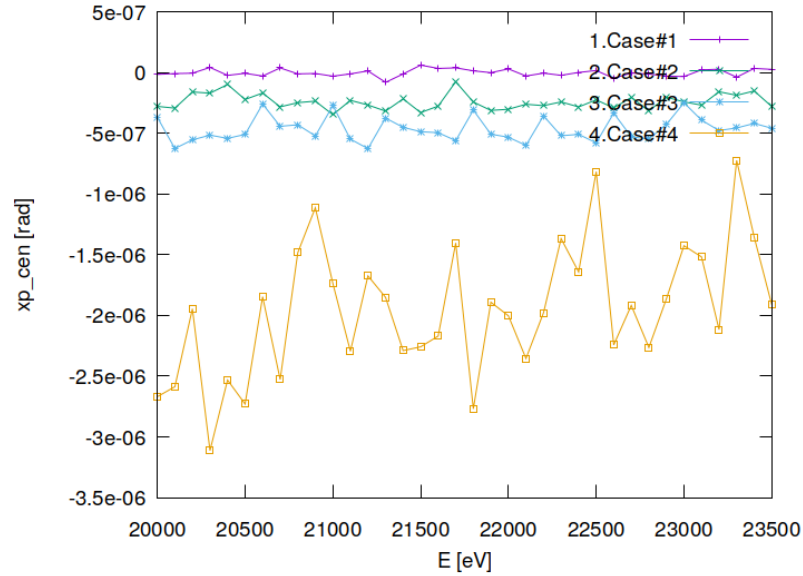


Figure 22.21: Sagittal coordinate of beam's centre of 'gravity' in angle space of optical element #04 (CM2).

"fig/BS\_choice\_C111\_Bragg/plot022.png" Lbl.:BS\_choice\_C111\_Bragg\_2d\_plot\_zp\_cen\_focstatavg\_oe04

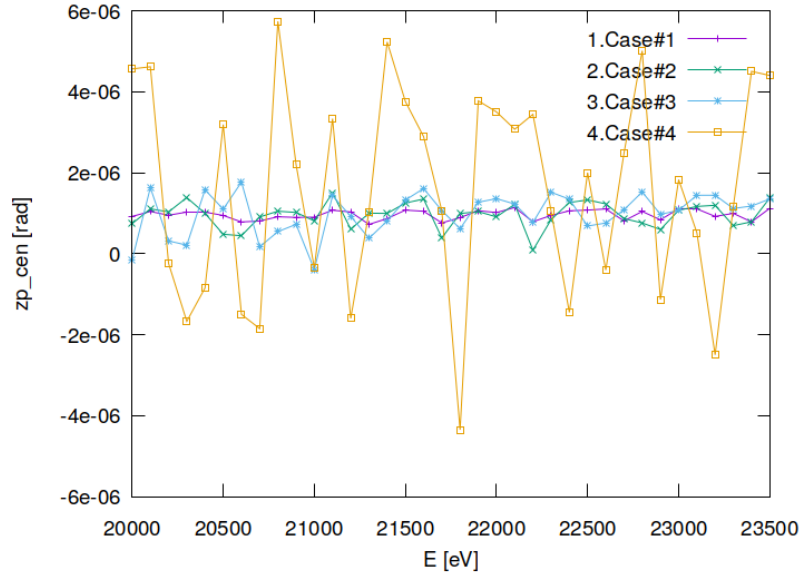


Figure 22.22: Meridional coordinate of beam's centre of 'gravity' in angle space of optical element #04 (CM2).

"fig/BS\_choice\_C111\_Bragg/plot023.png" Lbl.:BS\_choice\_C111\_Bragg\_2d\_plot\_dE\_fwhm\_focstatavg\_oe04

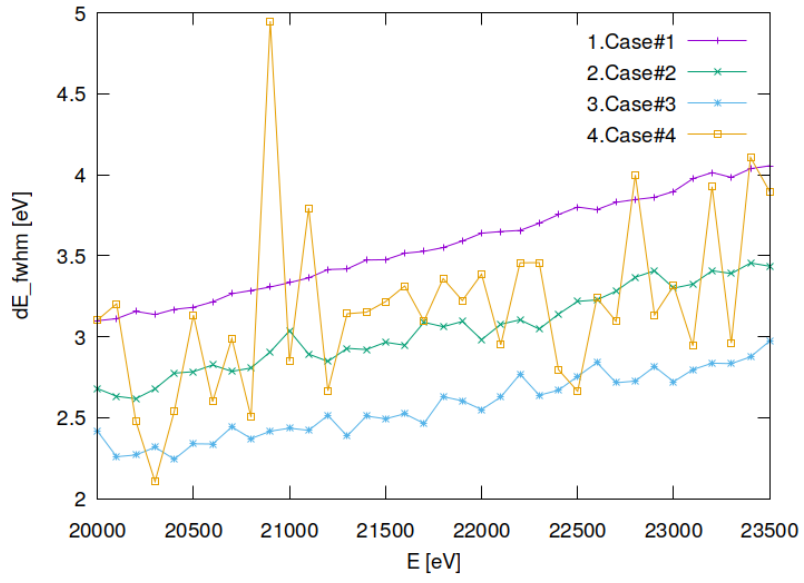


Figure 22.23: Bandwidth (FWHM) in beam cross section of optical element #04 (CM2).



## 22.8 Absorbed irradiance on surface

"fig/BS\_choice\_C111\_Bragg/plot024.png" Lbl.:BS\_choice\_C111\_Bragg\_false\_colour\_plot\_p\_abs\_foot\_oe03\_c2\_21800eV

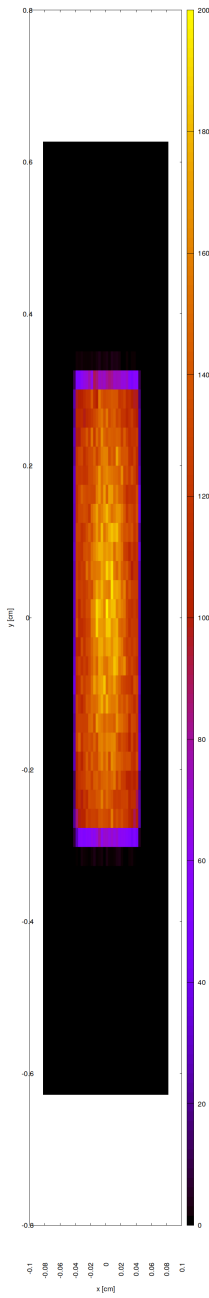


Figure 22.24: Absorbed irradiance on surface of optical element #03 (BS) for case #2 for 21800 eV photon energy setting.

```
"fig/BS_choice_C111_Bragg/plot025.png" Lbl.:BS_choice_C111_Bragg_false_colour_plot_p_abs_foot_oe03_c3_21800eV
```

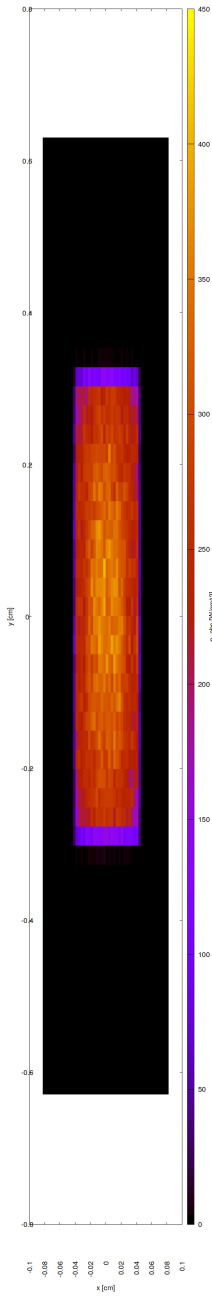


Figure 22.25: Absorbed irradiance on surface of optical element #03 (BS) for case #3 for 21800 eV photon energy setting.

```
"fig/BS_choice_C111_Bragg/plot026.png" Lbl.:BS_choice_C111_Bragg_false_colour_plot_p_abs_foot_oe03_c4_21800eV
```

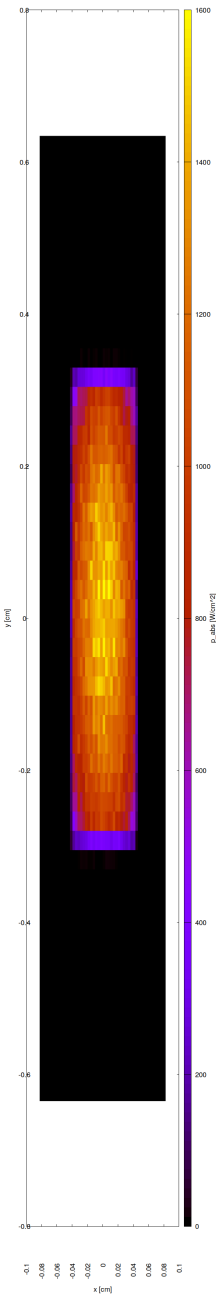


Figure 22.26: Absorbed irradiance on surface of optical element #03 (BS) for case #4 for 21800 eV photon energy setting.

## 22.9 Incident spectral flux on surface

"fig/BS\_choice\_C111\_Bragg/plot027.png" Lbl.:BS\_choice\_C111\_Bragg\_2d\_plot\_P\_spec\_spec\_oe03\_c2\_21800eV

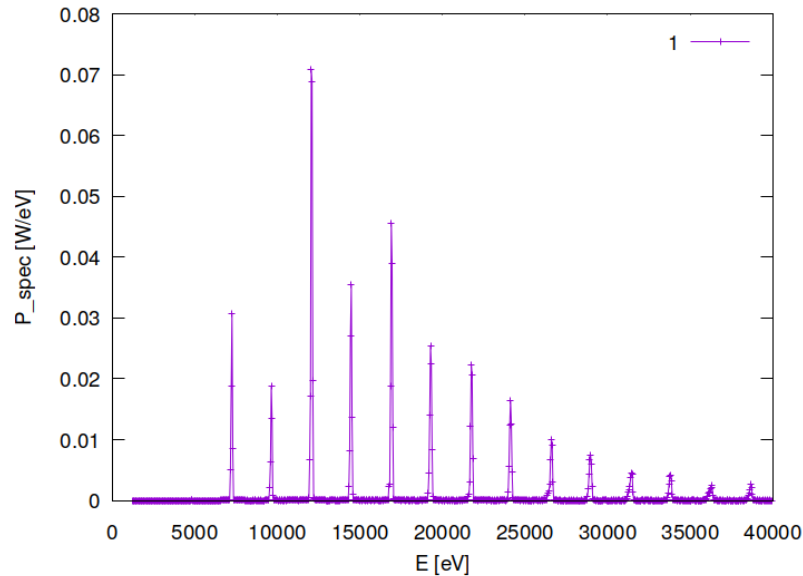


Figure 22.27: Incident spectral flux on surface of optical element #03 (BS) for case #2 for 21800 eV photon energy setting.

"fig/BS\_choice\_C111\_Bragg/plot028.png" Lbl.:BS\_choice\_C111\_Bragg\_2d\_plot\_P\_spec\_spec\_oe03\_c3\_21800eV

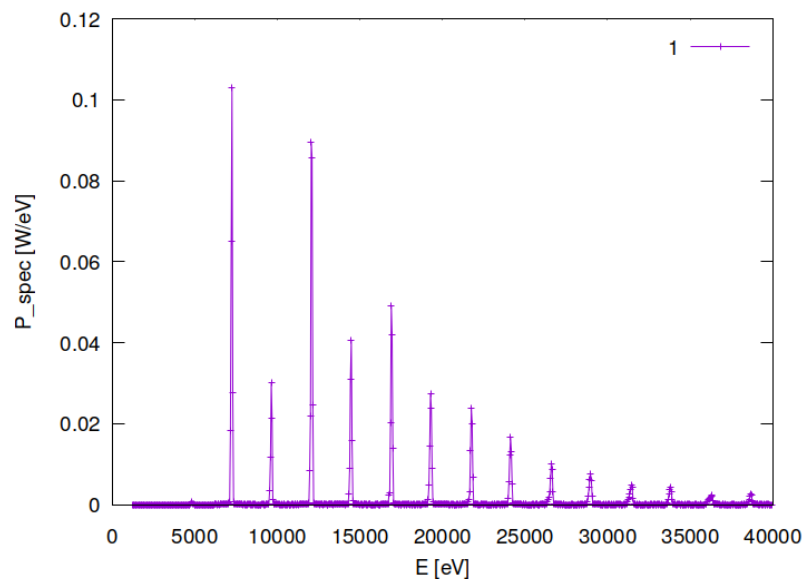


Figure 22.28: Incident spectral flux on surface of optical element #03 (BS) for case #3 for 21800 eV photon energy setting.

```
"fig/BS_choice_C111_Bragg/plot029.png" Lbl.:BS_choice_C111_Bragg_2d_plot_P_spec_spec_oe03_c4_21800eV
```

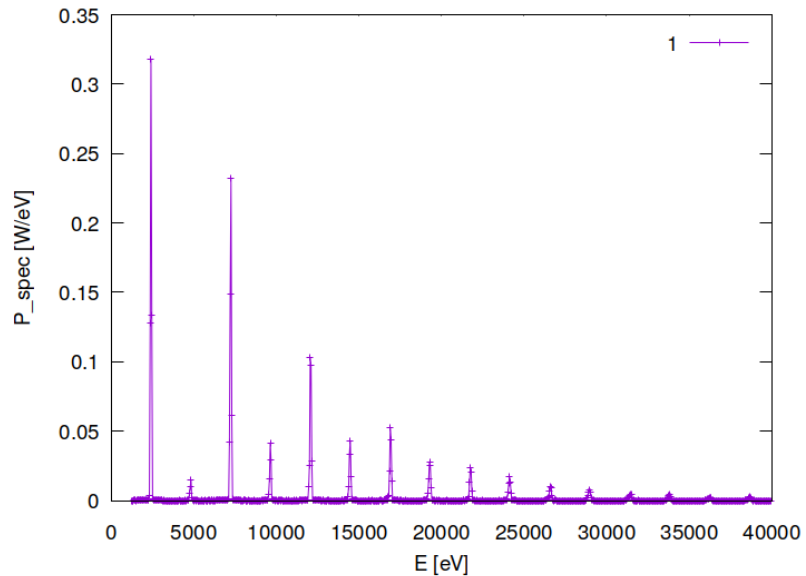


Figure 22.29: Incident spectral flux on surface of optical element #03 (BS) for case #4 for 21800 eV photon energy setting.



## 22.10 Temperature on surface

"fig/BS\_choice\_C111\_Bragg/plot030.png" Lbl.:BS\_choice\_C111\_Bragg\_false\_colour\_plot\_T\_oe03\_c2\_21800eV

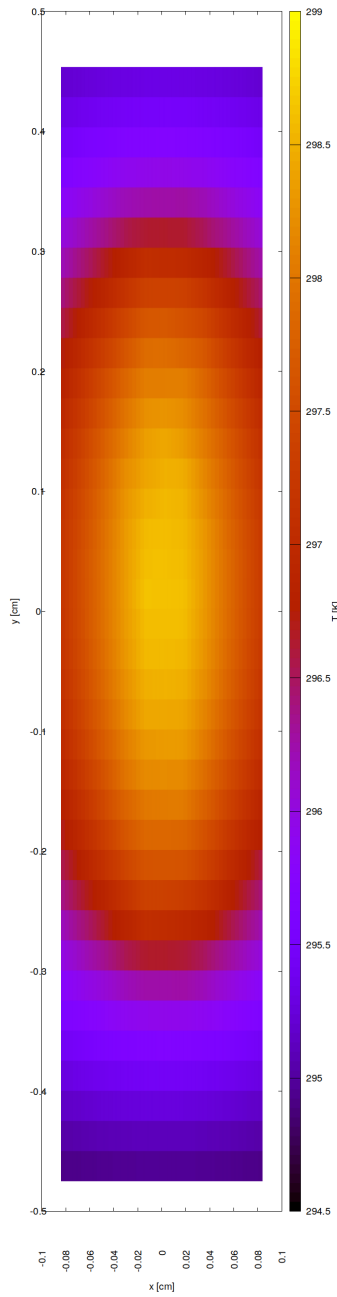


Figure 22.30: Temperature on surface of optical element #03 (BS) for case #2 for 21800 eV photon energy setting.

"fig/BS\_choice\_C111\_Bragg/plot031.png" Lbl.:BS\_choice\_C111\_Bragg\_false\_colour\_plot\_T\_oe03\_c3\_21800eV

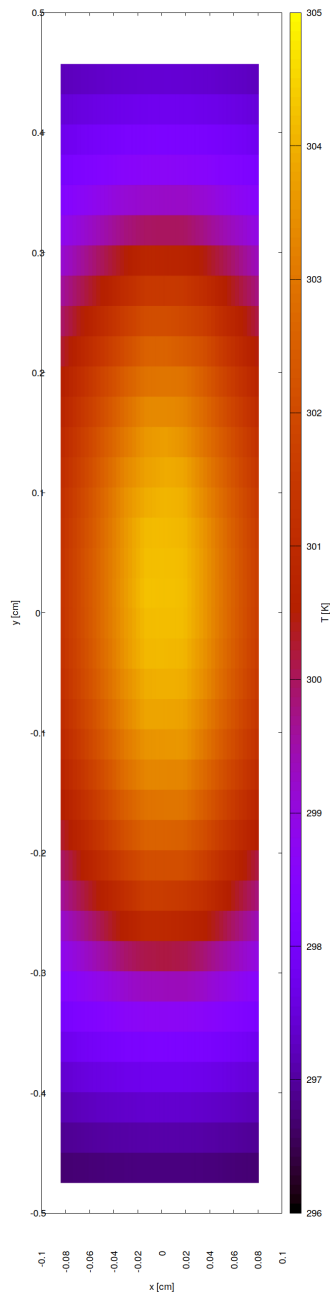


Figure 22.31: Temperature on surface of optical element #03 (BS) for case #3 for 21800 eV photon energy setting.

"fig/BS\_choice\_C111\_Bragg/plot032.png" Lbl.:BS\_choice\_C111\_Bragg\_false\_colour\_plot\_T\_oe03\_c4\_21800eV

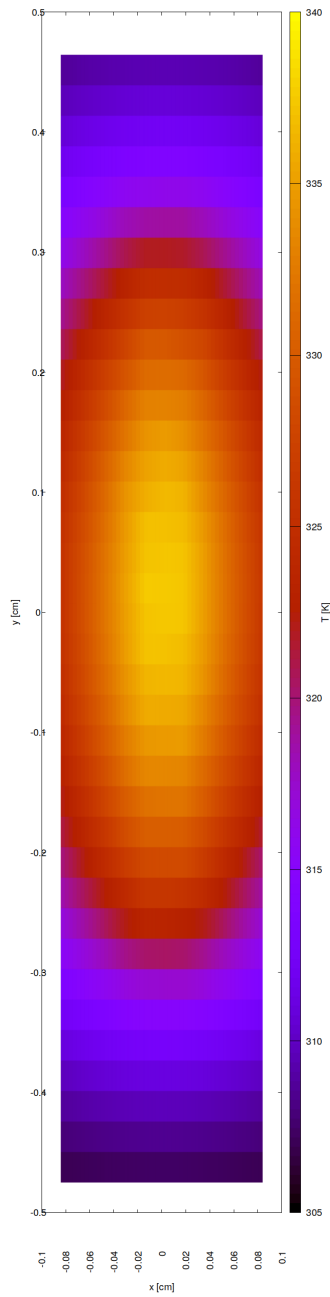


Figure 22.32: Temperature on surface of optical element #03 (BS) for case #4 for 21800 eV photon energy setting.



## 22.11 Mechanical stress (Von Mises stress) on surface

"fig/BS\_choice\_C111\_Bragg/plot033.png" Lbl.:BS\_choice\_C111\_Bragg\_false\_colour\_plot\_sigma\_oe03\_c2\_21800eV

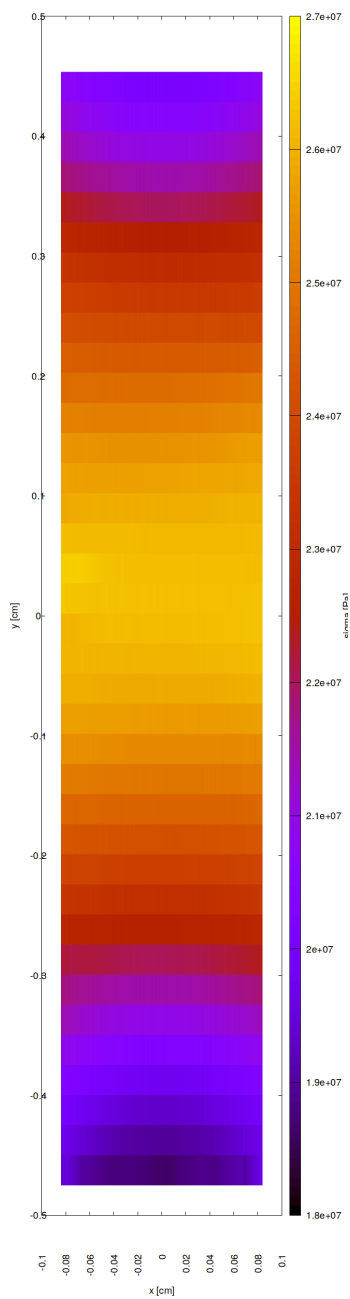


Figure 22.33: Mechanical stress (Von Mises stress) on surface of optical element #03 (BS) for case #2 for 21800 eV photon energy setting.  
287

"fig/BS\_choice\_C111\_Bragg/plot034.png" Lbl.:BS\_choice\_C111\_Bragg\_false\_colour\_plot\_sigma\_oe03\_c3\_21800eV

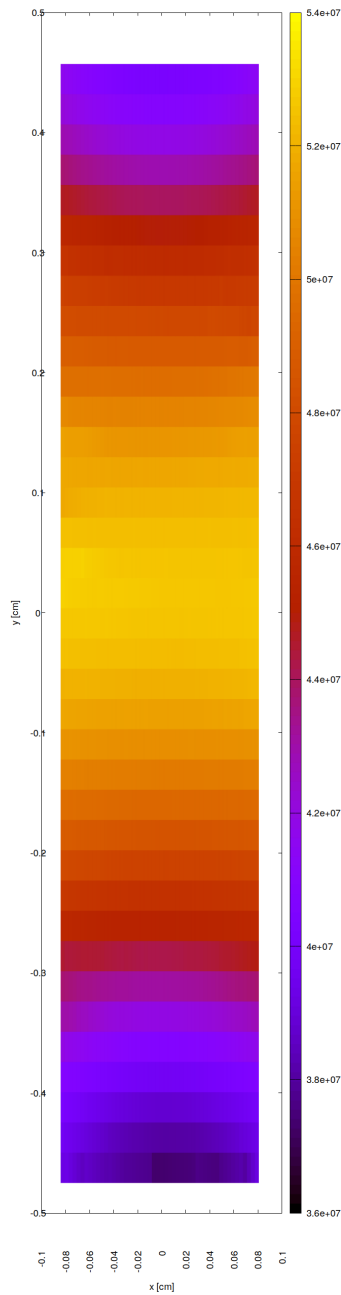


Figure 22.34: Mechanical stress (Von Mises stress) on surface of optical element #03 (BS) for case #3 for 21800 eV photon energy setting.

"fig/BS\_choice\_C111\_Bragg/plot035.png" Lbl.:BS\_choice\_C111\_Bragg\_false\_colour\_plot\_sigma\_oe03\_c4\_21800eV

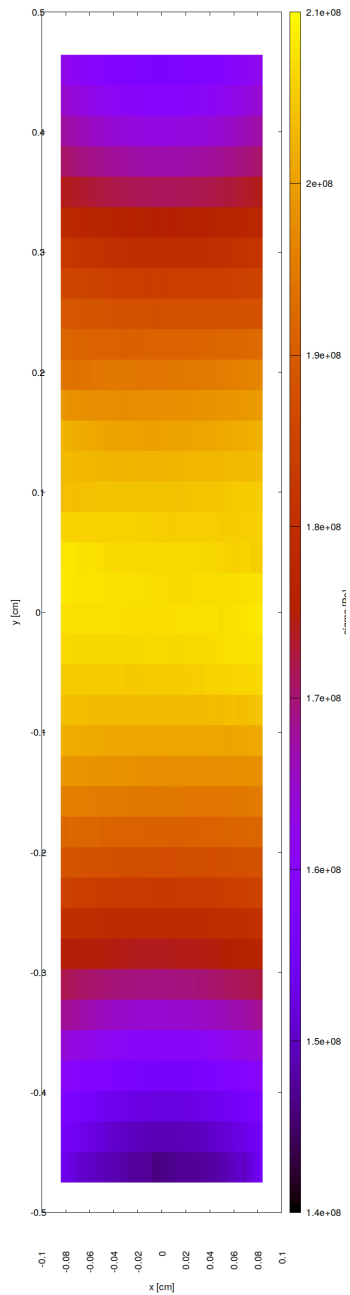


Figure 22.35: Mechanical stress (Von Mises stress) on surface of optical element #03 (BS) for case #4 for 21800 eV photon energy setting.



## 22.12 Surface slope error in meridional direction (y)

"fig/BS\_choice\_C111\_Bragg/plot036.png" Lbl.:BS\_choice\_C111\_Bragg\_false\_colour\_plot\_phi\_y\_oe03\_c2\_21800eV

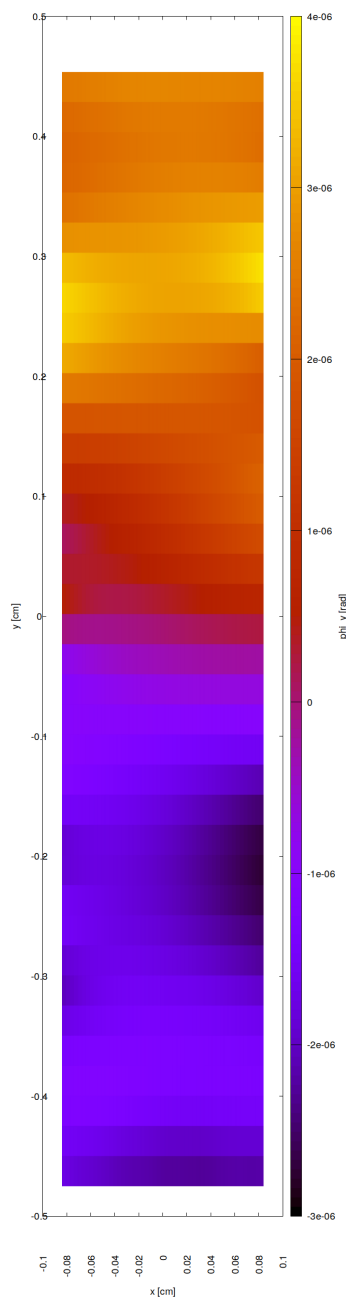


Figure 22.36: Surface slope error in meridional direction (y) of optical element #03 (BS) for case #2 for 21800 eV photon energy setting.

```
"fig/BS_choice_C111_Bragg/plot037.png" Lbl.:BS_choice_C111_Bragg_false_colour_plot_phi_y_oe03_c3_21800eV
```

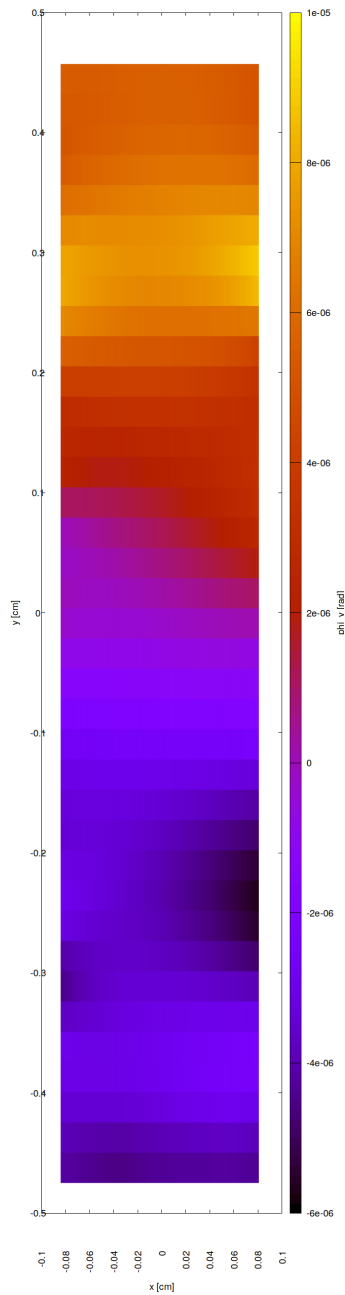


Figure 22.37: Surface slope error in meridional direction (y) of optical element #03 (BS) for case #3 for 21800 eV photon energy setting.

```
"fig/BS_choice_C111_Bragg/plot038.png" Lbl.:BS_choice_C111_Bragg_false_colour_plot_phi_y_oe03_c4_21800eV
```

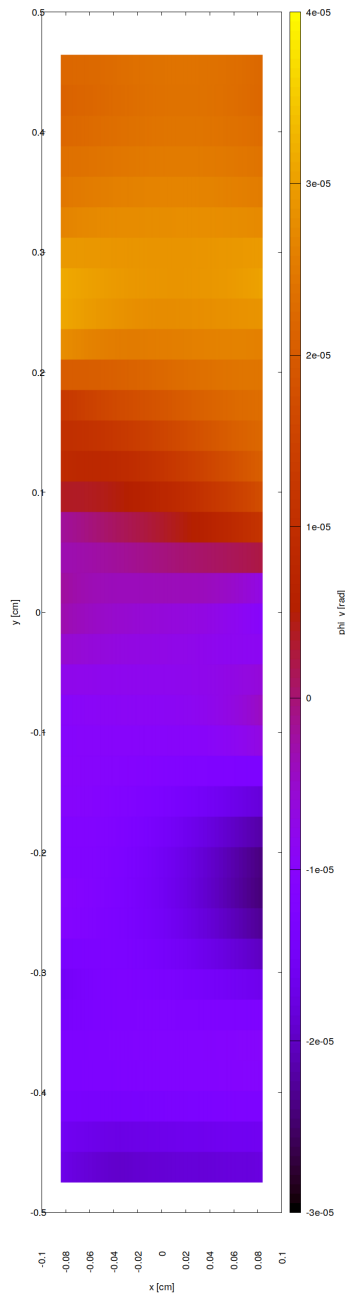


Figure 22.38: Surface slope error in meridional direction (y) of optical element #03 (BS) for case #4 for 21800 eV photon energy setting.



## 22.13 Incident photon irradiance on surface

"fig/BS\_choice\_C111\_Bragg/plot039.png" Lbl.:BS\_choice\_C111\_Bragg\_false\_colour\_plot\_I\_inc\_foot\_oe04\_c1\_21800eV

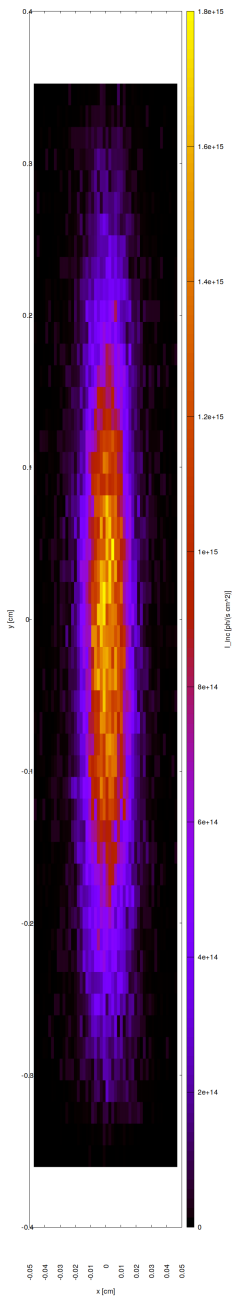


Figure 22.39: Incident photon irradiance on surface of optical element #04 (CM2) for case #1 for 21800 eV photon energy setting.

```
"fig/BS_choice_C111_Bragg/plot040.png" Lbl.:BS_choice_C111_Bragg_false_colour_plot_I_inc_foot_oe04_c2_21800eV
```

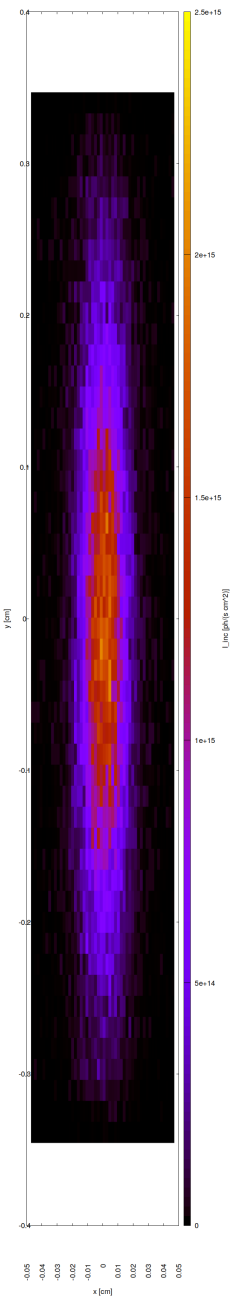


Figure 22.40: Incident photon irradiance on surface of optical element #04 (CM2) for case #2 for 21800 eV photon energy setting.

```
"fig/BS_choice_C111_Bragg/plot041.png" Lbl.:BS_choice_C111_Bragg_false_colour_plot_I_inc_foot_oe04_c3_21800eV
```

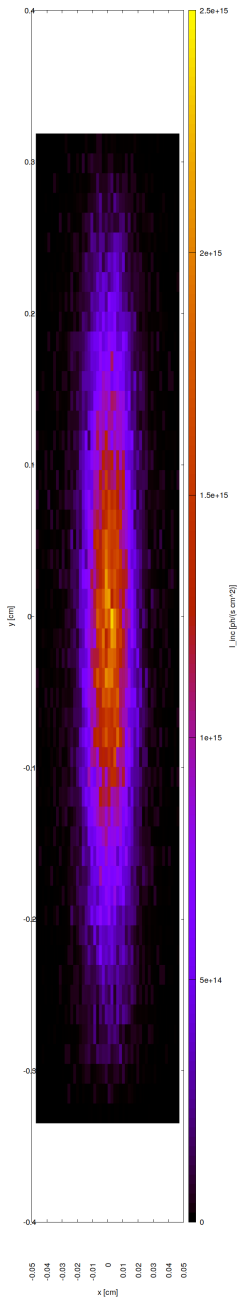


Figure 22.41: Incident photon irradiance on surface of optical element #04 (CM2) for case #3 for 21800 eV photon energy setting.

```
"fig/BS_choice_C111_Bragg/plot042.png" Lbl.:BS_choice_C111_Bragg_false_colour_plot_I_inc_foot_oe04_c4_21800eV
```

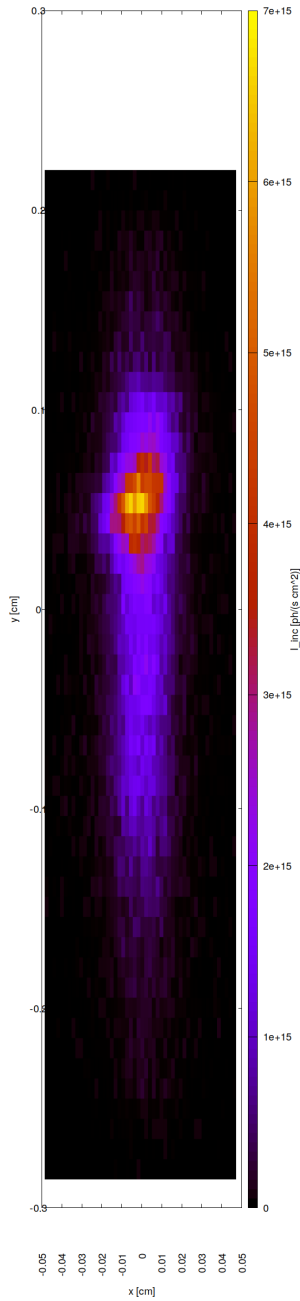


Figure 22.42: Incident photon irradiance on surface of optical element #04 (CM2) for case #4 for 21800 eV photon energy setting.

## 22.14 Photon irradiance in beam cross section

"fig/BS\_choice\_C111\_Bragg/plot043.png" Lbl.:BS\_choice\_C111\_Bragg\_false\_colour\_plot\_I\_foc\_oe04\_c1\_21800eV

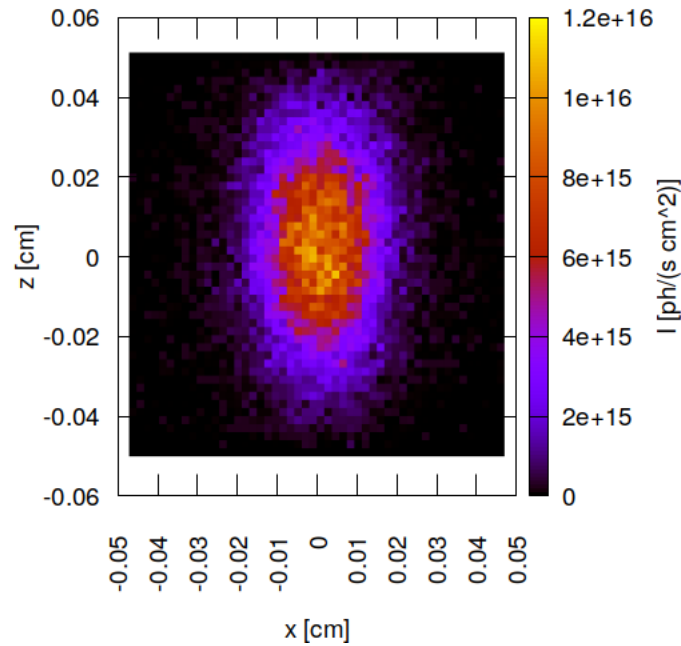


Figure 22.43: Photon irradiance in beam cross section of optical element #04 (CM2) for case #1 for 21800 eV photon energy setting.

"fig/BS\_choice\_C111\_Bragg/plot044.png" Lbl.:BS\_choice\_C111\_Bragg\_false\_colour\_plot\_I\_foc\_oe04\_c2\_21800eV

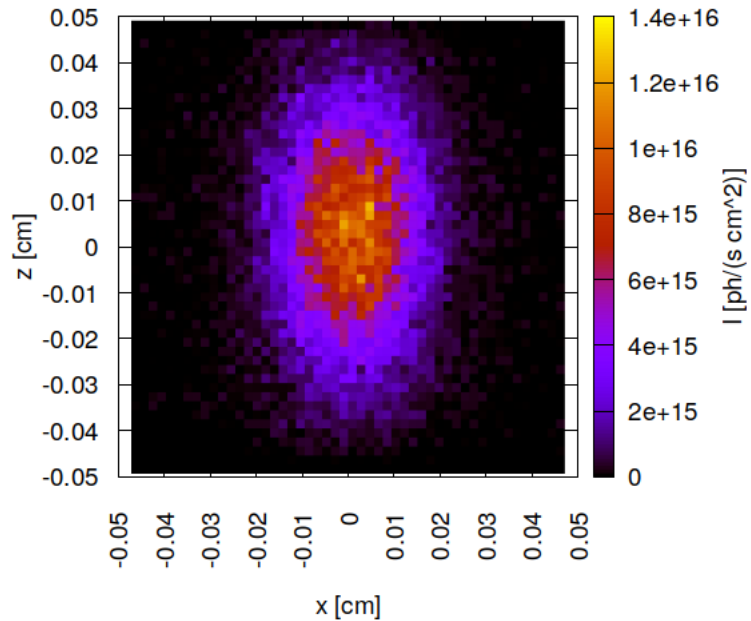


Figure 22.44: Photon irradiance in beam cross section of optical element #04 (CM2) for case #2 for 21800 eV photon energy setting.

"fig/BS\_choice\_C111\_Bragg/plot045.png" Lbl.:BS\_choice\_C111\_Bragg\_false\_colour\_plot\_I\_foc\_oe04\_c3\_21800eV

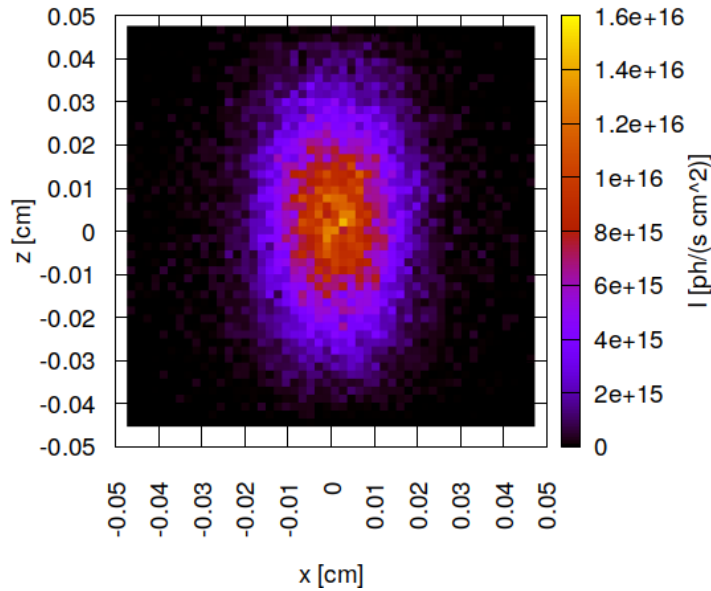


Figure 22.45: Photon irradiance in beam cross section of optical element #04 (CM2) for case #3 for 21800 eV photon energy setting.

"fig/BS\_choice\_C111\_Bragg/plot046.png" Lbl.:BS\_choice\_C111\_Bragg\_false\_colour\_plot\_I\_foc\_oe04\_c4\_21800eV

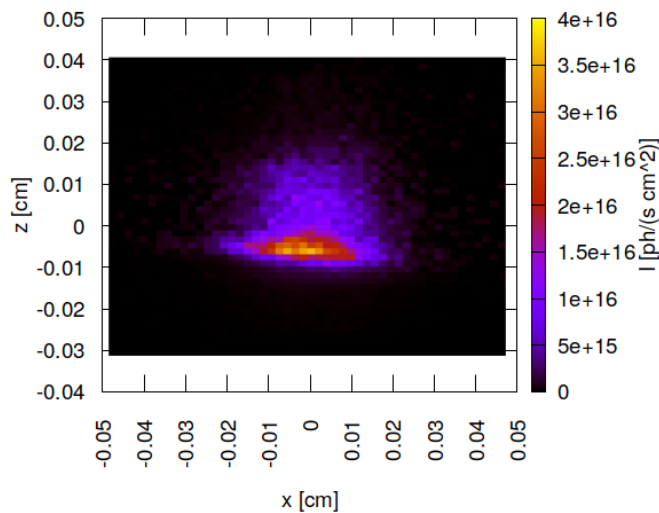


Figure 22.46: Photon irradiance in beam cross section of optical element #04 (CM2) for case #4 for 21800 eV photon energy setting.

## 22.15 Spectral photon flux in beam cross section

"fig/BS\_choice\_C111\_Bragg/plot047.png" Lbl.:BS\_choice\_C111\_Bragg\_2d\_plot\_I\_bandfoc\_oe04\_c1\_21800eV

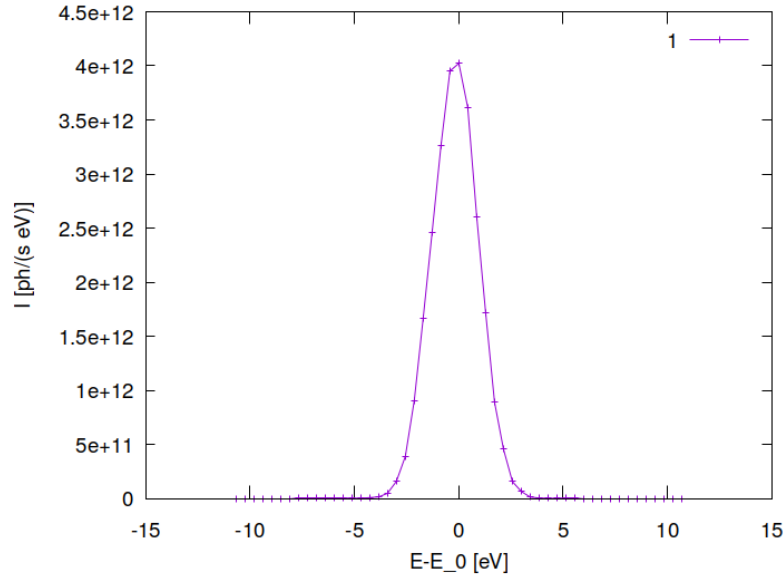


Figure 22.47: Spectral photon flux in beam cross section of optical element #04 (CM2) for case #1 for 21800 eV photon energy setting.

"fig/BS\_choice\_C111\_Bragg/plot048.png" Lbl.:BS\_choice\_C111\_Bragg\_2d\_plot\_I\_bandfoc\_oe04\_c2\_21800eV

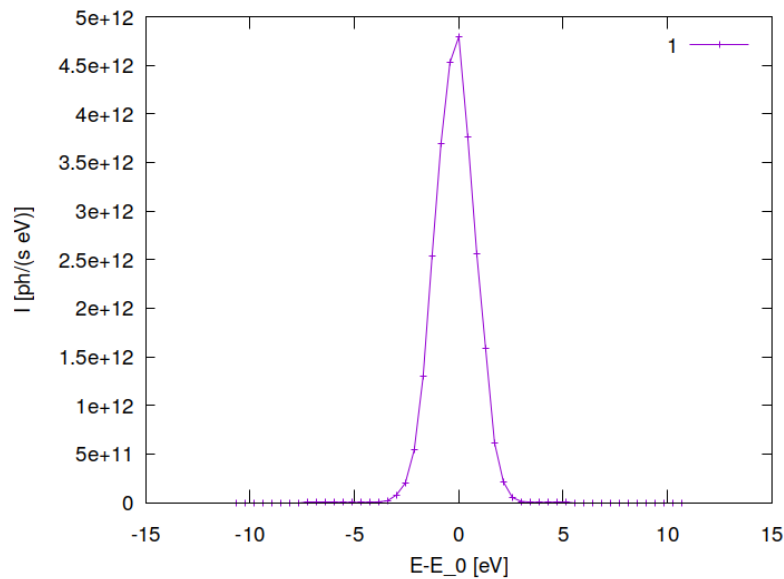


Figure 22.48: Spectral photon flux in beam cross section of optical element #04 (CM2) for case #2 for 21800 eV photon energy setting.

```
"fig/BS_choice_C111_Bragg/plot049.png" Lbl.:BS_choice_C111_Bragg_2d_plot_I_bandfoc_oe04_c3_21800eV
```

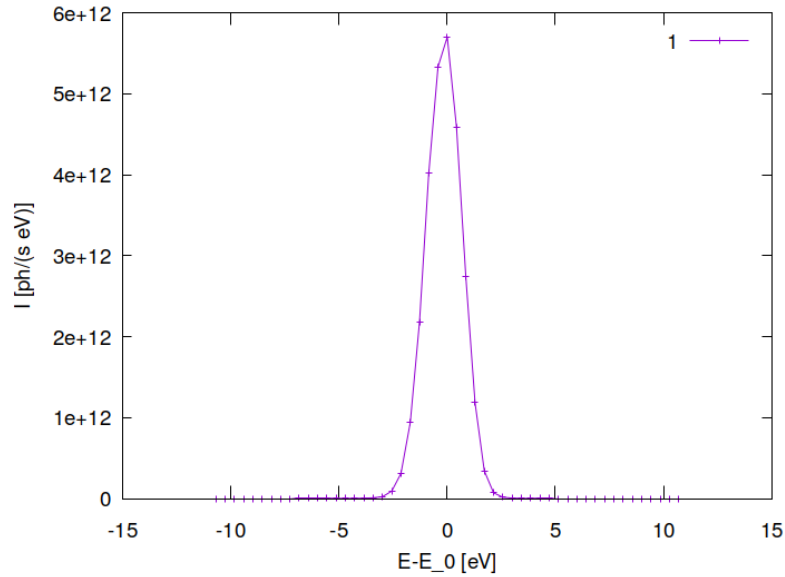


Figure 22.49: Spectral photon flux in beam cross section of optical element #04 (CM2) for case #3 for 21800 eV photon energy setting.

```
"fig/BS_choice_C111_Bragg/plot050.png" Lbl.:BS_choice_C111_Bragg_2d_plot_I_bandfoc_oe04_c4_21800eV
```

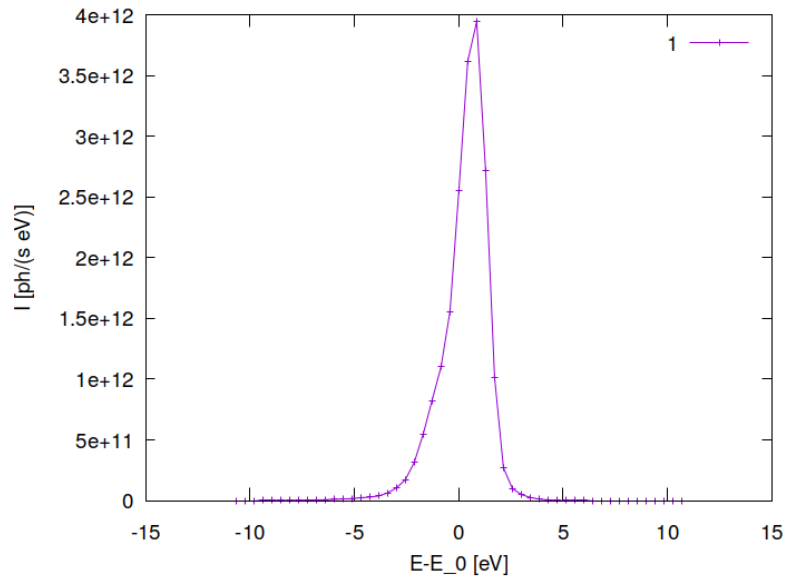


Figure 22.50: Spectral photon flux in beam cross section of optical element #04 (CM2) for case #4 for 21800 eV photon energy setting.

# Chapter 23

## Discussion of results

### 23.1 Silicon or diamond for the beam splitter

Silicon 333 provides nicely large deflection angles,  $2\theta_B \approx 32^\circ$ , but compared to diamond 111 or Si111 five to eight times lower reflectivity and thus five to ten times less flux in the monochromatized beam as shown in Figs. 7.32, 12.20, 17.20, and 22.20.<sup>1</sup> This is mainly due to Si333's small structure factor. This basically disqualifies Si333.

Silicon 111 on the other hand has the smallest deflection angle  $2\theta_B = 10.4^\circ$ , and would need 5.54 metres between first and second crystal to guarantee a minimum distance of one metre between the branches.

As absorption is much higher in silicon, deformation under heat load is much larger if it is not kept at cryogenic temperatures. Deformation reduces reflectivity considerably. Hence, both silicon variants need cryo-cooling otherwise their reflectivity lags behind that of diamond and temperatures rise above 200°Celsius (see Figs. 7.17 and 12.5). Above that, the thickness of the silicon beam splitters has been chosen to be ambitiously thin, as to give them a chance despite of their considerably higher absorption. Whilst silicon wafers of 30 or 20 microns thickness are not unheard of, the question remains, whether the crystal structure quality, the stability and longevity is sufficient for a monochromator. We are not aware of any monochromators with such thin crystals. Hence such a monochromator would be highly experimental.

Using diamond 111, either in Laue or Bragg geometry, seems to be the best option. The flux in the monochromatized beam is comparable to that of cryo cooled Si111, and the deflection angle is with  $2\theta_B \approx 16^\circ$  considerably larger, allowing for a moderate 3.66 metre distance between crystals. Above that diamond requires water cooling only.

### 23.2 Reduced filtering with diamond beam splitter

The stability of a diamond beam splitter under heat load and the match of materials allows to reduce upstream diamond filtering, thus keeping overall absorption the same or lower.

For the SinCrys side branch the gain in narrow band photon flux in Figs. 17.20 and 22.20 from reducing filtering is very small. Without any filters in the upstream beam path, flux is actually lowest, most likely due to a reduction in Bragg reflectivity by heat buckling. In this case, there are also many indications for a considerable

---

<sup>1</sup>Considering flux after the second crystal – here Ge220 – takes into account effects on throughput by the beam splitters deformation under heat load.

beam distortion. The false colour plots of the beam profile on the surface and in the continuation plane of optical element #4 in Figs. 22.42 and 22.46 respectively show this clearly. No filters in seems not to be a viable modus operandi.

The effect of reduced filtering on the transmitted beam to the main branch can be expected to be more pronounced, as photon energies there are lower and hence absorption generally higher. This will be discussed in a different part, where the transmitted beam is considered.

### 23.3 Germanium or diamond for the second crystal

In all previous simulations with a diamond 111 beam splitter Ge220 was used for the second crystal. Since Ge220 has a by 3% smaller inter-planar spacing compared to diamond 111, the deflection angle is off by the same order of magnitude. A large fraction of this mismatch can be caught by simply off-setting the germanium crystal and all downstream components by a small constant angle. This small permanent kink in the beamline would need to be around 8.2 milliradians for the given wavelength range.

Unfortunately, due to refraction the mismatch has a smaller, wavelength dependent part, too, as carbon and germanium differ in their dispersive properties. Over the given wavelength range this smaller part varies over a range of 1.4 milliradians. This can be derived from the Bragg angles given in Table 21.4. Bare in mind, the overall deflection angle is twice the Bragg angle and hence the angular offset is twice the difference of the Bragg angles. Over a distance of just one metre 1.4 milliradians correspond to an offset of 1.4 millimetres. This is of the order of the perimeter's diameter of the lens elements in the CRL. Therefore, one would have to tune the lateral positions of the CRLs, that will be following straight after the monochromator, and all other downstream components. If one would use focussing mirrors instead, only the mirror angle would need to be tuned, which is probably why Ge220 is a popular choice in combination with diamond beam splitters at other beamlines.

In combination with CRLs though choosing diamond 111 for the second crystal instead avoids a lot of complications in the form of extra actuators, motion control units and a generally large number of degrees of freedom that need to be adjusted. Therefore, in the following simulations diamond 111 is generally employed as a second monochromator crystal. For the sake of simplicity Bragg geometry is chosen, as in the case of the germanium crystal.

## **Part II**

# **Beam splitters effect on main beam**

## Chapter 24

# Setup for the modelling of the transmitted main branch in the case of Laue geometry

A thin CVD diamond crystal is employed as a diffractive beam splitter, using the 111 reflection in Laue geometry. The diamond 111 reflection diverts radiation within a narrow bandwidth of

$$\delta E/E = \delta\theta/\tan\theta$$

to the SinCrys side station. The thickness of the diamond crystal slab has been optimised in order to maximise 111 reflectivity under the constraint of keeping absorption of the transmitted main beam low.

This setup ends after the beam splitter, as the main task is to investigate the latter's effect on the transmitted main beam. Unfortunately the employed ray-tracing program, Shadow3 [15], cannot model transmission through a thin crystal where the beam is fulfilling or nearly fulfilling the Bragg condition. Hence, the transmitted part of the pendel-solution or anomalous absorption are beyond reach, unless considerable effort would be made to integrate another ray-tracing program.

Far from the Bragg condition though, the crystal acts like a normal absorber, like e.g. a thin sheet of metal. To include also refraction from front and rear surface, the model of a lens element was chosen as a substitute. Since a lens element consists of two optical surfaces, the employed ray tracing program Shadow3 uses a model with two consecutive optical elements. As the beam passes through the beam splitter at an angle, it is necessary to rotate both surfaces around a common centre, such that the deformations on both surfaces align correctly. The usual mechanism for that, by the definition of the incidence angle, rotates each surface around their respective intersection point with the optical axis a.k.a. node. To mimic a common rotation centre, the exit surface would need to be translated both along and transversal to the optical axis. An easier way, and hence the chosen one, is to rotate the source around the node of the first surface, which is possible in Shadow3, and requires a single parameter to be changed.

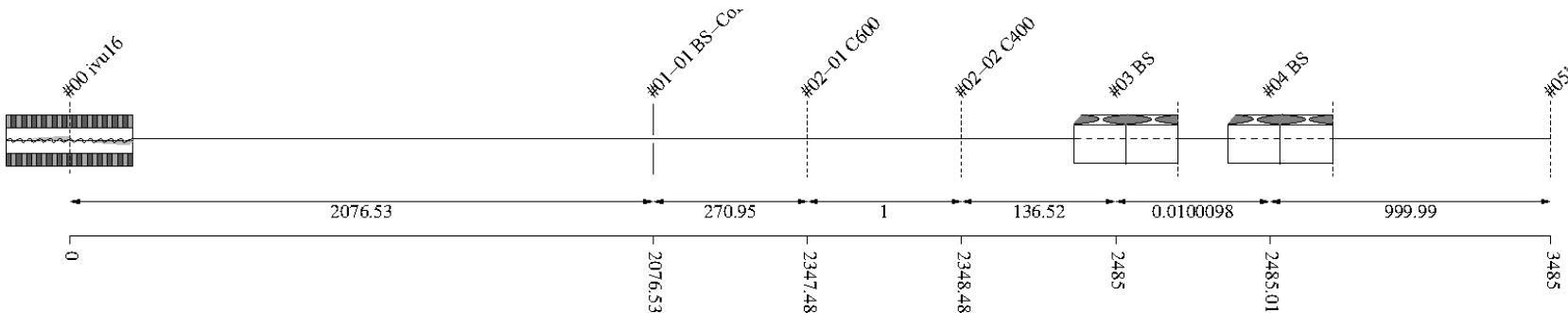


Figure 24.1: Schematic of optical setup

#	Name	Pathlen. cm	Descript.	Shape	Pitch* deg	Roll deg	Yaw deg	x_min cm	x_max cm	y_min cm	y_max cm	Thick. cm	Surface
0	ivu16	0	undulator	auto	0	0	0	-0.0027	0.0027	-0.0002	0.0002	auto	
1		2076.53	none	plane	0	0	0	-inf	inf	-inf	inf		perfect
1-1	BS-Collim	2076.53	aperture	rectangle	0	0	0	-0.035	0.035	-0.035	0.035		
2	Filter	2347.48	none	plane	0	0	0	-inf	inf	-inf	inf		perfect
2-1	C600	2347.48	C-filter	rectangle	0	0	0	-inf	inf	-inf	inf	0.06	
2-2	C400	2348.48	C-filter	rectangle	0	0	0	-inf	inf	-inf	inf	0.04	
3	BS	2485	vac/C-lens surface	cylinder	0+0	90+0	0+0	-0.15	0.15	-0.15	0.15		predefined
4	BS	2485.01	C/vac-lens surface	cylinder	0	0	0	-0.15	0.15	-0.15	0.15		heat bump
5	DanMAX	2485.01	none	plane	0+0	0+0	0+0	-inf	inf	-inf	inf		perfect
5'		3485	continuation plane		0	0	0						

Table 24.1: Setup parameters common to all components. (\*Glancing angle for mirrors, multilayers and crystals. Angle to surface normal otherwise.)

**Rays:** Polar type = total

Polar phase = 0 deg

Polar degree = 0

Is coherent = no

**Spectrum:** E min = 500 eV

E max = 40000 eV

Relative linewidth = 1

**Band:** Bandwidth = 0.0005

**Insertion Device:** lambda period = 1.6 cm

n period = 187

I electron = 0.5 A

E electron = 3 GeV

y horizontal waist = 0 cm

y vertical waist = 0 cm

epsilon x = 3.2E-08 cm rad

epsilon z = 8E-10 cm rad

K y = 1.66

K ymax = 1.7

Divergence limit = 5E-05 rad

**Undulator:** n harmonic max = 99

Tuning type = fixed gap

l aperture = 2076.53 cm

dx aperture = 0.07 cm

dz aperture = 0.07 cm

#1

**Screen:** Is absorbing[1] = no

**Shape:** Thickness = 0 cm

#2 Filter

**Screen:** Is absorbing[1] = yes

Is absorbing[2] = yes

Molecular formula[1] = C

Molecular formula[2] = C

Mass density[1] = 3.5 g/cm^3

Mass density[2] = 3.5 g/cm^3

Thickness[1] = 0.06 cm

Thickness[2] = 0.04 cm

**Shape:** Thickness = 0 cm

### #3 BS

**Dielectric:** Reflectivity type = polarisation

Is constant = no

Mass density = 3.5 g/cm<sup>3</sup>

**Geometry:** g = 0 cm

b = 0 cm

Is thin = yes

n clones = 1

Focus automatically = no

**Shape:** Defined by = user

Is convex = no

Is extruded = yes

Radius = 4177 cm

Thickness = 0.01 cm

**Boundary:** Type = rectangle

**Extruded:** Angle z = 0 deg

**Surface:** Is rough = no

### #4 BS

**Dielectric:** Reflectivity type = polarisation

Is constant = yes

delta refraction = 0

beta absorption = 0

**Geometry:** g = 0 cm

b = 0 cm

Is thin = yes

n clones = 1

Focus automatically = no

**Shape:** Defined by = user

Is convex = no

Is extruded = yes

Radius = 4177 cm

Thickness = 0.01 cm

**Boundary:** Type = rectangle

x rim = 0.5 cm

y rim = 0.5 cm

**Extruded:** Angle z = 0 deg

**Surface:** Is rough = no

**FEA:** Design type = type specific

Surface design = sheet with cooling loop

Is isotropic = no

Angle x = 45 deg

Angle y = 35.2644 deg

Angle z = 0 deg

Mass density = 3.516 g/cm<sup>3</sup>

**Heat:** Heat transfer type[1] = insulated

Heat transfer type[2] = heat transfer

Heat transfer type[3] = insulated

Heat transfer type[4] = insulated

Heat transfer type[5] = heat transfer

Heat transfer type[6] = flux

Heat transfer type[7] = insulated

Heat transfer type[8] = heat transfer

Heat transfer type[9] = heat sink

Heat transfer coefficient = 1 W/(cm<sup>2</sup>K)

Heat sink coefficient = 10 W/(cm<sup>2</sup>K)

T reference = 293.15 K

T cooling = 293.15 K

Heat capacity = 0.54 J/(gK)

Thermal conductivity[1] = 25 W/(cmK<sup>n</sup>)

**Stress and strain:** Constraint[1] = free

Constraint[2] = kinematic

Constraint[3] = free

Constraint[4] = free

Constraint[5] = free

Constraint[6] = free

Constraint[7] = free

Constraint[8] = free

Constraint[9] = free

Thermal expansion tensor[1] = 1.1E-06 1/K

Thermal expansion tensor[2] = 1.1E-06 1/K

Thermal expansion tensor[3] = 1.1E-06 1/K

Thermal expansion tensor[4] = 0 1/K

Thermal expansion tensor[5] = 0 1/K

Thermal expansion tensor[6] = 0 1/K

Stiffness tensor(1)(1) = 1.07861E+12 Pa

Stiffness tensor(2)[1] = 1.2663E+11 Pa

Stiffness tensor(2)[2] = 1.07861E+12 Pa

Stiffness tensor(3)[1] = 1.2663E+11 Pa

Stiffness tensor(3)[2] = 1.2663E+11 Pa

Stiffness tensor(3)[3] = 1.07861E+12 Pa

Stiffness tensor(4)[1] = 0 Pa

Stiffness tensor(4)[2] = 0 Pa

Stiffness tensor(4)[3] = 0 Pa  
Stiffness tensor(4)[4] = 5.7756E+11 Pa  
Stiffness tensor(5)[1] = 0 Pa  
Stiffness tensor(5)[2] = 0 Pa  
Stiffness tensor(5)[3] = 0 Pa  
Stiffness tensor(5)[4] = 0 Pa  
Stiffness tensor(5)[5] = 5.7756E+11 Pa  
Stiffness tensor(6)[1] = 0 Pa  
Stiffness tensor(6)[2] = 0 Pa  
Stiffness tensor(6)[3] = 0 Pa  
Stiffness tensor(6)[4] = 0 Pa  
Stiffness tensor(6)[5] = 0 Pa  
Stiffness tensor(6)[6] = 5.7756E+11 Pa

## #5 DanMAX

**Shape:** Thickness = 0 cm

# Chapter 25

## Finite element analysis (FEA)

Heat load, temperature gradients and subsequent deformation under thermal stress should be the same as for the equivalent crystal model described earlier 14. To show, that this is the case, is the purpose of this chapter.

### 25.1 FEA with both 600 and 400 micron diamond filters in

```
"fig/Main_beam_C111_Laue/fea_plot_geom_c02_16955eV_04.png" Lbl.:Main_beam_C111_Laue_Surface_plot_fea_plot_geom_c02_16955eV_04
```

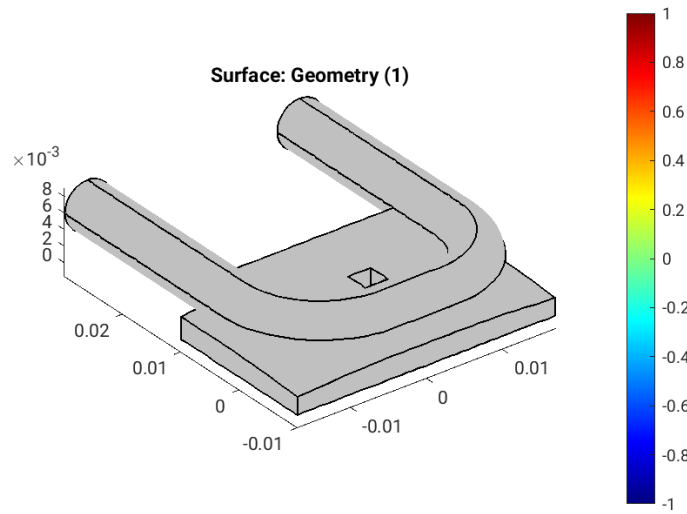


Figure 25.1: Geometry [m] of optical element #04, for case #02, at 16955 eV photon energy setting.

```
"fig/Main_beam_C111_Laue/fea_plot_cnstr_c02_16955eV_04.png" Lbl.:Main_beam_C111_Laue_Surface_plot_fea_plot_cnstr_c02_16955eV_04
```

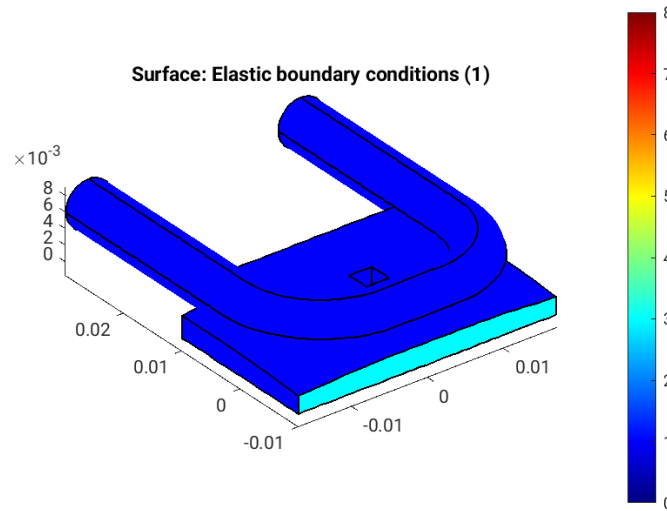


Figure 25.2: Elastic boundary conditions on the surfaces of optical element #04, for case #02, at 16955 eV photon energy setting. Color legend: Blue: Surface can move freely in all directions. Cyan: Tension free kinematic mounting. Minimalistic constraint for three points in surface. One point is fixed, the second can move in one direction, and the third in two, in a fashion that defines angular orientation without introducing stress if the surface expands.

```
"fig/Main_beam_C111_Laue/fea_plot_trans_c02_16955eV_04.png" Lbl.:Main_beam_C111_Laue_Surface_plot_fea_plot_trans_c02_16955eV_04
```

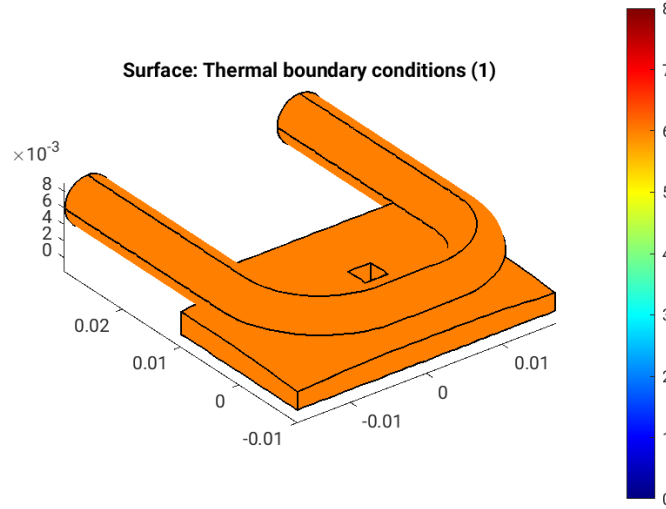


Figure 25.3: Thermal boundary conditions on the surfaces of optical element #04, for case #02, at 16955 eV photon energy setting. Color legend: Orange: No heat transfer at all. Blue: Heat transfer coefficient and temperature difference define heat current density,  $j_q = h(T - T_{cool})$ . Red: Forced heat flux from e.g. absorbed X-rays. Cyan: Heat transfer coefficient and temperature difference define heat current density,  $j_q = h^* \Delta T$  (only at inner surfaces).

```
"fig/Main_beam_C111_Laue/fea_plot_heattrans_c02_16955eV_04.png" Lbl.:Main_beam_C111_Laue_Surface_plot_fea_plot_heattrans_c02_16955eV_04
```

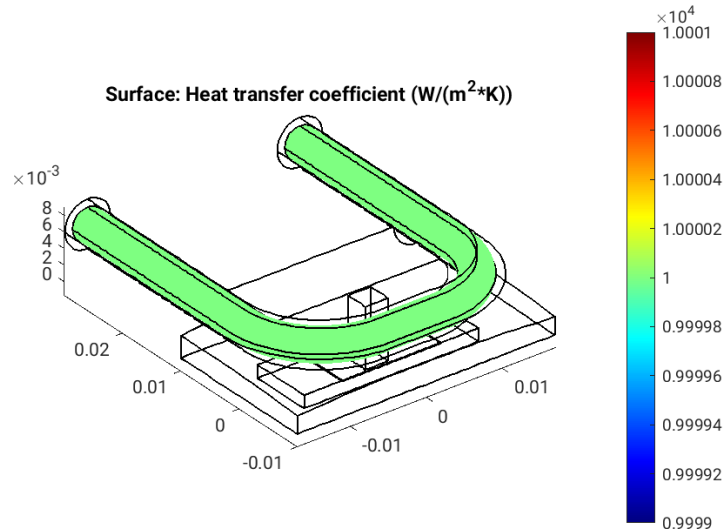


Figure 25.4: Heat transfer coefficient,  $h$  [W/(m<sup>2</sup> K)], on the surfaces of optical element #04, for case #02, at 16955 eV photon energy setting.

```
"fig/Main_beam_C111_Laue/fea_plot_heatflux_c02_16955eV_04.png" Lbl.:Main_beam_C111_Laue_Surface_plot_fea_plot_heatflux_c02_16955eV_04
```

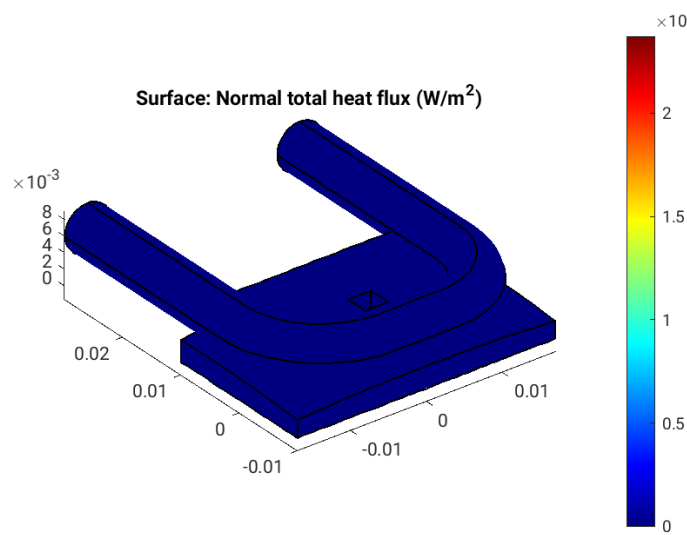


Figure 25.5: Absorbed irradiance,  $p_{\text{abs}}$  [W/m<sup>2</sup>], on the surfaces of optical element #04, for case #02, at 16955 eV photon energy setting.

```
"fig/Main_beam_C111_Laue/fea_plot_temp_c02_16955eV_04.png" Lbl.:Main_beam_C111_Laue_Surface_plot_fea_plot_temp_c02_16955eV_04
```

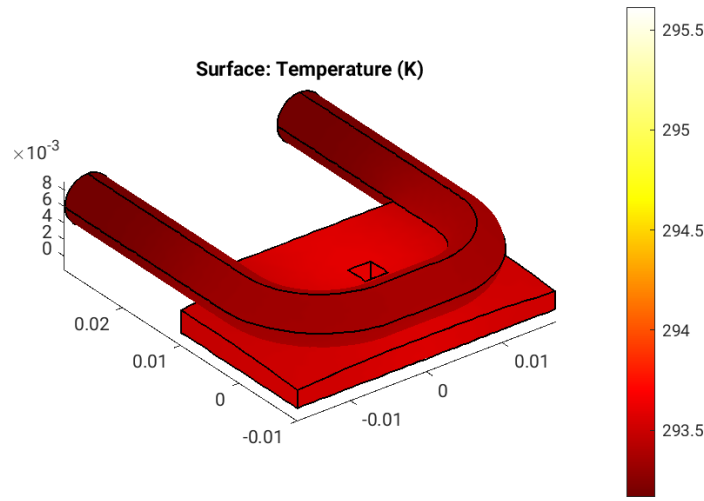


Figure 25.6: Temperature,  $T$  [K], on the surfaces of optical element #04, for case #02, at 16955 eV photon energy setting.

"fig/Main\_beam\_C111\_Laue/fea\_plot\_thermcond\_c02\_16955eV\_04.png" Lbl.:Main\_beam\_C111\_Laue\_Surface\_plot\_fea\_plot\_thermcond\_c02\_16955eV\_04

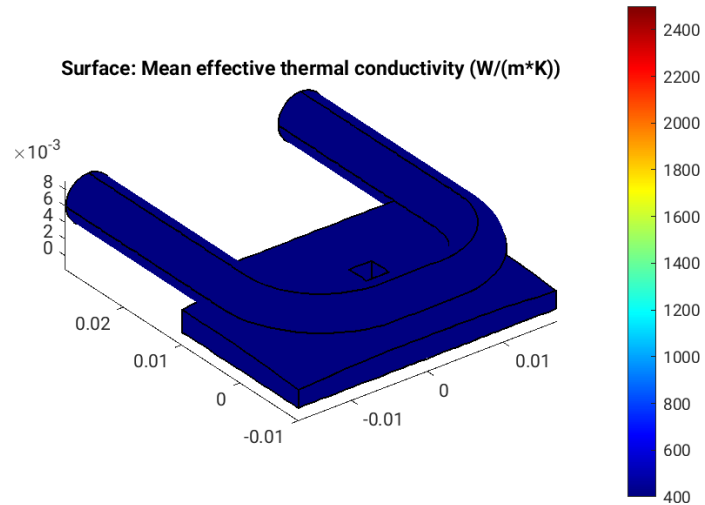


Figure 25.7: Thermal conductivity, lambda [W/(m K)], on the surfaces of optical element #04, for case #02, at 16955 eV photon energy setting.

"fig/Main\_beam\_C111\_Laue/fea\_plot\_stress\_c02\_16955eV\_04.png" Lbl.:Main\_beam\_C111\_Laue\_Surface\_plot\_fea\_plot\_stress\_c02\_16955eV\_04

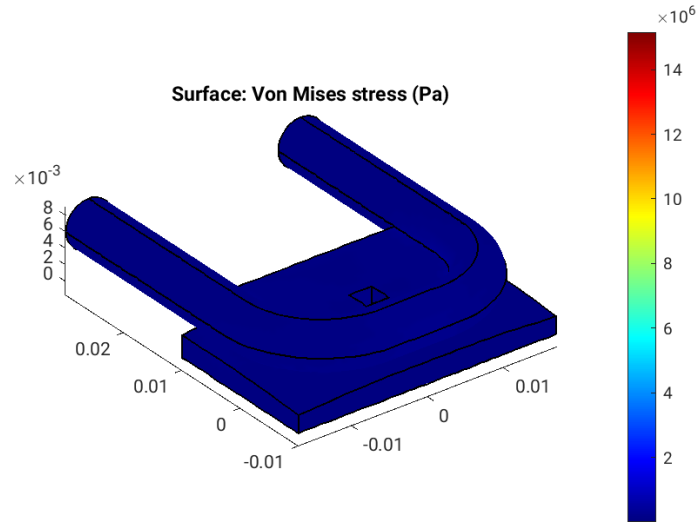


Figure 25.8: Von Mises stress, sigma [Pa], on the surfaces of optical element #04, for case #02, at 16955 eV photon energy setting.

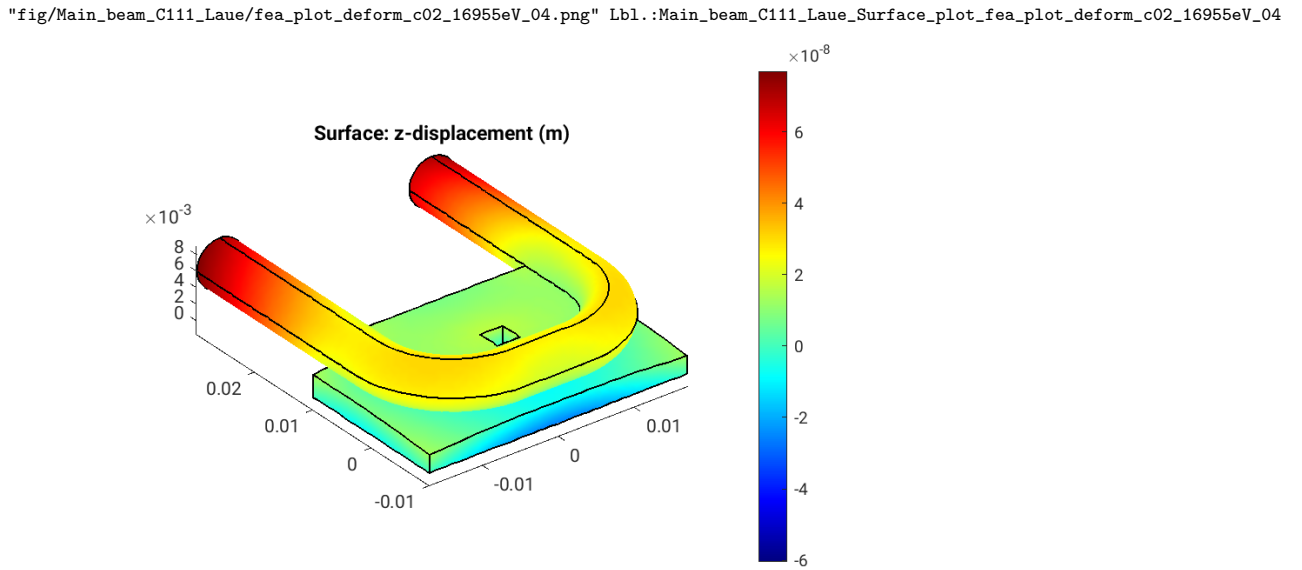


Figure 25.9: Thermoelastic deformation,  $dz$  [m], on the surfaces of optical element #04, for case #02, at 16955 eV photon energy setting.

## 25.2 FEA with only 400 micron diamond filter in

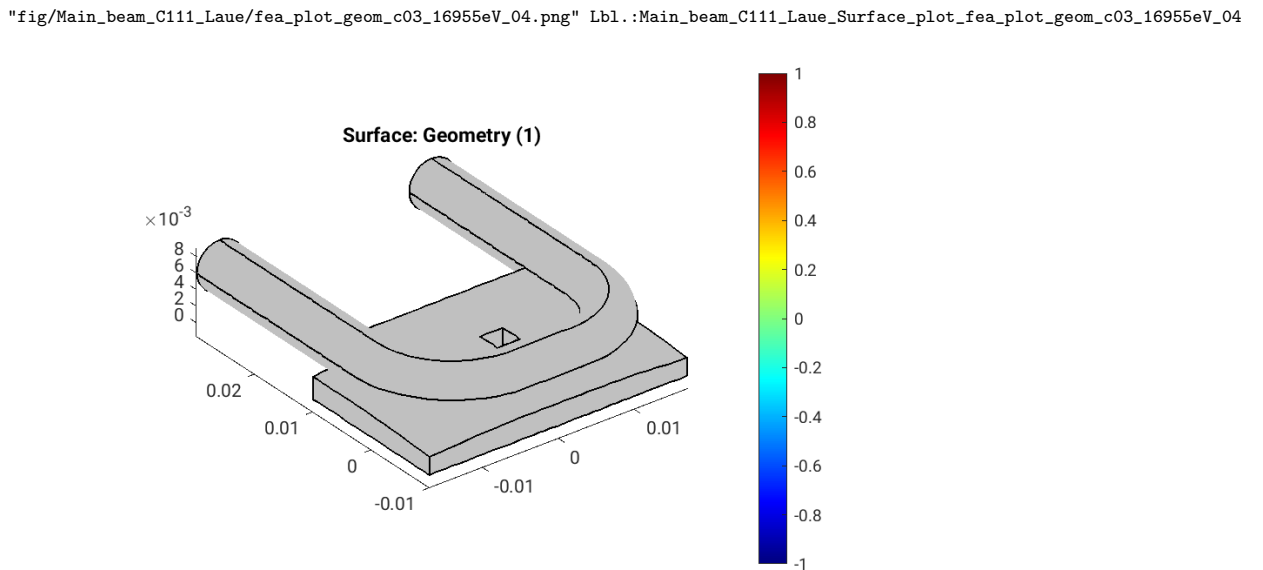


Figure 25.10: Geometry [m] of optical element #04, for case #03, at 16955 eV photon energy setting.

```
"fig/Main_beam_C111_Laue/fea_plot_cnstr_c03_16955eV_04.png" Lbl.:Main_beam_C111_Laue_Surface_plot_fea_plot_cnstr_c03_16955eV_04
```

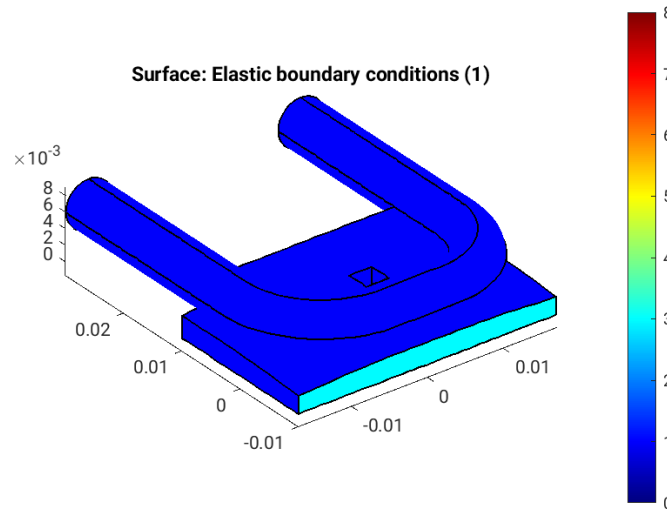


Figure 25.11: Elastic boundary conditions on the surfaces of optical element #04, for case #03, at 16955 eV photon energy setting. Color legend: Blue: Surface can move freely in all directions. Cyan: Tension free kinematic mounting. Minimalistic constraint for three points in surface. One point is fixed, the second can move in one direction, and the third in two, in a fashion that defines angular orientation without introducing stress if the surface expands.

```
"fig/Main_beam_C111_Laue/fea_plot_trans_c03_16955eV_04.png" Lbl.:Main_beam_C111_Laue_Surface_plot_fea_plot_trans_c03_16955eV_04
```

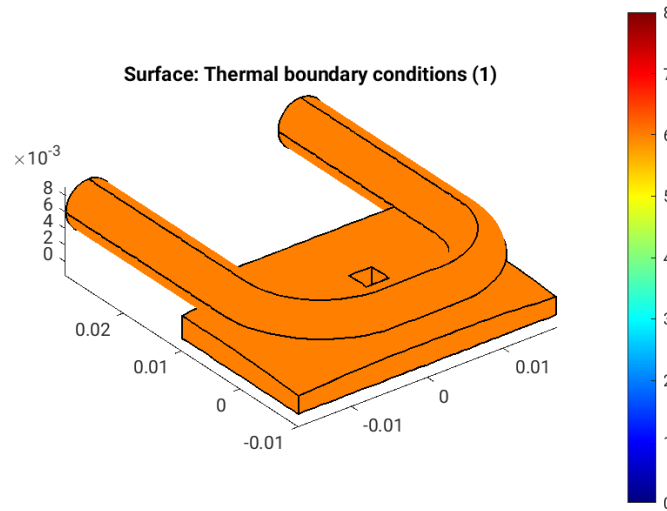


Figure 25.12: Thermal boundary conditions on the surfaces of optical element #04, for case #03, at 16955 eV photon energy setting. Color legend: Orange: No heat transfer at all. Blue: Heat transfer coefficient and temperature difference define heat current density,  $j_q = h(T - T_{cool})$ . Red: Forced heat flux from e.g. absorbed X-rays. Cyan: Heat transfer coefficient and temperature difference define heat current density,  $j_q = h^* \Delta T$  (only at inner surfaces).

```
"fig/Main_beam_C111_Laue/fea_plot_heattrans_c03_16955eV_04.png" Lbl.:Main_beam_C111_Laue_Surface_plot_fea_plot_heattrans_c03_16955eV_04
```

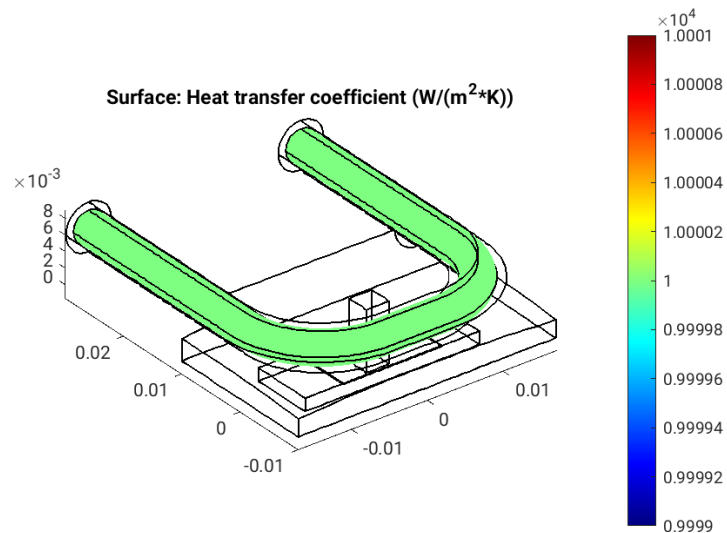


Figure 25.13: Heat transfer coefficient,  $h [W/(m^2 K)]$ , on the surfaces of optical element #04, for case #03, at 16955 eV photon energy setting.

```
"fig/Main_beam_C111_Laue/fea_plot_heatflux_c03_16955eV_04.png" Lbl.:Main_beam_C111_Laue_Surface_plot_fea_plot_heatflux_c03_16955eV_04
```

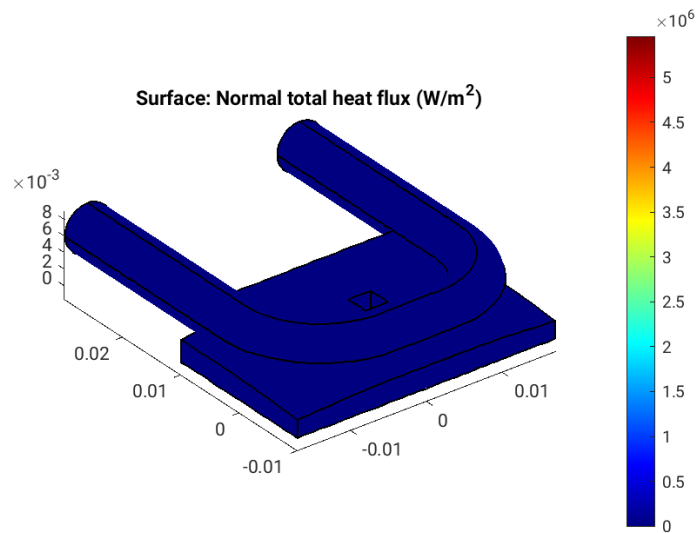


Figure 25.14: Absorbed irradiance,  $p_{\text{abs}}$  [W/m<sup>2</sup>], on the surfaces of optical element #04, for case #03, at 16955 eV photon energy setting.

```
"fig/Main_beam_C111_Laue/fea_plot_temp_c03_16955eV_04.png" Lbl.:Main_beam_C111_Laue_Surface_plot_fea_plot_temp_c03_16955eV_04
```

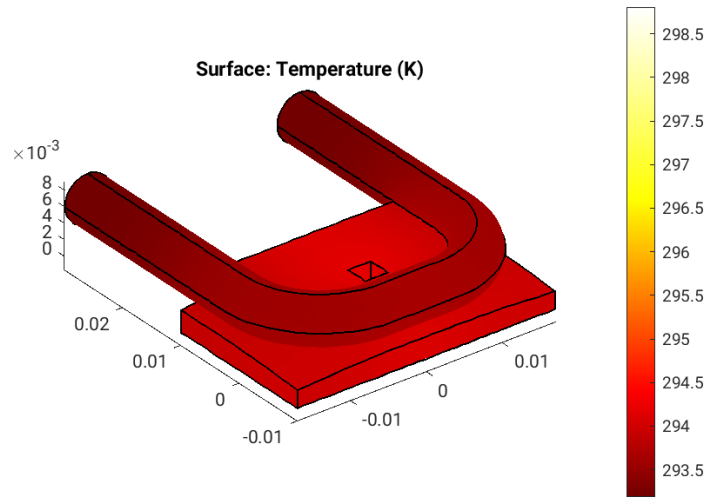


Figure 25.15: Temperature,  $T$  [K], on the surfaces of optical element #04, for case #03, at 16955 eV photon energy setting.

"fig/Main\_beam\_C111\_Laue/fea\_plot\_thermcond\_c03\_16955eV\_04.png" Lbl.:Main\_beam\_C111\_Laue\_Surface\_plot\_fea\_plot\_thermcond\_c03\_16955eV\_04

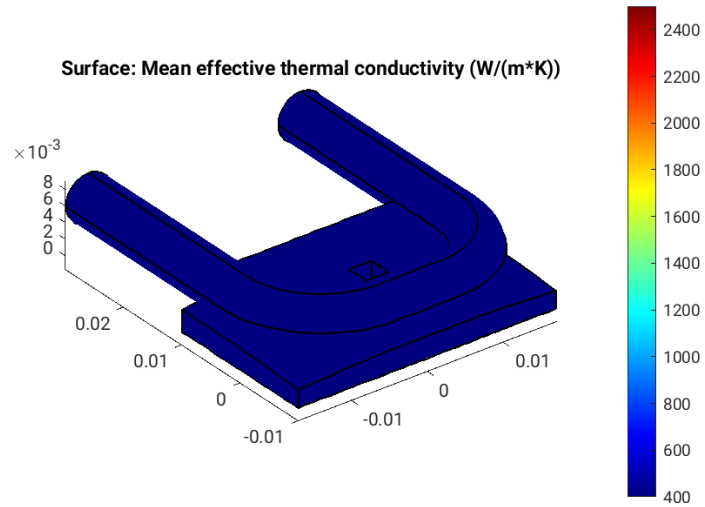


Figure 25.16: Thermal conductivity, lambda [W/(m K)], on the surfaces of optical element #04, for case #03, at 16955 eV photon energy setting.

"fig/Main\_beam\_C111\_Laue/fea\_plot\_stress\_c03\_16955eV\_04.png" Lbl.:Main\_beam\_C111\_Laue\_Surface\_plot\_fea\_plot\_stress\_c03\_16955eV\_04

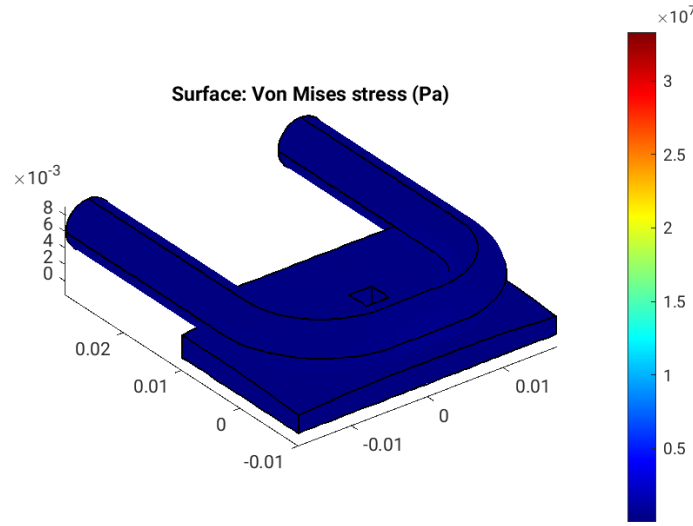


Figure 25.17: Von Mises stress, sigma [Pa], on the surfaces of optical element #04, for case #03, at 16955 eV photon energy setting.

```
"fig/Main_beam_C111_Laue/fea_plot_deform_c03_16955eV_04.png" Lbl.:Main_beam_C111_Laue_Surface_plot_fea_plot_deform_c03_16955eV_04
```

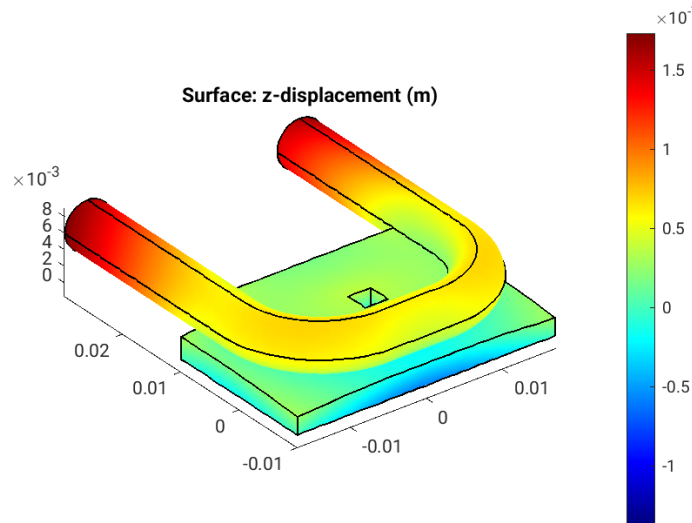


Figure 25.18: Thermoelastic deformation,  $dz$  [m], on the surfaces of optical element #04, for case #03, at 16955 eV photon energy setting.

### 25.3 FEA with no diamond filters in

```
"fig/Main_beam_C111_Laue/fea_plot_geom_c04_16955eV_04.png" Lbl.:Main_beam_C111_Laue_Surface_plot_fea_plot_geom_c04_16955eV_04
```

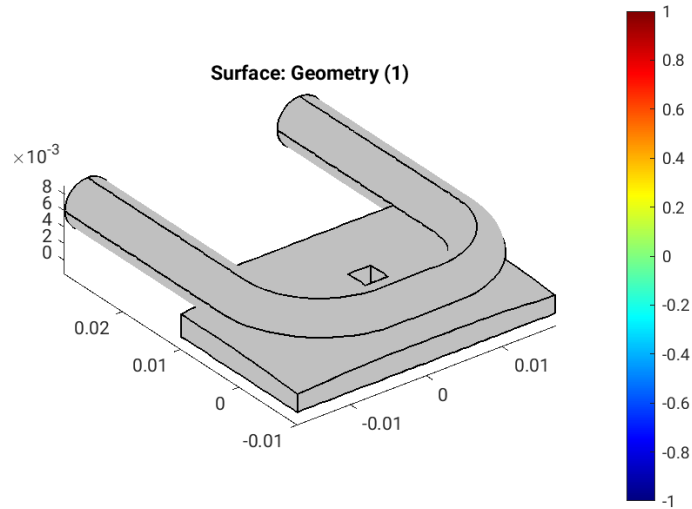


Figure 25.19: Geometry [m] of optical element #04, for case #04, at 16955 eV photon energy setting.

```
"fig/Main_beam_C111_Laue/fea_plot_cnstr_c04_16955eV_04.png" Lbl.:Main_beam_C111_Laue_Surface_plot_fea_plot_cnstr_c04_16955eV_04
```

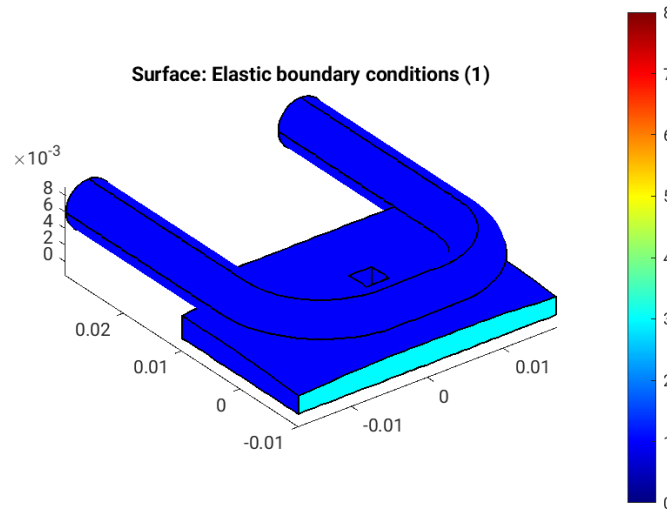


Figure 25.20: Elastic boundary conditions on the surfaces of optical element #04, for case #04, at 16955 eV photon energy setting. Color legend: Blue: Surface can move freely in all directions. Cyan: Tension free kinematic mounting. Minimalistic constraint for three points in surface. One point is fixed, the second can move in one direction, and the third in two, in a fashion that defines angular orientation without introducing stress if the surface expands.

```
"fig/Main_beam_C111_Laue/fea_plot_trans_c04_16955eV_04.png" Lbl.:Main_beam_C111_Laue_Surface_plot_fea_plot_trans_c04_16955eV_04
```

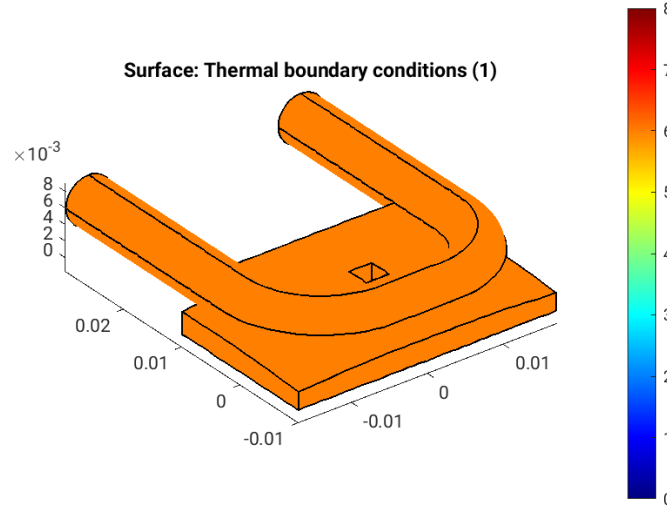


Figure 25.21: Thermal boundary conditions on the surfaces of optical element #04, for case #04, at 16955 eV photon energy setting. Color legend: Orange: No heat transfer at all. Blue: Heat transfer coefficient and temperature difference define heat current density,  $j_q = h(T - T_{cool})$ . Red: Forced heat flux from e.g. absorbed X-rays. Cyan: Heat transfer coefficient and temperature difference define heat current density,  $j_q = h^* \Delta T$  (only at inner surfaces).

```
"fig/Main_beam_C111_Laue/fea_plot_heattrans_c04_16955eV_04.png" Lbl.:Main_beam_C111_Laue_Surface_plot_fea_plot_heattrans_c04_16955eV_04
```

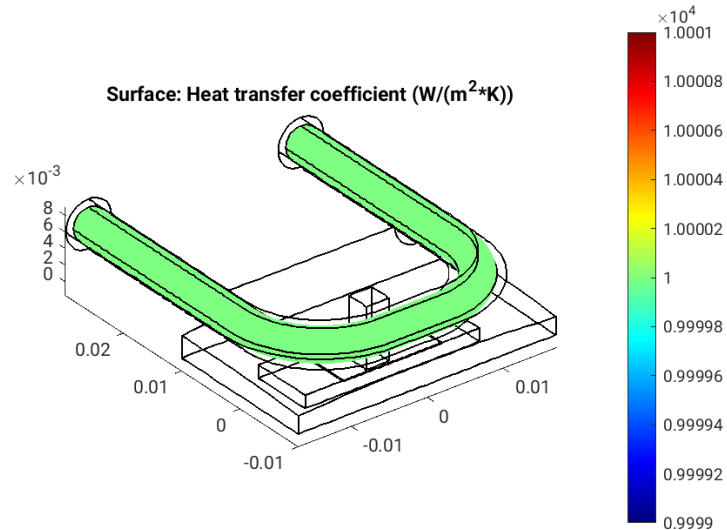


Figure 25.22: Heat transfer coefficient,  $h [W/(m^2 K)]$ , on the surfaces of optical element #04, for case #04, at 16955 eV photon energy setting.

```
"fig/Main_beam_C111_Laue/fea_plot_heatflux_c04_16955eV_04.png" Lbl.:Main_beam_C111_Laue_Surface_plot_fea_plot_heatflux_c04_16955eV_04
```

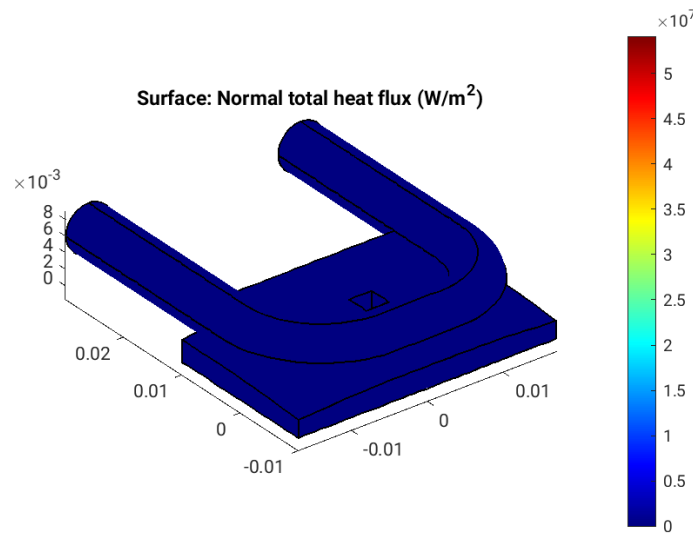


Figure 25.23: Absorbed irradiance,  $p_{\text{abs}}$  [W/m<sup>2</sup>], on the surfaces of optical element #04, for case #04, at 16955 eV photon energy setting.

```
"fig/Main_beam_C111_Laue/fea_plot_temp_c04_16955eV_04.png" Lbl.:Main_beam_C111_Laue_Surface_plot_fea_plot_temp_c04_16955eV_04
```

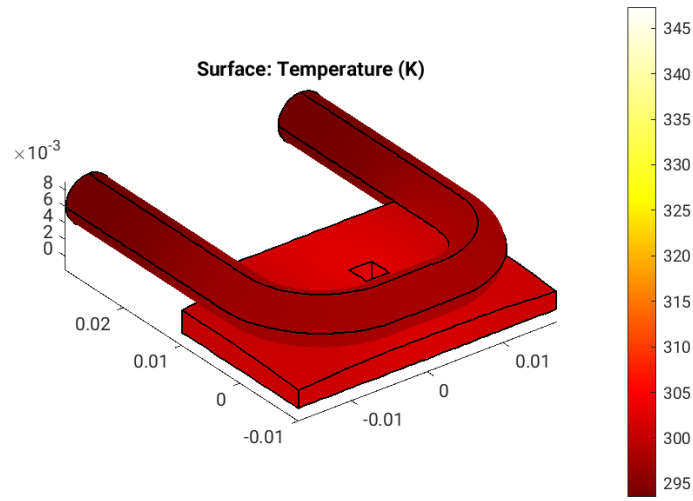


Figure 25.24: Temperature,  $T$  [K], on the surfaces of optical element #04, for case #04, at 16955 eV photon energy setting.

"fig/Main\_beam\_C111\_Laue/fea\_plot\_thermcond\_c04\_16955eV\_04.png" Lbl.:Main\_beam\_C111\_Laue\_Surface\_plot\_fea\_plot\_thermcond\_c04\_16955eV\_04

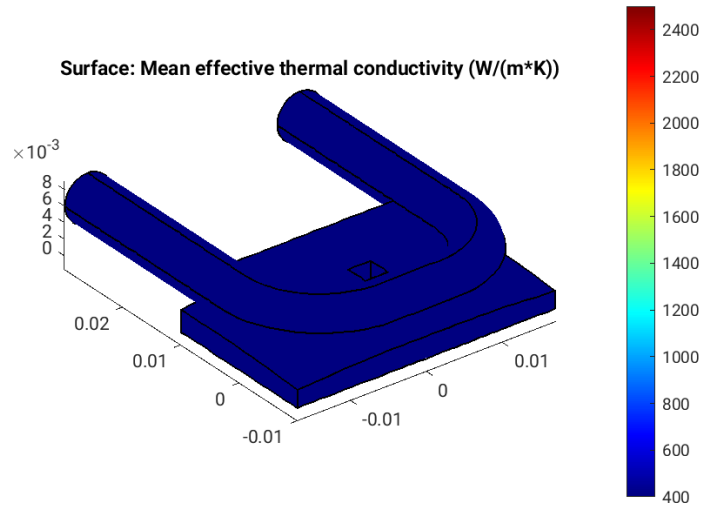


Figure 25.25: Thermal conductivity, lambda [W/(m K)], on the surfaces of optical element #04, for case #04, at 16955 eV photon energy setting.

"fig/Main\_beam\_C111\_Laue/fea\_plot\_stress\_c04\_16955eV\_04.png" Lbl.:Main\_beam\_C111\_Laue\_Surface\_plot\_fea\_plot\_stress\_c04\_16955eV\_04

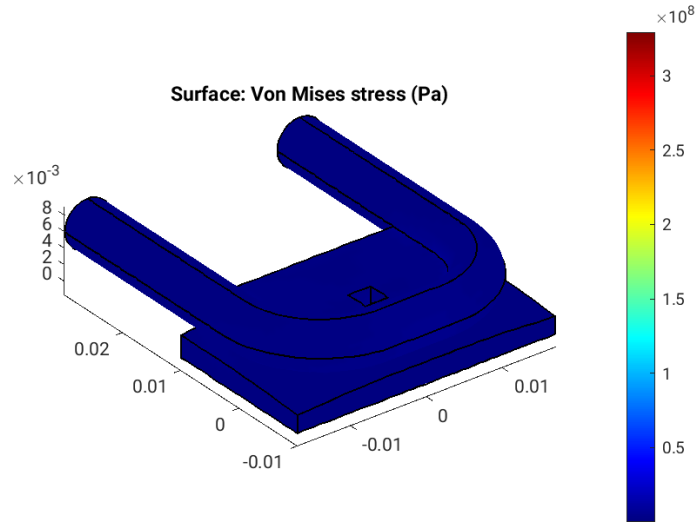


Figure 25.26: Von Mises stress, sigma [Pa], on the surfaces of optical element #04, for case #04, at 16955 eV photon energy setting.

"fig/Main\_beam\_C111\_Laue/fea\_plot\_deform\_c04\_16955eV\_04.png" Lbl.:Main\_beam\_C111\_Laue\_Surface\_plot\_fea\_plot\_deform\_c04\_16955eV\_04

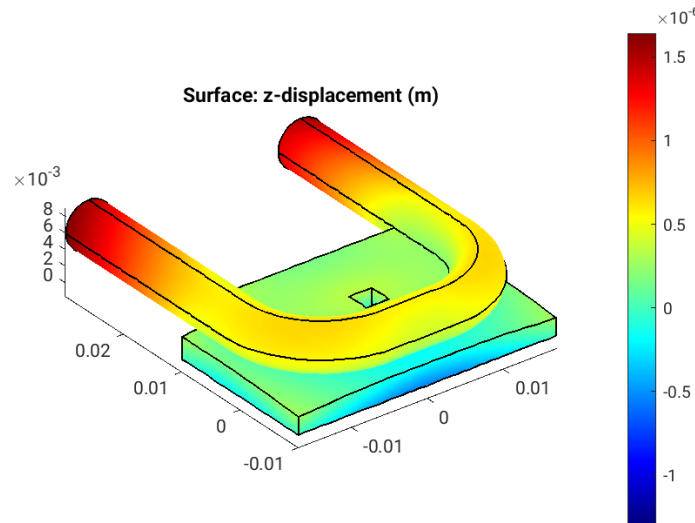


Figure 25.27: Thermoelastic deformation,  $dz$  [m], on the surfaces of optical element #04, for case #04, at 16955 eV photon energy setting.

# Chapter 26

## Parameter scan cases

There are four cases in total. Case #1 is the perfect crystal case with no heat load and consequently no deformation. This case serves as a reference, to discriminate against other beam deteriorating effects, such as source broadening or aberrations. Case #2 is with heat load and with both diamond filters – 600 and 400 micrometer in thickness – in the upstream beam path. Case #3 is with only the 400 micron thick filter in, and case #4 is without any filters.

Case	Thickness(1)_02 cm	Thickness(2)_02 cm	Has_slope_error_03	Skip_heatload
1	0.06	0.04	no	yes
2	0.06	0.04	yes	no
3	0.00001	0.04	yes	no
4	0.00001	0.00001	yes	no

Table 26.1: Parameter values for different cases in parameter scan

### Legend

**Case:** Case number in parameter scan

**Thickness(1)\_02:** Optical\_element\_#2.Type.Screen.Thickness(1) (Optical thickness of resp. screen with absorption.)

**Thickness(2)\_02:** Optical\_element\_#2.Type.Screen.Thickness(2) (Optical thickness of resp. screen with absorption.)

**Has\_slope\_error\_03:** Optical\_element\_#3.Surface.Has\_slope\_error (Has surface slope error?)

**Skip\_heatload:** Session.Skip\_heatload (Skip heat load calculation for all optical elements? (heat load parameters are kept))

## Chapter 27

# Photon energy scan

The  $K_y$ -values in the table below are those for optimised output between 15.6 and 18.3 keV used by DanMAX' main branch.

E eV	K_y	n_harm/step	dtheta_03 deg	dtheta_05 deg
<b>15556</b>	1.67551	7	-43.9164	43.9164
<b>15633.8</b>	1.66836	7	-43.873	43.873
<b>15711.5</b>	1.66125	7	-43.8301	43.8301
<b>15789.3</b>	1.65418	7	-43.7875	43.7875
<b>15867.1</b>	1.64714	7	-43.7454	43.7454
<b>15944.8</b>	1.64015	7	-43.7037	43.7037
<b>16022.6</b>	1.63319	7	-43.6625	43.6625
<b>16100.4</b>	1.62628	7	-43.6216	43.6216
<b>16178.2</b>	1.6194	7	-43.5811	43.5811
<b>16255.9</b>	1.61255	7	-43.541	43.541
<b>16333.7</b>	1.60575	7	-43.5013	43.5013
<b>16411.5</b>	1.59898	7	-43.462	43.462
<b>16489.2</b>	1.59224	7	-43.423	43.423
<b>16567</b>	1.58554	7	-43.3844	43.3844
<b>16644.8</b>	1.57887	7	-43.3462	43.3462
<b>16722.6</b>	1.57224	7	-43.3083	43.3083
<b>16800.3</b>	1.56564	7	-43.2708	43.2708
<b>16878.1</b>	1.55908	7	-43.2337	43.2337
<b>16955.9</b>	1.55255	7	-43.1969	43.1969
<b>17033.6</b>	1.54605	7	-43.1604	43.1604
<b>17111.4</b>	1.53958	7	-43.1243	43.1243
<b>17189.2</b>	1.53315	7	-43.0885	43.0885
<b>17266.9</b>	1.52674	7	-43.053	43.053
<b>17344.7</b>	1.52037	7	-43.0178	43.0178
<b>17422.5</b>	1.51402	7	-42.983	42.983
<b>17500.2</b>	1.50771	7	-42.9484	42.9484
<b>17578</b>	1.50143	7	-42.9142	42.9142
<b>17655.8</b>	1.49517	7	-42.8803	42.8803
<b>17733.6</b>	1.48895	7	-42.8467	42.8467
<b>17811.3</b>	1.48275	7	-42.8133	42.8133
<b>17889.1</b>	1.47658	7	-42.7803	42.7803
<b>17966.9</b>	1.47044	7	-42.7476	42.7476
<b>18044.6</b>	1.46433	7	-42.7151	42.7151
<b>18122.4</b>	1.45824	7	-42.6829	42.6829
<b>18200.2</b>	1.45218	7	-42.651	42.651
<b>18277.9</b>	1.44615	7	-42.6194	42.6194

Table 27.1: Scan values for different photon energies in energy scan

### Legend

**E:** photon energy

**K\_y:** deflection parameter for vertical field component of insertion device

**n\_harm/step:** number of undulator harmonic or number of energy slot for continuous source (e.g. wiggler)

**dtheta\_03:** Optical\_element\_#3.Move.Source.dangle\_x (Source rotation angle around x-axis (ccw).)

**dtheta\_05:** Optical\_element\_#5.Move.Source.dangle\_x (Source rotation angle around x-axis (ccw).)

<b>E eV</b>	<b>P_sum W</b>	<b>P_abs02-01 W</b>	<b>P_abs02-02 W</b>	<b>P_abs04 W</b>
<b>15556</b>	170.995	52.0318	7.06876	1.72629
<b>15633.8</b>	170.404	52.0256	7.06965	1.72807
<b>15711.5</b>	169.798	52.0361	7.07607	1.72712
<b>15789.3</b>	169.194	51.9484	7.06473	1.72716
<b>15867.1</b>	168.484	51.815	7.07956	1.72573
<b>15944.8</b>	167.889	52.111	7.0604	1.72307
<b>16022.6</b>	166.334	52.0951	7.06421	1.72098
<b>16100.4</b>	165.817	52.133	7.06212	1.71922
<b>16178.2</b>	165.215	52.1409	7.07774	1.71899
<b>16255.9</b>	164.545	52.109	7.04501	1.72213
<b>16333.7</b>	163.995	52.1534	7.05956	1.72047
<b>16411.5</b>	163.395	52.1383	7.05893	1.7158
<b>16489.2</b>	162.749	52.1822	7.04669	1.72065
<b>16567</b>	162.139	52.1891	7.04094	1.70877
<b>16644.8</b>	161.504	52.2041	7.04199	1.71266
<b>16722.6</b>	160.875	52.2082	7.00824	1.70741
<b>16800.3</b>	160.261	52.2376	6.98775	1.70404
<b>16878.1</b>	159.67	52.3483	7.00329	1.70891
<b>16955.9</b>	159.07	52.3613	6.9924	1.70125
<b>17033.6</b>	157.762	52.2884	6.96994	1.69651
<b>17111.4</b>	157.165	52.3616	6.97344	1.70075
<b>17189.2</b>	156.609	52.2949	6.93387	1.6928
<b>17266.9</b>	155.976	52.228	6.91572	1.68863
<b>17344.7</b>	155.424	52.4039	6.92508	1.68828
<b>17422.5</b>	154.752	52.3111	6.90511	1.69099
<b>17500.2</b>	154.186	52.3876	6.8797	1.69174
<b>17578</b>	153.627	52.3634	6.83383	1.68203
<b>17655.8</b>	153.017	52.3814	6.82953	1.68019
<b>17733.6</b>	152.421	52.5574	6.80424	1.67922
<b>17811.3</b>	151.837	52.5489	6.81447	1.67503
<b>17889.1</b>	151.22	52.4349	6.76967	1.66835
<b>17966.9</b>	150.624	52.5274	6.75092	1.66785
<b>18044.6</b>	150.012	52.4483	6.70439	1.66225
<b>18122.4</b>	148.856	52.3838	6.70795	1.65477
<b>18200.2</b>	148.268	52.423	6.66	1.65585
<b>18277.9</b>	147.713	52.2898	6.64233	1.65386

Table 27.2: Scan values for different photon energies with diamond filters of 1000 micron total thickness in

E eV	P_sum W	P_abs02-01 W	P_abs02-02 W	P_abs04 W
<b>15556</b>	170.995	0.199003	46.0659	4.08182
<b>15633.8</b>	170.404	0.198142	46.1393	4.08848
<b>15711.5</b>	169.798	0.195973	46.2296	4.06477
<b>15789.3</b>	169.194	0.195249	46.2747	4.06177
<b>15867.1</b>	168.484	0.193995	46.1987	4.04347
<b>15944.8</b>	167.889	0.192742	46.3658	4.04372
<b>16022.6</b>	166.334	0.190985	46.3433	4.033
<b>16100.4</b>	165.817	0.189802	46.4619	4.00575
<b>16178.2</b>	165.215	0.188711	46.5178	3.9934
<b>16255.9</b>	164.545	0.187069	46.4735	3.97889
<b>16333.7</b>	163.995	0.185827	46.3615	3.97048
<b>16411.5</b>	163.395	0.185417	46.5412	3.94557
<b>16489.2</b>	162.749	0.184051	46.5369	3.94517
<b>16567</b>	162.139	0.183317	46.7192	3.89832
<b>16644.8</b>	161.504	0.182185	46.6789	3.88405
<b>16722.6</b>	160.875	0.180403	46.601	3.87211
<b>16800.3</b>	160.261	0.179172	46.5892	3.84659
<b>16878.1</b>	159.67	0.178371	46.7264	3.83853
<b>16955.9</b>	159.07	0.177639	46.7724	3.81088
<b>17033.6</b>	157.762	0.177067	46.934	3.79845
<b>17111.4</b>	157.165	0.175692	46.896	3.78634
<b>17189.2</b>	156.609	0.174222	46.8324	3.74702
<b>17266.9</b>	155.976	0.172925	47.0087	3.74138
<b>17344.7</b>	155.424	0.172059	47.1191	3.71103
<b>17422.5</b>	154.752	0.170595	46.9618	3.68715
<b>17500.2</b>	154.186	0.170026	47.2036	3.68039
<b>17578</b>	153.627	0.169136	47.2662	3.64831
<b>17655.8</b>	153.017	0.167785	47.1985	3.62124
<b>17733.6</b>	152.421	0.166861	47.1806	3.61347
<b>17811.3</b>	151.837	0.165195	47.1884	3.59559
<b>17889.1</b>	151.22	0.163691	47.2653	3.5598
<b>17966.9</b>	150.624	0.163484	47.3456	3.52522
<b>18044.6</b>	150.012	0.162682	47.3026	3.49962
<b>18122.4</b>	148.856	0.161432	47.3836	3.47087
<b>18200.2</b>	148.268	0.159667	47.3216	3.44023
<b>18277.9</b>	147.713	0.159197	47.4511	3.42879

Table 27.3: Scan values for different photon energies with upstream diamond filter of 400 micron thickness in

E eV	P_sum W	P_abs02-01 W	P_abs02-02 W	P_abs04 W
<b>15556</b>	170.995	0.198797	0.197368	34.1728
<b>15633.8</b>	170.404	0.197268	0.196474	34.4301
<b>15711.5</b>	169.798	0.195916	0.195452	34.5809
<b>15789.3</b>	169.194	0.195088	0.194237	34.5934
<b>15867.1</b>	168.484	0.19439	0.192736	34.6885
<b>15944.8</b>	167.889	0.192597	0.191493	34.7599
<b>16022.6</b>	166.334	0.190614	0.190908	34.8645
<b>16100.4</b>	165.817	0.190945	0.189688	35.0248
<b>16178.2</b>	165.215	0.189017	0.187995	35.1117
<b>16255.9</b>	164.545	0.188192	0.187062	35.1432
<b>16333.7</b>	163.995	0.185893	0.186215	35.2493
<b>16411.5</b>	163.395	0.185556	0.18462	35.4244
<b>16489.2</b>	162.749	0.184425	0.183603	35.4296
<b>16567</b>	162.139	0.183439	0.182427	35.6431
<b>16644.8</b>	161.504	0.181836	0.181133	35.8133
<b>16722.6</b>	160.875	0.180841	0.179664	35.8728
<b>16800.3</b>	160.261	0.179911	0.179035	35.8131
<b>16878.1</b>	159.67	0.178404	0.178156	36.1114
<b>16955.9</b>	159.07	0.177536	0.176443	36.2171
<b>17033.6</b>	157.762	0.176257	0.175851	36.3345
<b>17111.4</b>	157.165	0.175341	0.174668	36.5037
<b>17189.2</b>	156.609	0.173727	0.173802	36.5464
<b>17266.9</b>	155.976	0.173538	0.172042	36.5999
<b>17344.7</b>	155.424	0.172467	0.171529	36.8631
<b>17422.5</b>	154.752	0.170241	0.169417	36.8754
<b>17500.2</b>	154.186	0.169842	0.168833	36.929
<b>17578</b>	153.627	0.168882	0.168305	37.1141
<b>17655.8</b>	153.017	0.167613	0.166765	37.2097
<b>17733.6</b>	152.421	0.166489	0.165576	37.2835
<b>17811.3</b>	151.837	0.164829	0.16517	37.5825
<b>17889.1</b>	151.22	0.164345	0.163241	37.6061
<b>17966.9</b>	150.624	0.162919	0.162802	37.6584
<b>18044.6</b>	150.012	0.162761	0.161843	37.9132
<b>18122.4</b>	148.856	0.160974	0.160793	37.8204
<b>18200.2</b>	148.268	0.160167	0.159572	37.9941
<b>18277.9</b>	147.713	0.159231	0.157902	38.1619

Table 27.4: Scan values for different photon energies with no upstream filters

### Legend

**E:** photon energy

**P\_sum:** sum of power in harmonics / energy intervals, P\_sum = P\_src

**P\_abs02-01:** total power absorbed by optical element 02-01

**P\_abs02-02:** total power absorbed by optical element 02-02

**P\_abs04:** total power absorbed by optical element 04

# Chapter 28

## Plots

### 28.1 Statistics of incident irradiance

```
"fig/Main_beam_C111_Laue/plot001.png" Lbl.:Main_beam_C111_Laue_2d_plot_I_peak_incstat_oe04
```

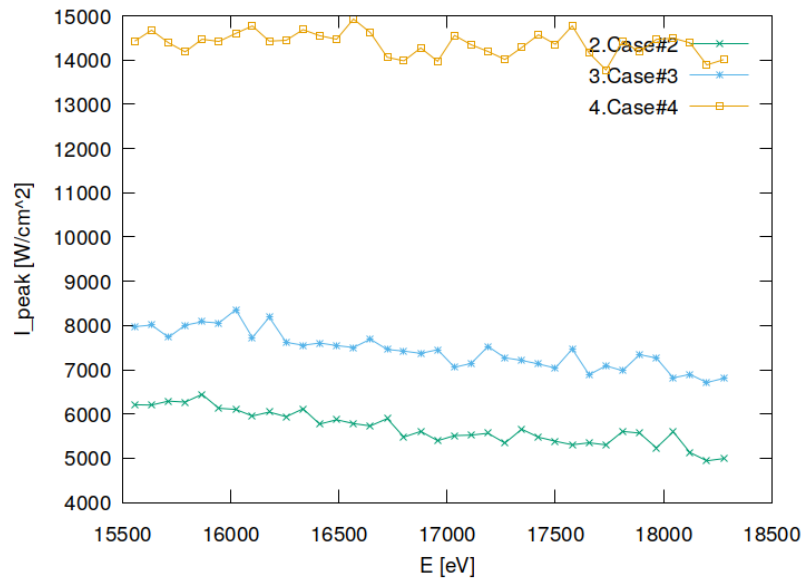


Figure 28.1: Incident peak irradiance of optical element #04 (BS).

```
"fig/Main_beam_C111_Laue/plot002.png" Lbl.:Main_beam_C111_Laue_2d_plot_I_int_incstat_oe04
```

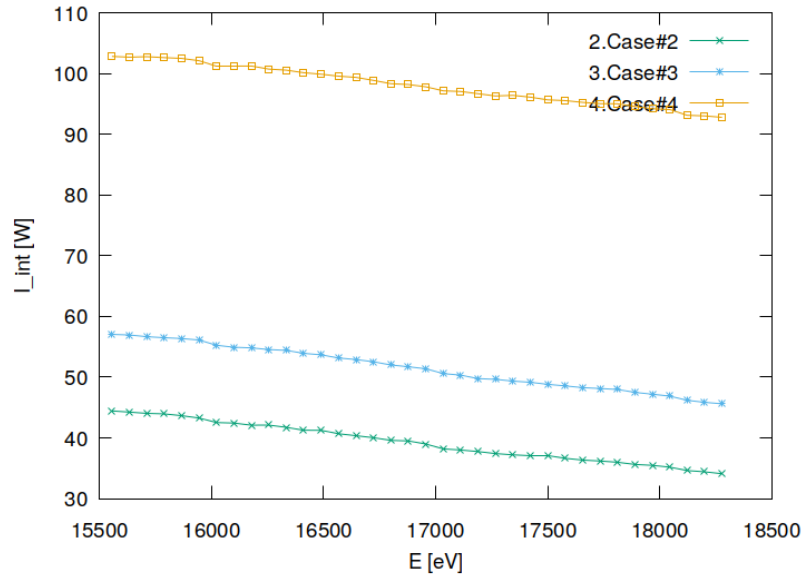


Figure 28.2: Incident flux of optical element #04 (BS).

## 28.2 Statistics of absorbed irradiance

```
"fig/Main_beam_C111_Laue/plot003.png" Lbl.:Main_beam_C111_Laue_2d_plot_I_peak_absstat_oe04
```

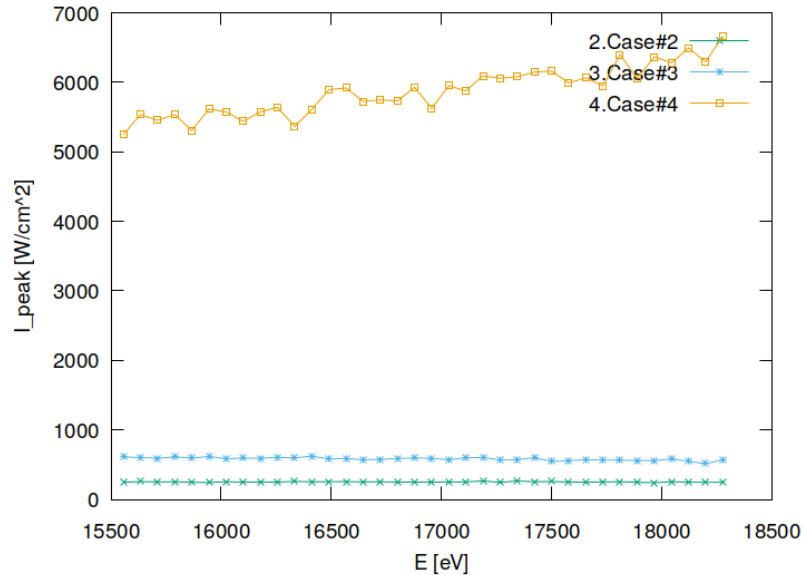


Figure 28.3: Absorbed peak irradiance of optical element #04 (BS).

```
"fig/Main_beam_C111_Laue/plot004.png" Lbl.:Main_beam_C111_Laue_2d_plot_I_int_absstat_oe04
```

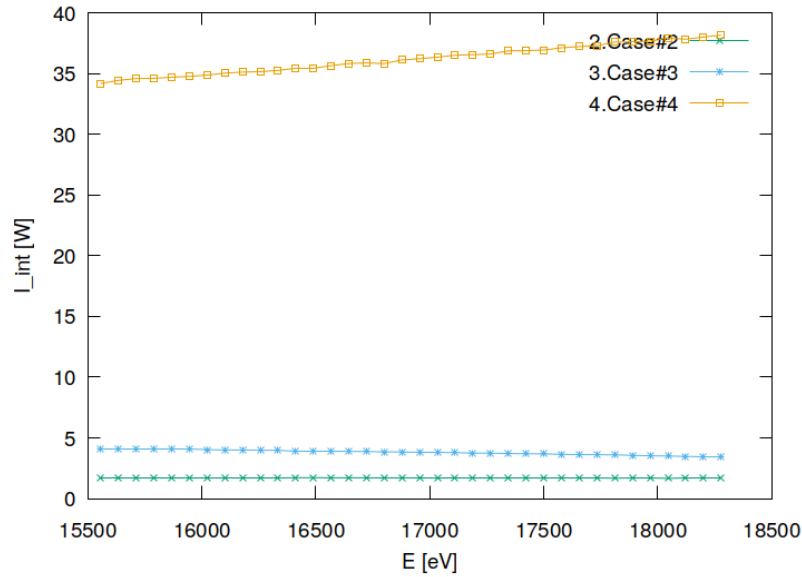


Figure 28.4: Absorbed flux of optical element #04 (BS).

### 28.3 Statistics of temperature

```
"fig/Main_beam_C111_Laue/plot005.png" Lbl.:Main_beam_C111_Laue_2d_plot_T_peak_stat_oe04
```

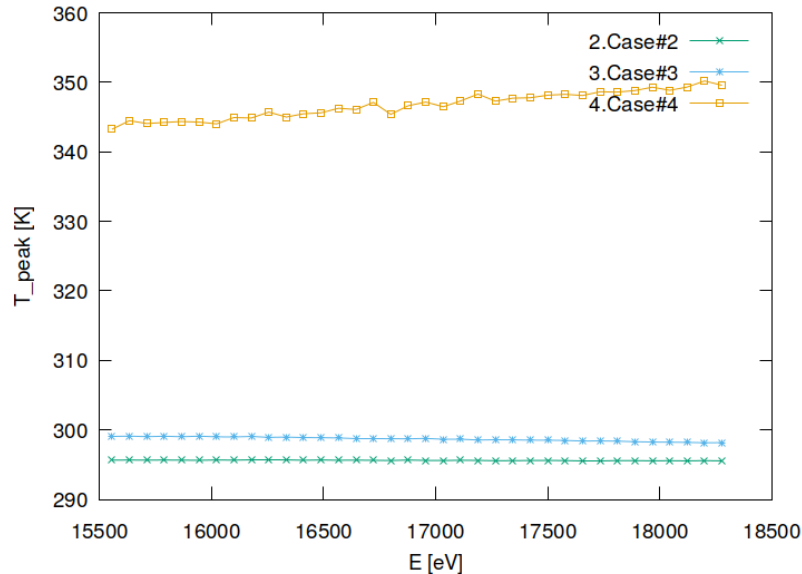


Figure 28.5: Peak temperature of optical element #04 (BS).

## 28.4 Statistics of mechanical stress (von Mises stress)

```
"fig/Main_beam_C111_Laue/plot006.png" Lbl.:Main_beam_C111_Laue_2d_plot_sigma_peak_stat_oe04
```

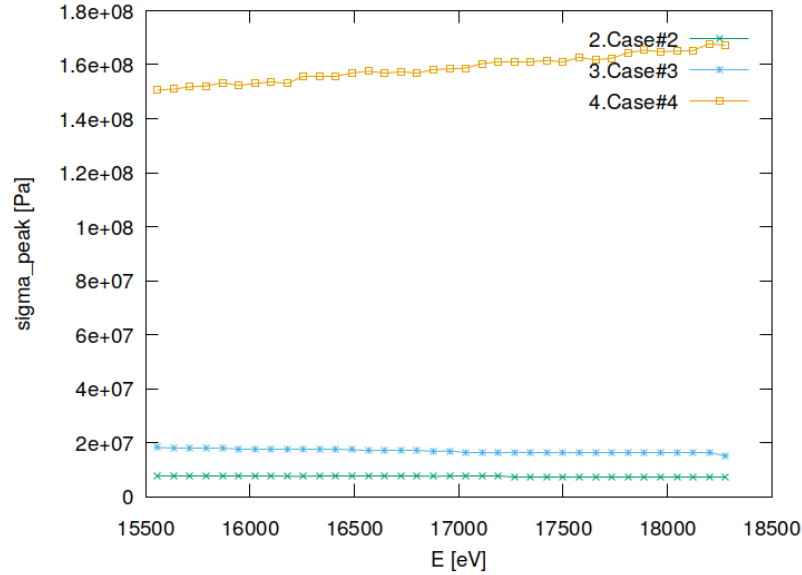


Figure 28.6: Peak mechanical stress (Von Mises stress) of optical element #04 (BS).

## 28.5 Statistics of optical surface deformation

```
"fig/Main_beam_C111_Laue/plot007.png" Lbl.:Main_beam_C111_Laue_2d_plot_dz_peak_stat_oe04
```

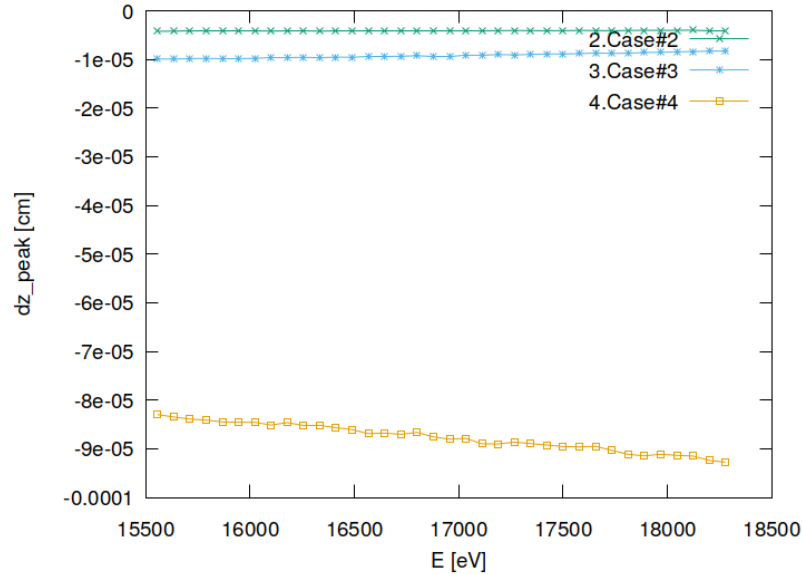


Figure 28.7: Peak deformation of optical element #04 (BS).

## 28.6 Statistics of photon irradiance on optical surface

"fig/Main\_beam\_C111\_Laue/plot008.png" Lbl.:Main\_beam\_C111\_Laue\_2d\_plot\_dx\_fwhm\_inc\_footstat\_oe04

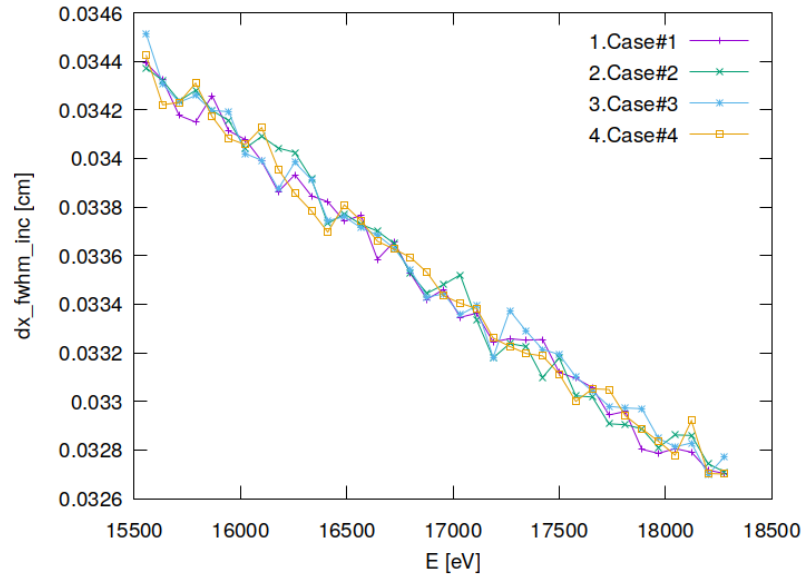


Figure 28.8: Sagittal footprint diameter (FWHM) of optical element #04 (BS).

"fig/Main\_beam\_C111\_Laue/plot009.png" Lbl.:Main\_beam\_C111\_Laue\_2d\_plot\_dx\_fwhm\_inc\_footstat\_oe05

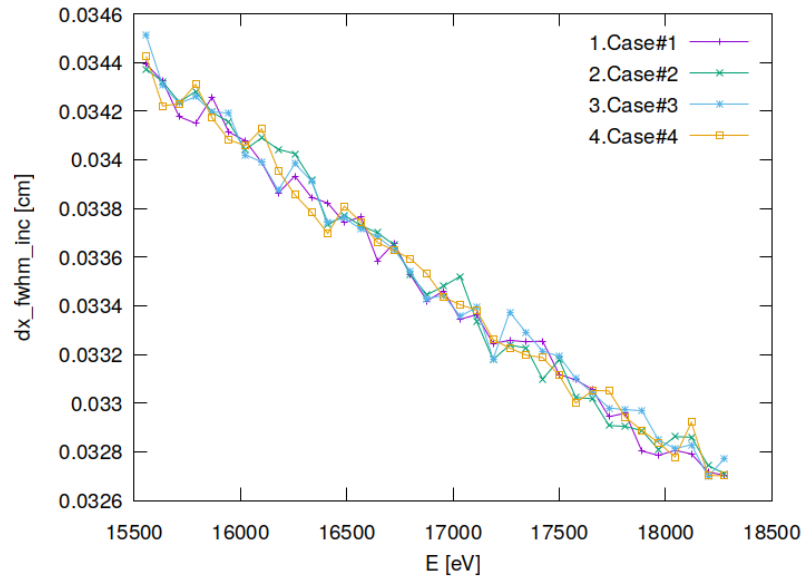


Figure 28.9: Sagittal footprint diameter (FWHM) of optical element #05 (Dan-MAX).

```
"fig/Main_beam_C111_Laue/plot010.png" Lbl.:Main_beam_C111_Laue_2d_plot_dy_fwhm_inc_footstat_oe04
```

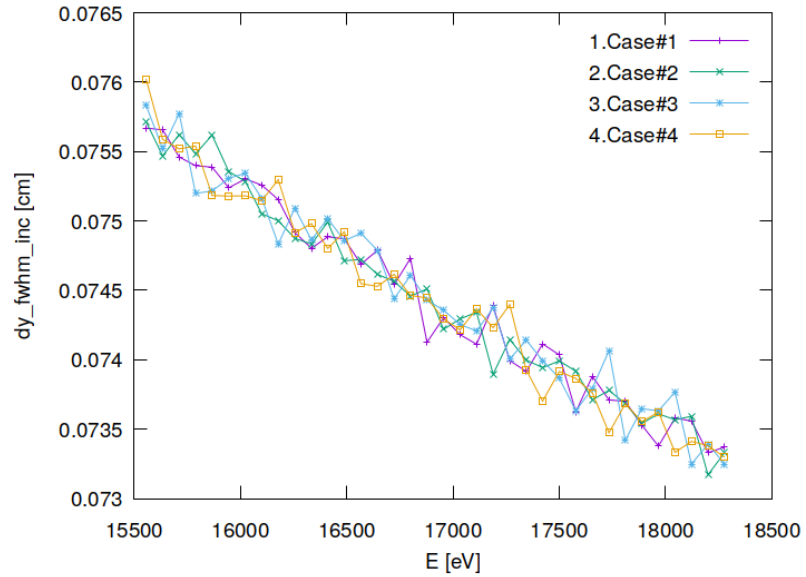


Figure 28.10: Meridional footprint diameter (FWHM) of optical element #04 (BS).

```
"fig/Main_beam_C111_Laue/plot011.png" Lbl.:Main_beam_C111_Laue_2d_plot_dy_fwhm_inc_footstat_oe05
```

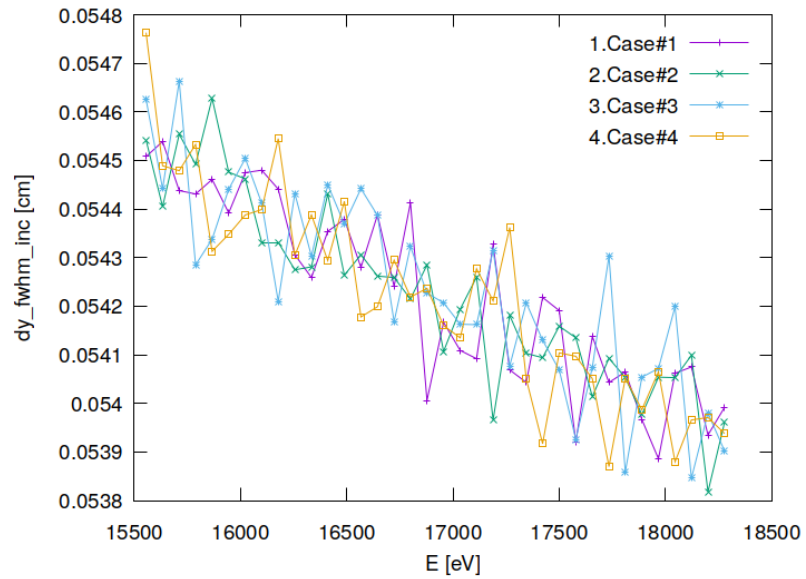


Figure 28.11: Meridional footprint diameter (FWHM) of optical element #05 (Dan-MAX).

```
"fig/Main_beam_C111_Laue/plot012.png" Lbl.:Main_beam_C111_Laue_2d_plot_I_inc_int_footstat_oe04
```

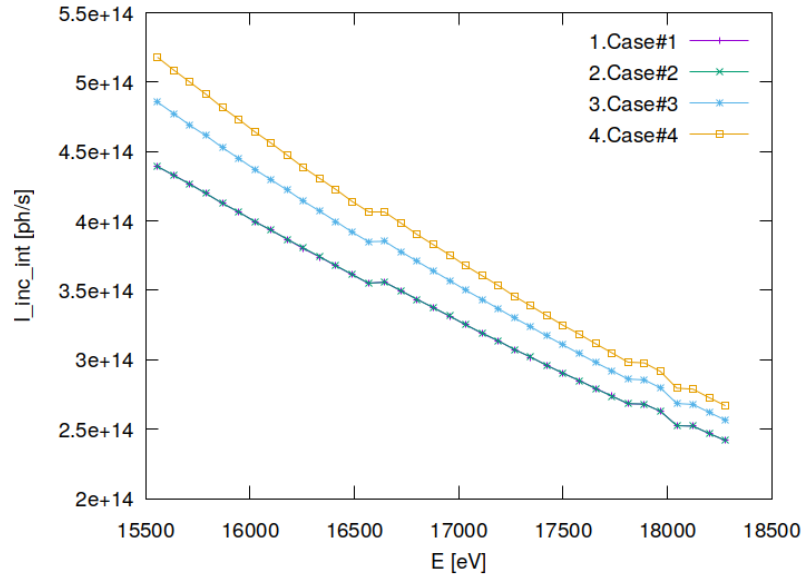


Figure 28.12: Incident photon flux on surface of optical element #04 (BS).

```
"fig/Main_beam_C111_Laue/plot013.png" Lbl.:Main_beam_C111_Laue_2d_plot_I_inc_int_footstat_oe05
```

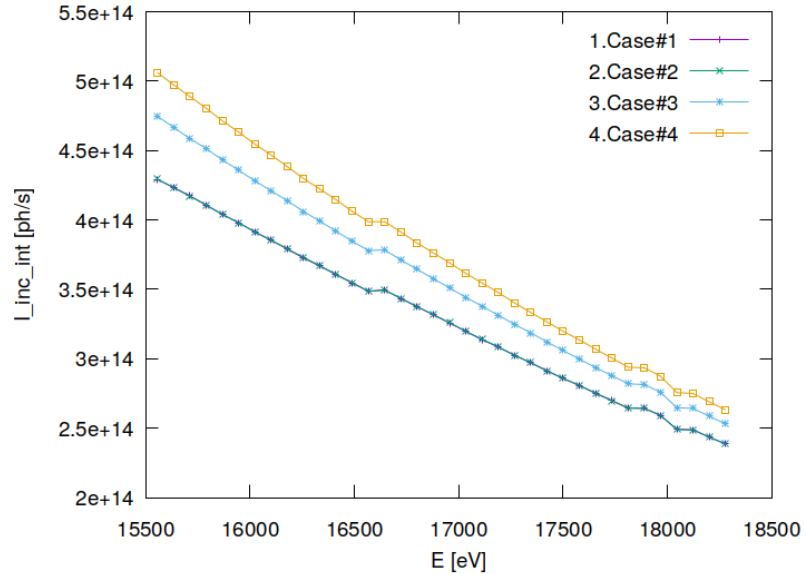


Figure 28.13: Incident photon flux on surface of optical element #05 (DanMAX).

"fig/Main\_beam\_C111\_Laue/plot014.png" Lbl.:Main\_beam\_C111\_Laue\_2d\_plot\_x\_cen\_inc\_footstat\_oe04

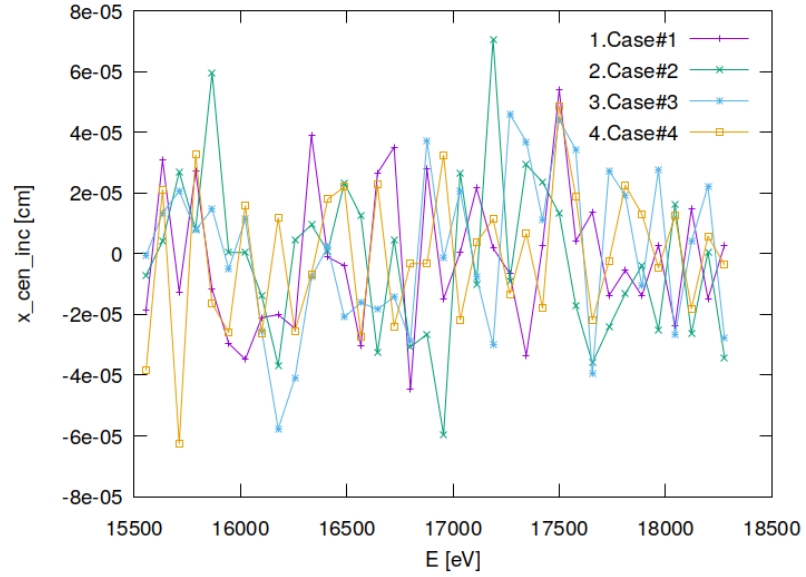


Figure 28.14: Sagittal coordinate of footprint's centre of 'gravity' on surface of optical element #04 (BS).

"fig/Main\_beam\_C111\_Laue/plot015.png" Lbl.:Main\_beam\_C111\_Laue\_2d\_plot\_x\_cen\_inc\_footstat\_oe05

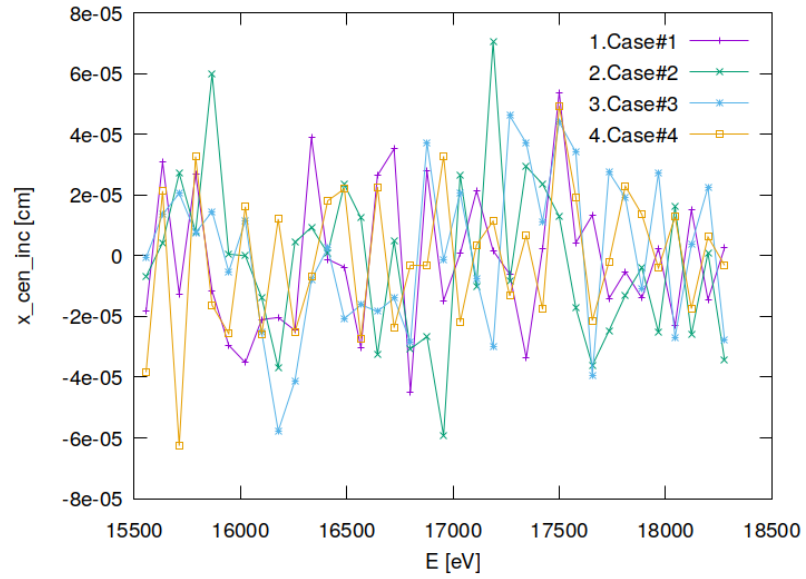


Figure 28.15: Sagittal coordinate of footprint's centre of 'gravity' on surface of optical element #05 (DanMAX).

"fig/Main\_beam\_C111\_Laue/plot016.png" Lbl.:Main\_beam\_C111\_Laue\_2d\_plot\_y\_cen\_inc\_footstat\_oe04

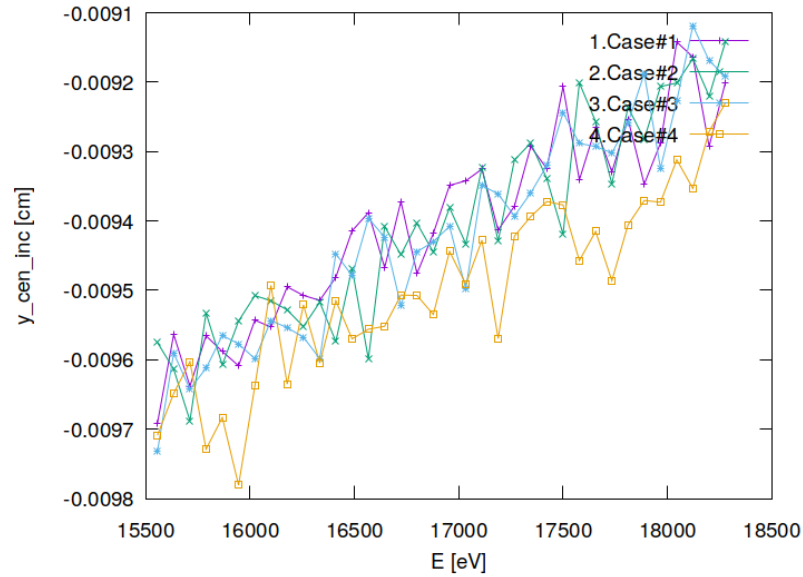


Figure 28.16: Meridional coordinate of footprint's centre of 'gravity' on surface of optical element #04 (BS).

"fig/Main\_beam\_C111\_Laue/plot017.png" Lbl.:Main\_beam\_C111\_Laue\_2d\_plot\_y\_cen\_inc\_footstat\_oe05

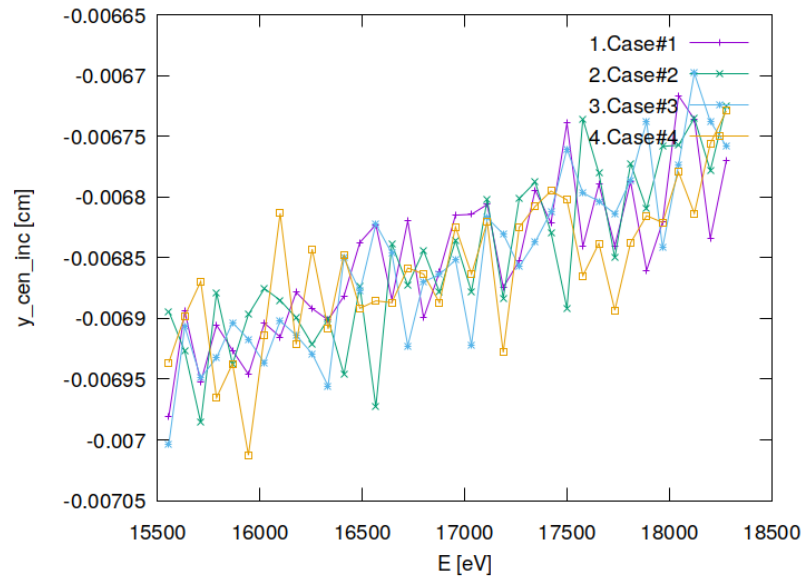


Figure 28.17: Meridional coordinate of footprint's centre of 'gravity' on surface of optical element #05 (DanMAX).

## 28.7 Statistics of photon irradiance in beam cross section

"fig/Main\_beam\_C111\_Laue/plot018.png" Lbl.:Main\_beam\_C111\_Laue\_2d\_plot\_dx\_fwhm\_focstatavg\_oe04

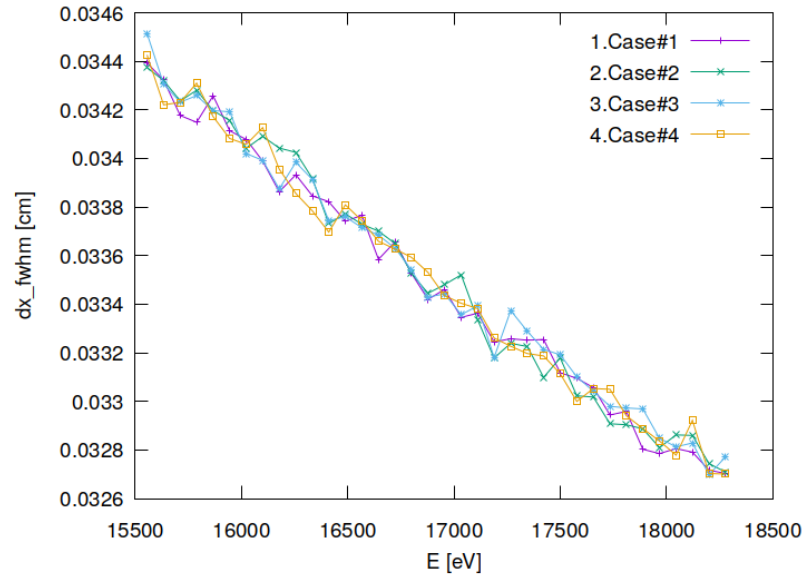


Figure 28.18: Sagittal beam diameter (FWHM) of optical element #04 (BS).

"fig/Main\_beam\_C111\_Laue/plot019.png" Lbl.:Main\_beam\_C111\_Laue\_2d\_plot\_dx\_fwhm\_focstatavg\_oe05

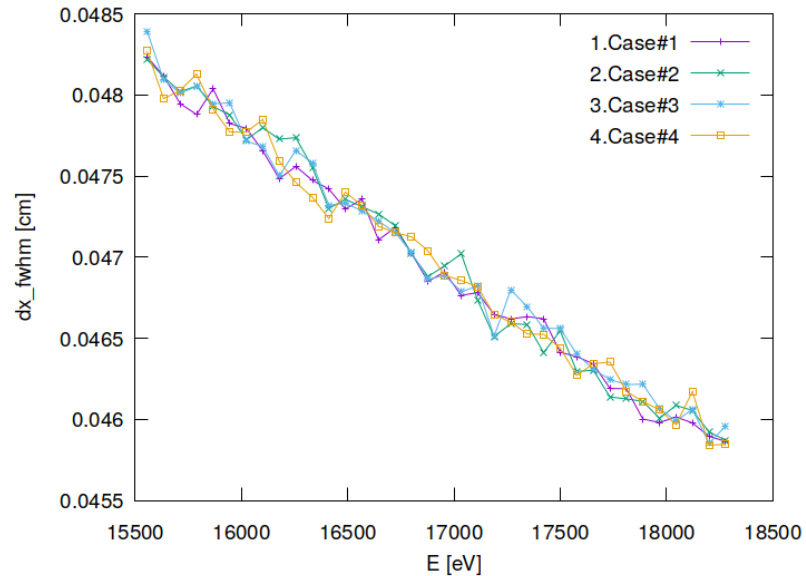


Figure 28.19: Sagittal beam diameter (FWHM) of optical element #05 (DanMAX).

"fig/Main\_beam\_C111\_Laue/plot020.png" Lbl.:Main\_beam\_C111\_Laue\_2d\_plot\_dz\_fwhm\_focstatavg\_oe04

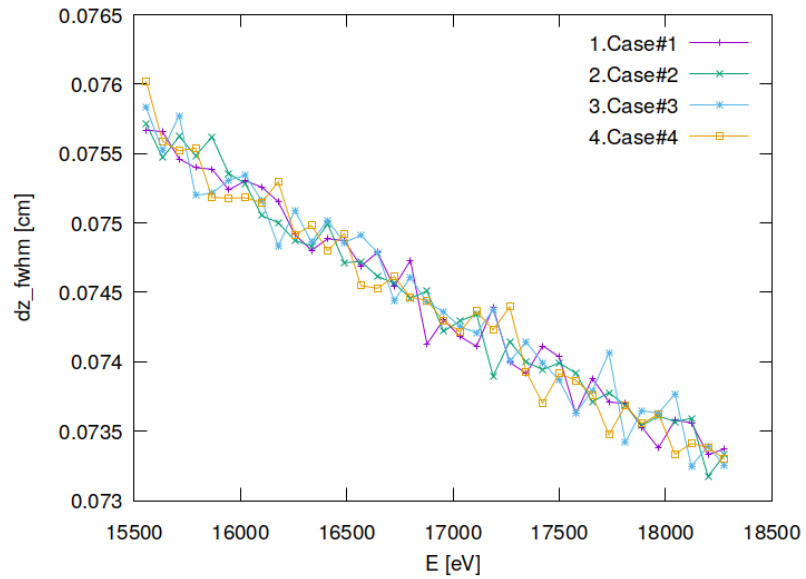


Figure 28.20: Meridional beam diameter (FWHM) of optical element #04 (BS).

"fig/Main\_beam\_C111\_Laue/plot021.png" Lbl.:Main\_beam\_C111\_Laue\_2d\_plot\_dz\_fwhm\_focstatavg\_oe05

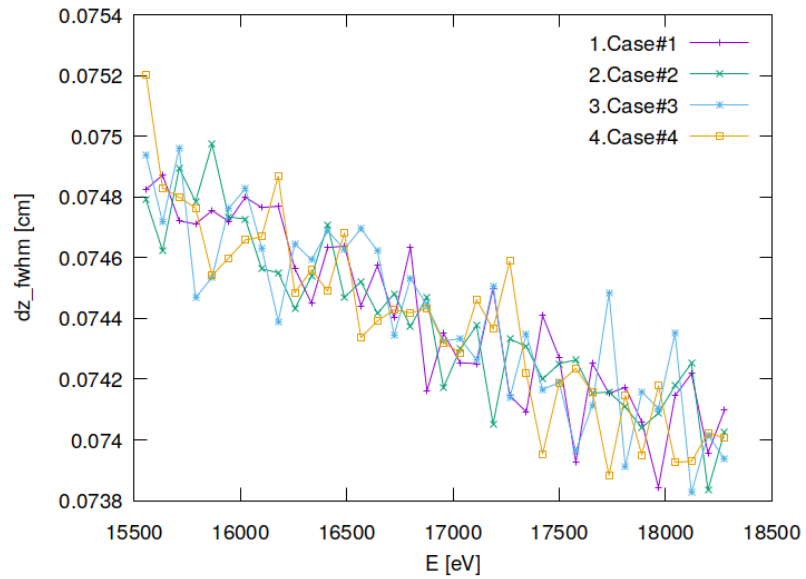


Figure 28.21: Meridional beam diameter (FWHM) of optical element #05 (Dan-MAX).

```
"fig/Main_beam_C111_Laue/plot022.png" Lbl.:Main_beam_C111_Laue_2d_plot_I_int_focstatavg_oe04
```

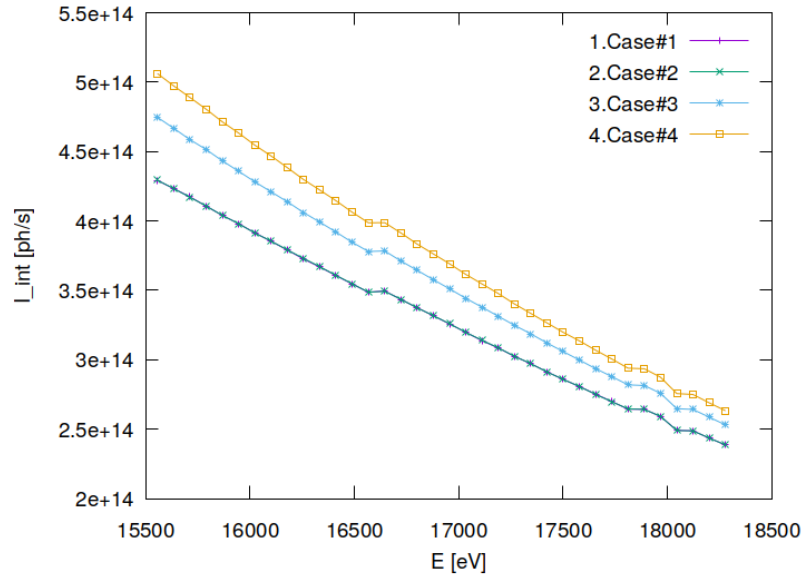


Figure 28.22: Photon flux in beam cross section of optical element #04 (BS).

```
"fig/Main_beam_C111_Laue/plot023.png" Lbl.:Main_beam_C111_Laue_2d_plot_I_int_focstatavg_oe05
```

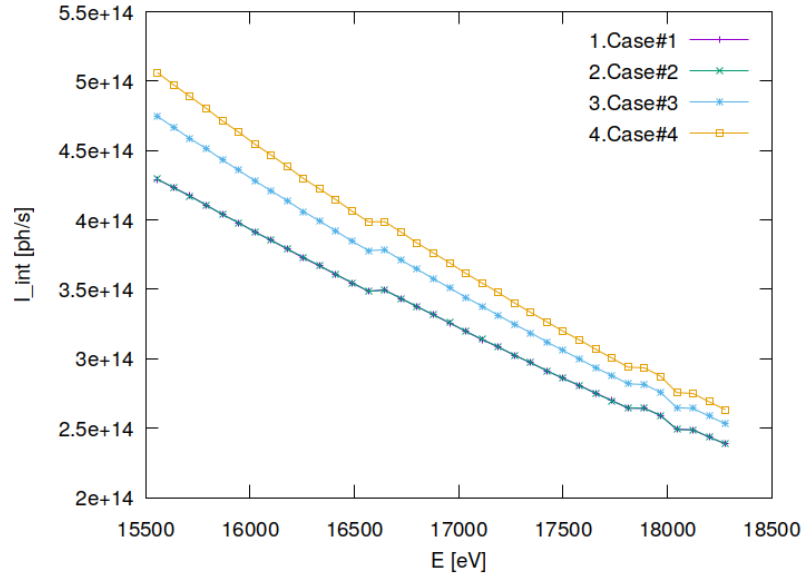


Figure 28.23: Photon flux in beam cross section of optical element #05 (DanMAX).

```
"fig/Main_beam_C111_Laue/plot024.png" Lbl.:Main_beam_C111_Laue_2d_plot_x_cen_focstatavg_oe04
```

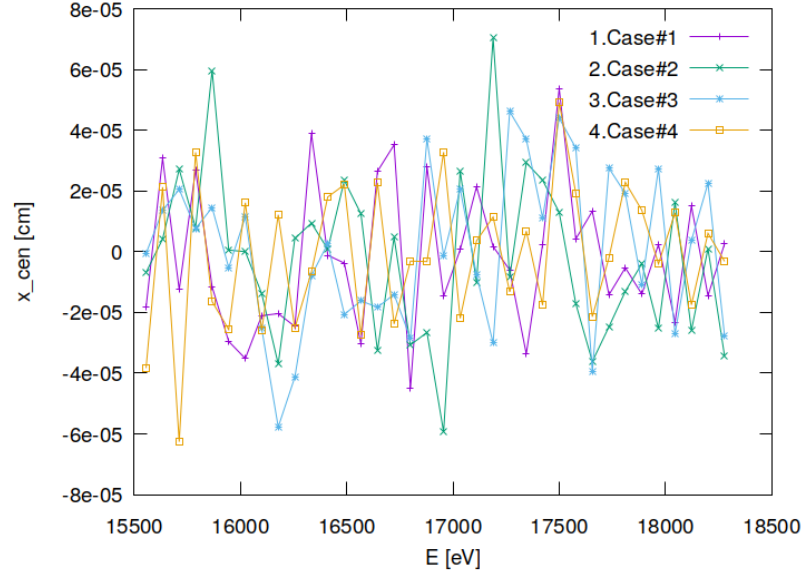


Figure 28.24: Sagittal coordinate of beam's centre of 'gravity' in beam cross section of optical element #04 (BS).

```
"fig/Main_beam_C111_Laue/plot025.png" Lbl.:Main_beam_C111_Laue_2d_plot_x_cen_focstatavg_oe05
```

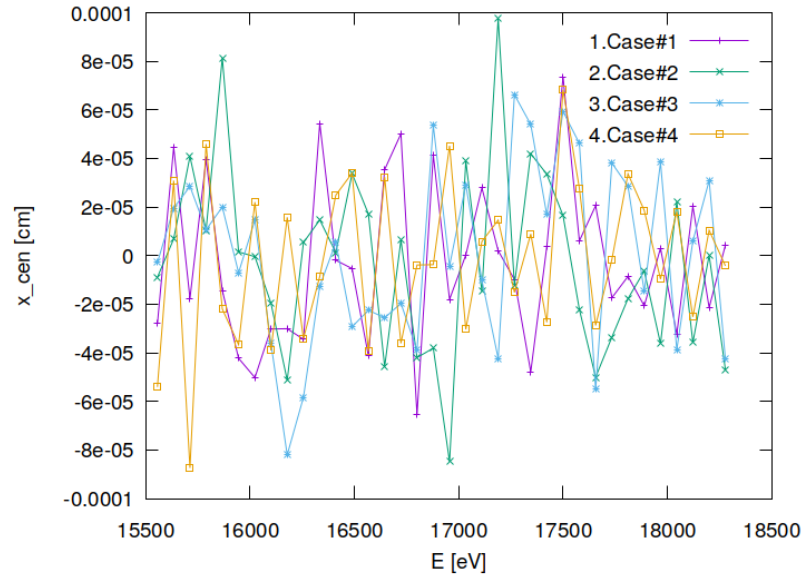


Figure 28.25: Sagittal coordinate of beam's centre of 'gravity' in beam cross section of optical element #05 (DanMAX).

```
"fig/Main_beam_C111_Laue/plot026.png" Lbl.:Main_beam_C111_Laue_2d_plot_z_cen_focstatavg_oe04
```

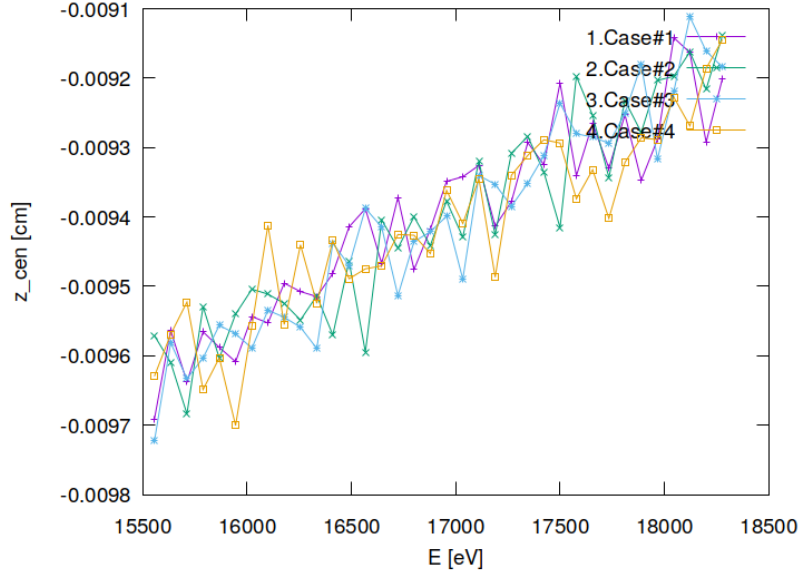


Figure 28.26: Meridional coordinate of beam's centre of 'gravity' in beam cross section of optical element #04 (BS).

```
"fig/Main_beam_C111_Laue/plot027.png" Lbl.:Main_beam_C111_Laue_2d_plot_z_cen_focstatavg_oe05
```

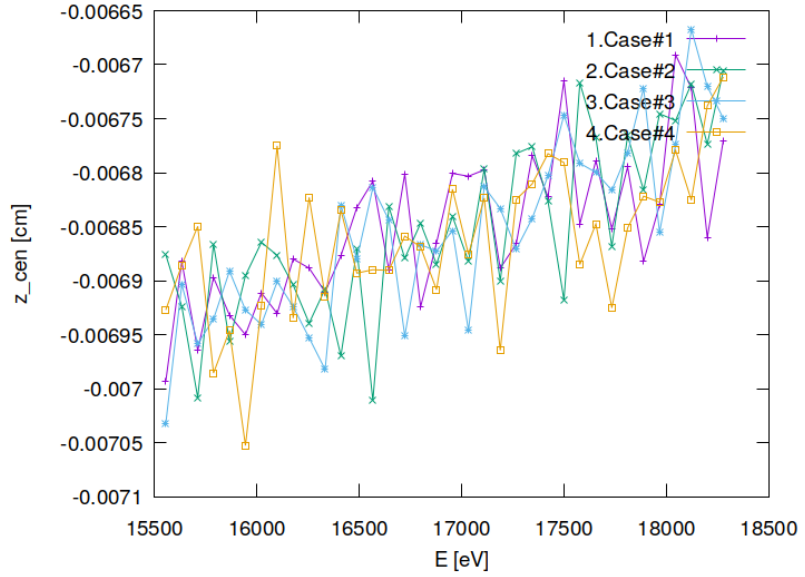


Figure 28.27: Meridional coordinate of beam's centre of 'gravity' in beam cross section of optical element #05 (DanMAX).

```
"fig/Main_beam_C111_Laue/plot028.png" Lbl.:Main_beam_C111_Laue_2d_plot_dxp_fwhm_focstatavg_oe04
```

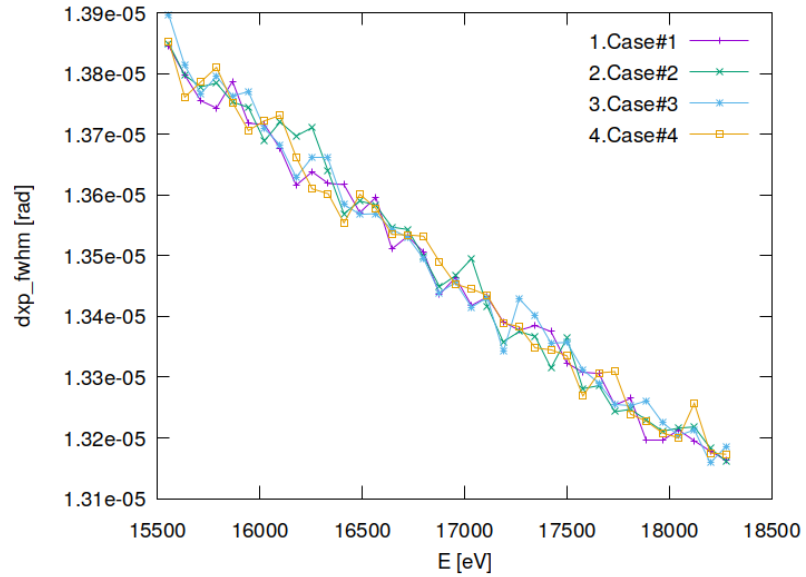


Figure 28.28: Sagittal beam divergence (FWHM) of optical element #04 (BS).

```
"fig/Main_beam_C111_Laue/plot029.png" Lbl.:Main_beam_C111_Laue_2d_plot_dxp_fwhm_focstatavg_oe05
```

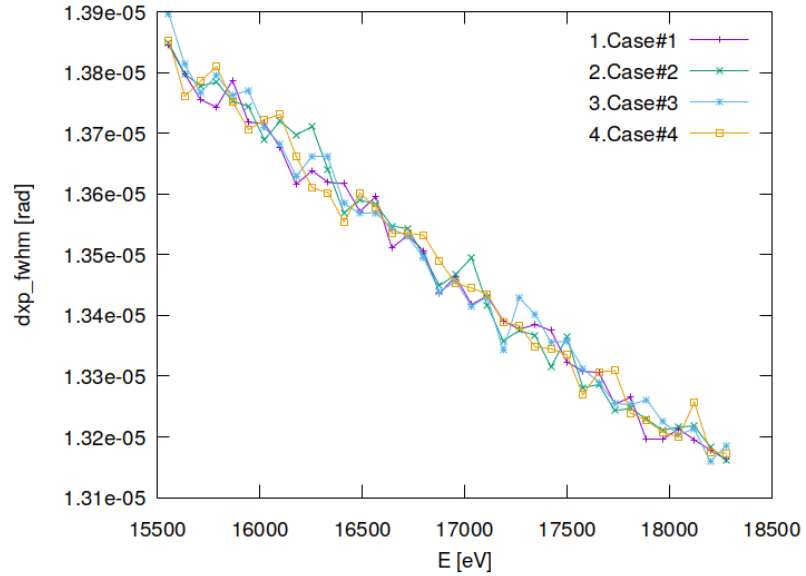


Figure 28.29: Sagittal beam divergence (FWHM) of optical element #05 (Dan-MAX).

```
"fig/Main_beam_C111_Laue/plot030.png" Lbl.:Main_beam_C111_Laue_2d_plot_dzp_fwhm_focstatavg_oe04
```

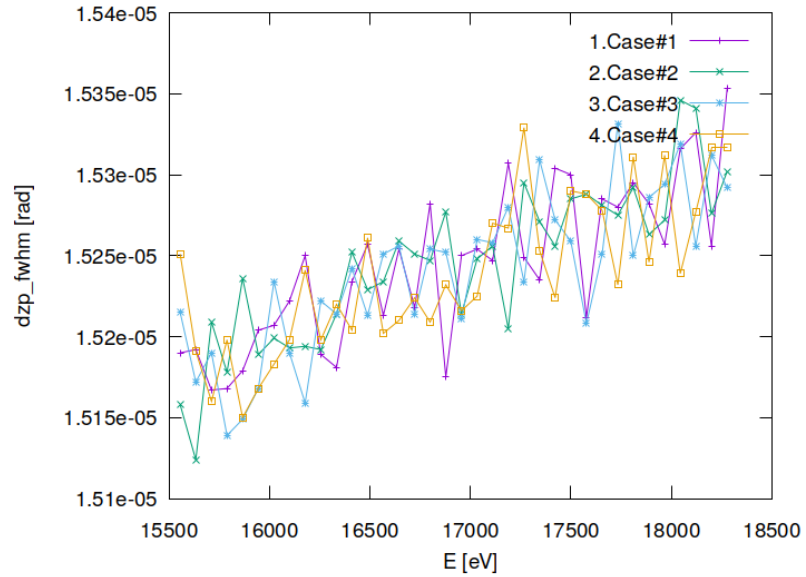


Figure 28.30: Meridional beam divergence (FWHM) of optical element #04 (BS).

```
"fig/Main_beam_C111_Laue/plot031.png" Lbl.:Main_beam_C111_Laue_2d_plot_dzp_fwhm_focstatavg_oe05
```

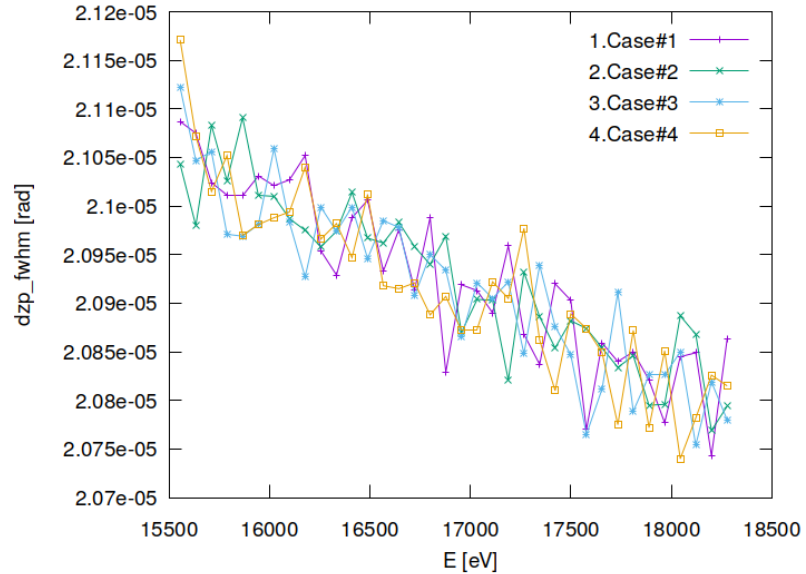


Figure 28.31: Meridional beam divergence (FWHM) of optical element #05 (Dan-MAX).

```
"fig/Main_beam_C111_Laue/plot032.png" Lbl.:Main_beam_C111_Laue_2d_plot_I_int_focstatavg_oe04
```

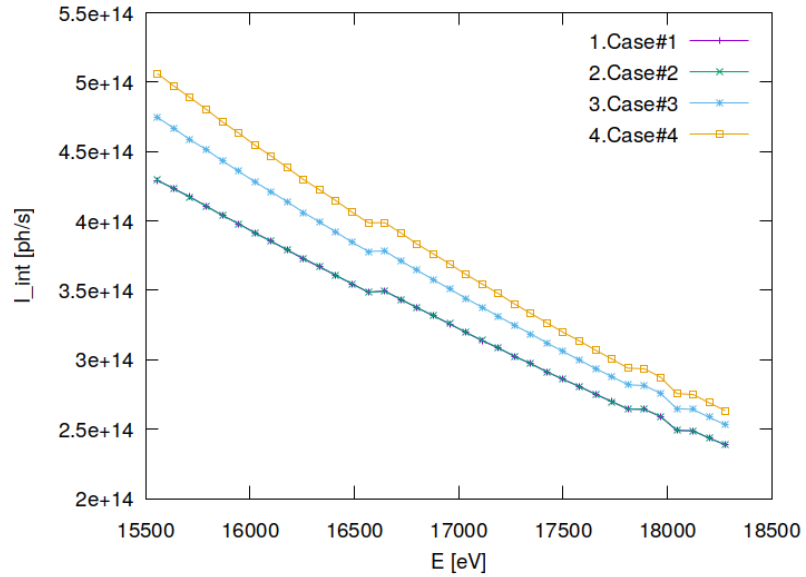


Figure 28.32: Photon flux in beam cross section of optical element #04 (BS).

```
"fig/Main_beam_C111_Laue/plot033.png" Lbl.:Main_beam_C111_Laue_2d_plot_I_int_focstatavg_oe05
```

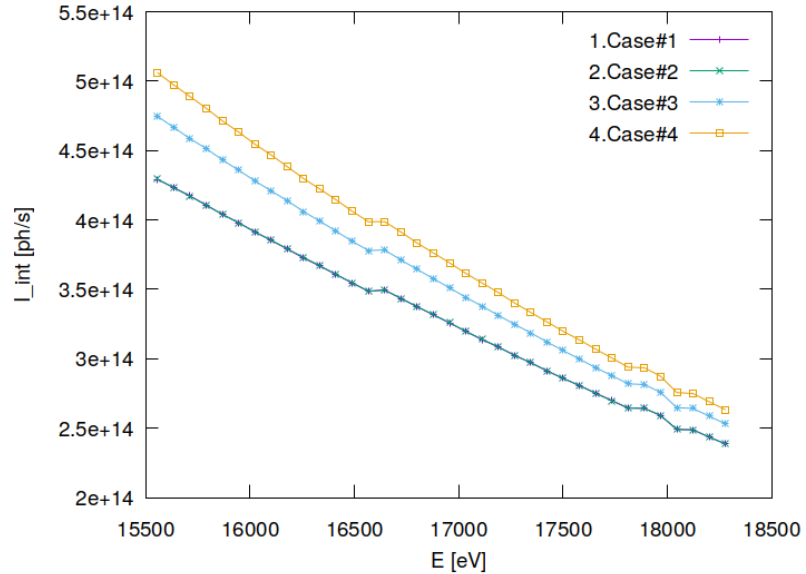


Figure 28.33: Photon flux in beam cross section of optical element #05 (DanMAX).

```
"fig/Main_beam_C111_Laue/plot034.png" Lbl.:Main_beam_C111_Laue_2d_plot_xp_cen_focstatavg_oe04
```

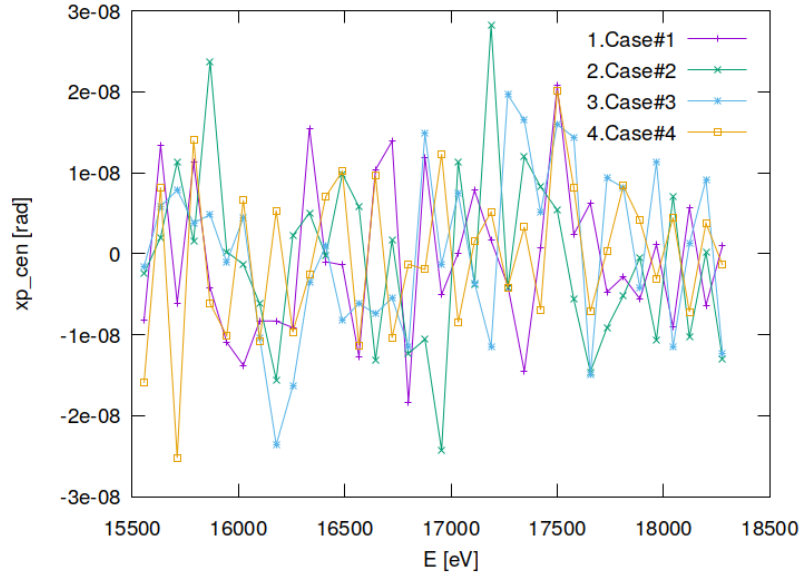


Figure 28.34: Sagittal coordinate of beam's centre of 'gravity' in angle space of optical element #04 (BS).

```
"fig/Main_beam_C111_Laue/plot035.png" Lbl.:Main_beam_C111_Laue_2d_plot_xp_cen_focstatavg_oe05
```

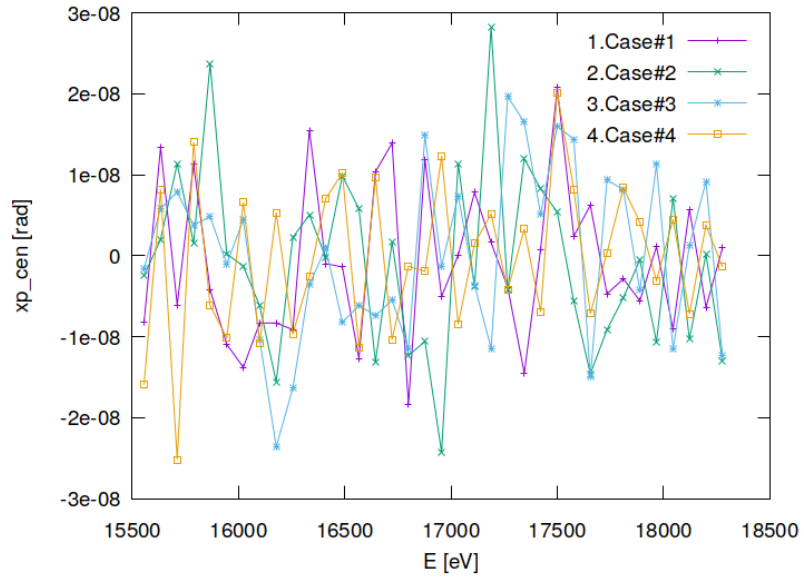


Figure 28.35: Sagittal coordinate of beam's centre of 'gravity' in angle space of optical element #05 (DanMAX).

```
"fig/Main_beam_C111_Laue/plot036.png" Lbl.:Main_beam_C111_Laue_2d_plot_zp_cen_focstatavg_oe04
```

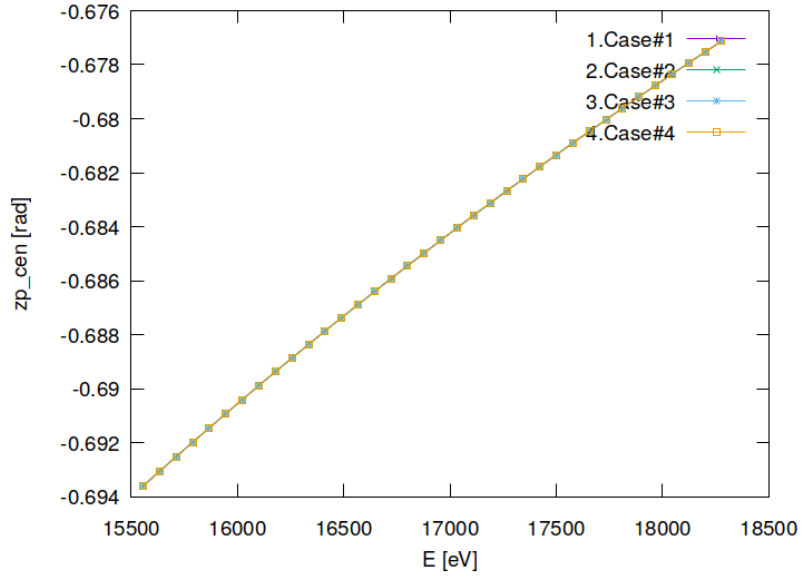


Figure 28.36: Meridional coordinate of beam's centre of 'gravity' in angle space of optical element #04 (BS).

```
"fig/Main_beam_C111_Laue/plot037.png" Lbl.:Main_beam_C111_Laue_2d_plot_zp_cen_focstatavg_oe05
```

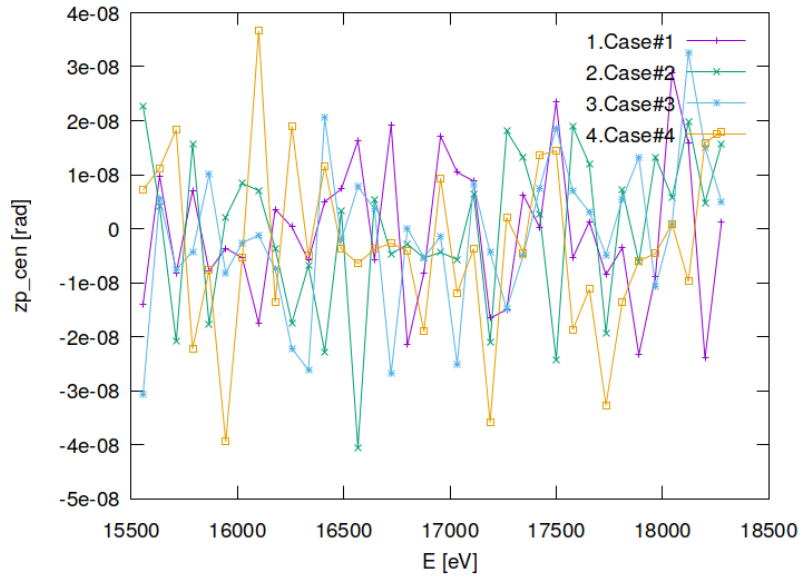


Figure 28.37: Meridional coordinate of beam's centre of 'gravity' in angle space of optical element #05 (DanMAX).

"fig/Main\_beam\_C111\_Laue/plot038.png" Lbl.:Main\_beam\_C111\_Laue\_2d\_plot\_dE\_fwhm\_focstatavg\_oe04

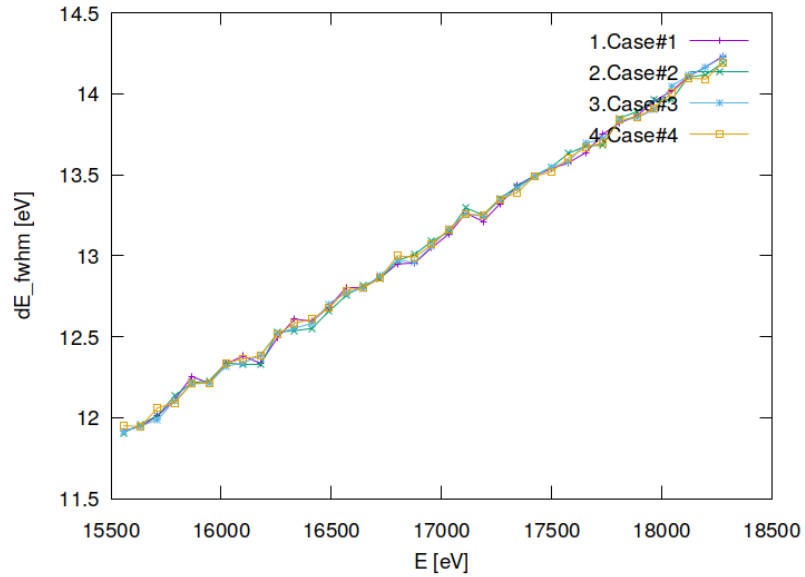


Figure 28.38: Bandwidth (FWHM) in beam cross section of optical element #04 (BS).

"fig/Main\_beam\_C111\_Laue/plot039.png" Lbl.:Main\_beam\_C111\_Laue\_2d\_plot\_dE\_fwhm\_focstatavg\_oe05

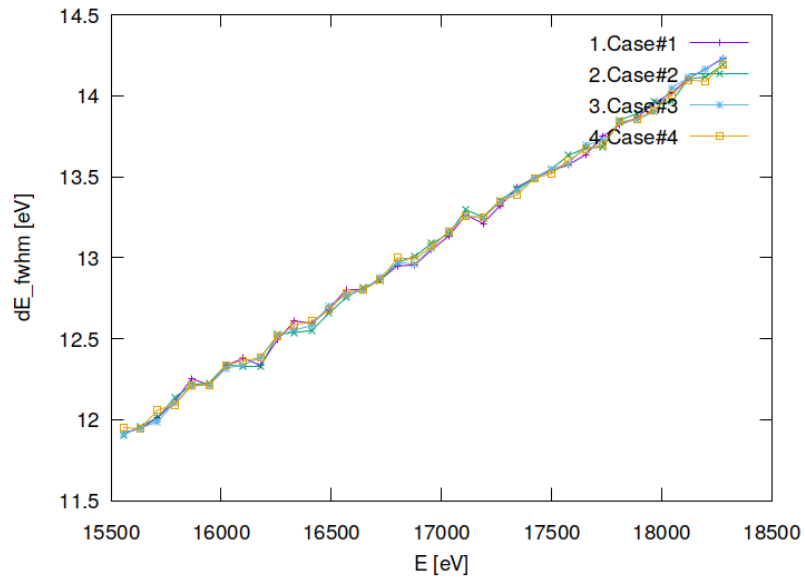


Figure 28.39: Bandwidth (FWHM) in beam cross section of optical element #05 (DanMAX).

## 28.8 Absorbed irradiance on surface

"fig/Main\_beam\_C111\_Laue/plot040.png" Lbl.:Main\_beam\_C111\_Laue\_false\_colour\_plot\_p\_abs\_foot\_oe04\_c2\_16955.9eV

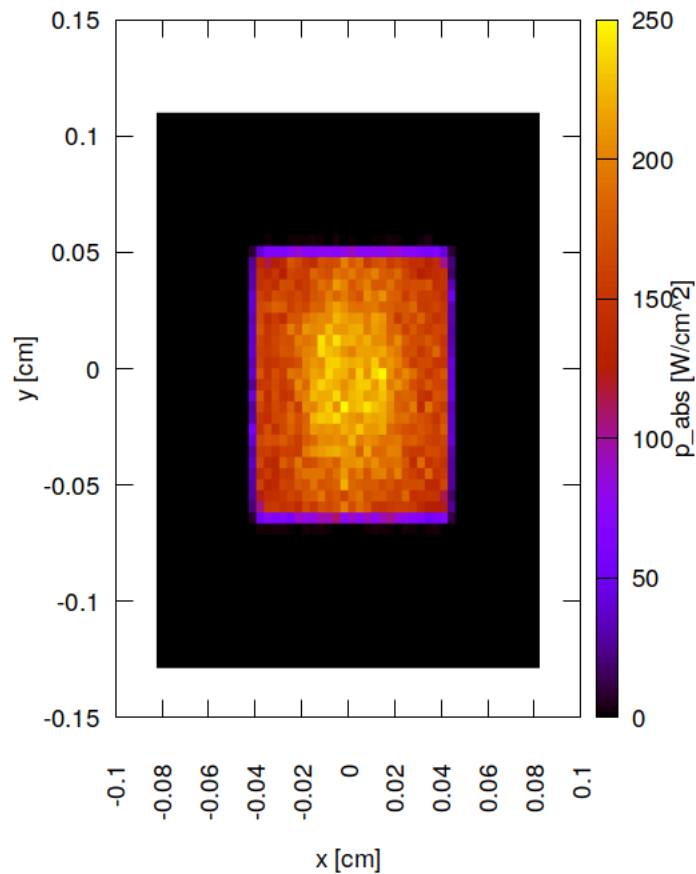


Figure 28.40: Absorbed irradiance on surface of optical element #04 (BS) for case #2 for 16955.9 eV photon energy setting.

"fig/Main\_beam\_C111\_Laue/plot041.png" Lbl.:Main\_beam\_C111\_Laue\_false\_colour\_plot\_p\_abs\_foot\_oe04\_c3\_16955.9eV

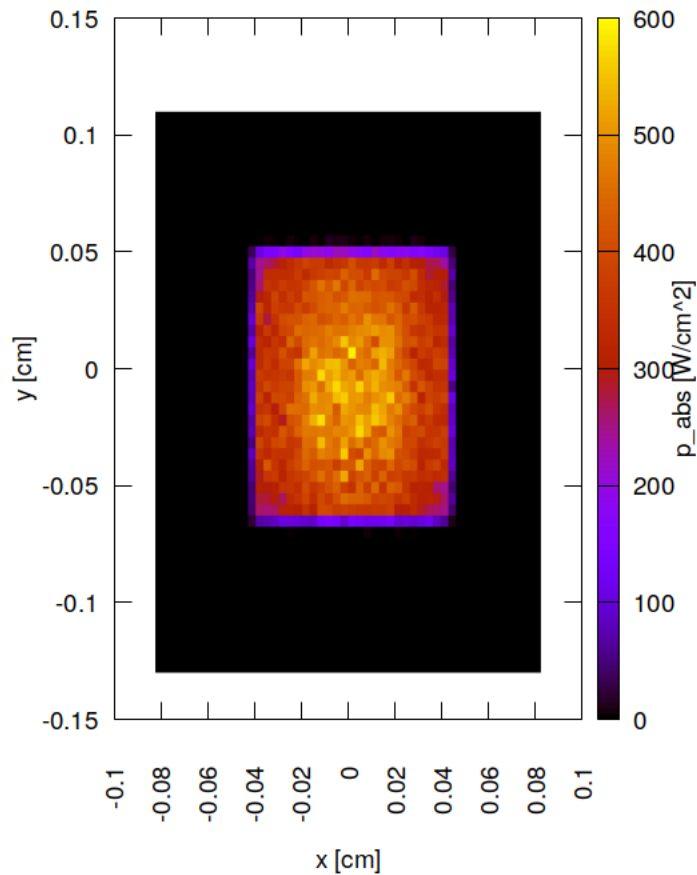


Figure 28.41: Absorbed irradiance on surface of optical element #04 (BS) for case #3 for 16955.9 eV photon energy setting.

"fig/Main\_beam\_C111\_Laue/plot042.png" Lbl.:Main\_beam\_C111\_Laue\_false\_colour\_plot\_p\_abs\_foot\_oe04\_c4\_16955.9eV

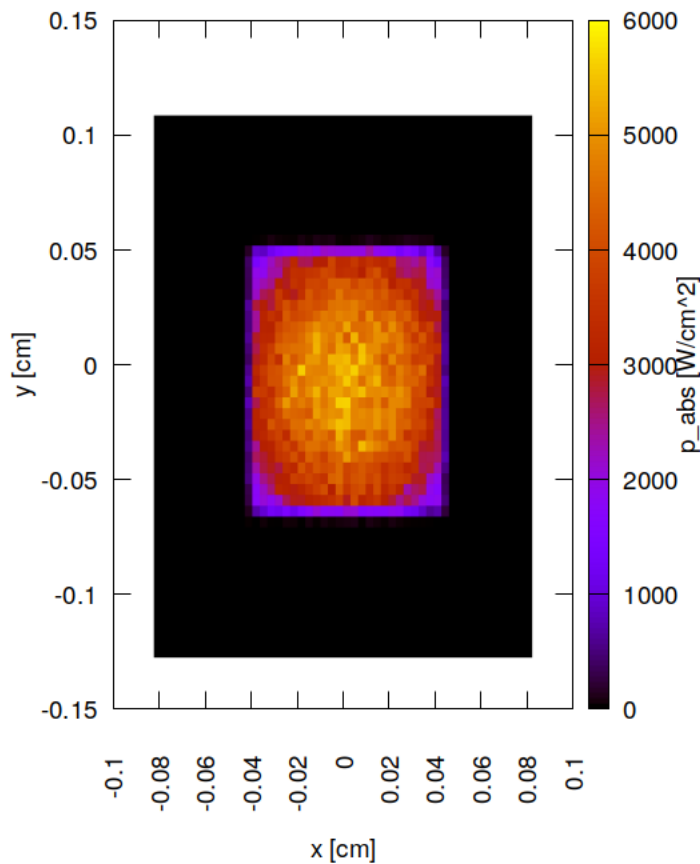


Figure 28.42: Absorbed irradiance on surface of optical element #04 (BS) for case #4 for 16955.9 eV photon energy setting.

## 28.9 Incident spectral flux on surface

"fig/Main\_beam\_C111\_Laue/plot043.png" Lbl.:Main\_beam\_C111\_Laue\_2d\_plot\_P\_spec\_spec\_oe04\_c2\_16955.9eV

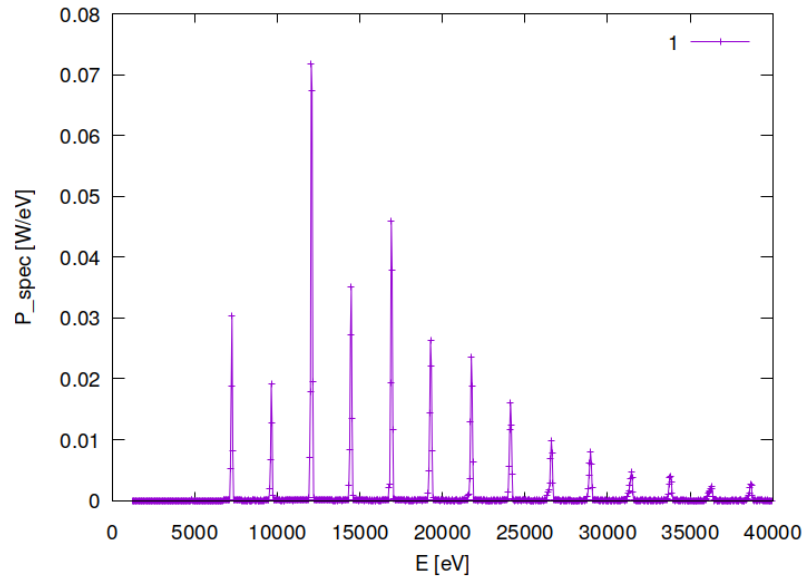


Figure 28.43: Incident spectral flux on surface of optical element #04 (BS) for case #2 for 16955.9 eV photon energy setting.

"fig/Main\_beam\_C111\_Laue/plot044.png" Lbl.:Main\_beam\_C111\_Laue\_2d\_plot\_P\_spec\_spec\_oe04\_c3\_16955.9eV

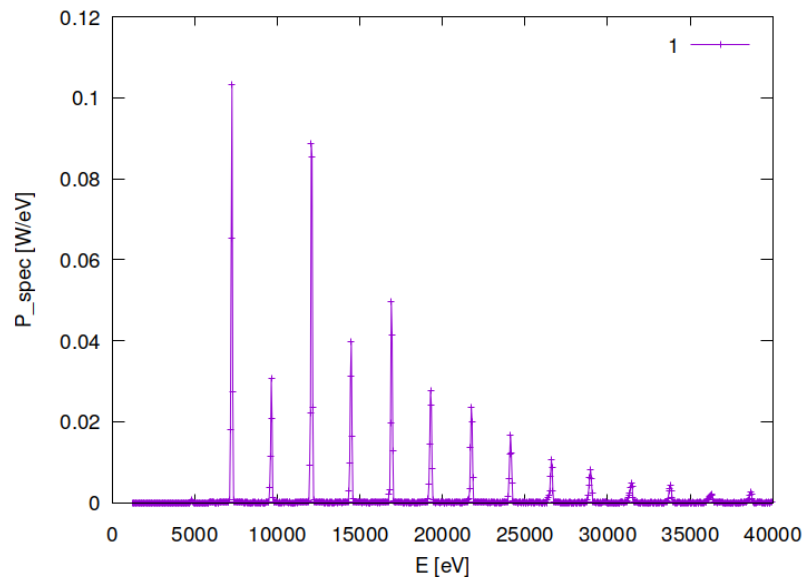


Figure 28.44: Incident spectral flux on surface of optical element #04 (BS) for case #3 for 16955.9 eV photon energy setting.

```
"fig/Main_beam_C111_Laue/plot045.png" Lbl.:Main_beam_C111_Laue_2d_plot_P_spec_spec_oe04_c4_16955.9eV
```

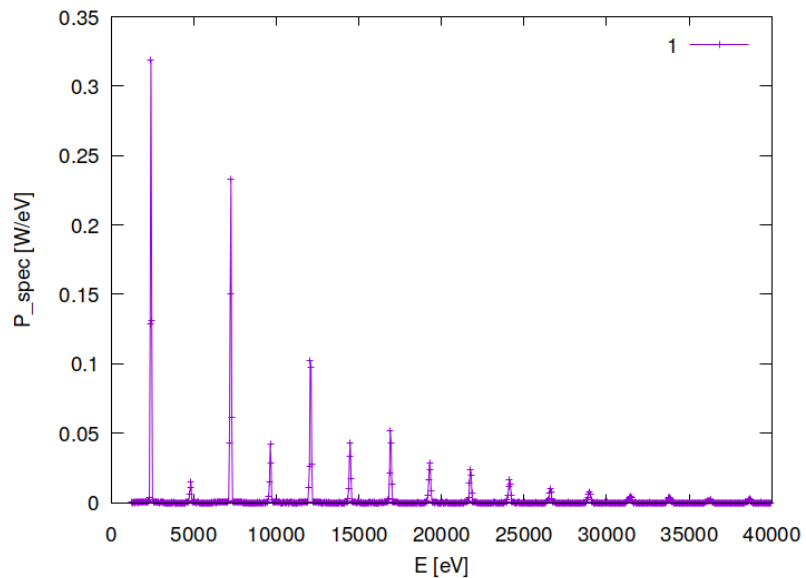


Figure 28.45: Incident spectral flux on surface of optical element #04 (BS) for case #4 for 16955.9 eV photon energy setting.

## 28.10 Temperature on surface

"fig/Main\_beam\_C111\_Laue/plot046.png" Lbl.:Main\_beam\_C111\_Laue\_false\_colour\_plot\_T\_oe04\_c2\_16955.9eV

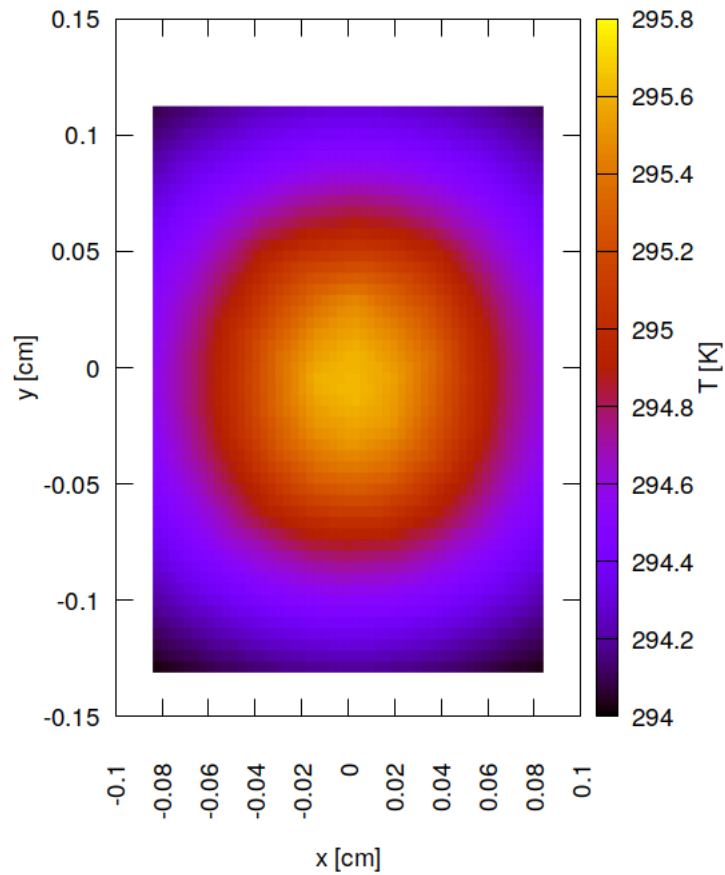


Figure 28.46: Temperature on surface of optical element #04 (BS) for case #2 for 16955.9 eV photon energy setting.

"fig/Main\_beam\_C111\_Laue/plot047.png" Lbl.:Main\_beam\_C111\_Laue\_false\_colour\_plot\_T\_oe04\_c3\_16955.9eV

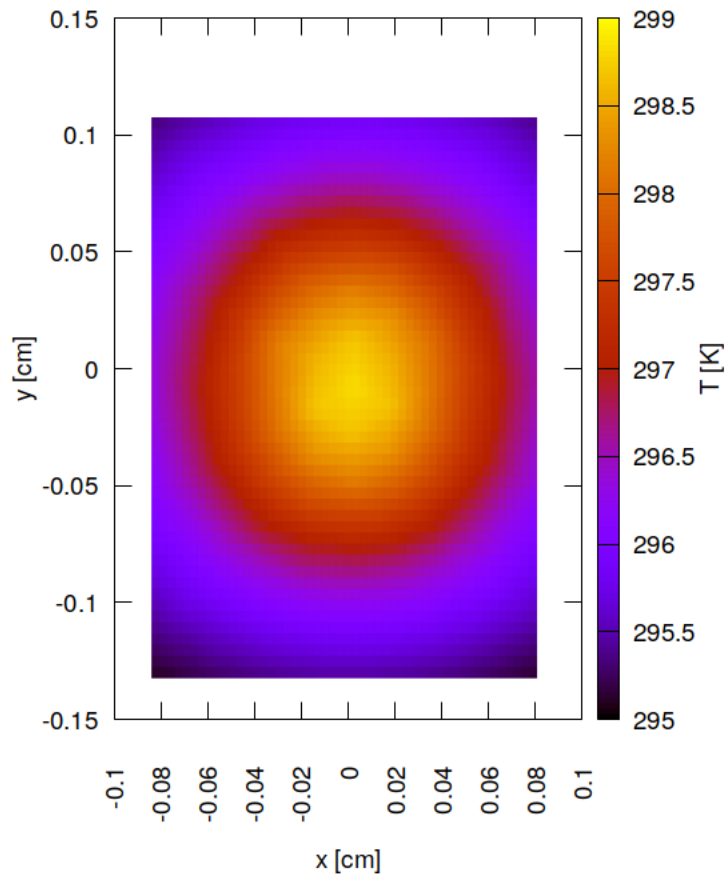


Figure 28.47: Temperature on surface of optical element #04 (BS) for case #3 for 16955.9 eV photon energy setting.

"fig/Main\_beam\_C111\_Laue/plot048.png" Lbl.:Main\_beam\_C111\_Laue\_false\_colour\_plot\_T\_oe04\_c4\_16955.9eV

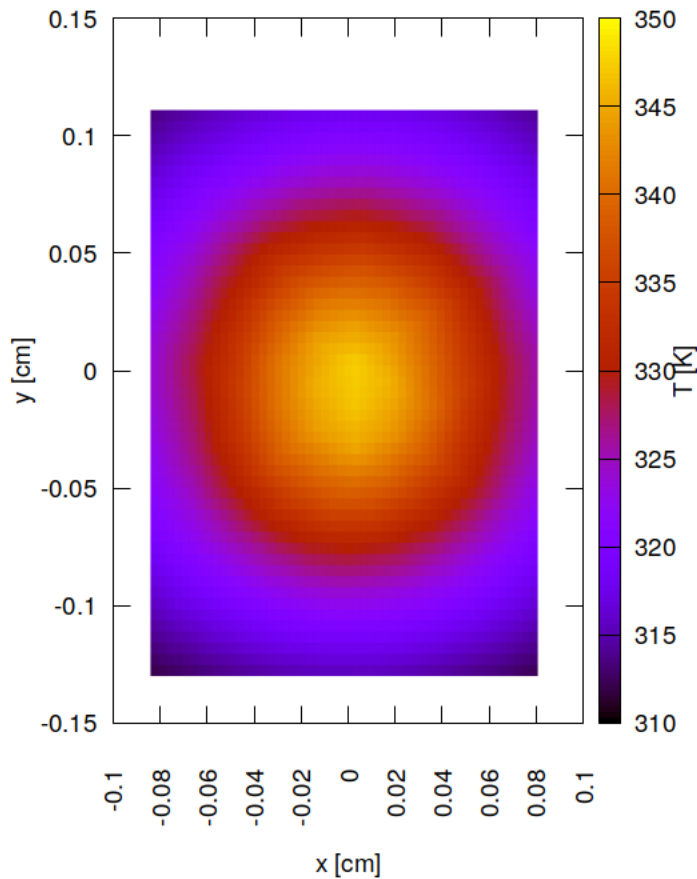


Figure 28.48: Temperature on surface of optical element #04 (BS) for case #4 for 16955.9 eV photon energy setting.

## 28.11 Mechanical stress (Von Mises stress) on surface

"fig/Main\_beam\_C111\_Laue/plot049.png" Lbl.:Main\_beam\_C111\_Laue\_false\_colour\_plot\_sigma\_oe04\_c2\_16955.9eV

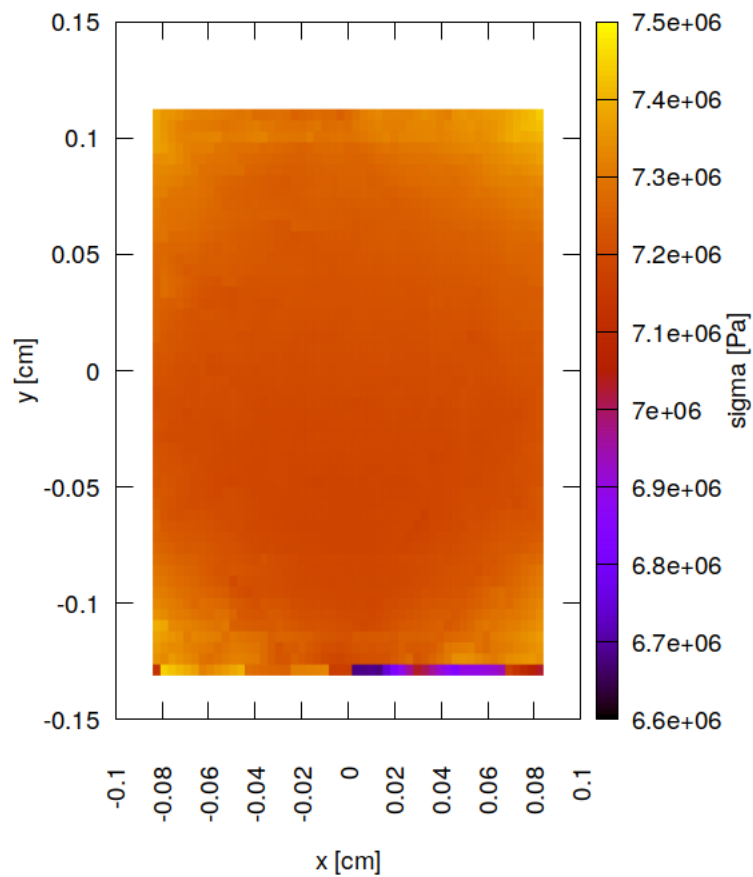


Figure 28.49: Mechanical stress (Von Mises stress) on surface of optical element #04 (BS) for case #2 for 16955.9 eV photon energy setting.

```
"fig/Main_beam_C111_Laue/plot050.png" Lbl.:Main_beam_C111_Laue_false_colour_plot_sigma_oe04_c3_16955.9eV
```

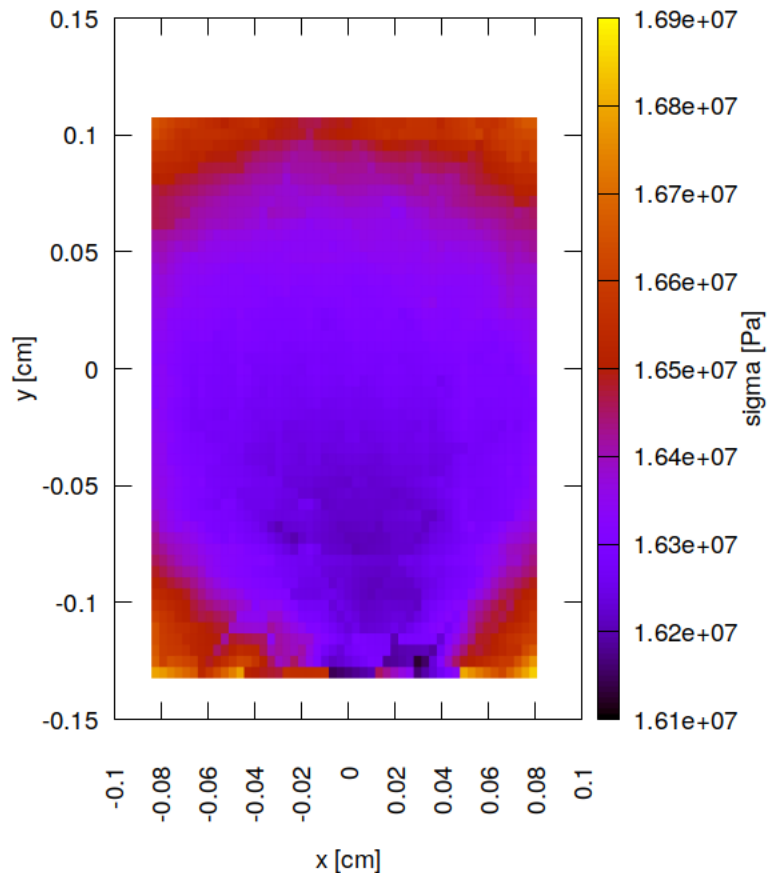


Figure 28.50: Mechanical stress (Von Mises stress) on surface of optical element #04 (BS) for case #3 for 16955.9 eV photon energy setting.

"fig/Main\_beam\_C111\_Laue/plot051.png" Lbl.:Main\_beam\_C111\_Laue\_false\_colour\_plot\_sigma\_oe04\_c4\_16955.9eV

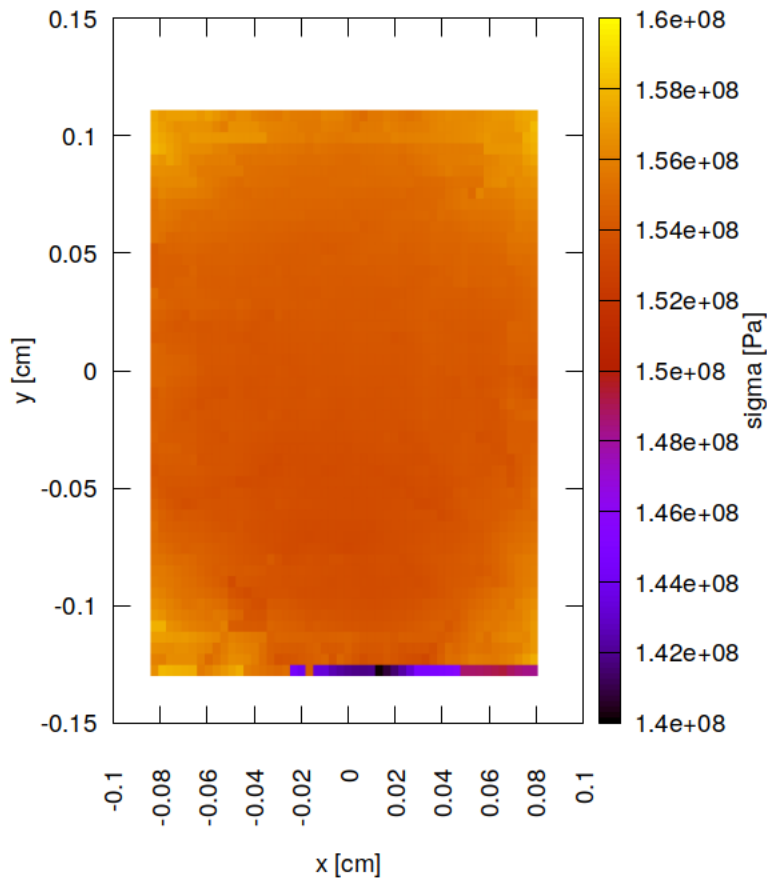


Figure 28.51: Mechanical stress (Von Mises stress) on surface of optical element #04 (BS) for case #4 for 16955.9 eV photon energy setting.

## 28.12 Surface slope error in meridional direction (y)

"fig/Main\_beam\_C111\_Laue/plot052.png" Lbl.:Main\_beam\_C111\_Laue\_false\_colour\_plot\_phi\_y\_oe04\_c2\_16955.9eV

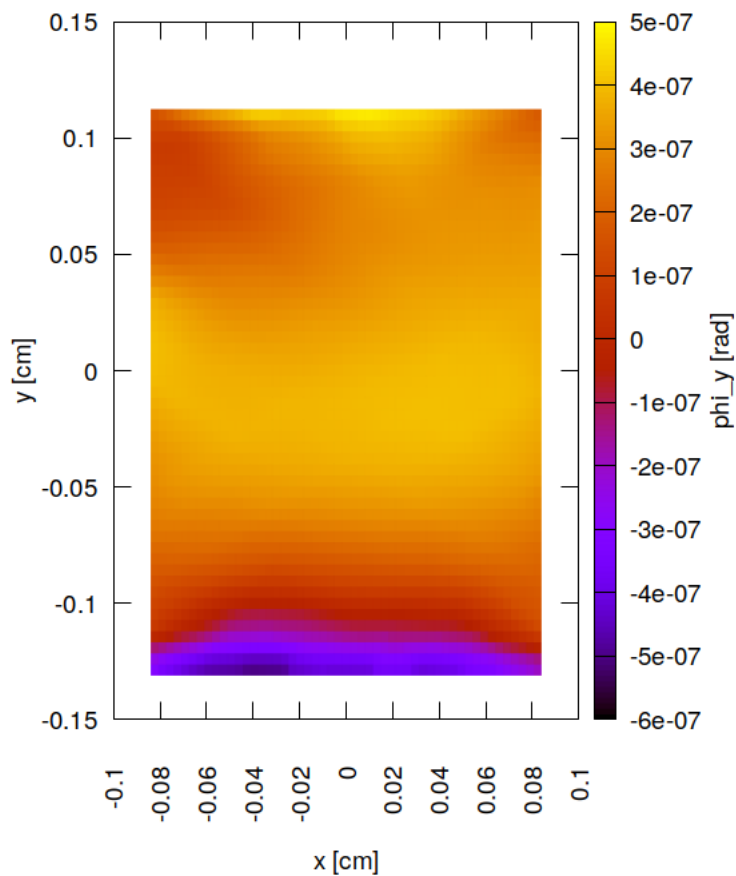


Figure 28.52: Surface slope error in meridional direction (y) of optical element #04 (BS) for case #2 for 16955.9 eV photon energy setting.

"fig/Main\_beam\_C111\_Laue/plot053.png" Lbl.:Main\_beam\_C111\_Laue\_false\_colour\_plot\_phi\_y\_oe04\_c3\_16955.9eV

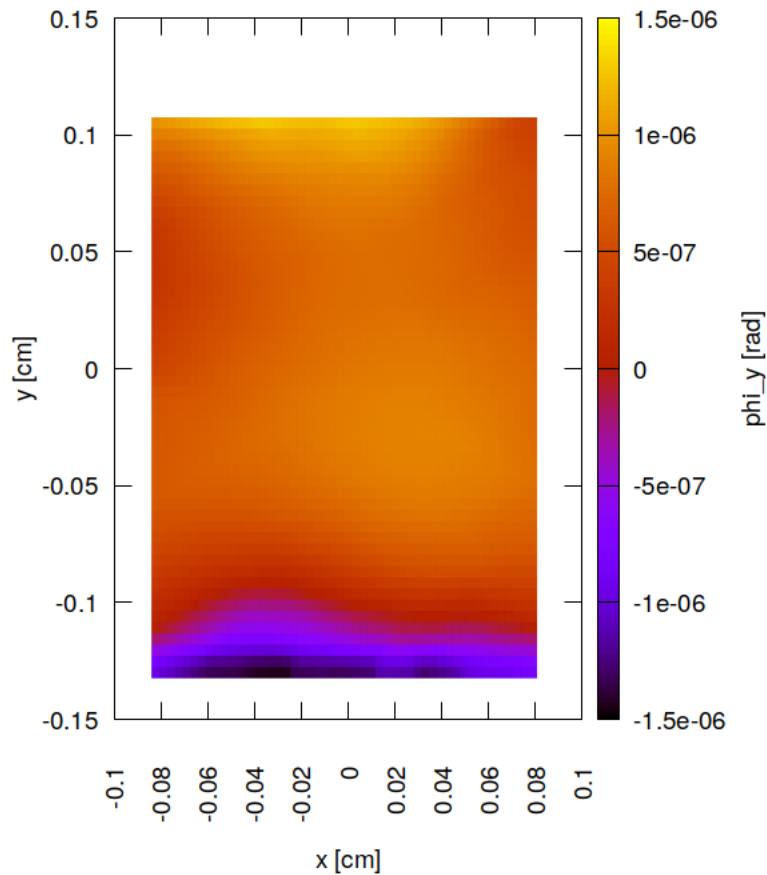


Figure 28.53: Surface slope error in meridional direction (y) of optical element #04 (BS) for case #3 for 16955.9 eV photon energy setting.

"fig/Main\_beam\_C111\_Laue/plot054.png" Lbl.:Main\_beam\_C111\_Laue\_false\_colour\_plot\_phi\_y\_oe04\_c4\_16955.9eV

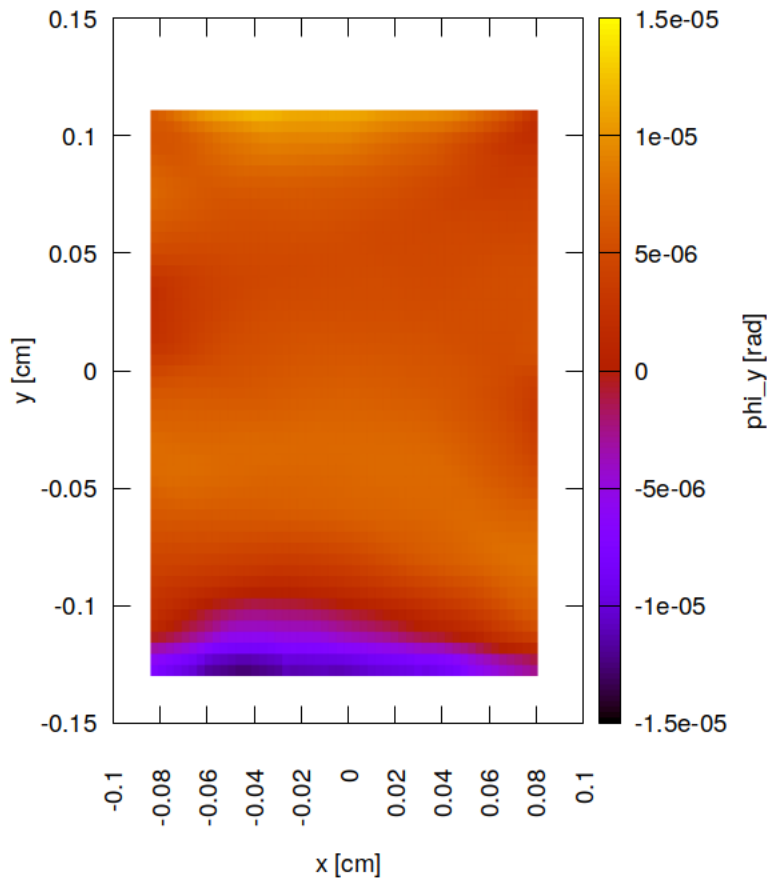


Figure 28.54: Surface slope error in meridional direction (y) of optical element #04 (BS) for case #4 for 16955.9 eV photon energy setting.

## 28.13 Incident photon irradiance on surface

"fig/Main\_beam\_C111\_Laue/plot055.png" Lbl.:Main\_beam\_C111\_Laue\_false\_colour\_plot\_I\_inc\_foot\_oe04\_c1\_16955.9eV

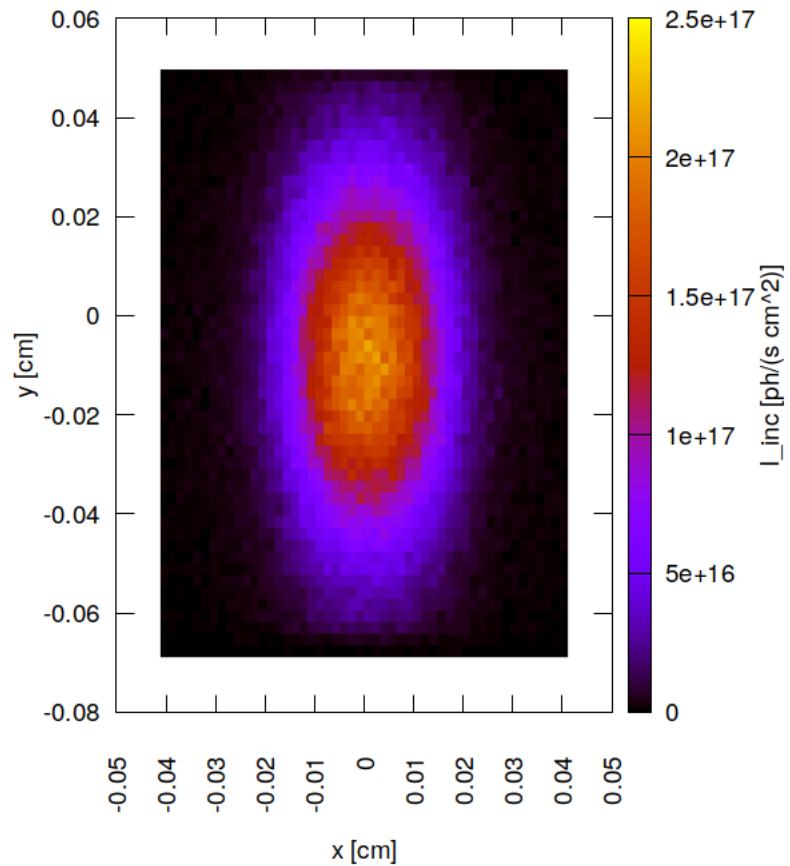


Figure 28.55: Incident photon irradiance on surface of optical element #04 (BS) for case #1 for 16955.9 eV photon energy setting.

"fig/Main\_beam\_C111\_Laue/plot056.png" Lbl.:Main\_beam\_C111\_Laue\_false\_colour\_plot\_I\_inc\_foot\_oe04\_c2\_16955.9eV

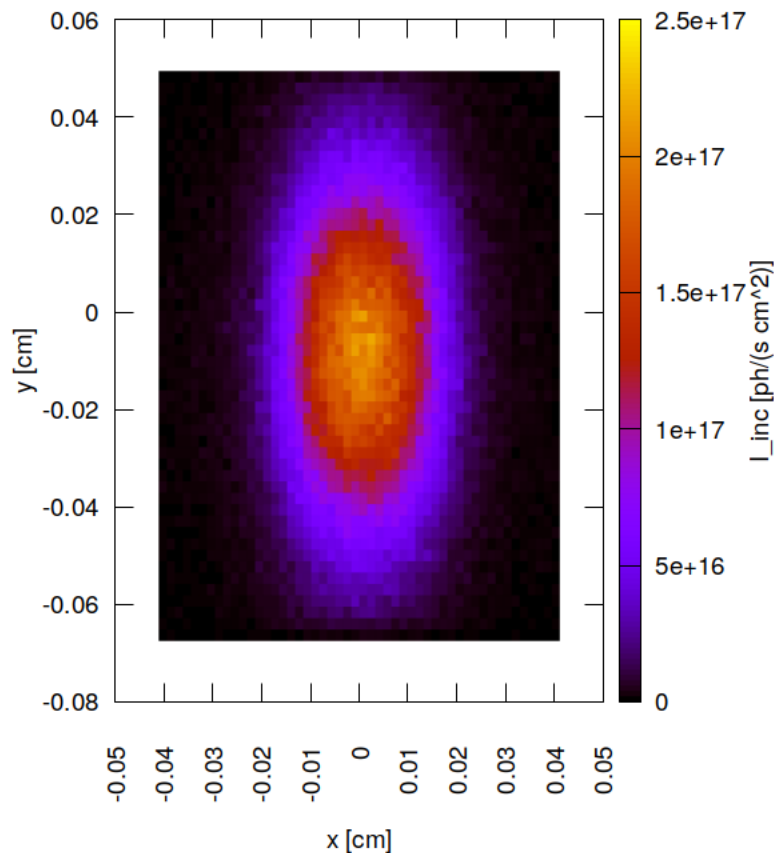


Figure 28.56: Incident photon irradiance on surface of optical element #04 (BS) for case #2 for 16955.9 eV photon energy setting.

"fig/Main\_beam\_C111\_Laue/plot057.png" Lbl.:Main\_beam\_C111\_Laue\_false\_colour\_plot\_I\_inc\_foot\_oe04\_c3\_16955.9eV

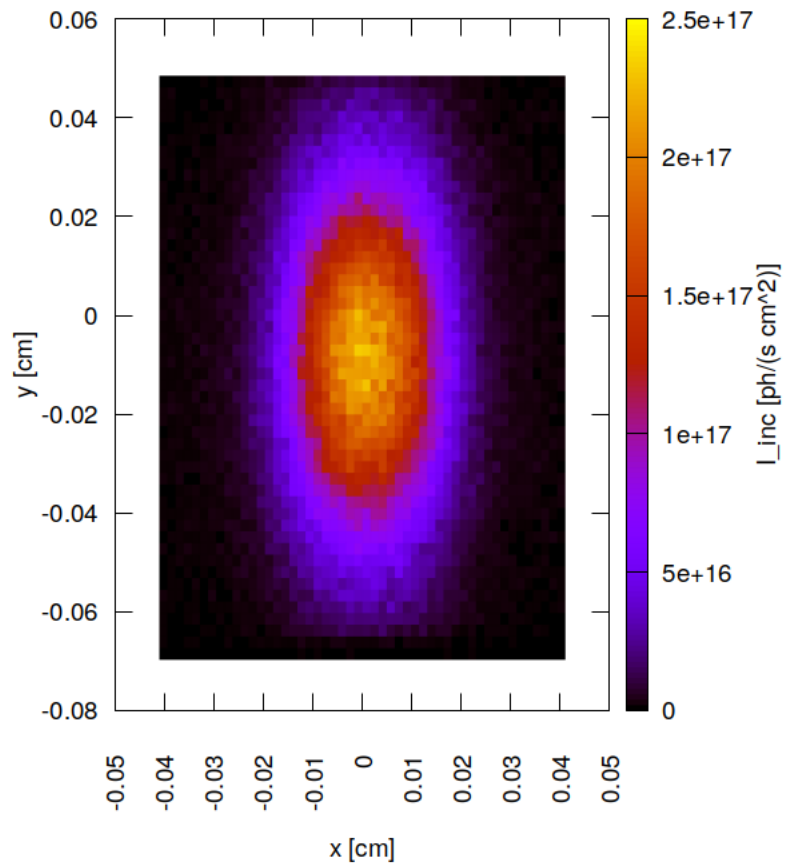


Figure 28.57: Incident photon irradiance on surface of optical element #04 (BS) for case #3 for 16955.9 eV photon energy setting.

"fig/Main\_beam\_C111\_Laue/plot058.png" Lbl.:Main\_beam\_C111\_Laue\_false\_colour\_plot\_I\_inc\_foot\_oe04\_c4\_16955.9eV

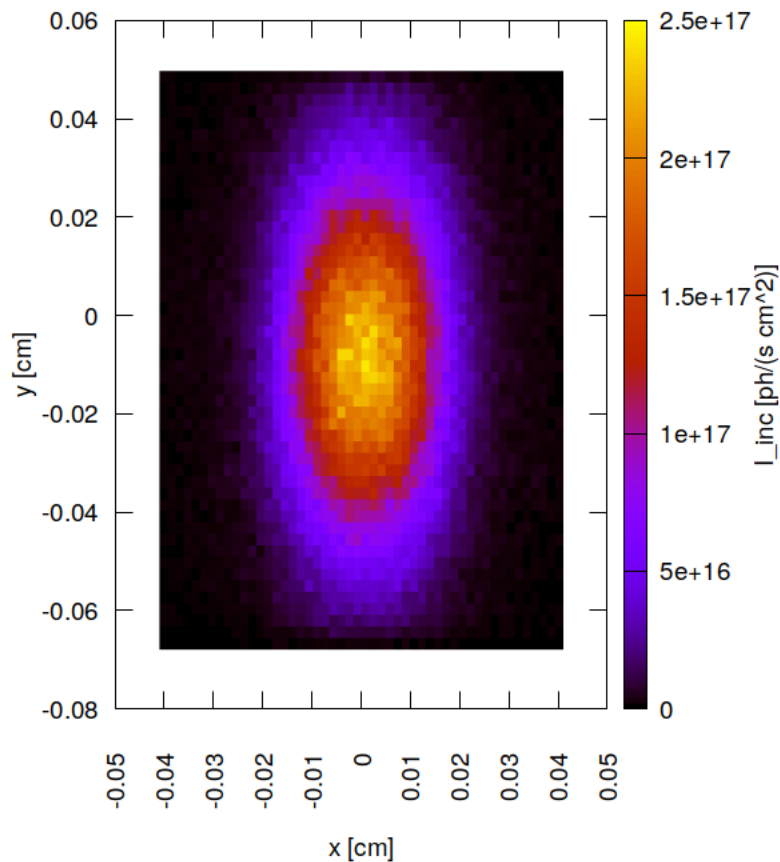


Figure 28.58: Incident photon irradiance on surface of optical element #04 (BS) for case #4 for 16955.9 eV photon energy setting.

"fig/Main\_beam\_C111\_Laue/plot059.png" Lbl.:Main\_beam\_C111\_Laue\_false\_colour\_plot\_I\_inc\_foot\_oe05\_c1\_16955.9eV

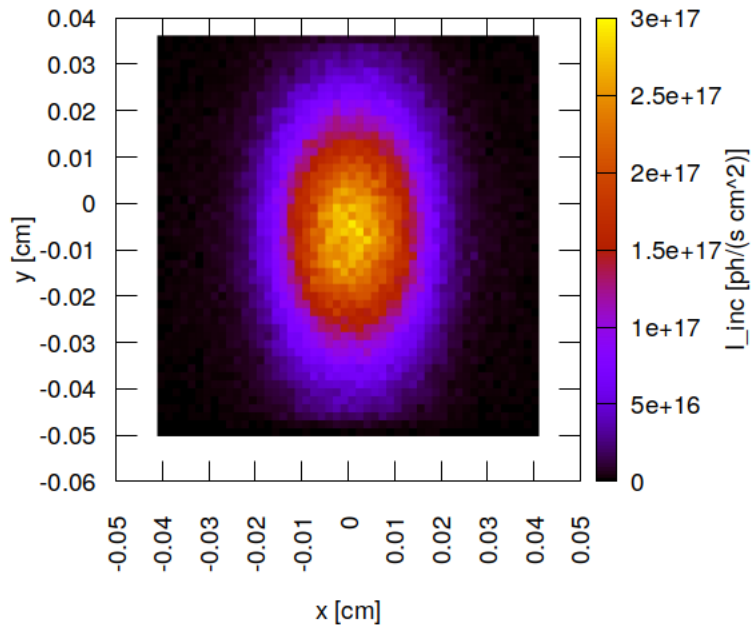


Figure 28.59: Incident photon irradiance on surface of optical element #05 (Dan-MAX) for case #1 for 16955.9 eV photon energy setting.

"fig/Main\_beam\_C111\_Laue/plot060.png" Lbl.:Main\_beam\_C111\_Laue\_false\_colour\_plot\_I\_inc\_foot\_oe05\_c2\_16955.9eV

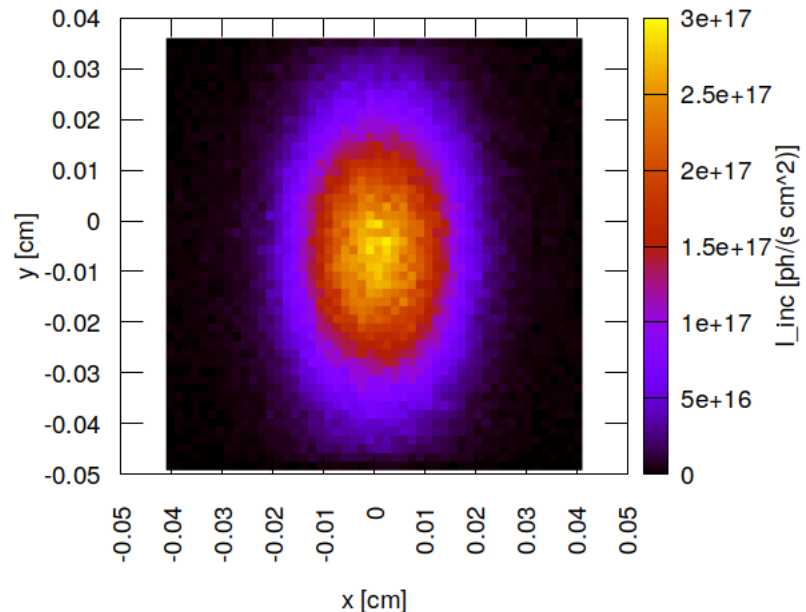


Figure 28.60: Incident photon irradiance on surface of optical element #05 (Dan-MAX) for case #2 for 16955.9 eV photon energy setting.

"fig/Main\_beam\_C111\_Laue/plot061.png" Lbl.:Main\_beam\_C111\_Laue\_false\_colour\_plot\_I\_inc\_foot\_oe05\_c3\_16955.9eV

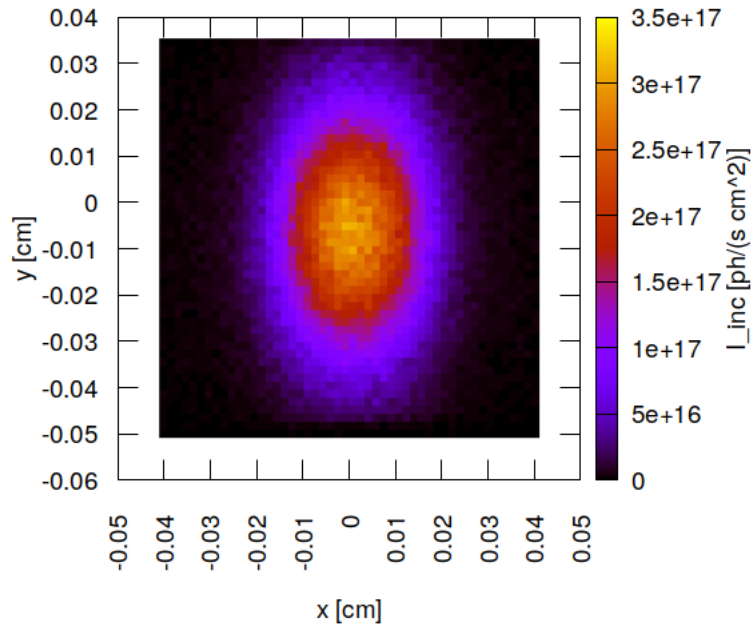


Figure 28.61: Incident photon irradiance on surface of optical element #05 (Dan-MAX) for case #3 for 16955.9 eV photon energy setting.

"fig/Main\_beam\_C111\_Laue/plot062.png" Lbl.:Main\_beam\_C111\_Laue\_false\_colour\_plot\_I\_inc\_oe05\_c4\_16955.9eV

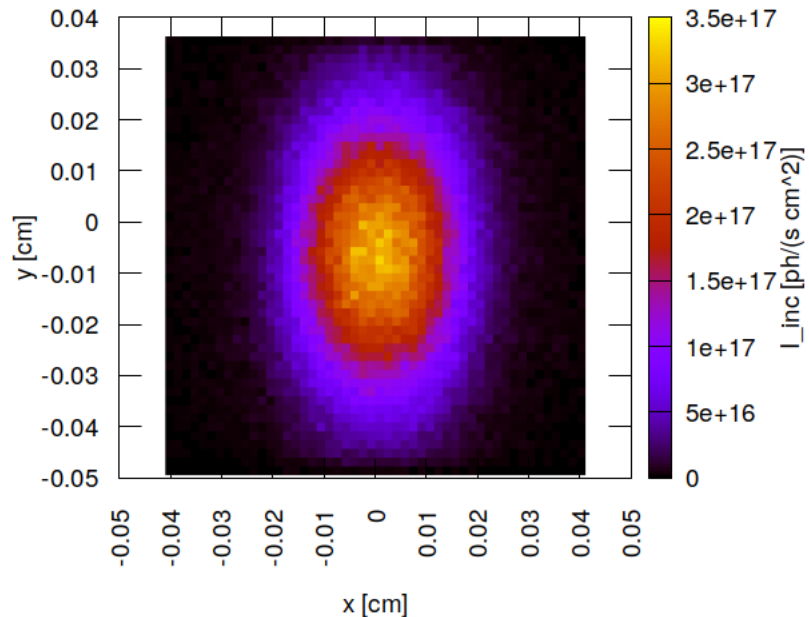


Figure 28.62: Incident photon irradiance on surface of optical element #05 (DanMAX) for case #4 for 16955.9 eV photon energy setting.

## 28.14 Photon irradiance in beam cross section

"fig/Main\_beam\_C111\_Laue/plot063.png" Lbl.:Main\_beam\_C111\_Laue\_false\_colour\_plot\_I\_foc\_oe04\_c1\_16955.9eV

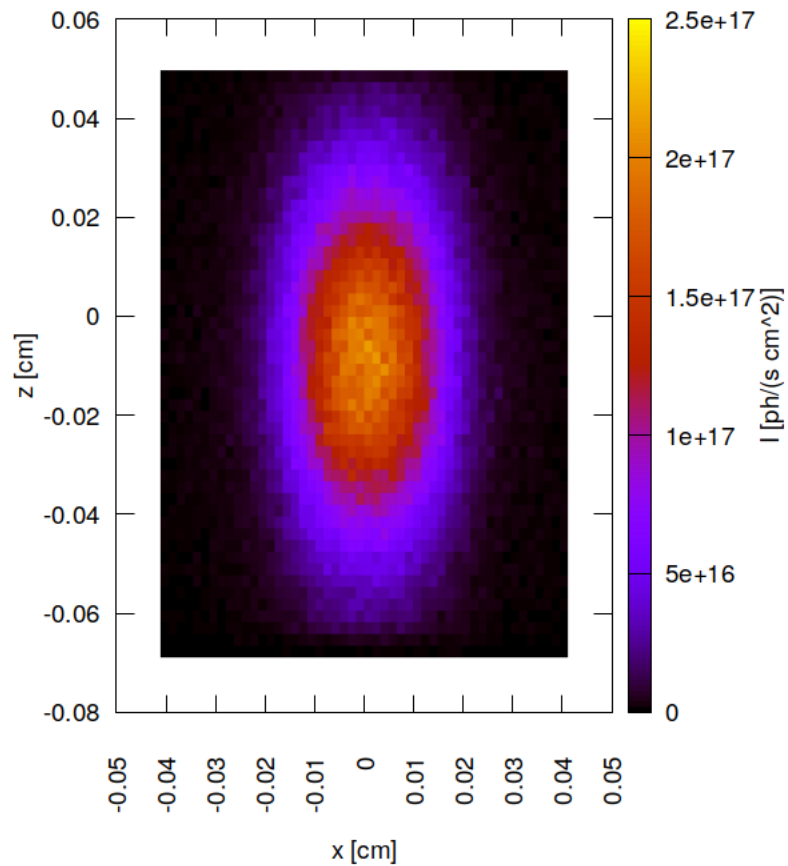


Figure 28.63: Photon irradiance in beam cross section of optical element #04 (BS) for case #1 for 16955.9 eV photon energy setting.

"fig/Main\_beam\_C111\_Laue/plot064.png" Lbl.:Main\_beam\_C111\_Laue\_false\_colour\_plot\_I\_foc\_oe04\_c2\_16955.9eV

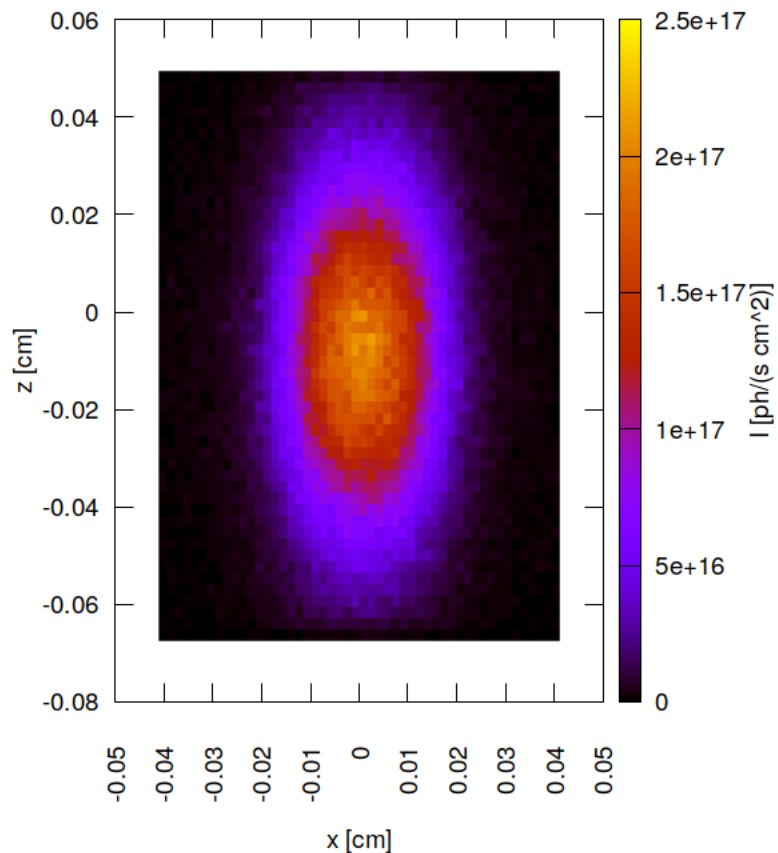


Figure 28.64: Photon irradiance in beam cross section of optical element #04 (BS) for case #2 for 16955.9 eV photon energy setting.

"fig/Main\_beam\_C111\_Laue/plot065.png" Lbl.:Main\_beam\_C111\_Laue\_false\_colour\_plot\_I\_foc\_oe04\_c3\_16955.9eV

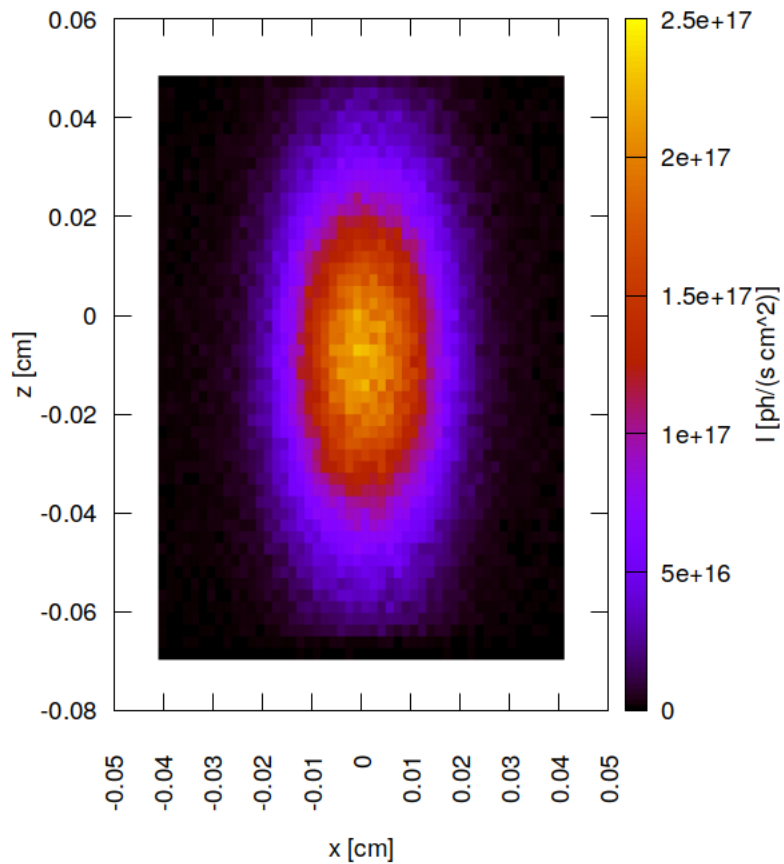


Figure 28.65: Photon irradiance in beam cross section of optical element #04 (BS) for case #3 for 16955.9 eV photon energy setting.

"fig/Main\_beam\_C111\_Laue/plot066.png" Lbl.:Main\_beam\_C111\_Laue\_false\_colour\_plot\_I\_foc\_oe04\_c4\_16955.9eV

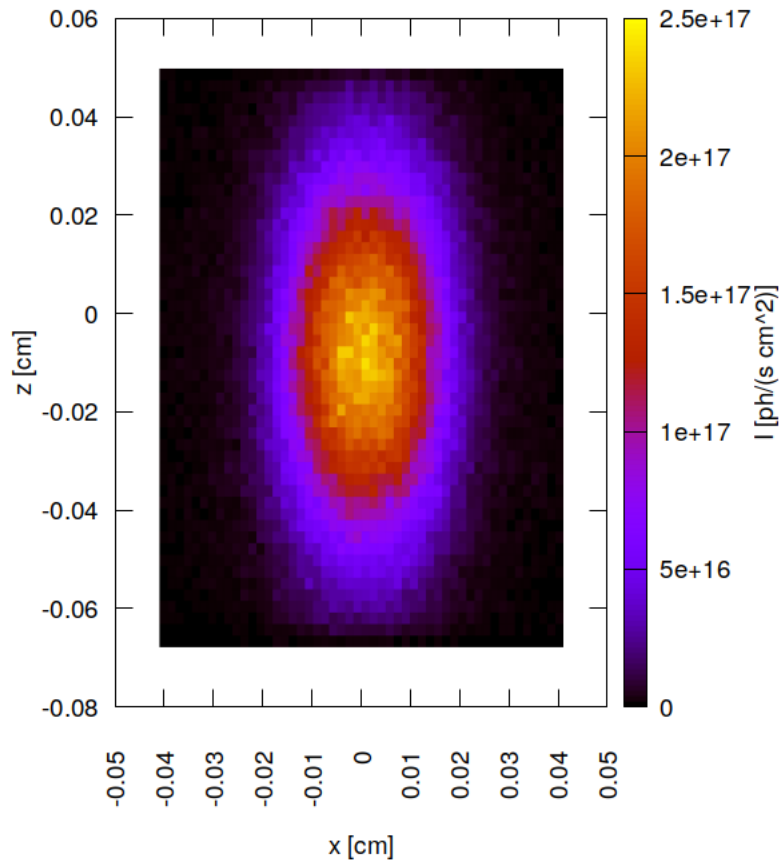


Figure 28.66: Photon irradiance in beam cross section of optical element #04 (BS) for case #4 for 16955.9 eV photon energy setting.

"fig/Main\_beam\_C111\_Laue/plot067.png" Lbl.:Main\_beam\_C111\_Laue\_false\_colour\_plot\_I\_foc\_oe05\_c1\_16955.9eV

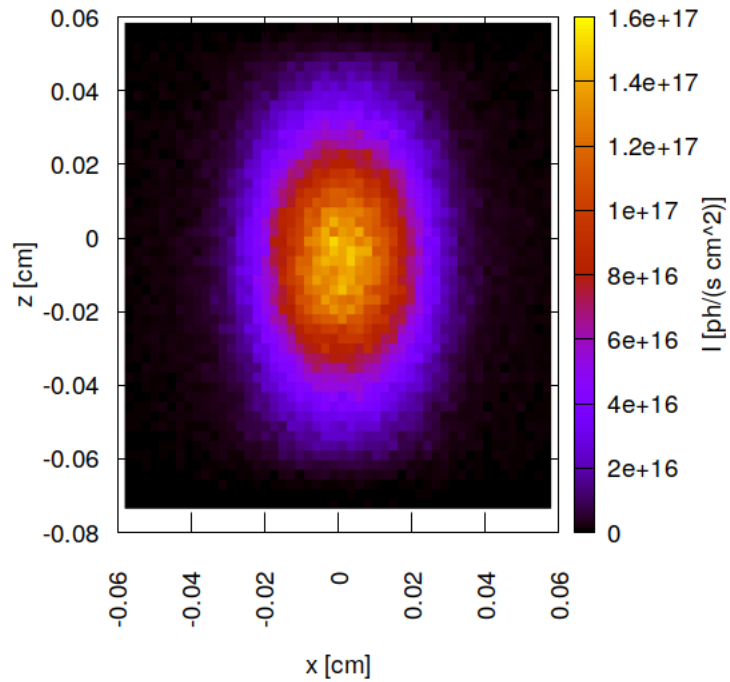


Figure 28.67: Photon irradiance in beam cross section of optical element #05 (Dan-MAX) for case #1 for 16955.9 eV photon energy setting.

"fig/Main\_beam\_C111\_Laue/plot068.png" Lbl.:Main\_beam\_C111\_Laue\_false\_colour\_plot\_I\_foc\_oe05\_c2\_16955.9eV

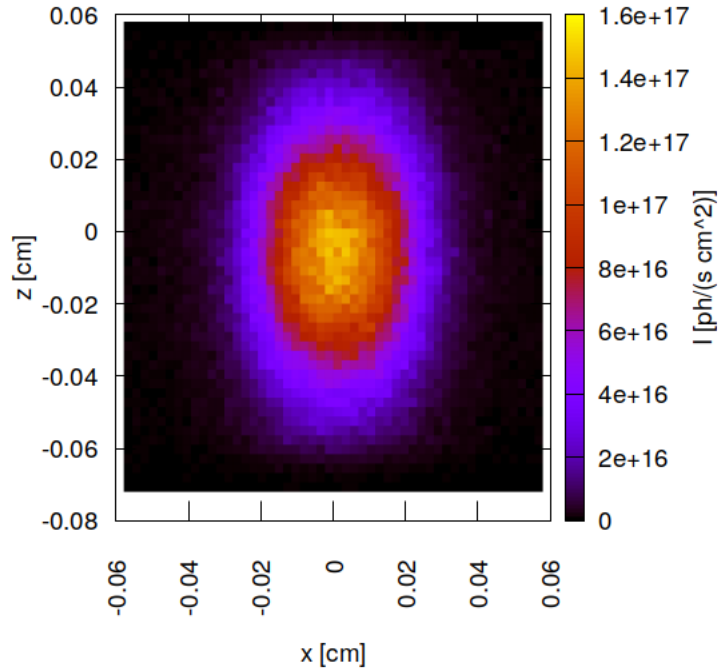


Figure 28.68: Photon irradiance in beam cross section of optical element #05 (Dan-MAX) for case #2 for 16955.9 eV photon energy setting.

"fig/Main\_beam\_C111\_Laue/plot069.png" Lbl.:Main\_beam\_C111\_Laue\_false\_colour\_plot\_I\_foc\_oe05\_c3\_16955.9eV

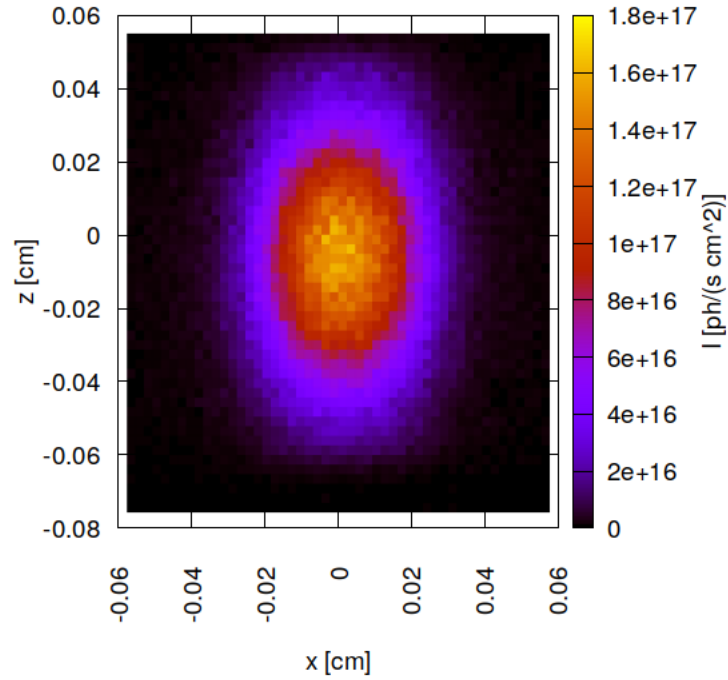


Figure 28.69: Photon irradiance in beam cross section of optical element #05 (Dan-MAX) for case #3 for 16955.9 eV photon energy setting.

"fig/Main\_beam\_C111\_Laue/plot070.png" Lbl.:Main\_beam\_C111\_Laue\_false\_colour\_plot\_I\_foc\_oe05\_c4\_16955.9eV

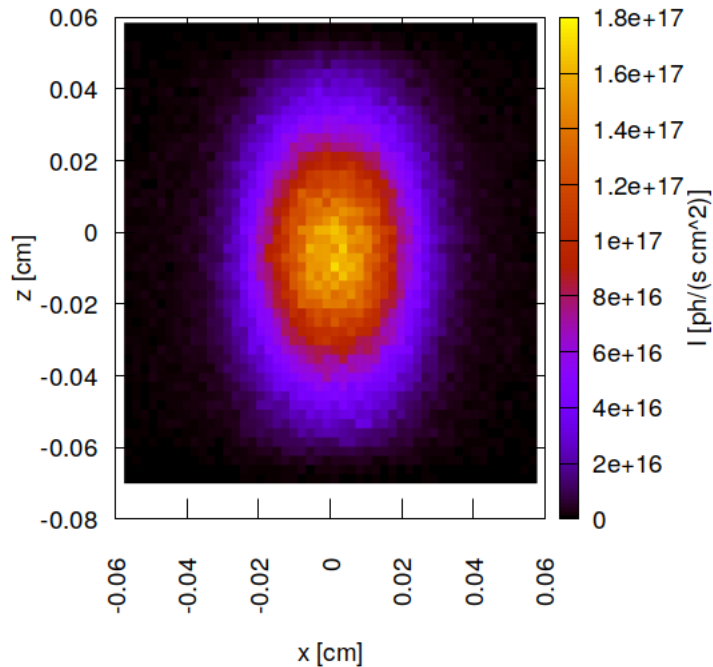


Figure 28.70: Photon irradiance in beam cross section of optical element #05 (Dan-MAX) for case #4 for 16955.9 eV photon energy setting.

## 28.15 Spectral photon flux in beam cross section

"fig/Main\_beam\_C111\_Laue/plot071.png" Lbl.:Main\_beam\_C111\_Laue\_2d\_plot\_I\_bandfoc\_oe04\_c1\_16955.9eV

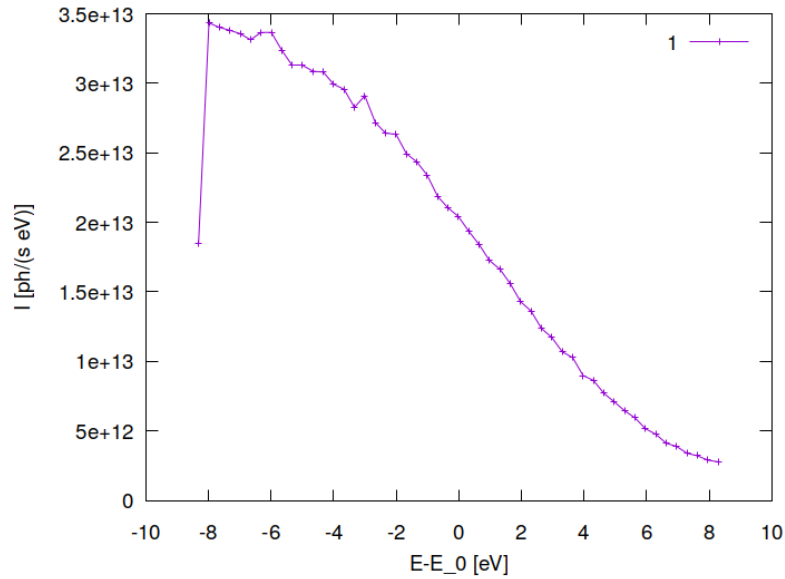


Figure 28.71: Spectral photon flux in beam cross section of optical element #04 (BS) for case #1 for 16955.9 eV photon energy setting.

"fig/Main\_beam\_C111\_Laue/plot072.png" Lbl.:Main\_beam\_C111\_Laue\_2d\_plot\_I\_bandfoc\_oe04\_c2\_16955.9eV

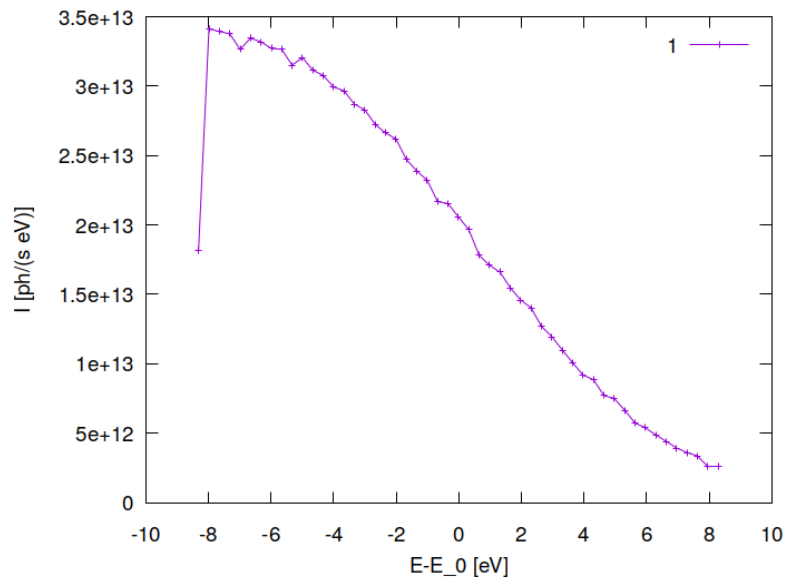


Figure 28.72: Spectral photon flux in beam cross section of optical element #04 (BS) for case #2 for 16955.9 eV photon energy setting.

```
"fig/Main_beam_C111_Laue/plot073.png" Lbl.:Main_beam_C111_Laue_2d_plot_I_bandfoc_oe04_c3_16955.9eV
```

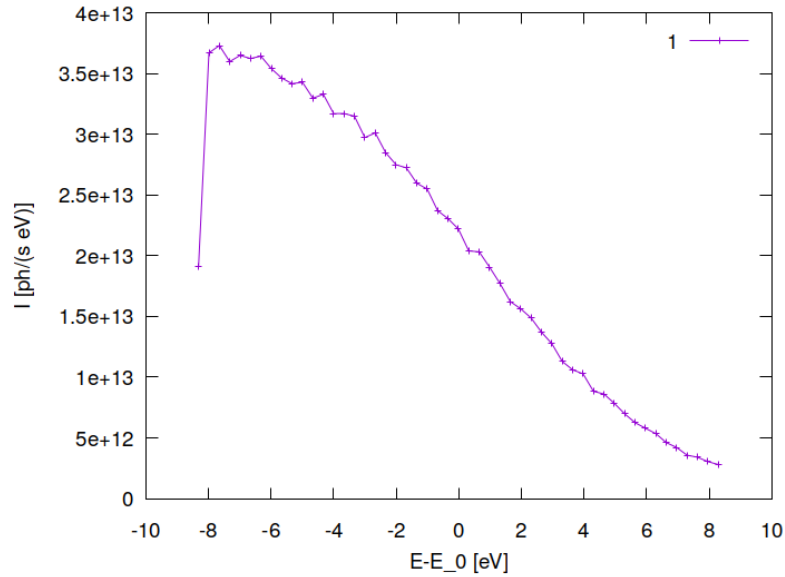


Figure 28.73: Spectral photon flux in beam cross section of optical element #04 (BS) for case #3 for 16955.9 eV photon energy setting.

```
"fig/Main_beam_C111_Laue/plot074.png" Lbl.:Main_beam_C111_Laue_2d_plot_I_bandfoc_oe04_c4_16955.9eV
```

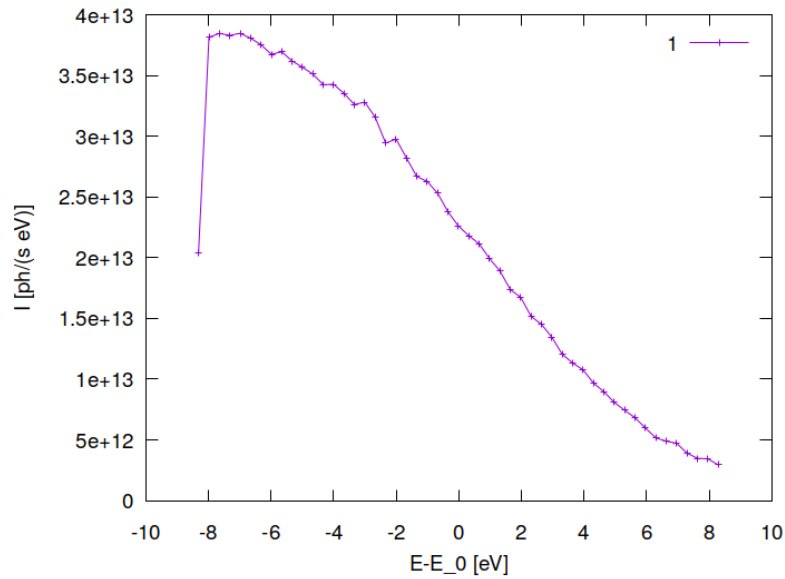


Figure 28.74: Spectral photon flux in beam cross section of optical element #04 (BS) for case #4 for 16955.9 eV photon energy setting.

```
"fig/Main_beam_C111_Laue/plot075.png" Lbl.:Main_beam_C111_Laue_2d_plot_I_bandfoc_oe05_c1_16955.9eV
```

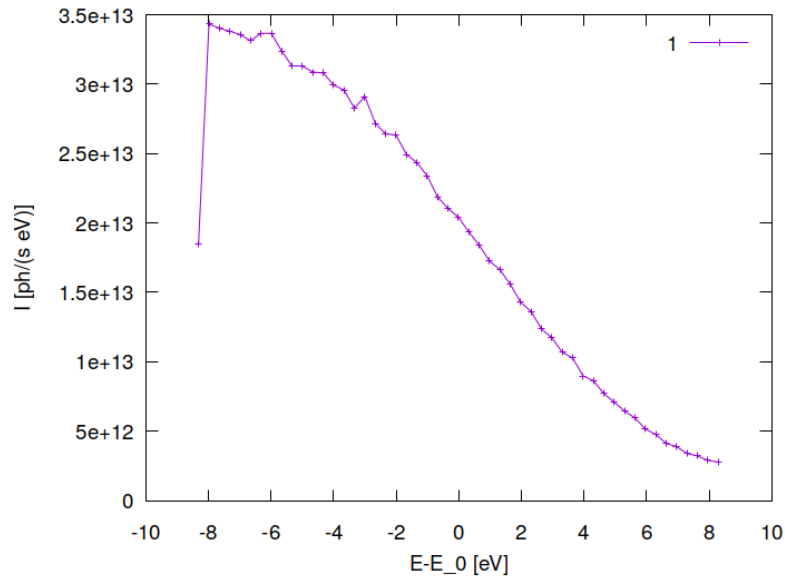


Figure 28.75: Spectral photon flux in beam cross section of optical element #05 (DanMAX) for case #1 for 16955.9 eV photon energy setting.

```
"fig/Main_beam_C111_Laue/plot076.png" Lbl.:Main_beam_C111_Laue_2d_plot_I_bandfoc_oe05_c2_16955.9eV
```

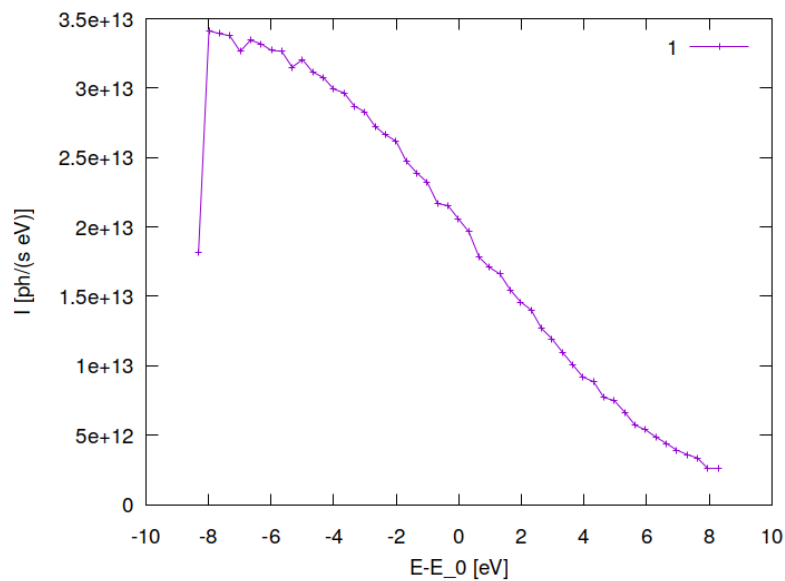


Figure 28.76: Spectral photon flux in beam cross section of optical element #05 (DanMAX) for case #2 for 16955.9 eV photon energy setting.

```
"fig/Main_beam_C111_Laue/plot077.png" Lbl.:Main_beam_C111_Laue_2d_plot_I_bandfoc_oe05_c3_16955.9eV
```

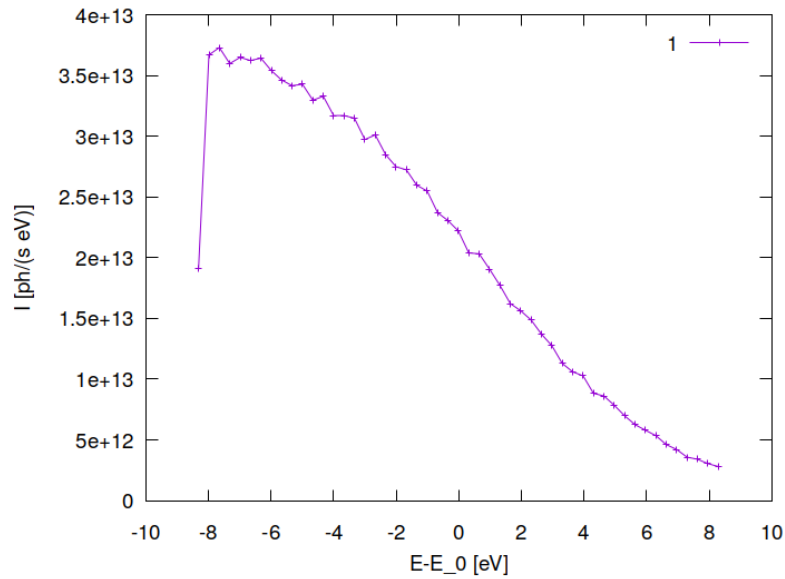


Figure 28.77: Spectral photon flux in beam cross section of optical element #05 (DanMAX) for case #3 for 16955.9 eV photon energy setting.

```
"fig/Main_beam_C111_Laue/plot078.png" Lbl.:Main_beam_C111_Laue_2d_plot_I_bandfoc_oe05_c4_16955.9eV
```

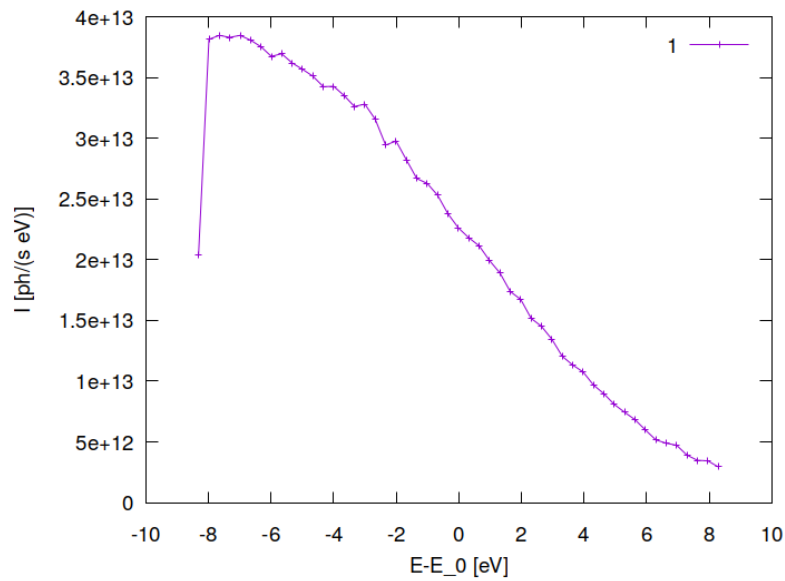


Figure 28.78: Spectral photon flux in beam cross section of optical element #05 (DanMAX) for case #4 for 16955.9 eV photon energy setting.

## Chapter 29

# Sharing the same harmonic in a Laue geometry beam splitter

The planned SinCrys side station of DanMAX uses a spectrally narrow portion of the synchrotron radiation from the shared insertion device via a diffractive diamond111 beam splitter. The 100 micrometre thin diamond sheet has only a marginal effect on the transmitted main beam, destined to be used at the DanMAX main station. Overall absorption at photon energies above 15 keV is small ( $\approx 15\%$ ) and above that can be compensated for by the removal of filtering, for which the same material, diamond – 300 micrometres in total – is used.

Refractive effects are negligible due to carbon's tiny refractive decrement ( $\delta < 10^5$ ) in this wavelength regime, and the fact that there are only two surfaces which are hardly bent and if so, remain mostly parallel. Temperature gradients inside the diamond sheet are small, and with its thickness gradients, thanks to diamond being the material with the highest thermal conductivity. Above that, any thinkable refractive effects would occur with commonly used diamond filters, too.

Nevertheless the beam splitter might affect the transmitted beam via diffraction, if by chance the same undulator harmonic is used at both stations. In the vicinity of the Bragg angle the beam splitter has a reflectivity close to 100%, thus effectively depleting the main beam of photons inside the spectral window it is set up for.

Simulating this effect turned out to be difficult, as ray tracing codes [15] focus on the diffracted beam and therefore omit the option to simulate the transmitted. Therefore a semi-quantitative approach is used here instead. It is going to be based on the DuMond diagram. The DuMond diagram is basically a graphical representation of Bragg's law,

$$\lambda = 2d \sin \theta_B$$

where wavelength  $\lambda$  is plotted as function of the ray's glancing angle  $\theta_B$  to the diffracting planes with inter-planar spacing  $d$ . In kinematic diffraction theory for (semi-)infinite crystals this is simply the line plot of a sine function, with an amplitude of  $2d$  as shown in Fig. 29.1.

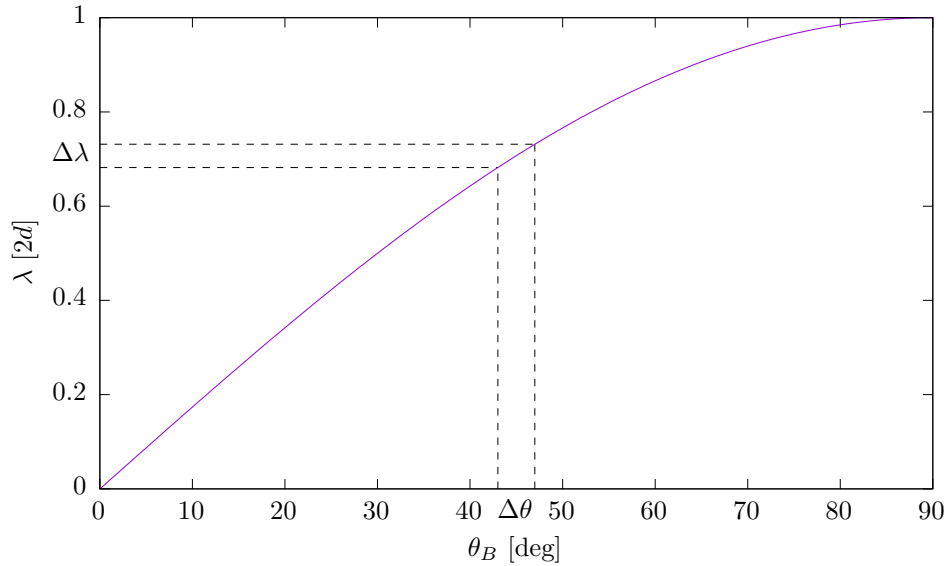


Figure 29.1: .

Small sections of the line plot in Fig. 29.1 are represented by the differential form of Bragg's law

$$\Delta\lambda = \lambda \frac{\Delta\theta_B}{\tan\theta_B}$$

with  $\partial\lambda/\partial\theta = \lambda/\tan\theta_B$  being the local slope.

The DuMond concept is also applicable to the dynamical theory of diffraction where the unequivocal mapping of angle and wavelength by the Bragg equation is replaced by the rocking curve,  $R(\theta - \theta_B, \lambda)$ , defining a range of angles at which Bragg diffraction is strong. The Bragg equation is of course still valid, but now describes a single point close to the centre of the rocking curve. The infinitely thin line of the sine function in Fig. 29.1 must be convoluted with the rocking curve,  $R(\theta - \theta_B, \lambda)$  at the given wavelength  $\lambda = 2d \sin \theta_B$ . This turns the line plot into a 2d density plot as shown in Fig. 29.2.

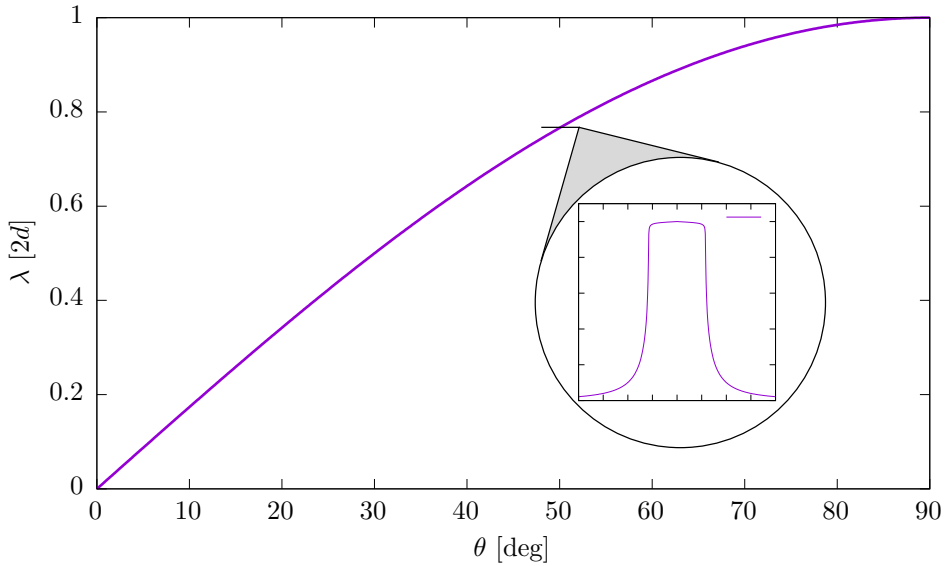


Figure 29.2

On a normal scale this is hardly visible though, as the rocking curve is typically very narrow, and in a plot showing the full angular range from 0 to 90 degrees is narrower than the typical line width in a diagram.

In Fig. 29.3 a small section of the DuMond diagram for Si111 is presented, where the actual shape of the Si111 rocking curve in Bragg geometry was used at a photon energy of 21.8 keV. Thanks to low absorption at this energy the rocking curve nearly has a top-hat profile. Additionally the plotted density is weighted with a 20  $\mu$ rad (RMS) wide Gaussian distribution,  $I_0(\theta)$  representing the angular distribution of synchrotron radiation at the position of DanMAX first monochromator crystal. Hence, the density values in the plot represent now reflected irradiance (in arbitrary units) rather than reflectivity.

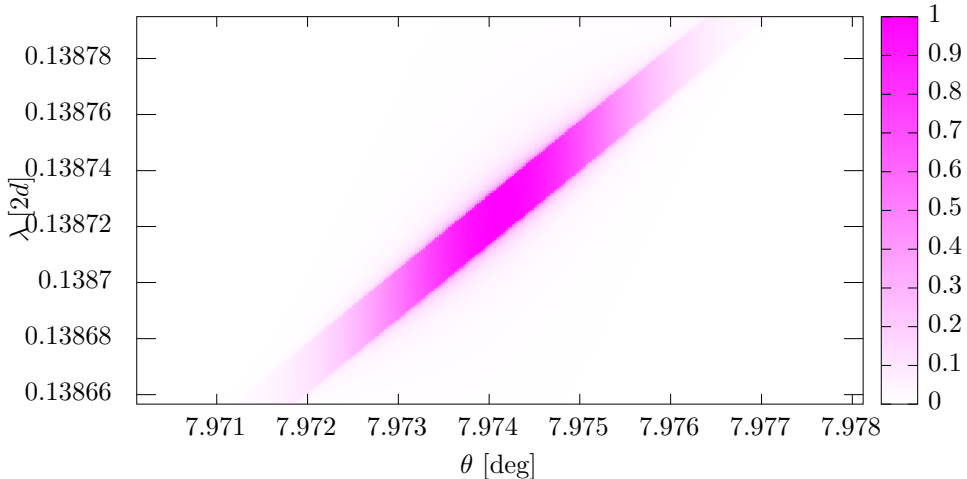


Figure 29.3

Thus, the density function in the plot – which is proportional to the reflected irradiance – is given by

$$I(\theta, \lambda) = I_0(\theta)R(\theta - \theta_B, \lambda) .$$

In Fig. 29.4 the density values are weighted additionally with the angle and wavelength dependent transmissivity  $T(\theta - \theta'_B, \lambda) \stackrel{\text{def}}{=} 1 - R'(\theta - \theta'_B, \lambda)$  through the preceding diamond beam splitter, where  $R'(\theta - \theta'_B, \lambda)$  is the diamond111 rocking curve:

$$I(\theta, \lambda) = I_0(\theta)T(\theta - \theta'_B, \lambda)R(\theta - \theta_B, \lambda) .$$

Thanks to the 'close to one' reflectivity of diamond111 the beam splitters angular-spectral transmission has basically a hole, where nearly all synchrotron radiation of a particular wavelength is reflected away to the SinCrys side branch.

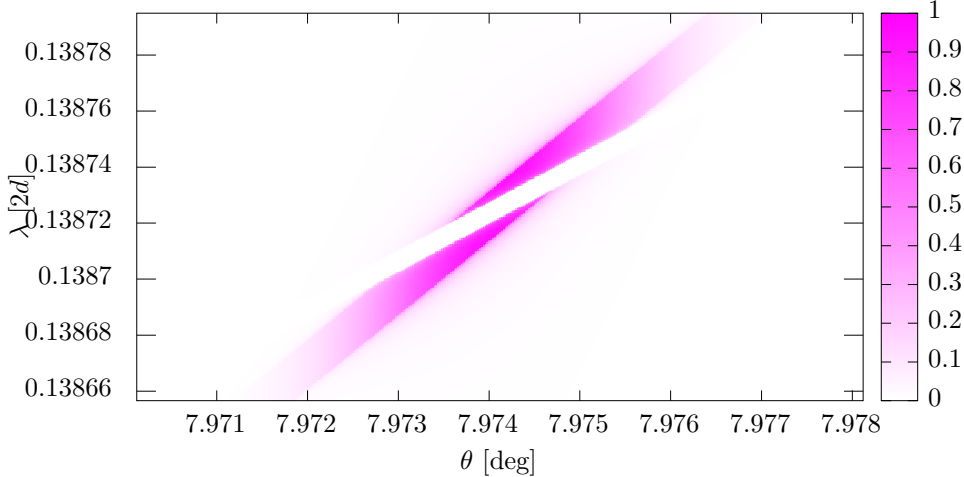


Figure 29.4

If both beamline branches are using the same harmonic, chances are that this hole aligns with the high reflectivity angular-spectral regime of the first crystal in the DanMAX Si111 monochromator. This is analogous to the double crystal DuMond diagram with two intersecting sine curves just with the first crystal curve being inverted.

As a consequence, the spectral distribution of the radiation shown in Fig. 29.5, derived from the DuMond diagram by integration over the angle coordinate, gets a dip so deep that it turns into a double peak shape and the overall throughput is considerably reduced.

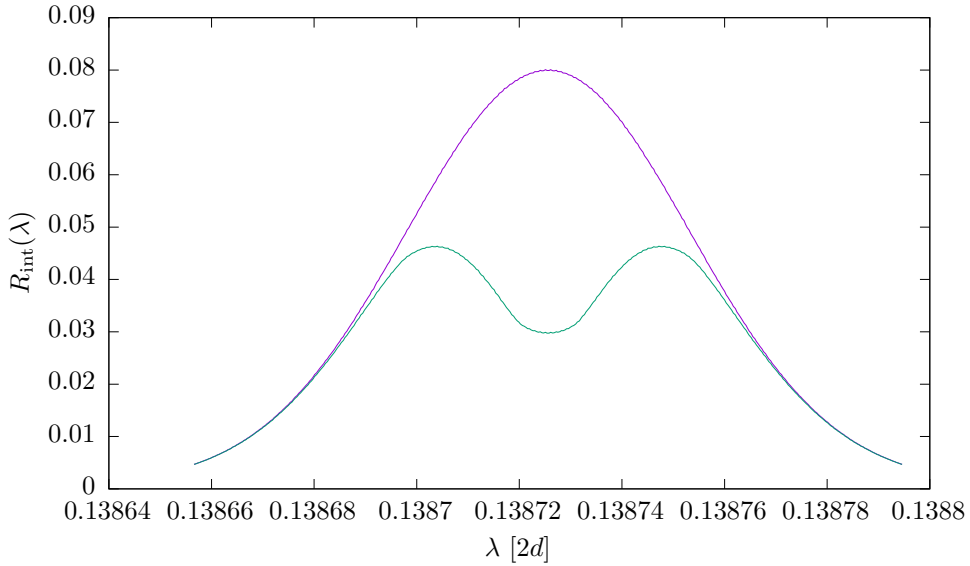


Figure 29.5: Integral of the density ( $\propto$ irradiance) in DuMond diagram over angle coordinate in Fig. 29.4. This represents the *spectral distribution* of the radiation transmitted by the diamond beam splitter and subsequently reflected from the first crystal in the DanMAX monochromator.

The angular distribution Fig. 29.6, derived from the DuMond diagram by integration over the wavelength coordinate, on the other hand keeps its single peak shape, but with the same reduced overall throughput of course.

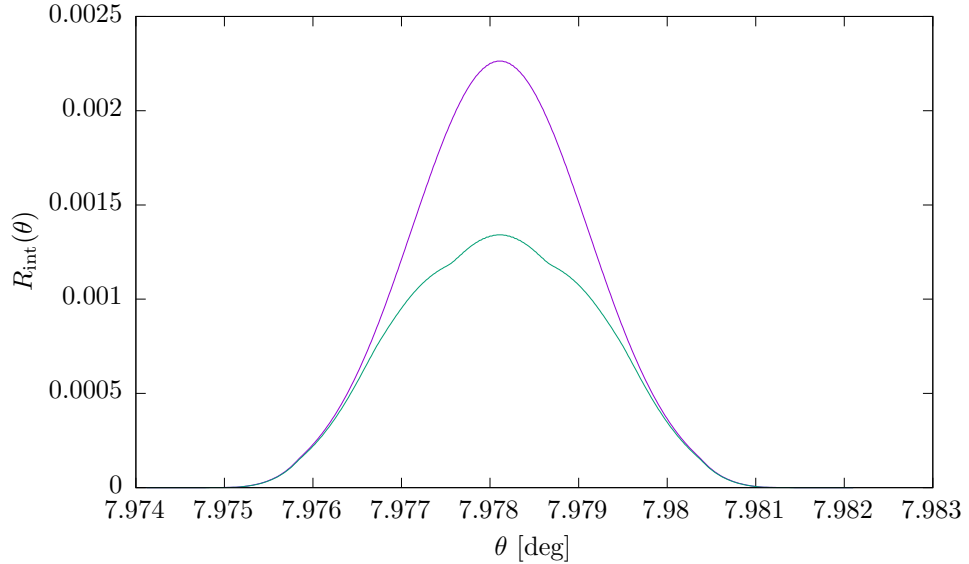


Figure 29.6: Integral of the density ( $\propto$ irradiance) in DuMond diagram over wavelength coordinate in Fig. 29.4. This represents the *angular distribution* of the radiation transmitted by the diamond beam splitter and subsequently reflected from the first crystal in the DanMAX monochromator.

Whether the spectral double peak introduced by the SinCrys beam splitter causes harm to a measurement at DanMAX depends very much on the type of

measurement. This spectral structure lies within the monochromator bandwidth and for many techniques that simply integrate over the bandwidth it probably doesn't matter. The reduction in overall throughput on the other hand is more likely to cause harm. DanMAX probably could live with a somewhat reduced flux provided it is constant over time. Though, any instability in the beam splitter or any adjustments to it that would lead to fluctuations of the total flux would in this configuration spoil any measurement with a probability bordering on certainty.

## Chapter 30

# Setup for the modelling of the transmitted main branch in the case of Bragg geometry

A thin CVD diamond crystal is employed as a diffractive beam splitter, using the 111 reflection in Bragg geometry. The diamond 111 reflection diverts radiation within a narrow bandwidth of

$$\delta E/E = \delta\theta/\tan\theta$$

to the SinCrys side station. A minimum thickness of 100 microns for the diamond crystal slab has been chosen which still provides sufficient mechanical stability. This happens to be the same thickness as in the Laue case. Though, absorption is worse in Bragg geometry due to the grazing incidence.

This setup ends after the beam splitter, as the main task is to investigate the latter's effect on the transmitted main beam. Unfortunately the employed ray-tracing program, Shadow3 [15], cannot model transmission through a thin crystal where the beam is fulfilling or nearly fulfilling the Bragg condition. Far from the Bragg condition though, the crystal acts like a normal absorber, like e.g. a thin sheet of metal. To include also refraction from front and rear surface, the model of a lens element was chosen as a substitute. To model the oblique incidence of the beam onto the beam splitter, the same trick was used as in Laue geometry (see section 24).

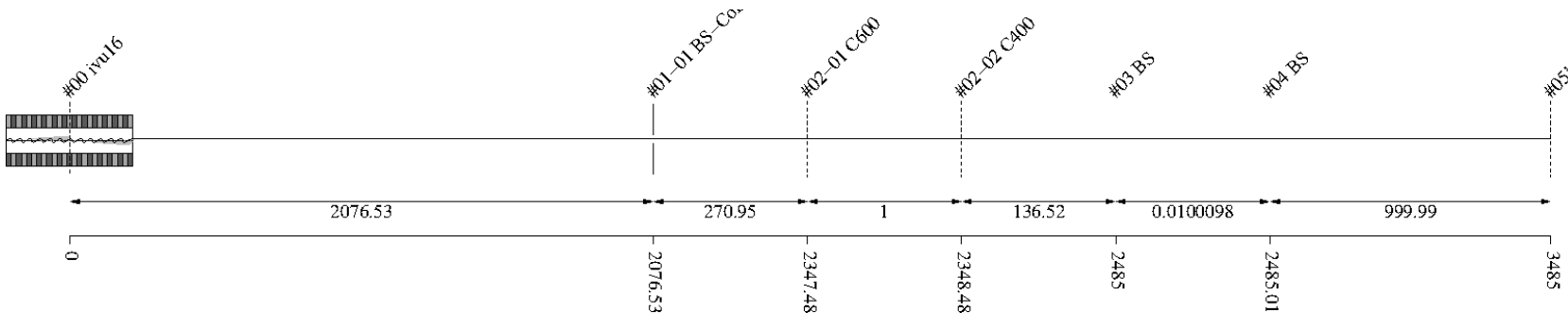


Figure 30.1: Schematic of optical setup

#	Name	Pathlen. cm	Descript.	Shape	Pitch* deg	Roll deg	Yaw deg	x_min cm	x_max cm	y_min cm	y_max cm	Thick. cm	Surface
<b>0</b>	ivu16	0	undulator	auto	0	0	0	-0.0027	0.0027	-0.0002	0.0002	auto	
<b>1</b>		2076.53	none	plane	0	0	0	-inf	inf	-inf	inf		perfect
<b>1-1</b>	BS-Collim	2076.53	aperture	rectangle	0	0	0	-0.035	0.035	-0.035	0.035		
<b>2</b>	Filter	2347.48	none	plane	0	0	0	-inf	inf	-inf	inf		perfect
<b>2-1</b>	C600	2347.48	C-filter	rectangle	0	0	0	-inf	inf	-inf	inf	0.06	
<b>2-2</b>	C400	2348.48	C-filter	rectangle	0	0	0	-inf	inf	-inf	inf	0.04	
<b>3</b>	BS	2485	vac/C-lens surface	plane	0+0	90+0	0+0	-0.15	0.15	-0.5	0.5		predefined
<b>4</b>	BS	2485.01	C/vac-lens surface	plane	0	0	0	-0.15	0.15	-0.5	0.5		heat bump
<b>5</b>	DanMAX	2485.01	none	plane	0+0	0+0	0+0	-inf	inf	-inf	inf		perfect
<b>5'</b>		3485	continuation plane		0	0	0						

Table 30.1: Setup parameters common to all components. (\*Glancing angle for mirrors, multilayers and crystals. Angle to surface normal otherwise.)

**Rays:** Polar type = total

Polar phase = 0 deg

Polar degree = 0

Is coherent = no

**Spectrum:** E min = 500 eV

E max = 40000 eV

Relative linewidth = 1

**Band:** Bandwidth = 0.0005

**Insertion Device:** lambda period = 1.6 cm

n period = 187

I electron = 0.5 A

E electron = 3 GeV

y horizontal waist = 0 cm

y vertical waist = 0 cm

epsilon x = 3.2E-08 cm rad

epsilon z = 8E-10 cm rad

K y = 1.66

K ymax = 1.7

Divergence limit = 5E-05 rad

**Undulator:** n harmonic max = 99

Tuning type = fixed gap

l aperture = 2076.53 cm

dx aperture = 0.07 cm

dz aperture = 0.07 cm

#1

**Screen:** Is absorbing[1] = no

**Shape:** Thickness = 0 cm

#2 Filter

**Screen:** Is absorbing[1] = yes

Is absorbing[2] = yes

Molecular formula[1] = C

Molecular formula[2] = C

Mass density[1] = 3.5 g/cm^3

Mass density[2] = 3.5 g/cm^3

Thickness[1] = 0.06 cm

Thickness[2] = 0.04 cm

**Shape:** Thickness = 0 cm

### #3 BS

**Dielectric:** Reflectivity type = polarisation

Is constant = no

Mass density = 3.5 g/cm<sup>3</sup>

**Geometry:** g = 0 cm

b = 0 cm

Is thin = yes

n clones = 1

Focus automatically = no

**Shape:** Thickness = 0.01 cm

**Boundary:** Type = rectangle

**Surface:** Is rough = no

### #4 BS

**Dielectric:** Reflectivity type = polarisation

Is constant = yes

delta refraction = 0

beta absorption = 0

**Geometry:** g = 0 cm

b = 0 cm

Is thin = yes

n clones = 1

Focus automatically = no

**Shape:** Thickness = 0.01 cm

**Boundary:** Type = rectangle

x rim = 0.5 cm

y rim = 0.5 cm

**Surface:** Is rough = no

**FEA:** Design type = type specific

Surface design = sheet with cooling loop

Is isotropic = no

Angle x = 0 deg

Angle y = 0 deg

Angle z = 0 deg

Mass density = 3.516 g/cm<sup>3</sup>

**Heat:** Heat transfer type[1] = insulated  
 Heat transfer type[2] = heat transfer  
 Heat transfer type[3] = insulated  
 Heat transfer type[4] = insulated  
 Heat transfer type[5] = heat transfer  
 Heat transfer type[6] = flux  
 Heat transfer type[7] = insulated  
 Heat transfer type[8] = heat transfer  
 Heat transfer type[9] = heat sink  
 Heat transfer coefficient = 1 W/(cm^2K)  
 Heat sink coefficient = 10 W/(cm^2K)  
 T reference = 293.15 K  
 T cooling = 293.15 K  
 Heat capacity = 0.54 J/(gK)  
 Thermal conductivity[1] = 25 W/(cmK^n)

**Stress and strain:** Constraint[1] = free  
 Constraint[2] = kinematic  
 Constraint[3] = free  
 Constraint[4] = free  
 Constraint[5] = free  
 Constraint[6] = free  
 Constraint[7] = free  
 Constraint[8] = free  
 Constraint[9] = free  
 Thermal expansion tensor[1] = 1.1E-06 1/K  
 Thermal expansion tensor[2] = 1.1E-06 1/K  
 Thermal expansion tensor[3] = 1.1E-06 1/K  
 Thermal expansion tensor[4] = 0 1/K  
 Thermal expansion tensor[5] = 0 1/K  
 Thermal expansion tensor[6] = 0 1/K  
 Stiffness tensor(1)(1) = 1.07861E+12 Pa  
 Stiffness tensor(2)[1] = 1.2663E+11 Pa  
 Stiffness tensor(2)[2] = 1.07861E+12 Pa  
 Stiffness tensor(3)[1] = 1.2663E+11 Pa  
 Stiffness tensor(3)[2] = 1.2663E+11 Pa  
 Stiffness tensor(3)[3] = 1.07861E+12 Pa  
 Stiffness tensor(4)[1] = 0 Pa  
 Stiffness tensor(4)[2] = 0 Pa  
 Stiffness tensor(4)[3] = 0 Pa  
 Stiffness tensor(4)[4] = 5.7756E+11 Pa  
 Stiffness tensor(5)[1] = 0 Pa  
 Stiffness tensor(5)[2] = 0 Pa  
 Stiffness tensor(5)[3] = 0 Pa  
 Stiffness tensor(5)[4] = 0 Pa  
 Stiffness tensor(5)[5] = 5.7756E+11 Pa  
 Stiffness tensor(6)[1] = 0 Pa  
 Stiffness tensor(6)[2] = 0 Pa  
 Stiffness tensor(6)[3] = 0 Pa  
 Stiffness tensor(6)[4] = 0 Pa  
 Stiffness tensor(6)[5] = 0 Pa  
 Stiffness tensor(6)[6] = 5.7756E+11 Pa

**#5 DanMAX**

**Shape:** Thickness = 0 cm

# Chapter 31

## Finite element analysis (FEA)

Heat load, temperature gradients and subsequent deformation under thermal stress should be the same as for the equivalent crystal model described earlier 19. To show, that this is the case, is the purpose of this chapter.

### 31.1 FEA with both 600 and 400 micron diamond filters in

```
"fig/Main_beam_C111_Bragg/fea_plot_geom_c02_16955eV_04.png" Lbl.:Main_beam_C111_Bragg_Surface_plot_fea_plot_geom_c02_16955eV_04
```

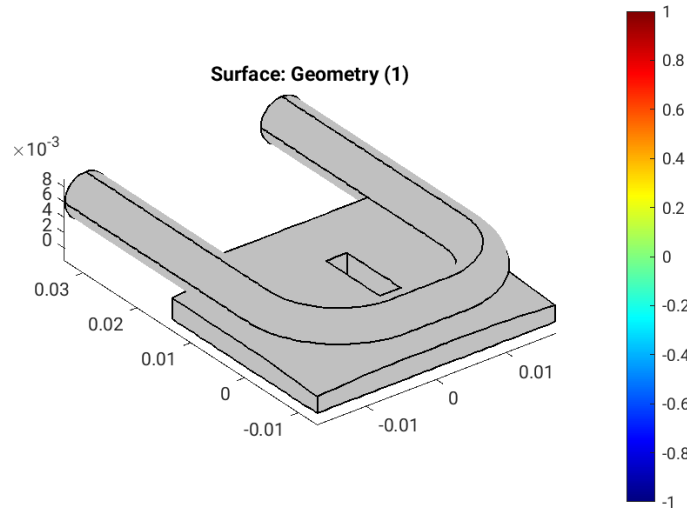


Figure 31.1: Geometry [m] of optical element #04, for case #02, at 16955 eV photon energy setting.

```
"fig/Main_beam_C111_Bragg/fea_plot_cnstr_c02_16955eV_04.png" Lbl.:Main_beam_C111_Bragg_Surface_plot_fea_plot_cnstr_c02_16955eV_04
```

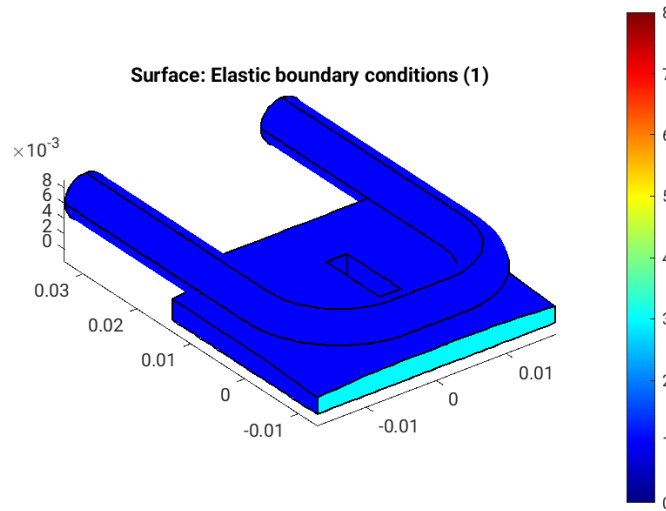


Figure 31.2: Elastic boundary conditions on the surfaces of optical element #04, for case #02, at 16955 eV photon energy setting. Color legend: Blue: Surface can move freely in all directions. Cyan: Tension free kinematic mounting. Minimalistic constraint for three points in surface. One point is fixed, the second can move in one direction, and the third in two, in a fashion that defines angular orientation without introducing stress if the surface expands.

```
"fig/Main_beam_C111_Bragg/fea_plot_trans_c02_16955eV_04.png" Lbl.:Main_beam_C111_Bragg_Surface_plot_fea_plot_trans_c02_16955eV_04
```

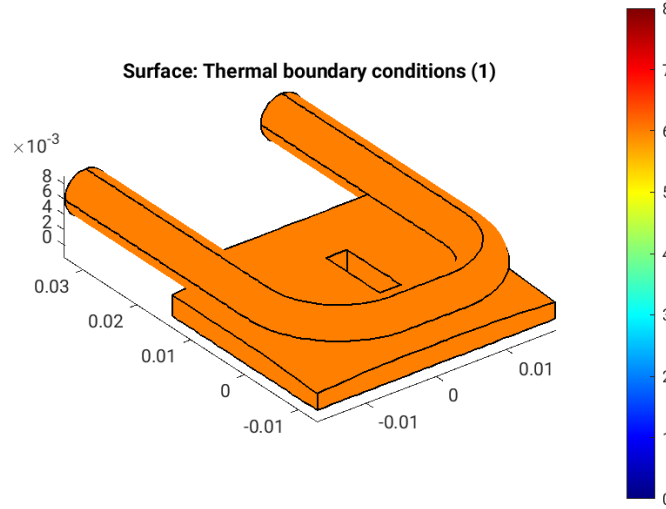


Figure 31.3: Thermal boundary conditions on the surfaces of optical element #04, for case #02, at 16955 eV photon energy setting. Color legend: Orange: No heat transfer at all. Blue: Heat transfer coefficient and temperature difference define heat current density,  $j_q = h(T - T_{cool})$ . Red: Forced heat flux from e.g. absorbed X-rays. Cyan: Heat transfer coefficient and temperature difference define heat current density,  $j_q = h^* \Delta T$  (only at inner surfaces).

```
"fig/Main_beam_C111_Bragg/fea_plot_heattrans_c02_16955eV_04.png" Lbl.:Main_beam_C111_Bragg_Surface_plot_fea_plot_heattrans_c02_16955eV_04
```

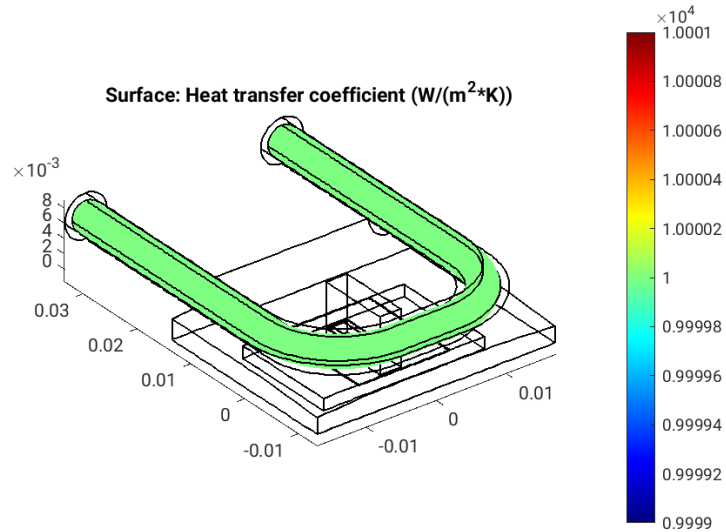


Figure 31.4: Heat transfer coefficient,  $h$  [ $W/(m^2 \cdot K)$ ], on the surfaces of optical element #04, for case #02, at 16955 eV photon energy setting.

```
"fig/Main_beam_C111_Braggfea_plot_heatflux_c02_16955eV_04.png" Lbl.:Main_beam_C111_Bragg_Surface_plot_fea_plot_heatflux_c02_16955eV_04
```

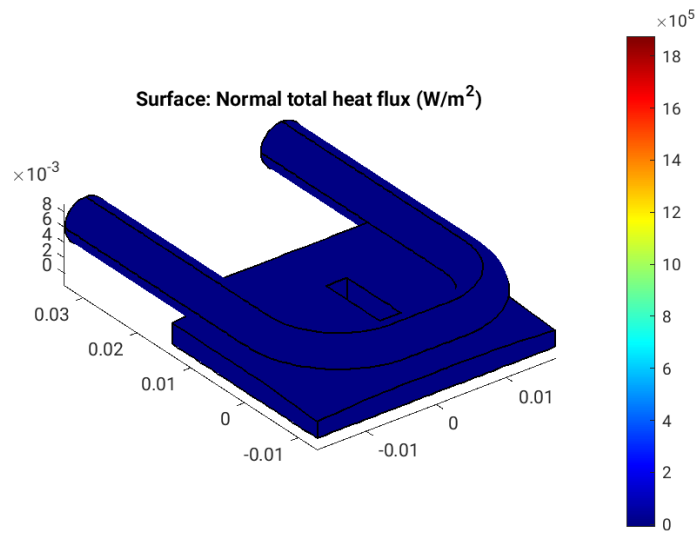


Figure 31.5: Absorbed irradiance,  $p_{\text{abs}}$  [W/m<sup>2</sup>], on the surfaces of optical element #04, for case #02, at 16955 eV photon energy setting.

```
"fig/Main_beam_C111_Braggfea_plot_temp_c02_16955eV_04.png" Lbl.:Main_beam_C111_Bragg_Surface_plot_fea_plot_temp_c02_16955eV_04
```

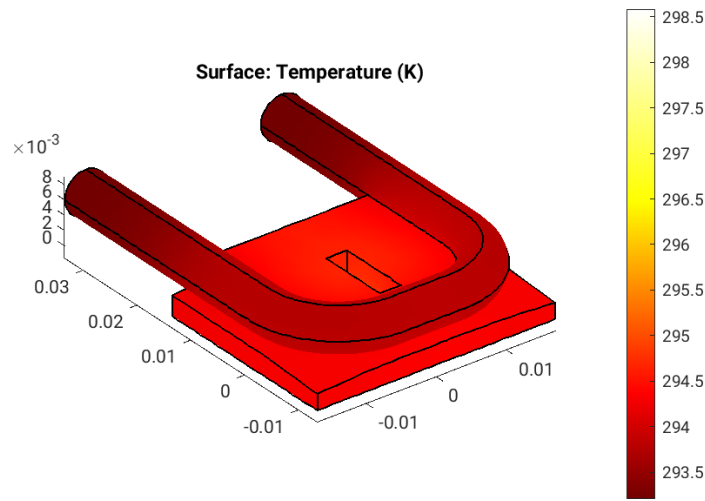


Figure 31.6: Temperature,  $T$  [K], on the surfaces of optical element #04, for case #02, at 16955 eV photon energy setting.

"fig/Main\_beam\_C111\_Braggfea\_plot\_thermcond\_c02\_16955eV\_04.png" Lbl.:Main\_beam\_C111\_Bragg\_Surface\_plot\_fea\_plot\_thermcond\_c02\_16955eV\_

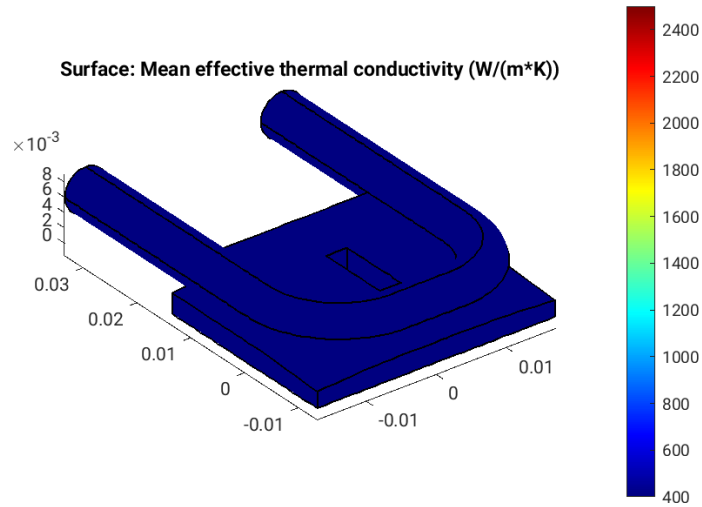


Figure 31.7: Thermal conductivity, lambda [W/(m K)], on the surfaces of optical element #04, for case #02, at 16955 eV photon energy setting.

"fig/Main\_beam\_C111\_Braggfea\_plot\_stress\_c02\_16955eV\_04.png" Lbl.:Main\_beam\_C111\_Bragg\_Surface\_plot\_fea\_plot\_stress\_c02\_16955eV\_04

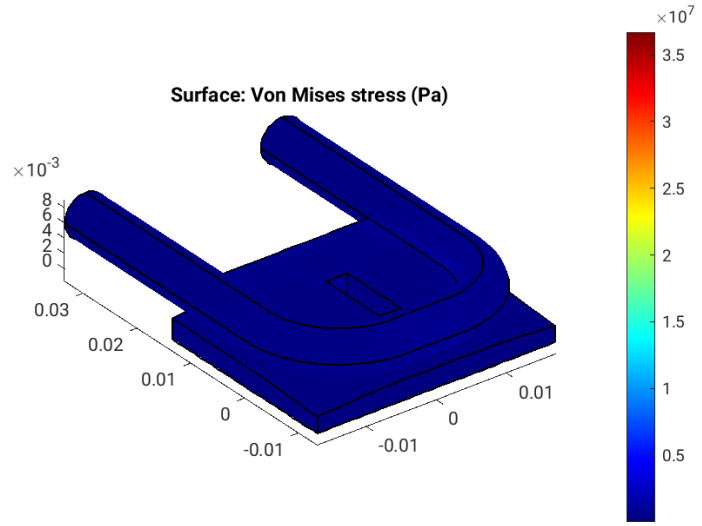


Figure 31.8: Von Mises stress, sigma [Pa], on the surfaces of optical element #04, for case #02, at 16955 eV photon energy setting.

```
"fig/Main_beam_C111_Bragg/fea_plot_deform_c02_16955eV_04.png" Lbl.:Main_beam_C111_Bragg_Surface_plot_fea_plot_deform_c02_16955eV_04
```

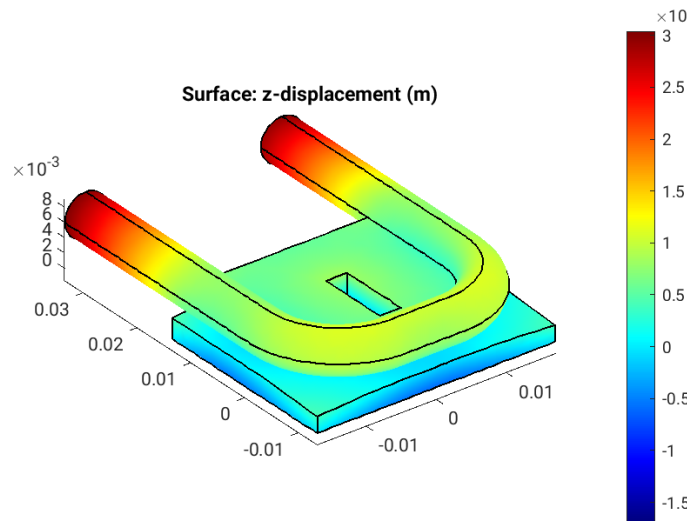


Figure 31.9: Thermoelastic deformation,  $dz$  [m], on the surfaces of optical element #04, for case #02, at 16955 eV photon energy setting.

## 31.2 FEA with only 400 micron diamond filter in

```
"fig/Main_beam_C111_Bragg/fea_plot_geom_c03_16955eV_04.png" Lbl.:Main_beam_C111_Bragg_Surface_plot_fea_plot_geom_c03_16955eV_04
```

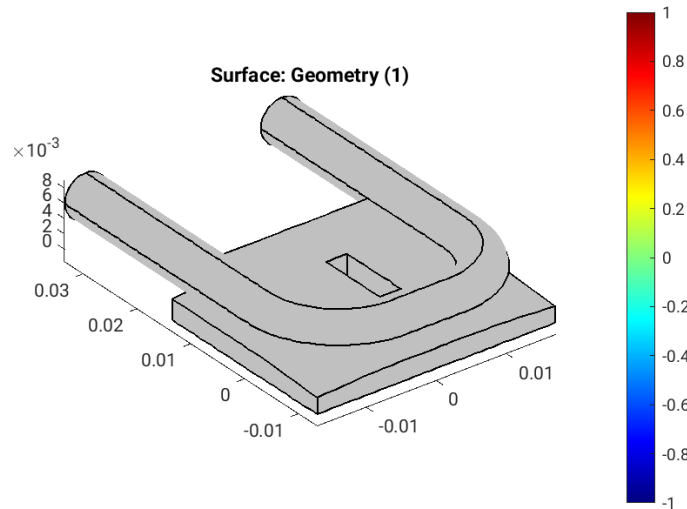


Figure 31.10: Geometry [m] of optical element #04, for case #03, at 16955 eV photon energy setting.

```
"fig/Main_beam_C111_Bragg/fea_plot_cnstr_c03_16955eV_04.png" Lbl.:Main_beam_C111_Bragg_Surface_plot_fea_plot_cnstr_c03_16955eV_04
```

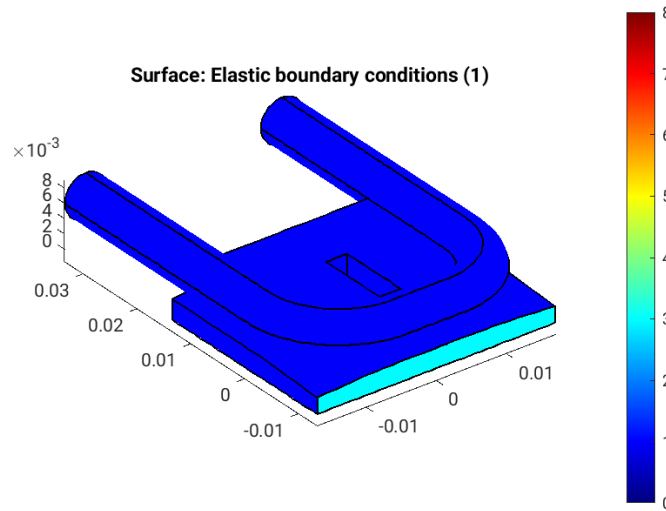


Figure 31.11: Elastic boundary conditions on the surfaces of optical element #04, for case #03, at 16955 eV photon energy setting. Color legend: Blue: Surface can move freely in all directions. Cyan: Tension free kinematic mounting. Minimalistic constraint for three points in surface. One point is fixed, the second can move in one direction, and the third in two, in a fashion that defines angular orientation without introducing stress if the surface expands.

```
"fig/Main_beam_C111_Bragg/fea_plot_trans_c03_16955eV_04.png" Lbl.:Main_beam_C111_Bragg_Surface_plot_fea_plot_trans_c03_16955eV_04
```

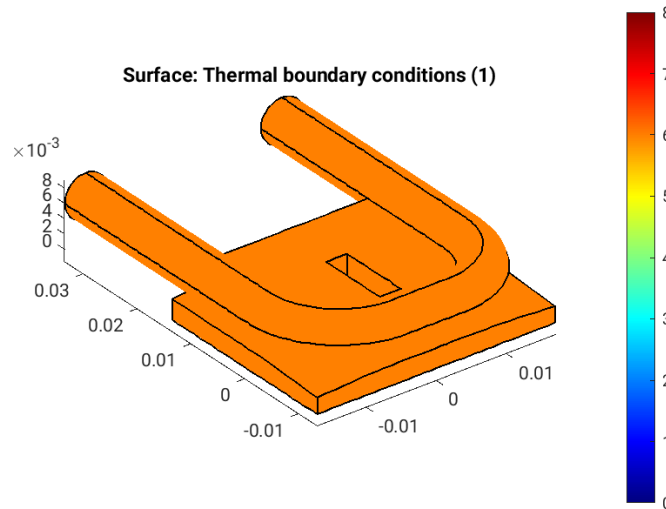


Figure 31.12: Thermal boundary conditions on the surfaces of optical element #04, for case #03, at 16955 eV photon energy setting. Color legend: Orange: No heat transfer at all. Blue: Heat transfer coefficient and temperature difference define heat current density,  $j_q = h(T - T_{cool})$ . Red: Forced heat flux from e.g. absorbed X-rays. Cyan: Heat transfer coefficient and temperature difference define heat current density,  $j_q = h^* \Delta T$  (only at inner surfaces).

```
"fig/Main_beam_C111_Bragg/fea_plot_heattrans_c03_16955eV_04.png" Lbl.:Main_beam_C111_Bragg_Surface_plot_fea_plot_heattrans_c03_16955eV_04
```

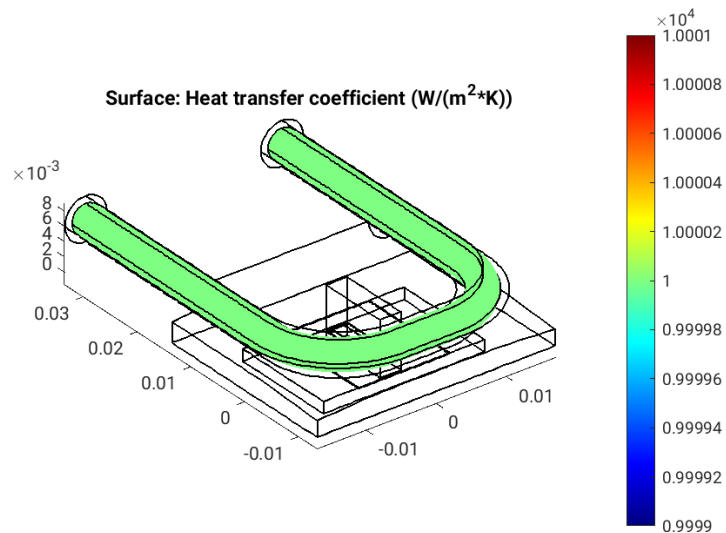


Figure 31.13: Heat transfer coefficient,  $h$  [ $W/(m^2 \cdot K)$ ], on the surfaces of optical element #04, for case #03, at 16955 eV photon energy setting.

```
"fig/Main_beam_C111_Bragg/fea_plot_heatflux_c03_16955eV_04.png" Lbl.:Main_beam_C111_Bragg_Surface_plot_fea_plot_heatflux_c03_16955eV_04
```

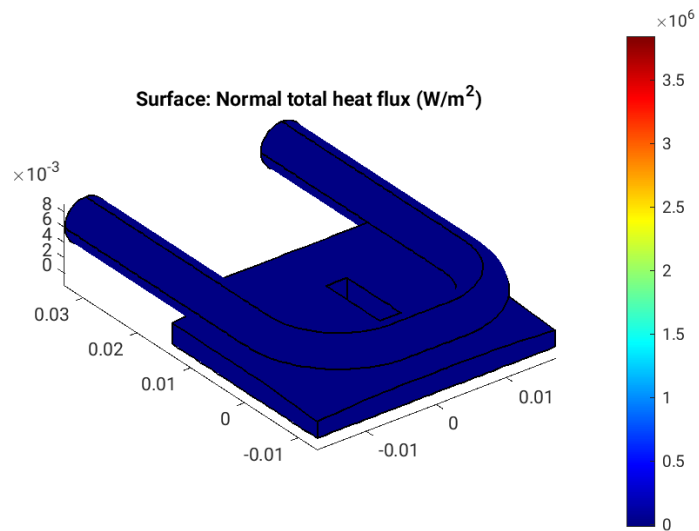


Figure 31.14: Absorbed irradiance,  $p_{\text{abs}}$  [W/m<sup>2</sup>], on the surfaces of optical element #04, for case #03, at 16955 eV photon energy setting.

```
"fig/Main_beam_C111_Bragg/fea_plot_temp_c03_16955eV_04.png" Lbl.:Main_beam_C111_Bragg_Surface_plot_fea_plot_temp_c03_16955eV_04
```

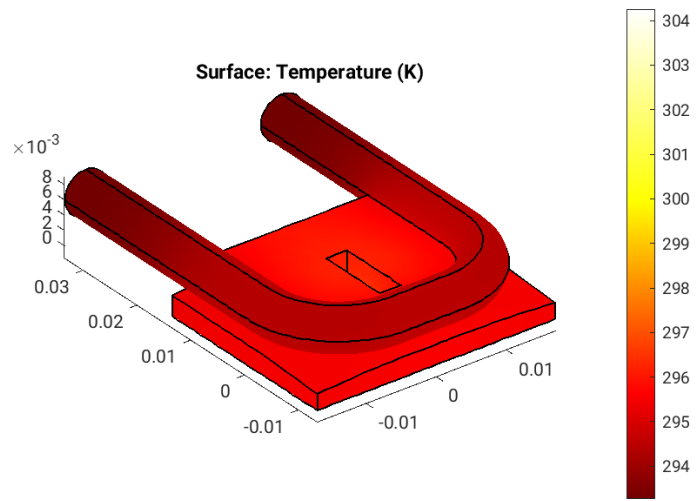


Figure 31.15: Temperature, T [K], on the surfaces of optical element #04, for case #03, at 16955 eV photon energy setting.

"fig/Main\_beam\_C111\_Braggfea\_plot\_thermcond\_c03\_16955eV\_04.png" Lbl.:Main\_beam\_C111\_Bragg\_Surface\_plot\_fea\_plot\_thermcond\_c03\_16955eV\_

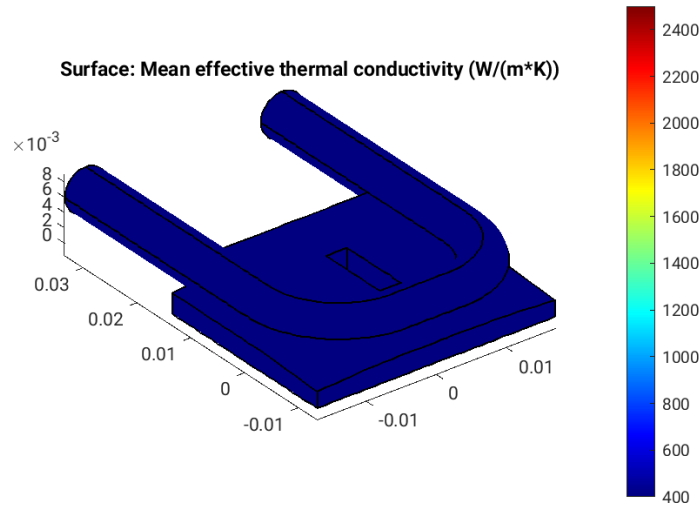


Figure 31.16: Thermal conductivity, lambda [W/(m K)], on the surfaces of optical element #04, for case #03, at 16955 eV photon energy setting.

"fig/Main\_beam\_C111\_Braggfea\_plot\_stress\_c03\_16955eV\_04.png" Lbl.:Main\_beam\_C111\_Bragg\_Surface\_plot\_fea\_plot\_stress\_c03\_16955eV\_04

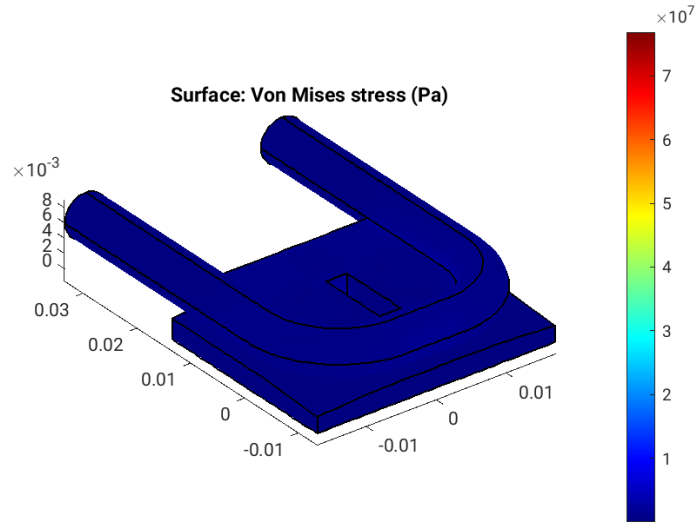


Figure 31.17: Von Mises stress, sigma [Pa], on the surfaces of optical element #04, for case #03, at 16955 eV photon energy setting.

```
"fig/Main_beam_C111_Bragg/fea_plot_deform_c03_16955eV_04.png" Lbl.:Main_beam_C111_Bragg_Surface_plot_fea_plot_deform_c03_16955eV_04
```

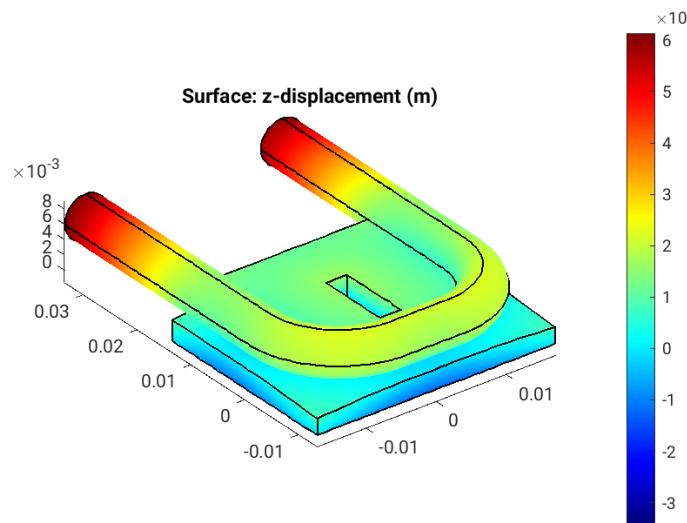


Figure 31.18: Thermoelastic deformation,  $dz$  [m], on the surfaces of optical element #04, for case #03, at 16955 eV photon energy setting.

### 31.3 FEA with no diamond filters in

```
"fig/Main_beam_C111_Bragg/fea_plot_geom_c04_16955eV_04.png" Lbl.:Main_beam_C111_Bragg_Surface_plot_fea_plot_geom_c04_16955eV_04
```

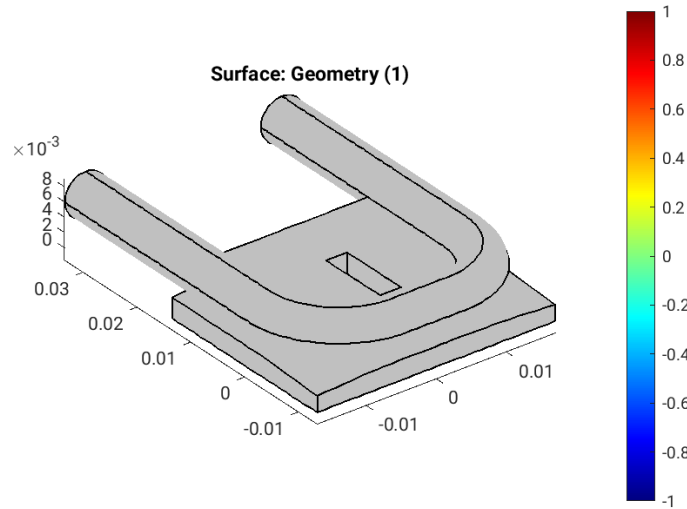


Figure 31.19: Geometry [m] of optical element #04, for case #04, at 16955 eV photon energy setting.

```
"fig/Main_beam_C111_Bragg/fea_plot_cnstr_c04_16955eV_04.png" Lbl.:Main_beam_C111_Bragg_Surface_plot_fea_plot_cnstr_c04_16955eV_04
```

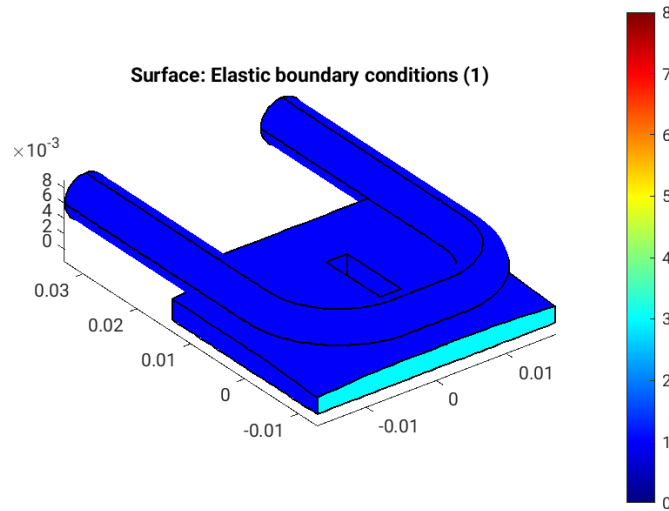


Figure 31.20: Elastic boundary conditions on the surfaces of optical element #04, for case #04, at 16955 eV photon energy setting. Color legend: Blue: Surface can move freely in all directions. Cyan: Tension free kinematic mounting. Minimalistic constraint for three points in surface. One point is fixed, the second can move in one direction, and the third in two, in a fashion that defines angular orientation without introducing stress if the surface expands.

```
"fig/Main_beam_C111_Bragg/fea_plot_trans_c04_16955eV_04.png" Lbl.:Main_beam_C111_Bragg_Surface_plot_fea_plot_trans_c04_16955eV_04
```

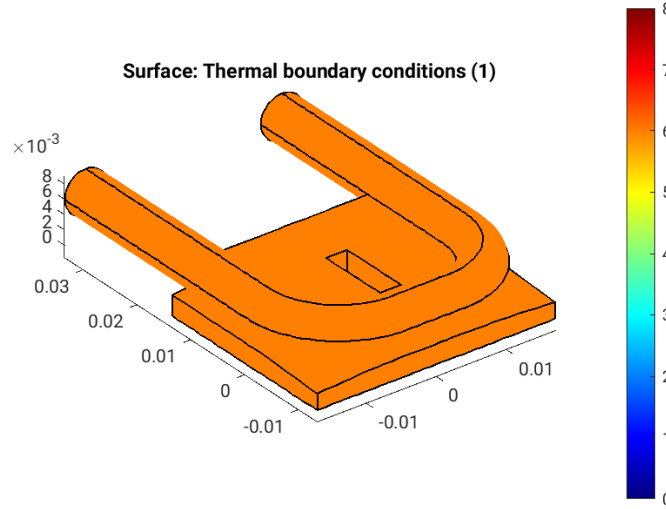


Figure 31.21: Thermal boundary conditions on the surfaces of optical element #04, for case #04, at 16955 eV photon energy setting. Color legend: Orange: No heat transfer at all. Blue: Heat transfer coefficient and temperature difference define heat current density,  $j_q = h(T - T_{cool})$ . Red: Forced heat flux from e.g. absorbed X-rays. Cyan: Heat transfer coefficient and temperature difference define heat current density,  $j_q = h^* \Delta T$  (only at inner surfaces).

```
"fig/Main_beam_C111_Bragg/fea_plot_heattrans_c04_16955eV_04.png" Lbl.:Main_beam_C111_Bragg_Surface_plot_fea_plot_heattrans_c04_16955eV_04
```

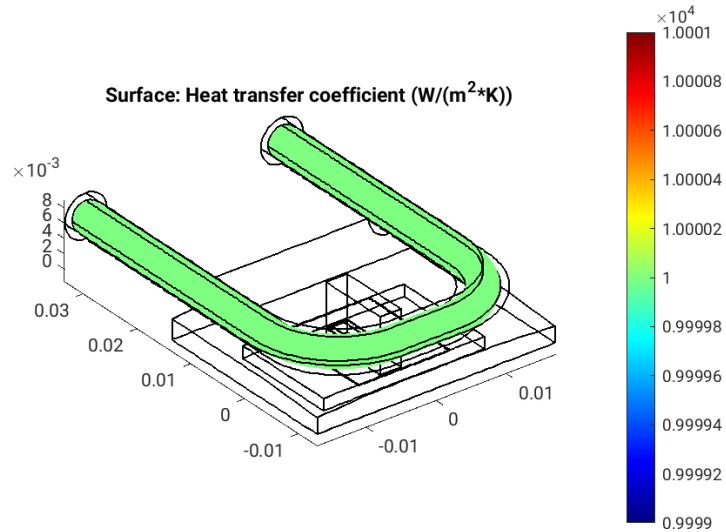


Figure 31.22: Heat transfer coefficient,  $h [W/(m^2 \cdot K)]$ , on the surfaces of optical element #04, for case #04, at 16955 eV photon energy setting.

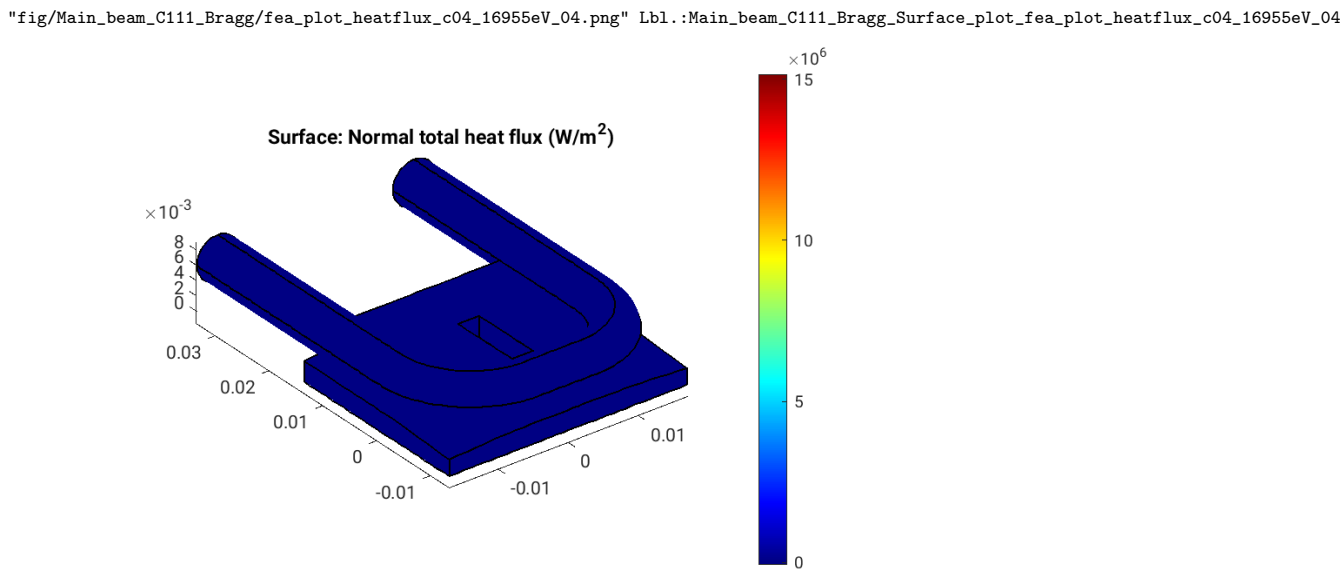


Figure 31.23: Absorbed irradiance,  $p_{\text{abs}}$  [ $\text{W}/\text{m}^2$ ], on the surfaces of optical element #04, for case #04, at 16955 eV photon energy setting.

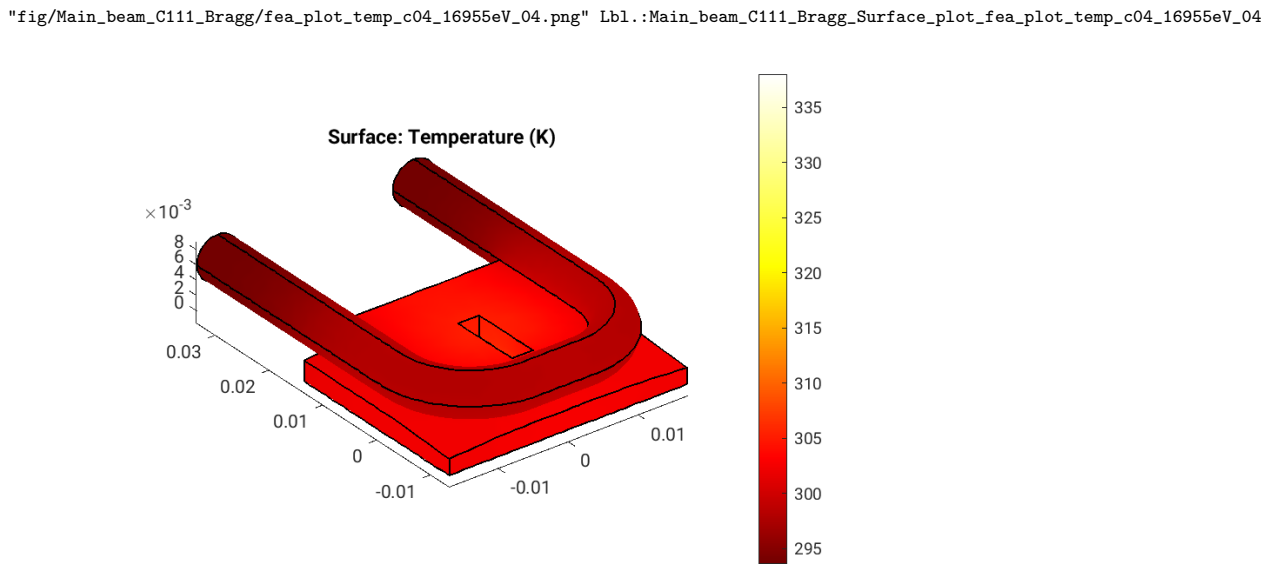


Figure 31.24: Temperature,  $T$  [K], on the surfaces of optical element #04, for case #04, at 16955 eV photon energy setting.

"fig/Main\_beam\_C111\_Braggfea\_plot\_thermcond\_c04\_16955eV\_04.png" Lbl.:Main\_beam\_C111\_Bragg\_Surface\_plot\_fea\_plot\_thermcond\_c04\_16955eV\_

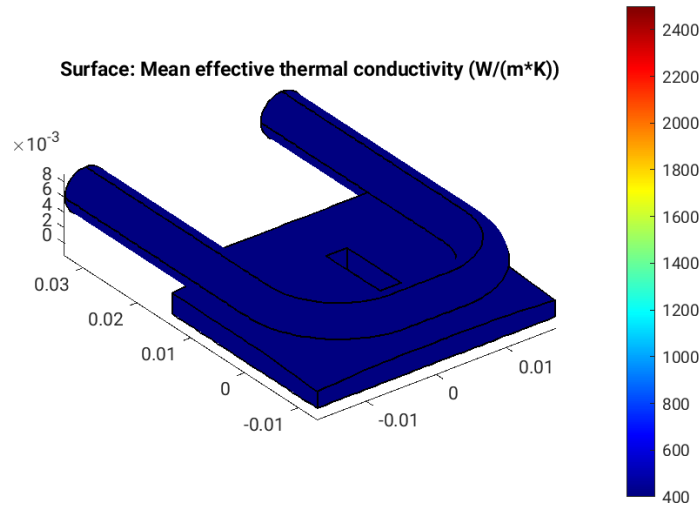


Figure 31.25: Thermal conductivity, lambda [W/(m K)], on the surfaces of optical element #04, for case #04, at 16955 eV photon energy setting.

"fig/Main\_beam\_C111\_Braggfea\_plot\_stress\_c04\_16955eV\_04.png" Lbl.:Main\_beam\_C111\_Bragg\_Surface\_plot\_fea\_plot\_stress\_c04\_16955eV\_04

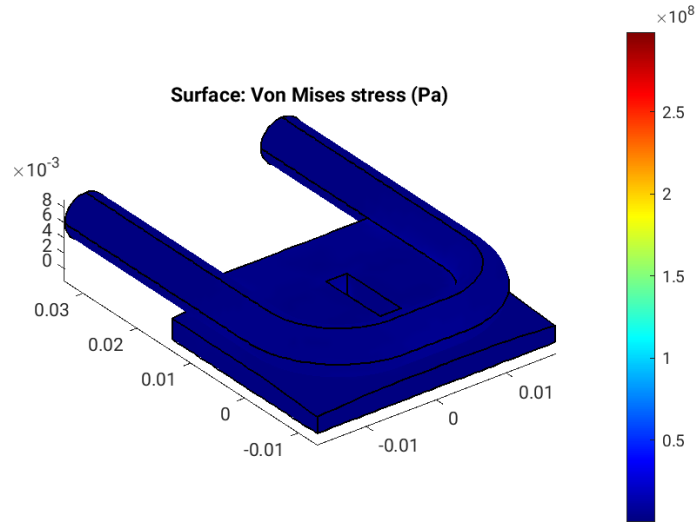


Figure 31.26: Von Mises stress, sigma [Pa], on the surfaces of optical element #04, for case #04, at 16955 eV photon energy setting.

```
"fig/Main_beam_C111_Bragg/fea_plot_deform_c04_16955eV_04.png" Lbl.:Main_beam_C111_Bragg_Surface_plot_fea_plot_deform_c04_16955eV_04
```

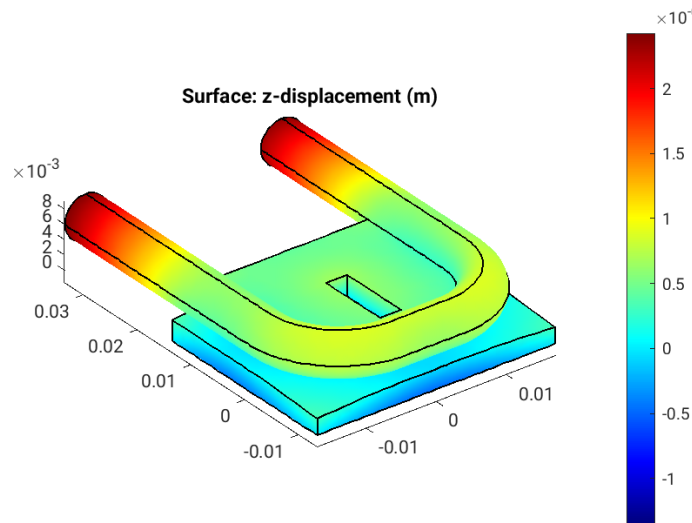


Figure 31.27: Thermoelastic deformation,  $dz$  [m], on the surfaces of optical element #04, for case #04, at 16955 eV photon energy setting.

# Chapter 32

## Parameter scan cases

There are four cases in total. Case #1 is the perfect crystal case with no heat load and consequently no deformation. This case serves as a reference, to discriminate against other beam deteriorating effects, such as source broadening or aberrations. Case #2 is with heat load and with both diamond filters – 600 and 400 micrometer in thickness – in the upstream beam path. Case #3 is with only the 400 micron thick filter in, and case #4 is without any filters.

Case	Thickness(1)_02 cm	Thickness(2)_02 cm	Has_slope_error_03	Skip_heatload
1	0.06	0.04	no	yes
2	0.06	0.04	yes	no
3	0.00001	0.04	yes	no
4	0.00001	0.00001	yes	no

Table 32.1: Parameter values for different cases in parameter scan

### Legend

**Case:** Case number in parameter scan

**Thickness(1)\_02:** Optical\_element\_#2.Type.Screen.Thickness(1) (Optical thickness of resp. screen with absorption.)

**Thickness(2)\_02:** Optical\_element\_#2.Type.Screen.Thickness(2) (Optical thickness of resp. screen with absorption.)

**Has\_slope\_error\_03:** Optical\_element\_#3.Surface.Has\_slope\_error (Has surface slope error?)

**Skip\_heatload:** Session.Skip\_heatload (Skip heat load calculation for all optical elements? (heat load parameters are kept))

## Chapter 33

# Photon energy scan

The  $K_y$ -values in the table below are those for optimised output between 15.6 and 18.3 keV used by DanMAX' main branch.

E eV	K_y	n_harm/step	dtheta_03 deg	dtheta_05 deg
<b>15556</b>	1.67551	7	81.3428	-81.3428
<b>15633.8</b>	1.66836	7	81.3862	-81.3862
<b>15711.5</b>	1.66125	7	81.4291	-81.4291
<b>15789.3</b>	1.65418	7	81.4717	-81.4717
<b>15867.1</b>	1.64714	7	81.5138	-81.5138
<b>15944.8</b>	1.64015	7	81.5555	-81.5555
<b>16022.6</b>	1.63319	7	81.5968	-81.5968
<b>16100.4</b>	1.62628	7	81.6377	-81.6377
<b>16178.2</b>	1.6194	7	81.6782	-81.6782
<b>16255.9</b>	1.61255	7	81.7182	-81.7182
<b>16333.7</b>	1.60575	7	81.758	-81.758
<b>16411.5</b>	1.59898	7	81.7973	-81.7973
<b>16489.2</b>	1.59224	7	81.8363	-81.8363
<b>16567</b>	1.58554	7	81.8748	-81.8748
<b>16644.8</b>	1.57887	7	81.9131	-81.9131
<b>16722.6</b>	1.57224	7	81.9509	-81.9509
<b>16800.3</b>	1.56564	7	81.9884	-81.9884
<b>16878.1</b>	1.55908	7	82.0256	-82.0256
<b>16955.9</b>	1.55255	7	82.0624	-82.0624
<b>17033.6</b>	1.54605	7	82.0989	-82.0989
<b>17111.4</b>	1.53958	7	82.135	-82.135
<b>17189.2</b>	1.53315	7	82.1708	-82.1708
<b>17266.9</b>	1.52674	7	82.2063	-82.2063
<b>17344.7</b>	1.52037	7	82.2415	-82.2415
<b>17422.5</b>	1.51402	7	82.2763	-82.2763
<b>17500.2</b>	1.50771	7	82.3109	-82.3109
<b>17578</b>	1.50143	7	82.3451	-82.3451
<b>17655.8</b>	1.49517	7	82.379	-82.379
<b>17733.6</b>	1.48895	7	82.4127	-82.4127
<b>17811.3</b>	1.48275	7	82.446	-82.446
<b>17889.1</b>	1.47658	7	82.479	-82.479
<b>17966.9</b>	1.47044	7	82.5117	-82.5117
<b>18044.6</b>	1.46433	7	82.5442	-82.5442
<b>18122.4</b>	1.45824	7	82.5764	-82.5764
<b>18200.2</b>	1.45218	7	82.6083	-82.6083
<b>18277.9</b>	1.44615	7	82.6399	-82.6399

Table 33.1: Scan values for different photon energies in energy scan

### Legend

**E:** photon energy

**K\_y:** deflection parameter for vertical field component of insertion device

**n\_harm/step:** number of undulator harmonic or number of energy slot for continuous source (e.g. wiggler)

**dtheta\_03:** Optical\_element\_#3.Move.Source.dangle\_x (Source rotation angle around x-axis (ccw).)

**dtheta\_05:** Optical\_element\_#5.Move.Source.dangle\_x (Source rotation angle around x-axis (ccw).)

<b>E eV</b>	<b>P_sum W</b>	<b>P_abs02-01 W</b>	<b>P_abs02-02 W</b>	<b>P_abs04 W</b>
<b>15556</b>	170.995	51.9769	7.05083	6.59549
<b>15633.8</b>	170.404	51.949	7.0837	6.63196
<b>15711.5</b>	169.798	52.0748	7.05706	6.62703
<b>15789.3</b>	169.194	51.9987	7.07543	6.65508
<b>15867.1</b>	168.484	51.9795	7.06573	6.69194
<b>15944.8</b>	167.889	51.9217	7.07069	6.69778
<b>16022.6</b>	166.334	51.9998	7.05796	6.72692
<b>16100.4</b>	165.817	52.1782	7.07352	6.74028
<b>16178.2</b>	165.215	52.2032	7.06336	6.76606
<b>16255.9</b>	164.545	52.162	7.06527	6.78467
<b>16333.7</b>	163.995	52.0964	7.06612	6.78898
<b>16411.5</b>	163.395	52.1926	7.06405	6.79061
<b>16489.2</b>	162.749	52.1043	7.07239	6.82654
<b>16567</b>	162.139	52.1979	7.04125	6.83321
<b>16644.8</b>	161.504	52.2588	7.04733	6.84111
<b>16722.6</b>	160.875	52.1824	6.99602	6.84651
<b>16800.3</b>	160.261	52.1519	6.99248	6.86852
<b>16878.1</b>	159.67	52.3506	6.98963	6.87326
<b>16955.9</b>	159.07	52.2182	6.99432	6.88688
<b>17033.6</b>	157.762	52.3385	6.97215	6.90132
<b>17111.4</b>	157.165	52.5377	6.94214	6.93146
<b>17189.2</b>	156.609	52.4502	6.92456	6.96578
<b>17266.9</b>	155.976	52.4055	6.94077	6.97452
<b>17344.7</b>	155.424	52.3575	6.89082	6.96481
<b>17422.5</b>	154.752	52.3428	6.88327	6.98424
<b>17500.2</b>	154.186	52.583	6.86883	6.99285
<b>17578</b>	153.627	52.3783	6.84528	6.99853
<b>17655.8</b>	153.017	52.2597	6.83217	7.00978
<b>17733.6</b>	152.421	52.4515	6.80568	7.02042
<b>17811.3</b>	151.837	52.4213	6.80604	7.06578
<b>17889.1</b>	151.22	52.4221	6.7624	7.0464
<b>17966.9</b>	150.624	52.3521	6.7503	7.07893
<b>18044.6</b>	150.012	52.3677	6.71321	7.06285
<b>18122.4</b>	148.856	52.3058	6.6708	7.06473
<b>18200.2</b>	148.268	52.5085	6.64877	7.11413
<b>18277.9</b>	147.713	52.3797	6.63649	7.11366

Table 33.2: Scan values for different photon energies with diamond filters of 1000 micron total thickness in

E eV	P_sum W	P_abs02-01 W	P_abs02-02 W	P_abs04 W
<b>15556</b>	170.995	0.199876	46.214	13.4692
<b>15633.8</b>	170.404	0.198201	46.2268	13.4919
<b>15711.5</b>	169.798	0.196733	46.2179	13.6018
<b>15789.3</b>	169.194	0.195437	46.2815	13.6414
<b>15867.1</b>	168.484	0.193832	46.1058	13.6121
<b>15944.8</b>	167.889	0.192226	46.3327	13.6301
<b>16022.6</b>	166.334	0.191175	46.2534	13.6806
<b>16100.4</b>	165.817	0.191025	46.3511	13.7163
<b>16178.2</b>	165.215	0.189237	46.4089	13.7552
<b>16255.9</b>	164.545	0.187045	46.3771	13.734
<b>16333.7</b>	163.995	0.186906	46.5221	13.7375
<b>16411.5</b>	163.395	0.185189	46.7073	13.8024
<b>16489.2</b>	162.749	0.183901	46.4038	13.8379
<b>16567</b>	162.139	0.183293	46.5693	13.8342
<b>16644.8</b>	161.504	0.182371	46.6411	13.8666
<b>16722.6</b>	160.875	0.180512	46.7029	13.831
<b>16800.3</b>	160.261	0.179437	46.7066	13.8147
<b>16878.1</b>	159.67	0.178716	46.8376	13.9134
<b>16955.9</b>	159.07	0.177226	46.8068	13.8681
<b>17033.6</b>	157.762	0.175799	46.7604	13.8152
<b>17111.4</b>	157.165	0.174844	46.7908	13.8603
<b>17189.2</b>	156.609	0.174226	47.0493	13.8412
<b>17266.9</b>	155.976	0.172755	46.8916	13.8341
<b>17344.7</b>	155.424	0.171957	46.9852	13.8663
<b>17422.5</b>	154.752	0.170686	47.0198	13.8124
<b>17500.2</b>	154.186	0.170273	47.2618	13.7983
<b>17578</b>	153.627	0.168795	47.1799	13.7953
<b>17655.8</b>	153.017	0.167499	47.1203	13.7418
<b>17733.6</b>	152.421	0.165929	47.2467	13.7644
<b>17811.3</b>	151.837	0.165783	47.219	13.7625
<b>17889.1</b>	151.22	0.163938	47.1545	13.7641
<b>17966.9</b>	150.624	0.163529	47.3366	13.6836
<b>18044.6</b>	150.012	0.162198	47.2734	13.6478
<b>18122.4</b>	148.856	0.161175	47.4925	13.7007
<b>18200.2</b>	148.268	0.160049	47.3221	13.652
<b>18277.9</b>	147.713	0.159337	47.3825	13.6259

Table 33.3: Scan values for different photon energies with upstream diamond filter of 400 micron thickness in

E eV	P_sum W	P_abs02-01 W	P_abs02-02 W	P_abs04 W
<b>15556</b>	170.995	0.19933	0.197664	52.913
<b>15633.8</b>	170.404	0.197907	0.196949	53.0649
<b>15711.5</b>	169.798	0.197016	0.194906	53.1474
<b>15789.3</b>	169.194	0.195459	0.193289	53.2309
<b>15867.1</b>	168.484	0.194026	0.192249	53.2044
<b>15944.8</b>	167.889	0.192323	0.191833	53.4137
<b>16022.6</b>	166.334	0.191417	0.190181	53.4452
<b>16100.4</b>	165.817	0.189909	0.189241	53.6663
<b>16178.2</b>	165.215	0.189181	0.188087	53.8675
<b>16255.9</b>	164.545	0.187226	0.186965	53.8422
<b>16333.7</b>	163.995	0.186123	0.185359	53.8573
<b>16411.5</b>	163.395	0.185729	0.185095	53.8666
<b>16489.2</b>	162.749	0.183779	0.182733	54.1031
<b>16567</b>	162.139	0.183131	0.181782	54.1281
<b>16644.8</b>	161.504	0.182218	0.180923	54.2746
<b>16722.6</b>	160.875	0.180624	0.179937	54.307
<b>16800.3</b>	160.261	0.17971	0.178548	54.3294
<b>16878.1</b>	159.67	0.178792	0.177538	54.5276
<b>16955.9</b>	159.07	0.177704	0.176177	54.5635
<b>17033.6</b>	157.762	0.176606	0.175323	54.4678
<b>17111.4</b>	157.165	0.175152	0.174677	54.6441
<b>17189.2</b>	156.609	0.174088	0.173153	54.8185
<b>17266.9</b>	155.976	0.173288	0.171849	54.8289
<b>17344.7</b>	155.424	0.171937	0.170818	54.8476
<b>17422.5</b>	154.752	0.169703	0.169584	55.0083
<b>17500.2</b>	154.186	0.169762	0.16927	55.0846
<b>17578</b>	153.627	0.169151	0.16811	55.1251
<b>17655.8</b>	153.017	0.167917	0.166619	55.0468
<b>17733.6</b>	152.421	0.16645	0.165469	55.2519
<b>17811.3</b>	151.837	0.165611	0.164788	55.3143
<b>17889.1</b>	151.22	0.163849	0.163433	55.1623
<b>17966.9</b>	150.624	0.163629	0.162556	55.4261
<b>18044.6</b>	150.012	0.162354	0.161764	55.3234
<b>18122.4</b>	148.856	0.160969	0.160443	55.3319
<b>18200.2</b>	148.268	0.159801	0.159281	55.4188
<b>18277.9</b>	147.713	0.158302	0.158074	55.5583

Table 33.4: Scan values for different photon energies with no upstream filters

### Legend

**E:** photon energy

**P\_sum:** sum of power in harmonics / energy intervals, P\_sum = P\_src

**P\_abs02-01:** total power absorbed by optical element 02-01

**P\_abs02-02:** total power absorbed by optical element 02-02

**P\_abs04:** total power absorbed by optical element 04

# Chapter 34

## Plots

### 34.1 Statistics of incident irradiance

```
"fig/Main_beam_C111_Bragg/plot001.png" Lbl.:Main_beam_C111_Bragg_2d_plot_I_peak_incstat_oe04
```

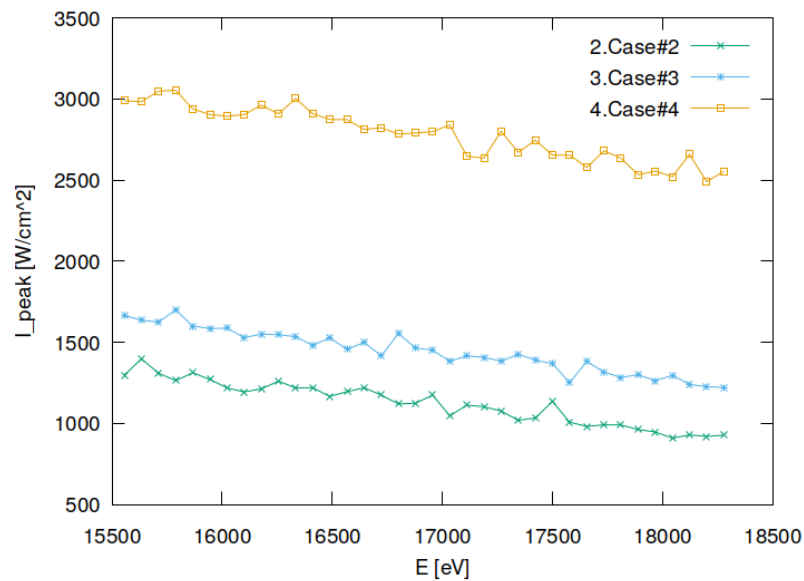


Figure 34.1: Incident peak irradiance of optical element #04 (BS).

```
"fig/Main_beam_C111_Bragg/plot002.png" Lbl.:Main_beam_C111_Bragg_2d_plot_I_int_incstat_oe04
```

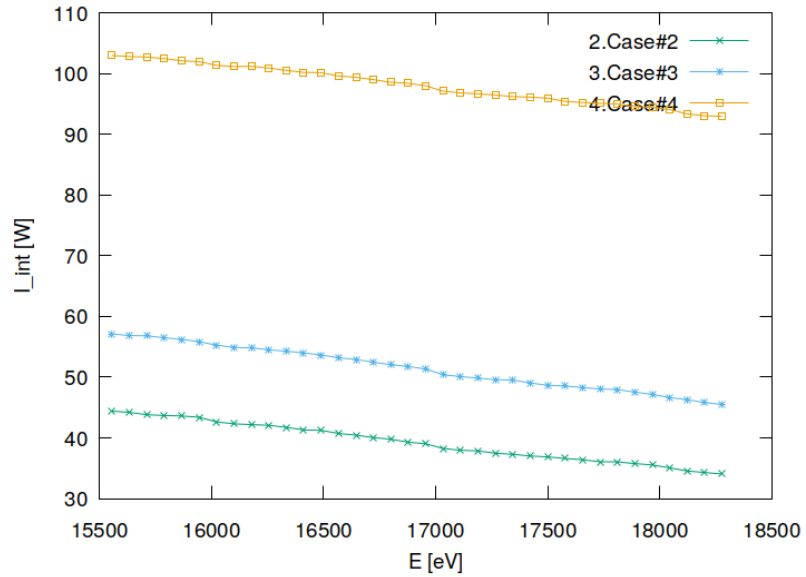


Figure 34.2: Incident flux of optical element #04 (BS).

## 34.2 Statistics of absorbed irradiance

```
"fig/Main_beam_C111_Bragg/plot003.png" Lbl.:Main_beam_C111_Bragg_2d_plot_I_peak_absstat_oe04
```

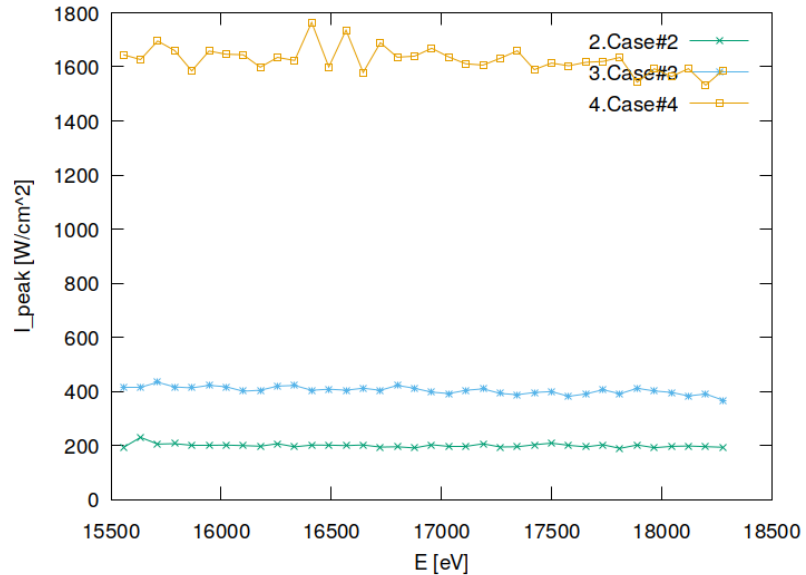


Figure 34.3: Absorbed peak irradiance of optical element #04 (BS).

```
"fig/Main_beam_C111_Bragg/plot004.png" Lbl.:Main_beam_C111_Bragg_2d_plot_I_int_absstat_oe04
```

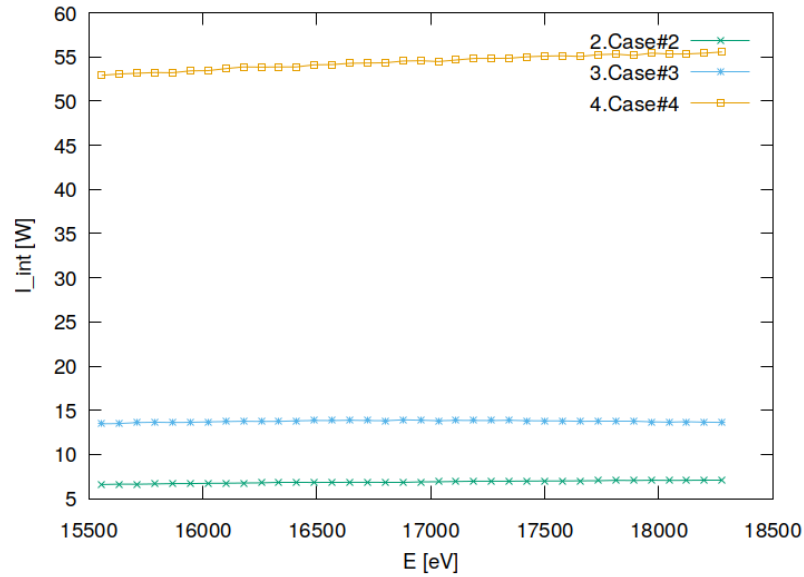


Figure 34.4: Absorbed flux of optical element #04 (BS).

### 34.3 Statistics of temperature

```
"fig/Main_beam_C111_Bragg/plot005.png" Lbl.:Main_beam_C111_Bragg_2d_plot_T_peak_stat_oe04
```

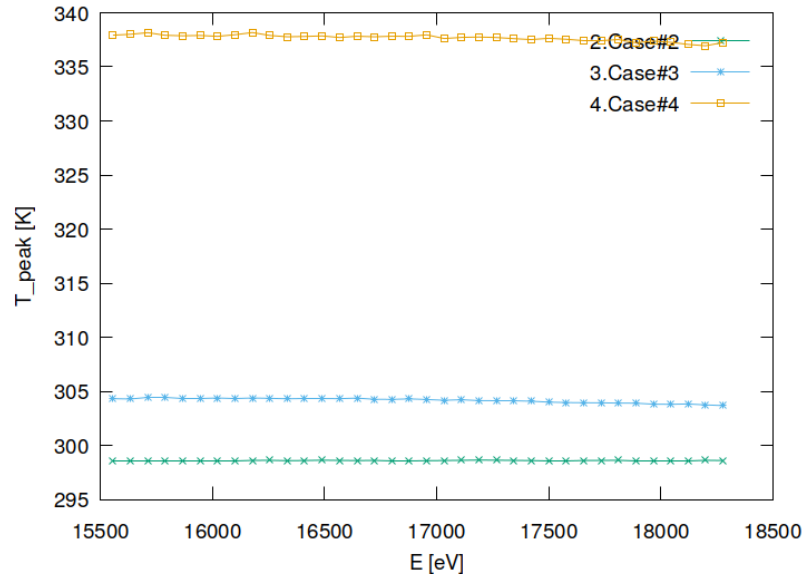


Figure 34.5: Peak temperature of optical element #04 (BS).

## 34.4 Statistics of mechanical stress (von Mises stress)

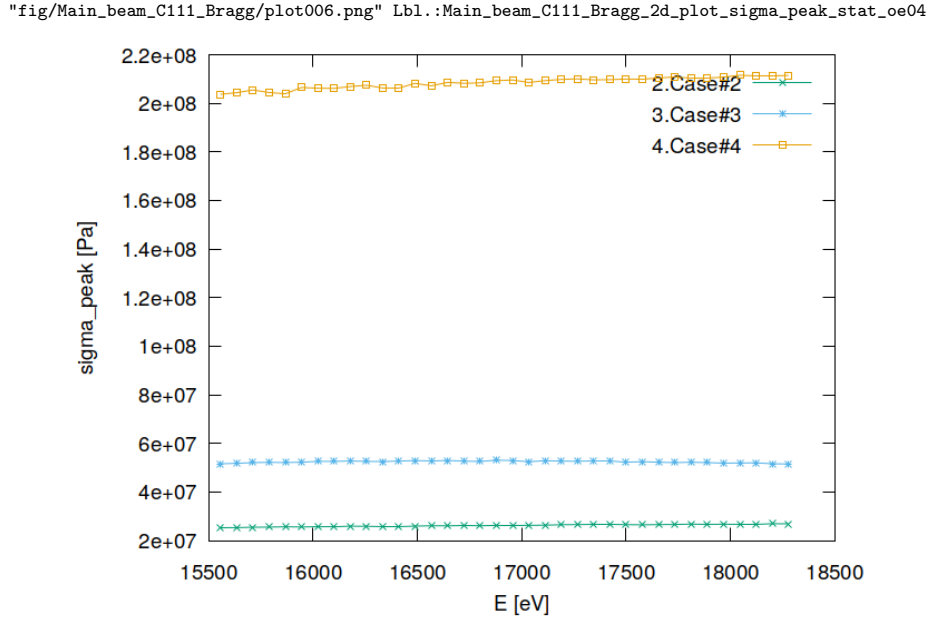


Figure 34.6: Peak mechanical stress (Von Mises stress) of optical element #04 (BS).

## 34.5 Statistics of optical surface deformation

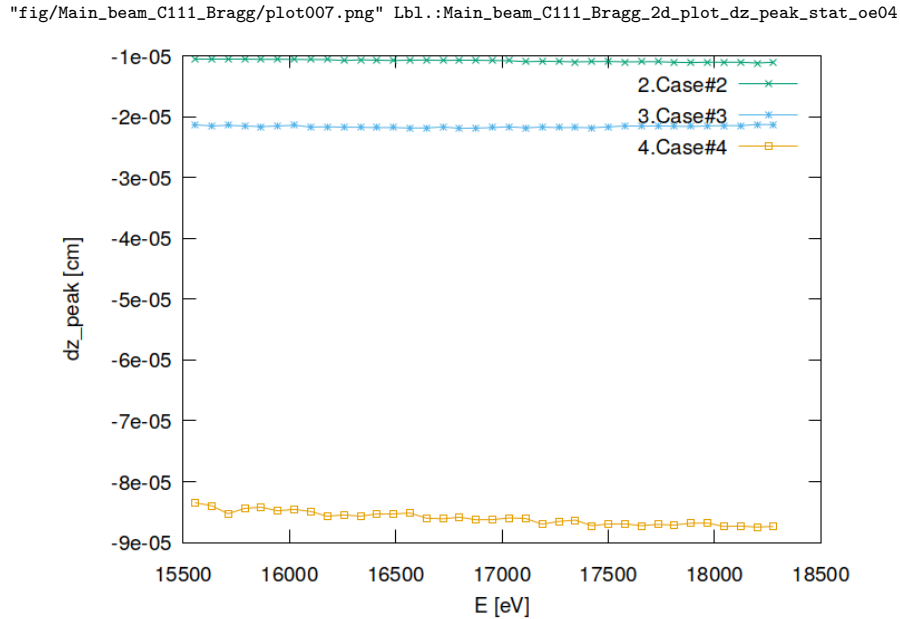


Figure 34.7: Peak deformation of optical element #04 (BS).

## 34.6 Statistics of photon irradiance on optical surface

"fig/Main\_beam\_C111\_Bragg/plot008.png" Lbl.:Main\_beam\_C111\_Bragg\_2d\_plot\_dx\_fwhm\_inc\_footstat\_oe04

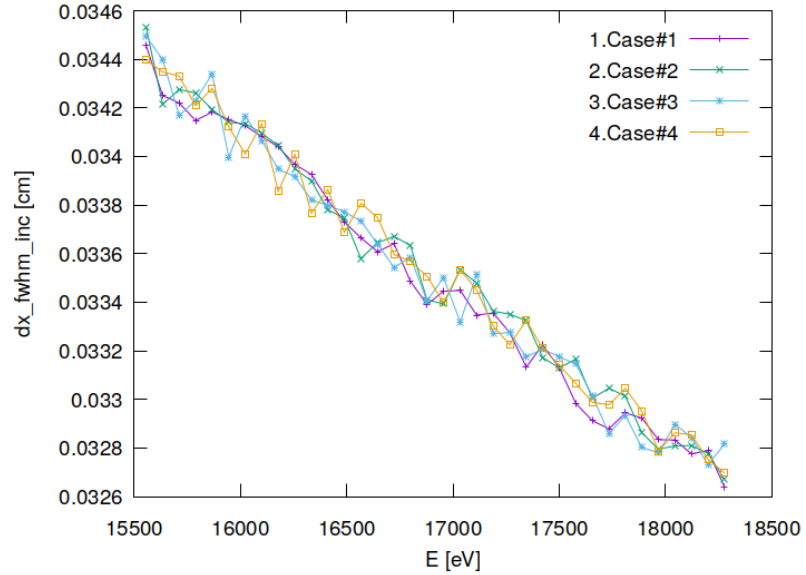


Figure 34.8: Sagittal footprint diameter (FWHM) of optical element #04 (BS).

"fig/Main\_beam\_C111\_Bragg/plot009.png" Lbl.:Main\_beam\_C111\_Bragg\_2d\_plot\_dx\_fwhm\_inc\_footstat\_oe05

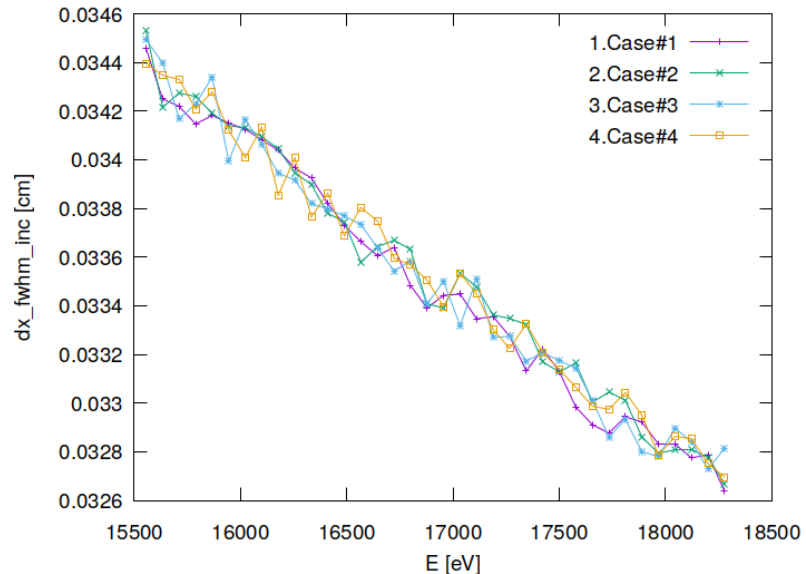


Figure 34.9: Sagittal footprint diameter (FWHM) of optical element #05 (Dan-MAX).

```
"fig/Main_beam_C111_Bragg/plot010.png" Lbl.:Main_beam_C111_Bragg_2d_plot_dy_fwhm_inc_footstat_oe04
```

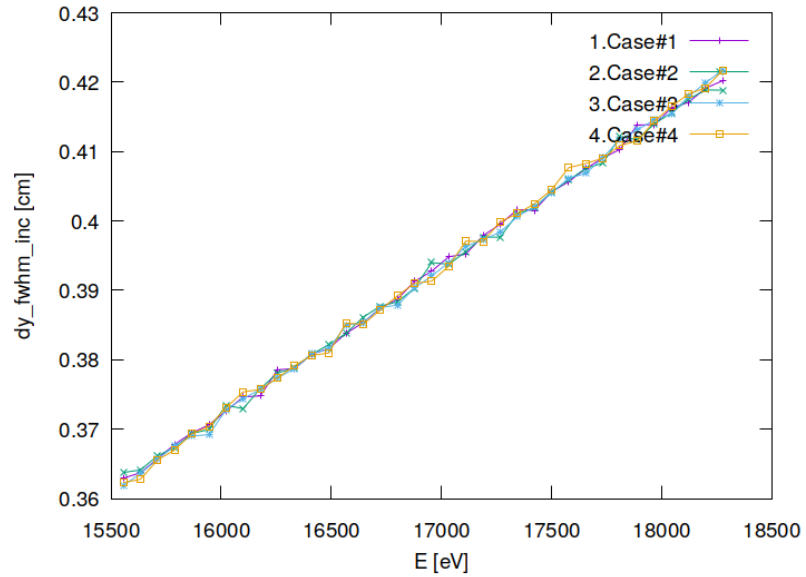


Figure 34.10: Meridional footprint diameter (FWHM) of optical element #04 (BS).

```
"fig/Main_beam_C111_Bragg/plot011.png" Lbl.:Main_beam_C111_Bragg_2d_plot_dy_fwhm_inc_footstat_oe05
```

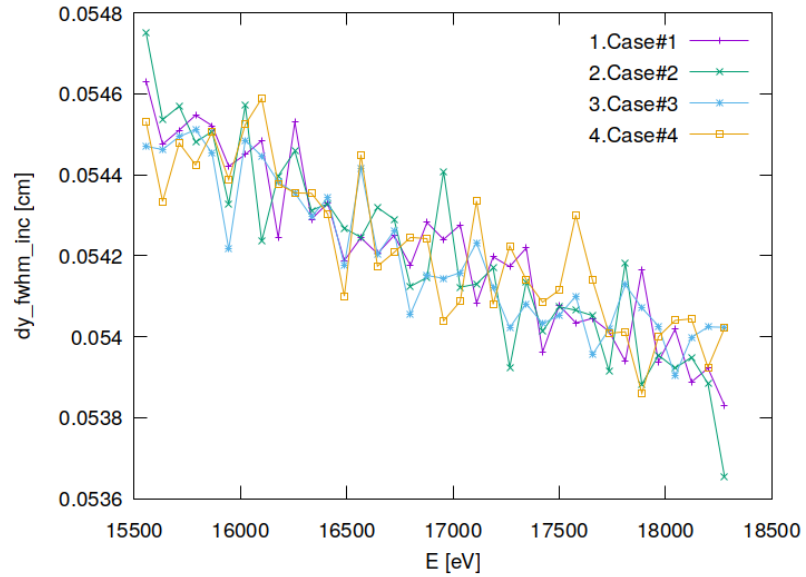


Figure 34.11: Meridional footprint diameter (FWHM) of optical element #05 (Dan-MAX).

```
"fig/Main_beam_C111_Bragg/plot012.png" Lbl.:Main_beam_C111_Bragg_2d_plot_I_inc_int_footstat_oe04
```

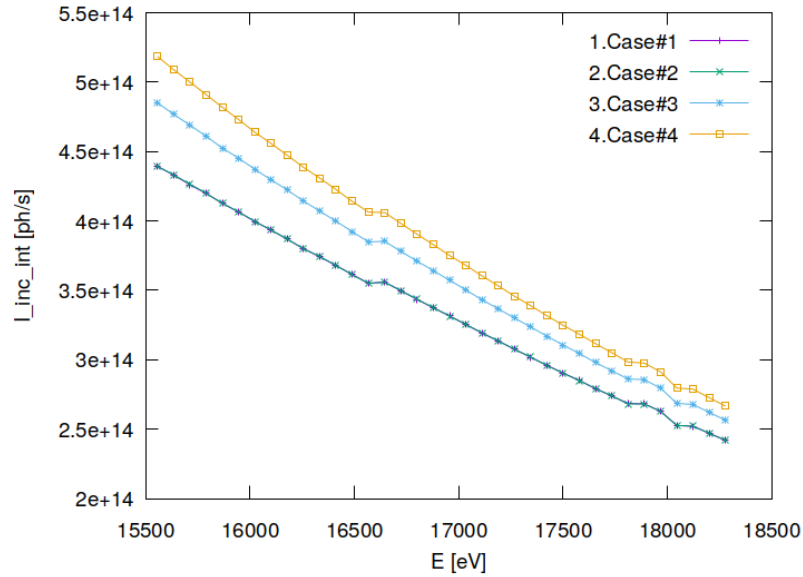


Figure 34.12: Incident photon flux on surface of optical element #04 (BS).

```
"fig/Main_beam_C111_Bragg/plot013.png" Lbl.:Main_beam_C111_Bragg_2d_plot_I_inc_int_footstat_oe05
```

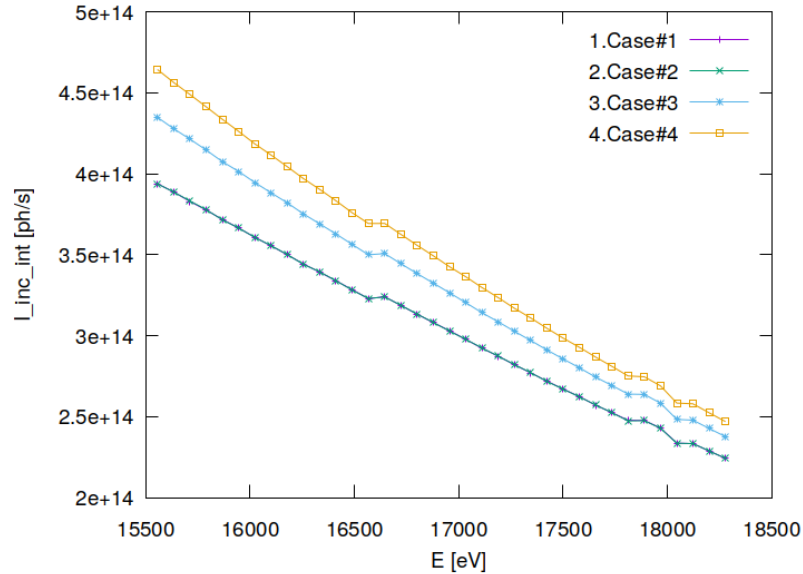


Figure 34.13: Incident photon flux on surface of optical element #05 (DanMAX).

```
"fig/Main_beam_C111_Bragg/plot014.png" Lbl.:Main_beam_C111_Bragg_2d_plot_x_cen_inc_footstat_oe04
```

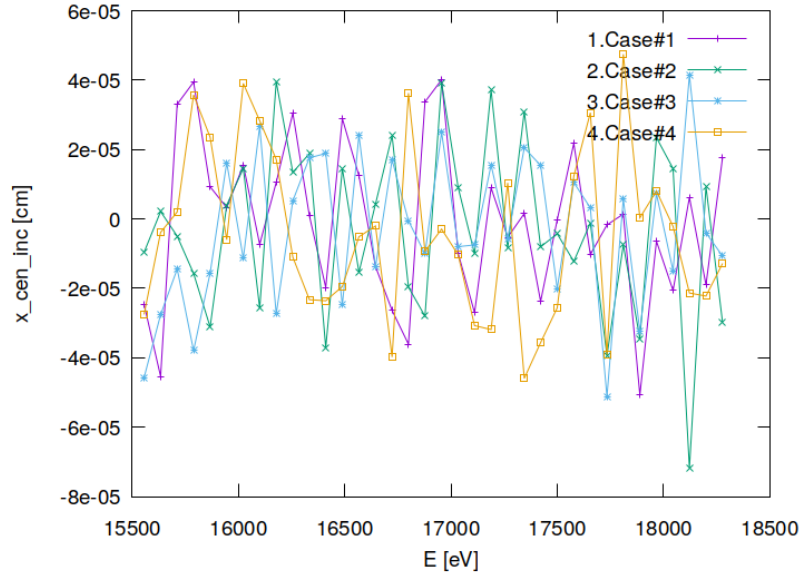


Figure 34.14: Sagittal coordinate of footprint's centre of 'gravity' on surface of optical element #04 (BS).

```
"fig/Main_beam_C111_Bragg/plot015.png" Lbl.:Main_beam_C111_Bragg_2d_plot_x_cen_inc_footstat_oe05
```

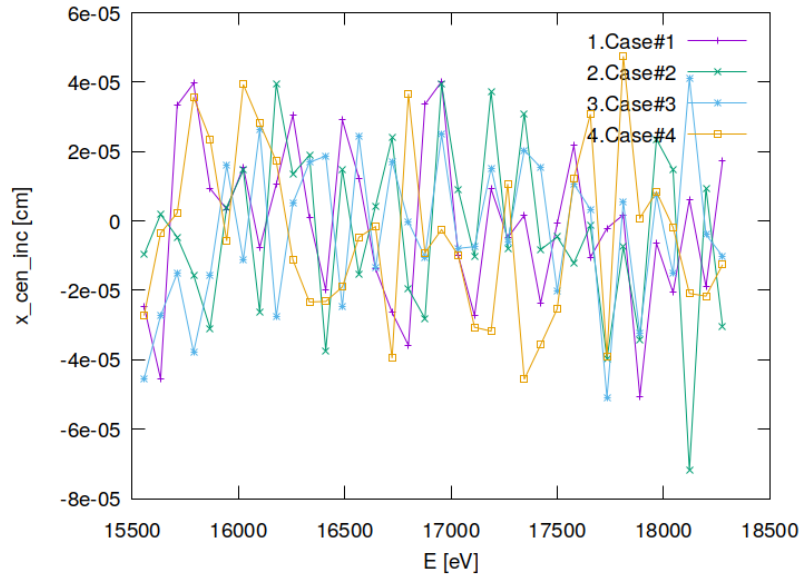


Figure 34.15: Sagittal coordinate of footprint's centre of 'gravity' on surface of optical element #05 (DanMAX).

```
"fig/Main_beam_C111_Bragg/plot016.png" Lbl.:Main_beam_C111_Bragg_2d_plot_y_cen_inc_footstat_oe04
```

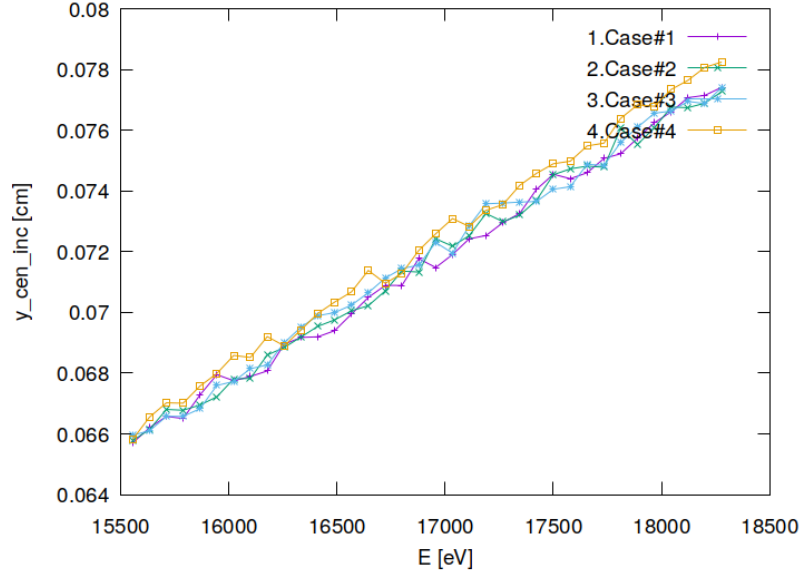


Figure 34.16: Meridional coordinate of footprint's centre of 'gravity' on surface of optical element #04 (BS).

```
"fig/Main_beam_C111_Bragg/plot017.png" Lbl.:Main_beam_C111_Bragg_2d_plot_y_cen_inc_footstat_oe05
```

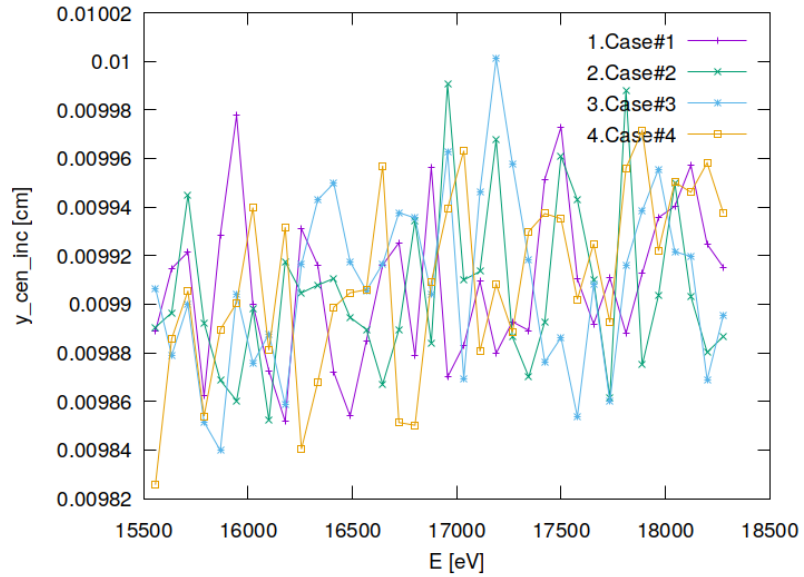


Figure 34.17: Meridional coordinate of footprint's centre of 'gravity' on surface of optical element #05 (DanMAX).

### 34.7 Statistics of photon irradiance in beam cross section

"fig/Main\_beam\_C111\_Bragg/plot018.png" Lbl.:Main\_beam\_C111\_Bragg\_2d\_plot\_dx\_fwhm\_focstatavg\_oe04

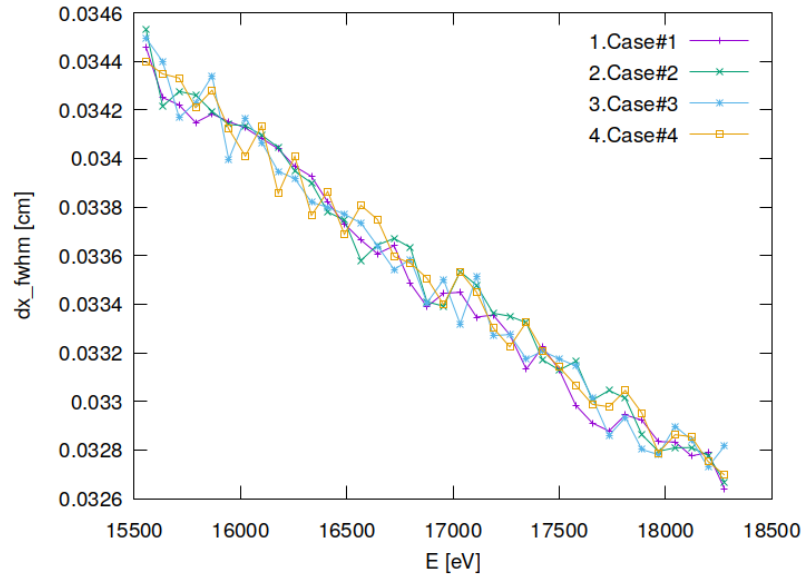


Figure 34.18: Sagittal beam diameter (FWHM) of optical element #04 (BS).

"fig/Main\_beam\_C111\_Bragg/plot019.png" Lbl.:Main\_beam\_C111\_Bragg\_2d\_plot\_dx\_fwhm\_focstatavg\_oe05

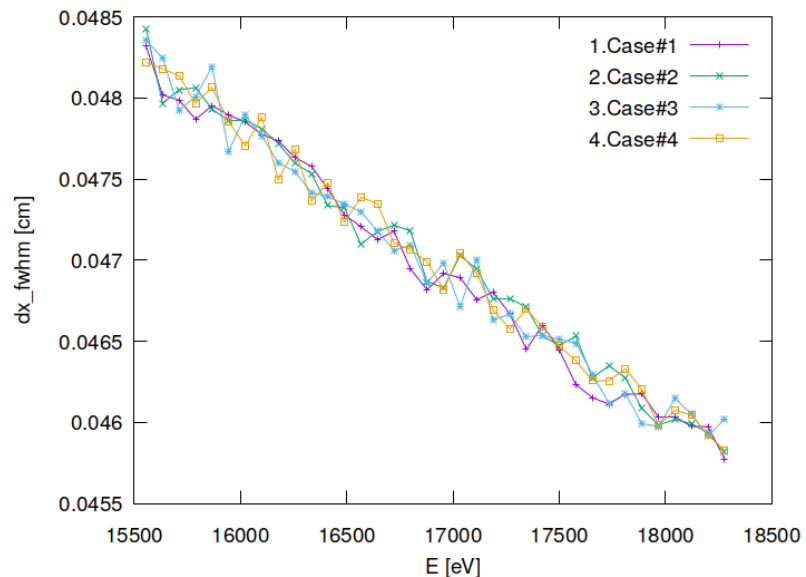


Figure 34.19: Sagittal beam diameter (FWHM) of optical element #05 (DanMAX).

```
"fig/Main_beam_C111_Bragg/plot020.png" Lbl.:Main_beam_C111_Bragg_2d_plot_dz_fwhm_focstatavg_oe04
```

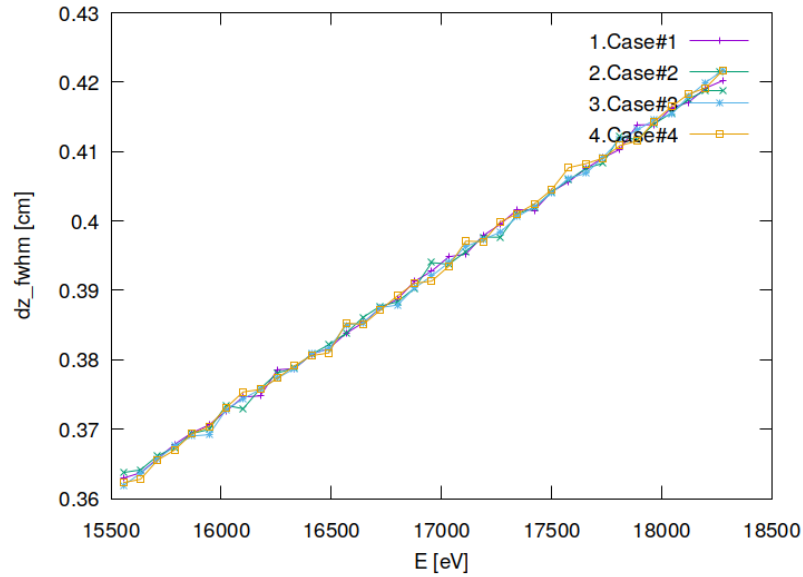


Figure 34.20: Meridional beam diameter (FWHM) of optical element #04 (BS).

```
"fig/Main_beam_C111_Bragg/plot021.png" Lbl.:Main_beam_C111_Bragg_2d_plot_dz_fwhm_focstatavg_oe05
```

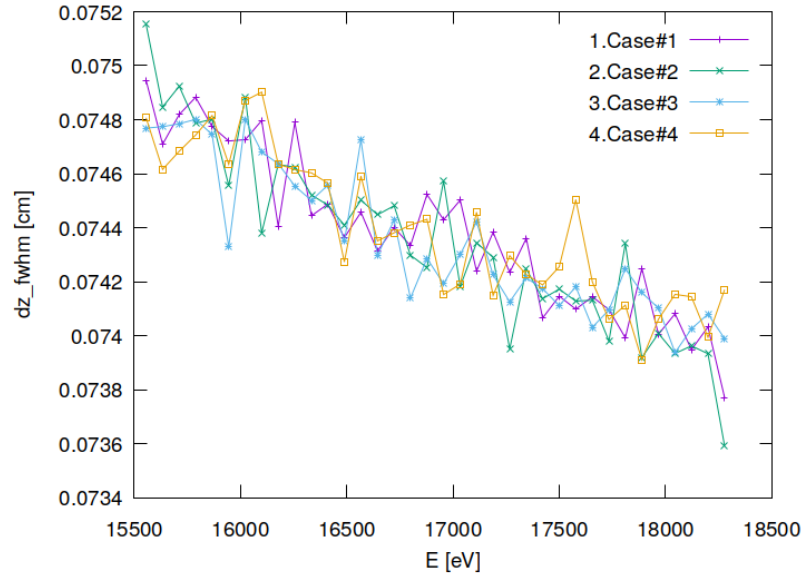


Figure 34.21: Meridional beam diameter (FWHM) of optical element #05 (Dan-MAX).

```
"fig/Main_beam_C111_Bragg/plot022.png" Lbl.:Main_beam_C111_Bragg_2d_plot_I_int_focstatavg_oe04
```

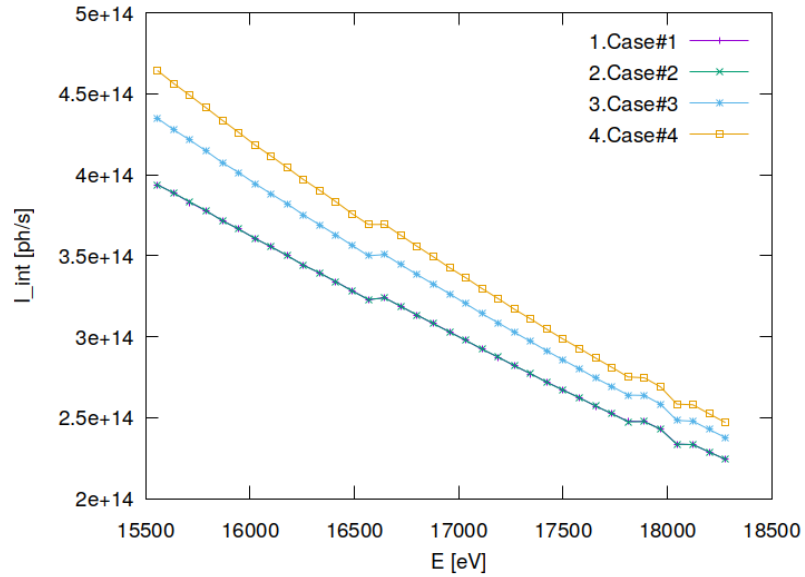


Figure 34.22: Photon flux in beam cross section of optical element #04 (BS).

```
"fig/Main_beam_C111_Bragg/plot023.png" Lbl.:Main_beam_C111_Bragg_2d_plot_I_int_focstatavg_oe05
```

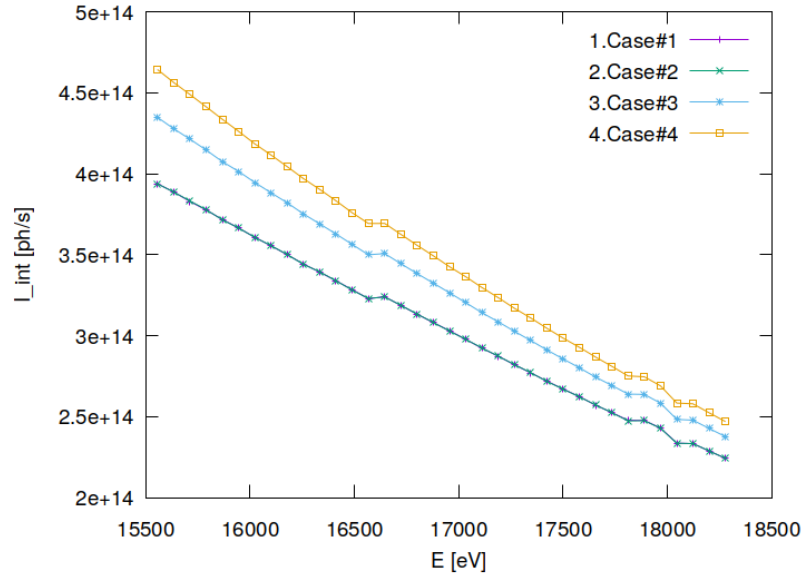


Figure 34.23: Photon flux in beam cross section of optical element #05 (DanMAX).

"fig/Main\_beam\_C111\_Bragg/plot024.png" Lbl.:Main\_beam\_C111\_Bragg\_2d\_plot\_x\_cen\_focstatavg\_oe04

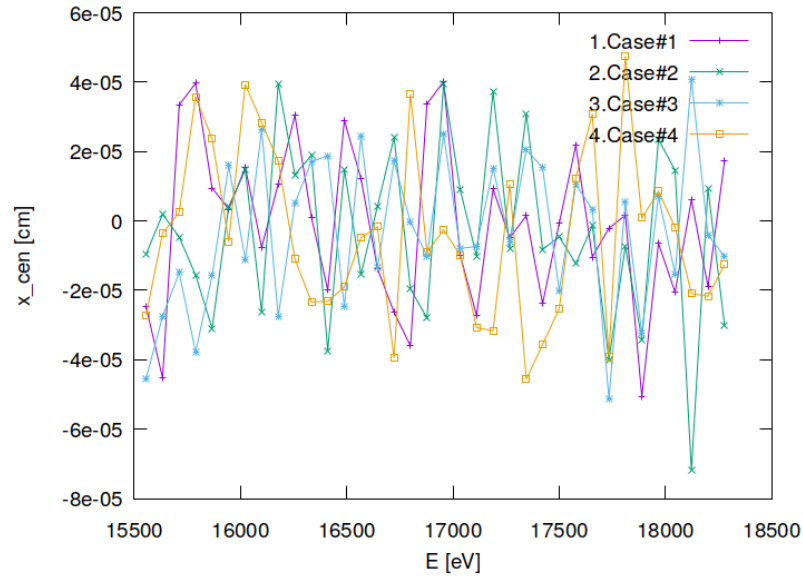


Figure 34.24: Sagittal coordinate of beam's centre of 'gravity' in beam cross section of optical element #04 (BS).

"fig/Main\_beam\_C111\_Bragg/plot025.png" Lbl.:Main\_beam\_C111\_Bragg\_2d\_plot\_x\_cen\_focstatavg\_oe05

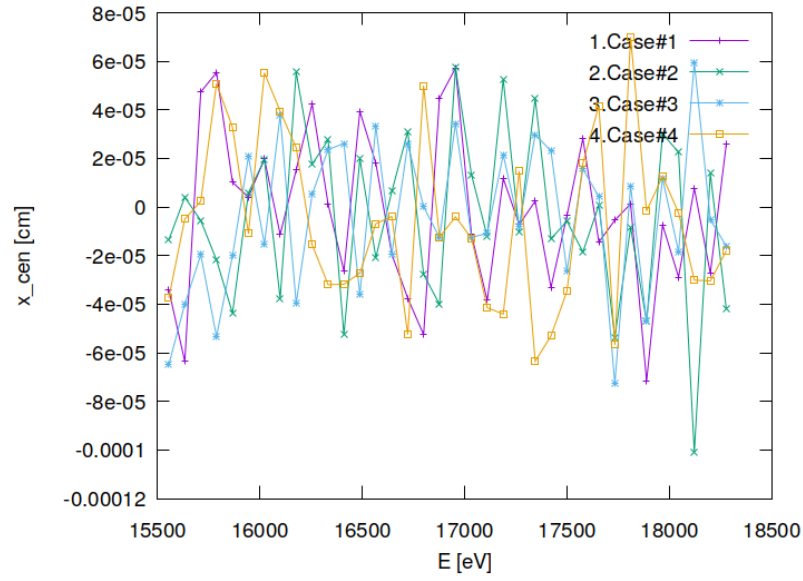


Figure 34.25: Sagittal coordinate of beam's centre of 'gravity' in beam cross section of optical element #05 (DanMAX).

"fig/Main\_beam\_C111\_Bragg/plot026.png" Lbl.:Main\_beam\_C111\_Bragg\_2d\_plot\_z\_cen\_focstatavg\_oe04

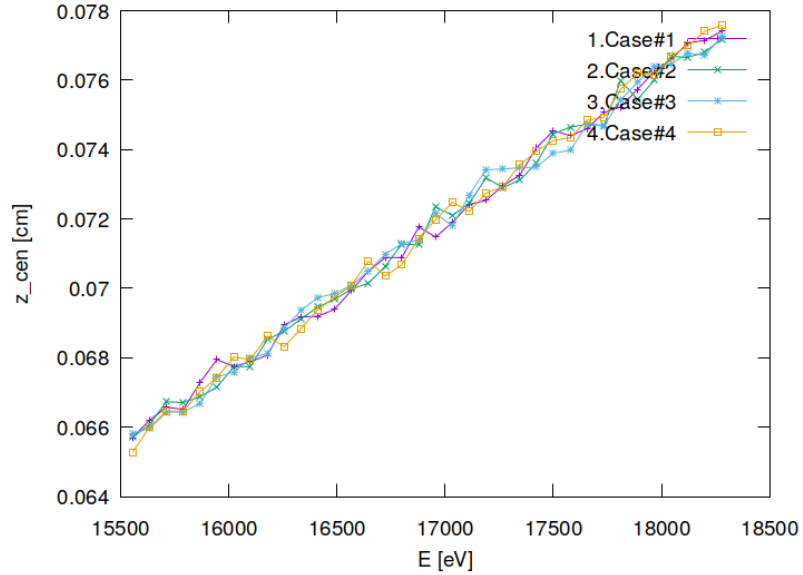


Figure 34.26: Meridional coordinate of beam's centre of 'gravity' in beam cross section of optical element #04 (BS).

"fig/Main\_beam\_C111\_Bragg/plot027.png" Lbl.:Main\_beam\_C111\_Bragg\_2d\_plot\_z\_cen\_focstatavg\_oe05

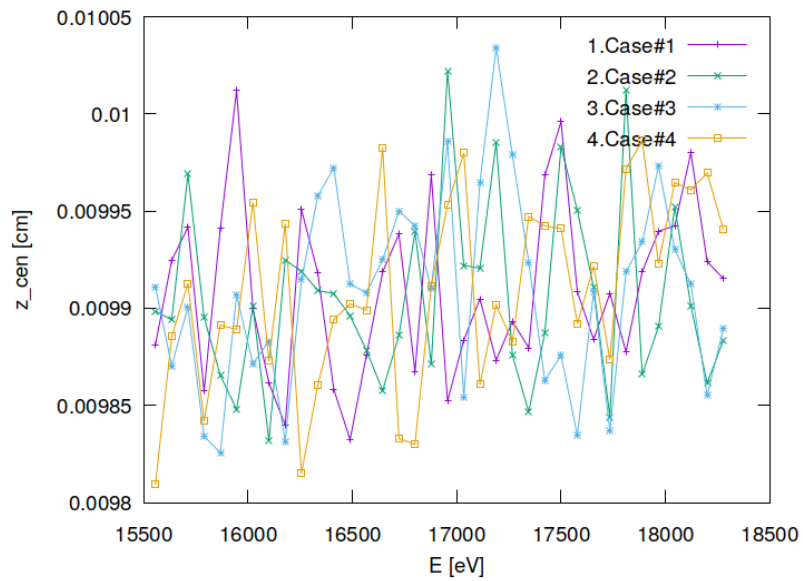


Figure 34.27: Meridional coordinate of beam's centre of 'gravity' in beam cross section of optical element #05 (DanMAX).

```
"fig/Main_beam_C111_Bragg/plot028.png" Lbl.:Main_beam_C111_Bragg_2d_plot_dxp_fwhm_focstatavg_oe04
```

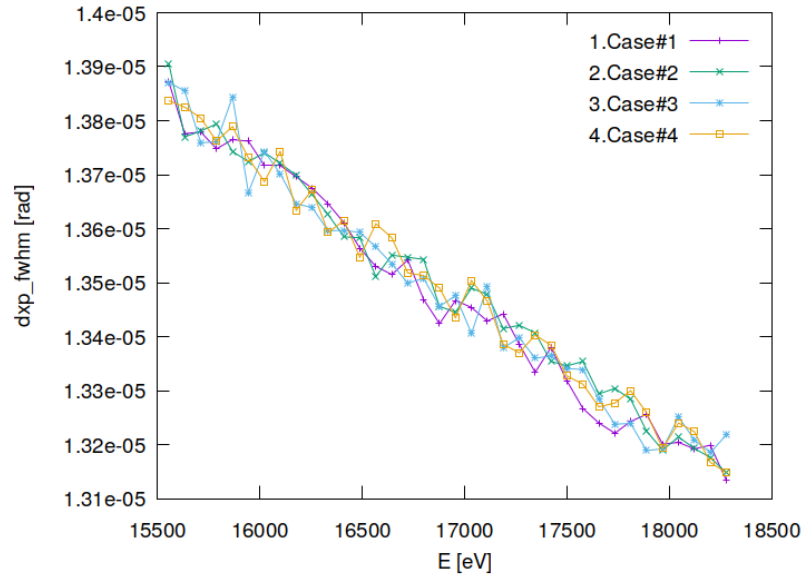


Figure 34.28: Sagittal beam divergence (FWHM) of optical element #04 (BS).

```
"fig/Main_beam_C111_Bragg/plot029.png" Lbl.:Main_beam_C111_Bragg_2d_plot_dxp_fwhm_focstatavg_oe05
```

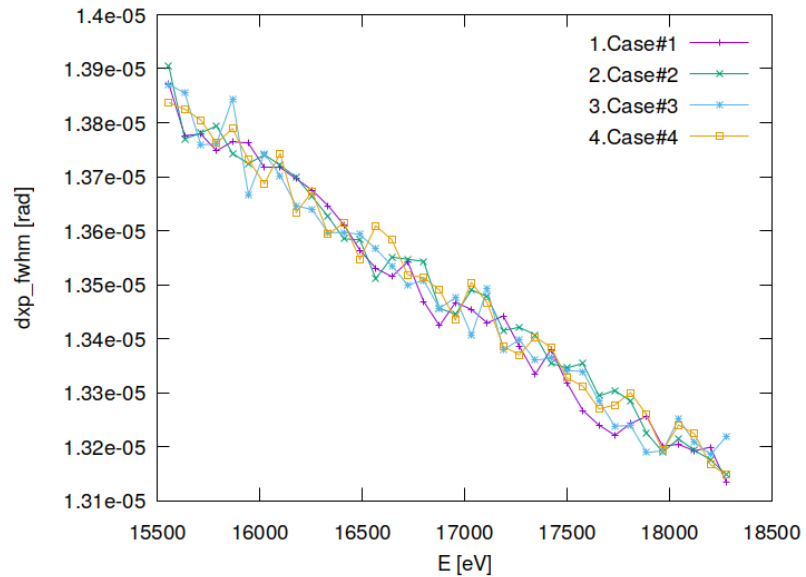


Figure 34.29: Sagittal beam divergence (FWHM) of optical element #05 (Dan-MAX).

```
"fig/Main_beam_C111_Bragg/plot030.png" Lbl.:Main_beam_C111_Bragg_2d_plot_dzp_fwhm_focstatavg_oe04
```

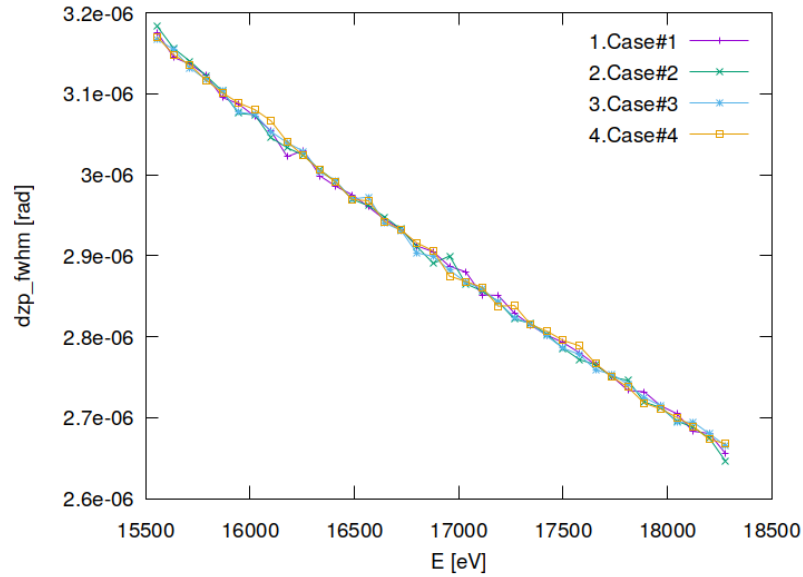


Figure 34.30: Meridional beam divergence (FWHM) of optical element #04 (BS).

```
"fig/Main_beam_C111_Bragg/plot031.png" Lbl.:Main_beam_C111_Bragg_2d_plot_dzp_fwhm_focstatavg_oe05
```

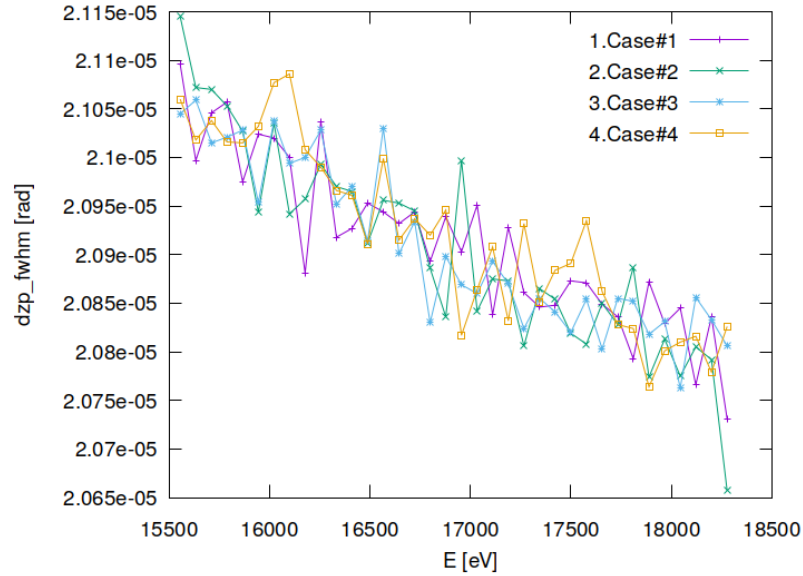


Figure 34.31: Meridional beam divergence (FWHM) of optical element #05 (Dan-MAX).

```
"fig/Main_beam_C111_Bragg/plot032.png" Lbl.:Main_beam_C111_Bragg_2d_plot_I_int_focstatavg_oe04
```

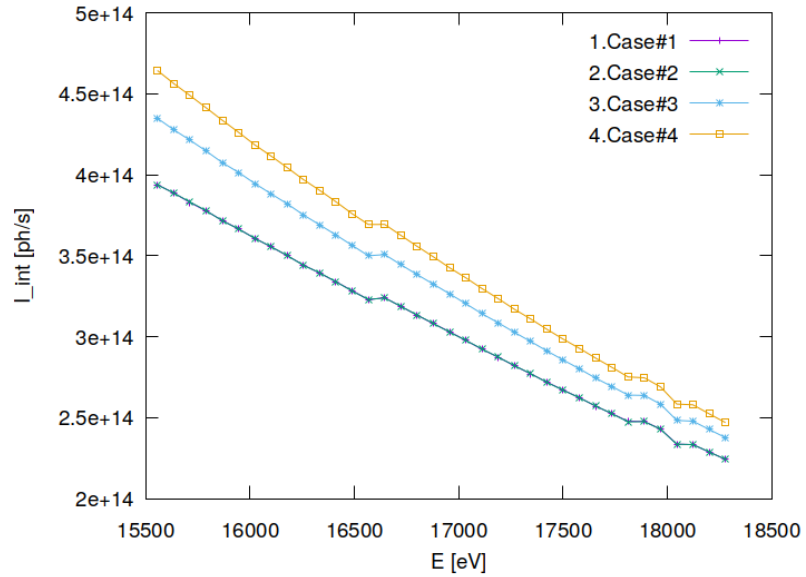


Figure 34.32: Photon flux in beam cross section of optical element #04 (BS).

```
"fig/Main_beam_C111_Bragg/plot033.png" Lbl.:Main_beam_C111_Bragg_2d_plot_I_int_focstatavg_oe05
```

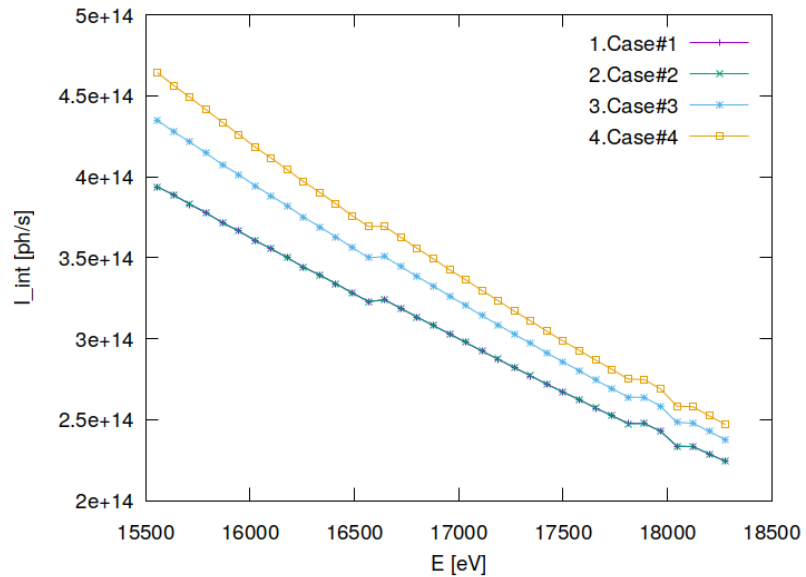


Figure 34.33: Photon flux in beam cross section of optical element #05 (DanMAX).

```
"fig/Main_beam_C111_Bragg/plot034.png" Lbl.:Main_beam_C111_Bragg_2d_plot_xp_cen_focstatavg_oe04
```

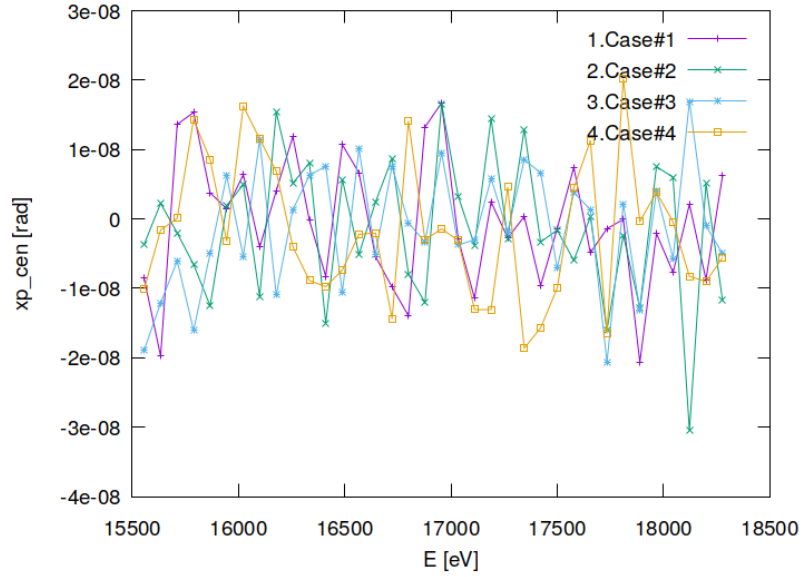


Figure 34.34: Sagittal coordinate of beam's centre of 'gravity' in angle space of optical element #04 (BS).

```
"fig/Main_beam_C111_Bragg/plot035.png" Lbl.:Main_beam_C111_Bragg_2d_plot_xp_cen_focstatavg_oe05
```

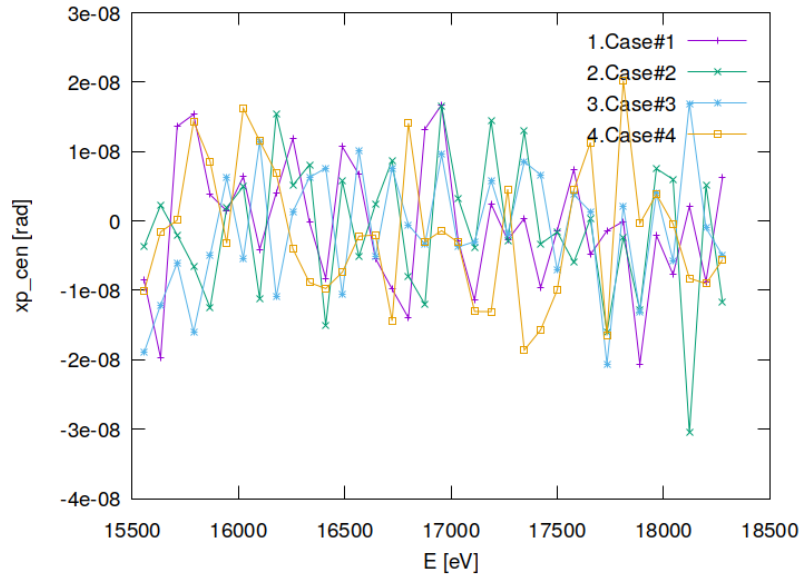


Figure 34.35: Sagittal coordinate of beam's centre of 'gravity' in angle space of optical element #05 (DanMAX).

```
"fig/Main_beam_C111_Bragg/plot036.png" Lbl.:Main_beam_C111_Bragg_2d_plot_zp_cen_focstatavg_oe04
```

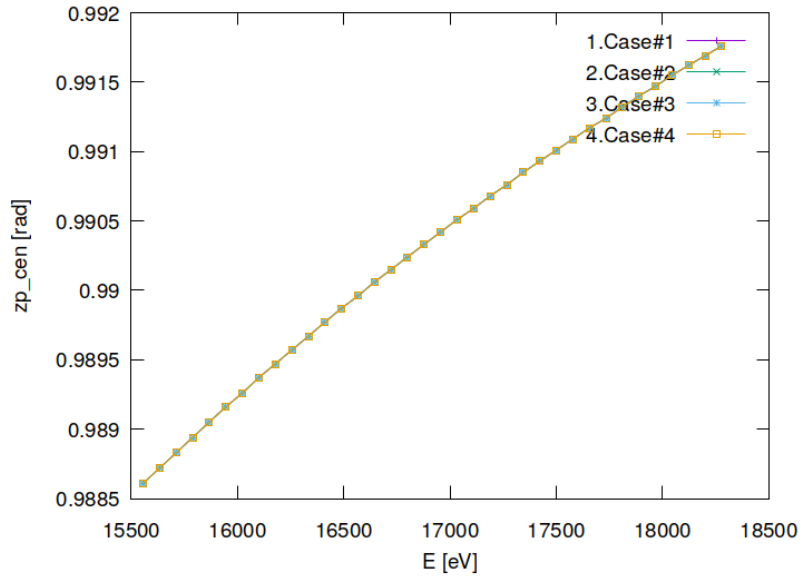


Figure 34.36: Meridional coordinate of beam's centre of 'gravity' in angle space of optical element #04 (BS).

```
"fig/Main_beam_C111_Bragg/plot037.png" Lbl.:Main_beam_C111_Bragg_2d_plot_zp_cen_focstatavg_oe05
```

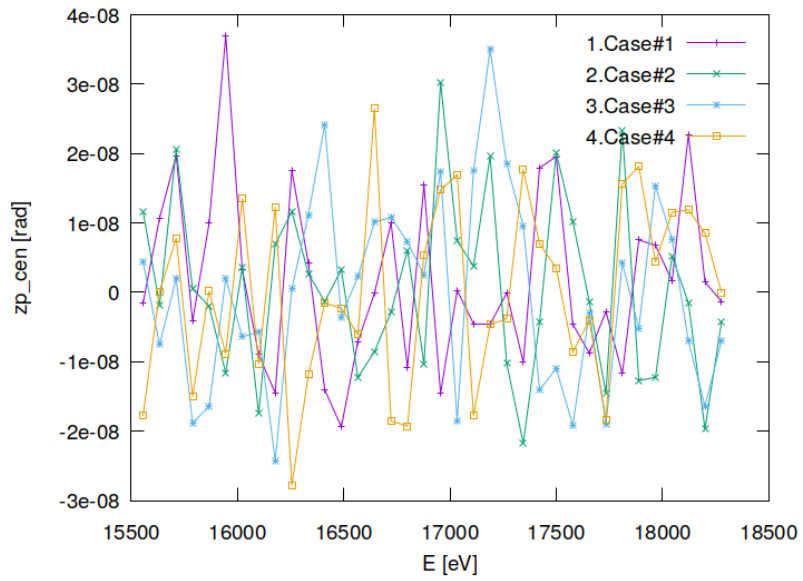


Figure 34.37: Meridional coordinate of beam's centre of 'gravity' in angle space of optical element #05 (DanMAX).

```
"fig/Main_beam_C111_Bragg/plot038.png" Lbl.:Main_beam_C111_Bragg_2d_plot_dE_fwhm_focstatavg_oe04
```

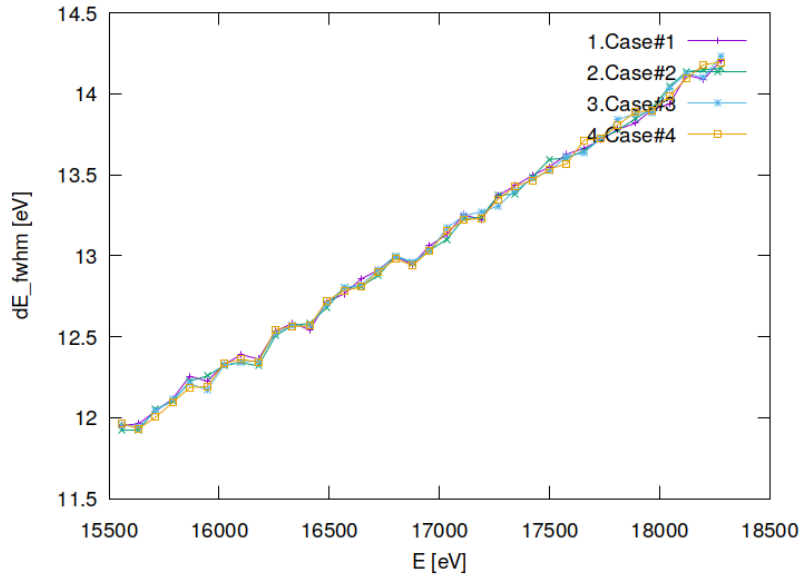


Figure 34.38: Bandwidth (FWHM) in beam cross section of optical element #04 (BS).

```
"fig/Main_beam_C111_Bragg/plot039.png" Lbl.:Main_beam_C111_Bragg_2d_plot_dE_fwhm_focstatavg_oe05
```

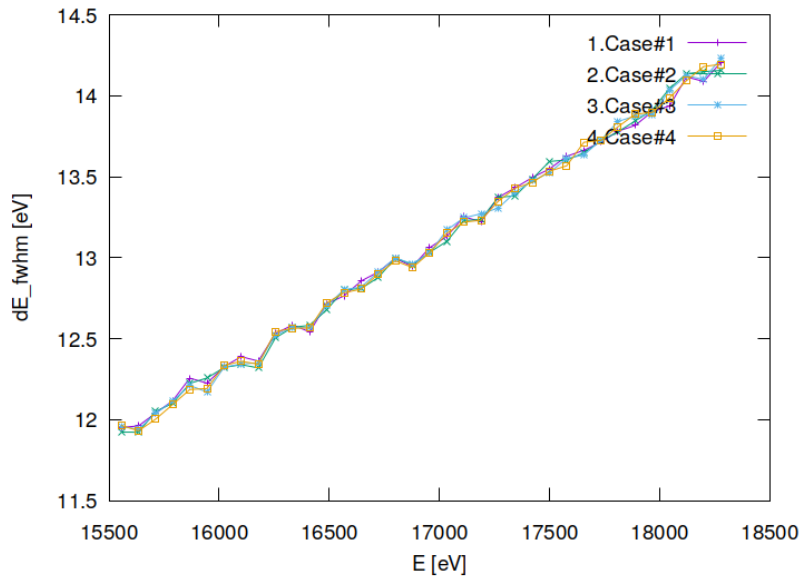


Figure 34.39: Bandwidth (FWHM) in beam cross section of optical element #05 (DanMAX).



## 34.8 Absorbed irradiance on surface

```
"fig/Main_beam_C111_Bragg/plot040.png" Lbl.:Main_beam_C111_Bragg_false_colour_plot_p_abs_foot_oe04_c2_16955.9eV
```

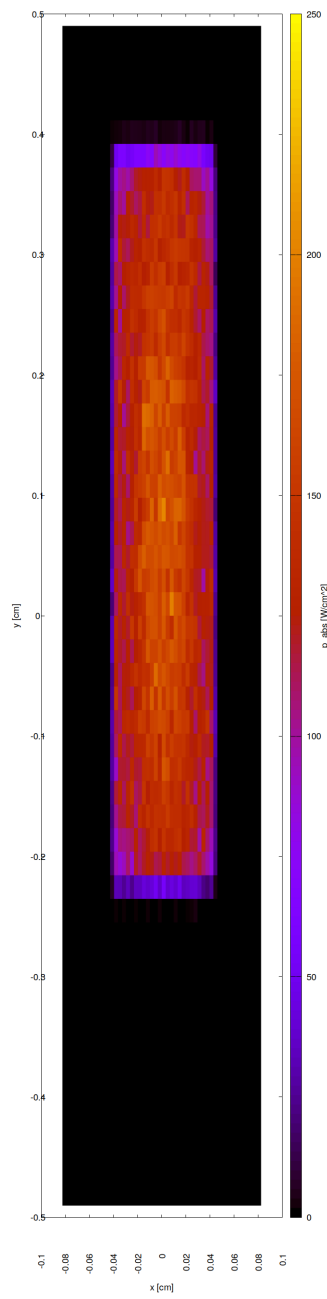


Figure 34.40: Absorbed irradiance on surface of optical element #04 (BS) for case #2 for 16955.9 eV photon energy setting.

"fig/Main\_beam\_C111\_Bragg/plot041.png" Lbl.:Main\_beam\_C111\_Bragg\_false\_colour\_plot\_p\_abs\_foot\_oe04\_c3\_16955.9eV

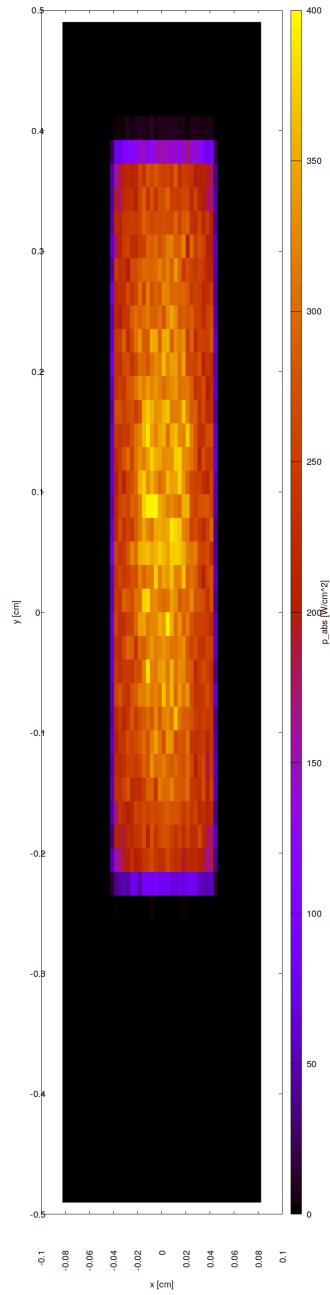


Figure 34.41: Absorbed irradiance on surface of optical element #04 (BS) for case #3 for 16955.9 eV photon energy setting.

```
"fig/Main_beam_C111_Bragg/plot042.png" Lbl.:Main_beam_C111_Bragg_false_colour_plot_p_abs_foot_oe04_c4_16955.9eV
```

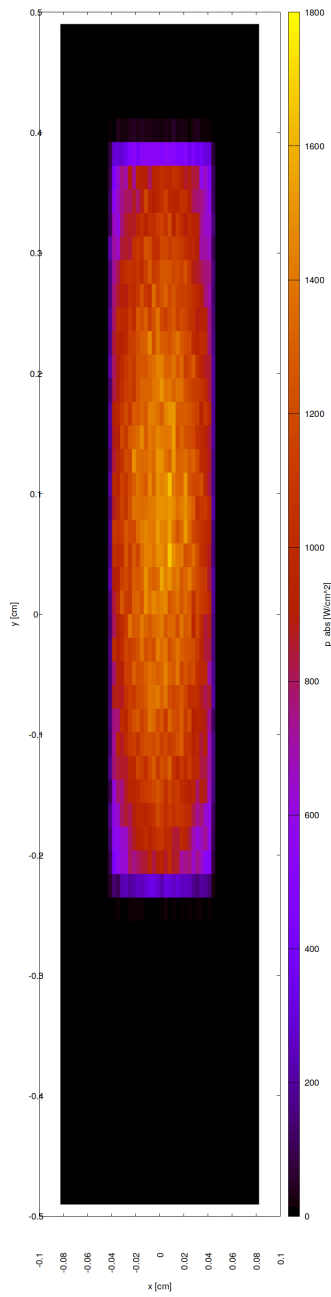


Figure 34.42: Absorbed irradiance on surface of optical element #04 (BS) for case #4 for 16955.9 eV photon energy setting.

### 34.9 Incident spectral flux on surface

"fig/Main\_beam\_C111\_Bragg/plot043.png" Lbl.:Main\_beam\_C111\_Bragg\_2d\_plot\_P\_spec\_spec\_oe04\_c2\_16955.9eV

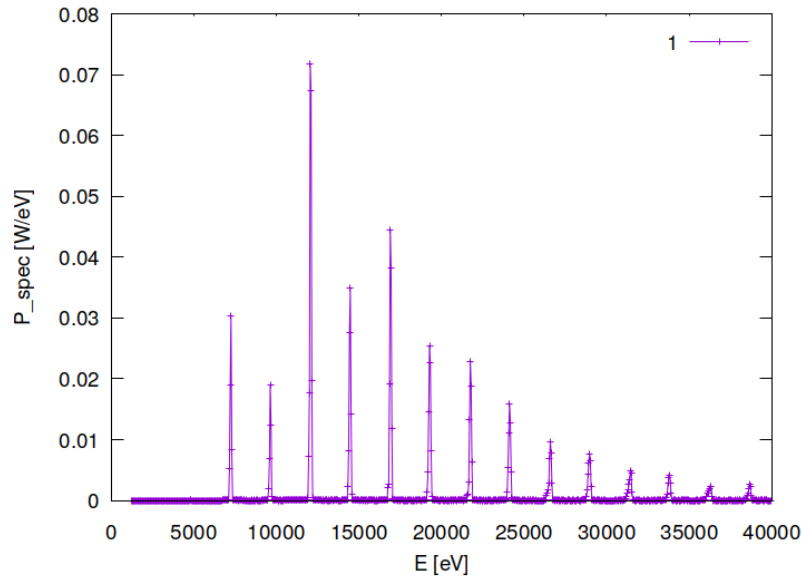


Figure 34.43: Incident spectral flux on surface of optical element #04 (BS) for case #2 for 16955.9 eV photon energy setting.

"fig/Main\_beam\_C111\_Bragg/plot044.png" Lbl.:Main\_beam\_C111\_Bragg\_2d\_plot\_P\_spec\_spec\_oe04\_c3\_16955.9eV

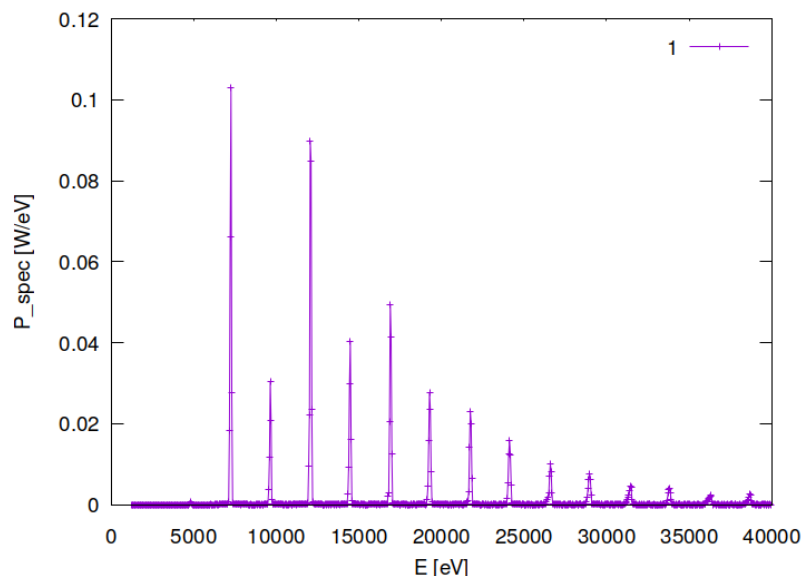


Figure 34.44: Incident spectral flux on surface of optical element #04 (BS) for case #3 for 16955.9 eV photon energy setting.

```
"fig/Main_beam_C111_Bragg/plot045.png" Lbl.:Main_beam_C111_Bragg_2d_plot_P_spec_spec_oe04_c4_16955.9eV
```

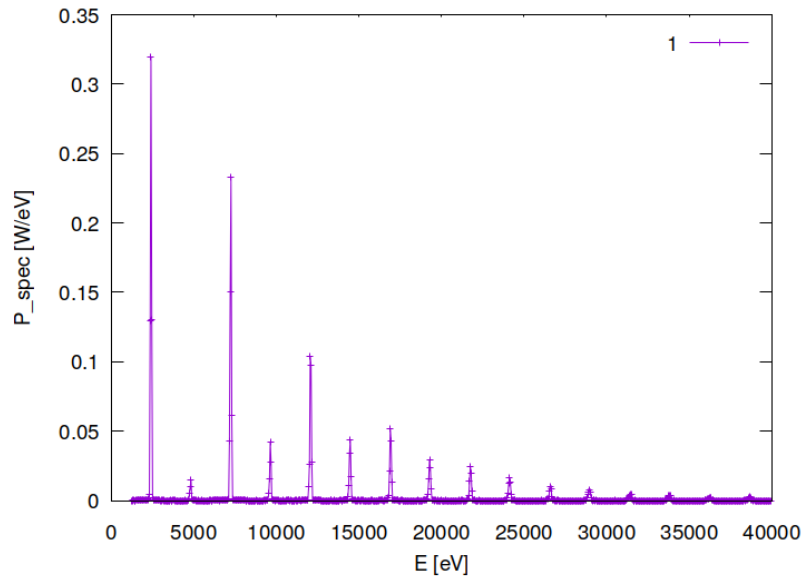


Figure 34.45: Incident spectral flux on surface of optical element #04 (BS) for case #4 for 16955.9 eV photon energy setting.



### 34.10 Temperature on surface

"fig/Main\_beam\_C111\_Bragg/plot046.png" Lbl.:Main\_beam\_C111\_Bragg\_false\_colour\_plot\_T\_oe04\_c2\_16955.9eV

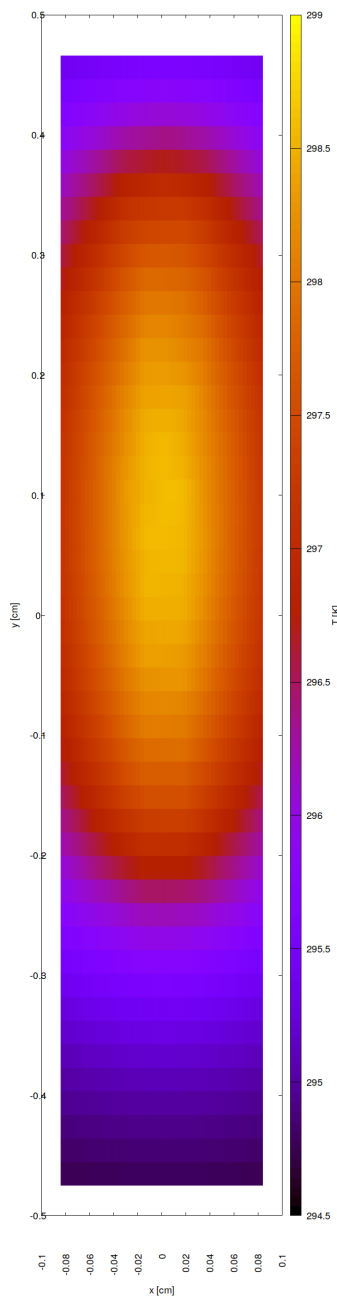


Figure 34.46: Temperature on surface of optical element #04 (BS) for case #2 for 16955.9 eV photon energy setting.

"fig/Main\_beam\_C111\_Bragg/plot047.png" Lbl.:Main\_beam\_C111\_Bragg\_false\_colour\_plot\_T\_oe04\_c3\_16955.9eV

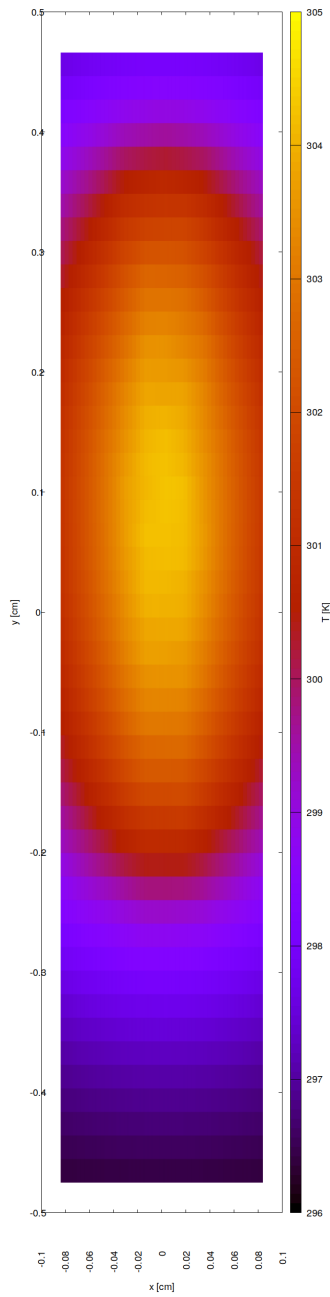


Figure 34.47: Temperature on surface of optical element #04 (BS) for case #3 for 16955.9 eV photon energy setting.

"fig/Main\_beam\_C111\_Bragg/plot048.png" Lbl.:Main\_beam\_C111\_Bragg\_false\_colour\_plot\_T\_oe04\_c4\_16955.9eV

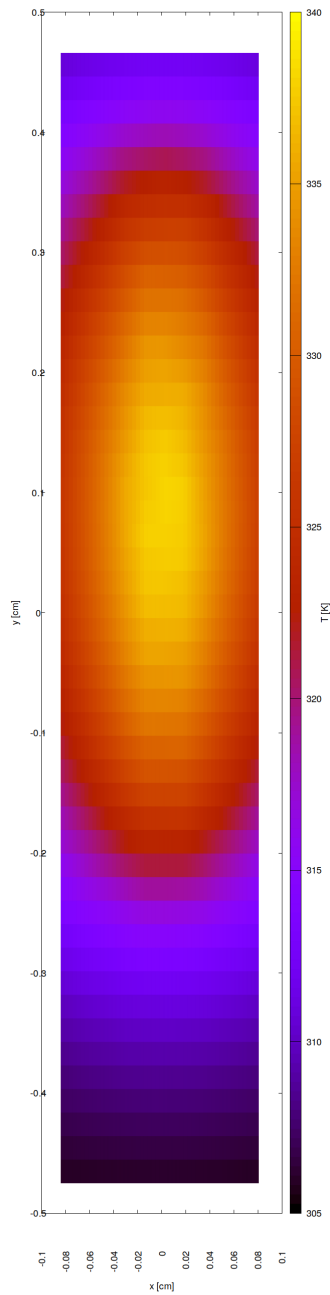


Figure 34.48: Temperature on surface of optical element #04 (BS) for case #4 for 16955.9 eV photon energy setting.



### 34.11 Mechanical stress (Von Mises stress) on surface

"fig/Main\_beam\_C111\_Bragg/plot049.png" Lbl.:Main\_beam\_C111\_Bragg\_false\_colour\_plot\_sigma\_oe04\_c2\_16955.9eV

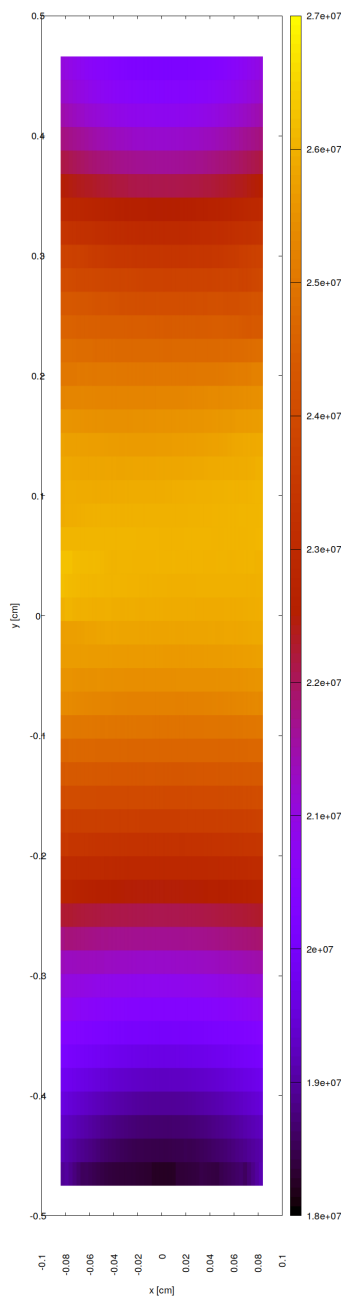


Figure 34.49: Mechanical stress (Von Mises stress) on surface of optical element #04 (BS) for case #2 for 16955.9 eV photon energy setting.  
452

"fig/Main\_beam\_C111\_Bragg/plot050.png" Lbl.:Main\_beam\_C111\_Bragg\_false\_colour\_plot\_sigma\_oe04\_c3\_16955.9eV

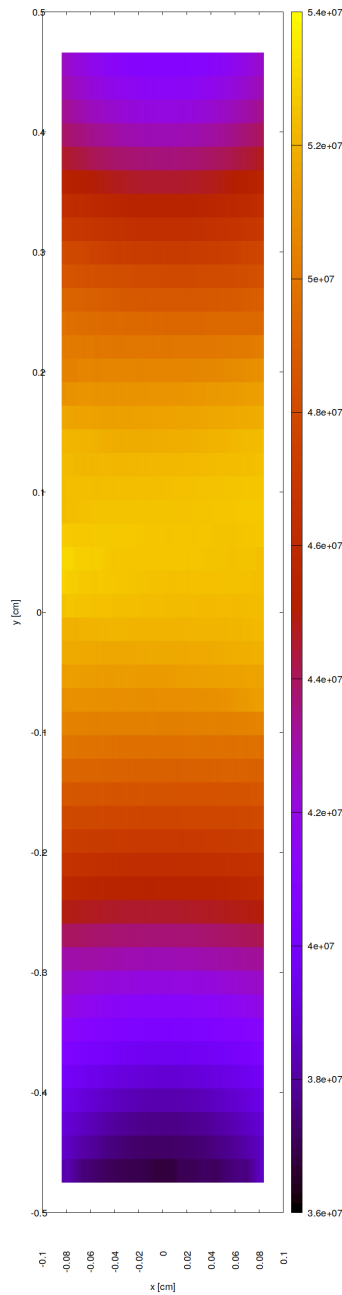


Figure 34.50: Mechanical stress (Von Mises stress) on surface of optical element #04 (BS) for case #3 for 16955.9 eV photon energy setting.

"fig/Main\_beam\_C111\_Bragg/plot051.png" Lbl.:Main\_beam\_C111\_Bragg\_false\_colour\_plot\_sigma\_oe04\_c4\_16955.9eV

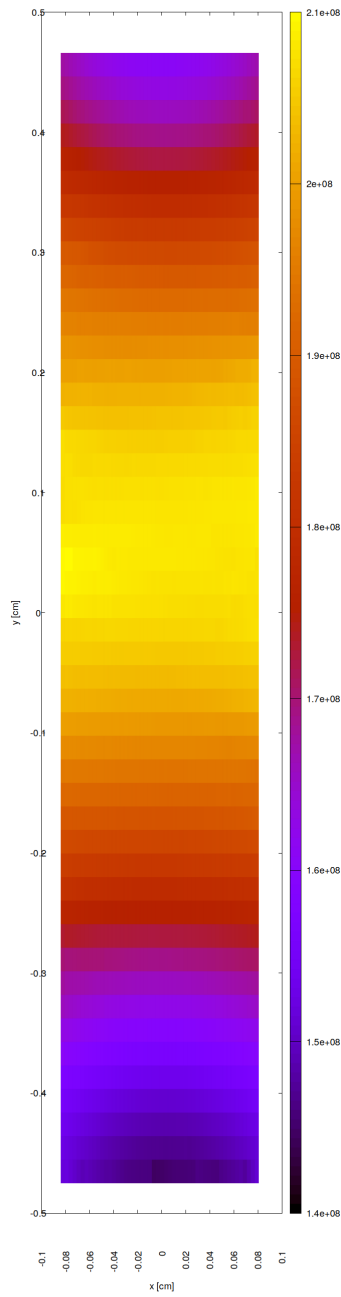


Figure 34.51: Mechanical stress (Von Mises stress) on surface of optical element #04 (BS) for case #4 for 16955.9 eV photon energy setting.



### 34.12 Surface slope error in meridional direction (y)

"fig/Main\_beam\_C111\_Bragg/plot052.png" Lbl.:Main\_beam\_C111\_Bragg\_false\_colour\_plot\_phi\_y\_oe04\_c2\_16955.9eV

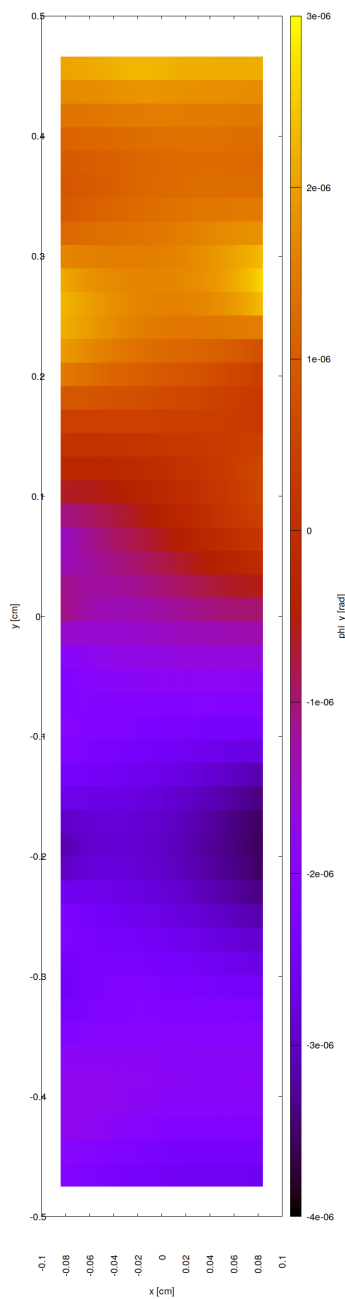


Figure 34.52: Surface slope error in meridional direction (y) of optical element #04 (BS) for case #2 for 16955.9 eV photon energy setting.  
456

"fig/Main\_beam\_C111\_Bragg/plot053.png" Lbl.:Main\_beam\_C111\_Bragg\_false\_colour\_plot\_phi\_y\_oe04\_c3\_16955.9eV

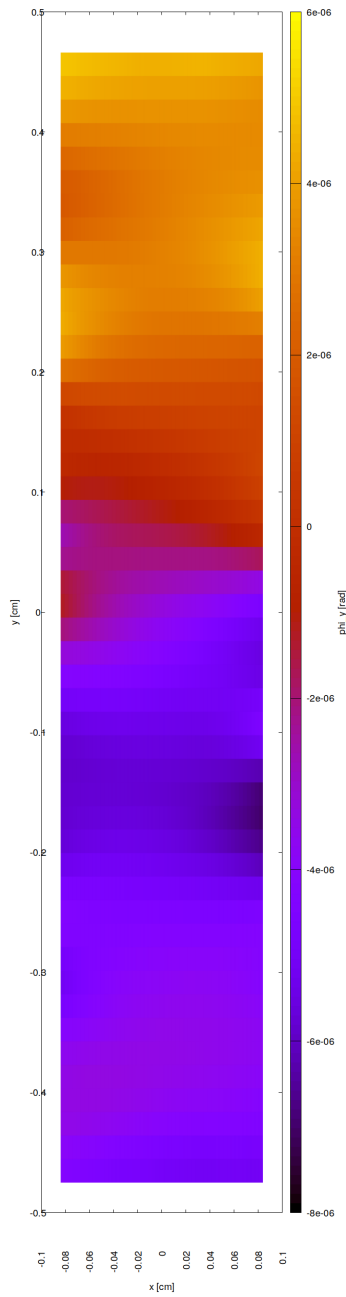


Figure 34.53: Surface slope error in meridional direction ( $y$ ) of optical element #04 (BS) for case #3 for 16955.9 eV photon energy setting.

"fig/Main\_beam\_C111\_Bragg/plot054.png" Lbl.:Main\_beam\_C111\_Bragg\_false\_colour\_plot\_phi\_y\_oe04\_c4\_16955.9eV

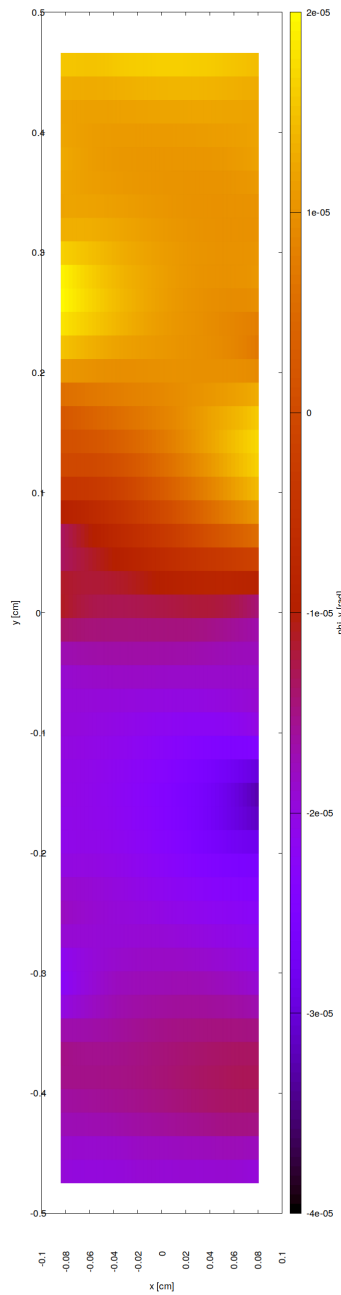


Figure 34.54: Surface slope error in meridional direction (y) of optical element #04 (BS) for case #4 for 16955.9 eV photon energy setting.



### 34.13 Incident photon irradiance on surface

```
"fig/Main_beam_C111_Bragg/plot055.png" Lbl.:Main_beam_C111_Bragg_false_colour_plot_I_inc_foot_oe04_c1_16955.9eV
```

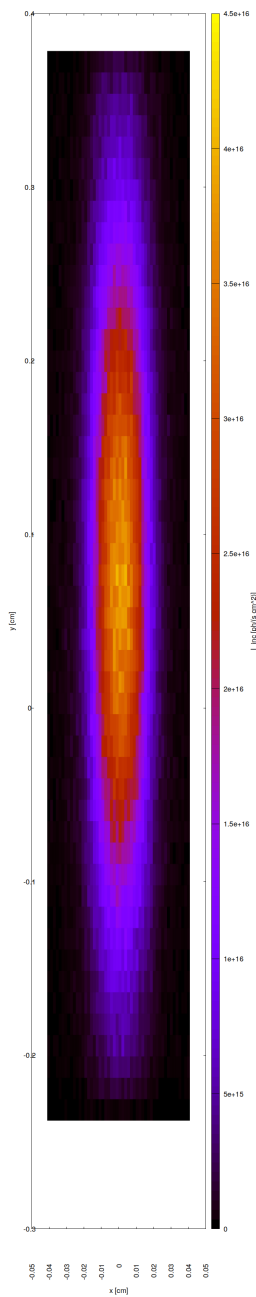


Figure 34.55: Incident photon irradiance on surface of optical element #04 (BS) for case #1 for 16955.9 eV photon energy setting.

```
"fig/Main_beam_C111_Bragg/plot056.png" Lbl.:Main_beam_C111_Bragg_false_colour_plot_I_inc_foot_oe04_c2_16955.9eV
```

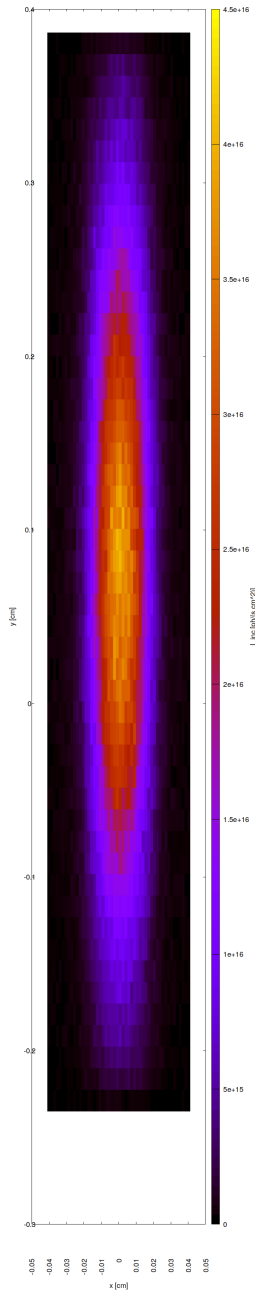


Figure 34.56: Incident photon irradiance on surface of optical element #04 (BS) for case #2 for 16955.9 eV photon energy setting.

```
"fig/Main_beam_C111_Bragg/plot057.png" Lbl.:Main_beam_C111_Bragg_false_colour_plot_I_inc_foot_oe04_c3_16955.9eV
```

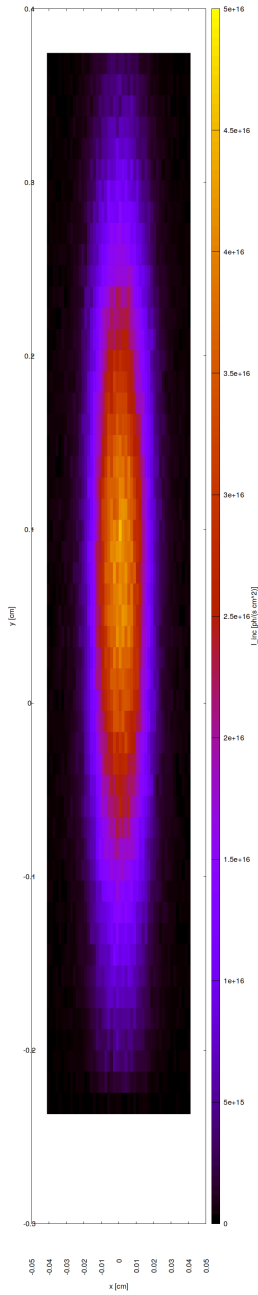


Figure 34.57: Incident photon irradiance on surface of optical element #04 (BS) for case #3 for 16955.9 eV photon energy setting.

```
"fig/Main_beam_C111_Bragg/plot058.png" Lbl.:Main_beam_C111_Bragg_false_colour_plot_I_inc_foot_oe04_c4_16955.9eV
```

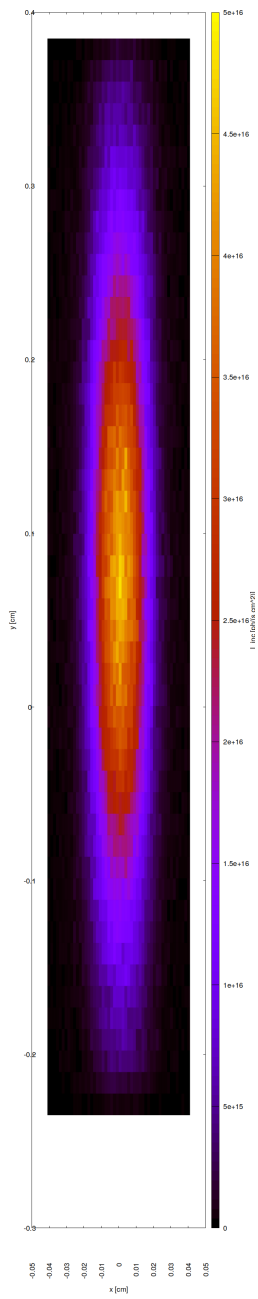


Figure 34.58: Incident photon irradiance on surface of optical element #04 (BS) for case #4 for 16955.9 eV photon energy setting.

"fig/Main\_beam\_C111\_Bragg/plot059.png" Lbl.:Main\_beam\_C111\_Bragg\_false\_colour\_plot\_I\_inc\_foot\_oe05\_c1\_16955.9eV

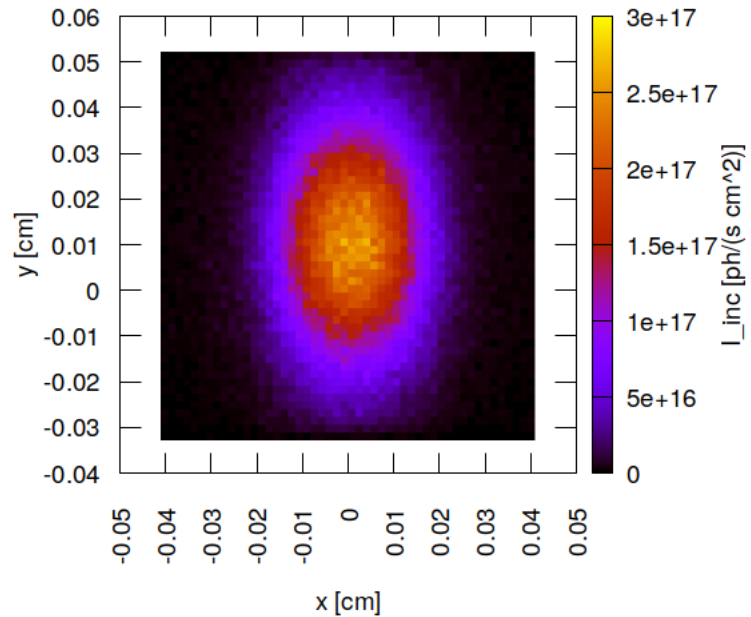


Figure 34.59: Incident photon irradiance on surface of optical element #05 (Dan-MAX) for case #1 for 16955.9 eV photon energy setting.

"fig/Main\_beam\_C111\_Bragg/plot060.png" Lbl.:Main\_beam\_C111\_Bragg\_false\_colour\_plot\_I\_inc\_foot\_oe05\_c2\_16955.9eV

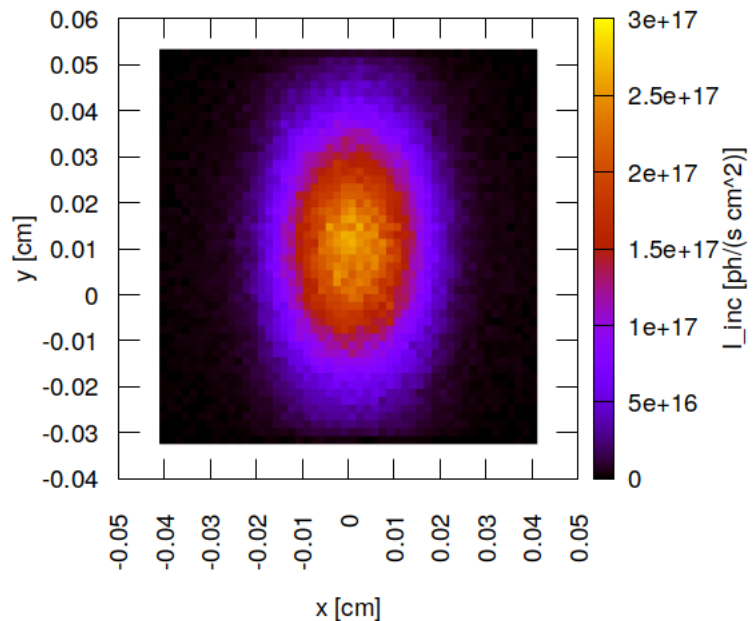


Figure 34.60: Incident photon irradiance on surface of optical element #05 (Dan-MAX) for case #2 for 16955.9 eV photon energy setting.

"fig/Main\_beam\_C111\_Bragg/plot061.png" Lbl.:Main\_beam\_C111\_Bragg\_false\_colour\_plot\_I\_inc\_foot\_oe05\_c3\_16955.9eV

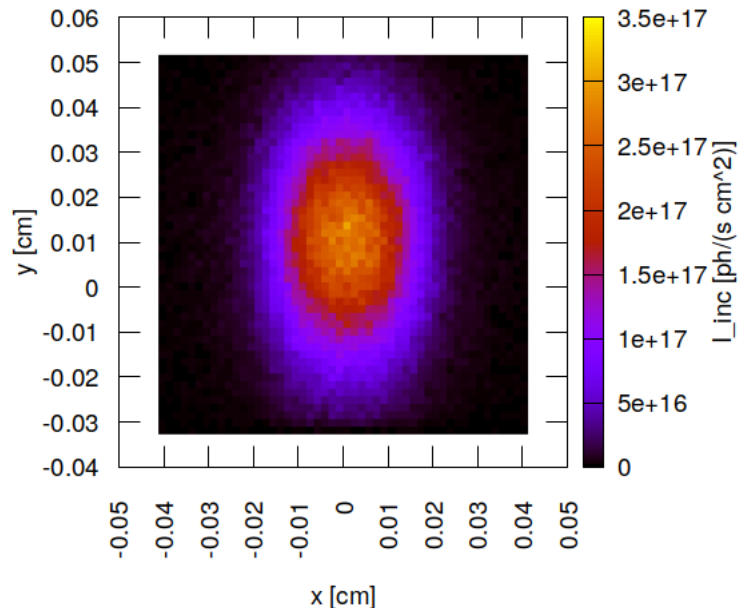


Figure 34.61: Incident photon irradiance on surface of optical element #05 (Dan-MAX) for case #3 for 16955.9 eV photon energy setting.

"fig/Main\_beam\_C111\_Bragg/plot062.png" Lbl.:Main\_beam\_C111\_Bragg\_false\_colour\_plot\_I\_inc\_foot\_oe05\_c4\_16955.9eV

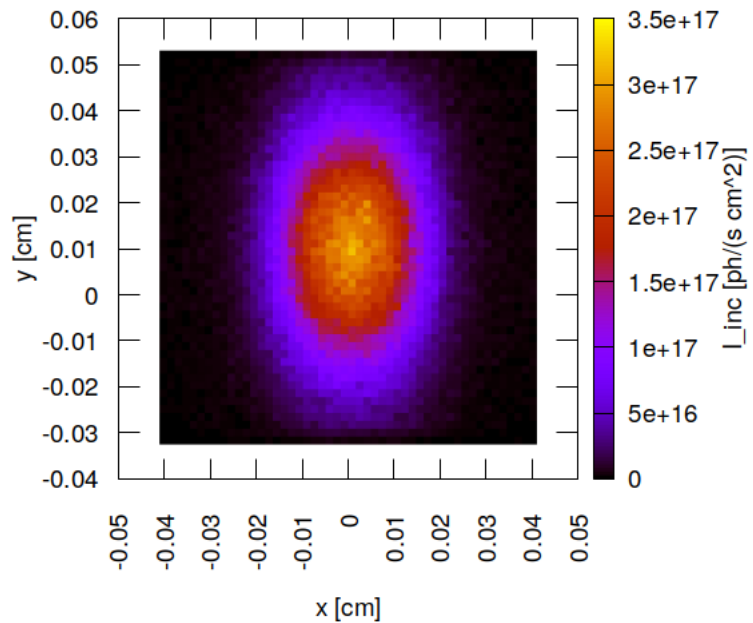


Figure 34.62: Incident photon irradiance on surface of optical element #05 (Dan-MAX) for case #4 for 16955.9 eV photon energy setting.



### 34.14 Photon irradiance in beam cross section

"fig/Main\_beam\_C111\_Bragg/plot063.png" Lbl.:Main\_beam\_C111\_Bragg\_false\_colour\_plot\_I\_foc\_oe04\_c1\_16955.9eV

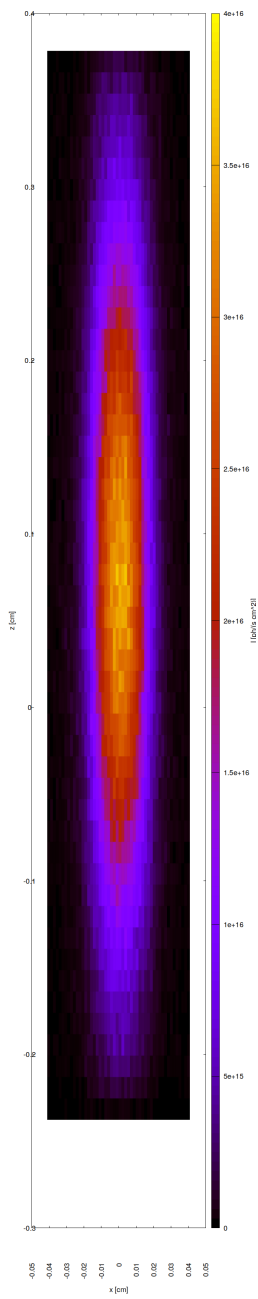


Figure 34.63: Photon irradiance in beam cross section of optical element #04 (BS) for case #1 for 16955.9 eV photon energy setting.

```
"fig/Main_beam_C111_Bragg/plot064.png" Lbl.:Main_beam_C111_Bragg_false_colour_plot_I_foc_oe04_c2_16955.9eV
```

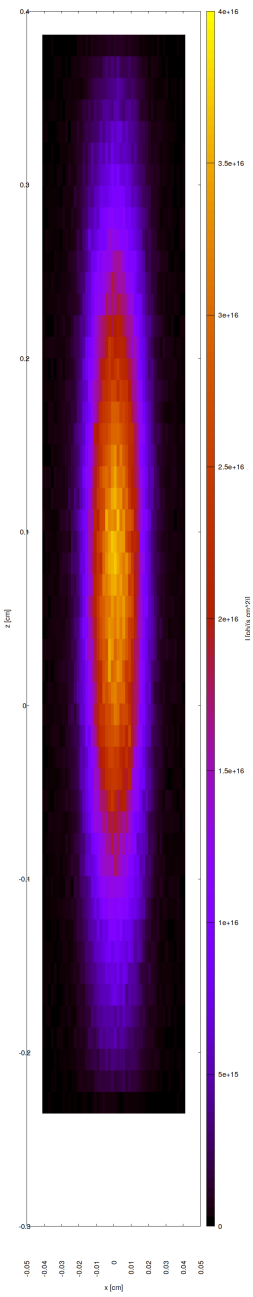


Figure 34.64: Photon irradiance in beam cross section of optical element #04 (BS) for case #2 for 16955.9 eV photon energy setting.

```
"fig/Main_beam_C111_Bragg/plot065.png" Lbl.:Main_beam_C111_Bragg_false_colour_plot_I_foc_oe04_c3_16955.9eV
```

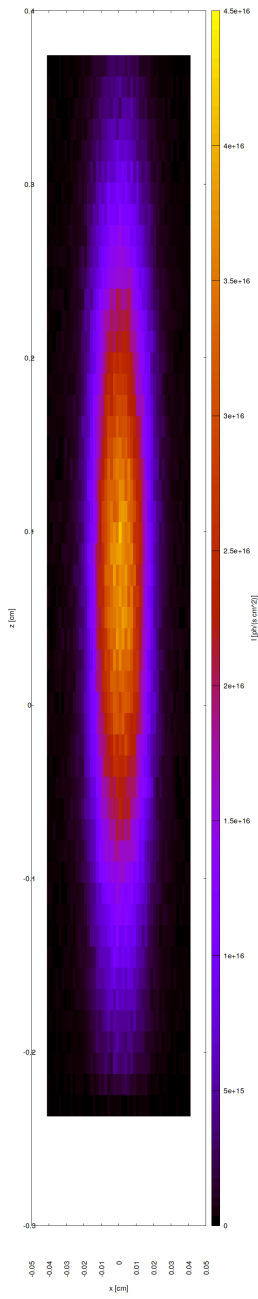


Figure 34.65: Photon irradiance in beam cross section of optical element #04 (BS) for case #3 for 16955.9 eV photon energy setting.

```
"fig/Main_beam_C111_Bragg/plot066.png" Lbl.:Main_beam_C111_Bragg_false_colour_plot_I_foc_oe04_c4_16955.9eV
```

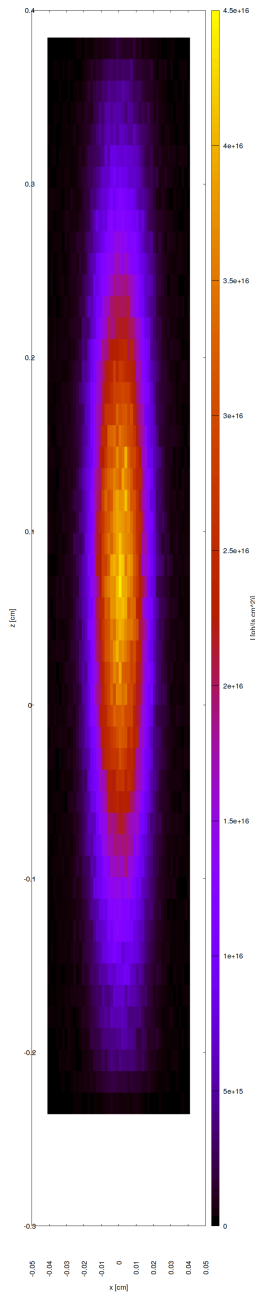


Figure 34.66: Photon irradiance in beam cross section of optical element #04 (BS) for case #4 for 16955.9 eV photon energy setting.

"fig/Main\_beam\_C111\_Bragg/plot067.png" Lbl.:Main\_beam\_C111\_Bragg\_false\_colour\_plot\_I\_foc\_oe05\_c1\_16955.9eV

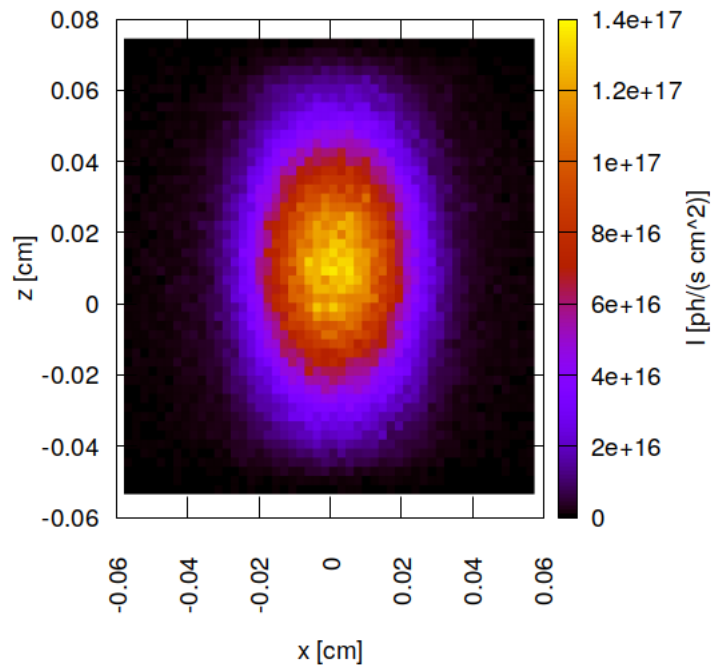


Figure 34.67: Photon irradiance in beam cross section of optical element #05 (Dan-MAX) for case #1 for 16955.9 eV photon energy setting.

"fig/Main\_beam\_C111\_Bragg/plot068.png" Lbl.:Main\_beam\_C111\_Bragg\_false\_colour\_plot\_I\_foc\_oe05\_c2\_16955.9eV

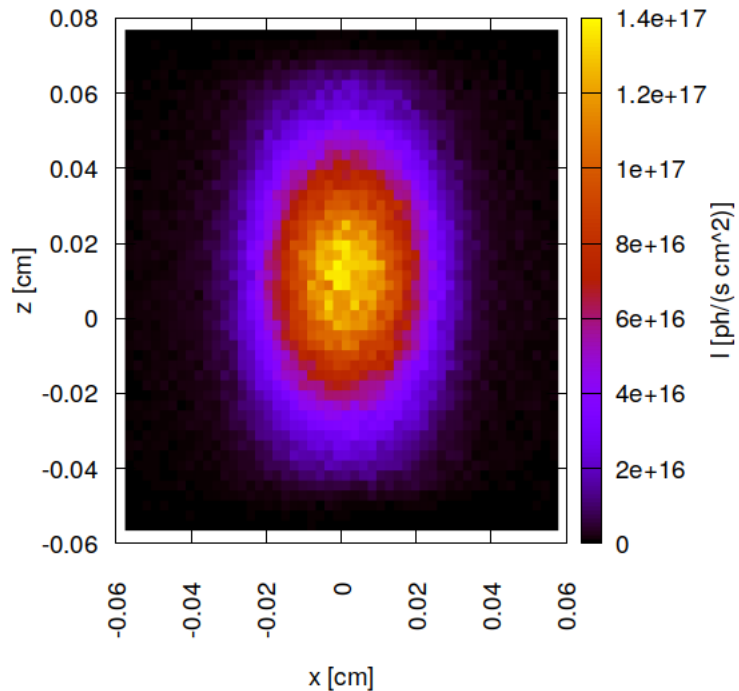


Figure 34.68: Photon irradiance in beam cross section of optical element #05 (Dan-MAX) for case #2 for 16955.9 eV photon energy setting.

"fig/Main\_beam\_C111\_Bragg/plot069.png" Lbl.:Main\_beam\_C111\_Bragg\_false\_colour\_plot\_I\_foc\_oe05\_c3\_16955.9eV

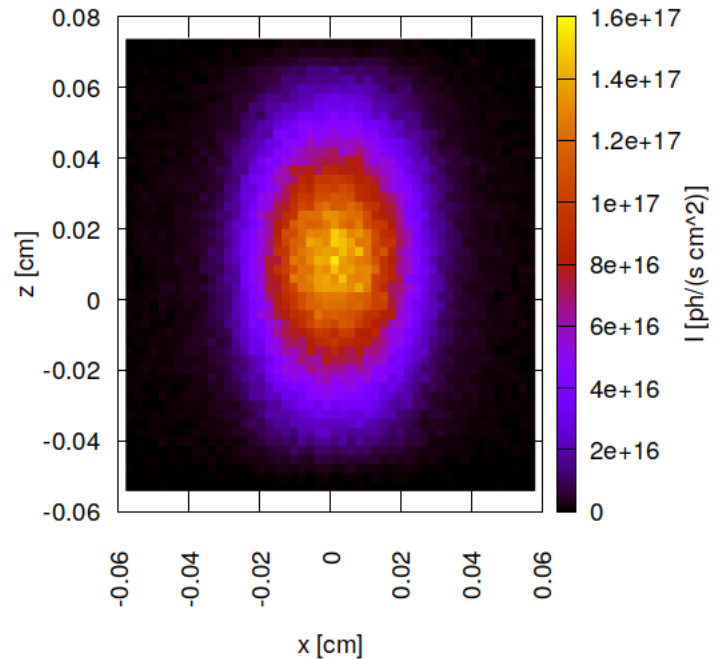


Figure 34.69: Photon irradiance in beam cross section of optical element #05 (Dan-MAX) for case #3 for 16955.9 eV photon energy setting.

"fig/Main\_beam\_C111\_Bragg/plot070.png" Lbl.:Main\_beam\_C111\_Bragg\_false\_colour\_plot\_I\_foc\_oe05\_c4\_16955.9eV

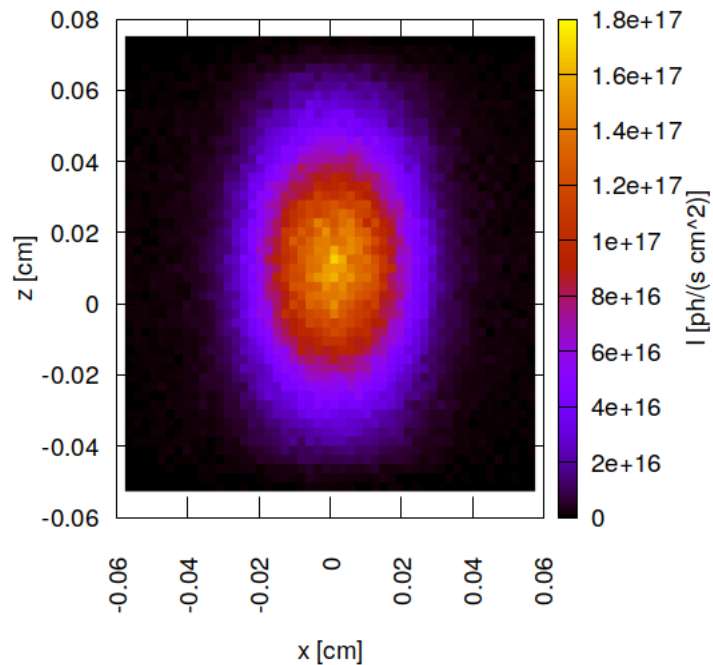


Figure 34.70: Photon irradiance in beam cross section of optical element #05 (Dan-MAX) for case #4 for 16955.9 eV photon energy setting.

### 34.15 Spectral photon flux in beam cross section

"fig/Main\_beam\_C111\_Bragg/plot071.png" Lbl.:Main\_beam\_C111\_Bragg\_2d\_plot\_I\_bandfoc\_oe04\_c1\_16955.9eV

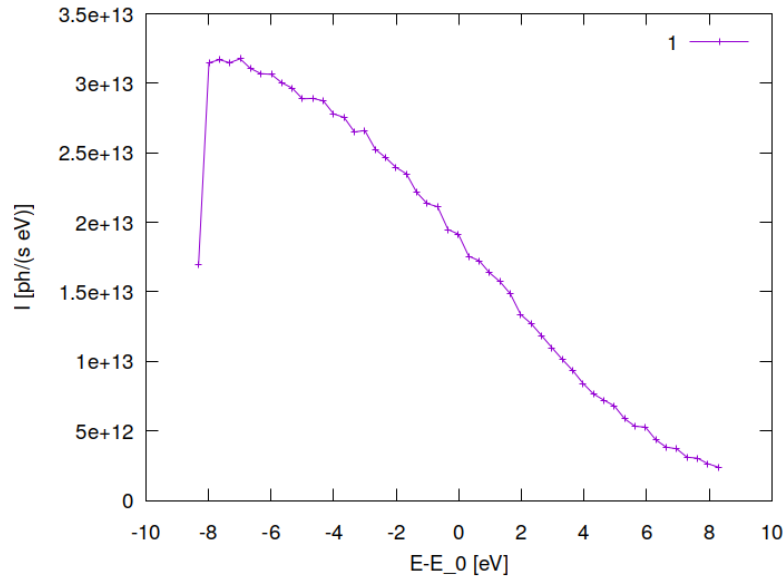


Figure 34.71: Spectral photon flux in beam cross section of optical element #04 (BS) for case #1 for 16955.9 eV photon energy setting.

"fig/Main\_beam\_C111\_Bragg/plot072.png" Lbl.:Main\_beam\_C111\_Bragg\_2d\_plot\_I\_bandfoc\_oe04\_c2\_16955.9eV

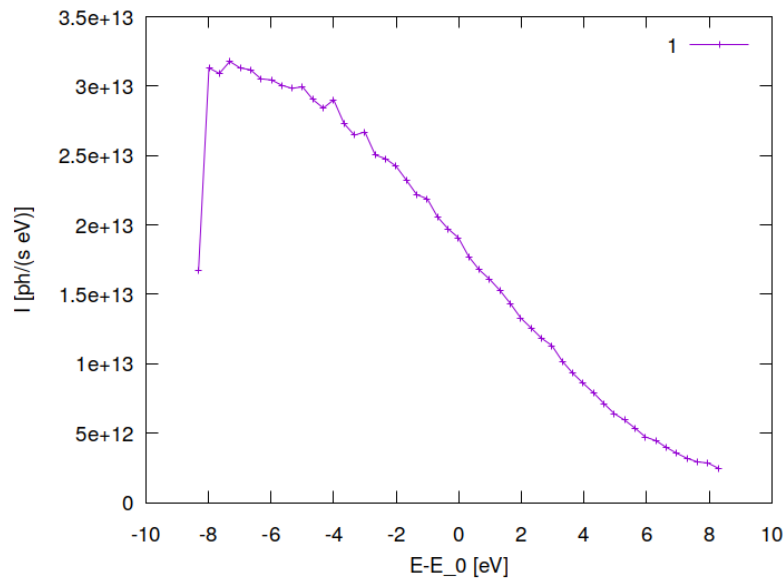


Figure 34.72: Spectral photon flux in beam cross section of optical element #04 (BS) for case #2 for 16955.9 eV photon energy setting.

```
"fig/Main_beam_C111_Bragg/plot073.png" Lbl.:Main_beam_C111_Bragg_2d_plot_I_bandfoc_oe04_c3_16955.9eV
```

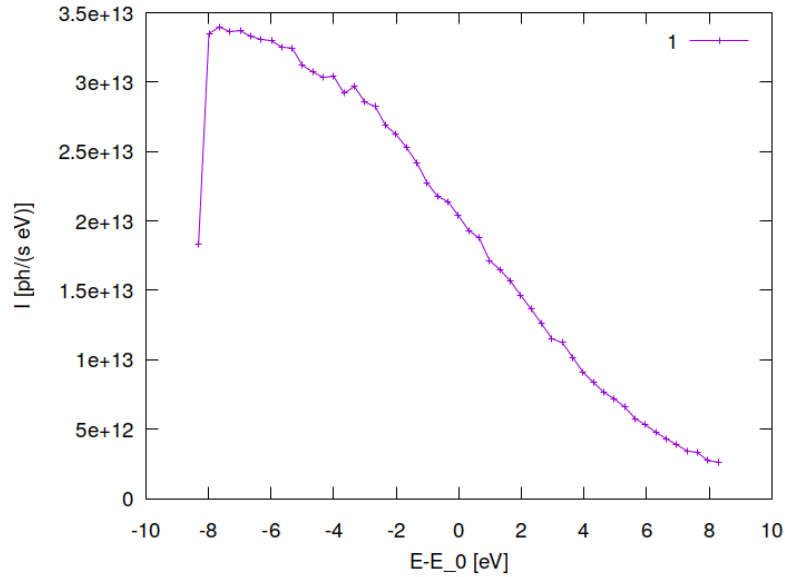


Figure 34.73: Spectral photon flux in beam cross section of optical element #04 (BS) for case #3 for 16955.9 eV photon energy setting.

```
"fig/Main_beam_C111_Bragg/plot074.png" Lbl.:Main_beam_C111_Bragg_2d_plot_I_bandfoc_oe04_c4_16955.9eV
```

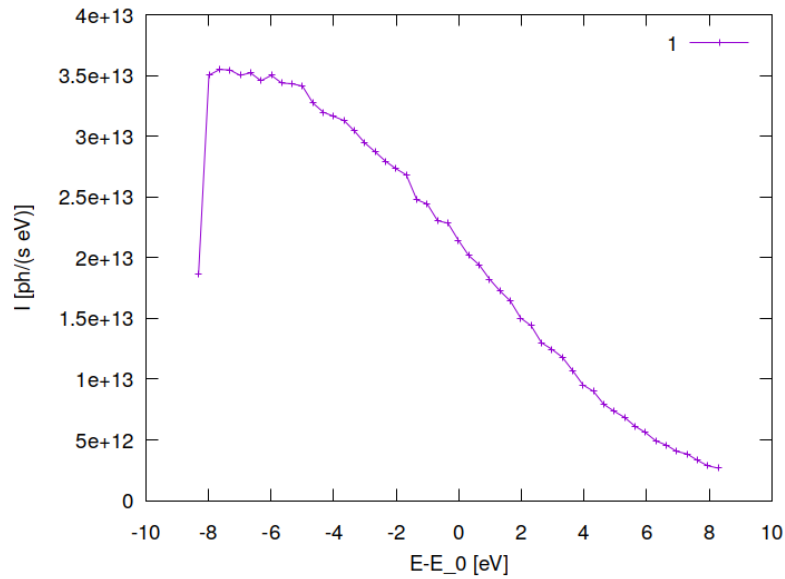


Figure 34.74: Spectral photon flux in beam cross section of optical element #04 (BS) for case #4 for 16955.9 eV photon energy setting.

```
"fig/Main_beam_C111_Bragg/plot075.png" Lbl.:Main_beam_C111_Bragg_2d_plot_I_bandfoc_oe05_c1_16955.9eV
```

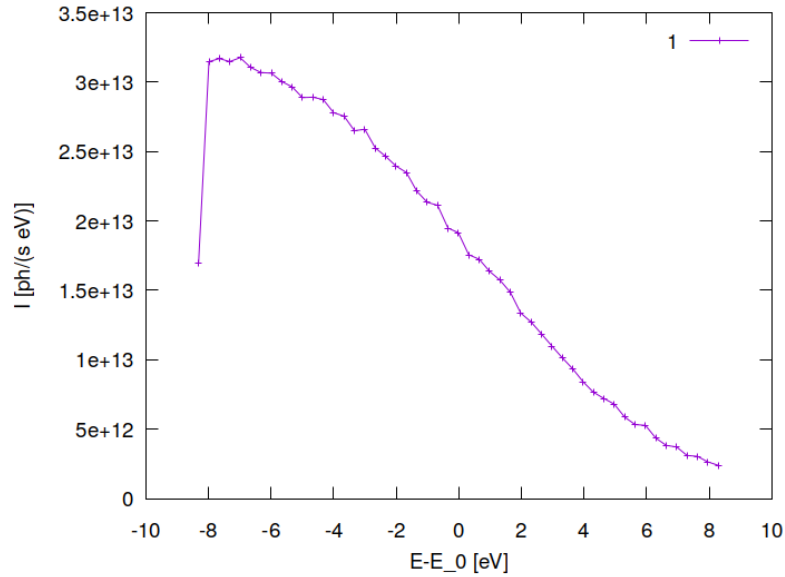


Figure 34.75: Spectral photon flux in beam cross section of optical element #05 (DanMAX) for case #1 for 16955.9 eV photon energy setting.

```
"fig/Main_beam_C111_Bragg/plot076.png" Lbl.:Main_beam_C111_Bragg_2d_plot_I_bandfoc_oe05_c2_16955.9eV
```

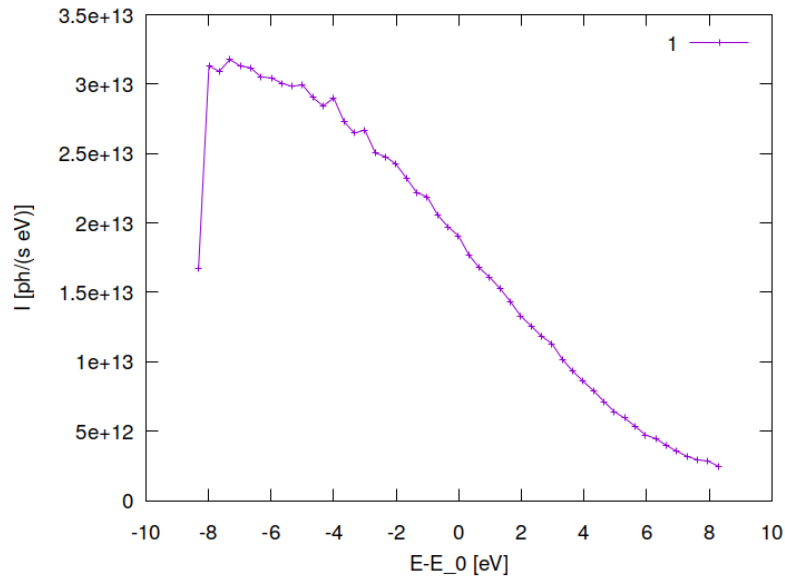


Figure 34.76: Spectral photon flux in beam cross section of optical element #05 (DanMAX) for case #2 for 16955.9 eV photon energy setting.

```
"fig/Main_beam_C111_Bragg/plot077.png" Lbl.:Main_beam_C111_Bragg_2d_plot_I_bandfoc_oe05_c3_16955.9eV
```

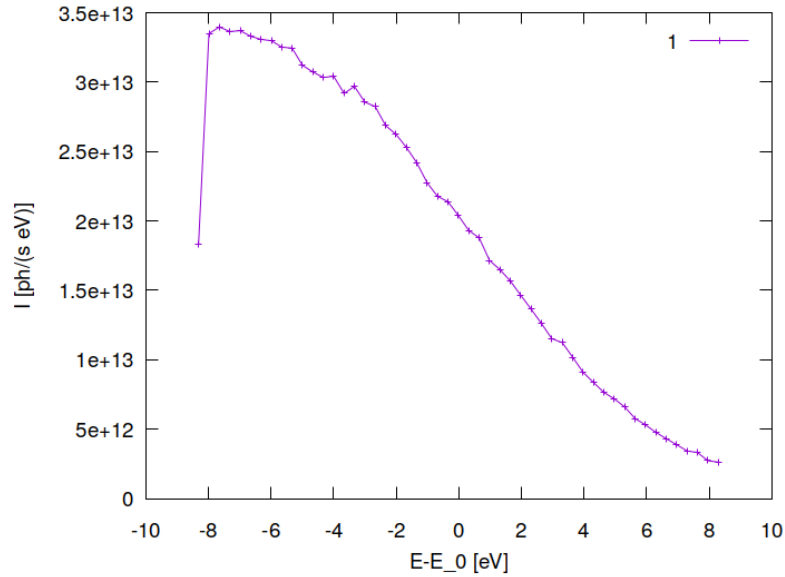


Figure 34.77: Spectral photon flux in beam cross section of optical element #05 (DanMAX) for case #3 for 16955.9 eV photon energy setting.

```
"fig/Main_beam_C111_Bragg/plot078.png" Lbl.:Main_beam_C111_Bragg_2d_plot_I_bandfoc_oe05_c4_16955.9eV
```

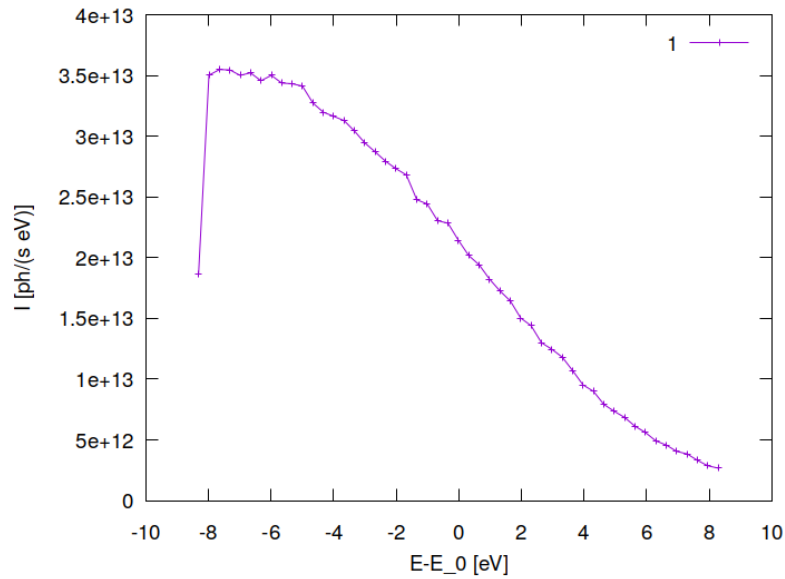


Figure 34.78: Spectral photon flux in beam cross section of optical element #05 (DanMAX) for case #4 for 16955.9 eV photon energy setting.

# Chapter 35

## Discussion of results

In general, the beam splitter has very little effect on the transmitted main beam, that is going to DanMAX. The only exception to this rule is, if both branches are using the same undulator harmonic. This has been discussed in an earlier analysis using analytical expressions for rocking curves and the DuMond diagram 29. Small changes in beam splitter angle then can have considerable changes in flux also in the transmitted beam, which by default is highly undesirable.

Far from fulfilling the Bragg condition, i.e. if using a different harmonic in the main branch, the beam splitter simply acts as a refractive element, altering the transmitted beam by refraction and absorption only.

### 35.1 Absorption

Here, absorption has the stronger, more obvious effect. There is a small reduction of total flux, in Laue geometry of the order of 1-2% (see 28.32) in Bragg geometry of about 10% (see 34.32). The considerably higher absorption in Bragg geometry is simply because of the longer path length in the beam splitter due to the shallower incidence.

### 35.2 Refraction

Refraction could refocus the beam or introduce aberrations. Refocussing should express itself directly by a change of divergence or indirectly by a change of beam diameter at a distance. If easily computable, the position of the focal spot on the optical axis is a very sensitive indicator for focussing. In ray-tracing, one is in the very fortunate situation that this position is indeed easily computable. By taking the first derivative of the ray position  $x$  as function of the ray direction  $x'$  one obtains directly the distance of the focus to this plane 2.6,  $dx/dx' = l$ . For a perfect beam in par-axial approximation originating from a point-like source the ray position is indeed a linear function of the ray direction and one obtains an unequivocal value for the first derivative, i.e. the slope of the straight line. For an imperfect beam one obtains a stretched and more or less straight point cloud. The slope has to be determined by linear regression. As a bonus, this approach delivers an indicator for the beam quality, namely the correlation coefficient  $r_{xx'}$  of the linear regression. It is one for a straight line, where  $x$  and  $x'$  are 100% correlated and gets smaller the further one is away from this ideal case. For example, due to the larger horizontal source size, the beam has a somewhat smaller correlation coefficient of  $r_{xx'} = 0.97$  in the horizontal compared to  $r_{yy'} = 0.9996$  in the vertical.

None of these indicators show any effect from the deformation of the beam splitter under heat load. Beam diameter ten metres behind the beam splitter is the same with and without deformation (Figs. 28.19, 28.21, 34.19 and 34.21) within noise level. The beam splitter represents only two slightly bent surfaces – smallest bending radius is of the order of hundreds of metres – which are also mostly parallel. Comparing this even to relatively weak compound refractive lenses consisting of dozens of biconcave lens elements with sub-millimetre radii of curvature, this is to be expected.

## **Part III**

# **Focussing with CRLs**

## Chapter 36

# Focussing setup with beam splitter in Laue geometry

A thin CVD diamond crystal is employed as a diffractive beam splitter, using the 111 reflection in Laue geometry. The diamond 111 reflection diverts radiation within a narrow bandwidth of

$$\delta E/E = \delta\theta/\tan\theta$$

to the SinCrys side station. The thickness of the diamond crystal slab has been optimised in order to maximise 111 reflectivity under the constraint of keeping absorption of the transmitted main beam low.

Subsequent reflection from a second crystal of the same material using the same set of diffracting planes which are parallel to the first is required to provide the necessary stability of the exit beam which has to hit the very small acceptance aperture of the CRLs (see chapter 23.3).

Putting the second crystal at a distance of around 3.66 metres behind the first provides the required offset of more than one metre between the twice deflected beam and the main beam.

Compound refractive lenses (CRL) are used to focus the monochromatised beam onto the sample. Even if flat, the beam splitter is focusing the beam in meridional direction due to its asymmetric transmission geometry 2.5. This generates an astigmatism that needs to be addressed in the design of the CRL. A stack of two-dimensionally focussing lenses has to be complemented by a stack of vertically focussing one-dimensional lenses compensating for the astigmatism.

Apart from focussing the beam splitter introduces aberrations to the beam which can be partially compensated by bending it meridionally to a concave cylindrical shape. The pragmatic approach was taken to vary the beam splitter's bending radius until the focal spot size was minimum at best focus of the CRLs. A radius of  $R = 41.77$  m was found to provide smallest focus.

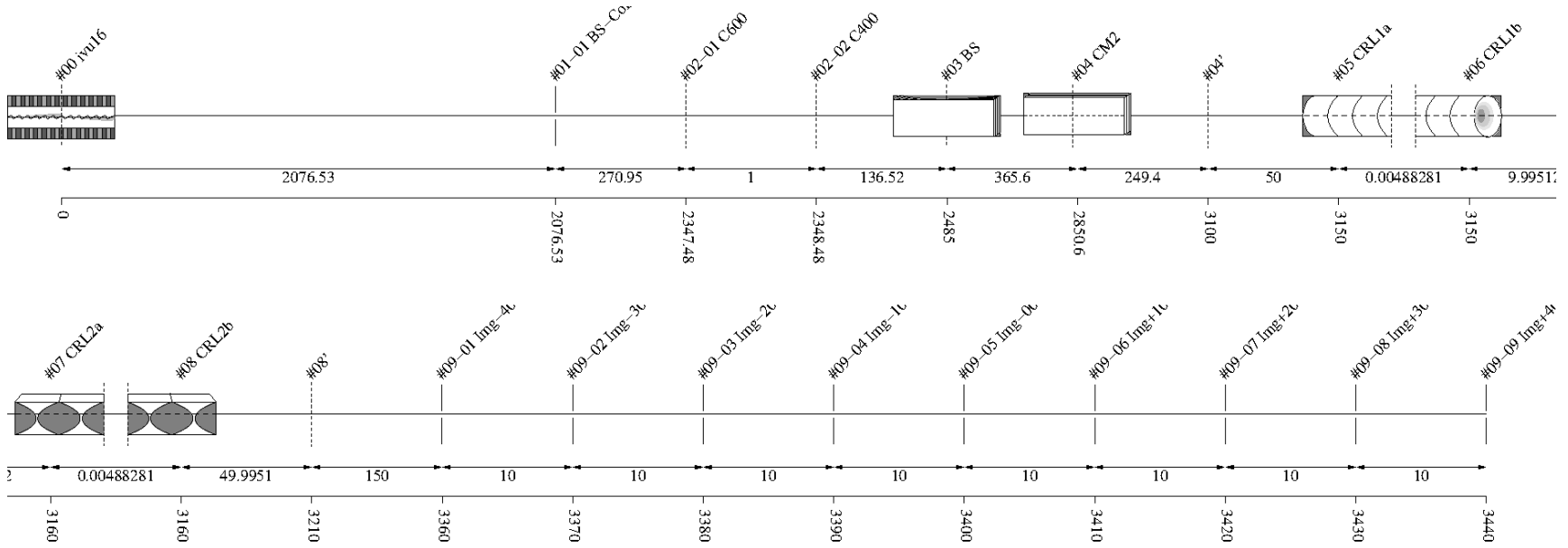


Figure 36.1: Schematic of optical setup

#	Name	Pathlen. cm	Descript.	Shape	Pitch* deg	Roll deg	Yaw deg	x_min cm	x_max cm	y_min cm	y_max cm	Thick. cm	Surface
0	ivu16	0	undulator	auto	0	0	0	-0.0027	0.0027	-0.0002	0.0002	auto	
1		2076.53	none	plane	0	0	0	-inf	inf	-inf	inf		perfect
1-1	BS-Collim	2076.53	aperture	rectangle	0	0	0	-0.035	0.035	-0.035	0.035		
2	Filter	2347.48	none	plane	0	0	0	-inf	inf	-inf	inf		perfect
2-1	C600	2347.48	C-filter	rectangle	0	0	0	-inf	inf	-inf	inf	0.06	

<b>2-2</b>	C400	2348.48	C-filter	rectangle	0	0	0	-inf	inf	-inf	inf	0.04	
<b>3</b>	BS	2485	C(1,1,1)-crystal	cylinder	133.197	90	0	-0.15	0.15	-0.15	0.15		heat bump
<b>4</b>	CM2	2850.6	C(1,1,1)-crystal	plane	7.93694	180	0	-inf	inf	-inf	inf		perfect
<b>4'</b>		3100	continuation plane		0	0	0						
<b>5</b>	CRL1a	3150	vac/Be-lens surface	parabola	0	0	0	-0.045	0.045	-0.045	0.045		perfect
<b>6</b>	CRL1b	3150	Be/vac-lens surface	parabola	0	0	0	-0.045	0.045	-0.045	0.045		perfect
<b>7</b>	CRL2a	3160	vac/Be-lens surface	extruded parabola	0	-90	0	-0.1	0.1	-0.085	0.085		perfect
<b>8</b>	CRL2b	3160	Be/vac-lens surface	extruded parabola	0	0	0	-0.1	0.1	-0.085	0.085		perfect
<b>8'</b>		3210	continuation plane		0	0	0						
<b>9</b>	sample	3400	none	plane	0	0	0	-inf	inf	-inf	inf		perfect
<b>9-1</b>	Img-40	3360	aperture	rectangle	0	0	0	-0.025	0.025	-0.025	0.025		
<b>9-2</b>	Img-30	3370	aperture	rectangle	0	0	0	-0.025	0.025	-0.025	0.025		
<b>9-3</b>	Img-20	3380	aperture	rectangle	0	0	0	-0.025	0.025	-0.025	0.025		
<b>9-4</b>	Img-10	3390	aperture	rectangle	0	0	0	-0.025	0.025	-0.025	0.025		
<b>9-5</b>	Img-00	3400	aperture	rectangle	0	0	0	-0.025	0.025	-0.025	0.025		
<b>9-6</b>	Img+10	3410	aperture	rectangle	0	0	0	-0.025	0.025	-0.025	0.025		
<b>9-7</b>	Img+20	3420	aperture	rectangle	0	0	0	-0.025	0.025	-0.025	0.025		
<b>9-8</b>	Img+30	3430	aperture	rectangle	0	0	0	-0.025	0.025	-0.025	0.025		
<b>9-9</b>	Img+40	3440	aperture	rectangle	0	0	0	-0.025	0.025	-0.025	0.025		

Table 36.1: Setup parameters common to all components. (\*Glancing angle for mirrors, multilayers and crystals. Angle to surface normal otherwise.)

**Rays:** Polar type = total

Polar phase = 0 deg

Polar degree = 0

Is coherent = no

**Spectrum:** E min = 500 eV

E max = 40000 eV

Relative linewidth = 1

**Band:** Bandwidth = 0.0005

**Insertion Device:** lambda period = 1.6 cm

n period = 187

I electron = 0.5 A

E electron = 3 GeV

y horizontal waist = 0 cm

y vertical waist = 0 cm

epsilon x = 3.2E-08 cm rad

epsilon z = 8E-10 cm rad

K y = 1.66

K ymax = 1.7

Divergence limit = 5E-05 rad

**Undulator:** n harmonic max = 99

Tuning type = fixed gap

l aperture = 2076.53 cm

dx aperture = 0.07 cm

dz aperture = 0.07 cm

#1

**Screen:** Is absorbing[1] = no

**Shape:** Thickness = 0 cm

#2 Filter

**Screen:** Is absorbing[1] = yes

Is absorbing[2] = yes

Molecular formula[1] = C

Molecular formula[2] = C

Mass density[1] = 3.5 g/cm^3

Mass density[2] = 3.5 g/cm^3

Thickness[1] = 0.06 cm

Thickness[2] = 0.04 cm

**Shape:** Thickness = 0 cm

### #3 BS

**Grating:** n order = -1

**Crystal:** Structure type = zincblende

Lattice constant[1] = 3.567 Angstrom  
Lattice constant[2] = 3.567 Angstrom  
Lattice constant[3] = 3.567 Angstrom  
Debye Waller factor = 1  
Is absorbing = yes  
Is asymmetric = yes  
Angle asymmetry = 125.26 deg  
Is inclined = no  
Is Johansson geometry = no  
Is mosaic = no

**Tune:** z rotation axis = 0 cm

**Geometry:** Is thin = yes

Tune automatic = yes

**Shape:** Defined by = user

Is convex = no  
Is extruded = yes  
Radius = 4177 cm  
Thickness = 0.01 cm

**Boundary:** Type = rectangle

x rim = 0.5 cm  
y rim = 0.5 cm

**Extruded:** Angle z = 0 deg

**Surface:** Is rough = no

**FEA:** Design type = type specific

Crystal design = laue with cooling loop  
Is isotropic = no  
Angle x = 45 deg  
Angle y = 35.2644 deg  
Angle z = 0 deg  
Mass density = 3.516 g/cm<sup>3</sup>

**Heat:** Heat transfer type[1] = insulated

Heat transfer type[2] = heat transfer  
Heat transfer type[3] = insulated  
Heat transfer type[4] = insulated

Heat transfer type[5] = heat transfer  
 Heat transfer type[6] = flux  
 Heat transfer type[7] = insulated  
 Heat transfer type[8] = heat transfer  
 Heat transfer type[9] = heat sink  
 Heat transfer coefficient = 1 W/(cm^2K)  
 Heat sink coefficient = 10 W/(cm^2K)  
 T reference = 293.15 K  
 T cooling = 293.15 K  
 Heat capacity = 0.54 J/(gK)  
 Thermal conductivity[1] = 25 W/(cmK^n)

**Stress and strain:** Constraint[1] = free  
 Constraint[2] = kinematic  
 Constraint[3] = free  
 Constraint[4] = free  
 Constraint[5] = free  
 Constraint[6] = free  
 Constraint[7] = free  
 Constraint[8] = free  
 Constraint[9] = free  
 Thermal expansion tensor[1] = 1.1E-06 1/K  
 Thermal expansion tensor[2] = 1.1E-06 1/K  
 Thermal expansion tensor[3] = 1.1E-06 1/K  
 Thermal expansion tensor[4] = 0 1/K  
 Thermal expansion tensor[5] = 0 1/K  
 Thermal expansion tensor[6] = 0 1/K  
 Stiffness tensor(1)(1) = 1.07861E+12 Pa  
 Stiffness tensor(2)[1] = 1.2663E+11 Pa  
 Stiffness tensor(2)[2] = 1.07861E+12 Pa  
 Stiffness tensor(3)[1] = 1.2663E+11 Pa  
 Stiffness tensor(3)[2] = 1.2663E+11 Pa  
 Stiffness tensor(3)[3] = 1.07861E+12 Pa  
 Stiffness tensor(4)[1] = 0 Pa  
 Stiffness tensor(4)[2] = 0 Pa  
 Stiffness tensor(4)[3] = 0 Pa  
 Stiffness tensor(4)[4] = 5.7756E+11 Pa  
 Stiffness tensor(5)[1] = 0 Pa  
 Stiffness tensor(5)[2] = 0 Pa  
 Stiffness tensor(5)[3] = 0 Pa  
 Stiffness tensor(5)[4] = 0 Pa  
 Stiffness tensor(5)[5] = 5.7756E+11 Pa  
 Stiffness tensor(6)[1] = 0 Pa  
 Stiffness tensor(6)[2] = 0 Pa  
 Stiffness tensor(6)[3] = 0 Pa  
 Stiffness tensor(6)[4] = 0 Pa  
 Stiffness tensor(6)[5] = 0 Pa  
 Stiffness tensor(6)[6] = 5.7756E+11 Pa

#### #4 CM2

**Crystal:** Structure type = zinblend  
 Lattice constant[1] = 3.567 Angstrom

Lattice constant[2] = 3.567 Angstrom  
Lattice constant[3] = 3.567 Angstrom  
Debye Waller factor = 1  
Is absorbing = yes  
Is asymmetric = no  
Is inclined = no  
Is Johansson geometry = no  
Is mosaic = no

**Tune:** Type = constant pathlength  
Are downstream elements fixed = no

**Geometry:** Is thin = no  
Tune automatic = yes

**Boundary:** Type = none

**Surface:** Is rough = no

## #5 CRL1a

**Dielectric:** Reflectivity type = polarisation  
Is constant = no  
Mass density = 1.85 g/cm<sup>3</sup>

**Geometry:** g = 3150 cm  
b = 250 cm  
Is thin = yes  
n clones = 5  
n originals = 2  
Focus automatically = yes

**Focus:** Type = chromatic  
Number variation method = cloning  
Vary distance = no

**Shape:** Defined by = user  
Is convex = no  
Is extruded = no  
Radius = 0.02 cm  
Thickness = 0.005 cm

**Boundary:** Type = ellipse

**Parabola:** Is source in infinity = no  
p semi = 0.02 cm

**Surface:** Is rough = no

### #6 CRL1b

**Dielectric:** Reflectivity type = polarisation

Is constant = yes

delta refraction = 0

beta absorption = 0

**Geometry:** g = 3150 cm

b = 250 cm

Is thin = yes

n clones = 5

n originals = 0

Focus automatically = yes

**Focus:** Type = chromatic

Number variation method = cloning

Vary distance = no

**Shape:** Defined by = user

Is convex = yes

Is extruded = no

Radius = 0.02 cm

Thickness = 0.005 cm

**Boundary:** Type = ellipse

**Parabola:** Is source in infinity = no

p semi = 0.02 cm

**Surface:** Is rough = no

### #7 CRL2a

**Dielectric:** Reflectivity type = polarisation

Is constant = no

Mass density = 1.85 g/cm<sup>3</sup>

**Geometry:** g = -255 cm

b = 240 cm

Is thin = yes

n clones = 6

n originals = 2

Focus automatically = yes

**Focus:** Type = chromatic

Number variation method = cloning

Vary distance = no

**Shape:** Defined by = user

Is convex = no

Is extruded = yes

Radius = 0.1 cm

Thickness = 0.005 cm

**Boundary:** Type = rectangle

**Parabola:** Is source in infinity = no

p semi = 0.1 cm

**Extruded:** Angle z = 0 deg

**Surface:** Is rough = no

## #8 CRL2b

**Dielectric:** Reflectivity type = polarisation

Is constant = yes

delta refraction = 0

beta absorption = 0

**Geometry:** g = -255 cm

b = 240 cm

Is thin = yes

n clones = 6

n originals = 0

Focus automatically = yes

**Focus:** Type = chromatic

Number variation method = cloning

Vary distance = no

**Shape:** Defined by = user

Is convex = yes

Is extruded = yes

Radius = 0.1 cm

Thickness = 0.005 cm

**Boundary:** Type = rectangle

**Parabola:** Is source in infinity = no  
p semi = 0.1 cm

**Extruded:** Angle z = 0 deg

**Surface:** Is rough = no

### #9 sample

**Screen:** Is absorbing[1] = no  
Is absorbing[2] = no  
Is absorbing[3] = no  
Is absorbing[4] = no  
Is absorbing[5] = no  
Is absorbing[6] = no  
Is absorbing[7] = no  
Is absorbing[8] = no  
Is absorbing[9] = no

**Shape:** Thickness = 0 cm

## Chapter 37

### Parameter scan cases

There are 48 cases in total, 24 without heat load on the beam splitter and 24 with. The number of 24 results from the combination of six 2D lens types and four 1D lens types, which were all tested for optimizing throughput and element numbers of the CRLs. Only two out of the 48 cases are finally relevant, i.e. cases #5 and #29. These are the cases without and with heat load respectively and the combination of lens types that provide high throughput with a reasonable number of elements.

Case	Has_slope_error_03	Skip_heatload	a_ellipse_05 cm	p_semi_05 cm	y_negative_07 cm	y_positive_07 cm	p_semi_07 cm
1	no	yes	0.02	0.005	0.03	0.03	0.02
2	no	yes	0.02	0.005	0.04	0.04	0.03
3	no	yes	0.02	0.005	0.05	0.05	0.05
4	no	yes	0.02	0.005	0.085	0.085	0.1
5	no	yes	0.03	0.01	0.03	0.03	0.02
6	no	yes	0.03	0.01	0.04	0.04	0.03
7	no	yes	0.03	0.01	0.05	0.05	0.05
8	no	yes	0.03	0.01	0.085	0.085	0.1
9	no	yes	0.045	0.02	0.03	0.03	0.02
10	no	yes	0.045	0.02	0.04	0.04	0.03
11	no	yes	0.045	0.02	0.05	0.05	0.05
12	no	yes	0.045	0.02	0.085	0.085	0.1
13	no	yes	0.055	0.03	0.03	0.03	0.02
14	no	yes	0.055	0.03	0.04	0.04	0.03
15	no	yes	0.055	0.03	0.05	0.05	0.05
16	no	yes	0.055	0.03	0.085	0.085	0.1
17	no	yes	0.07	0.05	0.03	0.03	0.02
18	no	yes	0.07	0.05	0.04	0.04	0.03
19	no	yes	0.07	0.05	0.05	0.05	0.05
20	no	yes	0.07	0.05	0.085	0.085	0.1
21	no	yes	0.095	0.1	0.03	0.03	0.02
22	no	yes	0.095	0.1	0.04	0.04	0.03
23	no	yes	0.095	0.1	0.05	0.05	0.05
24	no	yes	0.095	0.1	0.085	0.085	0.1
25	yes	no	0.02	0.005	0.03	0.03	0.02
26	yes	no	0.02	0.005	0.04	0.04	0.03
27	yes	no	0.02	0.005	0.05	0.05	0.05
28	yes	no	0.02	0.005	0.085	0.085	0.1
29	yes	no	0.03	0.01	0.03	0.03	0.02
30	yes	no	0.03	0.01	0.04	0.04	0.03
31	yes	no	0.03	0.01	0.05	0.05	0.05
32	yes	no	0.03	0.01	0.085	0.085	0.1
33	yes	no	0.045	0.02	0.03	0.03	0.02
34	yes	no	0.045	0.02	0.04	0.04	0.03
35	yes	no	0.045	0.02	0.05	0.05	0.05
36	yes	no	0.045	0.02	0.085	0.085	0.1
37	yes	no	0.055	0.03	0.03	0.03	0.02
38	yes	no	0.055	0.03	0.04	0.04	0.03
39	yes	no	0.055	0.03	0.05	0.05	0.05
40	yes	no	0.055	0.03	0.085	0.085	0.1
41	yes	no	0.07	0.05	0.03	0.03	0.02
42	yes	no	0.07	0.05	0.04	0.04	0.03
43	yes	no	0.07	0.05	0.05	0.05	0.05
44	yes	no	0.07	0.05	0.085	0.085	0.1
45	yes	no	0.095	0.1	0.03	0.03	0.02
46	yes	no	0.095	0.1	0.04	0.04	0.03
47	yes	no	0.095	0.1	0.05	0.05	0.05
48	yes	no	0.095	0.1	0.085	0.085	0.1

Table 37.1: Parameter values for different cases in parameter scan

### Legend

**Case:** Case number in parameter scan

**Has\_slope\_error\_03:** Optical\_element\_#3.Surface.Has\_slope\_error (Has surface slope error?)

**Skip\_heatload:** Session.Skip\_heatload (Skip heat load calculation for all optical elements? (heat load parameters are kept))

**a\_ellipse\_05:** Optical\_element\_#5.Shape.Boundary.a\_ellipse (External outline semi-axis in meridional direction.)

**p\_semi\_05:** Optical\_element\_#5.Shape.Parabola.p\_semi (Semilatus rectum p of parabola:  
 $y = x^2/2p$  in cartesian or  $r = p/(1+\cos(\phi))$  in polar coordinates. The radius of curvature in the lens center is  $R_0 = p$ .)

**y\_negative\_07:** Optical\_element\_#7.Shape.Boundary.y\_negative (Lateral extension  
in neg. y-direction.)

**y\_positive\_07:** Optical\_element\_#7.Shape.Boundary.y\_positive (Lateral extension  
in pos. y-direction.)

**p\_semi\_07:** Optical\_element\_#7.Shape.Parabola.p\_semi (Semilatus rectum p of parabola:  
 $y = x^2/2p$  in cartesian or  $r = p/(1+\cos(\phi))$  in polar coordinates. The radius of curvature in the lens center is  $R_0 = p$ .)

## Chapter 38

# Photon energy scan

The  $K_y$ -values in the table below are those for optimised output between 15.6 and 18.3 keV used by DanMAX' main branch. The number of required 2D and 1D focussing lens elements of the type that provided maximum throughput under realistic conditions are also provided here. These are the 2D and 1D lens types used in case #5, with central radius of curvature of 100 and 200 microns respectively.

E eV	K_y	n_harm/step	P_sum W	theta_B03 deg	nMult_05	nMult_07
<b>20000</b>	1.67551	9	0	8.6565237	24	4
<b>20100</b>	1.66836	9	0	8.6131277	24	4
<b>20200</b>	1.66125	9	0	8.5701675	24	4
<b>20300</b>	1.65418	9	0	8.5276346	24	4
<b>20400</b>	1.64714	9	0	8.4855232	24	4
<b>20500</b>	1.64015	9	0	8.4438276	25	4
<b>20600</b>	1.63319	9	0	8.4025402	25	4
<b>20700</b>	1.62628	9	0	8.3616571	25	4
<b>20800</b>	1.6194	9	0	8.3211708	25	4
<b>20900</b>	1.61255	9	0	8.2810764	26	4
<b>21000</b>	1.60575	9	0	8.2413683	26	4
<b>21100</b>	1.59898	9	0	8.2020397	26	4
<b>21200</b>	1.59224	9	0	8.1630869	26	4
<b>21300</b>	1.58554	9	0	8.1245022	27	4
<b>21400</b>	1.57887	9	0	8.0862827	27	4
<b>21500</b>	1.57224	9	0	8.0484219	27	5
<b>21600</b>	1.56564	9	0	8.0109158	27	5
<b>21700</b>	1.55908	9	0	7.9737582	28	5
<b>21800</b>	1.55255	9	0	7.936945	28	5
<b>21900</b>	1.54605	9	0	7.9004712	28	5
<b>22000</b>	1.53958	9	0	7.8643322	28	5
<b>22100</b>	1.53315	9	0	7.8285236	29	5
<b>22200</b>	1.52674	9	0	7.7930403	29	5
<b>22300</b>	1.52037	9	0	7.7578783	29	5
<b>22400</b>	1.51402	9	0	7.7230334	30	5
<b>22500</b>	1.50771	9	0	7.6885004	30	5
<b>22600</b>	1.50143	9	0	7.6542764	30	5
<b>22700</b>	1.49517	9	0	7.6203566	30	5
<b>22800</b>	1.48895	9	0	7.5867367	31	5
<b>22900</b>	1.48275	9	0	7.5534129	31	5
<b>23000</b>	1.47658	9	0	7.5203819	31	5
<b>23100</b>	1.47044	9	0	7.487639	31	5
<b>23200</b>	1.46433	9	0	7.4551811	32	5
<b>23300</b>	1.45824	9	0	7.4230037	32	5
<b>23400</b>	1.45218	9	0	7.3911042	32	5
<b>23500</b>	1.44615	9	0	7.359478	32	5

Table 38.1: Scan values for different photon energies in energy scan of setup without heat load

E eV	P_sum W	theta_B03 deg	nMult_05	nMult_07
20000	170.798	8.6565237	25	1
20100	170.209	8.6131277	25	1
20200	169.47	8.5701675	25	1
20300	168.879	8.5276346	25	1
20400	168.315	8.4855232	26	1
20500	167.588	8.4438276	26	1
20600	166.189	8.4025402	26	1
20700	165.542	8.3616571	26	1
20800	164.949	8.3211708	27	1
20900	164.413	8.2810764	27	1
21000	163.752	8.2413683	27	1
21100	163.16	8.2020397	27	1
21200	162.507	8.1630869	28	1
21300	161.904	8.1245022	28	1
21400	161.386	8.0862827	28	1
21500	160.797	8.0484219	29	1
21600	160.163	8.0109158	29	1
21700	159.473	7.9737582	29	1
21800	158.884	7.936945	29	1
21900	157.585	7.9004712	30	1
22000	157.101	7.8643322	30	1
22100	156.451	7.8285236	30	1
22200	155.93	7.7930403	30	1
22300	155.254	7.7578783	31	1
22400	154.716	7.7230334	31	1
22500	154.16	7.6885004	31	2
22600	153.484	7.6542764	32	2
22700	152.951	7.6203566	32	2
22800	152.294	7.5867367	32	2
22900	151.786	7.5534129	32	2
23000	151.176	7.5203819	33	2
23100	150.589	7.487639	33	2
23200	149.911	7.4551811	33	2
23300	148.827	7.4230037	34	2
23400	148.246	7.3911042	34	2
23500	147.698	7.359478	34	2

Table 38.2: Scan values for different photon energies in energy scan of setup with heat load

### Legend

**E:** photon energy

**P\_sum:** sum of power in harmonics / energy intervals, P\_sum = P\_src

**theta\_B03:** Bragg angle, i.e. glancing angle of incident and reflected beam w.r.t. the set of diffracting planes of optical element 03

**nMult\_05:** number of elements in compound refractive lens optical element 05

**nMult\_07:** number of elements in compound refractive lens optical element 07

# Chapter 39

## Plots

### 39.1 Statistics of incident irradiance

```
"fig/CRL_optim_C111_Laue/plot001.png" Lbl.:CRL_optim_C111_Laue_2d_plot_I_peak_incstat_oe03
```

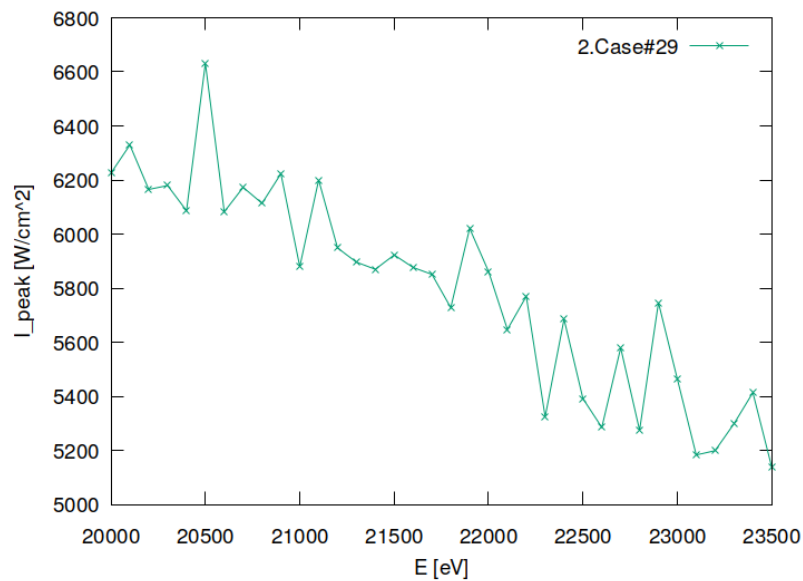


Figure 39.1: Incident peak irradiance of optical element #03 (BS).

```
"fig/CRL_optim_C111_Laue/plot002.png" Lbl.:CRL_optim_C111_Laue_2d_plot_I_int_incstat_oe03
```

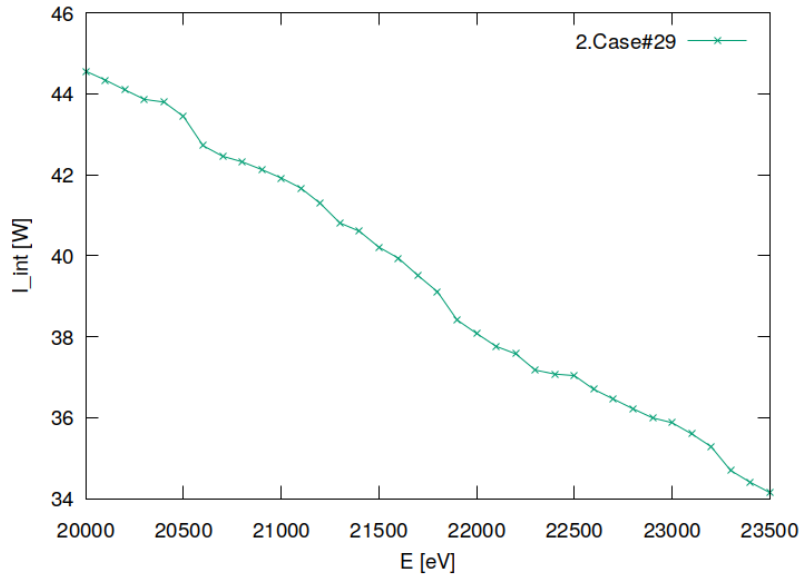


Figure 39.2: Incident flux of optical element #03 (BS).

## 39.2 Statistics of absorbed irradiance

```
"fig/CRL_optim_C111_Laue/plot003.png" Lbl.:CRL_optim_C111_Laue_2d_plot_I_peak_absstat_oe03
```

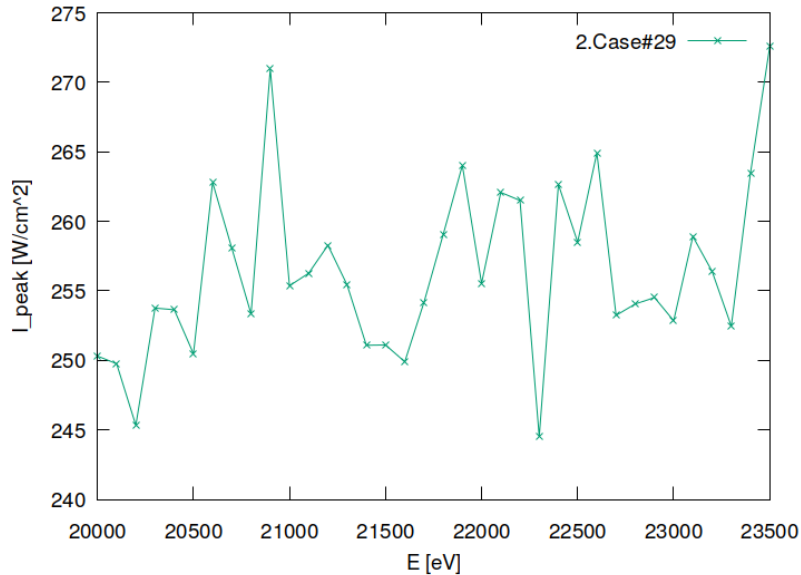


Figure 39.3: Absorbed peak irradiance of optical element #03 (BS).

```
"fig/CRL_optim_C111_Laue/plot004.png" Lbl.:CRL_optim_C111_Laue_2d_plot_I_int_absstat_oe03
```

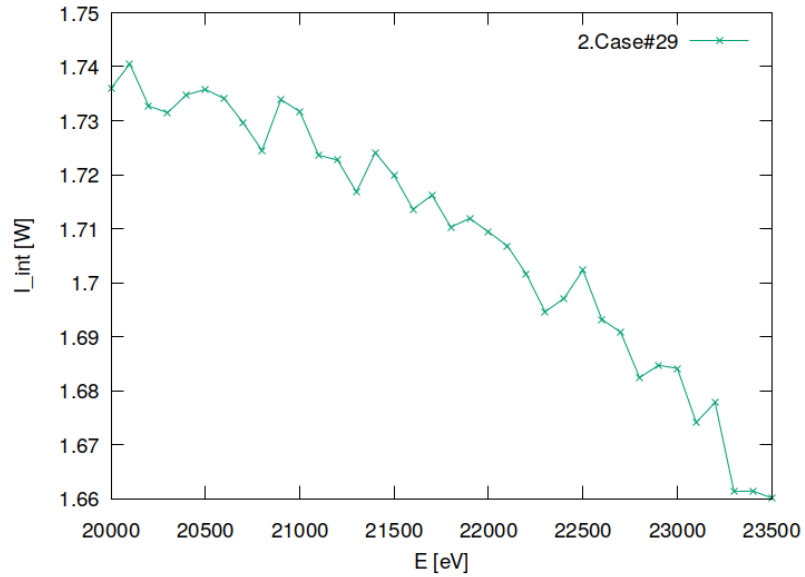


Figure 39.4: Absorbed flux of optical element #03 (BS).

### 39.3 Statistics of temperature

```
"fig/CRL_optim_C111_Laue/plot005.png" Lbl.:CRL_optim_C111_Laue_2d_plot_T_peak_stat_oe03
```

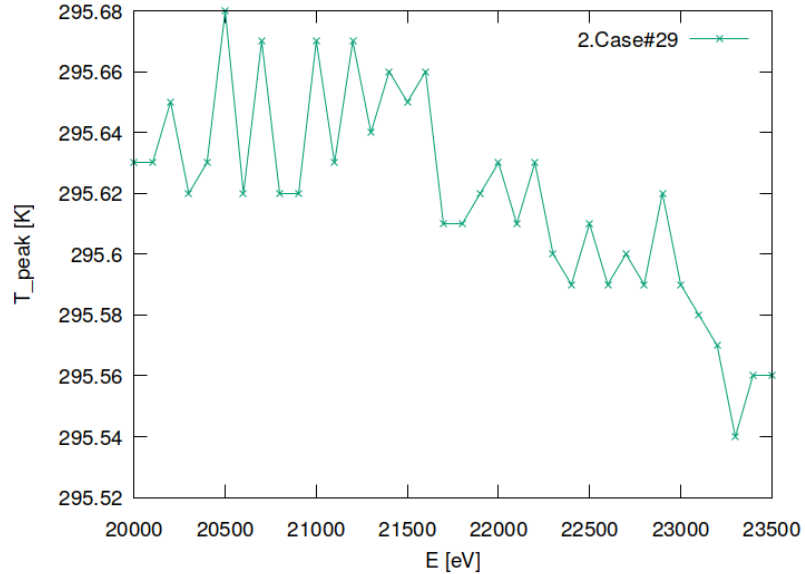


Figure 39.5: Peak temperature of optical element #03 (BS).

## 39.4 Statistics of mechanical stress (von Mises stress)

```
"fig/CRL_optim_C111_Laue/plot006.png" Lbl.:CRL_optim_C111_Laue_2d_plot_sigma_peak_stat_oe03
```

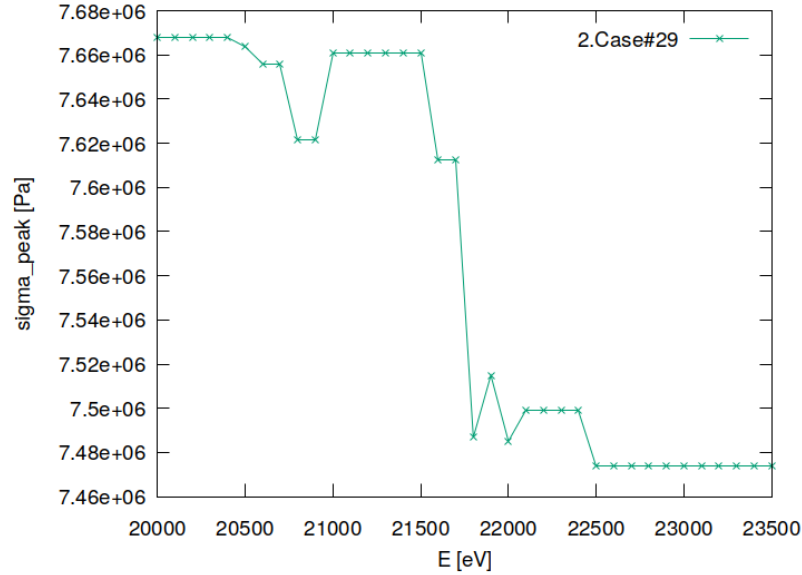


Figure 39.6: Peak mechanical stress (Von Mises stress) of optical element #03 (BS).

## 39.5 Statistics of optical surface deformation

```
"fig/CRL_optim_C111_Laue/plot007.png" Lbl.:CRL_optim_C111_Laue_2d_plot_dz_peak_stat_oe03
```

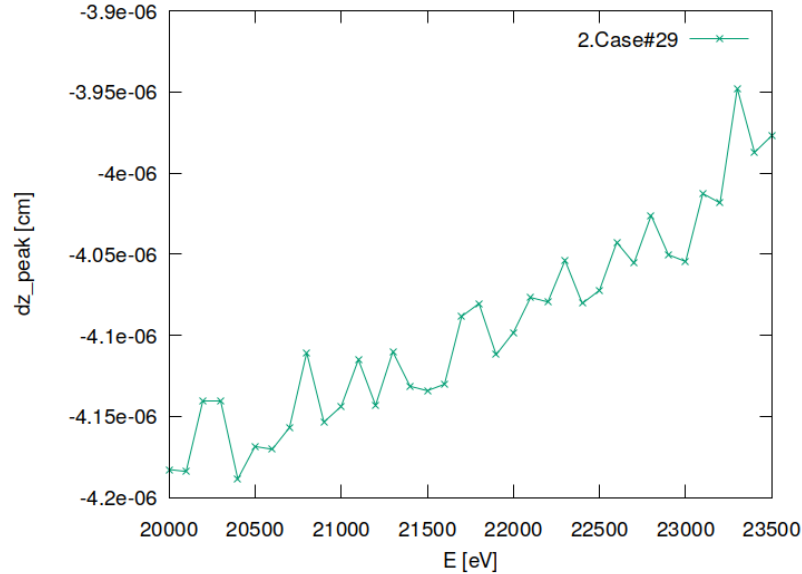


Figure 39.7: Peak deformation of optical element #03 (BS).

## 39.6 Statistics of photon irradiance on optical surface

```
"fig/CRL_optim_C111_Laue/plot008.png" Lbl.:CRL_optim_C111_Laue_2d_plot_dx_fwhm_inc_footstat_oe04
```

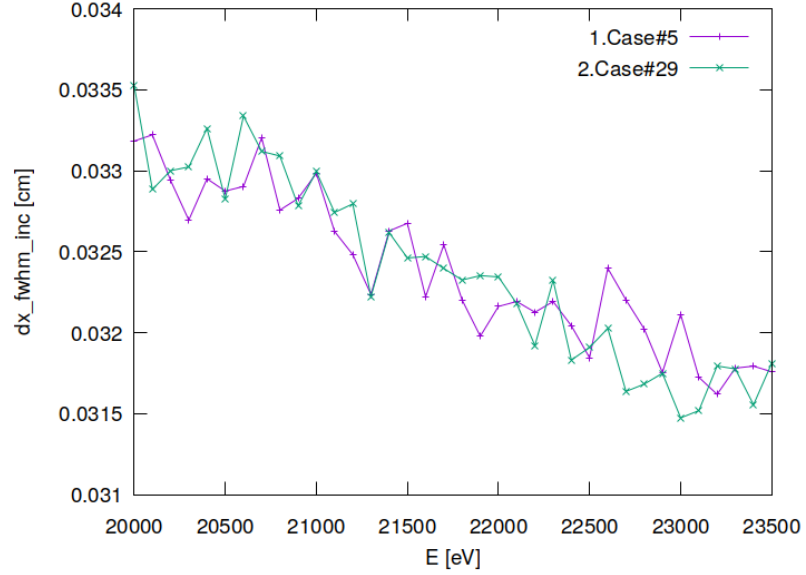


Figure 39.8: Sagittal footprint diameter (FWHM) of optical element #04 (CM2).

```
"fig/CRL_optim_C111_Laue/plot009.png" Lbl.:CRL_optim_C111_Laue_2d_plot_dx_fwhm_inc_footstat_oe09
```

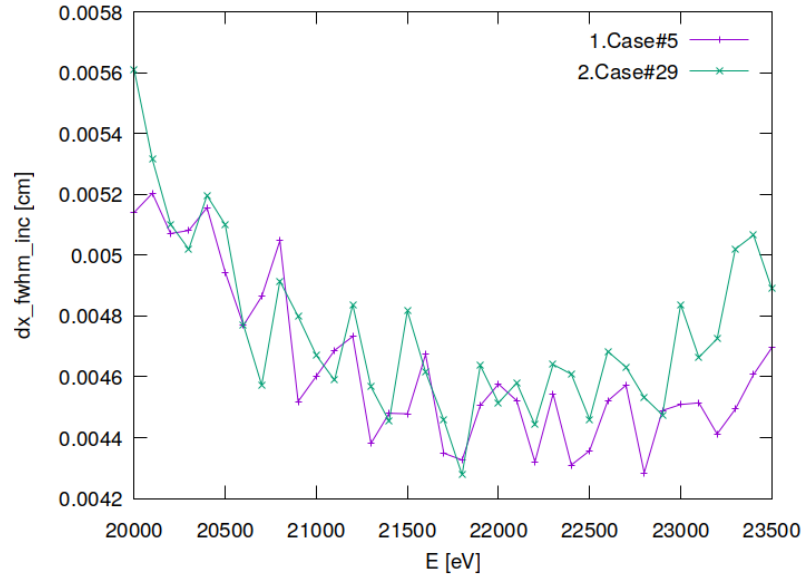


Figure 39.9: Sagittal footprint diameter (FWHM) of optical element #09 (sample).

```
"fig/CRL_optim_C111_Laue/plot010.png" Lbl.:CRL_optim_C111_Laue_2d_plot_dy_fwhm_inc_footstat_oe04
```

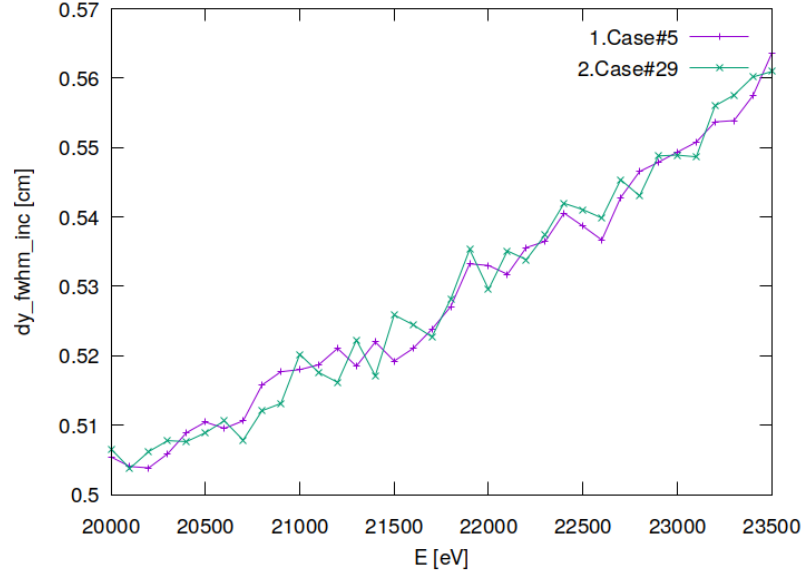


Figure 39.10: Meridional footprint diameter (FWHM) of optical element #04 (CM2).

```
"fig/CRL_optim_C111_Laue/plot011.png" Lbl.:CRL_optim_C111_Laue_2d_plot_dy_fwhm_inc_footstat_oe09
```

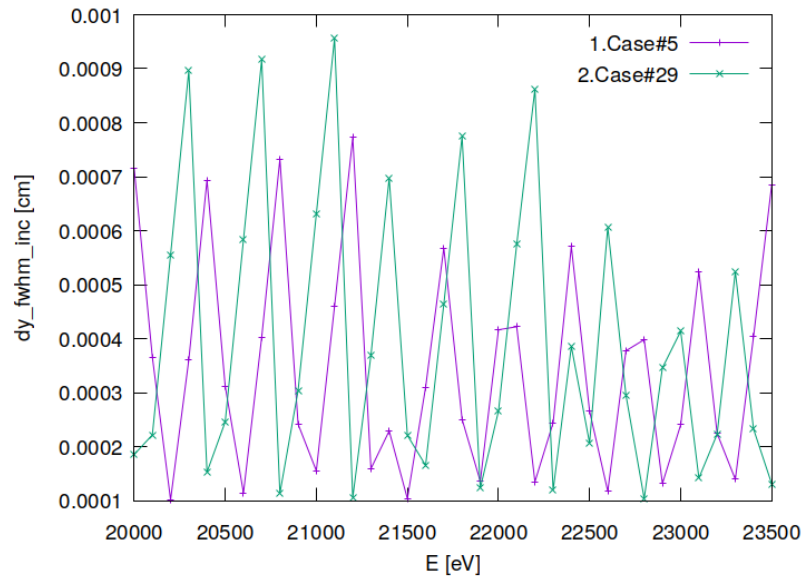


Figure 39.11: Meridional footprint diameter (FWHM) of optical element #09 (sample).

```
"fig/CRL_optim_C111_Laue/plot012.png" Lbl.:CRL_optim_C111_Laue_2d_plot_I_inc_int_footstat_oe04
```

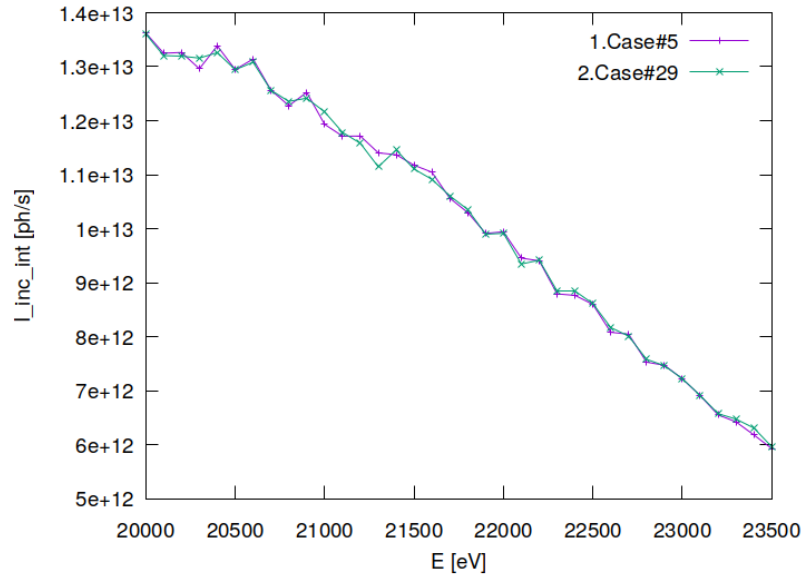


Figure 39.12: Incident photon flux on surface of optical element #04 (CM2).

```
"fig/CRL_optim_C111_Laue/plot013.png" Lbl.:CRL_optim_C111_Laue_2d_plot_I_inc_int_footstat_oe09
```

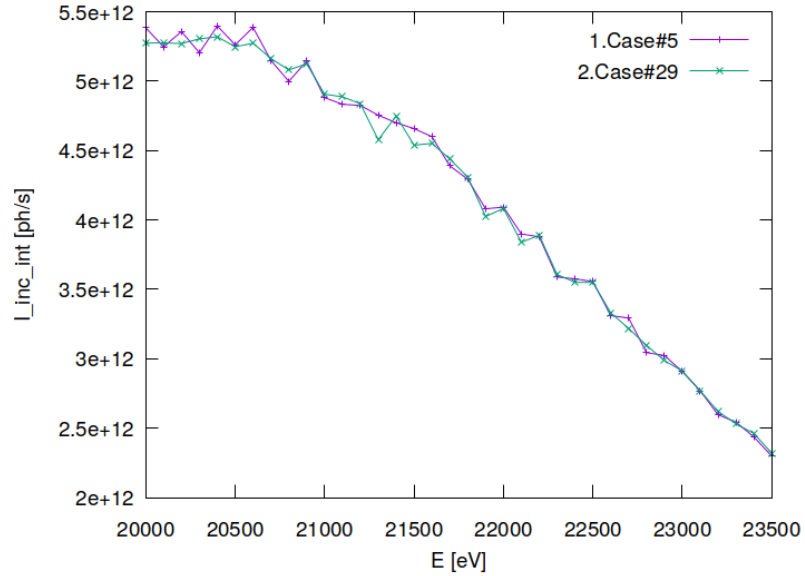


Figure 39.13: Incident photon flux on surface of optical element #09 (sample).

"fig/CRL\_optim\_C111\_Laue/plot014.png" Lbl.:CRL\_optim\_C111\_Laue\_2d\_plot\_x\_cen\_inc\_footstat\_oe04

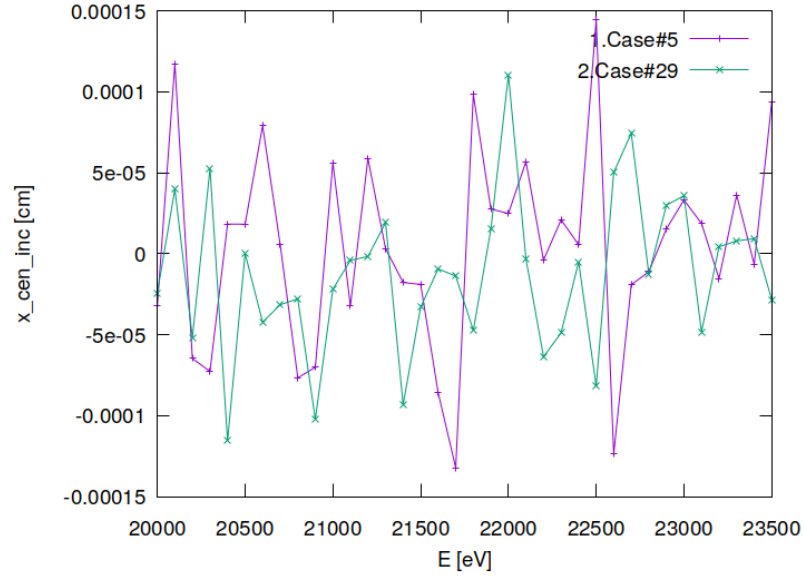


Figure 39.14: Sagittal coordinate of footprint's centre of 'gravity' on surface of optical element #04 (CM2).

"fig/CRL\_optim\_C111\_Laue/plot015.png" Lbl.:CRL\_optim\_C111\_Laue\_2d\_plot\_x\_cen\_inc\_footstat\_oe09

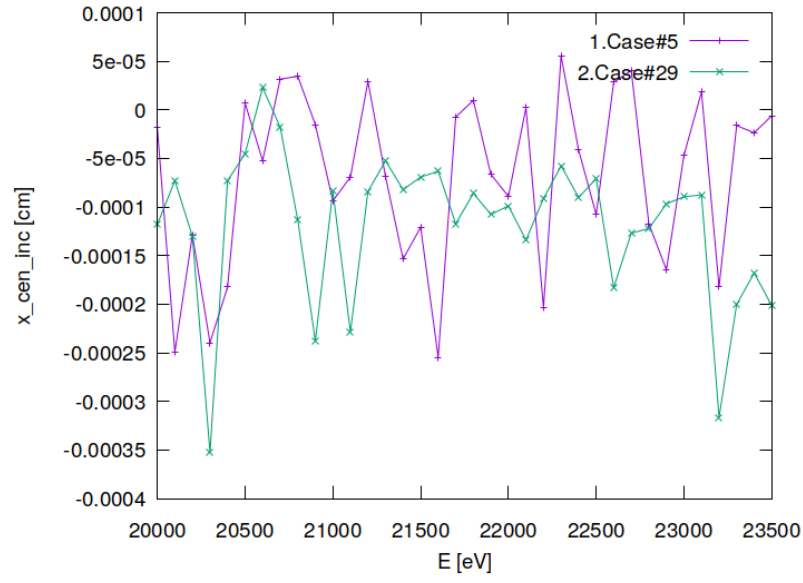


Figure 39.15: Sagittal coordinate of footprint's centre of 'gravity' on surface of optical element #09 (sample).

```
"fig/CRL_optim_C111_Laue/plot016.png" Lbl.:CRL_optim_C111_Laue_2d_plot_y_cen_inc_footstat_oe04
```

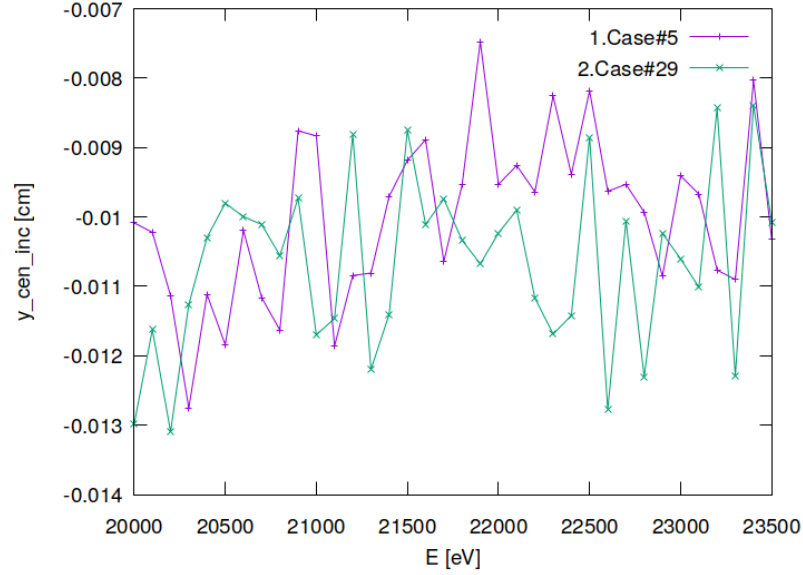


Figure 39.16: Meridional coordinate of footprint's centre of 'gravity' on surface of optical element #04 (CM2).

```
"fig/CRL_optim_C111_Laue/plot017.png" Lbl.:CRL_optim_C111_Laue_2d_plot_y_cen_inc_footstat_oe09
```

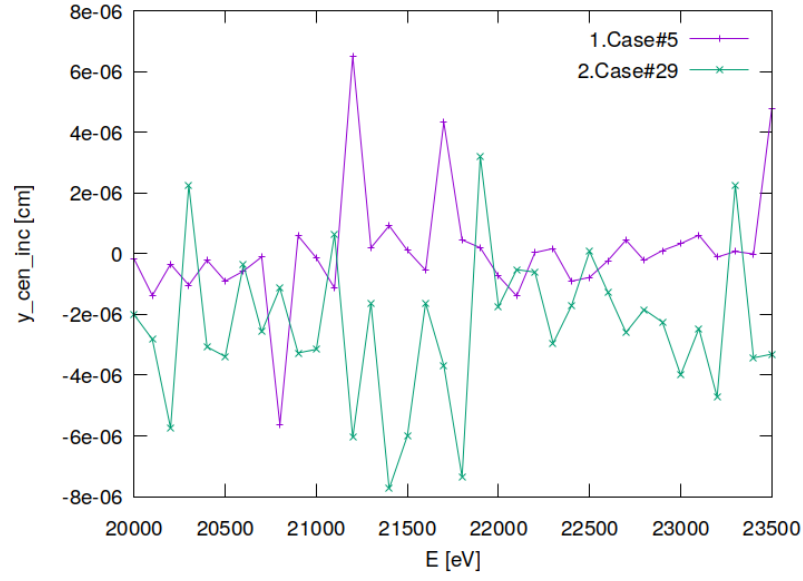


Figure 39.17: Meridional coordinate of footprint's centre of 'gravity' on surface of optical element #09 (sample).

## 39.7 Statistics of photon irradiance in beam cross section

"fig/CRL\_optim\_C111\_Laue/plot018.png" Lbl.:CRL\_optim\_C111\_Laue\_2d\_plot\_dx\_fwhm\_focstatavg\_oe04

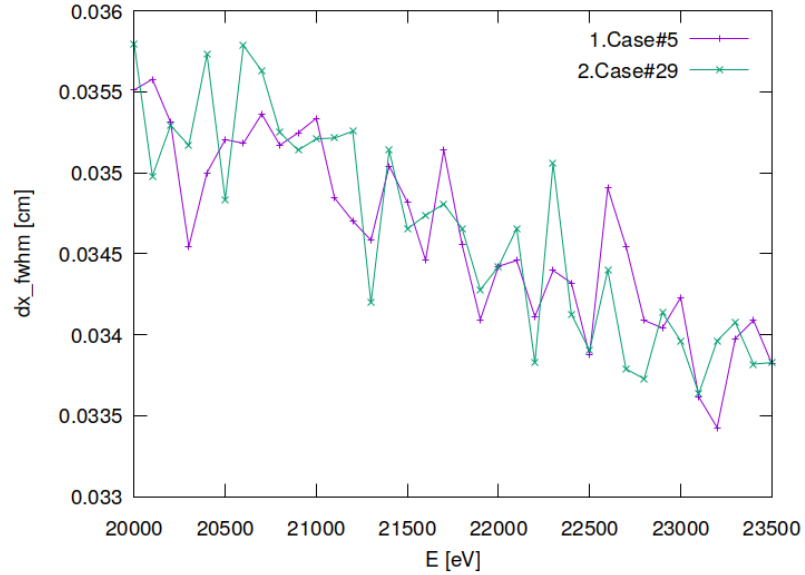


Figure 39.18: Sagittal beam diameter (FWHM) of optical element #04 (CM2).

"fig/CRL\_optim\_C111\_Laue/plot019.png" Lbl.:CRL\_optim\_C111\_Laue\_2d\_plot\_dx\_fwhm\_focstatavg\_oe09

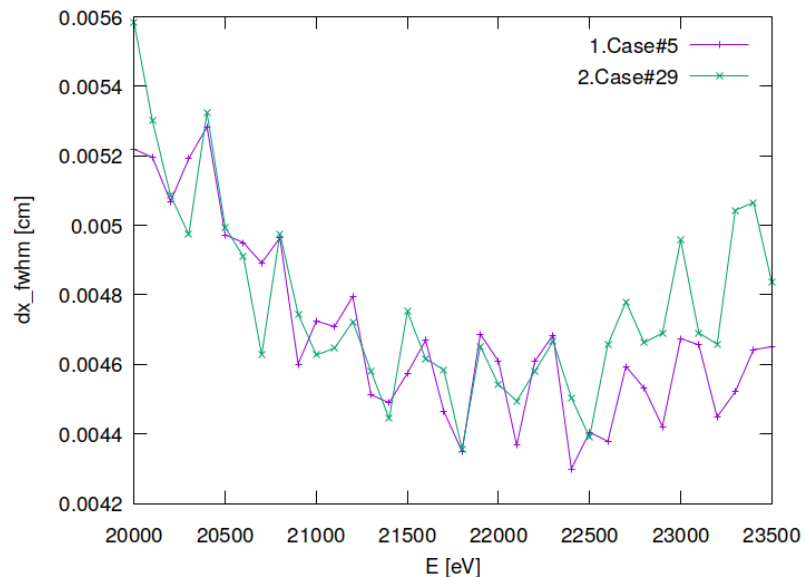


Figure 39.19: Sagittal beam diameter (FWHM) of optical element #09 (sample).

```
"fig/CRL_optim_C111_Laue/plot020.png" Lbl.:CRL_optim_C111_Laue_2d_plot_dz_fwhm_focstatavg_oe04
```

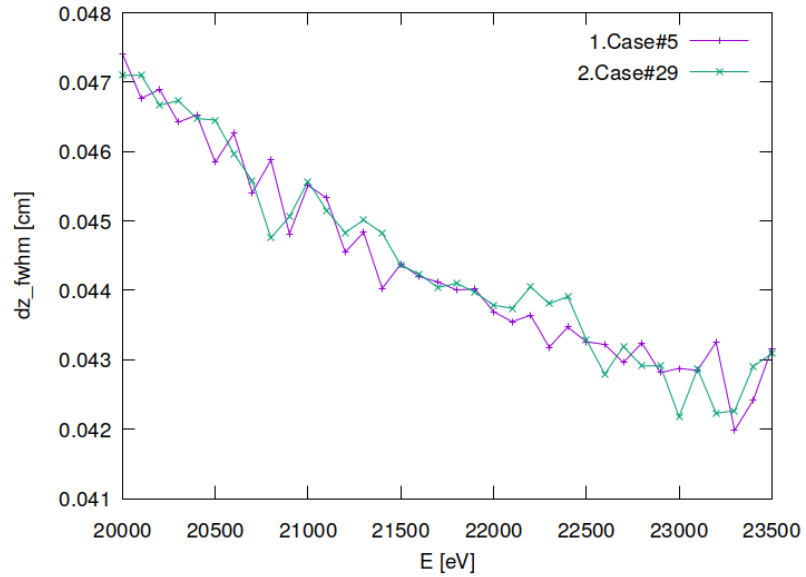


Figure 39.20: Meridional beam diameter (FWHM) of optical element #04 (CM2).

```
"fig/CRL_optim_C111_Laue/plot021.png" Lbl.:CRL_optim_C111_Laue_2d_plot_dz_fwhm_focstatavg_oe09
```

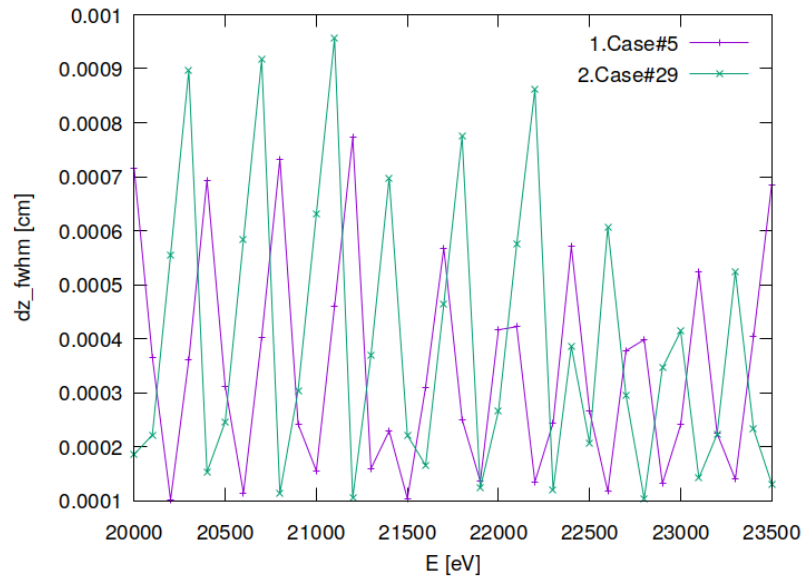


Figure 39.21: Meridional beam diameter (FWHM) of optical element #09 (sample).

```
"fig/CRL_optim_C111_Laue/plot022.png" Lbl.:CRL_optim_C111_Laue_2d_plot_I_int_focstatavg_oe04
```

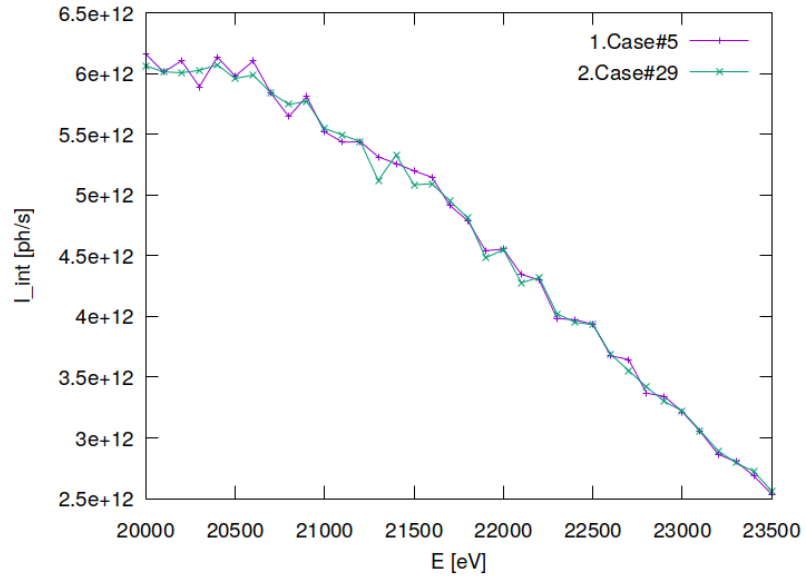


Figure 39.22: Photon flux in beam cross section of optical element #04 (CM2).

```
"fig/CRL_optim_C111_Laue/plot023.png" Lbl.:CRL_optim_C111_Laue_2d_plot_I_int_focstatavg_oe09
```

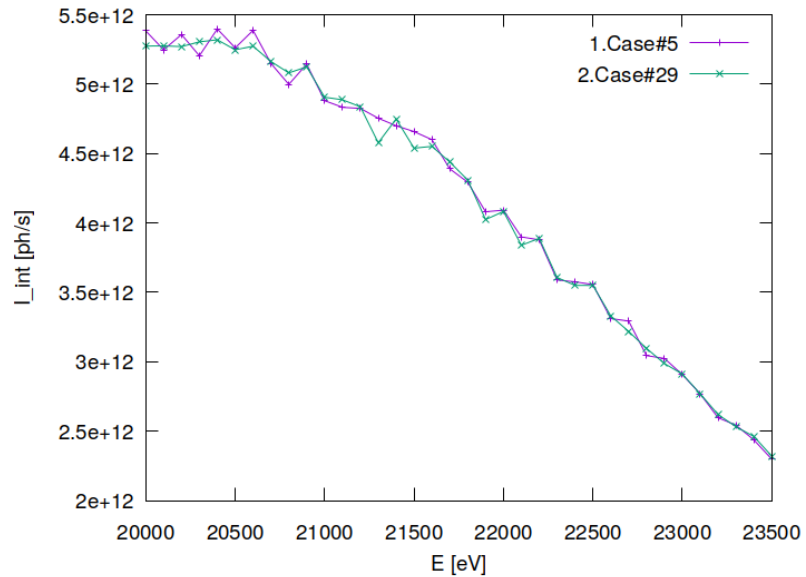


Figure 39.23: Photon flux in beam cross section of optical element #09 (sample).

```
"fig/CRL_optim_C111_Laue/plot024.png" Lbl.:CRL_optim_C111_Laue_2d_plot_x_cen_focstatavg_oe04
```

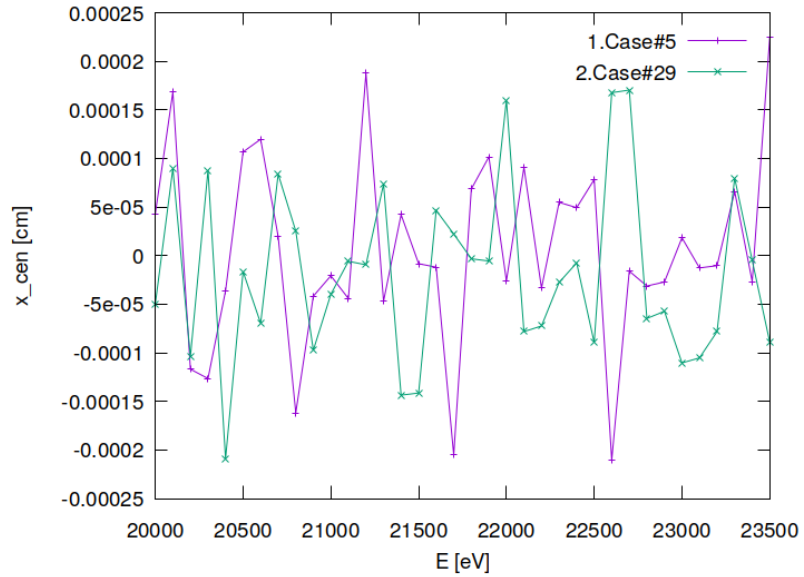


Figure 39.24: Sagittal coordinate of beam's centre of 'gravity' in beam cross section of optical element #04 (CM2).

```
"fig/CRL_optim_C111_Laue/plot025.png" Lbl.:CRL_optim_C111_Laue_2d_plot_x_cen_focstatavg_oe09
```

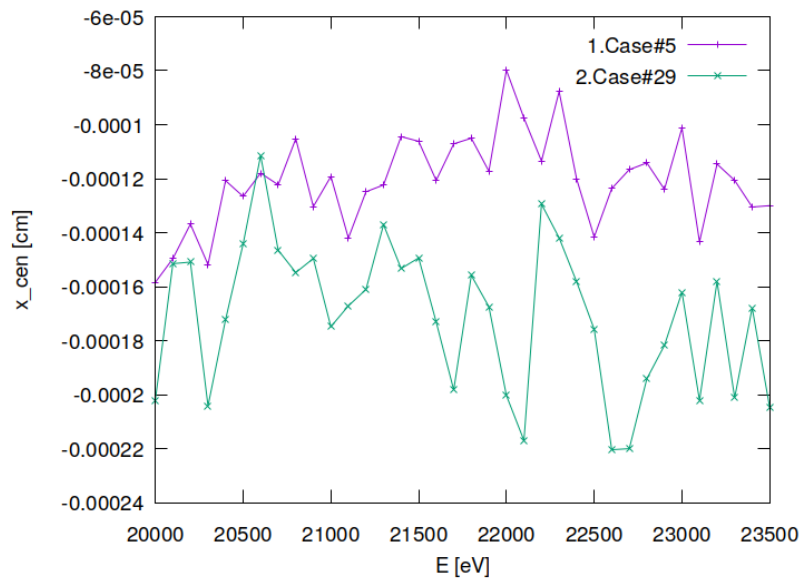


Figure 39.25: Sagittal coordinate of beam's centre of 'gravity' in beam cross section of optical element #09 (sample).

```
"fig/CRL_optim_C111_Laue/plot026.png" Lbl.:CRL_optim_C111_Laue_2d_plot_z_cen_focstatavg_oe04
```

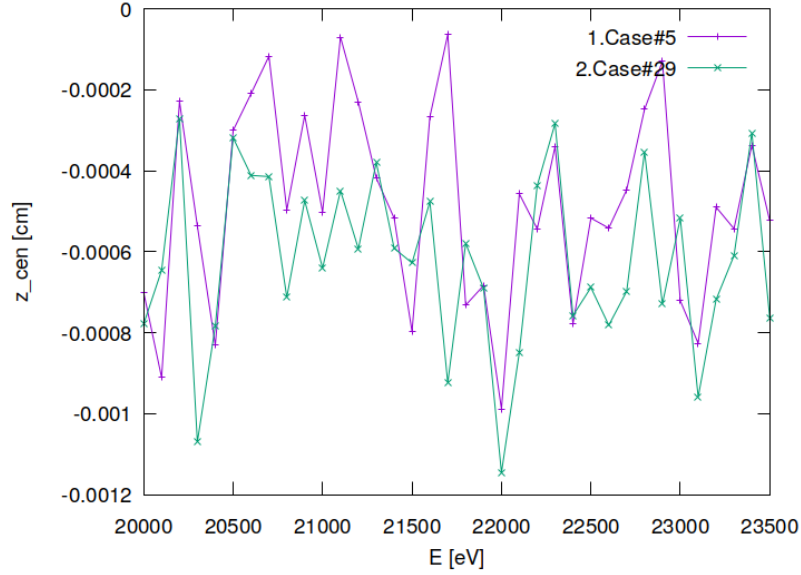


Figure 39.26: Meridional coordinate of beam's centre of 'gravity' in beam cross section of optical element #04 (CM2).

```
"fig/CRL_optim_C111_Laue/plot027.png" Lbl.:CRL_optim_C111_Laue_2d_plot_z_cen_focstatavg_oe09
```

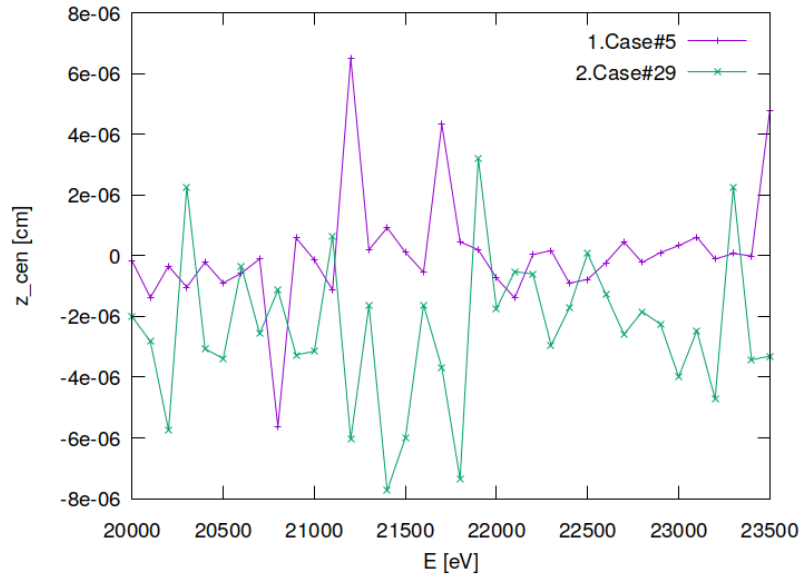


Figure 39.27: Meridional coordinate of beam's centre of 'gravity' in beam cross section of optical element #09 (sample).

```
"fig/CRL_optim_C111_Laue/plot028.png" Lbl.:CRL_optim_C111_Laue_2d_plot_dxp_fwhm_focstatavg_oe04
```

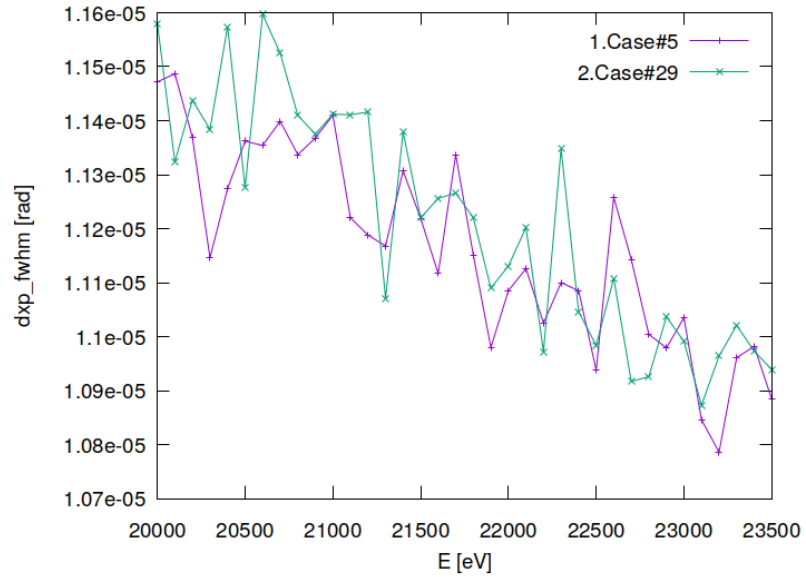


Figure 39.28: Sagittal beam divergence (FWHM) of optical element #04 (CM2).

```
"fig/CRL_optim_C111_Laue/plot029.png" Lbl.:CRL_optim_C111_Laue_2d_plot_dxp_fwhm_focstatavg_oe09
```

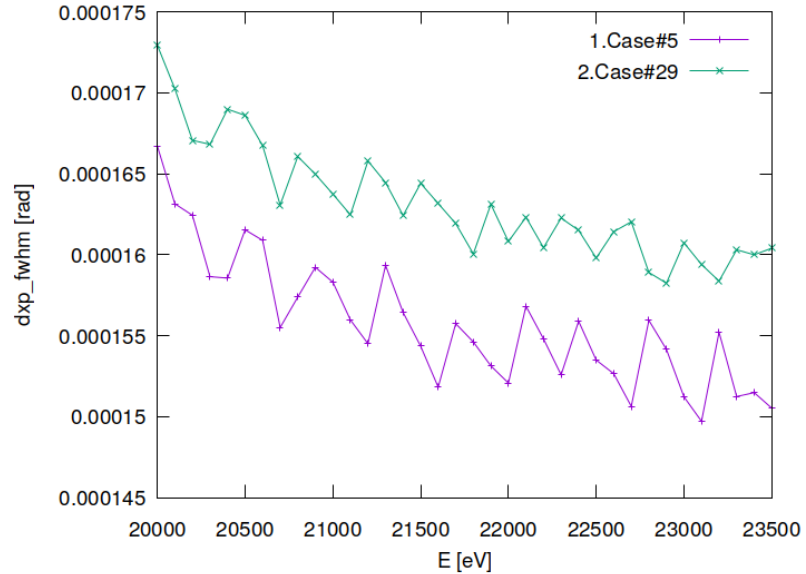


Figure 39.29: Sagittal beam divergence (FWHM) of optical element #09 (sample).

```
"fig/CRL_optim_C111_Laue/plot030.png" Lbl.:CRL_optim_C111_Laue_2d_plot_dzp_fwhm_focstatavg_oe04
```

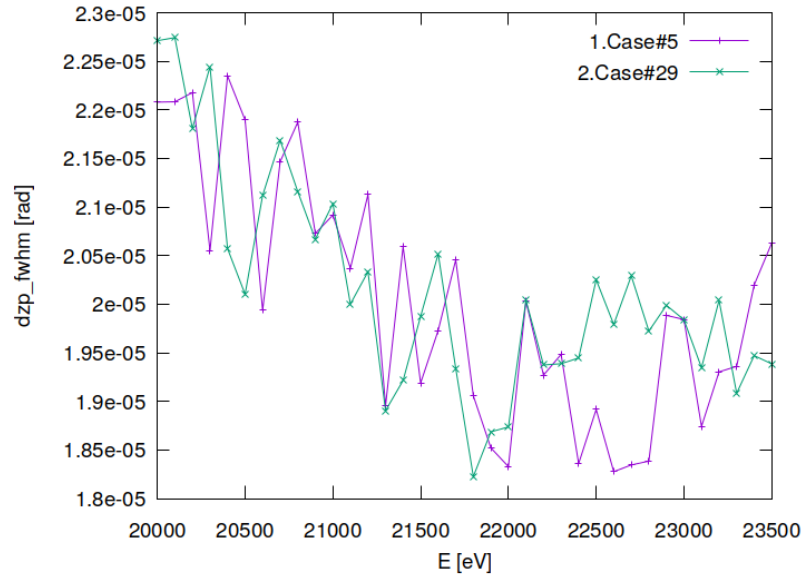


Figure 39.30: Meridional beam divergence (FWHM) of optical element #04 (CM2).

```
"fig/CRL_optim_C111_Laue/plot031.png" Lbl.:CRL_optim_C111_Laue_2d_plot_dzp_fwhm_focstatavg_oe09
```

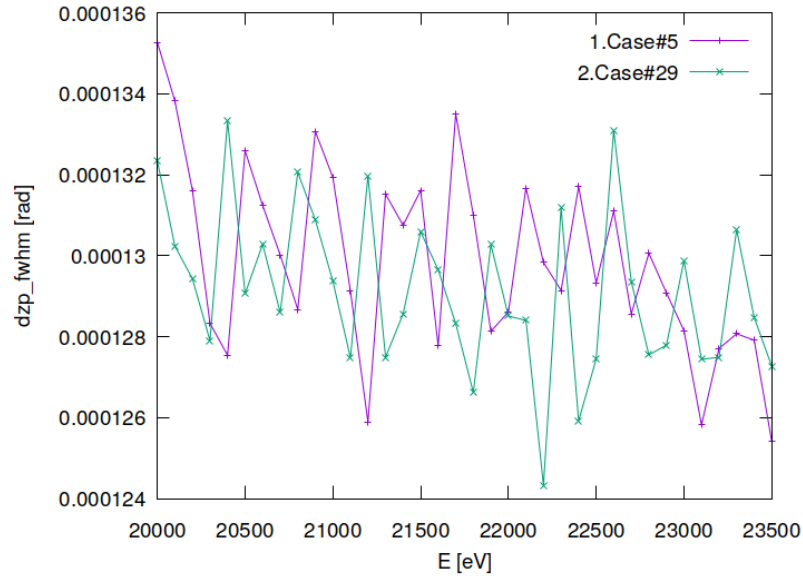


Figure 39.31: Meridional beam divergence (FWHM) of optical element #09 (sample).

```
"fig/CRL_optim_C111_Laue/plot032.png" Lbl.:CRL_optim_C111_Laue_2d_plot_I_int_focstatavg_oe04
```

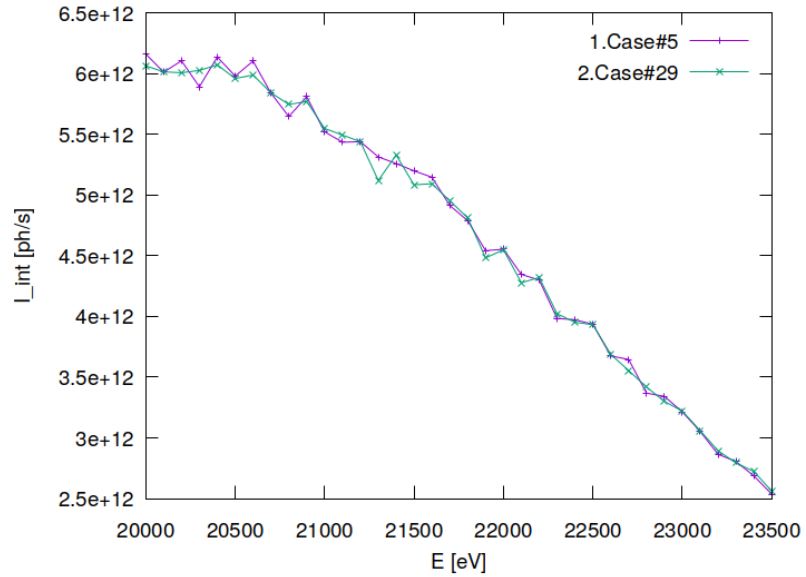


Figure 39.32: Photon flux in beam cross section of optical element #04 (CM2).

```
"fig/CRL_optim_C111_Laue/plot033.png" Lbl.:CRL_optim_C111_Laue_2d_plot_I_int_focstatavg_oe09
```

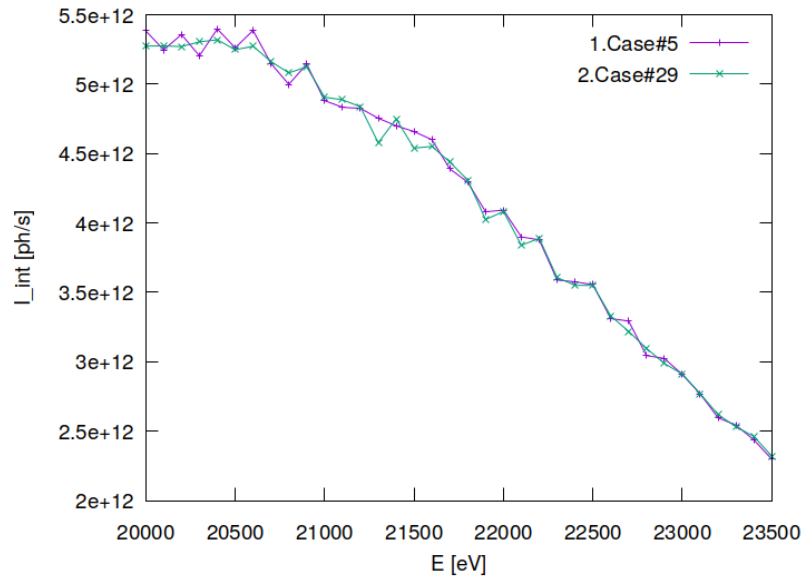


Figure 39.33: Photon flux in beam cross section of optical element #09 (sample).

"fig/CRL\_optim\_C111\_Laue/plot034.png" Lbl.:CRL\_optim\_C111\_Laue\_2d\_plot\_xp\_cen\_focstatavg\_oe04

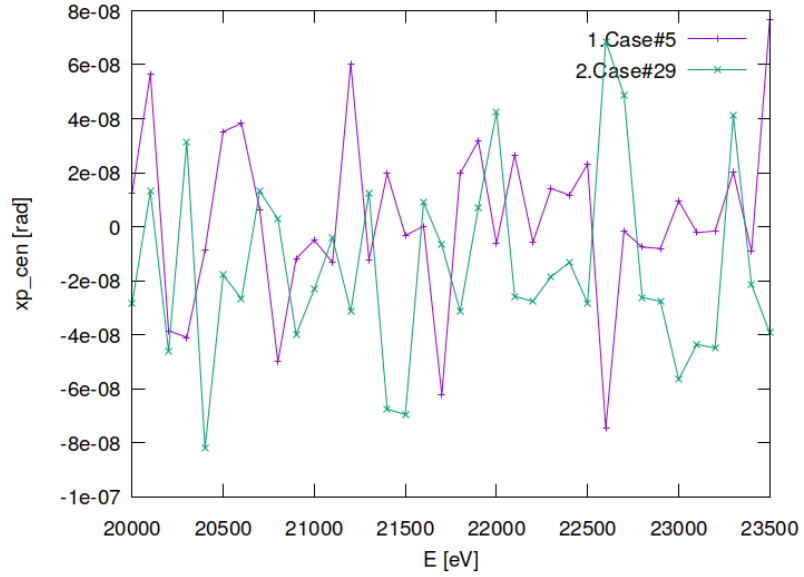


Figure 39.34: Sagittal coordinate of beam's centre of 'gravity' in angle space of optical element #04 (CM2).

"fig/CRL\_optim\_C111\_Laue/plot035.png" Lbl.:CRL\_optim\_C111\_Laue\_2d\_plot\_xp\_cen\_focstatavg\_oe09

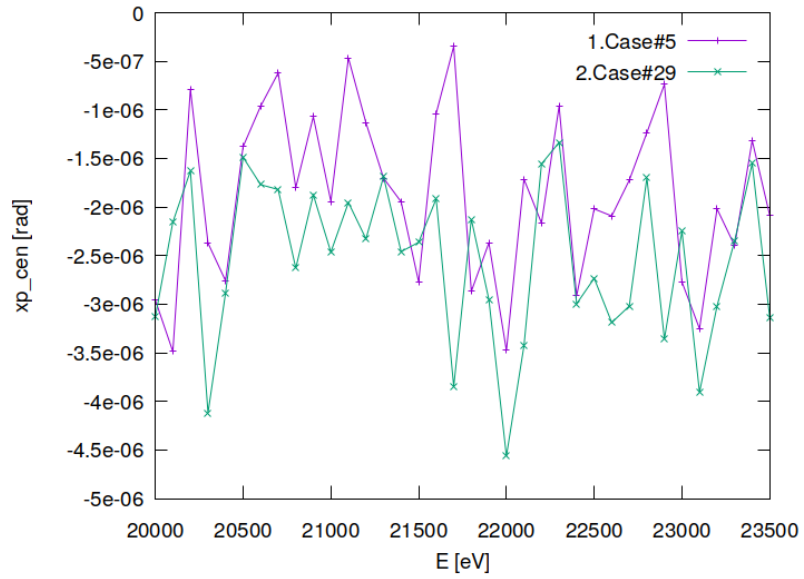


Figure 39.35: Sagittal coordinate of beam's centre of 'gravity' in angle space of optical element #09 (sample).

```
"fig/CRL_optim_C111_Laue/plot036.png" Lbl.:CRL_optim_C111_Laue_2d_plot_zp_cen_focstatavg_oe04
```

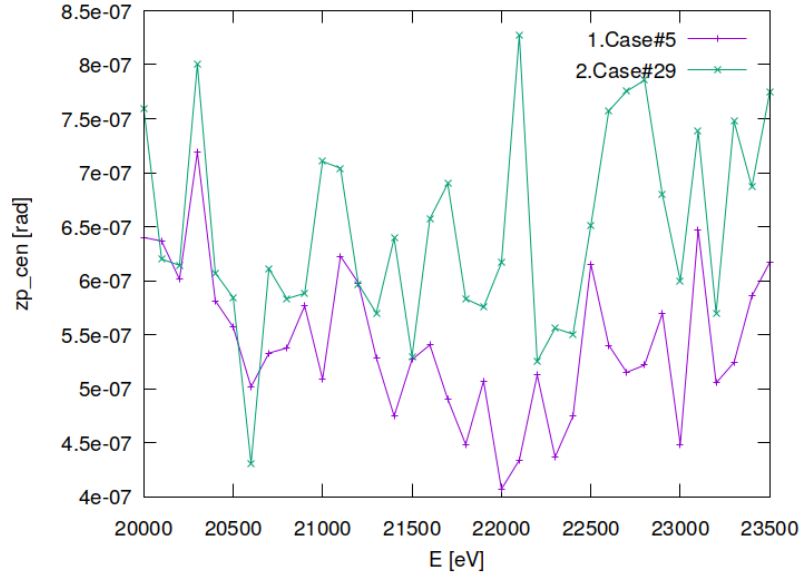


Figure 39.36: Meridional coordinate of beam's centre of 'gravity' in angle space of optical element #04 (CM2).

```
"fig/CRL_optim_C111_Laue/plot037.png" Lbl.:CRL_optim_C111_Laue_2d_plot_zp_cen_focstatavg_oe09
```

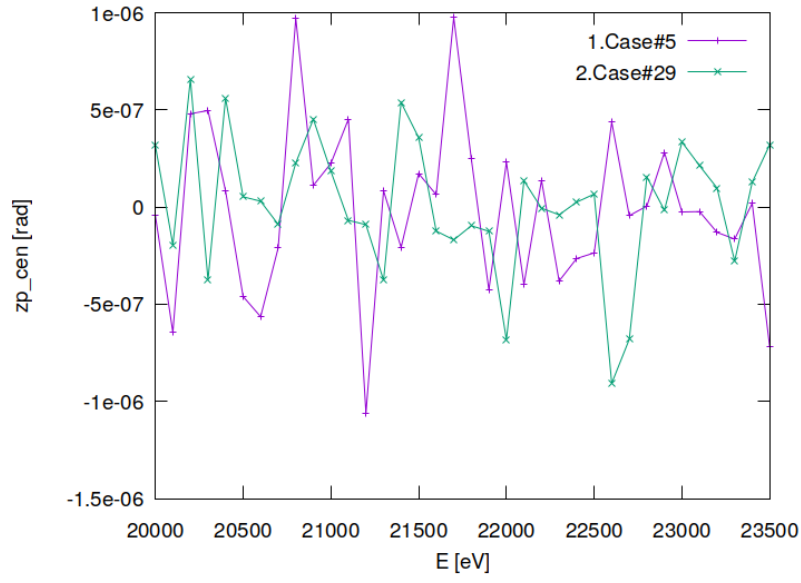


Figure 39.37: Meridional coordinate of beam's centre of 'gravity' in angle space of optical element #09 (sample).

"fig/CRL\_optim\_C111\_Laue/plot038.png" Lbl.:CRL\_optim\_C111\_Laue\_2d\_plot\_dE\_fwhm\_focstatavg\_oe04

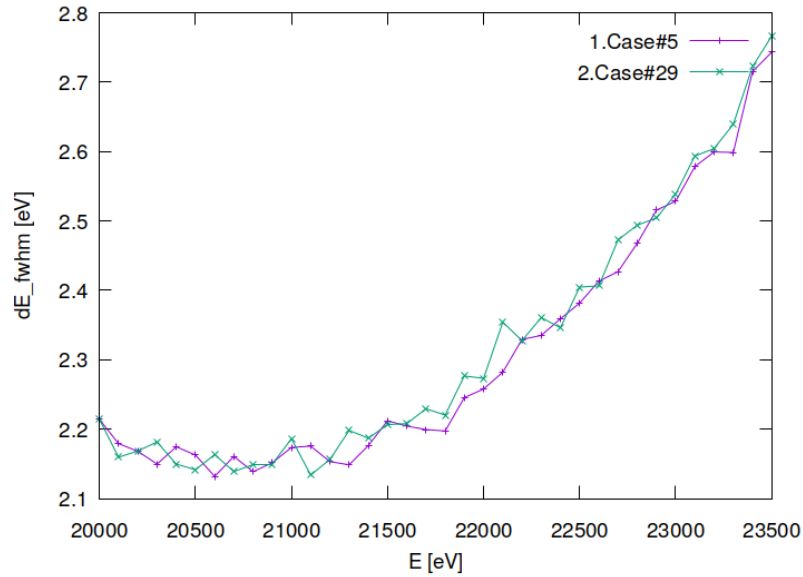


Figure 39.38: Bandwidth (FWHM) in beam cross section of optical element #04 (CM2).

"fig/CRL\_optim\_C111\_Laue/plot039.png" Lbl.:CRL\_optim\_C111\_Laue\_2d\_plot\_dE\_fwhm\_focstatavg\_oe09

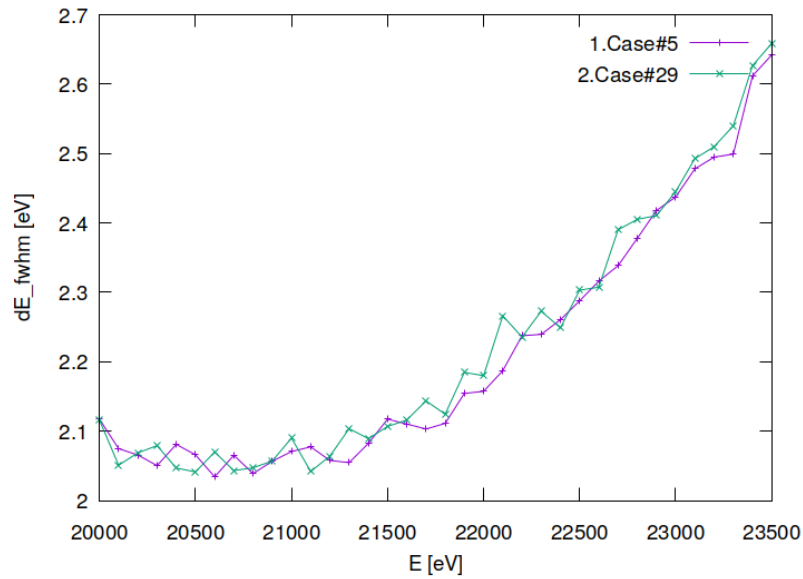


Figure 39.39: Bandwidth (FWHM) in beam cross section of optical element #09 (sample).

## 39.8 Absorbed irradiance on surface

"fig/CRL\_optim\_C111\_Laue/plot040.png" Lbl.:CRL\_optim\_C111\_Laue\_false\_colour\_plot\_p\_abs\_foot\_oe03\_c29\_21800eV

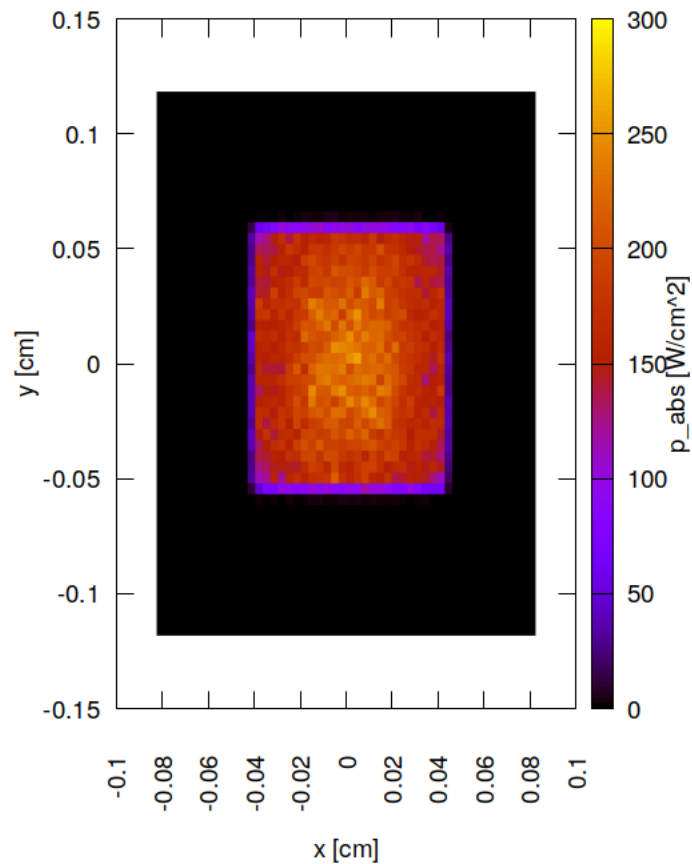


Figure 39.40: Absorbed irradiance on surface of optical element #03 (BS) for case #29 for 21800 eV photon energy setting.

### 39.9 Incident spectral flux on surface

"fig/CRL\_optim\_C111\_Laue/plot041.png" Lbl.:CRL\_optim\_C111\_Laue\_2d\_plot\_P\_spec\_spec\_oe03\_c29\_21800eV

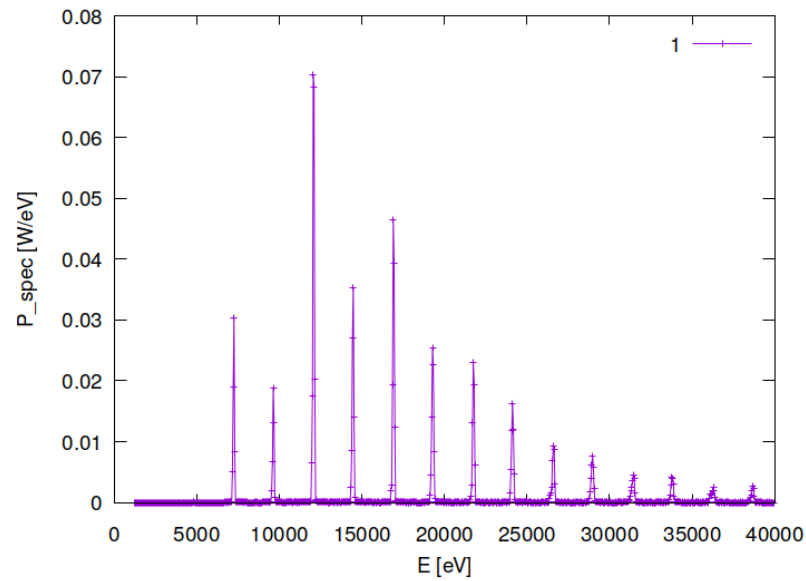


Figure 39.41: Incident spectral flux on surface of optical element #03 (BS) for case #29 for 21800 eV photon energy setting.

## 39.10 Temperature on surface

"fig/CRL\_optim\_C111\_Laue/plot042.png" Lbl.:CRL\_optim\_C111\_Laue\_false\_colour\_plot\_T\_oe03\_c29\_21800eV

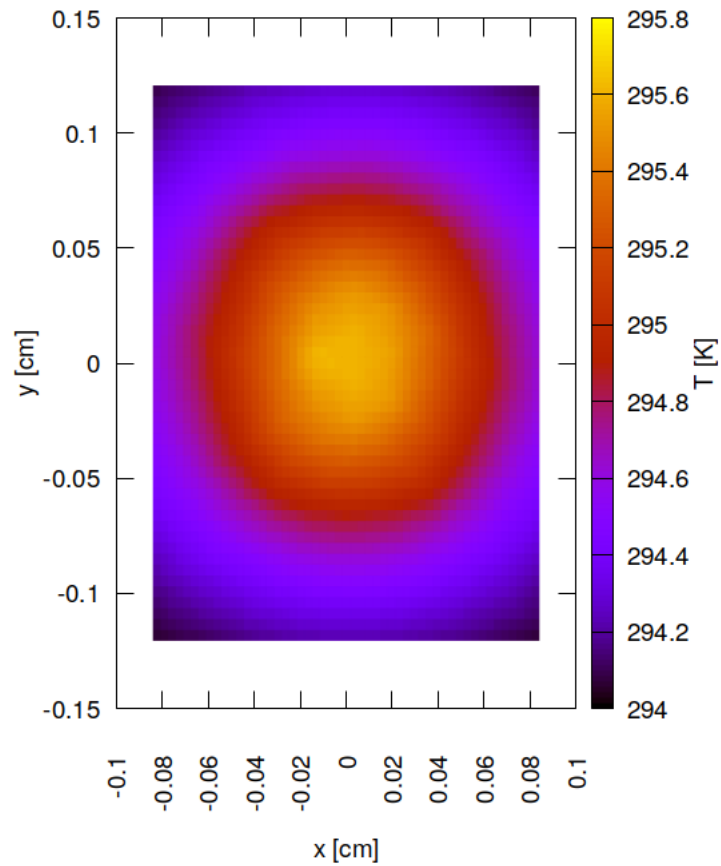


Figure 39.42: Temperature on surface of optical element #03 (BS) for case #29 for 21800 eV photon energy setting.

### 39.11 Mechanical stress (Von Mises stress) on surface

"fig/CRL\_optim\_C111\_Laue/plot043.png" Lbl.:CRL\_optim\_C111\_Laue\_false\_colour\_plot\_sigma\_oe03\_c29\_21800eV

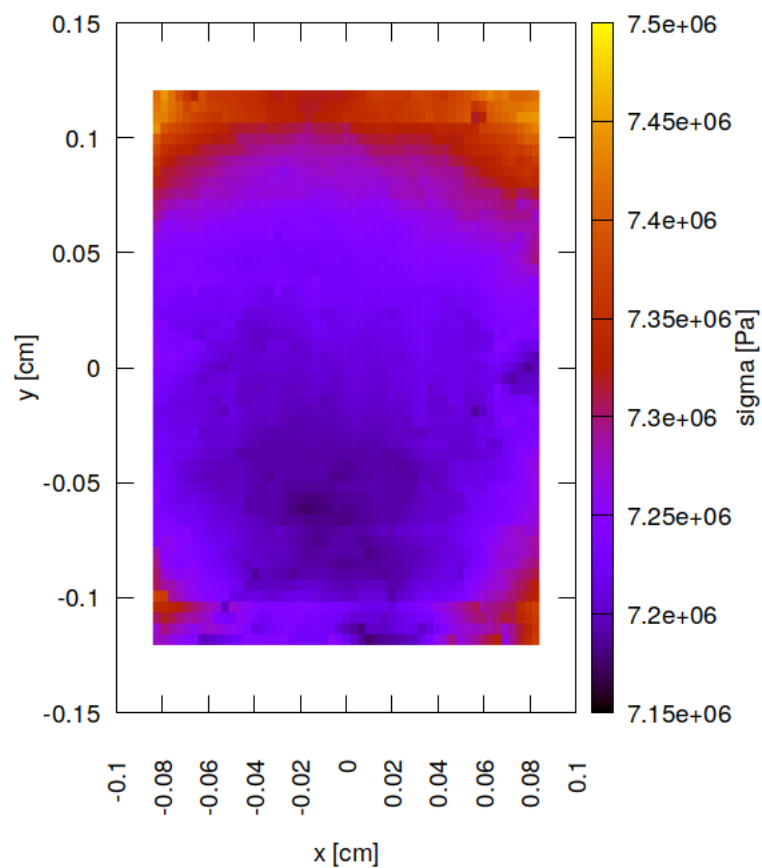


Figure 39.43: Mechanical stress (Von Mises stress) on surface of optical element #03 (BS) for case #29 for 21800 eV photon energy setting.

### 39.12 Surface slope error in meridional direction (y)

"fig/CRL\_optim\_C111\_Laue/plot044.png" Lbl.:CRL\_optim\_C111\_Laue\_false\_colour\_plot\_phi\_y\_oe03\_c29\_21800eV

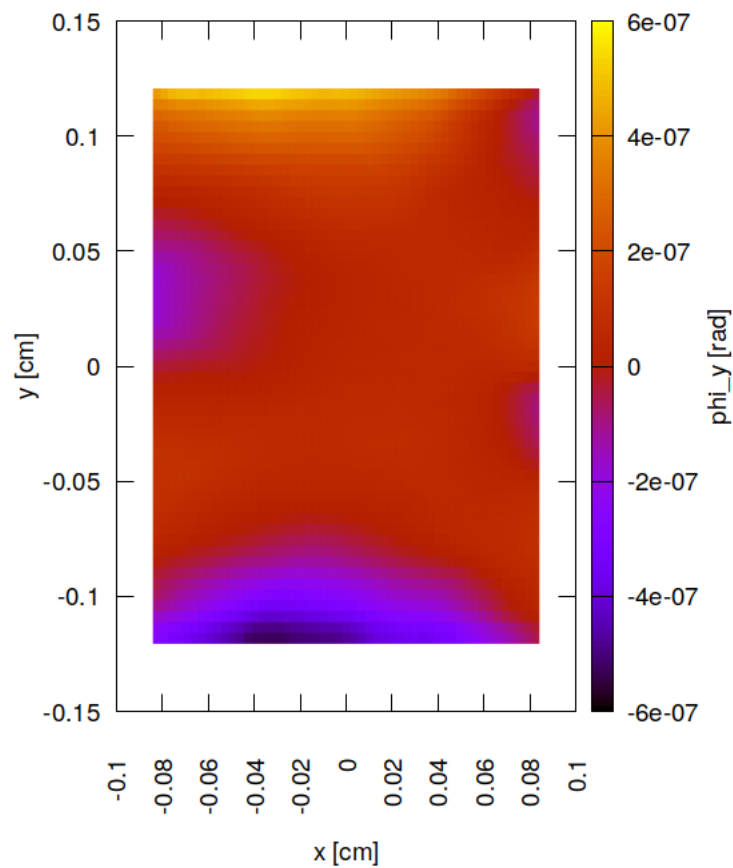


Figure 39.44: Surface slope error in meridional direction (y) of optical element #03 (BS) for case #29 for 21800 eV photon energy setting.



### 39.13 Incident photon irradiance on surface

"fig/CRL\_optim\_C111\_Laue/plot045.png" Lbl.:CRL\_optim\_C111\_Laue\_false\_colour\_plot\_I\_inc\_foot\_oe04\_c5\_21800eV



Figure 39.45: Incident photon irradiance on surface of optical element #04 (CM2) for case #5 for 21800 eV photon energy setting.

```
"fig/CRL_optim_C111_Laue/plot046.png" Lbl.:CRL_optim_C111_Laue_false_colour_plot_I_inc_foot_oe04_c29_21800eV
```

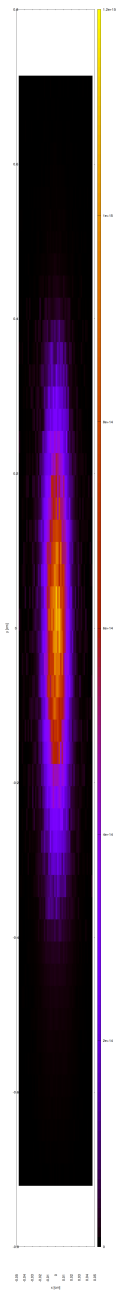


Figure 39.46: Incident photon irradiance on surface of optical element #04 (CM2) for case #29 for 21800 eV photon energy setting.

```
"fig/CRL_optim_C111_Laue/plot047.png" Lbl.:CRL_optim_C111_Laue_false_colour_plot_I_inc_foot_oe09_c5_21800eV
```



Figure 39.47: Incident photon irradiance on surface of optical element #09 (sample) for case #5 for 21800 eV photon energy setting.

```
"fig/CRL_optim_C111_Laue/plot048.png" Lbl.:CRL_optim_C111_Laue_false_colour_plot_I_inc_foot_oe09_c29_21800eV
```



Figure 39.48: Incident photon irradiance on surface of optical element #09 (sample) for case #29 for 21800 eV photon energy setting.



### 39.14 Photon irradiance in beam cross section

"fig/CRL\_optim\_C111\_Laue/plot049.png" Lbl.:CRL\_optim\_C111\_Laue\_false\_colour\_plot\_I\_foc\_oe04\_c5\_21800eV

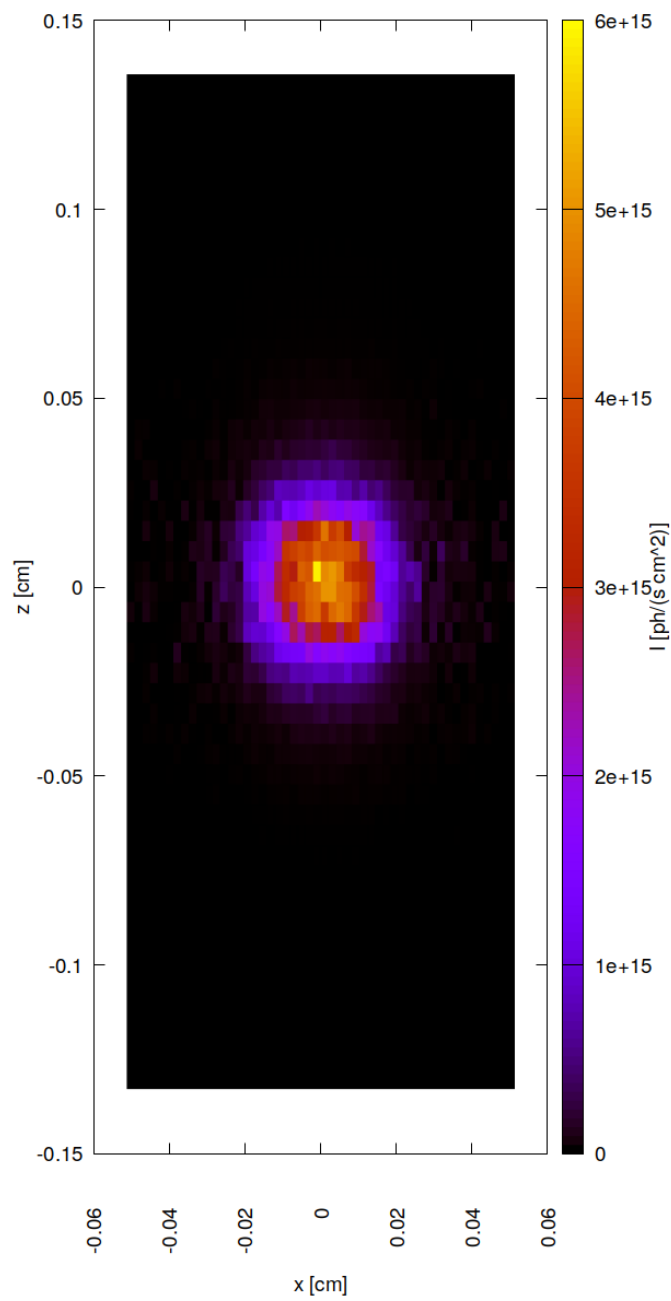


Figure 39.49: Photon irradiance in beam cross section of optical element #04 (CM2) for case #5 for 21800 eV photon energy setting.

"fig/CRL\_optim\_C111\_Laue/plot050.png" Lbl.:CRL\_optim\_C111\_Laue\_false\_colour\_plot\_I\_foc\_oe04\_c29\_21800eV

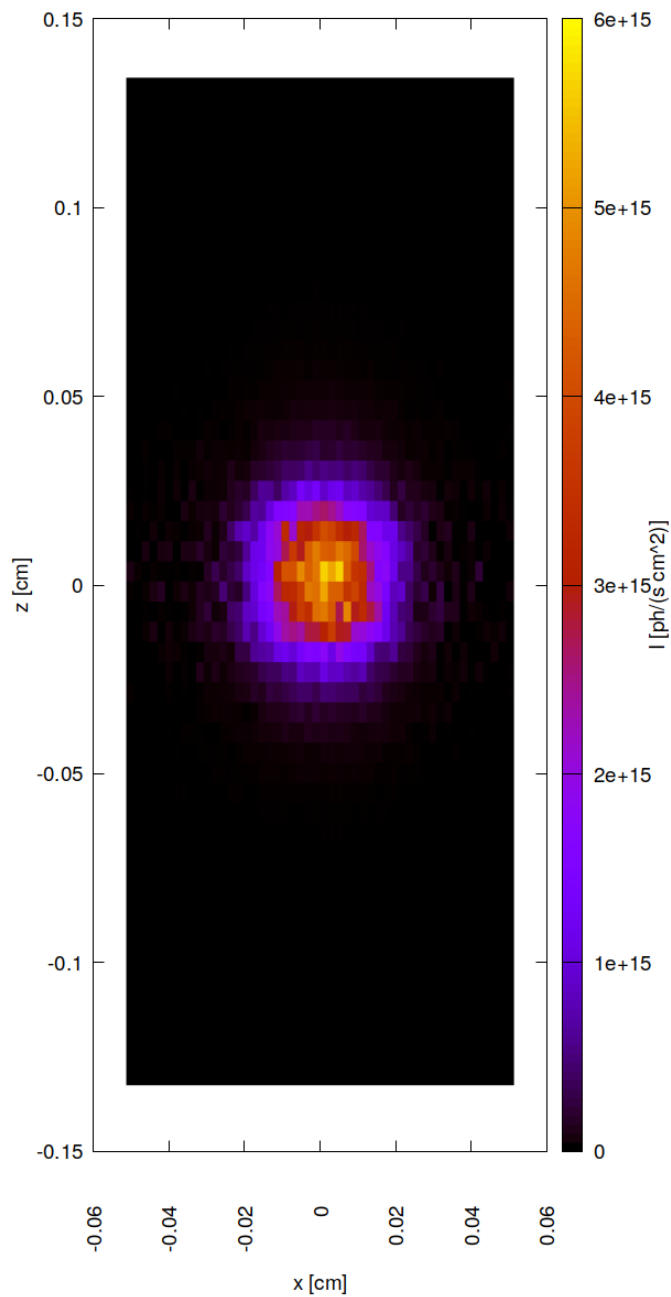


Figure 39.50: Photon irradiance in beam cross section of optical element #04 (CM2) for case #29 for 21800 eV photon energy setting.

```
"fig/CRL_optim_C111_Laue/plot051.png" Lbl.:CRL_optim_C111_Laue_false_colour_plot_I_foc_oe09_c5_21800eV
```

Figure 39.51: Photon irradiance in beam cross section of optical element #09 (sample) for case #5 for 21800 eV photon energy setting.

```
"fig/CRL_optim_C111_Laue/plot052.png" Lbl.:CRL_optim_C111_Laue_false_colour_plot_I_foc_oe09_c29_21800eV
```

Figure 39.52: Photon irradiance in beam cross section of optical element #09 (sample) for case #29 for 21800 eV photon energy setting.

## 39.15 Spectral photon flux in beam cross section

```
"fig/CRL_optim_C111_Laue/plot053.png" Lbl.:CRL_optim_C111_Laue_2d_plot_I_bandfoc_oe04_c5_21800eV
```

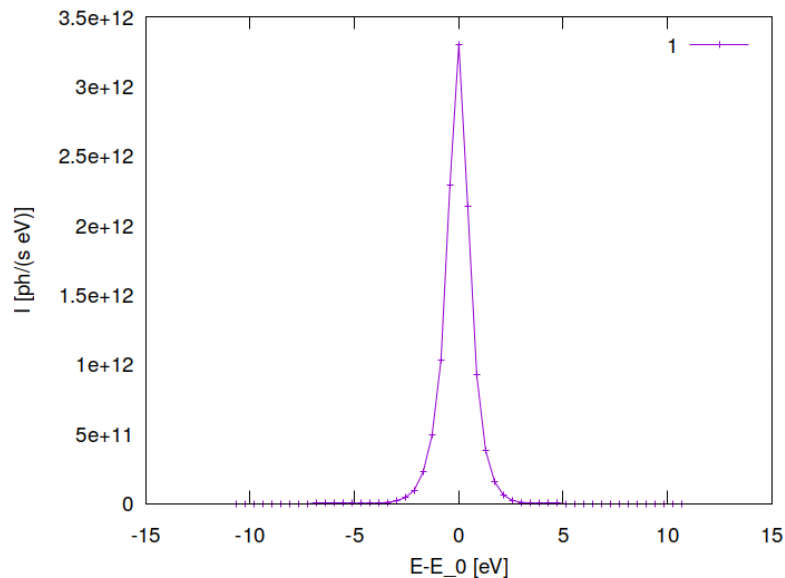


Figure 39.53: Spectral photon flux in beam cross section of optical element #04 (CM2) for case #5 for 21800 eV photon energy setting.

```
"fig/CRL_optim_C111_Laue/plot054.png" Lbl.:CRL_optim_C111_Laue_2d_plot_I_bandfoc_oe04_c29_21800eV
```

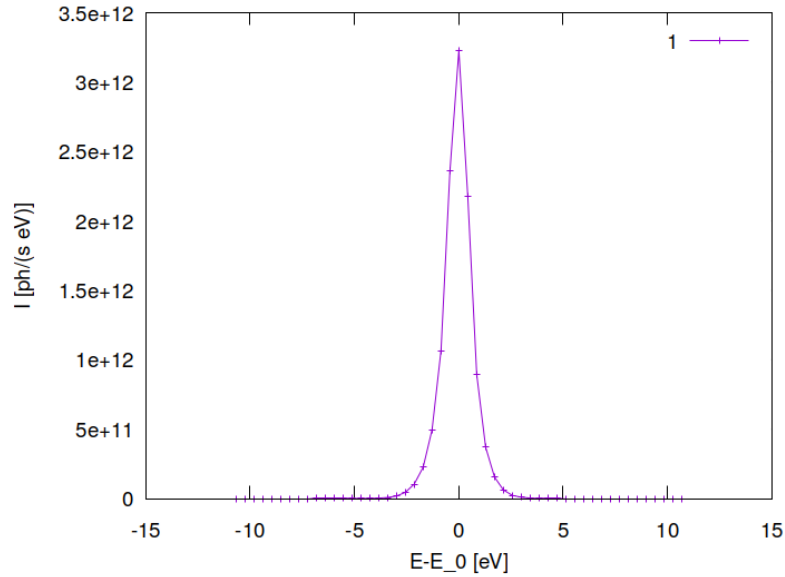


Figure 39.54: Spectral photon flux in beam cross section of optical element #04 (CM2) for case #29 for 21800 eV photon energy setting.

```
"fig/CRL_optim_C111_Laue/plot055.png" Lbl.:CRL_optim_C111_Laue_2d_plot_I_bandfoc_oe09_c5_21800eV
```

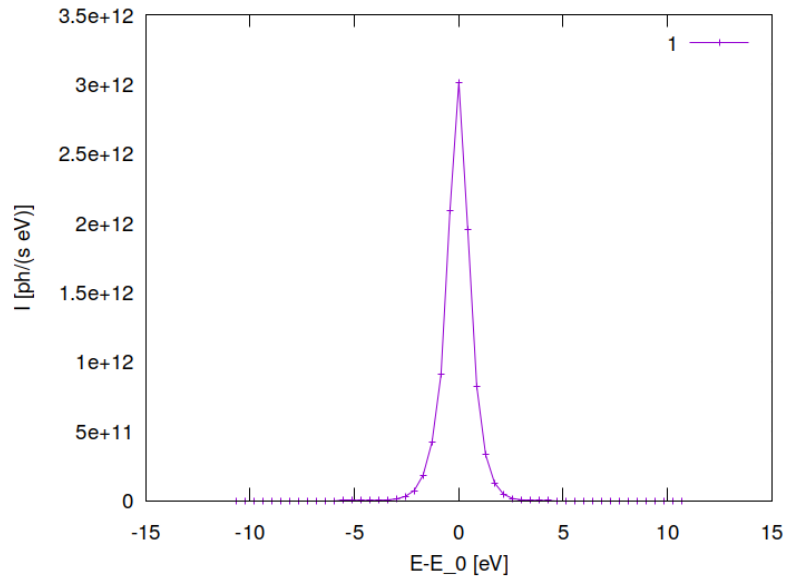


Figure 39.55: Spectral photon flux in beam cross section of optical element #09 (sample) for case #5 for 21800 eV photon energy setting.

```
"fig/CRL_optim_C111_Laue/plot056.png" Lbl.:CRL_optim_C111_Laue_2d_plot_I_bandfoc_oe09_c29_21800eV
```

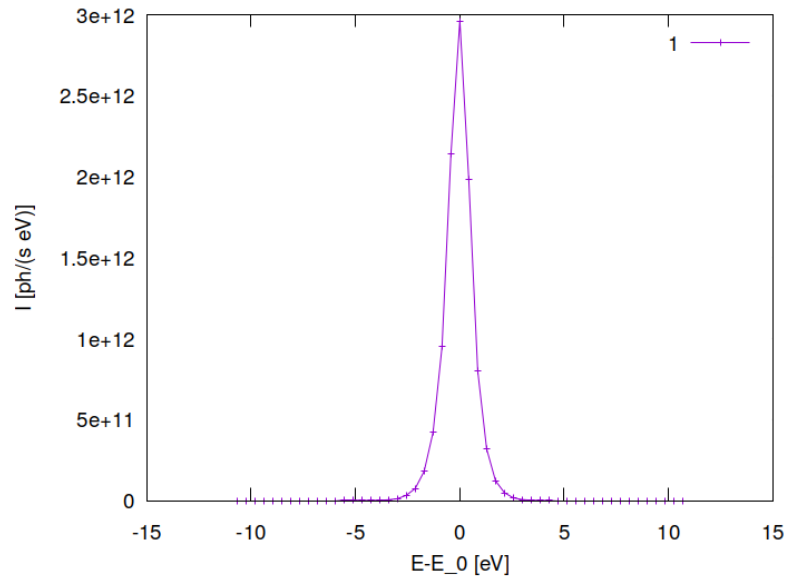


Figure 39.56: Spectral photon flux in beam cross section of optical element #09 (sample) for case #29 for 21800 eV photon energy setting.

## Chapter 40

# Focussing setup with beam splitter in Bragg geometry

A thin CVD diamond crystal is employed as a diffractive beam splitter, using the 111 reflection in Bragg geometry. The diamond 111 reflection diverts radiation within a narrow bandwidth of

$$\delta E/E = \delta\theta/\tan\theta$$

to the SinCrys side station.

Subsequent reflection from a second crystal of the same material using the same set of diffracting planes which are parallel to the first is required to provide the necessary stability of the exit beam which has to hit the very small acceptance aperture of the CRLs (see chapter 23.3).

Putting the second crystal at a distance of around 3.66 metres behind the first provides the required offset of more than one metre between the twice deflected beam and the main beam.

Compound refractive lenses (CRL) are used to focus the monochromatised beam onto the sample. Despite of the beam splitter in Bragg geometry not intrinsically focusing, unlike in Laue geometry, it still produces astigmatism due to deformation under heat load. The effects of deformation on the beam are more pronounced in Bragg geometry due to the more grazing incidence. This generates an astigmatism that needs to be addressed in the design of the CRL. A stack of two-dimensionally focussing lenses has to be complemented by a stack of horizontally focussing one-dimensional lenses compensating for the astigmatism.

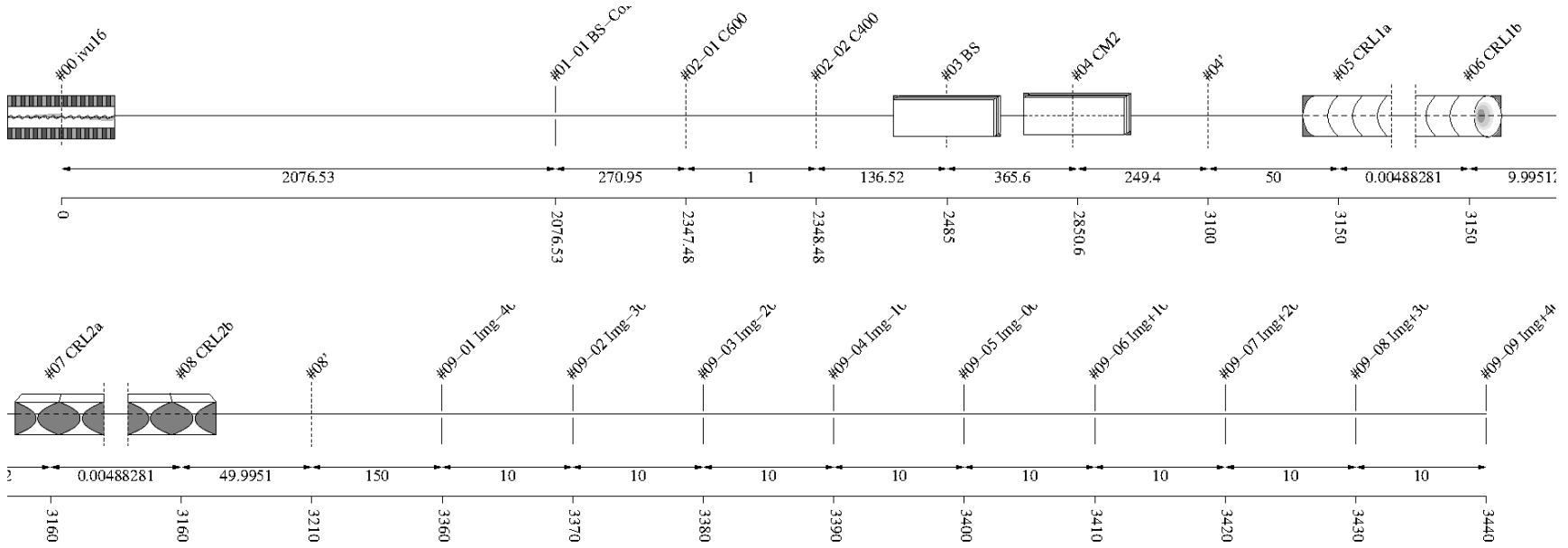


Figure 40.1: Schematic of optical setup

#	Name	Pathlen. cm	Descript.	Shape	Pitch* deg	Roll deg	Yaw deg	x_min cm	x_max cm	y_min cm	y_max cm	Thick. cm	Surface
0	ivu16	0	undulator	auto	0	0	0	-0.0027	0.0027	-0.0002	0.0002	auto	
1		2076.53	none	plane	0	0	0	-inf	inf	-inf	inf		perfect
1-1	BS-Collim	2076.53	aperture	rectangle	0	0	0	-0.035	0.035	-0.035	0.035		
2	Filter	2347.48	none	plane	0	0	0	-inf	inf	-inf	inf		perfect
2-1	C600	2347.48	C-filter	rectangle	0	0	0	-inf	inf	-inf	inf	0.06	

<b>2-2</b>	C400	2348.48	C-filter	rectangle	0	0	0	-inf	inf	-inf	inf	0.04	
<b>3</b>	BS	2485	C(1,1,1)-crystal	plane	7.93694	90	0	-0.15	0.15	-0.5	0.5		heat bump
<b>4</b>	CM2	2850.6	C(1,1,1)-crystal	plane	7.93694	180	0	-inf	inf	-inf	inf		perfect
<b>4'</b>		3100	continuation plane		0	0	0						
<b>5</b>	CRL1a	3150	vac/Be-lens surface	parabola	0	0	0	-0.045	0.045	-0.045	0.045		perfect
<b>6</b>	CRL1b	3150	Be/vac-lens surface	parabola	0	0	0	-0.045	0.045	-0.045	0.045		perfect
<b>7</b>	CRL2a	3160	vac/Be-lens surface	extruded parabola	0	-90	0	-0.1	0.1	-0.085	0.085		perfect
<b>8</b>	CRL2b	3160	Be/vac-lens surface	extruded parabola	0	0	0	-0.1	0.1	-0.085	0.085		perfect
<b>8'</b>		3210	continuation plane		0	0	0						
<b>9</b>	sample	3400	none	plane	0	0	0	-inf	inf	-inf	inf		perfect
<b>9-1</b>	Img-40	3360	aperture	rectangle	0	0	0	-0.025	0.025	-0.025	0.025		
<b>9-2</b>	Img-30	3370	aperture	rectangle	0	0	0	-0.025	0.025	-0.025	0.025		
<b>9-3</b>	Img-20	3380	aperture	rectangle	0	0	0	-0.025	0.025	-0.025	0.025		
<b>9-4</b>	Img-10	3390	aperture	rectangle	0	0	0	-0.025	0.025	-0.025	0.025		
<b>9-5</b>	Img-00	3400	aperture	rectangle	0	0	0	-0.025	0.025	-0.025	0.025		
<b>9-6</b>	Img+10	3410	aperture	rectangle	0	0	0	-0.025	0.025	-0.025	0.025		
<b>9-7</b>	Img+20	3420	aperture	rectangle	0	0	0	-0.025	0.025	-0.025	0.025		
<b>9-8</b>	Img+30	3430	aperture	rectangle	0	0	0	-0.025	0.025	-0.025	0.025		
<b>9-9</b>	Img+40	3440	aperture	rectangle	0	0	0	-0.025	0.025	-0.025	0.025		

Table 40.1: Setup parameters common to all components. (\*Glancing angle for mirrors, multilayers and crystals. Angle to surface normal otherwise.)

**Rays:** Polar type = total

Polar phase = 0 deg

Polar degree = 0

Is coherent = no

**Spectrum:** E min = 500 eV

E max = 40000 eV

Relative linewidth = 1

**Band:** Bandwidth = 0.0005

**Insertion Device:** lambda period = 1.6 cm

n period = 187

I electron = 0.5 A

E electron = 3 GeV

y horizontal waist = 0 cm

y vertical waist = 0 cm

epsilon x = 3.2E-08 cm rad

epsilon z = 8E-10 cm rad

K y = 1.66

K ymax = 1.7

Divergence limit = 5E-05 rad

**Undulator:** n harmonic max = 99

Tuning type = fixed gap

l aperture = 2076.53 cm

dx aperture = 0.07 cm

dz aperture = 0.07 cm

#1

**Screen:** Is absorbing[1] = no

**Shape:** Thickness = 0 cm

#2 Filter

**Screen:** Is absorbing[1] = yes

Is absorbing[2] = yes

Molecular formula[1] = C

Molecular formula[2] = C

Mass density[1] = 3.5 g/cm^3

Mass density[2] = 3.5 g/cm^3

Thickness[1] = 0.06 cm

Thickness[2] = 0.04 cm

**Shape:** Thickness = 0 cm

### #3 BS

**Crystal:** Structure type = zinblend

Lattice constant[1] = 3.567 Angstrom  
Lattice constant[2] = 3.567 Angstrom  
Lattice constant[3] = 3.567 Angstrom  
Debye Waller factor = 1  
Is absorbing = yes  
Is asymmetric = no  
Is inclined = no  
Is Johansson geometry = no  
Is mosaic = no

**Tune:** z rotation axis = 0 cm

**Geometry:** Is thin = yes

Tune automatic = yes

**Shape:** Thickness = 0.01 cm

**Boundary:** Type = rectangle

x rim = 0.5 cm  
y rim = 0.5 cm

**Surface:** Is rough = no

**FEA:** Design type = type specific

Crystal design = laue with cooling loop  
Is isotropic = no  
Angle x = 0 deg  
Angle y = 0 deg  
Angle z = 0 deg  
Mass density = 3.516 g/cm<sup>3</sup>

**Heat:** Heat transfer type[1] = insulated

Heat transfer type[2] = heat transfer  
Heat transfer type[3] = insulated  
Heat transfer type[4] = insulated  
Heat transfer type[5] = heat transfer  
Heat transfer type[6] = flux  
Heat transfer type[7] = insulated  
Heat transfer type[8] = heat transfer  
Heat transfer type[9] = heat sink  
Heat transfer coefficient = 1 W/(cm<sup>2</sup>K)  
Heat sink coefficient = 10 W/(cm<sup>2</sup>K)  
T reference = 293.15 K  
T cooling = 293.15 K  
Heat capacity = 0.54 J/(gK)  
Thermal conductivity[1] = 25 W/(cmK<sup>n</sup>)

**Stress and strain:** Constraint[1] = free  
 Constraint[2] = kinematic  
 Constraint[3] = free  
 Constraint[4] = free  
 Constraint[5] = free  
 Constraint[6] = free  
 Constraint[7] = free  
 Constraint[8] = free  
 Constraint[9] = free  
 Thermal expansion tensor[1] = 1.1E-06 1/K  
 Thermal expansion tensor[2] = 1.1E-06 1/K  
 Thermal expansion tensor[3] = 1.1E-06 1/K  
 Thermal expansion tensor[4] = 0 1/K  
 Thermal expansion tensor[5] = 0 1/K  
 Thermal expansion tensor[6] = 0 1/K  
 Stiffness tensor(1)(1) = 1.07861E+12 Pa  
 Stiffness tensor(2)[1] = 1.2663E+11 Pa  
 Stiffness tensor(2)[2] = 1.07861E+12 Pa  
 Stiffness tensor(3)[1] = 1.2663E+11 Pa  
 Stiffness tensor(3)[2] = 1.2663E+11 Pa  
 Stiffness tensor(3)[3] = 1.07861E+12 Pa  
 Stiffness tensor(4)[1] = 0 Pa  
 Stiffness tensor(4)[2] = 0 Pa  
 Stiffness tensor(4)[3] = 0 Pa  
 Stiffness tensor(4)[4] = 5.7756E+11 Pa  
 Stiffness tensor(5)[1] = 0 Pa  
 Stiffness tensor(5)[2] = 0 Pa  
 Stiffness tensor(5)[3] = 0 Pa  
 Stiffness tensor(5)[4] = 0 Pa  
 Stiffness tensor(5)[5] = 5.7756E+11 Pa  
 Stiffness tensor(6)[1] = 0 Pa  
 Stiffness tensor(6)[2] = 0 Pa  
 Stiffness tensor(6)[3] = 0 Pa  
 Stiffness tensor(6)[4] = 0 Pa  
 Stiffness tensor(6)[5] = 0 Pa  
 Stiffness tensor(6)[6] = 5.7756E+11 Pa

#### #4 CM2

**Crystal:** Structure type = zinblend  
 Lattice constant[1] = 3.567 Angstrom  
 Lattice constant[2] = 3.567 Angstrom  
 Lattice constant[3] = 3.567 Angstrom  
 Debye Waller factor = 1  
 Is absorbing = yes  
 Is asymmetric = no  
 Is inclined = no  
 Is Johansson geometry = no  
 Is mosaic = no

**Tune:** Type = constant pathlength  
 Are downstream elements fixed = no

**Geometry:** Is thin = no  
Tune automatic = yes

**Boundary:** Type = none

**Surface:** Is rough = no

### #5 CRL1a

**Dielectric:** Reflectivity type = polarisation  
Is constant = no  
Mass density = 1.85 g/cm<sup>3</sup>

**Geometry:** g = 3150 cm  
b = 250 cm  
Is thin = yes  
n clones = 5  
n originals = 2  
Focus automatically = yes

**Focus:** Type = chromatic  
Number variation method = cloning  
Vary distance = no

**Shape:** Defined by = user  
Is convex = no  
Is extruded = no  
Radius = 0.02 cm  
Thickness = 0.005 cm

**Boundary:** Type = ellipse

**Parabola:** Is source in infinity = no  
p semi = 0.02 cm

**Surface:** Is rough = no

### #6 CRL1b

**Dielectric:** Reflectivity type = polarisation  
Is constant = yes  
delta refraction = 0  
beta absorption = 0

**Geometry:** g = 3150 cm  
b = 250 cm  
Is thin = yes  
n clones = 5  
n originals = 0  
Focus automatically = yes

**Focus:** Type = chromatic  
Number variation method = cloning  
Vary distance = no

**Shape:** Defined by = user  
Is convex = yes  
Is extruded = no  
Radius = 0.02 cm  
Thickness = 0.005 cm

**Boundary:** Type = ellipse

**Parabola:** Is source in infinity = no  
p semi = 0.02 cm

**Surface:** Is rough = no

## #7 CRL2a

**Dielectric:** Reflectivity type = polarisation  
Is constant = no  
Mass density = 1.85 g/cm<sup>3</sup>

**Geometry:** g = -255 cm  
b = 240 cm  
Is thin = yes  
n clones = 6  
n originals = 2  
Focus automatically = yes

**Focus:** Type = chromatic  
Number variation method = cloning  
Vary distance = no

**Shape:** Defined by = user  
Is convex = no  
Is extruded = yes  
Radius = 0.1 cm  
Thickness = 0.005 cm

**Boundary:** Type = rectangle

**Parabola:** Is source in infinity = no  
p semi = 0.1 cm

**Extruded:** Angle z = 0 deg

**Surface:** Is rough = no

### #8 CRL2b

**Dielectric:** Reflectivity type = polarisation  
Is constant = yes  
delta refraction = 0  
beta absorption = 0

**Geometry:** g = -255 cm  
b = 240 cm  
Is thin = yes  
n clones = 6  
n originals = 0  
Focus automatically = yes

**Focus:** Type = chromatic  
Number variation method = cloning  
Vary distance = no

**Shape:** Defined by = user  
Is convex = yes  
Is extruded = yes  
Radius = 0.1 cm  
Thickness = 0.005 cm

**Boundary:** Type = rectangle

**Parabola:** Is source in infinity = no  
p semi = 0.1 cm

**Extruded:** Angle z = 0 deg

**Surface:** Is rough = no

### #9 sample

**Screen:** Is absorbing[1] = no  
Is absorbing[2] = no  
Is absorbing[3] = no  
Is absorbing[4] = no  
Is absorbing[5] = no  
Is absorbing[6] = no  
Is absorbing[7] = no  
Is absorbing[8] = no  
Is absorbing[9] = no

**Shape:** Thickness = 0 cm

## **Chapter 41**

### **Parameter scan cases**

There are 48 cases in total, 24 without heat load on the beam splitter and 24 with. The number of 24 results from the combination of six 2D lens types and four 1D lens types, which were all tested for optimizing throughput and element numbers of the CRLs. Only two out of the 48 cases are finally relevant, i.e. cases #5 and #29. These are the cases without and with heat load respectively and a combination of lens types that provide high throughput with a reasonable number of elements.

Case	Has_slope_error_03	Skip_heatload	a_ellipse_05 cm	p_semi_05 cm	y_negative_07 cm	y_positive_07 cm	p_semi_07 cm
1	no	yes	0.02	0.005	0.03	0.03	0.02
2	no	yes	0.02	0.005	0.04	0.04	0.03
3	no	yes	0.02	0.005	0.05	0.05	0.05
4	no	yes	0.02	0.005	0.085	0.085	0.1
5	no	yes	0.03	0.01	0.03	0.03	0.02
6	no	yes	0.03	0.01	0.04	0.04	0.03
7	no	yes	0.03	0.01	0.05	0.05	0.05
8	no	yes	0.03	0.01	0.085	0.085	0.1
9	no	yes	0.045	0.02	0.03	0.03	0.02
10	no	yes	0.045	0.02	0.04	0.04	0.03
11	no	yes	0.045	0.02	0.05	0.05	0.05
12	no	yes	0.045	0.02	0.085	0.085	0.1
13	no	yes	0.055	0.03	0.03	0.03	0.02
14	no	yes	0.055	0.03	0.04	0.04	0.03
15	no	yes	0.055	0.03	0.05	0.05	0.05
16	no	yes	0.055	0.03	0.085	0.085	0.1
17	no	yes	0.07	0.05	0.03	0.03	0.02
18	no	yes	0.07	0.05	0.04	0.04	0.03
19	no	yes	0.07	0.05	0.05	0.05	0.05
20	no	yes	0.07	0.05	0.085	0.085	0.1
21	no	yes	0.095	0.1	0.03	0.03	0.02
22	no	yes	0.095	0.1	0.04	0.04	0.03
23	no	yes	0.095	0.1	0.05	0.05	0.05
24	no	yes	0.095	0.1	0.085	0.085	0.1
25	yes	no	0.02	0.005	0.03	0.03	0.02
26	yes	no	0.02	0.005	0.04	0.04	0.03
27	yes	no	0.02	0.005	0.05	0.05	0.05
28	yes	no	0.02	0.005	0.085	0.085	0.1
29	yes	no	0.03	0.01	0.03	0.03	0.02
30	yes	no	0.03	0.01	0.04	0.04	0.03
31	yes	no	0.03	0.01	0.05	0.05	0.05
32	yes	no	0.03	0.01	0.085	0.085	0.1
33	yes	no	0.045	0.02	0.03	0.03	0.02
34	yes	no	0.045	0.02	0.04	0.04	0.03
35	yes	no	0.045	0.02	0.05	0.05	0.05
36	yes	no	0.045	0.02	0.085	0.085	0.1
37	yes	no	0.055	0.03	0.03	0.03	0.02
38	yes	no	0.055	0.03	0.04	0.04	0.03
39	yes	no	0.055	0.03	0.05	0.05	0.05
40	yes	no	0.055	0.03	0.085	0.085	0.1
41	yes	no	0.07	0.05	0.03	0.03	0.02
42	yes	no	0.07	0.05	0.04	0.04	0.03
43	yes	no	0.07	0.05	0.05	0.05	0.05
44	yes	no	0.07	0.05	0.085	0.085	0.1
45	yes	no	0.095	0.1	0.03	0.03	0.02
46	yes	no	0.095	0.1	0.04	0.04	0.03
47	yes	no	0.095	0.1	0.05	0.05	0.05
48	yes	no	0.095	0.1	0.085	0.085	0.1

Table 41.1: Parameter values for different cases in parameter scan

### Legend

**Case:** Case number in parameter scan

**Has\_slope\_error\_03:** Optical\_element\_#3.Surface.Has\_slope\_error (Has surface slope error?)

**Skip\_heatload:** Session.Skip\_heatload (Skip heat load calculation for all optical elements? (heat load parameters are kept))

**a\_ellipse\_05:** Optical\_element\_#5.Shape.Boundary.a\_ellipse (External outline semi-axis in meridional direction.)

**p\_semi\_05:** Optical\_element\_#5.Shape.Parabola.p\_semi (Semilatus rectum p of parabola:  
 $y = x^2/2p$  in cartesian or  $r = p/(1+\cos(\phi))$  in polar coordinates. The radius of curvature in the lens center is  $R_0 = p$ .)

**y\_negative\_07:** Optical\_element\_#7.Shape.Boundary.y\_negative (Lateral extension  
in neg. y-direction.)

**y\_positive\_07:** Optical\_element\_#7.Shape.Boundary.y\_positive (Lateral extension  
in pos. y-direction.)

**p\_semi\_07:** Optical\_element\_#7.Shape.Parabola.p\_semi (Semilatus rectum p of parabola:  
 $y = x^2/2p$  in cartesian or  $r = p/(1+\cos(\phi))$  in polar coordinates. The radius of curvature in the lens center is  $R_0 = p$ .)

## Chapter 42

# Photon energy scan

The  $K_y$ -values in the table below are those for optimised output between 15.6 and 18.3 keV used by DanMAX' main branch. The number of required 2D and 1D focussing lens elements of the type that provided maximum throughput under realistic conditions are also provided here. These are the 2D and 1D lens types used in case #5, with central radius of curvature of 100 and 200 microns respectively.

E eV	K_y	n_harm/step	theta_B03 deg	nMult_05	nMult_07
<b>20000</b>	1.67551	9	8.6565237	25	0
<b>20100</b>	1.66836	9	8.6131277	25	0
<b>20200</b>	1.66125	9	8.5701675	26	0
<b>20300</b>	1.65418	9	8.5276346	26	0
<b>20400</b>	1.64714	9	8.4855232	26	0
<b>20500</b>	1.64015	9	8.4438276	27	0
<b>20600</b>	1.63319	9	8.4025402	27	0
<b>20700</b>	1.62628	9	8.3616571	27	0
<b>20800</b>	1.6194	9	8.3211708	27	0
<b>20900</b>	1.61255	9	8.2810764	28	0
<b>21000</b>	1.60575	9	8.2413683	28	0
<b>21100</b>	1.59898	9	8.2020397	28	0
<b>21200</b>	1.59224	9	8.1630869	28	0
<b>21300</b>	1.58554	9	8.1245022	29	0
<b>21400</b>	1.57887	9	8.0862827	29	0
<b>21500</b>	1.57224	9	8.0484219	29	0
<b>21600</b>	1.56564	9	8.0109158	29	0
<b>21700</b>	1.55908	9	7.9737582	30	0
<b>21800</b>	1.55255	9	7.936945	30	0
<b>21900</b>	1.54605	9	7.9004712	30	0
<b>22000</b>	1.53958	9	7.8643322	31	0
<b>22100</b>	1.53315	9	7.8285236	31	0
<b>22200</b>	1.52674	9	7.7930403	31	0
<b>22300</b>	1.52037	9	7.7578783	31	0
<b>22400</b>	1.51402	9	7.7230334	32	0
<b>22500</b>	1.50771	9	7.6885004	32	0
<b>22600</b>	1.50143	9	7.6542764	32	0
<b>22700</b>	1.49517	9	7.6203566	33	0
<b>22800</b>	1.48895	9	7.5867367	33	0
<b>22900</b>	1.48275	9	7.5534129	33	0
<b>23000</b>	1.47658	9	7.5203819	33	0
<b>23100</b>	1.47044	9	7.487639	34	0
<b>23200</b>	1.46433	9	7.4551811	34	0
<b>23300</b>	1.45824	9	7.4230037	34	0
<b>23400</b>	1.45218	9	7.3911042	35	0
<b>23500</b>	1.44615	9	7.359478	35	0

Table 42.1: Scan values for different photon energies in energy scan of setup without heat load

E eV	P_sum W	theta_B03 deg	nMult_05	nMult_07
20000	170.798	8.6565237	25	2
20100	170.209	8.6131277	25	2
20200	169.47	8.5701675	25	2
20300	168.879	8.5276346	25	2
20400	168.315	8.4855232	26	2
20500	167.588	8.4438276	26	2
20600	166.189	8.4025402	26	2
20700	165.542	8.3616571	26	2
20800	164.949	8.3211708	27	2
20900	164.413	8.2810764	27	2
21000	163.752	8.2413683	27	2
21100	163.16	8.2020397	27	2
21200	162.507	8.1630869	28	2
21300	161.904	8.1245022	28	2
21400	161.386	8.0862827	28	2
21500	160.797	8.0484219	28	2
21600	160.163	8.0109158	29	2
21700	159.473	7.9737582	29	2
21800	158.884	7.936945	29	2
21900	157.585	7.9004712	29	2
22000	157.101	7.8643322	30	2
22100	156.451	7.8285236	30	2
22200	155.93	7.7930403	30	2
22300	155.254	7.7578783	31	2
22400	154.716	7.7230334	31	2
22500	154.16	7.6885004	31	2
22600	153.484	7.6542764	31	2
22700	152.951	7.6203566	32	2
22800	152.294	7.5867367	32	2
22900	151.786	7.5534129	32	2
23000	151.176	7.5203819	32	2
23100	150.589	7.487639	33	2
23200	149.911	7.4551811	33	2
23300	148.827	7.4230037	33	2
23400	148.246	7.3911042	34	2
23500	147.698	7.359478	34	2

Table 42.2: Scan values for different photon energies in energy scan with heat load on the beam splitter.

### Legend

**E:** photon energy

**P\_sum:** sum of power in harmonics / energy intervals, P\_sum = P\_src

**theta\_B03:** Bragg angle, i.e. glancing angle of incident and reflected beam w.r.t. the set of diffracting planes of optical element 03

**nMult\_05:** number of elements in compound refractive lens optical element 05

**nMult\_07:** number of elements in compound refractive lens optical element 07

# Chapter 43

## Plots

### 43.1 Statistics of incident irradiance

```
"fig/CRL_optim_C111_Bragg/plot001.png" Lbl.:CRL_optim_C111_Bragg_2d_plot_I_peak_incstat_oe03
```

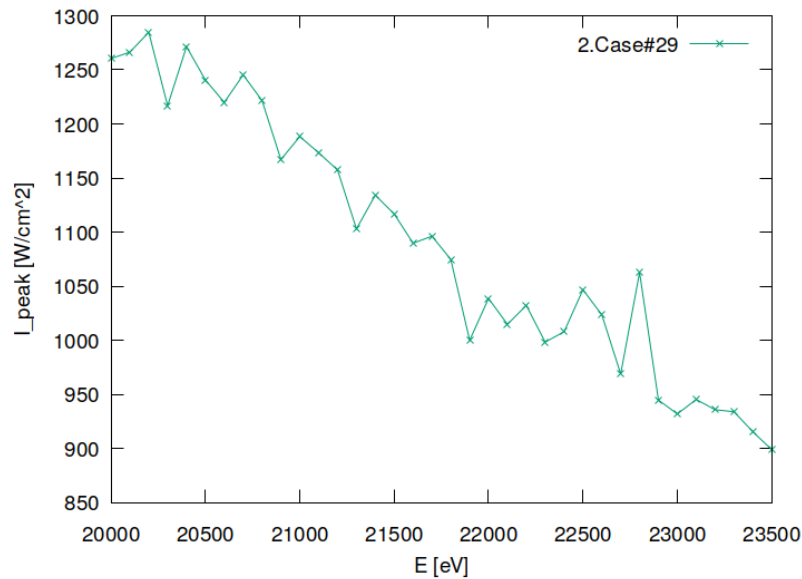


Figure 43.1: Incident peak irradiance of optical element #03 (BS).

```
"fig/CRL_optim_C111_Bragg/plot002.png" Lbl.:CRL_optim_C111_Bragg_2d_plot_I_int_incstat_oe03
```

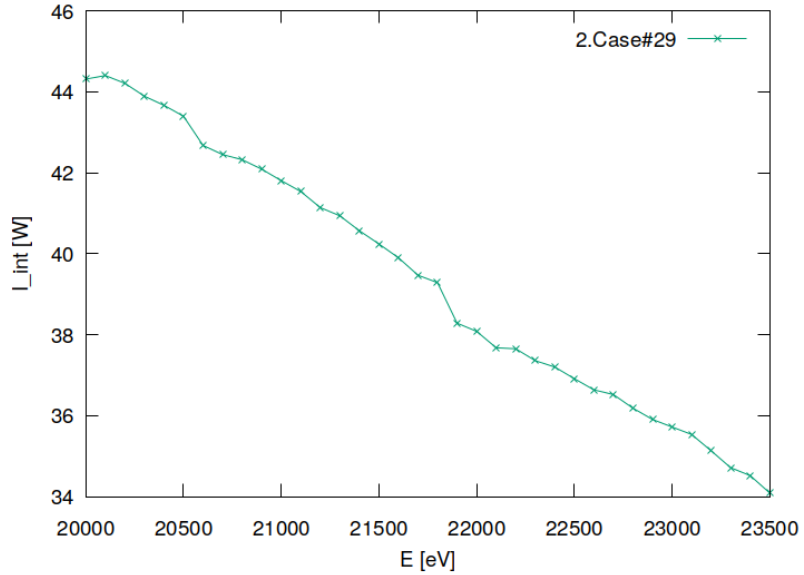


Figure 43.2: Incident flux of optical element #03 (BS).

## 43.2 Statistics of absorbed irradiance

```
"fig/CRL_optim_C111_Bragg/plot003.png" Lbl.:CRL_optim_C111_Bragg_2d_plot_I_peak_absstat_oe03
```

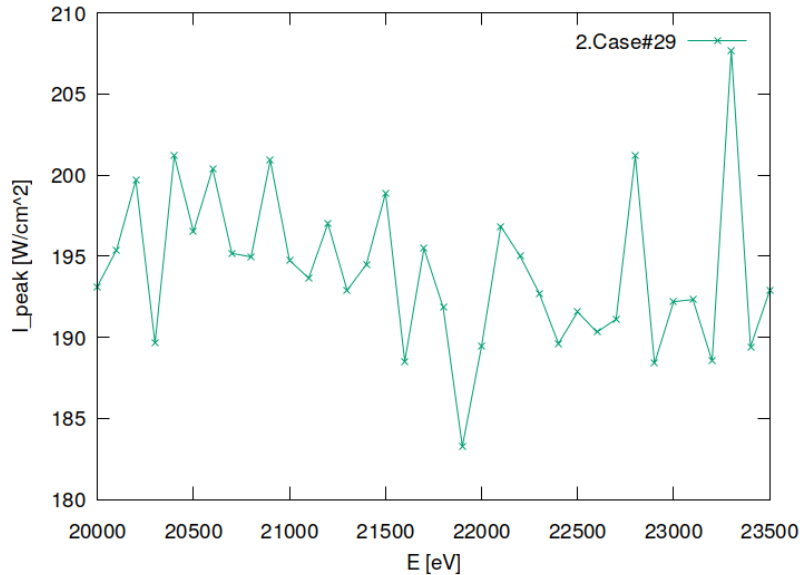


Figure 43.3: Absorbed peak irradiance of optical element #03 (BS).

```
"fig/CRL_optim_C111_Bragg/plot004.png" Lbl.:CRL_optim_C111_Bragg_2d_plot_I_int_absstat_oe03
```

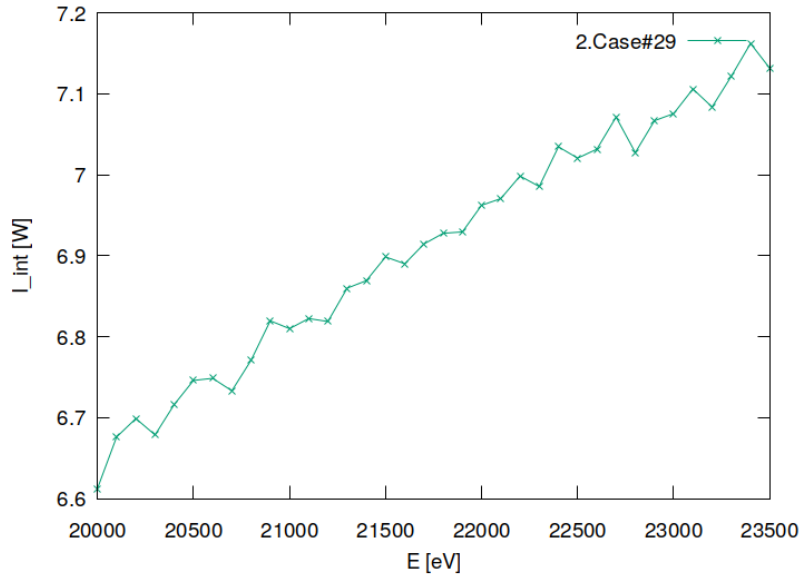


Figure 43.4: Absorbed flux of optical element #03 (BS).

### 43.3 Statistics of temperature

```
"fig/CRL_optim_C111_Bragg/plot005.png" Lbl.:CRL_optim_C111_Bragg_2d_plot_T_peak_stat_oe03
```

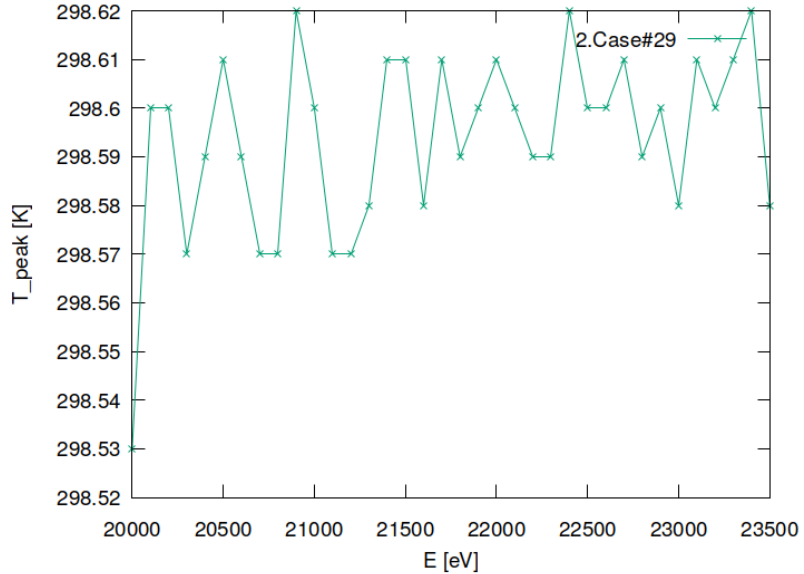


Figure 43.5: Peak temperature of optical element #03 (BS).

## 43.4 Statistics of mechanical stress (von Mises stress)

"fig/CRL\_optim\_C111\_Bragg/plot006.png" Lbl.:CRL\_optim\_C111\_Bragg\_2d\_plot\_sigma\_peak\_stat\_oe03

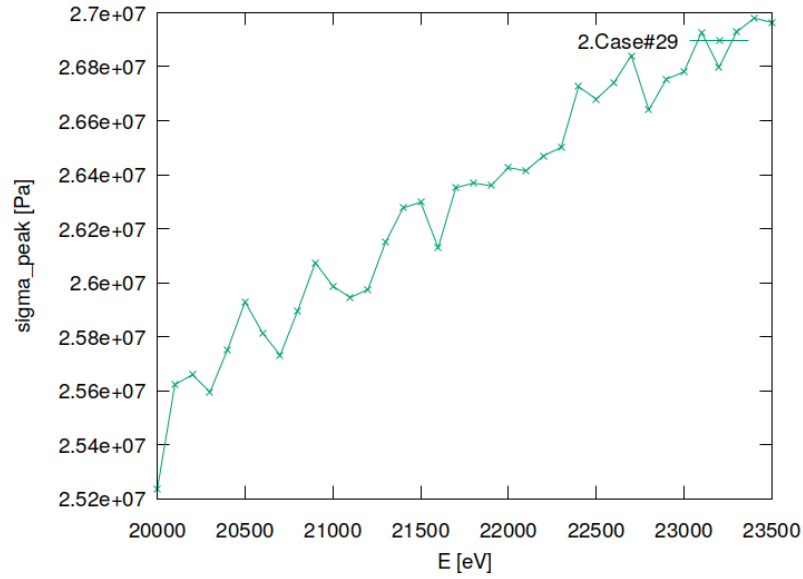


Figure 43.6: Peak mechanical stress (Von Mises stress) of optical element #03 (BS).

## 43.5 Statistics of optical surface deformation

"fig/CRL\_optim\_C111\_Bragg/plot007.png" Lbl.:CRL\_optim\_C111\_Bragg\_2d\_plot\_dz\_peak\_stat\_oe03

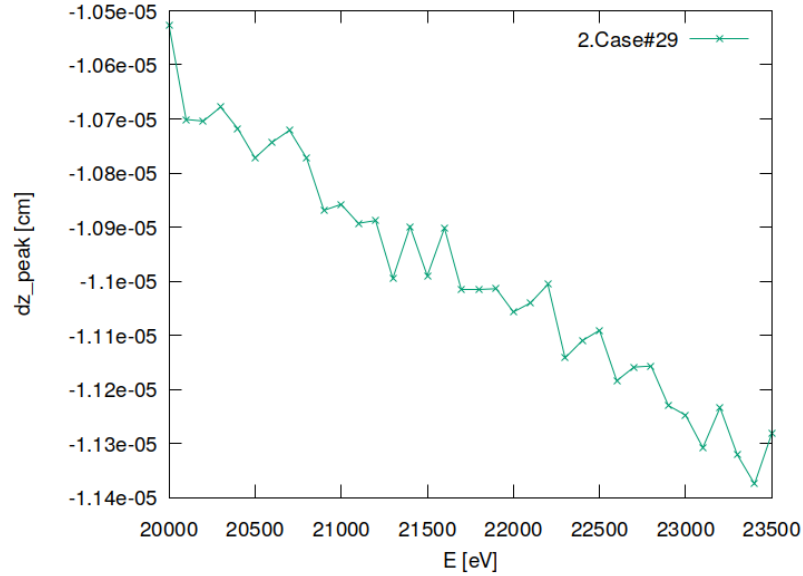


Figure 43.7: Peak deformation of optical element #03 (BS).

## 43.6 Statistics of photon irradiance on optical surface

"fig/CRL\_optim\_C111\_Bragg/plot008.png" Lbl.:CRL\_optim\_C111\_Bragg\_2d\_plot\_dx\_fwhm\_inc\_footstat\_oe04

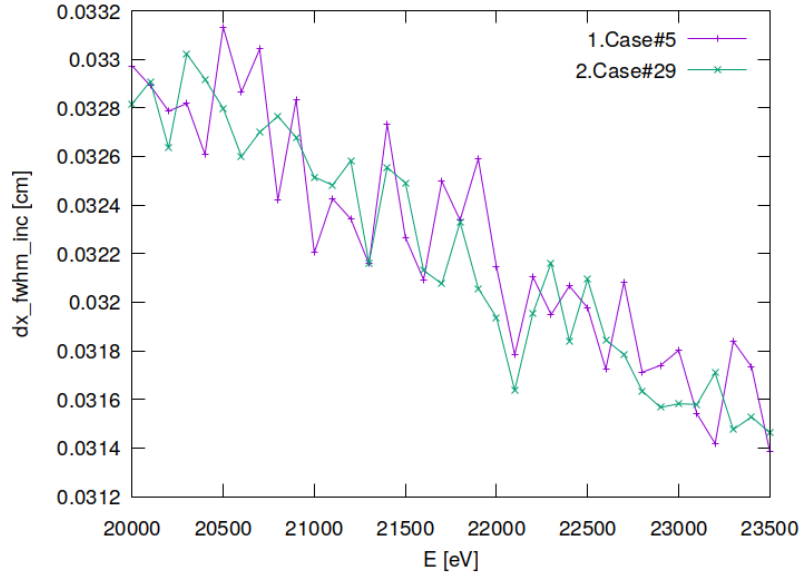


Figure 43.8: Sagittal footprint diameter (FWHM) of optical element #04 (CM2).

"fig/CRL\_optim\_C111\_Bragg/plot009.png" Lbl.:CRL\_optim\_C111\_Bragg\_2d\_plot\_dx\_fwhm\_inc\_footstat\_oe09

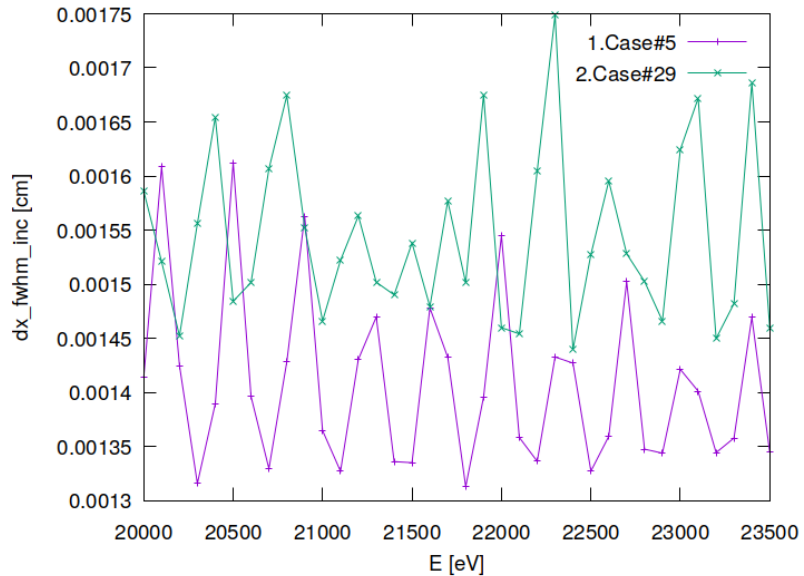


Figure 43.9: Sagittal footprint diameter (FWHM) of optical element #09 (sample).

```
"fig/CRL_optim_C111_Bragg/plot010.png" Lbl.:CRL_optim_C111_Bragg_2d_plot_dy_fwhm_inc_footstat_oe04
```

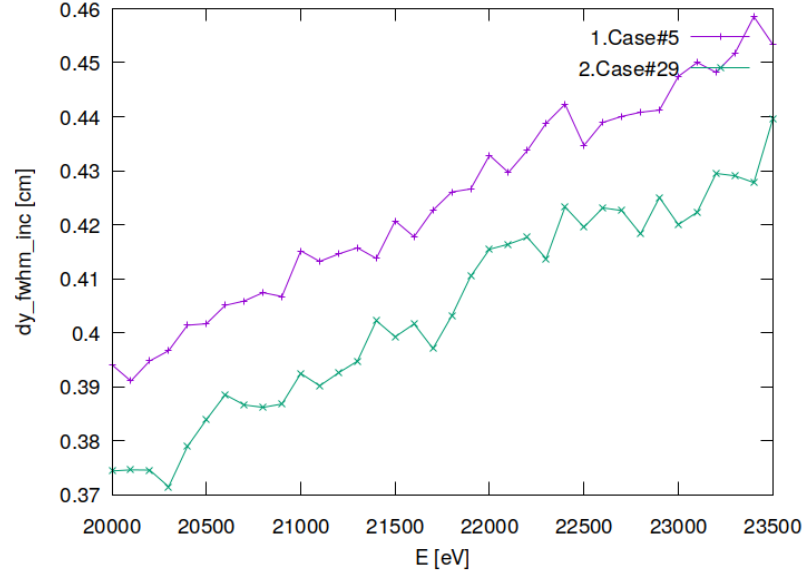


Figure 43.10: Meridional footprint diameter (FWHM) of optical element #04 (CM2).

```
"fig/CRL_optim_C111_Bragg/plot011.png" Lbl.:CRL_optim_C111_Bragg_2d_plot_dy_fwhm_inc_footstat_oe09
```

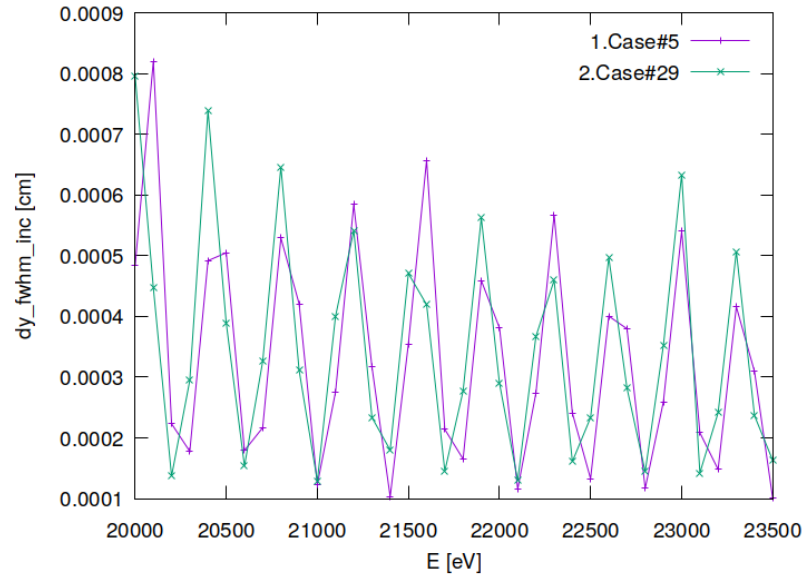


Figure 43.11: Meridional footprint diameter (FWHM) of optical element #09 (sample).

```
"fig/CRL_optim_C111_Bragg/plot012.png" Lbl.:CRL_optim_C111_Bragg_2d_plot_I_inc_int_footstat_oe04
```

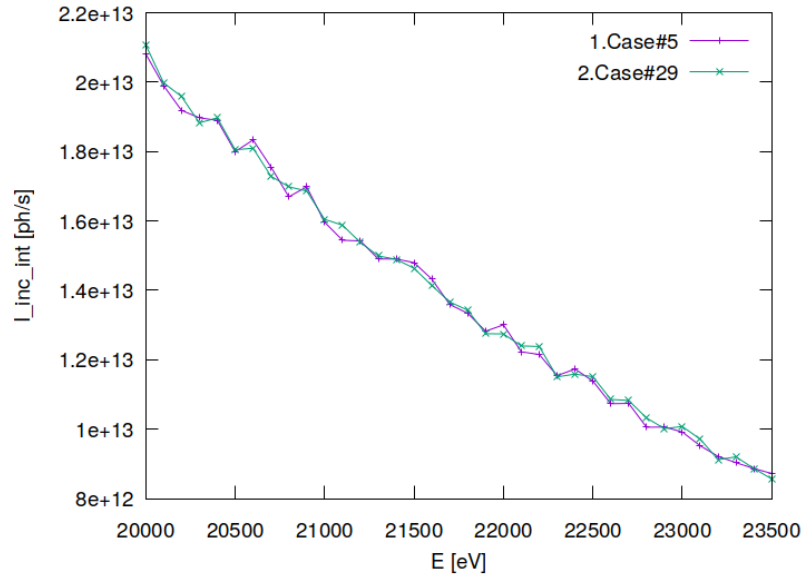


Figure 43.12: Incident photon flux on surface of optical element #04 (CM2).

```
"fig/CRL_optim_C111_Bragg/plot013.png" Lbl.:CRL_optim_C111_Bragg_2d_plot_I_inc_int_footstat_oe09
```

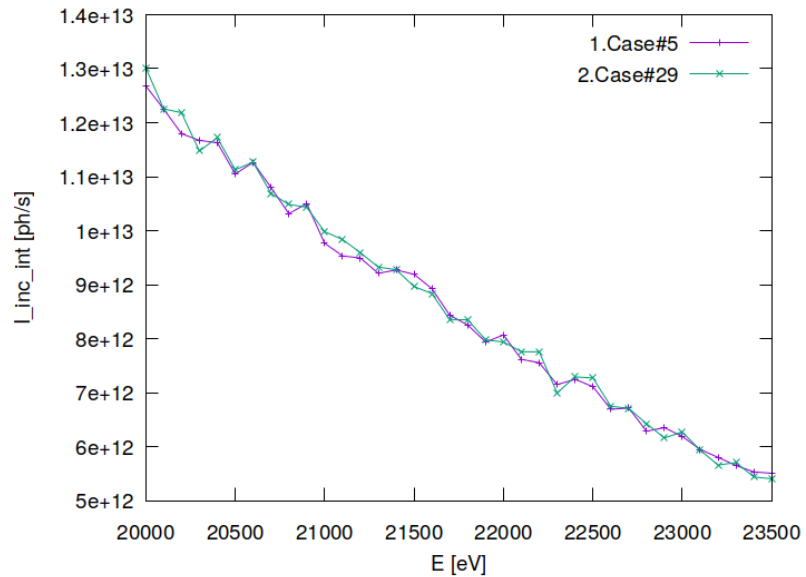


Figure 43.13: Incident photon flux on surface of optical element #09 (sample).

```
"fig/CRL_optim_C111_Bragg/plot014.png" Lbl.:CRL_optim_C111_Bragg_2d_plot_x_cen_inc_footstat_oe04
```

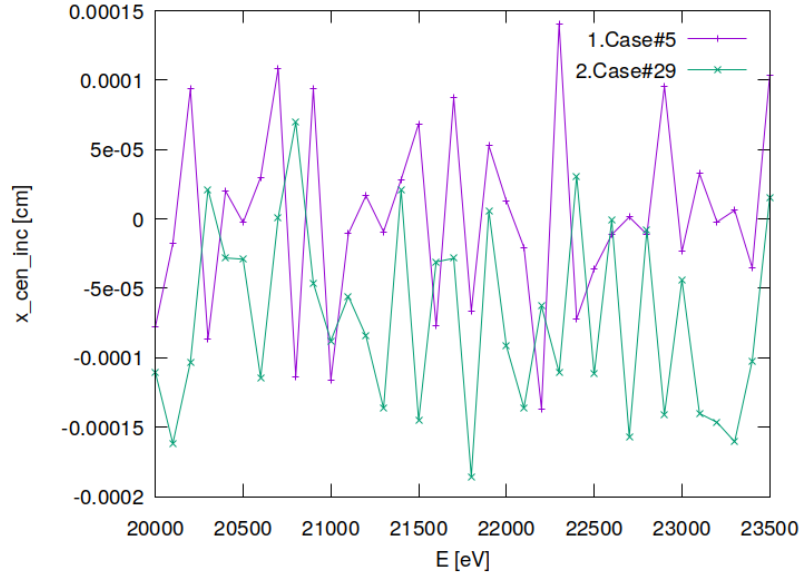


Figure 43.14: Sagittal coordinate of footprint's centre of 'gravity' on surface of optical element #04 (CM2).

```
"fig/CRL_optim_C111_Bragg/plot015.png" Lbl.:CRL_optim_C111_Bragg_2d_plot_x_cen_inc_footstat_oe09
```

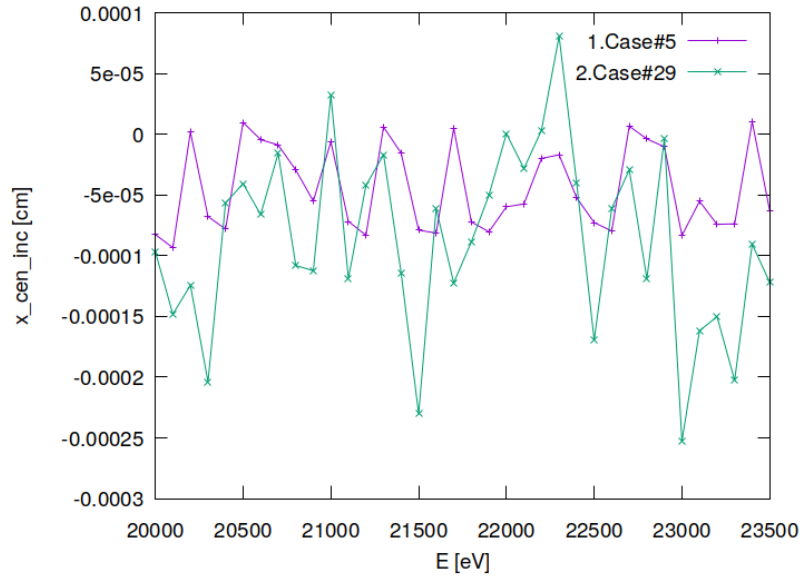


Figure 43.15: Sagittal coordinate of footprint's centre of 'gravity' on surface of optical element #09 (sample).

```
"fig/CRL_optim_C111_Bragg/plot016.png" Lbl.:CRL_optim_C111_Bragg_2d_plot_y_cen_inc_footstat_oe04
```

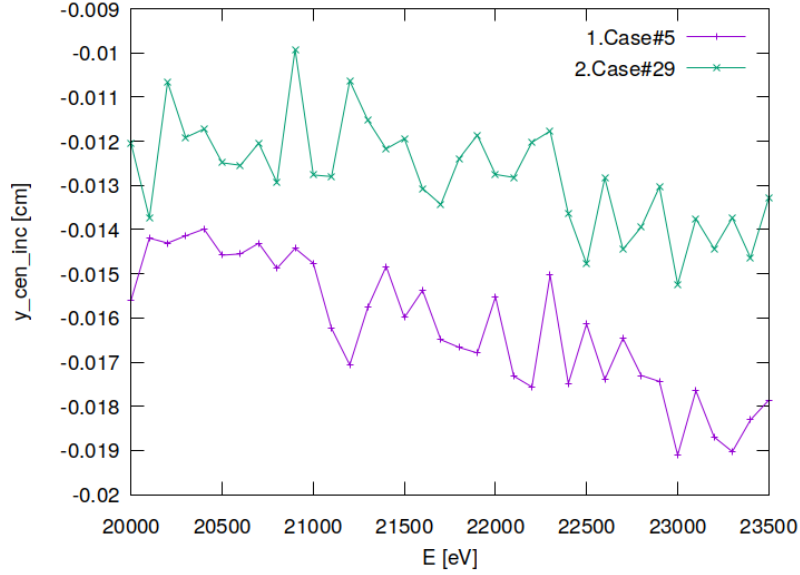


Figure 43.16: Meridional coordinate of footprint's centre of 'gravity' on surface of optical element #04 (CM2).

```
"fig/CRL_optim_C111_Bragg/plot017.png" Lbl.:CRL_optim_C111_Bragg_2d_plot_y_cen_inc_footstat_oe09
```

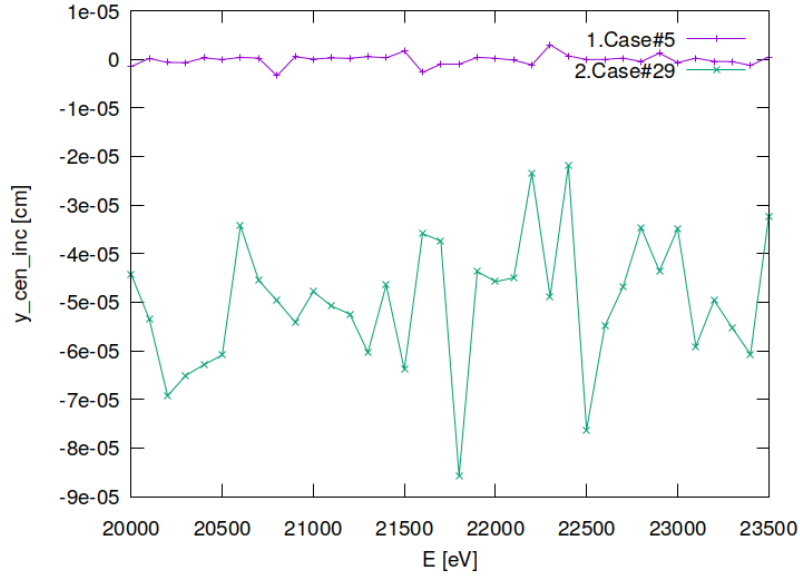


Figure 43.17: Meridional coordinate of footprint's centre of 'gravity' on surface of optical element #09 (sample).

## 43.7 Statistics of photon irradiance in beam cross section

"fig/CRL\_optim\_C111\_Bragg/plot018.png" Lbl.:CRL\_optim\_C111\_Bragg\_2d\_plot\_dx\_fwhm\_focstatavg\_oe04

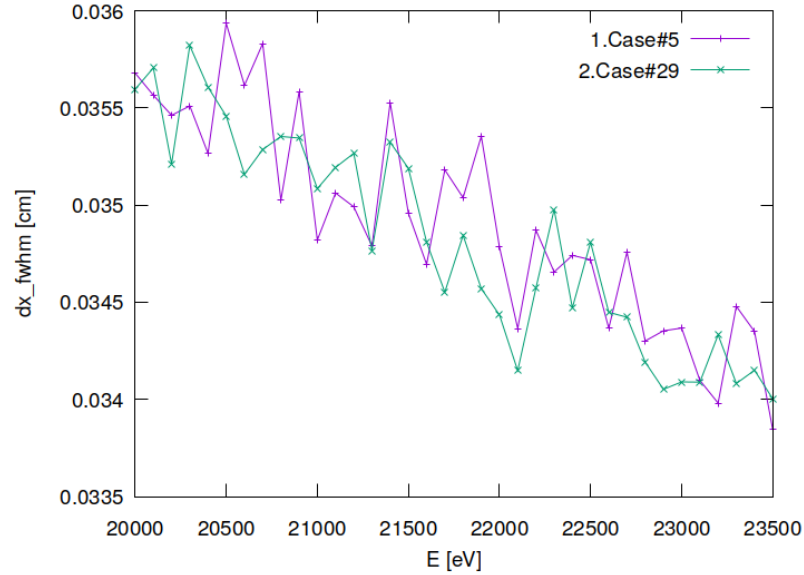


Figure 43.18: Sagittal beam diameter (FWHM) of optical element #04 (CM2).

"fig/CRL\_optim\_C111\_Bragg/plot019.png" Lbl.:CRL\_optim\_C111\_Bragg\_2d\_plot\_dx\_fwhm\_focstatavg\_oe09

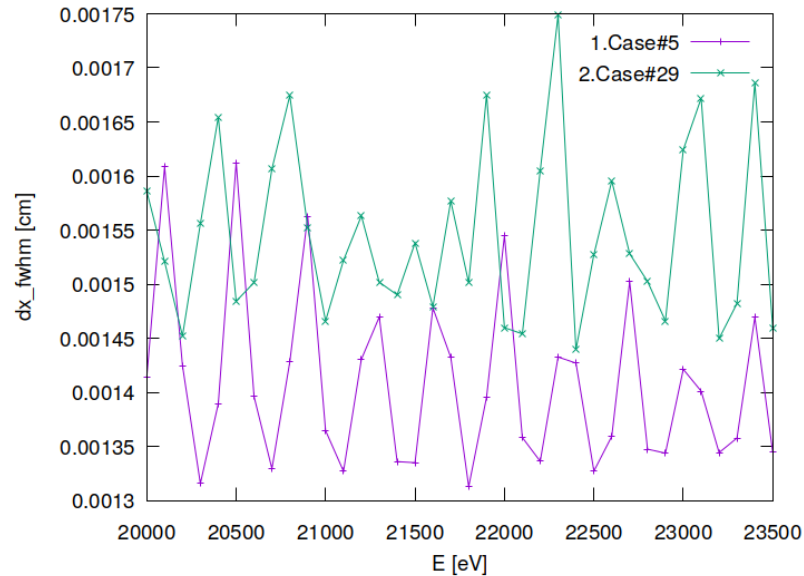


Figure 43.19: Sagittal beam diameter (FWHM) of optical element #09 (sample).

```
"fig/CRL_optim_C111_Bragg/plot020.png" Lbl.:CRL_optim_C111_Bragg_2d_plot_dz_fwhm_focstatavg_oe04
```

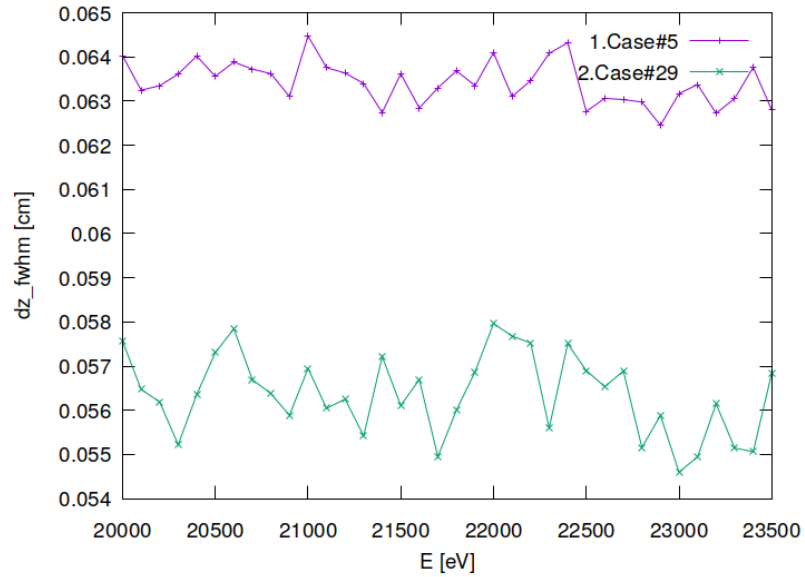


Figure 43.20: Meridional beam diameter (FWHM) of optical element #04 (CM2).

```
"fig/CRL_optim_C111_Bragg/plot021.png" Lbl.:CRL_optim_C111_Bragg_2d_plot_dz_fwhm_focstatavg_oe09
```

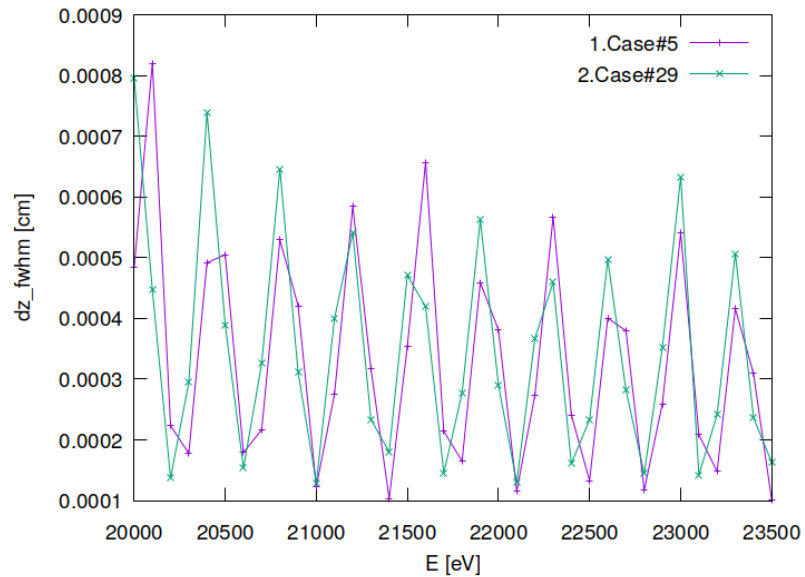


Figure 43.21: Meridional beam diameter (FWHM) of optical element #09 (sample).

"fig/CRL\_optim\_C111\_Bragg/plot022.png" Lbl.:CRL\_optim\_C111\_Bragg\_2d\_plot\_I\_int\_focstatavg\_oe04

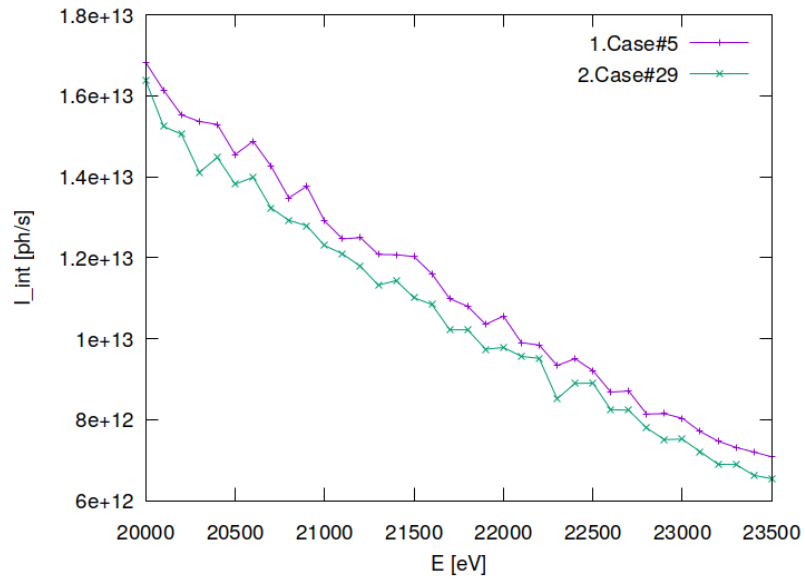


Figure 43.22: Photon flux in beam cross section of optical element #04 (CM2).

"fig/CRL\_optim\_C111\_Bragg/plot023.png" Lbl.:CRL\_optim\_C111\_Bragg\_2d\_plot\_I\_int\_focstatavg\_oe09

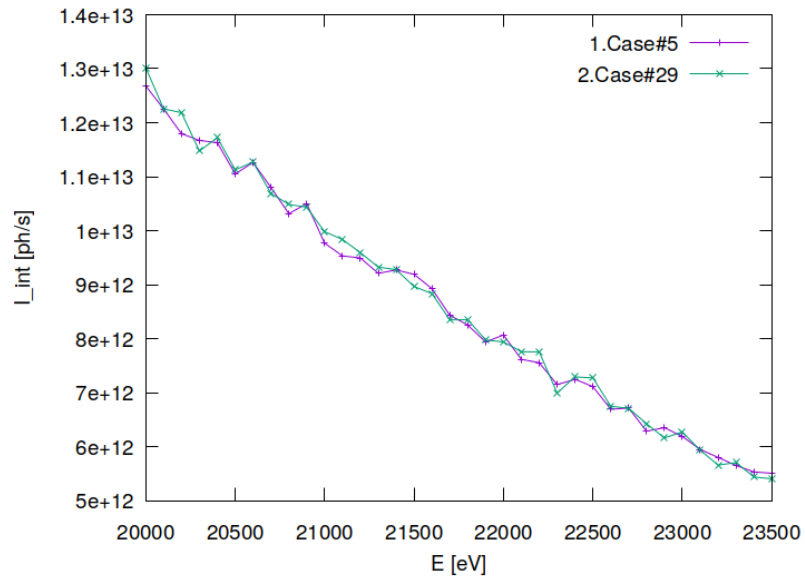


Figure 43.23: Photon flux in beam cross section of optical element #09 (sample).

"fig/CRL\_optim\_C111\_Bragg/plot024.png" Lbl.:CRL\_optim\_C111\_Bragg\_2d\_plot\_x\_cen\_focstatavg\_oe04

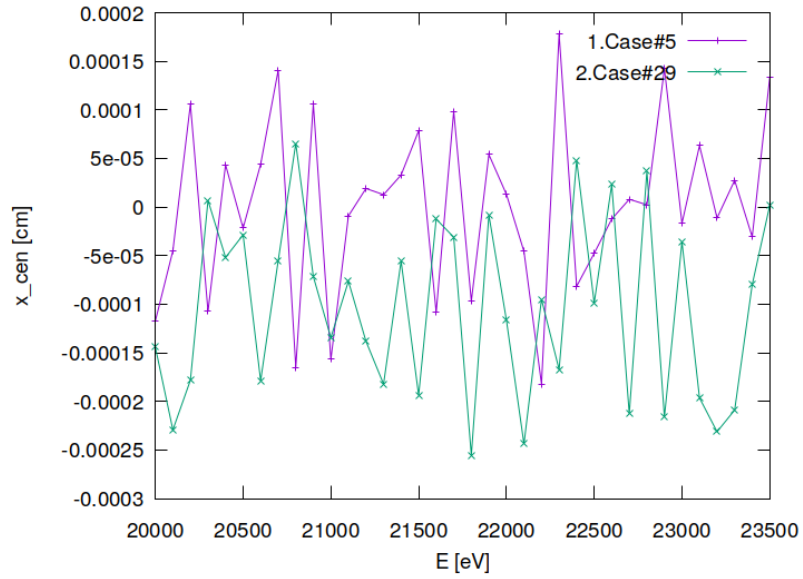


Figure 43.24: Sagittal coordinate of beam's centre of 'gravity' in beam cross section of optical element #04 (CM2).

"fig/CRL\_optim\_C111\_Bragg/plot025.png" Lbl.:CRL\_optim\_C111\_Bragg\_2d\_plot\_x\_cen\_focstatavg\_oe09

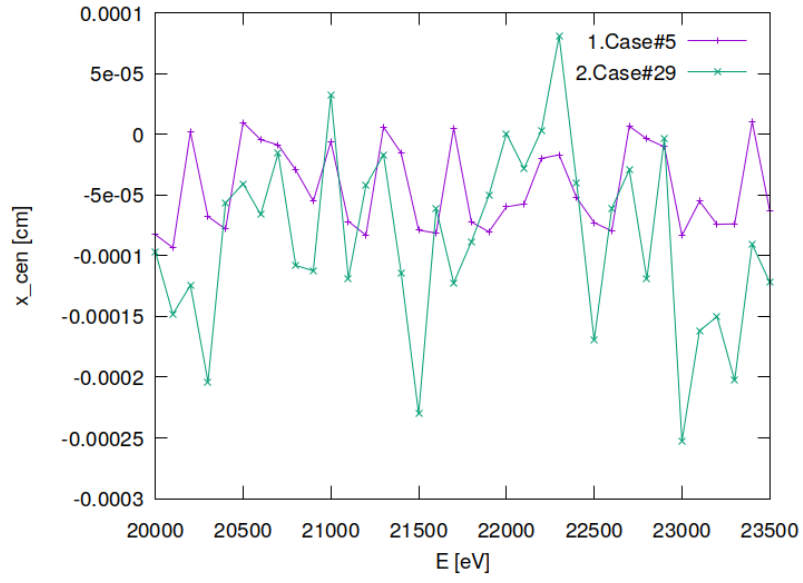


Figure 43.25: Sagittal coordinate of beam's centre of 'gravity' in beam cross section of optical element #09 (sample).

"fig/CRL\_optim\_C111\_Bragg/plot026.png" Lbl.:CRL\_optim\_C111\_Bragg\_2d\_plot\_z\_cen\_focstatavg\_oe04

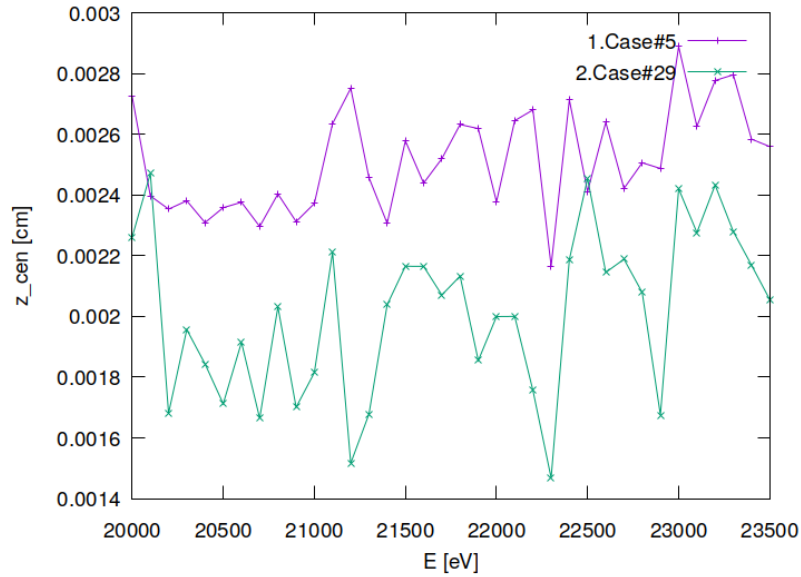


Figure 43.26: Meridional coordinate of beam's centre of 'gravity' in beam cross section of optical element #04 (CM2).

"fig/CRL\_optim\_C111\_Bragg/plot027.png" Lbl.:CRL\_optim\_C111\_Bragg\_2d\_plot\_z\_cen\_focstatavg\_oe09

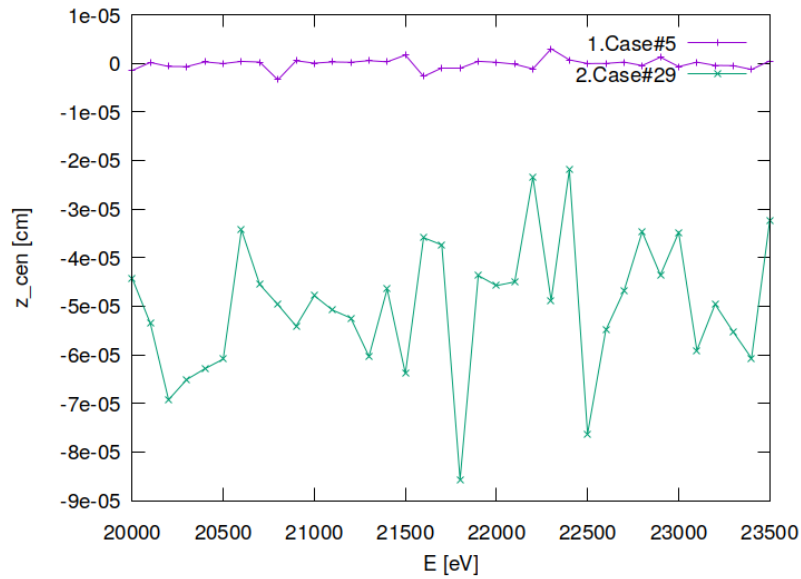


Figure 43.27: Meridional coordinate of beam's centre of 'gravity' in beam cross section of optical element #09 (sample).

```
"fig/CRL_optim_C111_Bragg/plot028.png" Lbl.:CRL_optim_C111_Bragg_2d_plot_dxp_fwhm_focstatavg_oe04
```

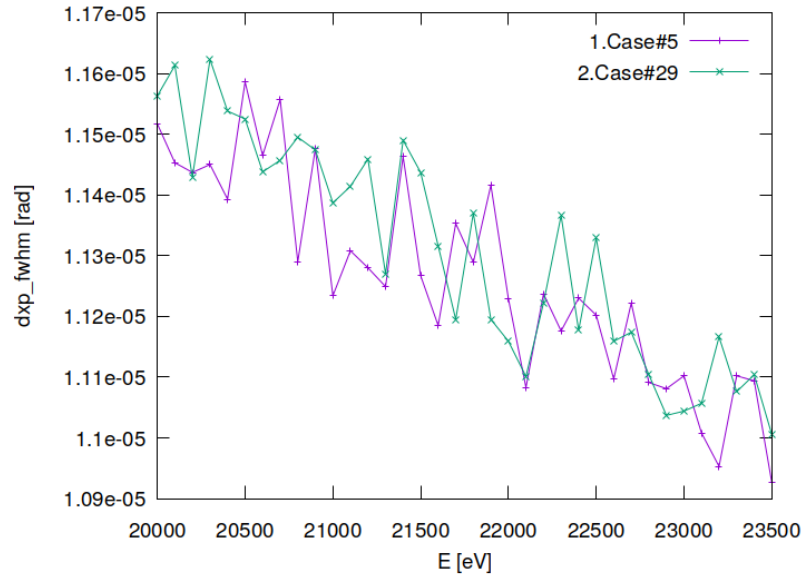


Figure 43.28: Sagittal beam divergence (FWHM) of optical element #04 (CM2).

```
"fig/CRL_optim_C111_Bragg/plot029.png" Lbl.:CRL_optim_C111_Bragg_2d_plot_dxp_fwhm_focstatavg_oe09
```

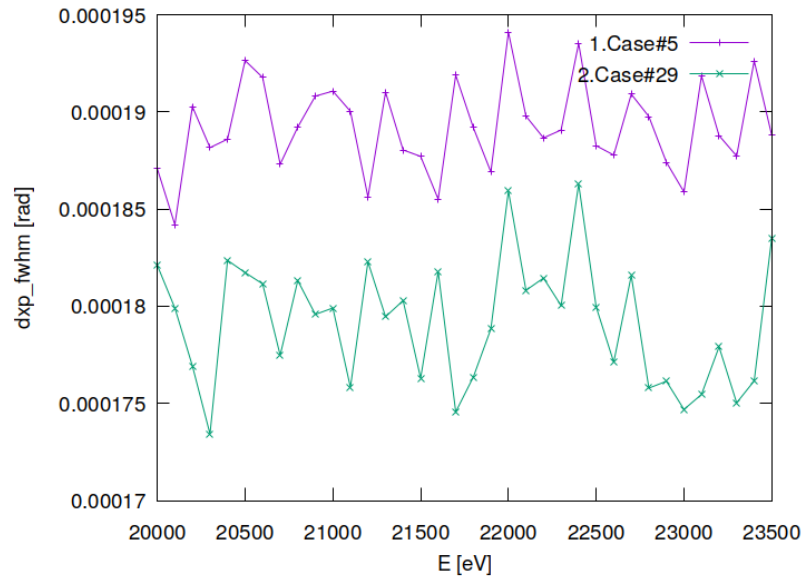


Figure 43.29: Sagittal beam divergence (FWHM) of optical element #09 (sample).

```
"fig/CRL_optim_C111_Bragg/plot030.png" Lbl.:CRL_optim_C111_Bragg_2d_plot_dzp_fwhm_focstatavg_oe04
```

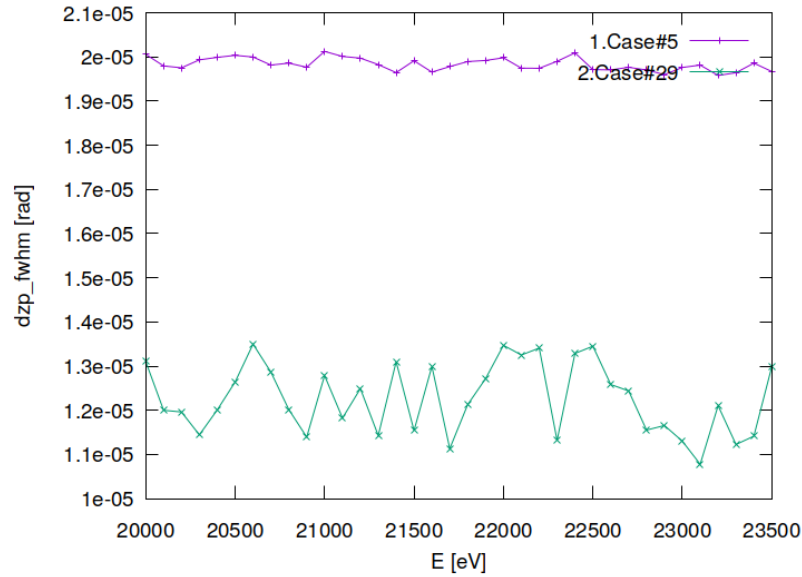


Figure 43.30: Meridional beam divergence (FWHM) of optical element #04 (CM2).

```
"fig/CRL_optim_C111_Bragg/plot031.png" Lbl.:CRL_optim_C111_Bragg_2d_plot_dzp_fwhm_focstatavg_oe09
```

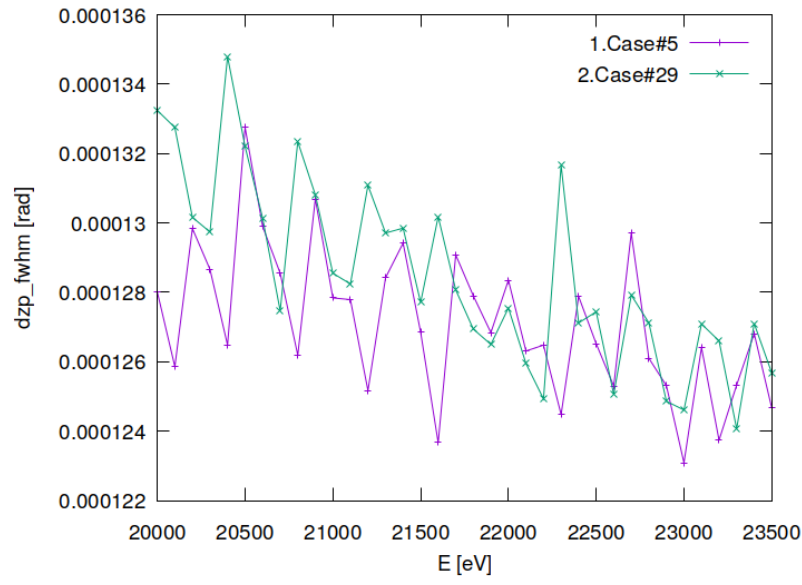


Figure 43.31: Meridional beam divergence (FWHM) of optical element #09 (sample).

```
"fig/CRL_optim_C111_Bragg/plot032.png" Lbl.:CRL_optim_C111_Bragg_2d_plot_I_int_focstatavg_oe04
```

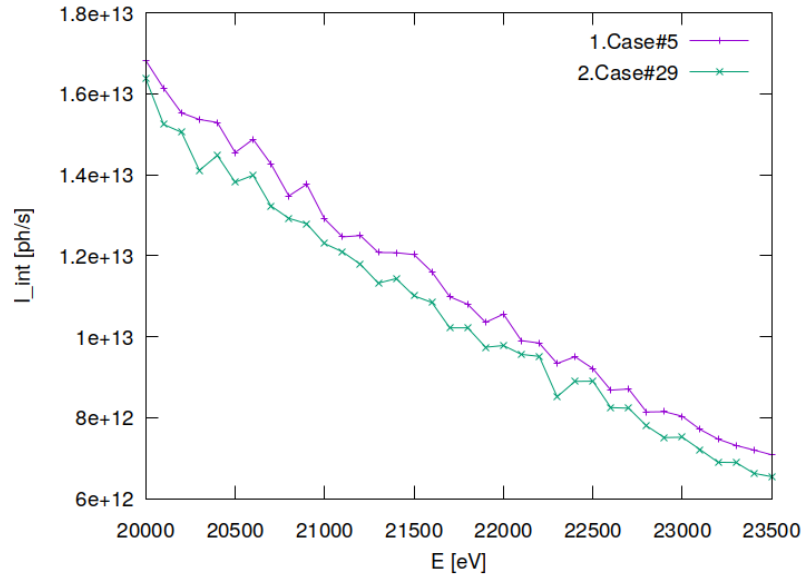


Figure 43.32: Photon flux in beam cross section of optical element #04 (CM2).

```
"fig/CRL_optim_C111_Bragg/plot033.png" Lbl.:CRL_optim_C111_Bragg_2d_plot_I_int_focstatavg_oe09
```

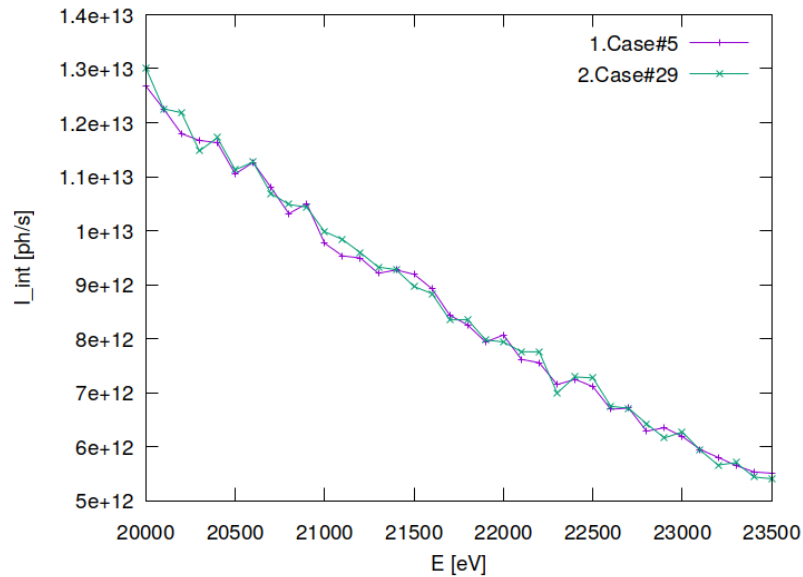


Figure 43.33: Photon flux in beam cross section of optical element #09 (sample).

"fig/CRL\_optim\_C111\_Bragg/plot034.png" Lbl.:CRL\_optim\_C111\_Bragg\_2d\_plot\_xp\_cen\_focstatavg\_oe04

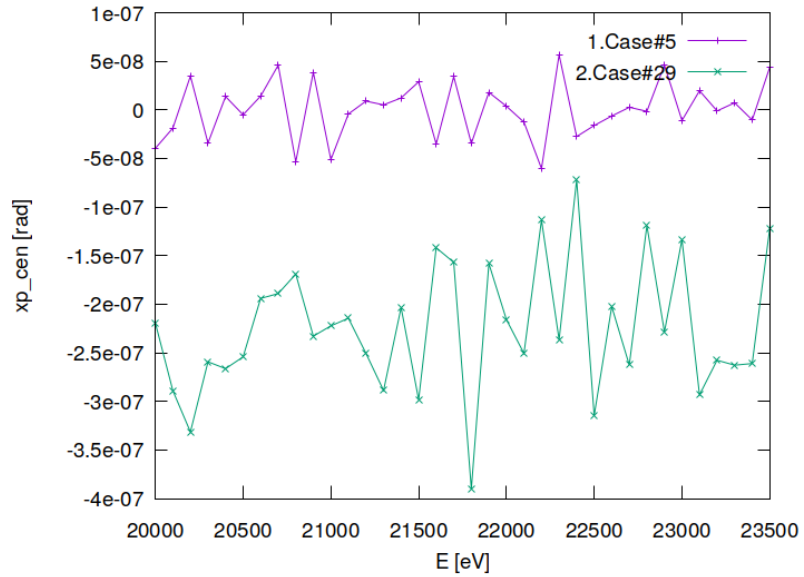


Figure 43.34: Sagittal coordinate of beam's centre of 'gravity' in angle space of optical element #04 (CM2).

"fig/CRL\_optim\_C111\_Bragg/plot035.png" Lbl.:CRL\_optim\_C111\_Bragg\_2d\_plot\_xp\_cen\_focstatavg\_oe09

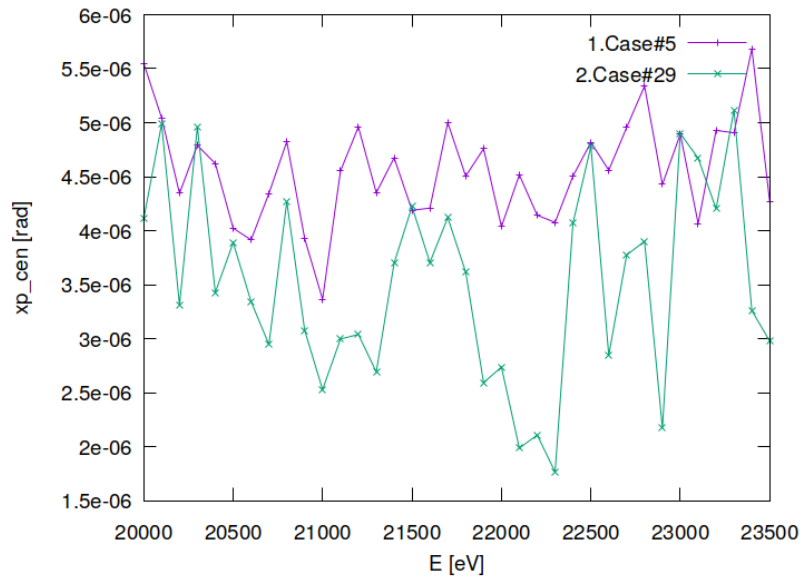


Figure 43.35: Sagittal coordinate of beam's centre of 'gravity' in angle space of optical element #09 (sample).

"fig/CRL\_optim\_C111\_Bragg/plot036.png" Lbl.:CRL\_optim\_C111\_Bragg\_2d\_plot\_zp\_cen\_focstatavg\_oe04

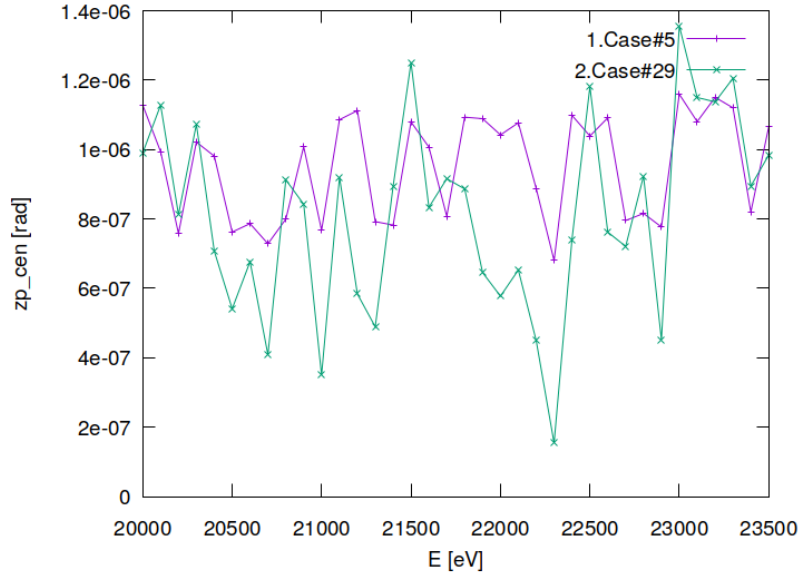


Figure 43.36: Meridional coordinate of beam's centre of 'gravity' in angle space of optical element #04 (CM2).

"fig/CRL\_optim\_C111\_Bragg/plot037.png" Lbl.:CRL\_optim\_C111\_Bragg\_2d\_plot\_zp\_cen\_focstatavg\_oe09

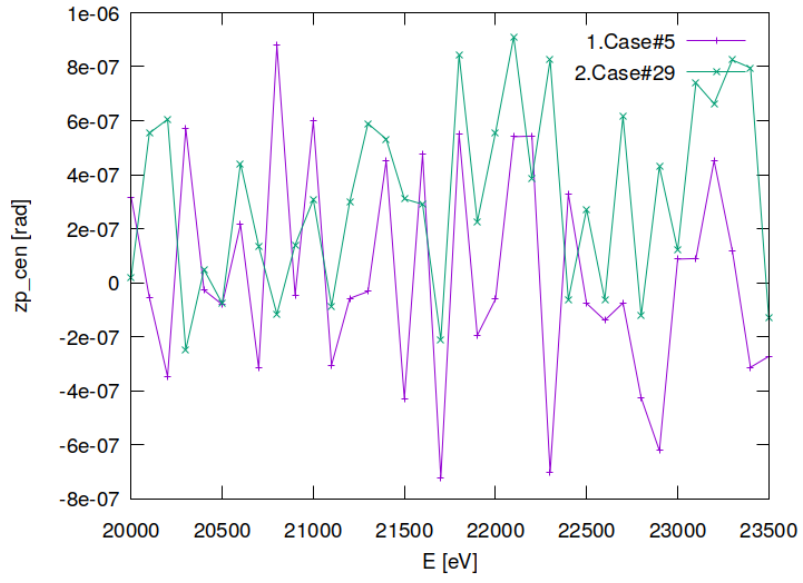


Figure 43.37: Meridional coordinate of beam's centre of 'gravity' in angle space of optical element #09 (sample).

```
"fig/CRL_optim_C111_Bragg/plot038.png" Lbl.:CRL_optim_C111_Bragg_2d_plot_dE_fwhm_focstatavg_oe04
```

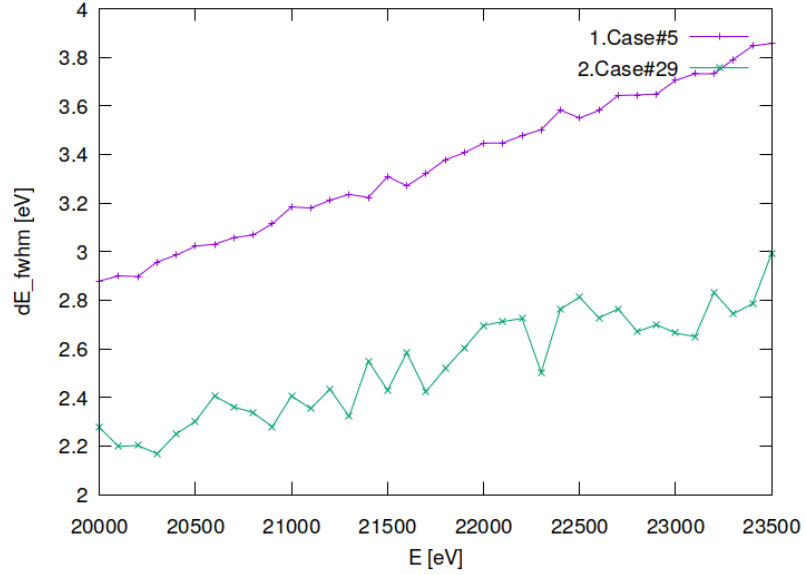


Figure 43.38: Bandwidth (FWHM) in beam cross section of optical element #04 (CM2).

```
"fig/CRL_optim_C111_Bragg/plot039.png" Lbl.:CRL_optim_C111_Bragg_2d_plot_dE_fwhm_focstatavg_oe09
```

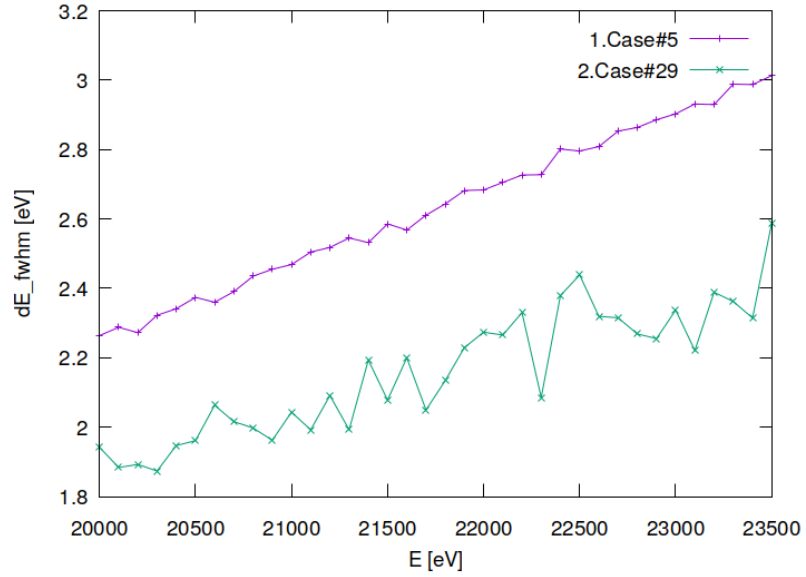


Figure 43.39: Bandwidth (FWHM) in beam cross section of optical element #09 (sample).



## 43.8 Absorbed irradiance on surface

"fig/CRL\_optim\_C111\_Bragg/plot040.png" Lbl.:CRL\_optim\_C111\_Bragg\_false\_colour\_plot\_p\_abs\_foot\_oe03\_c29\_21800eV

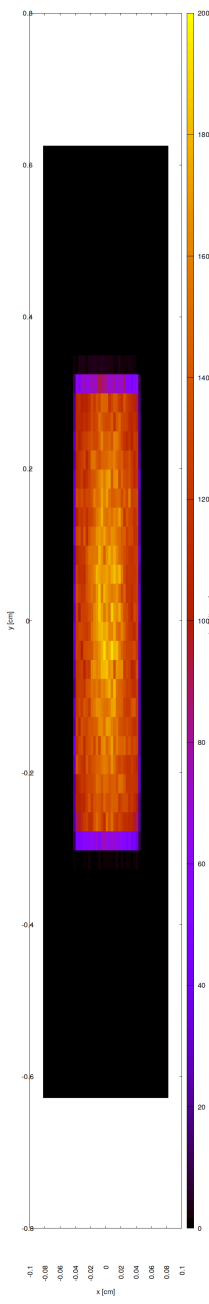


Figure 43.40: Absorbed irradiance on surface of optical element #03 (BS) for case #29 for 21800 eV photon energy setting.

### 43.9 Incident spectral flux on surface

"fig/CRL\_optim\_C111\_Bragg/plot041.png" Lbl.:CRL\_optim\_C111\_Bragg\_2d\_plot\_P\_spec\_spec\_oe03\_c29\_21800eV

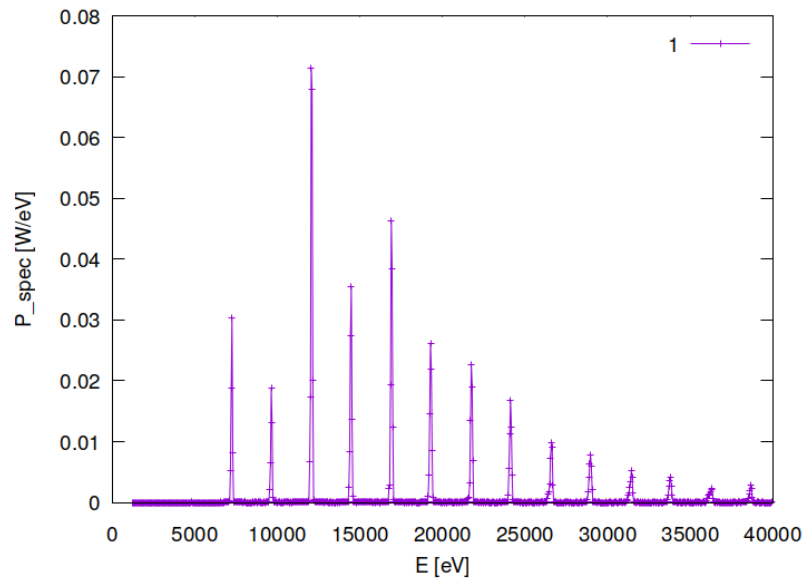


Figure 43.41: Incident spectral flux on surface of optical element #03 (BS) for case #29 for 21800 eV photon energy setting.



## 43.10 Temperature on surface

"fig/CRL\_optim\_C111\_Bragg/plot042.png" Lbl.:CRL\_optim\_C111\_Bragg\_false\_colour\_plot\_T\_oe03\_c29\_21800eV

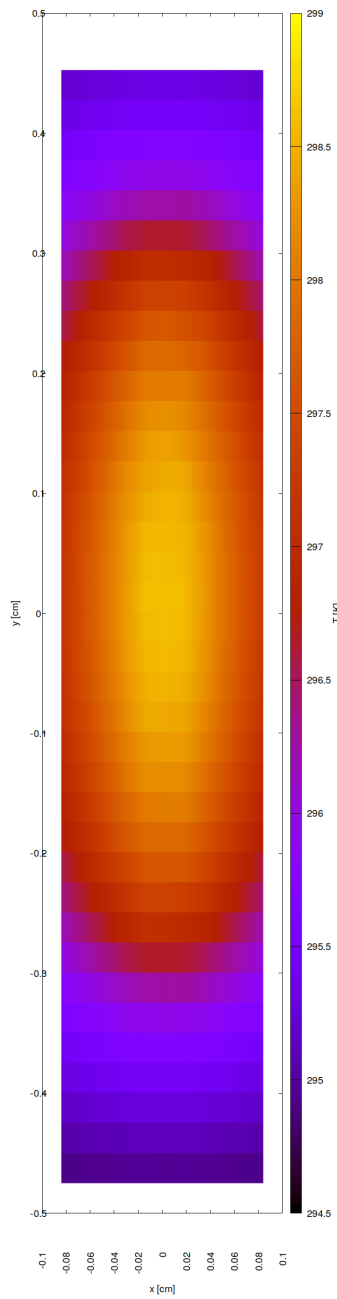


Figure 43.42: Temperature on surface of optical element #03 (BS) for case #29 for 21800 eV photon energy setting.



### 43.11 Mechanical stress (Von Mises stress) on surface

"fig/CRL\_optim\_C111\_Bragg/plot043.png" Lbl.:CRL\_optim\_C111\_Bragg\_false\_colour\_plot\_sigma\_oe03\_c29\_21800eV

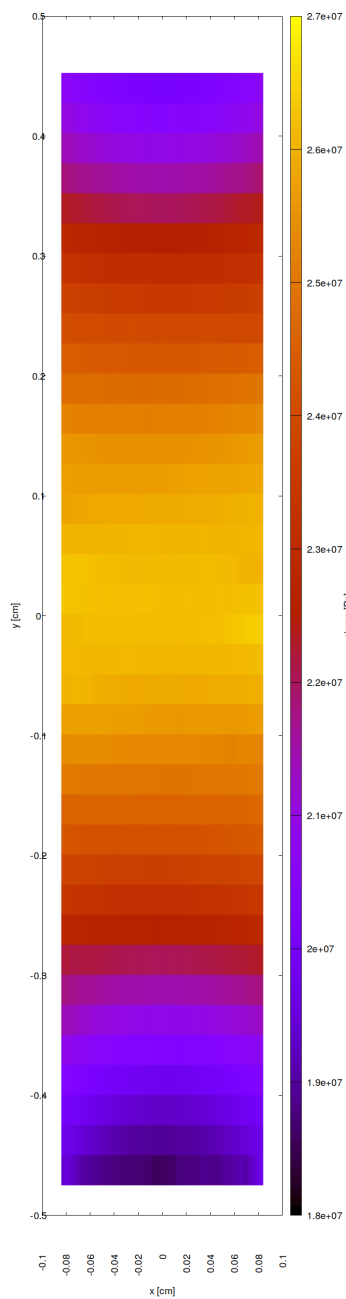


Figure 43.43: Mechanical stress (Von Mises stress) on surface of optical element #03 (BS) for case #29 for 21800 eV photon energy setting.  
577



### 43.12 Surface slope error in meridional direction (y)

"fig/CRL\_optim\_C111\_Bragg/plot044.png" Lbl.:CRL\_optim\_C111\_Bragg\_false\_colour\_plot\_phi\_y\_oe03\_c29\_21800eV

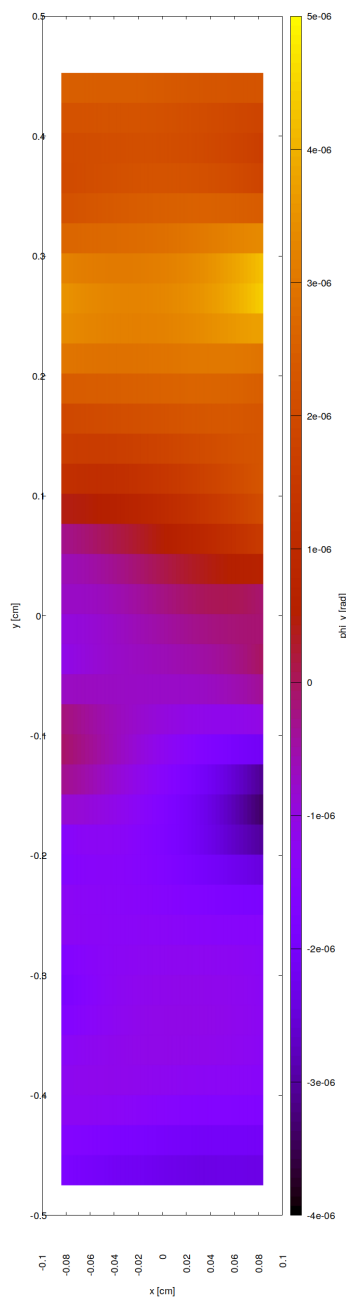


Figure 43.44: Surface slope error in meridional direction (y) of optical element #03 (BS) for case #29 for 21800 eV photon energy setting.



### 43.13 Incident photon irradiance on surface

"fig/CRL\_optim\_C111\_Bragg/plot045.png" Lbl.:CRL\_optim\_C111\_Bragg\_false\_colour\_plot\_I\_inc\_foot\_oe04\_c5\_21800eV

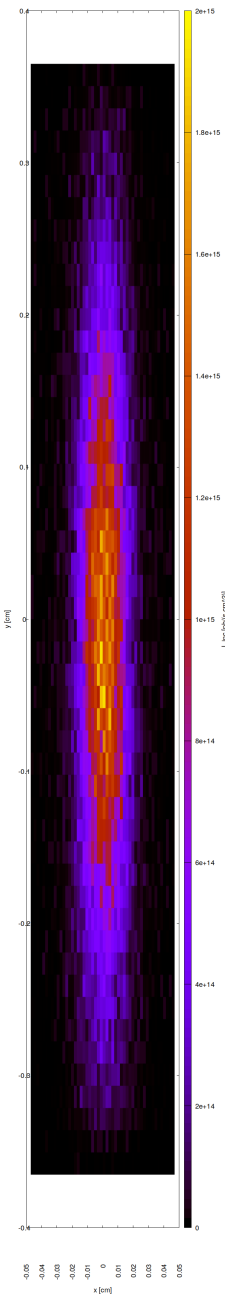


Figure 43.45: Incident photon irradiance on surface of optical element #04 (CM2) for case #5 for 21800 eV photon energy setting.

```
"fig/CRL_optim_C111_Bragg/plot046.png" Lbl.:CRL_optim_C111_Bragg_false_colour_plot_I_inc_foot_oe04_c29_21800eV
```

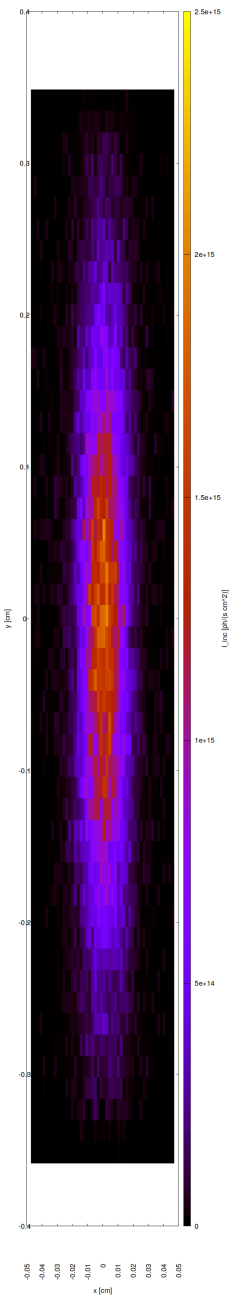


Figure 43.46: Incident photon irradiance on surface of optical element #04 (CM2) for case #29 for 21800 eV photon energy setting.

```
"fig/CRL_optim_C111_Bragg/plot047.png" Lbl.:CRL_optim_C111_Bragg_false_colour_plot_I_inc_foot_oe09_c5_21800eV
```

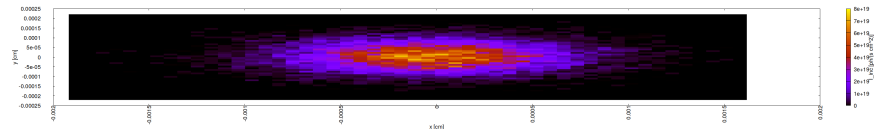


Figure 43.47: Incident photon irradiance on surface of optical element #09 (sample) for case #5 for 21800 eV photon energy setting.

```
"fig/CRL_optim_C111_Bragg/plot048.png" Lbl.:CRL_optim_C111_Bragg_false_colour_plot_I_inc_foot_oe09_c29_21800eV
```

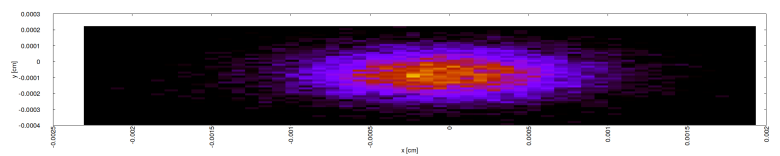


Figure 43.48: Incident photon irradiance on surface of optical element #09 (sample) for case #29 for 21800 eV photon energy setting.

### 43.14 Photon irradiance in beam cross section

```
"fig/CRL_optim_C111_Bragg/plot049.png" Lbl.:CRL_optim_C111_Bragg_false_colour_plot_I_foc_oe04_c5_21800eV
```

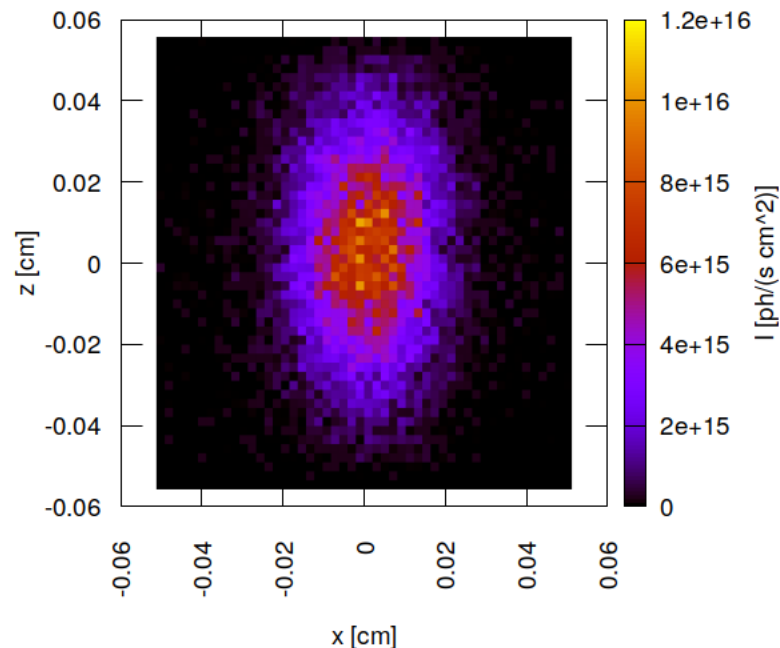


Figure 43.49: Photon irradiance in beam cross section of optical element #04 (CM2) for case #5 for 21800 eV photon energy setting.

"fig/CRL\_optim\_C111\_Bragg/plot050.png" Lbl.:CRL\_optim\_C111\_Bragg\_false\_colour\_plot\_I\_foc\_oe04\_c29\_21800eV

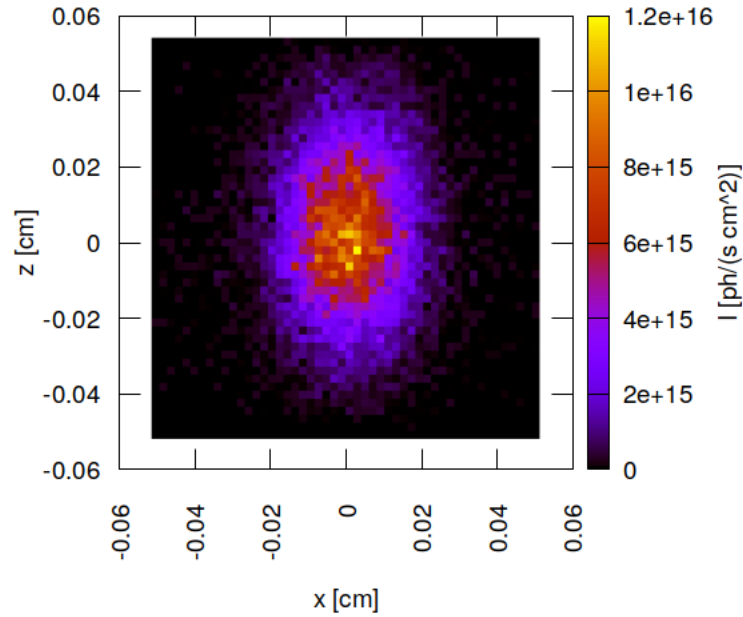


Figure 43.50: Photon irradiance in beam cross section of optical element #04 (CM2) for case #29 for 21800 eV photon energy setting.

"fig/CRL\_optim\_C111\_Bragg/plot051.png" Lbl.:CRL\_optim\_C111\_Bragg\_false\_colour\_plot\_I\_foc\_oe09\_c5\_21800eV

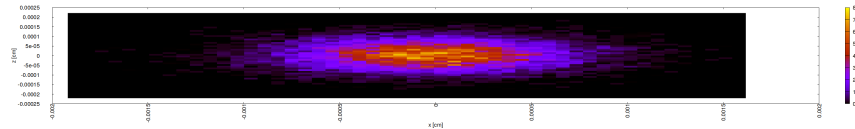


Figure 43.51: Photon irradiance in beam cross section of optical element #09 (sample) for case #5 for 21800 eV photon energy setting.

"fig/CRL\_optim\_C111\_Bragg/plot052.png" Lbl.:CRL\_optim\_C111\_Bragg\_false\_colour\_plot\_I\_foc\_oe09\_c29\_21800eV

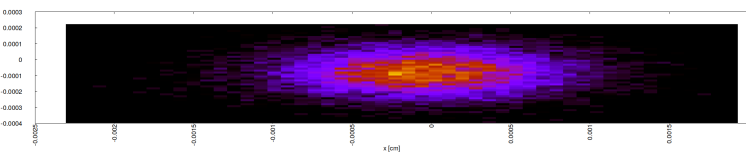


Figure 43.52: Photon irradiance in beam cross section of optical element #09 (sample) for case #29 for 21800 eV photon energy setting.

### 43.15 Spectral photon flux in beam cross section

"fig/CRL\_optim\_C111\_Bragg/plot053.png" Lbl.:CRL\_optim\_C111\_Bragg\_2d\_plot\_I\_bandfoc\_oe04\_c5\_21800eV

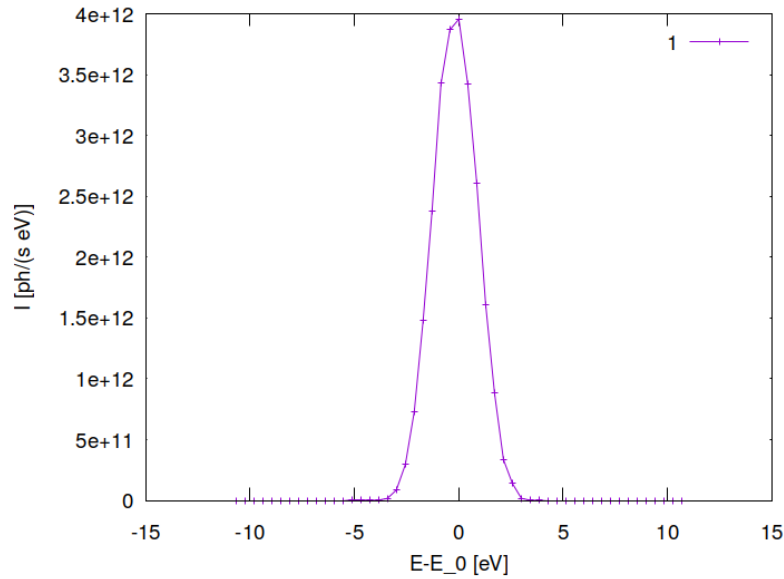


Figure 43.53: Spectral photon flux in beam cross section of optical element #04 (CM2) for case #5 for 21800 eV photon energy setting.

"fig/CRL\_optim\_C111\_Bragg/plot054.png" Lbl.:CRL\_optim\_C111\_Bragg\_2d\_plot\_I\_bandfoc\_oe04\_c29\_21800eV

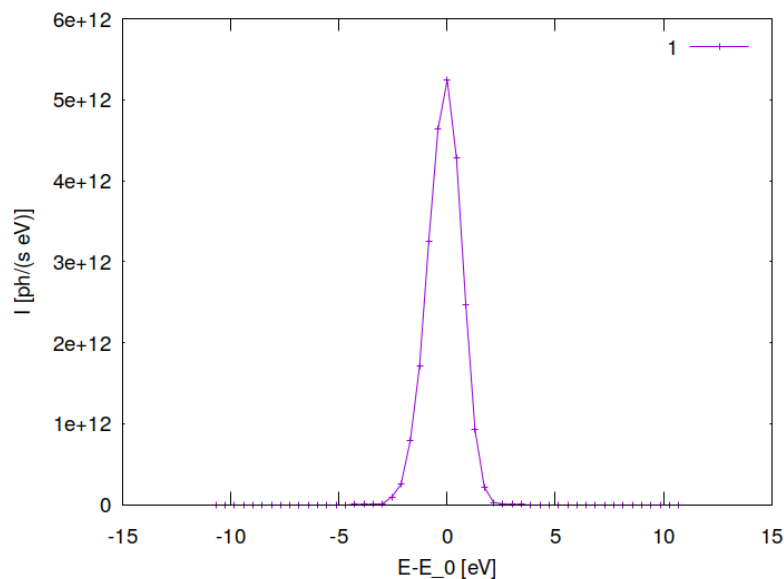


Figure 43.54: Spectral photon flux in beam cross section of optical element #04 (CM2) for case #29 for 21800 eV photon energy setting.

```
"fig/CRL_optim_C111_Bragg/plot055.png" Lbl.:CRL_optim_C111_Bragg_2d_plot_I_bandfoc_oe09_c5_21800eV
```

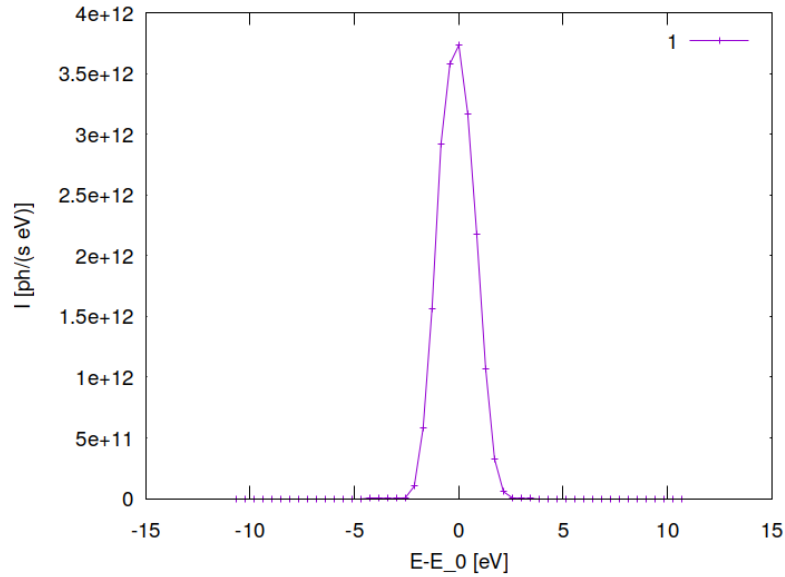


Figure 43.55: Spectral photon flux in beam cross section of optical element #09 (sample) for case #5 for 21800 eV photon energy setting.

```
"fig/CRL_optim_C111_Bragg/plot056.png" Lbl.:CRL_optim_C111_Bragg_2d_plot_I_bandfoc_oe09_c29_21800eV
```

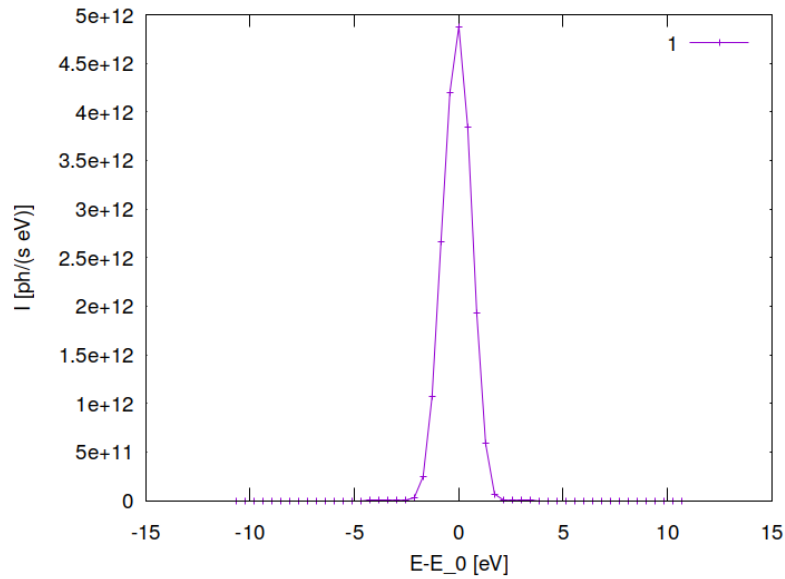


Figure 43.56: Spectral photon flux in beam cross section of optical element #09 (sample) for case #29 for 21800 eV photon energy setting.

# Chapter 44

## Discussion of results

The difference in throughput between different lens element types are small. Only for the 2D lens type with smallest central radius of curvature is the throughput remarkably lower. This is because these lenses haven an aperture significantly smaller than the beam. This leaves a lot of freedom for the choice of the lens type with regard to total lens numbers and step size when adding or removing a single element. Case #5 – #29 if heat load is to be included – was chosen, as it requires the smallest number of lens elements.

### 44.1 Beam splitter in Laue geometry

For the beam splitter in Laue geometry this corresponds to up to 34 2D elements with 100 micron and up to five 1D elements with 200 micron central radius.

This setup creates a focal spot with dimensions 50 times 5 microns (FWHM) in the horizontal, Fig. 39.19, and the vertical, Fig. 39.21, respectively. The horizontal size is considerably larger than one would naively expect from source size and imaging geometry of the CRLs alone. With source and image on axis CRL aberrations are low, hence source size and demagnification by the given imaging geometry should define the focal spot size. Though, this neglects the lensing effect and the large aberration of the asymmetric diffraction by the diamond 111 beam splitter in Laue geometry. This effect is described in section 2.5.

Beam divergence (FWHM) in the focal spot is 160 microradians horizontally, Fig. 39.29, and slightly smaller, 130 microradians, vertically, Fig. 39.31.

The in-focus flux of the monochromatised synchrotron radiation with a (FWHM) bandwidth of about  $1.1 \times 10^{-4}$ , Fig. 39.39, is expected to be at maximum  $5.5 \times 10^{12} \text{ ph/s}$ , Fig. 39.33.

### 44.2 Beam splitter in Bragg geometry

For the beam splitter in Bragg geometry this corresponds to up to 35 2D elements with 100 micron and one 1D element with 200 micron central radius.

The setup creates a focal spot with dimensions 15 times 5 microns (FWHM) in the horizontal, Fig. 43.19, and the vertical, Fig. 43.21, respectively.

Beam divergence (FWHM) in the focal spot is 190 microradians horizontally, Fig. 43.29, and slightly smaller, 130 microradians, vertically, Fig. 43.31.

The in-focus flux of the monochromatised synchrotron radiation with a (FWHM) bandwidth of about  $1.1 \times 10^{-4}$ , Fig. 43.39, is expected to be up to  $1.2 \times 10^{13} \text{ ph/s}$ , Fig. 43.33.

## **Part IV**

# **Defocussing with CRLs**

## Chapter 45

# Focusing test setup with diamond 111 beam splitter in Laue geometry

A thin CVD diamond crystal is employed as a diffractive beam splitter, using the 111 reflection in Laue geometry. The diamond 111 reflection diverts radiation within a narrow bandwidth of

$$\delta E/E = \delta\theta/\tan\theta$$

to the SinCrys side station. The thickness of the diamond crystal slab has been optimised in order to maximise 111 reflectivity under the constraint of keeping absorption of the transmitted main beam low.

Subsequent reflection from a second crystal of the same material using the same set of diffracting planes which are parallel to the first is required to provide the necessary stability of the exit beam which has to hit the very small acceptance aperture of the CRLs (see chapter 23.3).

Putting the second crystal at a distance of around 3.66 metres behind the first provides the required offset of more than one metre between the twice deflected beam and the main beam.

Compound refractive lenses (CRL) are used to focus the monochromatised beam onto the sample. A stack of two-dimensionally focussing lenses has to be complemented by a stack of vertically focussing one-dimensional lenses in order to compensate for the astigmatism generated by the asymmetry and the Laue geometry of the beam splitter and its deformation under the heat load from absorption. Furthermore, the beam splitter is bent meridionally to a concave cylindrical shape with radius  $R = 41.77$  m to partially compensate for aberrations introduced by the beam splitter.

Due to the deterioration of the beam by the beam splitter in Laue geometry, the focal spot diameter in the horizontal exceeds 5 microns even at best focus. So in order to achieve an illuminated area five microns wide the beam has to be apertured down to that size which consequently sacrifices flux. In order to register size and flux of the beam at the sample position both with and without aperture an aperture is inserted just one micron behind the optical plane a.k.a. footprint of (empty) optical element 9. This way, one obtains the full beam in the footprint of optical element 9 and the apertured beam in the continuation plane of the same which is chosen to be at the same location.<sup>1</sup>

---

<sup>1</sup>The continuation plane collects all rays after passing through the optical element including all its screens and apertures. This is even true in the somewhat unphysical case that the continuation plane is located before one or more apertures.

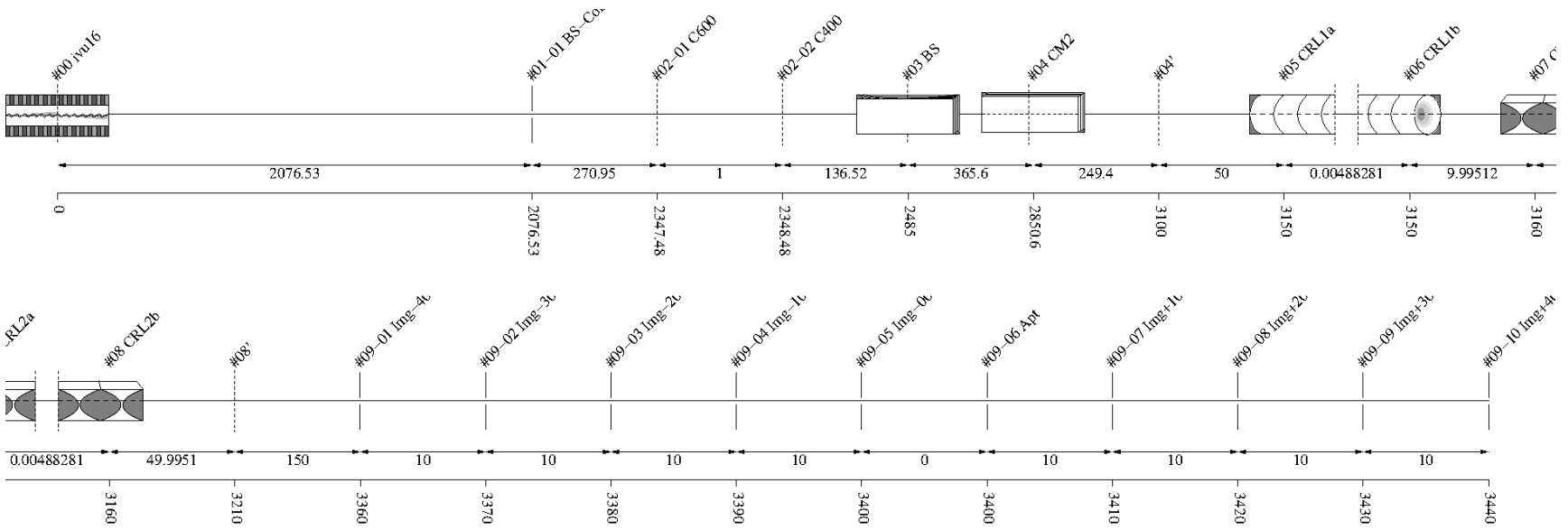


Figure 45.1: Schematic of optical setup

#	Name	Pathlen. cm	Descript.	Shape	Pitch* deg	Roll deg	Yaw deg	x_min cm	x_max cm	y_min cm	y_max cm	Thick. cm	Surface
<b>0</b>	ivu16	0	undulator	auto	0	0	0	-0.0027	0.0027	-0.0002	0.0002	auto	
<b>1</b>		2076.53	none	plane	0	0	0	-inf	inf	-inf	inf		perfect
<b>1-1</b>	BS-Collim	2076.53	aperture	rectangle	0	0	0	-0.035	0.035	-0.035	0.035		
<b>2</b>	Filter	2347.48	none	plane	0	0	0	-inf	inf	-inf	inf		perfect
<b>2-1</b>	C600	2347.48	C-filter	rectangle	0	0	0	-inf	inf	-inf	inf	0.06	
<b>2-2</b>	C400	2348.48	C-filter	rectangle	0	0	0	-inf	inf	-inf	inf	0.04	

<b>3</b>	BS	2485	C(1,1,1)-crystal	cylinder	133.197	90	0	-0.15	0.15	-0.15	0.15		heat bump
<b>4</b>	CM2	2850.6	C(1,1,1)-crystal	plane	7.93694	180	0	-inf	inf	-inf	inf		perfect
<b>4'</b>		3100	continuation plane		0	0	0						
<b>5</b>	CRL1a	3150	vac/Be-lens surface	parabola	0	0	0	-0.03	0.03	-0.03	0.03		perfect
<b>6</b>	CRL1b	3150	Be/vac-lens surface	parabola	0	0	0	-0.03	0.03	-0.03	0.03		perfect
<b>7</b>	CRL2a	3160	vac/Be-lens surface	extruded parabola	0	-90	0	-0.1	0.1	-0.03	0.03		perfect
<b>8</b>	CRL2b	3160	Be/vac-lens surface	extruded parabola	0	0	0	-0.1	0.1	-0.03	0.03		perfect
<b>8'</b>		3210	continuation plane		0	0	0						
<b>9</b>	sample	3400	none	plane	0	0	0	-inf	inf	-inf	inf		perfect
<b>9-1</b>	Img-40	3360	aperture	rectangle	0	0	0	-0.025	0.025	-0.025	0.025		
<b>9-2</b>	Img-30	3370	aperture	rectangle	0	0	0	-0.025	0.025	-0.025	0.025		
<b>9-3</b>	Img-20	3380	aperture	rectangle	0	0	0	-0.025	0.025	-0.025	0.025		
<b>9-4</b>	Img-10	3390	aperture	rectangle	0	0	0	-0.025	0.025	-0.025	0.025		
<b>9-5</b>	Img-00	3400	aperture	rectangle	0	0	0	-0.025	0.025	-0.025	0.025		
<b>9-6</b>	Apt	3400	aperture	rectangle	0	0	0	-0.025	0.025	-0.025	0.025		
<b>9-7</b>	Img+10	3410	aperture	rectangle	0	0	0	-0.025	0.025	-0.025	0.025		
<b>9-8</b>	Img+20	3420	aperture	rectangle	0	0	0	-0.025	0.025	-0.025	0.025		
<b>9-9</b>	Img+30	3430	aperture	rectangle	0	0	0	-0.025	0.025	-0.025	0.025		
<b>9-10</b>	Img+40	3440	aperture	rectangle	0	0	0	-0.025	0.025	-0.025	0.025		

Table 45.1: Setup parameters common to all components. (\*Glancing angle for mirrors, multilayers and crystals. Angle to surface normal otherwise.)

**Rays:** Polar type = total

Polar phase = 0 deg

Polar degree = 0

Is coherent = no

**Spectrum:** E min = 500 eV

E max = 40000 eV

Relative linewidth = 1

**Band:** Bandwidth = 0.0005

**Insertion Device:** lambda period = 1.6 cm

n period = 187

I electron = 0.5 A

E electron = 3 GeV

y horizontal waist = 0 cm

y vertical waist = 0 cm

epsilon x = 3.2E-08 cm rad

epsilon z = 8E-10 cm rad

K y = 1.66

K ymax = 1.7

Divergence limit = 5E-05 rad

**Undulator:** n harmonic max = 99

Tuning type = fixed gap

l aperture = 2076.53 cm

dx aperture = 0.07 cm

dz aperture = 0.07 cm

#1

**Screen:** Is absorbing[1] = no

**Shape:** Thickness = 0 cm

#2 Filter

**Screen:** Is absorbing[1] = yes

Is absorbing[2] = yes

Molecular formula[1] = C

Molecular formula[2] = C

Mass density[1] = 3.5 g/cm^3

Mass density[2] = 3.5 g/cm^3

Thickness[1] = 0.06 cm

Thickness[2] = 0.04 cm

**Shape:** Thickness = 0 cm

### #3 BS

**Grating:** n order = -1

**Crystal:** Structure type = zincblende

Lattice constant[1] = 3.567 Angstrom  
Lattice constant[2] = 3.567 Angstrom  
Lattice constant[3] = 3.567 Angstrom  
Debye Waller factor = 1  
Is absorbing = yes  
Is asymmetric = yes  
Angle asymmetry = 125.26 deg  
Is inclined = no  
Is Johansson geometry = no  
Is mosaic = no

**Tune:** z rotation axis = 0 cm

**Geometry:** Is thin = yes

Tune automatic = yes

**Shape:** Defined by = user

Is convex = no  
Is extruded = yes  
Radius = 4177 cm  
Thickness = 0.01 cm

**Boundary:** Type = rectangle

x rim = 0.5 cm  
y rim = 0.5 cm

**Extruded:** Angle z = 0 deg

**Surface:** Is rough = no

**FEA:** Design type = type specific

Crystal design = laue with cooling loop  
Is isotropic = no  
Angle x = 0 deg  
Angle y = 0 deg  
Angle z = 0 deg  
Mass density = 3.516 g/cm<sup>3</sup>

**Heat:** Heat transfer type[1] = insulated

Heat transfer type[2] = heat transfer  
Heat transfer type[3] = insulated  
Heat transfer type[4] = insulated

Heat transfer type[5] = heat transfer  
 Heat transfer type[6] = flux  
 Heat transfer type[7] = insulated  
 Heat transfer type[8] = heat transfer  
 Heat transfer type[9] = heat sink  
 Heat transfer coefficient = 1 W/(cm^2K)  
 Heat sink coefficient = 10 W/(cm^2K)  
 T reference = 293.15 K  
 T cooling = 293.15 K  
 Heat capacity = 0.54 J/(gK)  
 Thermal conductivity[1] = 25 W/(cmK^n)

**Stress and strain:** Constraint[1] = free  
 Constraint[2] = kinematic  
 Constraint[3] = free  
 Constraint[4] = free  
 Constraint[5] = free  
 Constraint[6] = free  
 Constraint[7] = free  
 Constraint[8] = free  
 Constraint[9] = free  
 Thermal expansion tensor[1] = 1.1E-06 1/K  
 Thermal expansion tensor[2] = 1.1E-06 1/K  
 Thermal expansion tensor[3] = 1.1E-06 1/K  
 Thermal expansion tensor[4] = 0 1/K  
 Thermal expansion tensor[5] = 0 1/K  
 Thermal expansion tensor[6] = 0 1/K  
 Stiffness tensor(1)(1) = 1.07861E+12 Pa  
 Stiffness tensor(2)[1] = 1.2663E+11 Pa  
 Stiffness tensor(2)[2] = 1.07861E+12 Pa  
 Stiffness tensor(3)[1] = 1.2663E+11 Pa  
 Stiffness tensor(3)[2] = 1.2663E+11 Pa  
 Stiffness tensor(3)[3] = 1.07861E+12 Pa  
 Stiffness tensor(4)[1] = 0 Pa  
 Stiffness tensor(4)[2] = 0 Pa  
 Stiffness tensor(4)[3] = 0 Pa  
 Stiffness tensor(4)[4] = 5.7756E+11 Pa  
 Stiffness tensor(5)[1] = 0 Pa  
 Stiffness tensor(5)[2] = 0 Pa  
 Stiffness tensor(5)[3] = 0 Pa  
 Stiffness tensor(5)[4] = 0 Pa  
 Stiffness tensor(5)[5] = 5.7756E+11 Pa  
 Stiffness tensor(6)[1] = 0 Pa  
 Stiffness tensor(6)[2] = 0 Pa  
 Stiffness tensor(6)[3] = 0 Pa  
 Stiffness tensor(6)[4] = 0 Pa  
 Stiffness tensor(6)[5] = 0 Pa  
 Stiffness tensor(6)[6] = 5.7756E+11 Pa

#### #4 CM2

**Crystal:** Structure type = zinblend  
 Lattice constant[1] = 3.567 Angstrom

Lattice constant[2] = 3.567 Angstrom  
Lattice constant[3] = 3.567 Angstrom  
Debye Waller factor = 1  
Is absorbing = yes  
Is asymmetric = no  
Is inclined = no  
Is Johansson geometry = no  
Is mosaic = no

**Tune:** Type = constant pathlength  
Are downstream elements fixed = no

**Geometry:** Is thin = no  
Tune automatic = yes

**Boundary:** Type = none

**Surface:** Is rough = no

## #5 CRL1a

**Dielectric:** Reflectivity type = polarisation  
Is constant = no  
Mass density = 1.85 g/cm<sup>3</sup>

**Geometry:** g = 3150 cm  
b = 250 cm  
Is thin = yes  
n clones = 5  
n originals = 2  
Focus automatically = yes

**Focus:** Type = chromatic  
Number variation method = cloning  
Vary distance = no

**Shape:** Defined by = user  
Is convex = no  
Is extruded = no  
Radius = 0.01 cm  
Thickness = 0.005 cm

**Boundary:** Type = ellipse

**Parabola:** Is source in infinity = no  
p semi = 0.01 cm

**Surface:** Is rough = no

### #6 CRL1b

**Dielectric:** Reflectivity type = polarisation

Is constant = yes

delta refraction = 0

beta absorption = 0

**Geometry:** g = 3150 cm

b = 250 cm

Is thin = yes

n clones = 5

n originals = 0

Focus automatically = yes

**Focus:** Type = chromatic

Number variation method = cloning

Vary distance = no

**Shape:** Defined by = user

Is convex = yes

Is extruded = no

Radius = 0.01 cm

Thickness = 0.005 cm

**Boundary:** Type = ellipse

**Parabola:** Is source in infinity = no

p semi = 0.01 cm

**Surface:** Is rough = no

### #7 CRL2a

**Dielectric:** Reflectivity type = polarisation

Is constant = no

Mass density = 1.85 g/cm<sup>3</sup>

**Geometry:** g = -255 cm

b = 240 cm

Is thin = yes

n clones = 6

n originals = 2

Focus automatically = yes

**Focus:** Type = chromatic

Number variation method = cloning

Vary distance = no

**Shape:** Defined by = user

Is convex = no

Is extruded = yes

Radius = 0.02 cm

Thickness = 0.005 cm

**Boundary:** Type = rectangle

**Parabola:** Is source in infinity = no

p semi = 0.02 cm

**Extruded:** Angle z = 0 deg

**Surface:** Is rough = no

## #8 CRL2b

**Dielectric:** Reflectivity type = polarisation

Is constant = yes

delta refraction = 0

beta absorption = 0

**Geometry:** g = -255 cm

b = 240 cm

Is thin = yes

n clones = 6

n originals = 0

Focus automatically = yes

**Focus:** Type = chromatic

Number variation method = cloning

Vary distance = no

**Shape:** Defined by = user

Is convex = yes

Is extruded = yes

Radius = 0.02 cm

Thickness = 0.005 cm

**Boundary:** Type = rectangle

**Parabola:** Is source in infinity = no  
p semi = 0.02 cm

**Extruded:** Angle z = 0 deg

**Surface:** Is rough = no

### #9 sample

**Screen:** Is absorbing[1] = no  
Is absorbing[2] = no  
Is absorbing[3] = no  
Is absorbing[4] = no  
Is absorbing[5] = no  
Is absorbing[6] = no  
Is absorbing[7] = no  
Is absorbing[8] = no  
Is absorbing[9] = no  
Is absorbing[10] = no

**Shape:** Thickness = 0 cm

# Chapter 46

## Parameter scan cases

Only the first five of the six cases are relevant, all five without heat load. These cases represent different focussing settings. In the first case the CRLs are set up for best focus. In the second case the CRLs focus behind the sample position, such that the beam cross-section at the sample position is at least  $5 \times 5$  microns large. In the third and fourth case one aims for a  $15 \times 15$  and  $100 \times 100$  microns large beam cross section.

Case	Has_slope_error_03	b_05 cm	g_07 cm	Skip_heatload
1	no	270	-261	yes
2	no	270	-267	yes
3	no	270	-274	yes
4	no	370	-240	yes
5	no	-3150	-240	yes
6	yes	249	-242	no

Table 46.1: Parameter values for different cases in parameter scan

### Legend

**Case:** Case number in parameter scan

**Has\_slope\_error\_03:** Optical\_element\_#3.Surface.Has\_slope\_error (Has surface slope error?)

**b\_05:** Optical\_element\_#5.Geometry.b (Distance from optical element's pole to meridional image focus.)

**g\_07:** Optical\_element\_#7.Geometry.g (Distance btw. meridional object focus and optical element's pole.)

**Skip\_heatload:** Session.Skip\_heatload (Skip heat load calculation for all optical elements? (heat load parameters are kept))

## Chapter 47

# Photon energy scan

The  $K_y$ -values in the table below are those for optimized output between 15.6 and 18.3 keV used by DanMAX' main branch. The number of 2D and 1D focussing lens elements needed for the required beam properties in the SinCrys side branch are also provided here.

E eV	K_y	n_harm/step	theta_B03 deg	nMult_05	nMult_07
<b>20000</b>	1.67551	9	8.6565237	24	4
<b>20100</b>	1.66836	9	8.6131277	24	4
<b>20200</b>	1.66125	9	8.5701675	24	4
<b>20300</b>	1.65418	9	8.5276346	24	4
<b>20400</b>	1.64714	9	8.4855232	24	4
<b>20500</b>	1.64015	9	8.4438276	25	4
<b>20600</b>	1.63319	9	8.4025402	25	4
<b>20700</b>	1.62628	9	8.3616571	25	4
<b>20800</b>	1.6194	9	8.3211708	25	4
<b>20900</b>	1.61255	9	8.2810764	26	4
<b>21000</b>	1.60575	9	8.2413683	26	4
<b>21100</b>	1.59898	9	8.2020397	26	4
<b>21200</b>	1.59224	9	8.1630869	26	4
<b>21300</b>	1.58554	9	8.1245022	27	4
<b>21400</b>	1.57887	9	8.0862827	27	4
<b>21500</b>	1.57224	9	8.0484219	27	5
<b>21600</b>	1.56564	9	8.0109158	27	5
<b>21700</b>	1.55908	9	7.9737582	28	5
<b>21800</b>	1.55255	9	7.936945	28	5
<b>21900</b>	1.54605	9	7.9004712	28	5
<b>22000</b>	1.53958	9	7.8643322	28	5
<b>22100</b>	1.53315	9	7.8285236	29	5
<b>22200</b>	1.52674	9	7.7930403	29	5
<b>22300</b>	1.52037	9	7.7578783	29	5
<b>22400</b>	1.51402	9	7.7230334	30	5
<b>22500</b>	1.50771	9	7.6885004	30	5
<b>22600</b>	1.50143	9	7.6542764	30	5
<b>22700</b>	1.49517	9	7.6203566	30	5
<b>22800</b>	1.48895	9	7.5867367	31	5
<b>22900</b>	1.48275	9	7.5534129	31	5
<b>23000</b>	1.47658	9	7.5203819	31	5
<b>23100</b>	1.47044	9	7.487639	31	5
<b>23200</b>	1.46433	9	7.4551811	32	5
<b>23300</b>	1.45824	9	7.4230037	32	5
<b>23400</b>	1.45218	9	7.3911042	32	5
<b>23500</b>	1.44615	9	7.359478	32	5

Table 47.1: Scan values for different photon energies in energy scan of case #1 (best focus)

E eV	nMult_05	nMult_07
<b>20000</b>	24	5
<b>20100</b>	24	5
<b>20200</b>	24	5
<b>20300</b>	24	5
<b>20400</b>	24	5
<b>20500</b>	25	5
<b>20600</b>	25	5
<b>20700</b>	25	5
<b>20800</b>	25	5
<b>20900</b>	26	5
<b>21000</b>	26	5
<b>21100</b>	26	5
<b>21200</b>	26	6
<b>21300</b>	27	6
<b>21400</b>	27	6
<b>21500</b>	27	6
<b>21600</b>	27	6
<b>21700</b>	28	6
<b>21800</b>	28	6
<b>21900</b>	28	6
<b>22000</b>	28	6
<b>22100</b>	29	6
<b>22200</b>	29	6
<b>22300</b>	29	6
<b>22400</b>	30	6
<b>22500</b>	30	6
<b>22600</b>	30	6
<b>22700</b>	30	6
<b>22800</b>	31	6
<b>22900</b>	31	6
<b>23000</b>	31	7
<b>23100</b>	31	7
<b>23200</b>	32	7
<b>23300</b>	32	7
<b>23400</b>	32	7
<b>23500</b>	32	7

Table 47.2: Scan values for different photon energies in energy scan of case #2 ( $5 \times 5$  microns)

E eV	nMult_05	nMult_07
<b>20000</b>	24	6
<b>20100</b>	24	6
<b>20200</b>	24	6
<b>20300</b>	24	6
<b>20400</b>	24	6
<b>20500</b>	25	6
<b>20600</b>	25	6
<b>20700</b>	25	6
<b>20800</b>	25	7
<b>20900</b>	26	7
<b>21000</b>	26	7
<b>21100</b>	26	7
<b>21200</b>	26	7
<b>21300</b>	27	7
<b>21400</b>	27	7
<b>21500</b>	27	7
<b>21600</b>	27	7
<b>21700</b>	28	7
<b>21800</b>	28	7
<b>21900</b>	28	7
<b>22000</b>	28	7
<b>22100</b>	29	7
<b>22200</b>	29	7
<b>22300</b>	29	8
<b>22400</b>	30	8
<b>22500</b>	30	8
<b>22600</b>	30	8
<b>22700</b>	30	8
<b>22800</b>	31	8
<b>22900</b>	31	8
<b>23000</b>	31	8
<b>23100</b>	31	8
<b>23200</b>	32	8
<b>23300</b>	32	8
<b>23400</b>	32	8
<b>23500</b>	32	8

Table 47.3: Scan values for different photon energies in energy scan of case #3  
(15 × 15 microns)

E eV	nMult_05	nMult_07
<b>20000</b>	18	0
<b>20100</b>	18	0
<b>20200</b>	18	0
<b>20300</b>	18	0
<b>20400</b>	18	0
<b>20500</b>	19	0
<b>20600</b>	19	0
<b>20700</b>	19	0
<b>20800</b>	19	0
<b>20900</b>	19	0
<b>21000</b>	19	0
<b>21100</b>	20	0
<b>21200</b>	20	0
<b>21300</b>	20	0
<b>21400</b>	20	0
<b>21500</b>	20	0
<b>21600</b>	21	0
<b>21700</b>	21	0
<b>21800</b>	21	0
<b>21900</b>	21	0
<b>22000</b>	21	0
<b>22100</b>	22	0
<b>22200</b>	22	0
<b>22300</b>	22	0
<b>22400</b>	22	0
<b>22500</b>	22	0
<b>22600</b>	23	0
<b>22700</b>	23	0
<b>22800</b>	23	0
<b>22900</b>	23	0
<b>23000</b>	23	0
<b>23100</b>	24	0
<b>23200</b>	24	0
<b>23300</b>	24	0
<b>23400</b>	24	0
<b>23500</b>	24	0

Table 47.4: Scan values for different photon energies in energy scan of case #4 (100 × 100 microns)

E eV	nMult_05	nMult_07
<b>20000</b>	0	0
<b>20100</b>	0	0
<b>20200</b>	0	0
<b>20300</b>	0	0
<b>20400</b>	0	0
<b>20500</b>	0	0
<b>20600</b>	0	0
<b>20700</b>	0	0
<b>20800</b>	0	0
<b>20900</b>	0	0
<b>21000</b>	0	0
<b>21100</b>	0	0
<b>21200</b>	0	0
<b>21300</b>	0	0
<b>21400</b>	0	0
<b>21500</b>	0	0
<b>21600</b>	0	0
<b>21700</b>	0	0
<b>21800</b>	0	0
<b>21900</b>	0	0
<b>22000</b>	0	0
<b>22100</b>	0	0
<b>22200</b>	0	0
<b>22300</b>	0	0
<b>22400</b>	0	0
<b>22500</b>	0	0
<b>22600</b>	0	0
<b>22700</b>	0	0
<b>22800</b>	0	0
<b>22900</b>	0	0
<b>23000</b>	0	0
<b>23100</b>	0	0
<b>23200</b>	0	0
<b>23300</b>	0	0
<b>23400</b>	0	0
<b>23500</b>	0	0

Table 47.5: Scan values for different photon energies in energy scan of case #5 (unfocussed)

#### Legend

**E:** photon energy

**nMult\_05:** number of elements in compound refractive lens optical element 05

**nMult\_07:** number of elements in compound refractive lens optical element 07

# Chapter 48

## Plots

### 48.1 Statistics of photon irradiance on optical surface

```
"fig/Defocus_C111_Laue/plot001.png" Lbl.:Defocus_C111_Laue_2d_plot_dx_fwhm_inc_footstat_oe09
```

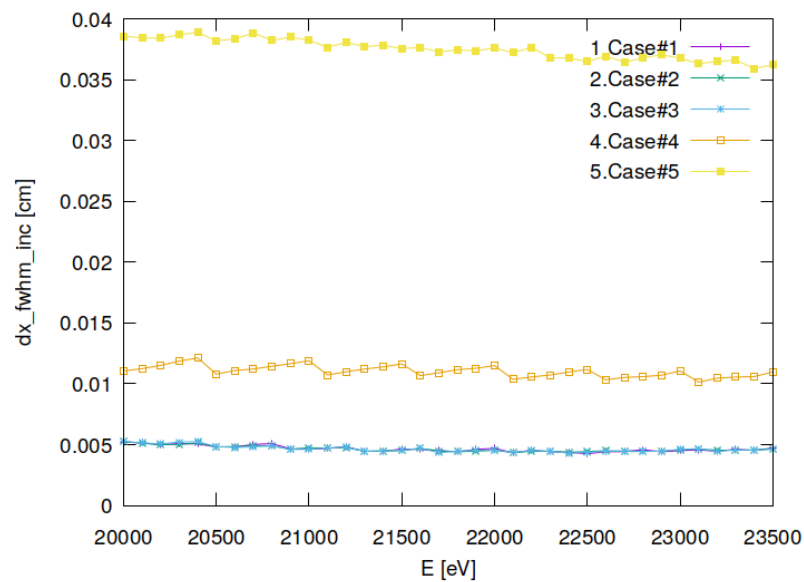


Figure 48.1: Sagittal footprint diameter (FWHM) of optical element #09 (sample).

```
"fig/Defocus_C111_Laue/plot002.png" Lbl.:Defocus_C111_Laue_2d_plot_dy_fwhm_inc_footstat_oe09
```

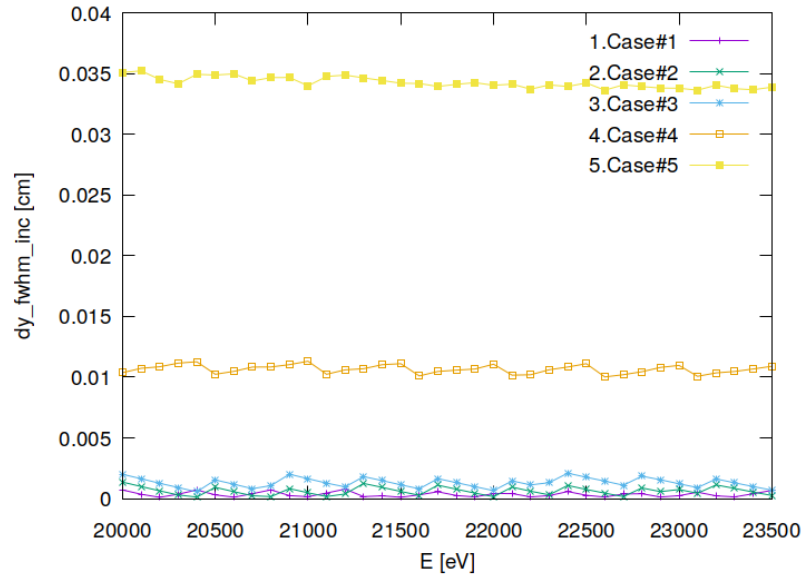


Figure 48.2: Meridional footprint diameter (FWHM) of optical element #09 (sample).

```
"fig/Defocus_C111_Laue/plot003.png" Lbl.:Defocus_C111_Laue_2d_plot_I_inc_int_footstat_oe09
```

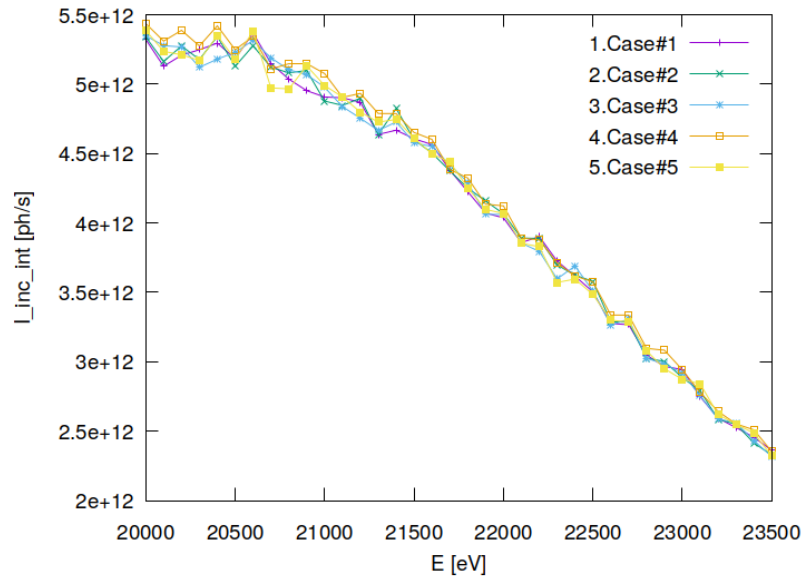


Figure 48.3: Incident photon flux on surface of optical element #09 (sample).

"fig/Defocus\_C111\_Laue/plot004.png" Lbl.:Defocus\_C111\_Laue\_2d\_plot\_x\_cen\_inc\_footstat\_oe09

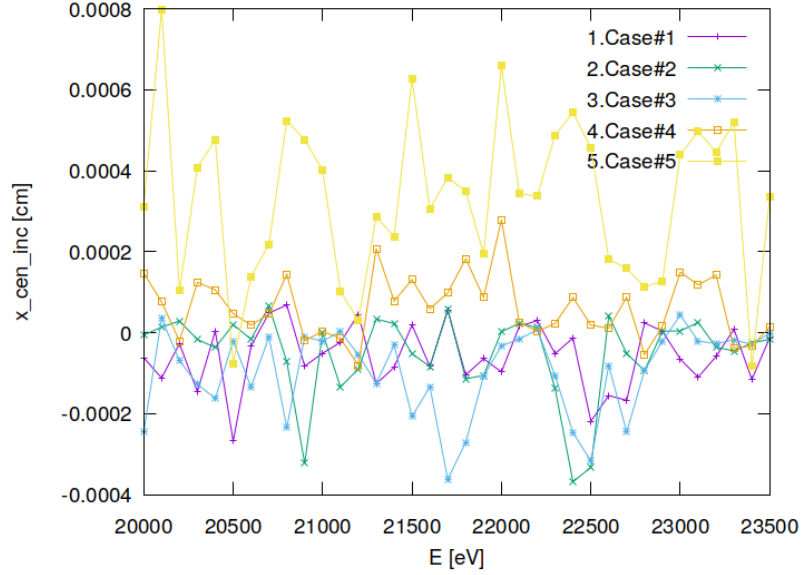


Figure 48.4: Sagittal coordinate of footprint's centre of 'gravity' on surface of optical element #09 (sample).

"fig/Defocus\_C111\_Laue/plot005.png" Lbl.:Defocus\_C111\_Laue\_2d\_plot\_y\_cen\_inc\_footstat\_oe09

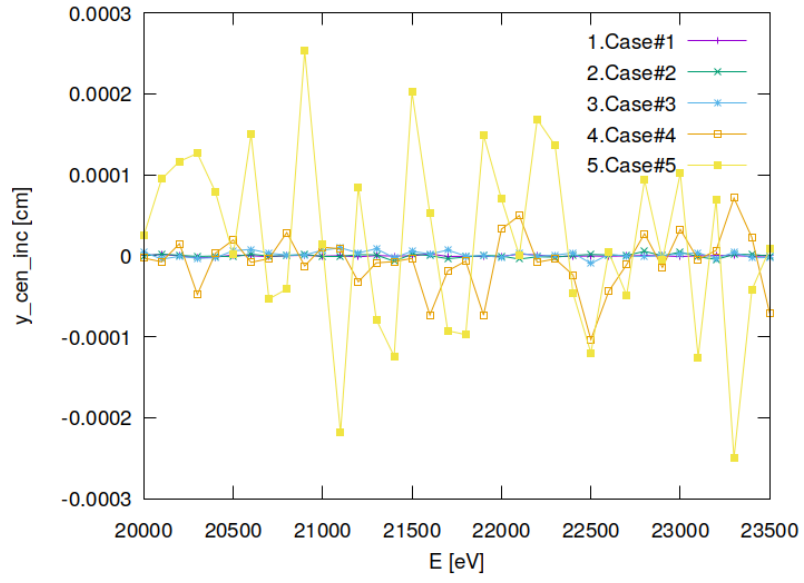


Figure 48.5: Meridional coordinate of footprint's centre of 'gravity' on surface of optical element #09 (sample).

## 48.2 Statistics of photon irradiance in beam cross section

"fig/Defocus\_C111\_Laue/plot006.png" Lbl.:Defocus\_C111\_Laue\_2d\_plot\_dx\_fwhm\_focstatavg\_oe09

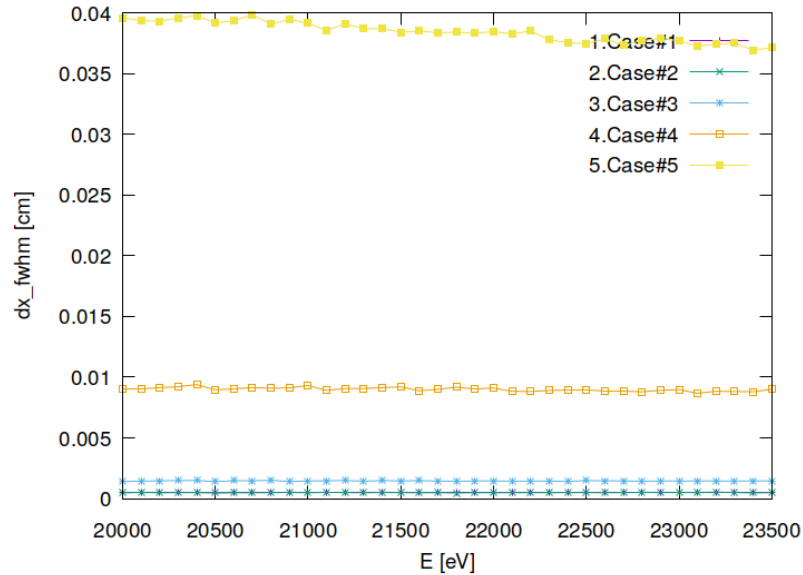


Figure 48.6: Sagittal beam diameter (FWHM) of optical element #09 (sample).

"fig/Defocus\_C111\_Laue/plot007.png" Lbl.:Defocus\_C111\_Laue\_2d\_plot\_dz\_fwhm\_focstatavg\_oe09

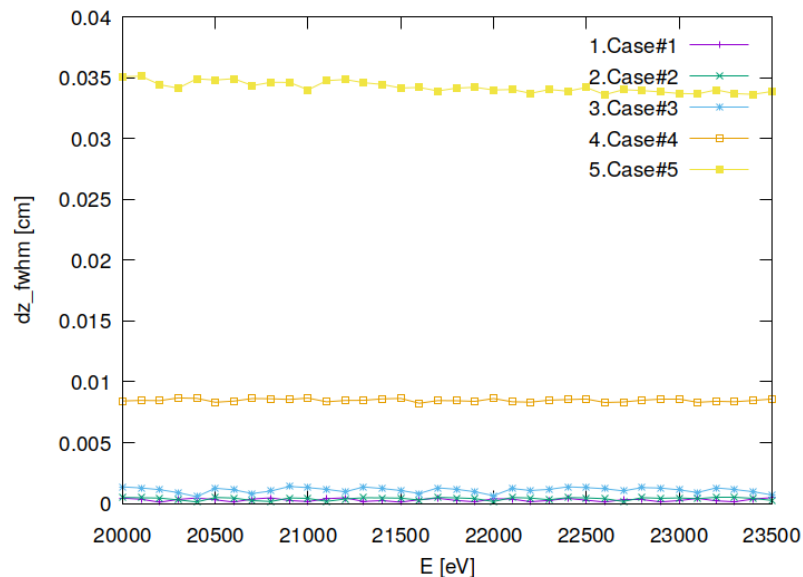


Figure 48.7: Meridional beam diameter (FWHM) of optical element #09 (sample).

```
"fig/Defocus_C111_Laue/plot008.png" Lbl.:Defocus_C111_Laue_2d_plot_I_int_focstatavg_oe09
```

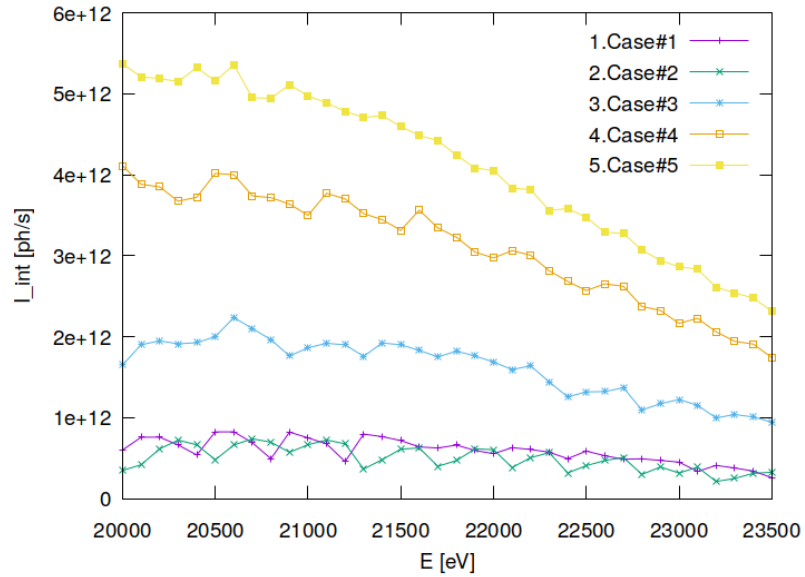


Figure 48.8: Photon flux in beam cross section of optical element #09 (sample).

```
"fig/Defocus_C111_Laue/plot009.png" Lbl.:Defocus_C111_Laue_2d_plot_x_cen_focstatavg_oe09
```

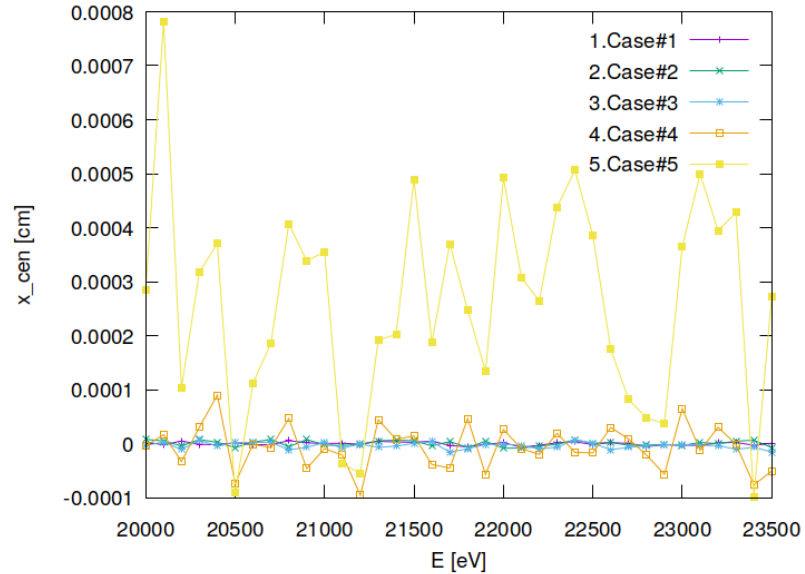


Figure 48.9: Sagittal coordinate of beam's centre of 'gravity' in beam cross section of optical element #09 (sample).

```
"fig/Defocus_C111_Laue/plot010.png" Lbl.:Defocus_C111_Laue_2d_plot_z_cen_focstatavg_oe09
```

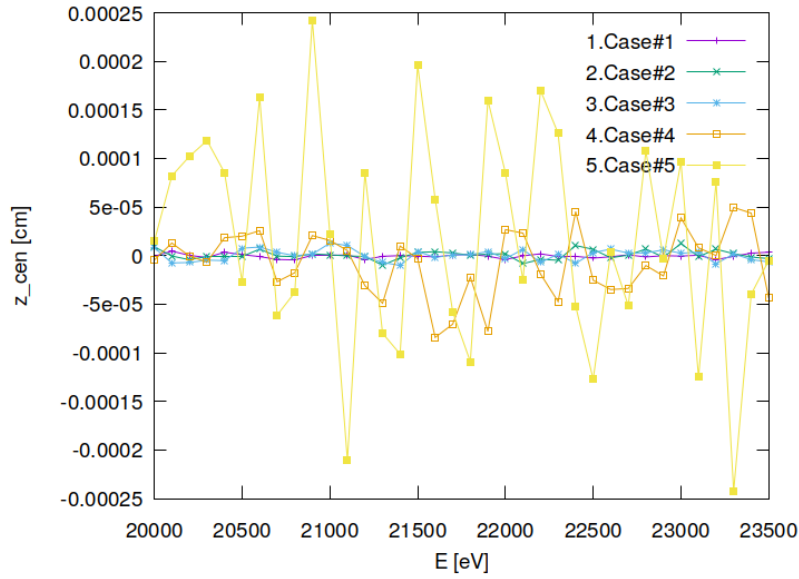


Figure 48.10: Meridional coordinate of beam's centre of 'gravity' in beam cross section of optical element #09 (sample).

```
"fig/Defocus_C111_Laue/plot011.png" Lbl.:Defocus_C111_Laue_2d_plot_dxpx_fwhm_focstatavg_oe09
```

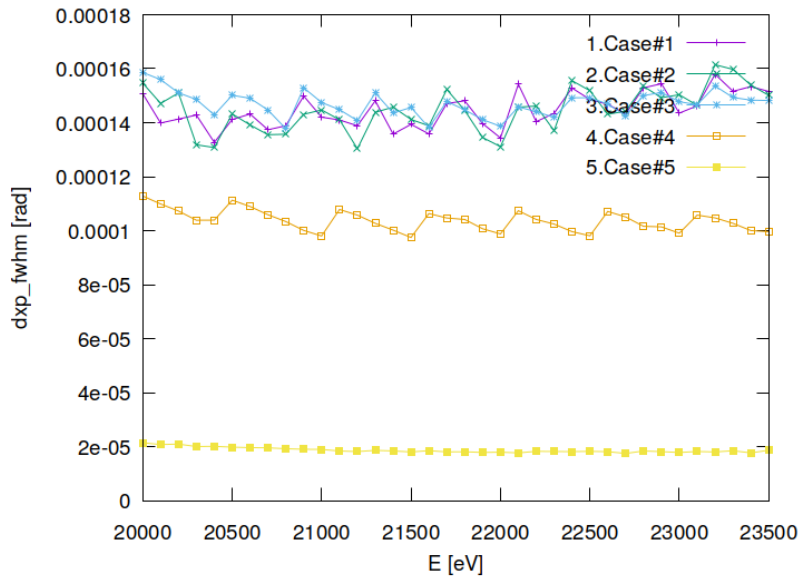


Figure 48.11: Sagittal beam divergence (FWHM) of optical element #09 (sample).

```
"fig/Defocus_C111_Laue/plot012.png" Lbl.:Defocus_C111_Laue_2d_plot_dzp_fwhm_focstatavg_oe09
```

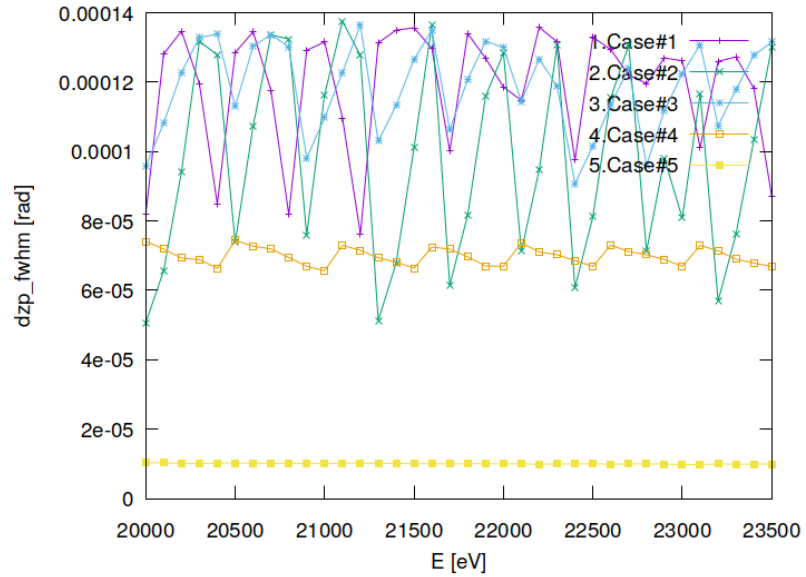


Figure 48.12: Meridional beam divergence (FWHM) of optical element #09 (sample).

```
"fig/Defocus_C111_Laue/plot013.png" Lbl.:Defocus_C111_Laue_2d_plot_I_int_focstatavg_oe09
```

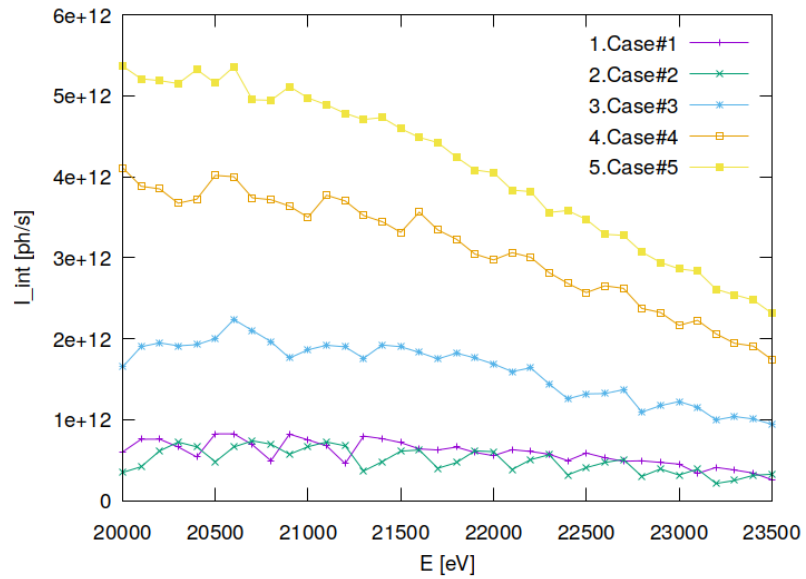


Figure 48.13: Photon flux in beam cross section of optical element #09 (sample).

```
"fig/Defocus_C111_Laue/plot014.png" Lbl.:Defocus_C111_Laue_2d_plot_xp_cen_focstatavg_oe09
```

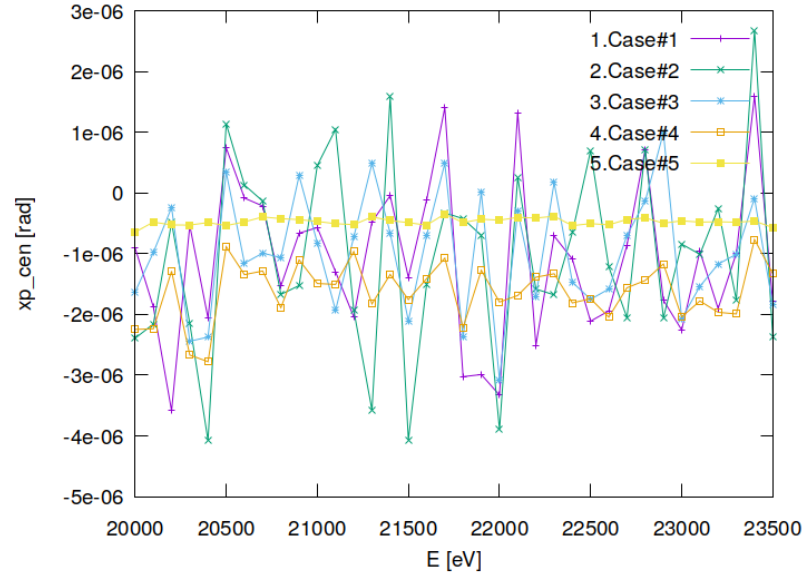


Figure 48.14: Sagittal coordinate of beam's centre of 'gravity' in angle space of optical element #09 (sample).

```
"fig/Defocus_C111_Laue/plot015.png" Lbl.:Defocus_C111_Laue_2d_plot_zp_cen_focstatavg_oe09
```

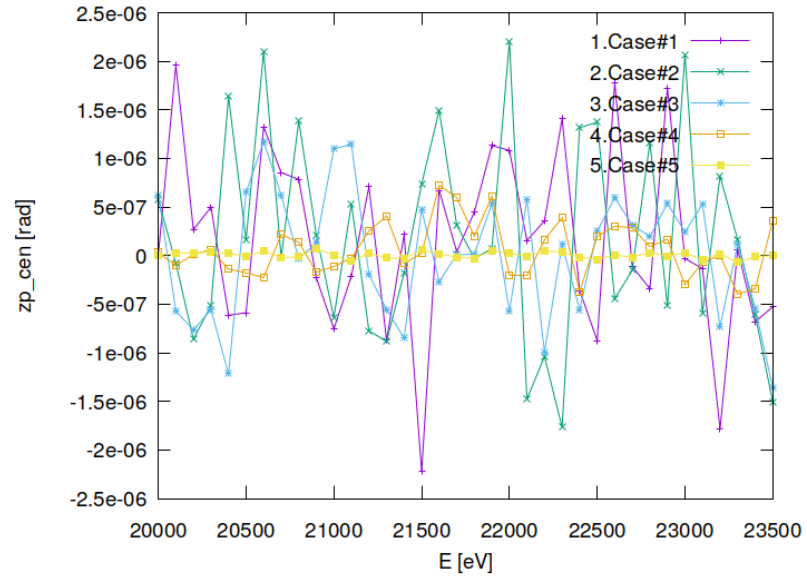


Figure 48.15: Meridional coordinate of beam's centre of 'gravity' in angle space of optical element #09 (sample).

```
"fig/Defocus_C111_Laue/plot016.png" Lbl.:Defocus_C111_Laue_2d_plot_dE_fwhm_focstatavg_oe09
```

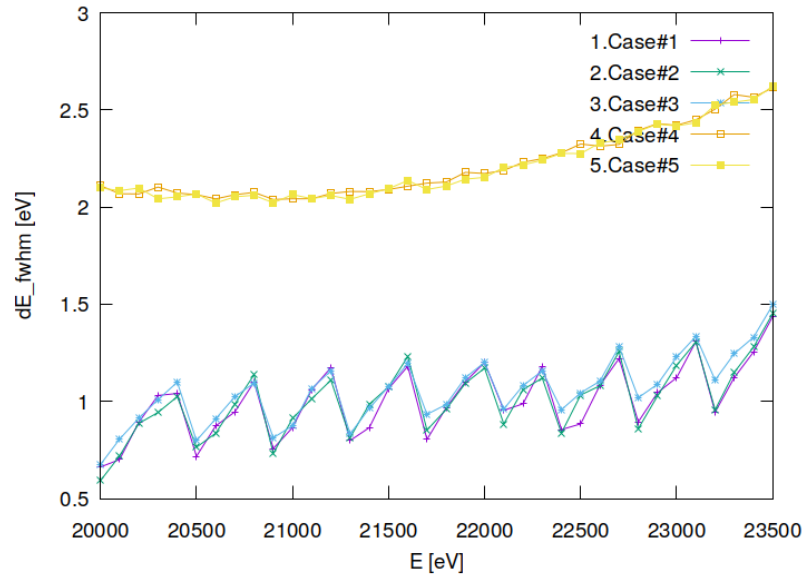


Figure 48.16: Bandwidth (FWHM) in beam cross section of optical element #09 (sample).

### 48.3 Incident photon irradiance on surface

```
"fig/Defocus_C111_Laue/plot017.png" Lbl.:Defocus_C111_Laue_false_colour_plot_I_inc_foot_oe09_c1_21800eV
```

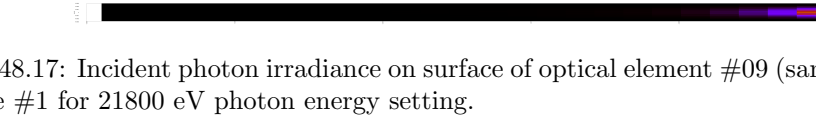


Figure 48.17: Incident photon irradiance on surface of optical element #09 (sample) for case #1 for 21800 eV photon energy setting.

```
"fig/Defocus_C111_Laue/plot018.png" Lbl.:Defocus_C111_Laue_false_colour_plot_I_inc_foot_oe09_c2_21800eV
```



Figure 48.18: Incident photon irradiance on surface of optical element #09 (sample) for case #2 for 21800 eV photon energy setting.

```
"fig/Defocus_C111_Laue/plot019.png" Lbl.:Defocus_C111_Laue_false_colour_plot_I_inc_foot_oe09_c3_21800eV
```

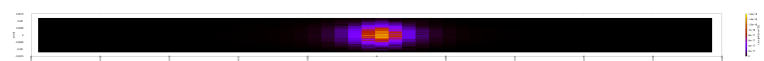


Figure 48.19: Incident photon irradiance on surface of optical element #09 (sample) for case #3 for 21800 eV photon energy setting.

```
"fig/Defocus_C111_Laue/plot020.png" Lbl.:Defocus_C111_Laue_false_colour_plot_I_inc_foot_oe09_c4_21800eV
```

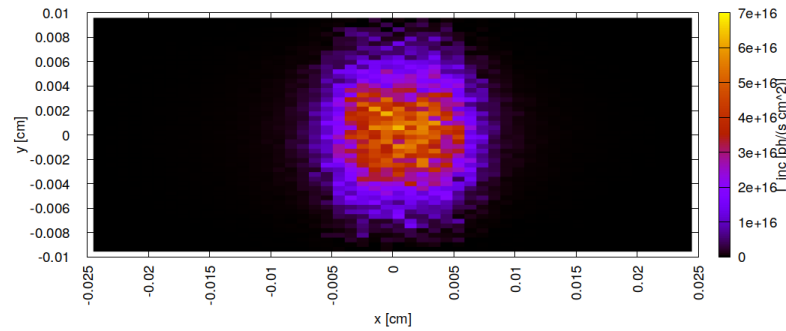


Figure 48.20: Incident photon irradiance on surface of optical element #09 (sample) for case #4 for 21800 eV photon energy setting.

```
"fig/Defocus_C111_Laue/plot021.png" Lbl.:Defocus_C111_Laue_false_colour_plot_I_inc_foot_oe09_c5_21800eV
```

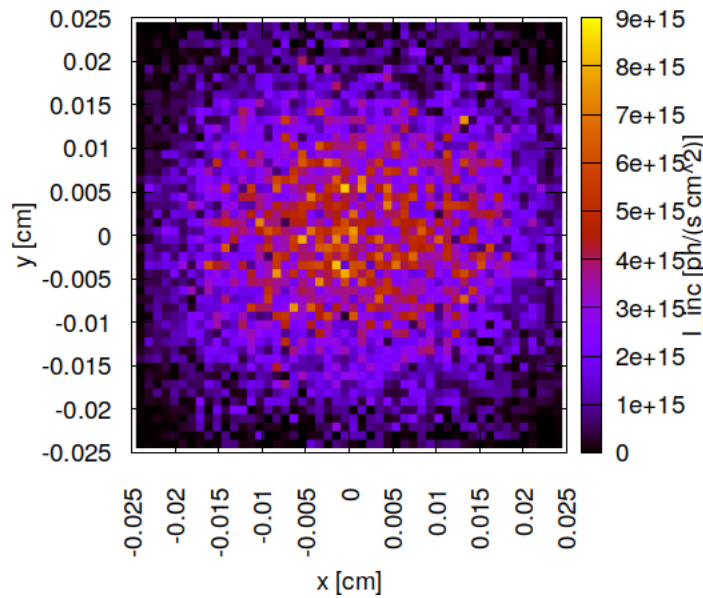


Figure 48.21: Incident photon irradiance on surface of optical element #09 (sample) for case #5 for 21800 eV photon energy setting.

## 48.4 Photon irradiance in beam cross section

"fig/Defocus\_C111\_Laue/plot022.png" Lbl.:Defocus\_C111\_Laue\_false\_colour\_plot\_I\_foc\_oe09\_c1\_21800eV

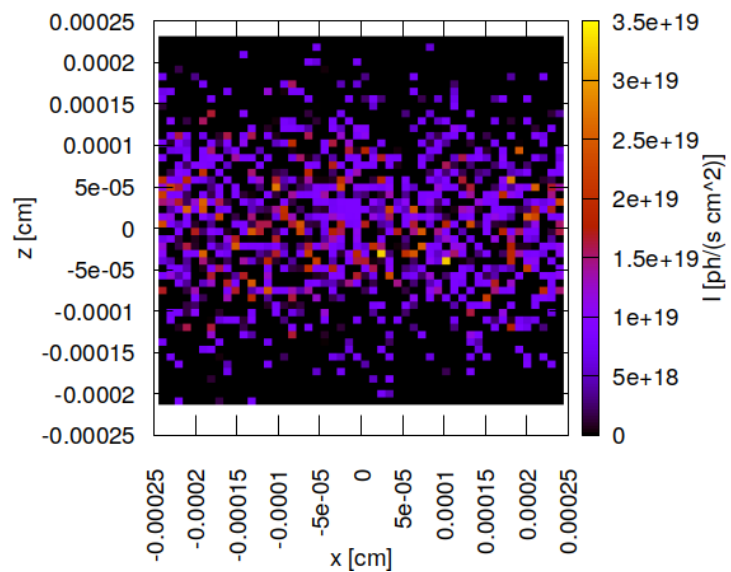


Figure 48.22: Photon irradiance in beam cross section of optical element #09 (sample) for case #1 for 21800 eV photon energy setting.

"fig/Defocus\_C111\_Laue/plot023.png" Lbl.:Defocus\_C111\_Laue\_false\_colour\_plot\_I\_foc\_oe09\_c2\_21800eV

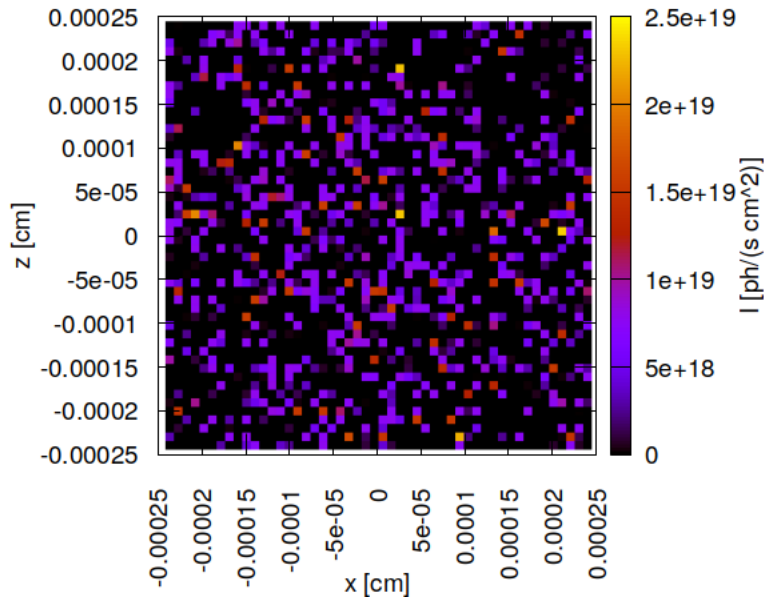


Figure 48.23: Photon irradiance in beam cross section of optical element #09 (sample) for case #2 for 21800 eV photon energy setting.

```
"fig/Defocus_C111_Laue/plot024.png" Lbl.:Defocus_C111_Laue_false_colour_plot_I_foc_oe09_c3_21800eV
```

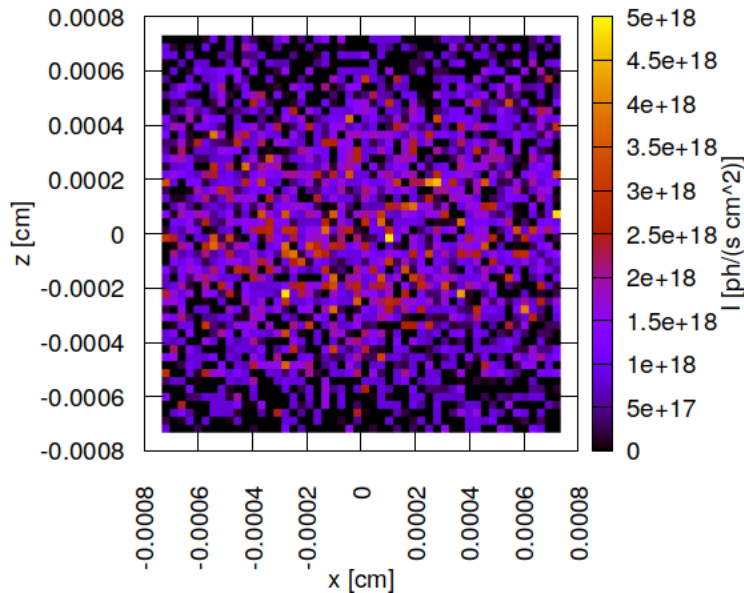


Figure 48.24: Photon irradiance in beam cross section of optical element #09 (sample) for case #3 for 21800 eV photon energy setting.

```
"fig/Defocus_C111_Laue/plot025.png" Lbl.:Defocus_C111_Laue_false_colour_plot_I_foc_oe09_c4_21800eV
```

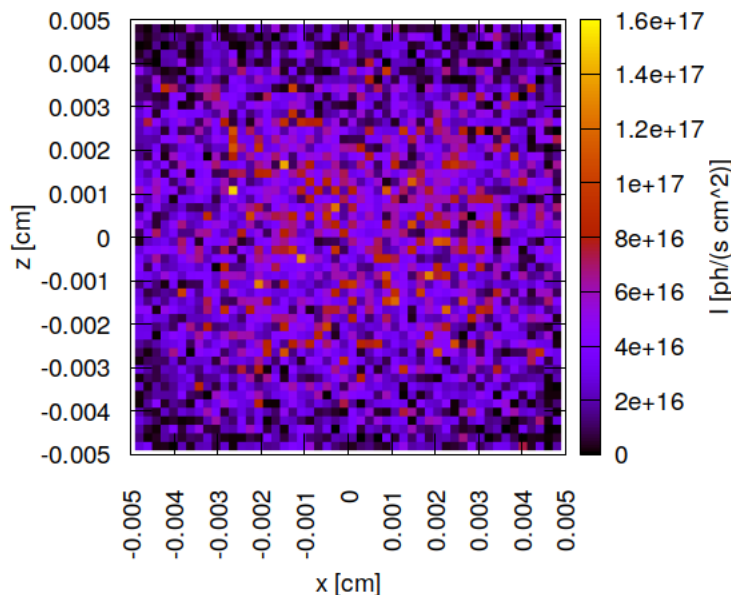


Figure 48.25: Photon irradiance in beam cross section of optical element #09 (sample) for case #4 for 21800 eV photon energy setting.

```
"fig/Defocus_C111_Laue/plot026.png" Lbl.:Defocus_C111_Laue_false_colour_plot_I_foc_oe09_c5_21800eV
```

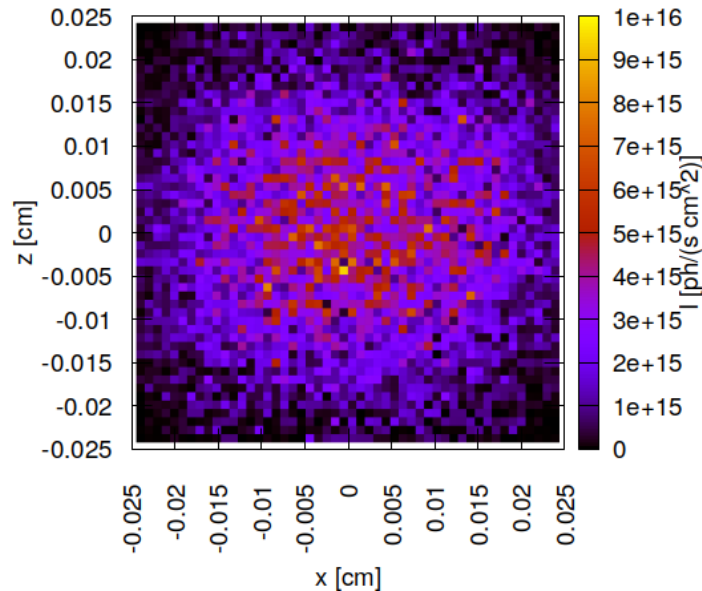


Figure 48.26: Photon irradiance in beam cross section of optical element #09 (sample) for case #5 for 21800 eV photon energy setting.

## 48.5 Spectral photon flux in beam cross section

```
"fig/Defocus_C111_Laue/plot027.png" Lbl.:Defocus_C111_Laue_2d_plot_I_bandfoc_oe09_c1_21800eV
```

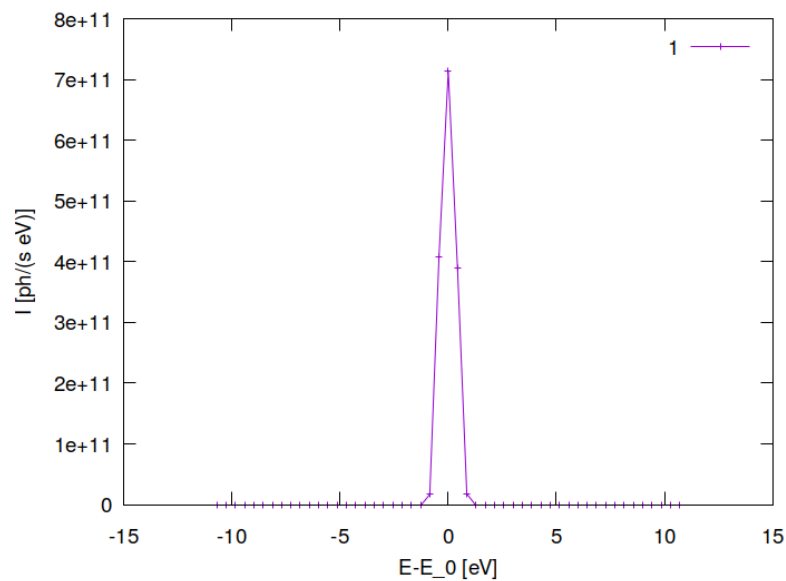


Figure 48.27: Spectral photon flux in beam cross section of optical element #09 (sample) for case #1 for 21800 eV photon energy setting.

```
"fig/Defocus_C111_Laue/plot028.png" Lbl.:Defocus_C111_Laue_2d_plot_I_bandfoc_oe09_c2_21800eV
```

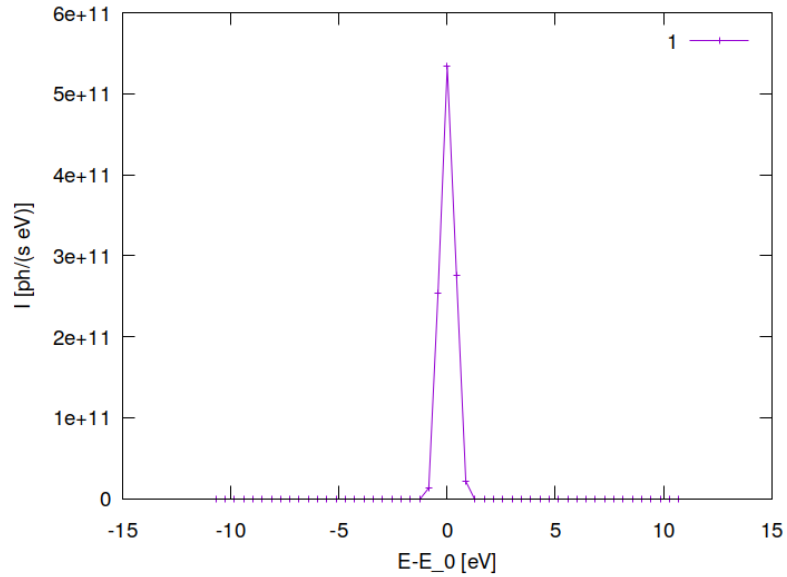


Figure 48.28: Spectral photon flux in beam cross section of optical element #09 (sample) for case #2 for 21800 eV photon energy setting.

```
"fig/Defocus_C111_Laue/plot029.png" Lbl.:Defocus_C111_Laue_2d_plot_I_bandfoc_oe09_c3_21800eV
```

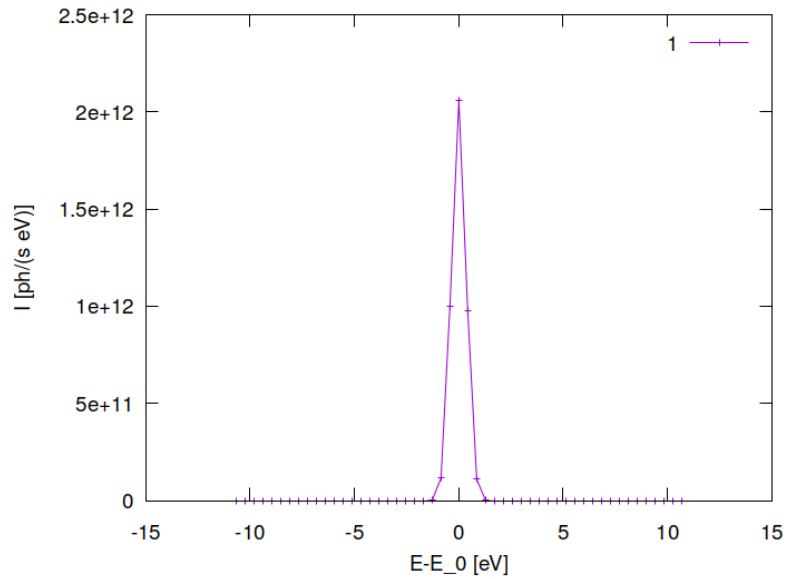


Figure 48.29: Spectral photon flux in beam cross section of optical element #09 (sample) for case #3 for 21800 eV photon energy setting.

```
"fig/Defocus_C111_Laue/plot030.png" Lbl.:Defocus_C111_Laue_2d_plot_I_bandfoc_oe09_c4_21800eV
```

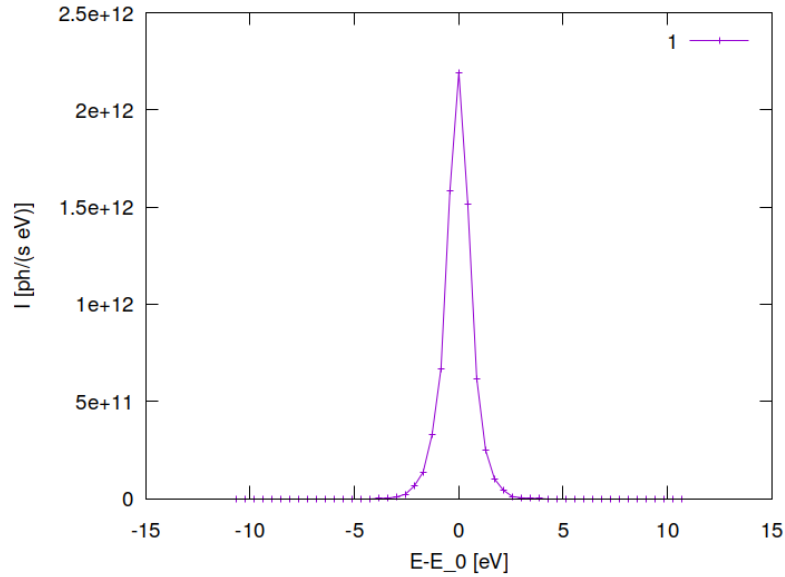


Figure 48.30: Spectral photon flux in beam cross section of optical element #09 (sample) for case #4 for 21800 eV photon energy setting.

```
"fig/Defocus_C111_Laue/plot031.png" Lbl.:Defocus_C111_Laue_2d_plot_I_bandfoc_oe09_c5_21800eV
```

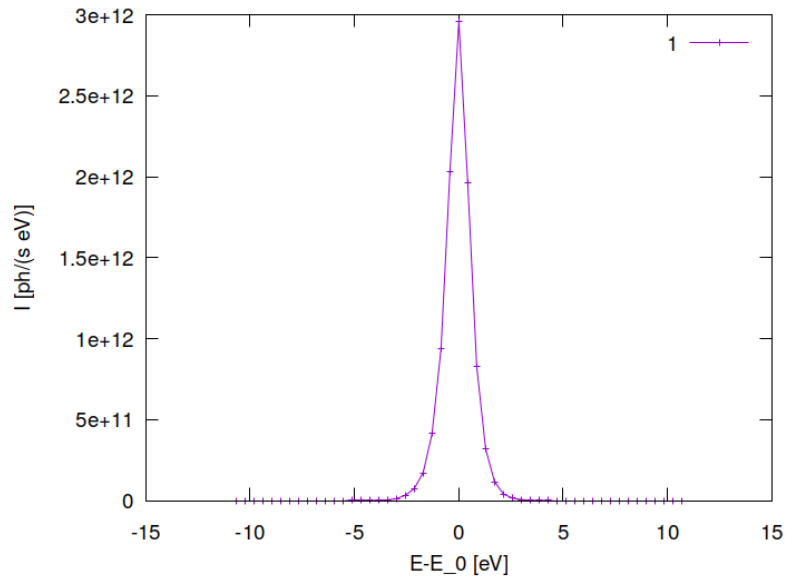


Figure 48.31: Spectral photon flux in beam cross section of optical element #09 (sample) for case #5 for 21800 eV photon energy setting.

## Chapter 49

# Focusing test setup with diamond 111 beam splitter in Bragg geometry

A thin CVD diamond crystal is employed as a diffractive beam splitter, using the 111 reflection in Bragg geometry. The diamond 111 reflection diverts radiation within a narrow bandwidth of

$$\delta E/E = \delta\theta/\tan\theta$$

to the SinCrys side station.

Subsequent reflection from a second crystal of the same material using the same set of diffracting planes which are parallel to the first is required to provide the necessary stability of the exit beam which has to hit the very small acceptance aperture of the CRLs (see chapter 23.3).

Putting the second crystal at a distance of around 3.66 metres behind the first provides the required offset of more than one metre between the twice deflected beam and the main beam.

Compound refractive lenses (CRL) are used to focus the monochromatised beam onto the sample. A stack of two-dimensionally focussing lenses has to be complemented by a stack of one-dimensional lenses in order to compensate for the astigmatism generated by the deformation of the beam splitter under the heat load from absorption.

Even for the beam splitter in Bragg geometry the horizontal beam diameter (FWHM) exceeds five microns, the largest contribution coming from source broadening. Therefore an aperture of the size of the requested illuminated area is inserted at the sample position in the same way as in the Laue case. Correspondingly, one obtains the full beam in the footprint of optical element 9 and the apertured beam in the continuation plane of the same.

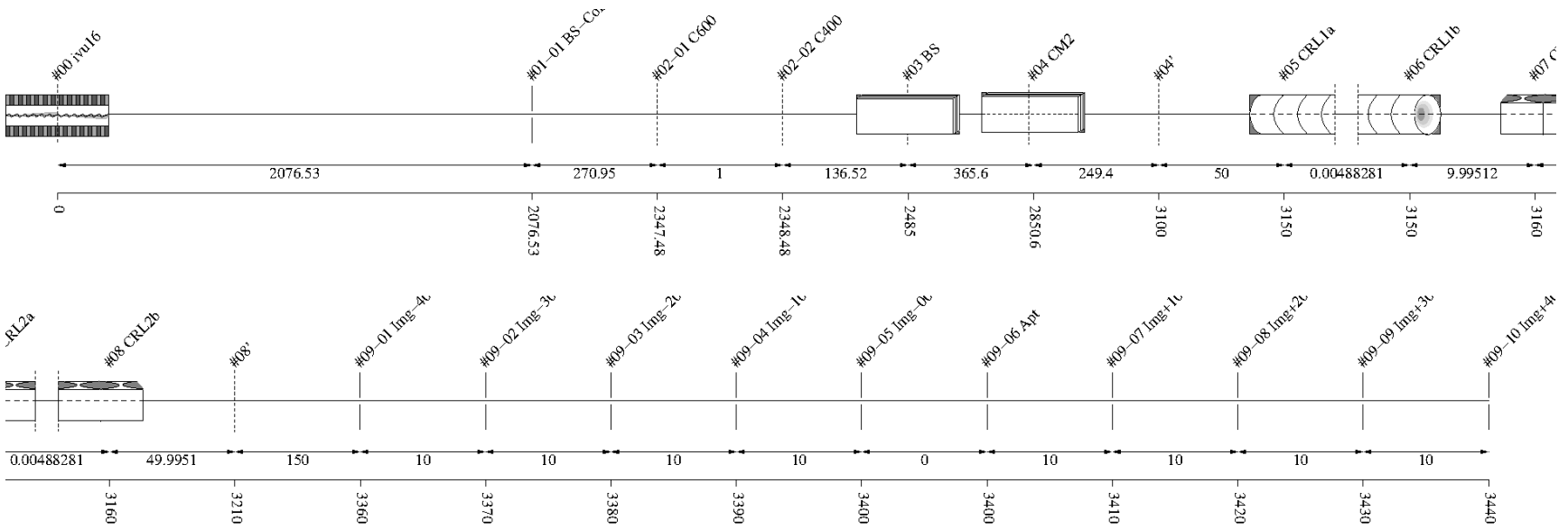


Figure 49.1: Schematic of optical setup

#	Name	Pathlen. cm	Descript.	Shape	Pitch* deg	Roll deg	Yaw deg	x_min cm	x_max cm	y_min cm	y_max cm	Thick. cm	Surface
<b>0</b>	ivu16	0	undulator	auto	0	0	0	-0.0027	0.0027	-0.0002	0.0002	auto	
<b>1</b>		2076.53	none	plane	0	0	0	-inf	inf	-inf	inf		perfect
<b>1-1</b>	BS-Collim	2076.53	aperture	rectangle	0	0	0	-0.035	0.035	-0.035	0.035		
<b>2</b>	Filter	2347.48	none	plane	0	0	0	-inf	inf	-inf	inf		perfect
<b>2-1</b>	C600	2347.48	C-filter	rectangle	0	0	0	-inf	inf	-inf	inf	0.06	
<b>2-2</b>	C400	2348.48	C-filter	rectangle	0	0	0	-inf	inf	-inf	inf	0.04	

<b>3</b>	BS	2485	C(1,1,1)-crystal	plane	7.93694	90	0	-0.15	0.15	-0.5	0.5		heat bump
<b>4</b>	CM2	2850.6	C(1,1,1)-crystal	plane	7.93694	180	0	-inf	inf	-inf	inf		perfect
<b>4'</b>		3100	continuation plane		0	0	0						
<b>5</b>	CRL1a	3150	vac/Be-lens surface	parabola	0	0	0	-0.03	0.03	-0.03	0.03		perfect
<b>6</b>	CRL1b	3150	Be/vac-lens surface	parabola	0	0	0	-0.03	0.03	-0.03	0.03		perfect
<b>7</b>	CRL2a	3160	vac/Be-lens surface	extruded parabola	0	0	0	-0.1	0.1	-0.03	0.03		perfect
<b>8</b>	CRL2b	3160	Be/vac-lens surface	extruded parabola	0	0	0	-0.1	0.1	-0.03	0.03		perfect
<b>8'</b>		3210	continuation plane		0	0	0						
<b>9</b>	sample	3400	none	plane	0	-90	0	-inf	inf	-inf	inf		perfect
<b>9-1</b>	Img-40	3360	aperture	rectangle	0	0	0	-0.025	0.025	-0.025	0.025		
<b>9-2</b>	Img-30	3370	aperture	rectangle	0	0	0	-0.025	0.025	-0.025	0.025		
<b>9-3</b>	Img-20	3380	aperture	rectangle	0	0	0	-0.025	0.025	-0.025	0.025		
<b>9-4</b>	Img-10	3390	aperture	rectangle	0	0	0	-0.025	0.025	-0.025	0.025		
<b>9-5</b>	Img-00	3400	aperture	rectangle	0	0	0	-0.025	0.025	-0.025	0.025		
<b>9-6</b>	Apt	3400	aperture	rectangle	0	0	0	-0.025	0.025	-0.025	0.025		
<b>9-7</b>	Img+10	3410	aperture	rectangle	0	0	0	-0.025	0.025	-0.025	0.025		
<b>9-8</b>	Img+20	3420	aperture	rectangle	0	0	0	-0.025	0.025	-0.025	0.025		
<b>9-9</b>	Img+30	3430	aperture	rectangle	0	0	0	-0.025	0.025	-0.025	0.025		
<b>9-10</b>	Img+40	3440	aperture	rectangle	0	0	0	-0.025	0.025	-0.025	0.025		

Table 49.1: Setup parameters common to all components. (\*Glancing angle for mirrors, multilayers and crystals. Angle to surface normal otherwise.)

**Rays:** Polar type = total

Polar phase = 0 deg

Polar degree = 0

Is coherent = no

**Spectrum:** E min = 500 eV

E max = 40000 eV

Relative linewidth = 1

**Band:** Bandwidth = 0.0005

**Insertion Device:** lambda period = 1.6 cm

n period = 187

I electron = 0.5 A

E electron = 3 GeV

y horizontal waist = 0 cm

y vertical waist = 0 cm

epsilon x = 3.2E-08 cm rad

epsilon z = 8E-10 cm rad

K y = 1.66

K ymax = 1.7

Divergence limit = 5E-05 rad

**Undulator:** n harmonic max = 99

Tuning type = fixed gap

l aperture = 2076.53 cm

dx aperture = 0.07 cm

dz aperture = 0.07 cm

#1

**Screen:** Is absorbing[1] = no

**Shape:** Thickness = 0 cm

#2 Filter

**Screen:** Is absorbing[1] = yes

Is absorbing[2] = yes

Molecular formula[1] = C

Molecular formula[2] = C

Mass density[1] = 3.5 g/cm^3

Mass density[2] = 3.5 g/cm^3

Thickness[1] = 0.06 cm

Thickness[2] = 0.04 cm

**Shape:** Thickness = 0 cm

### #3 BS

**Crystal:** Structure type = zinblend

Lattice constant[1] = 3.567 Angstrom  
Lattice constant[2] = 3.567 Angstrom  
Lattice constant[3] = 3.567 Angstrom  
Debye Waller factor = 1  
Is absorbing = yes  
Is asymmetric = no  
Is inclined = no  
Is Johansson geometry = no  
Is mosaic = no

**Tune:** z rotation axis = 0 cm

**Geometry:** Is thin = yes

Tune automatic = yes

**Shape:** Thickness = 0.01 cm

**Boundary:** Type = rectangle

x rim = 0.5 cm  
y rim = 0.5 cm

**Surface:** Is rough = no

**FEA:** Design type = type specific

Crystal design = laue with cooling loop  
Is isotropic = no  
Angle x = 0 deg  
Angle y = 0 deg  
Angle z = 0 deg  
Mass density = 3.516 g/cm<sup>3</sup>

**Heat:** Heat transfer type[1] = insulated

Heat transfer type[2] = heat transfer  
Heat transfer type[3] = insulated  
Heat transfer type[4] = insulated  
Heat transfer type[5] = heat transfer  
Heat transfer type[6] = flux  
Heat transfer type[7] = insulated  
Heat transfer type[8] = heat transfer  
Heat transfer type[9] = heat sink  
Heat transfer coefficient = 1 W/(cm<sup>2</sup>K)  
Heat sink coefficient = 10 W/(cm<sup>2</sup>K)  
T reference = 293.15 K  
T cooling = 293.15 K  
Heat capacity = 0.54 J/(gK)  
Thermal conductivity[1] = 25 W/(cmK<sup>n</sup>)

**Stress and strain:** Constraint[1] = free  
 Constraint[2] = kinematic  
 Constraint[3] = free  
 Constraint[4] = free  
 Constraint[5] = free  
 Constraint[6] = free  
 Constraint[7] = free  
 Constraint[8] = free  
 Constraint[9] = free  
 Thermal expansion tensor[1] = 1.1E-06 1/K  
 Thermal expansion tensor[2] = 1.1E-06 1/K  
 Thermal expansion tensor[3] = 1.1E-06 1/K  
 Thermal expansion tensor[4] = 0 1/K  
 Thermal expansion tensor[5] = 0 1/K  
 Thermal expansion tensor[6] = 0 1/K  
 Stiffness tensor(1)(1) = 1.07861E+12 Pa  
 Stiffness tensor(2)[1] = 1.2663E+11 Pa  
 Stiffness tensor(2)[2] = 1.07861E+12 Pa  
 Stiffness tensor(3)[1] = 1.2663E+11 Pa  
 Stiffness tensor(3)[2] = 1.2663E+11 Pa  
 Stiffness tensor(3)[3] = 1.07861E+12 Pa  
 Stiffness tensor(4)[1] = 0 Pa  
 Stiffness tensor(4)[2] = 0 Pa  
 Stiffness tensor(4)[3] = 0 Pa  
 Stiffness tensor(4)[4] = 5.7756E+11 Pa  
 Stiffness tensor(5)[1] = 0 Pa  
 Stiffness tensor(5)[2] = 0 Pa  
 Stiffness tensor(5)[3] = 0 Pa  
 Stiffness tensor(5)[4] = 0 Pa  
 Stiffness tensor(5)[5] = 5.7756E+11 Pa  
 Stiffness tensor(6)[1] = 0 Pa  
 Stiffness tensor(6)[2] = 0 Pa  
 Stiffness tensor(6)[3] = 0 Pa  
 Stiffness tensor(6)[4] = 0 Pa  
 Stiffness tensor(6)[5] = 0 Pa  
 Stiffness tensor(6)[6] = 5.7756E+11 Pa

#### #4 CM2

**Crystal:** Structure type = zinblend  
 Lattice constant[1] = 3.567 Angstrom  
 Lattice constant[2] = 3.567 Angstrom  
 Lattice constant[3] = 3.567 Angstrom  
 Debye Waller factor = 1  
 Is absorbing = yes  
 Is asymmetric = no  
 Is inclined = no  
 Is Johansson geometry = no  
 Is mosaic = no

**Tune:** Type = constant pathlength  
 Are downstream elements fixed = no

**Geometry:** Is thin = no  
Tune automatic = yes

**Boundary:** Type = none

**Surface:** Is rough = no

### #5 CRL1a

**Dielectric:** Reflectivity type = polarisation  
Is constant = no  
Mass density = 1.85 g/cm<sup>3</sup>

**Geometry:** g = 3150 cm  
b = 250 cm  
Is thin = yes  
n clones = 5  
n originals = 2  
Focus automatically = yes

**Focus:** Type = chromatic  
Number variation method = cloning  
Vary distance = no

**Shape:** Defined by = user  
Is convex = no  
Is extruded = no  
Radius = 0.01 cm  
Thickness = 0.005 cm

**Boundary:** Type = ellipse

**Parabola:** Is source in infinity = no  
p semi = 0.01 cm

**Surface:** Is rough = no

### #6 CRL1b

**Dielectric:** Reflectivity type = polarisation  
Is constant = yes  
delta refraction = 0  
beta absorption = 0

**Geometry:** g = 3150 cm  
b = 250 cm  
Is thin = yes  
n clones = 5  
n originals = 0  
Focus automatically = yes

**Focus:** Type = chromatic  
Number variation method = cloning  
Vary distance = no

**Shape:** Defined by = user  
Is convex = yes  
Is extruded = no  
Radius = 0.01 cm  
Thickness = 0.005 cm

**Boundary:** Type = ellipse

**Parabola:** Is source in infinity = no  
p semi = 0.01 cm

**Surface:** Is rough = no

## #7 CRL2a

**Dielectric:** Reflectivity type = polarisation  
Is constant = no  
Mass density = 1.85 g/cm<sup>3</sup>

**Geometry:** g = -255 cm  
b = 240 cm  
Is thin = yes  
n clones = 6  
n originals = 2  
Focus automatically = yes

**Focus:** Type = chromatic  
Number variation method = cloning  
Vary distance = no

**Shape:** Defined by = user  
Is convex = no  
Is extruded = yes  
Radius = 0.02 cm  
Thickness = 0.005 cm

**Boundary:** Type = rectangle

**Parabola:** Is source in infinity = no  
p semi = 0.02 cm

**Extruded:** Angle z = 0 deg

**Surface:** Is rough = no

### #8 CRL2b

**Dielectric:** Reflectivity type = polarisation  
Is constant = yes  
delta refraction = 0  
beta absorption = 0

**Geometry:** g = -255 cm  
b = 240 cm  
Is thin = yes  
n clones = 6  
n originals = 0  
Focus automatically = yes

**Focus:** Type = chromatic  
Number variation method = cloning  
Vary distance = no

**Shape:** Defined by = user  
Is convex = yes  
Is extruded = yes  
Radius = 0.02 cm  
Thickness = 0.005 cm

**Boundary:** Type = rectangle

**Parabola:** Is source in infinity = no  
p semi = 0.02 cm

**Extruded:** Angle z = 0 deg

**Surface:** Is rough = no

### #9 sample

**Screen:** Is absorbing[1] = no  
Is absorbing[2] = no  
Is absorbing[3] = no  
Is absorbing[4] = no  
Is absorbing[5] = no  
Is absorbing[6] = no  
Is absorbing[7] = no  
Is absorbing[8] = no  
Is absorbing[9] = no  
Is absorbing[10] = no

**Shape:** Thickness = 0 cm

# Chapter 50

## Parameter scan cases

Only the first five of the six cases are relevant, all five without heat load. These cases represent different focussing settings. In the first case the CRLs are set up for best focus. In the second case the CRLs focus behind the sample position, such that the beam cross-section at the sample position is at least  $5 \times 5$  microns large. In the third and fourth case one aims for a  $15 \times 15$  and  $100 \times 100$  microns large beam cross section. Finally, case #5 is without any focussing. Due to the somewhat smaller but still large focal spot even in Bragg geometry the third case – one earlier than in Laue geometry – represents the smallest aperture size that does not clip the beam, i.e. where no flux is lost.

Case	Has_slope_error_03	b_05 cm	g_07 cm	Skip_heatload
1	no	249	-240	yes
2	no	254	-240	yes
3	no	264	-253	yes
4	no	410	-280	yes
5	no	-3150	-240	yes
6	yes	249	-242	no

Table 50.1: Parameter values for different cases in parameter scan

### Legend

**Case:** Case number in parameter scan

**Has\_slope\_error\_03:** Optical\_element\_#3.Surface.Has\_slope\_error (Has surface slope error?)

**b\_05:** Optical\_element\_#5.Geometry.b (Distance from optical element's pole to meridional image focus.)

**g\_07:** Optical\_element\_#7.Geometry.g (Distance btw. meridional object focus and optical element's pole.)

**Skip\_heatload:** Session.Skip\_heatload (Skip heat load calculation for all optical elements? (heat load parameters are kept))

## Chapter 51

# Photon energy scan

The  $K_y$ -values in the table below are those for optimised output between 15.6 and 18.3 keV used by DanMAX' main branch. The number of 2D and 1D focussing lens elements needed for the required beam properties in the SinCrys side branch are also provided here.

E eV	K_y	n_harm/step	theta_B03 deg	nMult_05	nMult_07
<b>20000</b>	1.67551	9	8.6565237	25	0
<b>20100</b>	1.66836	9	8.6131277	26	0
<b>20200</b>	1.66125	9	8.5701675	26	0
<b>20300</b>	1.65418	9	8.5276346	26	0
<b>20400</b>	1.64714	9	8.4855232	26	0
<b>20500</b>	1.64015	9	8.4438276	27	0
<b>20600</b>	1.63319	9	8.4025402	27	0
<b>20700</b>	1.62628	9	8.3616571	27	0
<b>20800</b>	1.6194	9	8.3211708	27	0
<b>20900</b>	1.61255	9	8.2810764	28	0
<b>21000</b>	1.60575	9	8.2413683	28	0
<b>21100</b>	1.59898	9	8.2020397	28	0
<b>21200</b>	1.59224	9	8.1630869	28	0
<b>21300</b>	1.58554	9	8.1245022	29	0
<b>21400</b>	1.57887	9	8.0862827	29	0
<b>21500</b>	1.57224	9	8.0484219	29	0
<b>21600</b>	1.56564	9	8.0109158	30	0
<b>21700</b>	1.55908	9	7.9737582	30	0
<b>21800</b>	1.55255	9	7.936945	30	0
<b>21900</b>	1.54605	9	7.9004712	30	0
<b>22000</b>	1.53958	9	7.8643322	31	0
<b>22100</b>	1.53315	9	7.8285236	31	0
<b>22200</b>	1.52674	9	7.7930403	31	0
<b>22300</b>	1.52037	9	7.7578783	32	0
<b>22400</b>	1.51402	9	7.7230334	32	0
<b>22500</b>	1.50771	9	7.6885004	32	0
<b>22600</b>	1.50143	9	7.6542764	32	0
<b>22700</b>	1.49517	9	7.6203566	33	0
<b>22800</b>	1.48895	9	7.5867367	33	0
<b>22900</b>	1.48275	9	7.5534129	33	0
<b>23000</b>	1.47658	9	7.5203819	34	0
<b>23100</b>	1.47044	9	7.487639	34	0
<b>23200</b>	1.46433	9	7.4551811	34	0
<b>23300</b>	1.45824	9	7.4230037	34	0
<b>23400</b>	1.45218	9	7.3911042	35	0
<b>23500</b>	1.44615	9	7.359478	35	0

Table 51.1: Scan values for different photon energies in energy scan of case #1 (best focus)

E eV	nMult_05	nMult_07
<b>20000</b>	25	0
<b>20100</b>	25	0
<b>20200</b>	25	0
<b>20300</b>	26	0
<b>20400</b>	26	0
<b>20500</b>	26	0
<b>20600</b>	26	0
<b>20700</b>	27	0
<b>20800</b>	27	0
<b>20900</b>	27	0
<b>21000</b>	27	0
<b>21100</b>	28	0
<b>21200</b>	28	0
<b>21300</b>	28	0
<b>21400</b>	28	0
<b>21500</b>	29	0
<b>21600</b>	29	0
<b>21700</b>	29	0
<b>21800</b>	30	0
<b>21900</b>	30	0
<b>22000</b>	30	0
<b>22100</b>	30	0
<b>22200</b>	31	0
<b>22300</b>	31	0
<b>22400</b>	31	0
<b>22500</b>	32	0
<b>22600</b>	32	0
<b>22700</b>	32	0
<b>22800</b>	32	0
<b>22900</b>	33	0
<b>23000</b>	33	0
<b>23100</b>	33	0
<b>23200</b>	34	0
<b>23300</b>	34	0
<b>23400</b>	34	0
<b>23500</b>	34	0

Table 51.2: Scan values for different photon energies in energy scan of case #2 ( $5 \times 5$  microns)

E eV	nMult_05	nMult_07
<b>20000</b>	24	3
<b>20100</b>	24	3
<b>20200</b>	24	3
<b>20300</b>	25	3
<b>20400</b>	25	3
<b>20500</b>	25	3
<b>20600</b>	25	3
<b>20700</b>	26	3
<b>20800</b>	26	3
<b>20900</b>	26	3
<b>21000</b>	26	3
<b>21100</b>	27	3
<b>21200</b>	27	3
<b>21300</b>	27	3
<b>21400</b>	27	3
<b>21500</b>	28	3
<b>21600</b>	28	3
<b>21700</b>	28	3
<b>21800</b>	29	3
<b>21900</b>	29	3
<b>22000</b>	29	3
<b>22100</b>	29	3
<b>22200</b>	30	3
<b>22300</b>	30	3
<b>22400</b>	30	3
<b>22500</b>	30	3
<b>22600</b>	31	3
<b>22700</b>	31	3
<b>22800</b>	31	3
<b>22900</b>	31	3
<b>23000</b>	32	3
<b>23100</b>	32	3
<b>23200</b>	32	3
<b>23300</b>	33	3
<b>23400</b>	33	3
<b>23500</b>	33	3

Table 51.3: Scan values for different photon energies in energy scan of case #3  
(15 × 15 microns)

E eV	nMult_05	nMult_07
<b>20000</b>	16	7
<b>20100</b>	16	7
<b>20200</b>	16	7
<b>20300</b>	17	7
<b>20400</b>	17	7
<b>20500</b>	17	7
<b>20600</b>	17	7
<b>20700</b>	17	7
<b>20800</b>	17	8
<b>20900</b>	18	8
<b>21000</b>	18	8
<b>21100</b>	18	8
<b>21200</b>	18	8
<b>21300</b>	18	8
<b>21400</b>	18	8
<b>21500</b>	19	8
<b>21600</b>	19	8
<b>21700</b>	19	8
<b>21800</b>	19	8
<b>21900</b>	19	8
<b>22000</b>	20	8
<b>22100</b>	20	9
<b>22200</b>	20	9
<b>22300</b>	20	9
<b>22400</b>	20	9
<b>22500</b>	20	9
<b>22600</b>	21	9
<b>22700</b>	21	9
<b>22800</b>	21	9
<b>22900</b>	21	9
<b>23000</b>	21	9
<b>23100</b>	22	9
<b>23200</b>	22	9
<b>23300</b>	22	9
<b>23400</b>	22	10
<b>23500</b>	22	10

Table 51.4: Scan values for different photon energies in energy scan of case #4 (100 × 100 microns)

E eV	nMult_05	nMult_07
<b>20000</b>	0	0
<b>20100</b>	0	0
<b>20200</b>	0	0
<b>20300</b>	0	0
<b>20400</b>	0	0
<b>20500</b>	0	0
<b>20600</b>	0	0
<b>20700</b>	0	0
<b>20800</b>	0	0
<b>20900</b>	0	0
<b>21000</b>	0	0
<b>21100</b>	0	0
<b>21200</b>	0	0
<b>21300</b>	0	0
<b>21400</b>	0	0
<b>21500</b>	0	0
<b>21600</b>	0	0
<b>21700</b>	0	0
<b>21800</b>	0	0
<b>21900</b>	0	0
<b>22000</b>	0	0
<b>22100</b>	0	0
<b>22200</b>	0	0
<b>22300</b>	0	0
<b>22400</b>	0	0
<b>22500</b>	0	0
<b>22600</b>	0	0
<b>22700</b>	0	0
<b>22800</b>	0	0
<b>22900</b>	0	0
<b>23000</b>	0	0
<b>23100</b>	0	0
<b>23200</b>	0	0
<b>23300</b>	0	0
<b>23400</b>	0	0
<b>23500</b>	0	0

Table 51.5: Scan values for different photon energies in energy scan of case #5 (unfocussed)

#### Legend

**E:** photon energy

**nMult\_05:** number of elements in compound refractive lens optical element 05

**nMult\_07:** number of elements in compound refractive lens optical element 07

# Chapter 52

## Plots

### 52.1 Statistics of photon irradiance on optical surface

```
"fig/Defocus_C111_Bragg/plot001.png" Lbl.:Defocus_C111_Bragg_2d_plot_dx_fwhm_inc_footstat_oe09
```

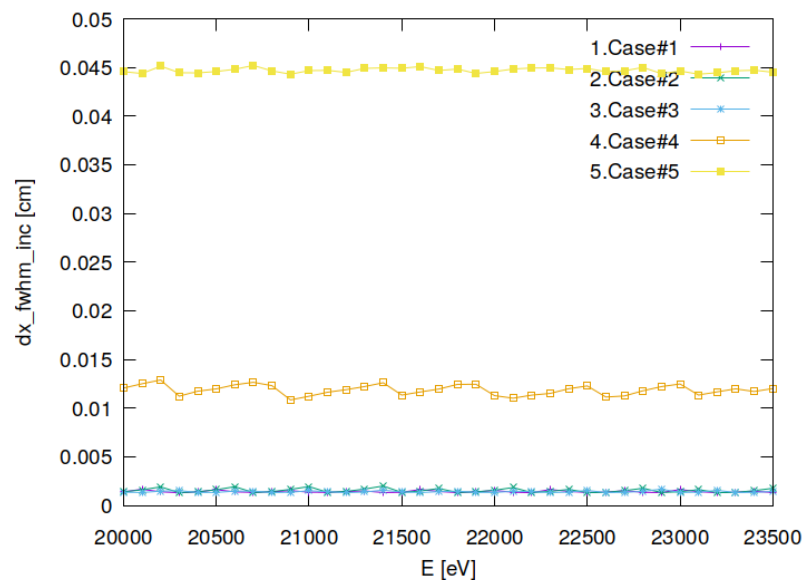


Figure 52.1: Sagittal footprint diameter (FWHM) of optical element #09 (sample).

```
"fig/Defocus_C111_Bragg/plot002.png" Lbl.:Defocus_C111_Bragg_2d_plot_dy_fwhm_inc_footstat_oe09
```

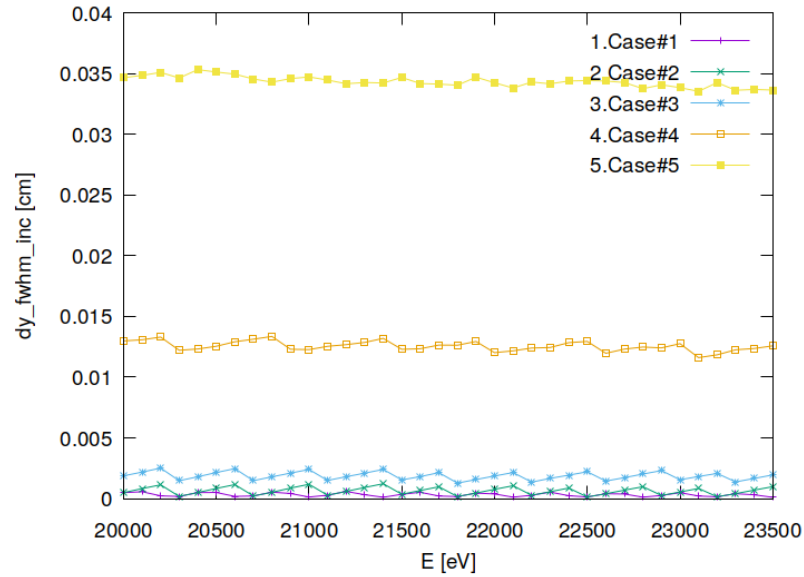


Figure 52.2: Meridional footprint diameter (FWHM) of optical element #09 (sample).

```
"fig/Defocus_C111_Bragg/plot003.png" Lbl.:Defocus_C111_Bragg_2d_plot_I_inc_int_footstat_oe09
```

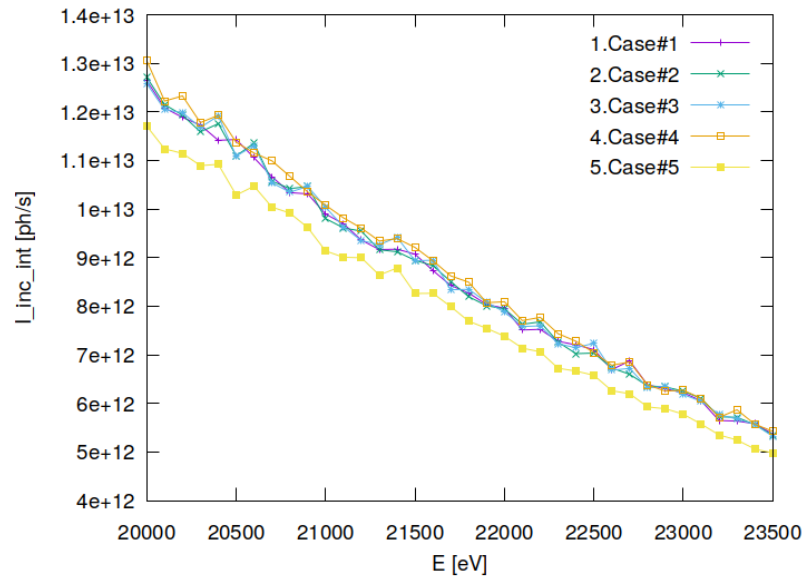


Figure 52.3: Incident photon flux on surface of optical element #09 (sample).

"fig/Defocus\_C111\_Bragg/plot004.png" Lbl.:Defocus\_C111\_Bragg\_2d\_plot\_x\_cen\_inc\_footstat\_oe09

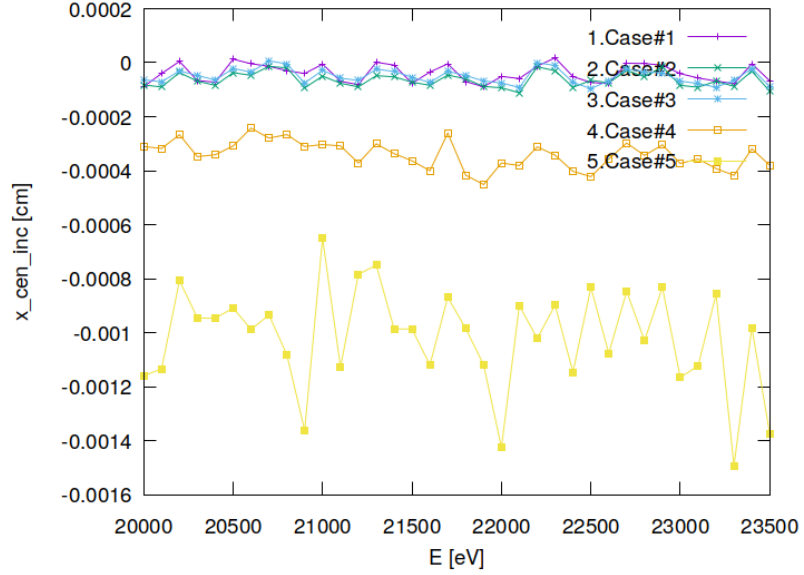


Figure 52.4: Sagittal coordinate of footprint's centre of 'gravity' on surface of optical element #09 (sample).

"fig/Defocus\_C111\_Bragg/plot005.png" Lbl.:Defocus\_C111\_Bragg\_2d\_plot\_y\_cen\_inc\_footstat\_oe09

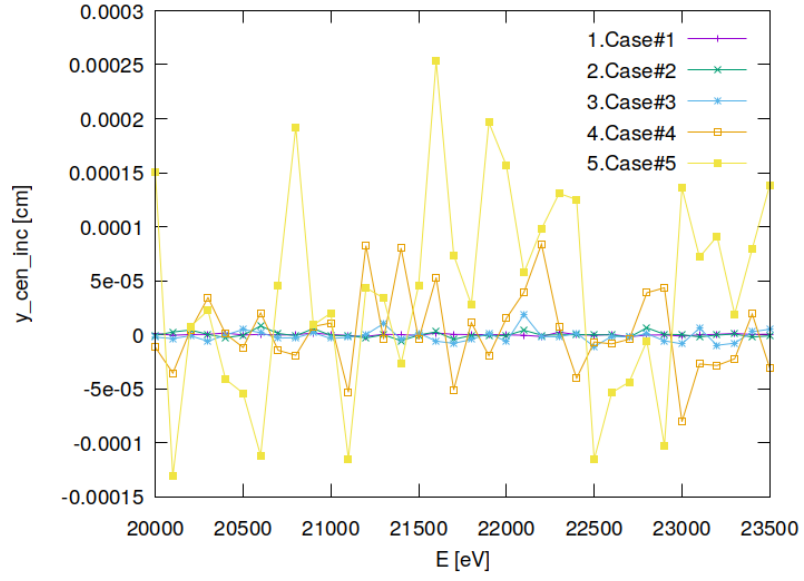


Figure 52.5: Meridional coordinate of footprint's centre of 'gravity' on surface of optical element #09 (sample).

## 52.2 Statistics of photon irradiance in beam cross section

"fig/Defocus\_C111\_Bragg/plot006.png" Lbl.:Defocus\_C111\_Bragg\_2d\_plot\_dx\_fwhm\_focstatavg\_oe09

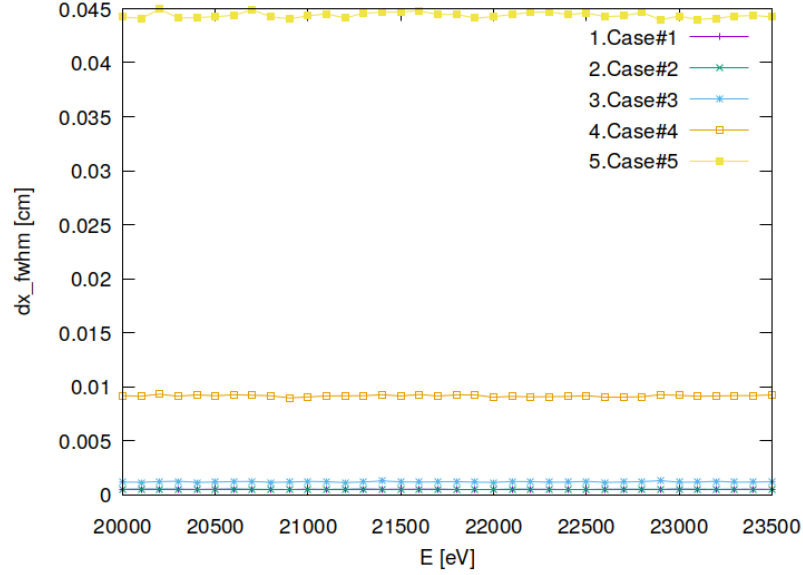


Figure 52.6: Sagittal beam diameter (FWHM) of optical element #09 (sample).

"fig/Defocus\_C111\_Bragg/plot007.png" Lbl.:Defocus\_C111\_Bragg\_2d\_plot\_dz\_fwhm\_focstatavg\_oe09

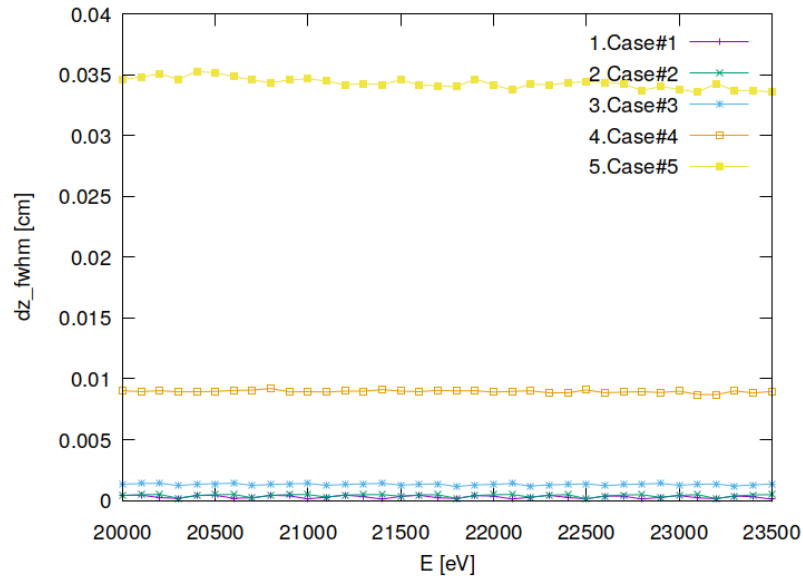


Figure 52.7: Meridional beam diameter (FWHM) of optical element #09 (sample).

"fig/Defocus\_C111\_Bragg/plot008.png" Lbl.:Defocus\_C111\_Bragg\_2d\_plot\_I\_int\_focstatavg\_oe09

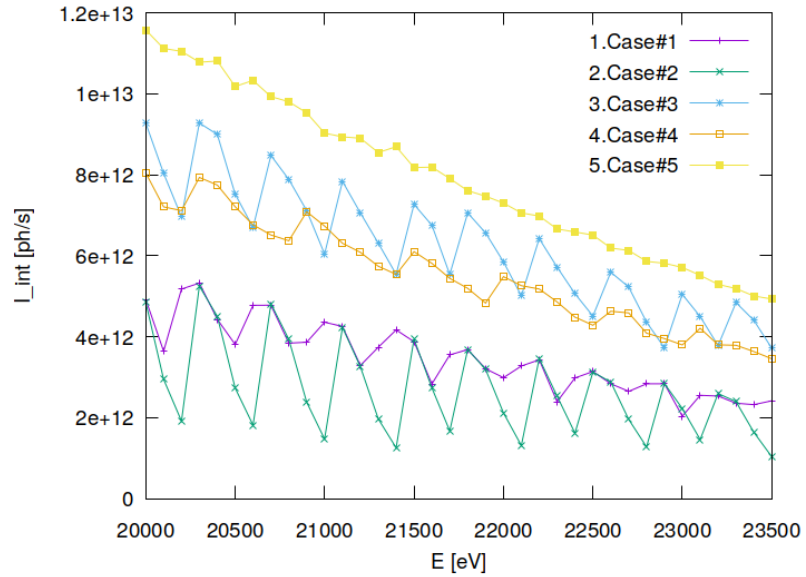


Figure 52.8: Photon flux in beam cross section of optical element #09 (sample).

"fig/Defocus\_C111\_Bragg/plot009.png" Lbl.:Defocus\_C111\_Bragg\_2d\_plot\_x\_cen\_focstatavg\_oe09

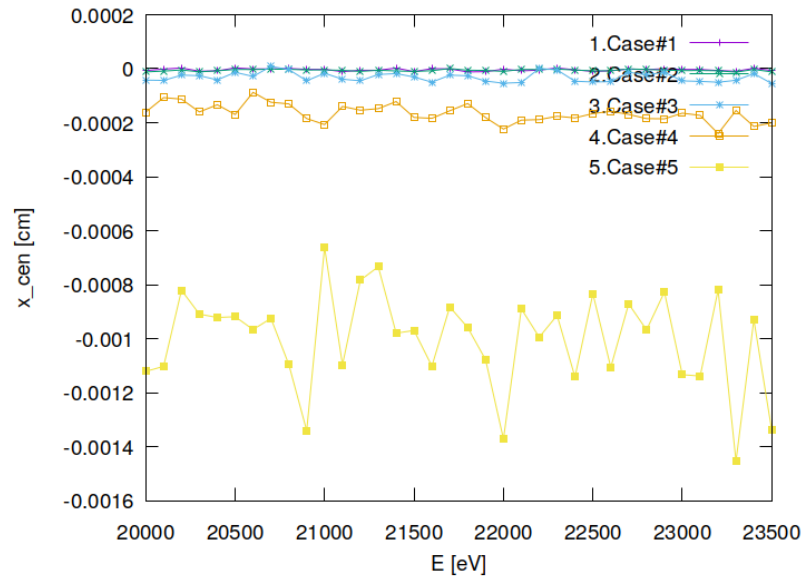


Figure 52.9: Sagittal coordinate of beam's centre of 'gravity' in beam cross section of optical element #09 (sample).

"fig/Defocus\_C111\_Bragg/plot010.png" Lbl.:Defocus\_C111\_Bragg\_2d\_plot\_z\_cen\_focstatavg\_oe09

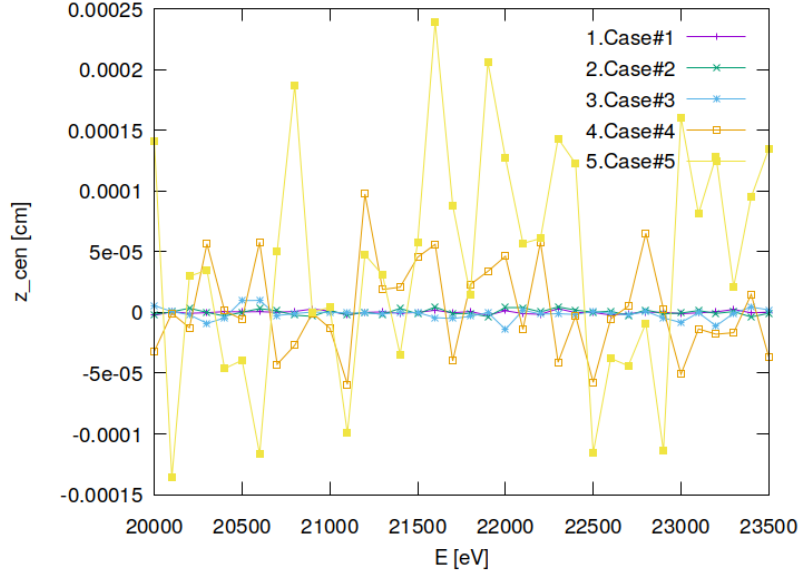


Figure 52.10: Meridional coordinate of beam's centre of 'gravity' in beam cross section of optical element #09 (sample).

"fig/Defocus\_C111\_Bragg/plot011.png" Lbl.:Defocus\_C111\_Bragg\_2d\_plot\_dxp\_fwhm\_focstatavg\_oe09

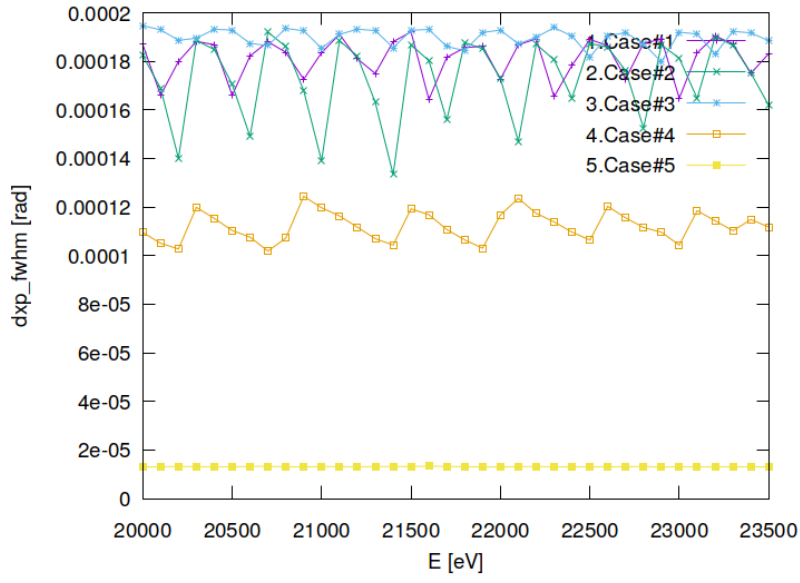


Figure 52.11: Sagittal beam divergence (FWHM) of optical element #09 (sample).

"fig/Defocus\_C111\_Bragg/plot012.png" Lbl.:Defocus\_C111\_Bragg\_2d\_plot\_dzp\_fwhm\_focstatavg\_oe09

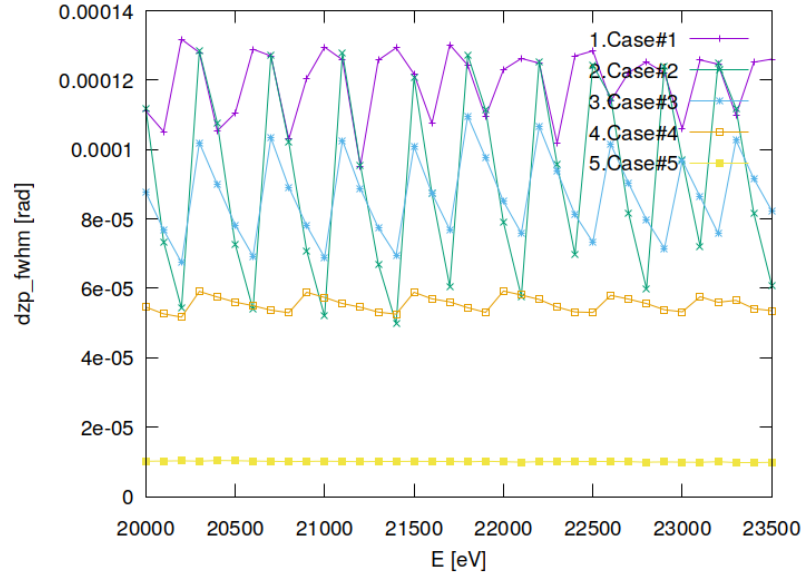


Figure 52.12: Meridional beam divergence (FWHM) of optical element #09 (sample).

"fig/Defocus\_C111\_Bragg/plot013.png" Lbl.:Defocus\_C111\_Bragg\_2d\_plot\_I\_int\_focstatavg\_oe09

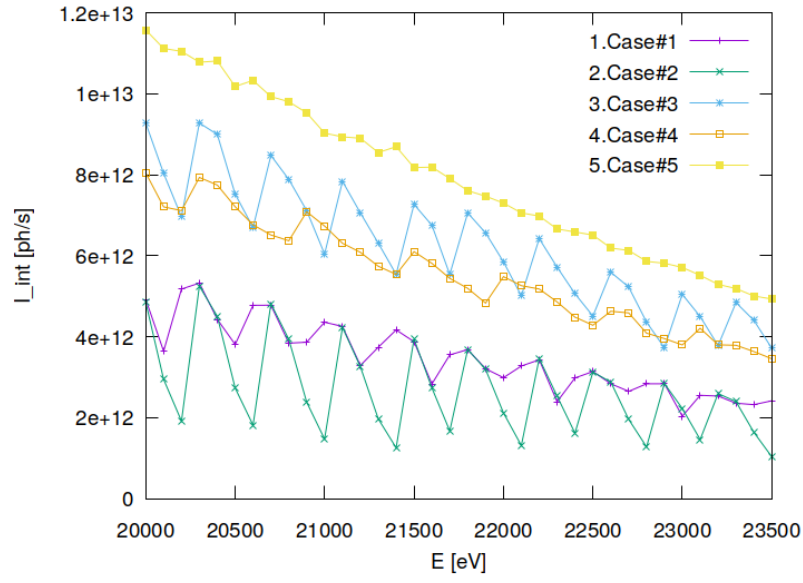


Figure 52.13: Photon flux in beam cross section of optical element #09 (sample).

```
"fig/Defocus_C111_Bragg/plot014.png" Lbl.:Defocus_C111_Bragg_2d_plot_xp_cen_focstatavg_oe09
```

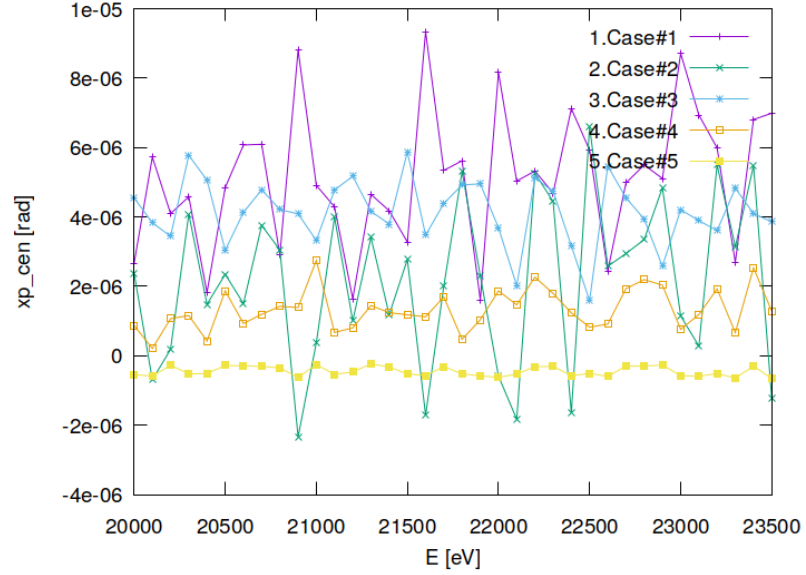


Figure 52.14: Sagittal coordinate of beam's centre of 'gravity' in angle space of optical element #09 (sample).

```
"fig/Defocus_C111_Bragg/plot015.png" Lbl.:Defocus_C111_Bragg_2d_plot_zp_cen_focstatavg_oe09
```

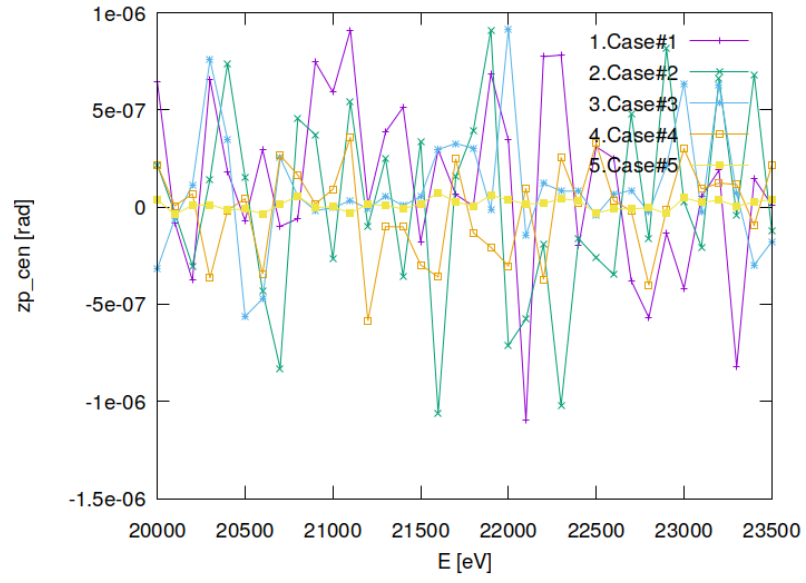


Figure 52.15: Meridional coordinate of beam's centre of 'gravity' in angle space of optical element #09 (sample).

```
"fig/Defocus_C111_Bragg/plot016.png" Lbl.:Defocus_C111_Bragg_2d_plot_dE_fwhm_focstatavg_oe09
```

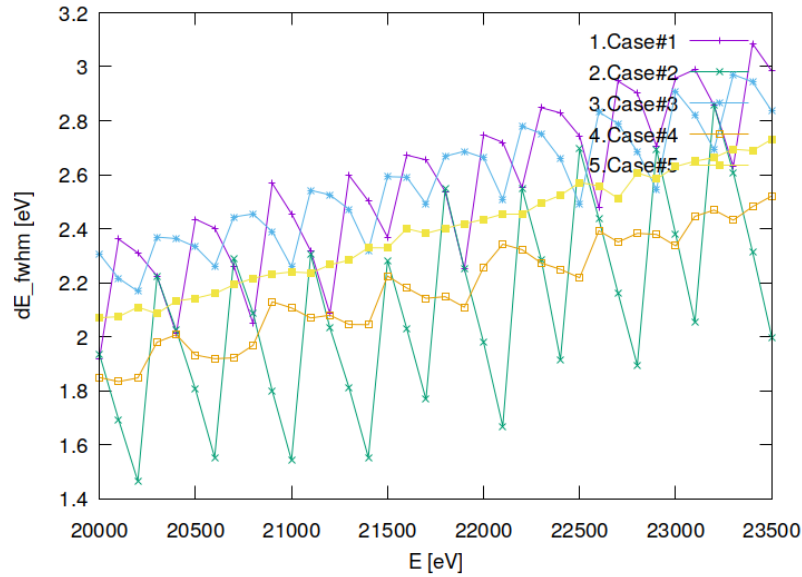


Figure 52.16: Bandwidth (FWHM) in beam cross section of optical element #09 (sample).

### 52.3 Incident photon irradiance on surface

```
"fig/Defocus_C111_Bragg/plot017.png" Lbl.:Defocus_C111_Bragg_false_colour_plot_I_inc_foot_oe09_c1_21800eV
```

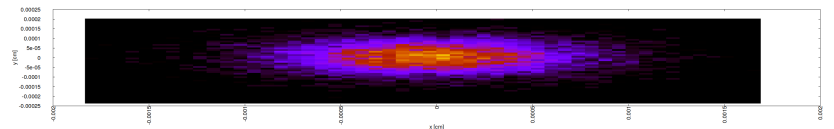


Figure 52.17: Incident photon irradiance on surface of optical element #09 (sample) for case #1 for 21800 eV photon energy setting.

```
"fig/Defocus_C111_Bragg/plot018.png" Lbl.:Defocus_C111_Bragg_false_colour_plot_I_inc_foot_oe09_c2_21800eV
```

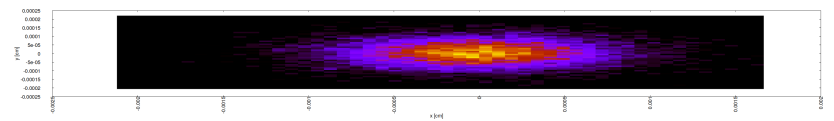


Figure 52.18: Incident photon irradiance on surface of optical element #09 (sample) for case #2 for 21800 eV photon energy setting.

"fig/Defocus\_C111\_Bragg/plot019.png" Lbl.:Defocus\_C111\_Bragg\_false\_colour\_plot\_I\_inc\_foot\_oe09\_c3\_21800eV

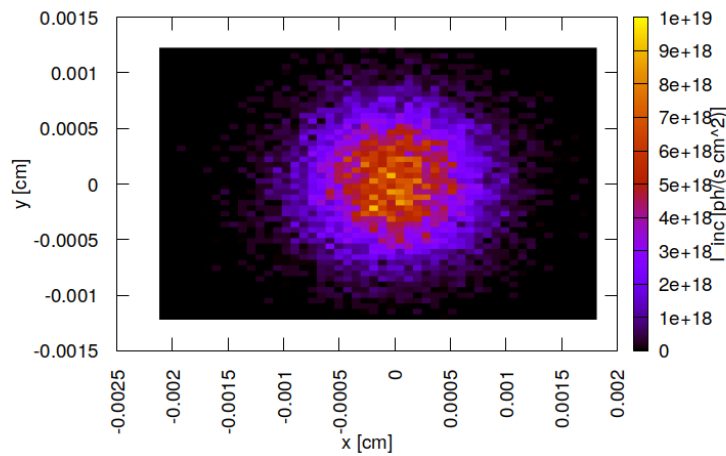


Figure 52.19: Incident photon irradiance on surface of optical element #09 (sample) for case #3 for 21800 eV photon energy setting.

"fig/Defocus\_C111\_Bragg/plot020.png" Lbl.:Defocus\_C111\_Bragg\_false\_colour\_plot\_I\_inc\_foot\_oe09\_c4\_21800eV

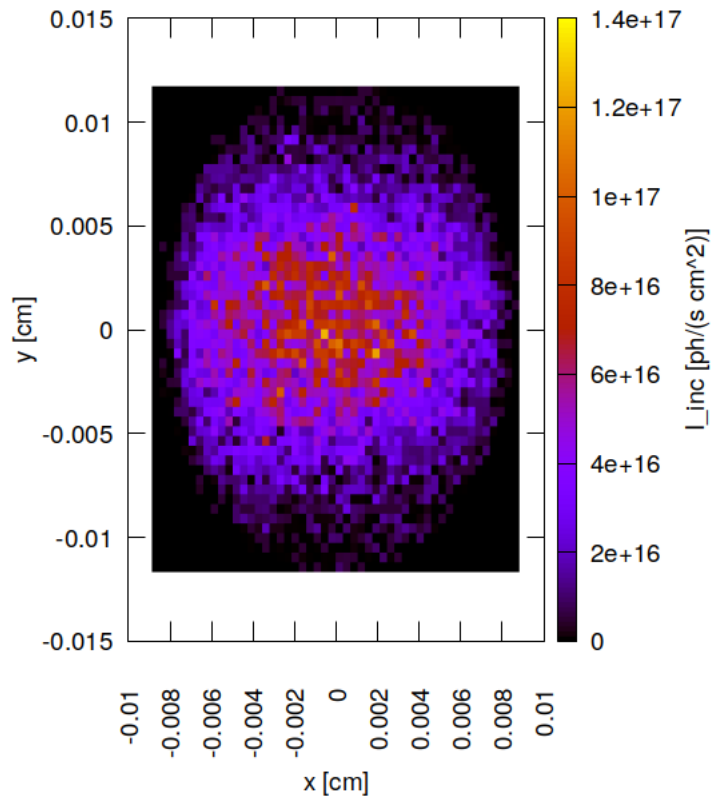


Figure 52.20: Incident photon irradiance on surface of optical element #09 (sample) for case #4 for 21800 eV photon energy setting.

```
"fig/Defocus_C111_Bragg/plot021.png" Lbl.:Defocus_C111_Bragg_false_colour_plot_I_inc_foot_oe09_c5_21800eV
```

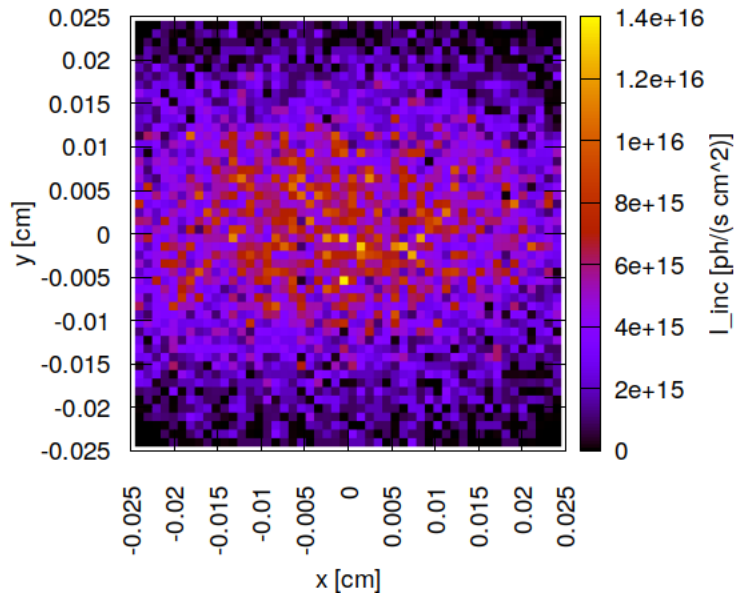


Figure 52.21: Incident photon irradiance on surface of optical element #09 (sample) for case #5 for 21800 eV photon energy setting.

## 52.4 Photon irradiance in beam cross section

"fig/Defocus\_C111\_Bragg/plot022.png" Lbl.:Defocus\_C111\_Bragg\_false\_colour\_plot\_I\_foc\_oe09\_c1\_21800eV

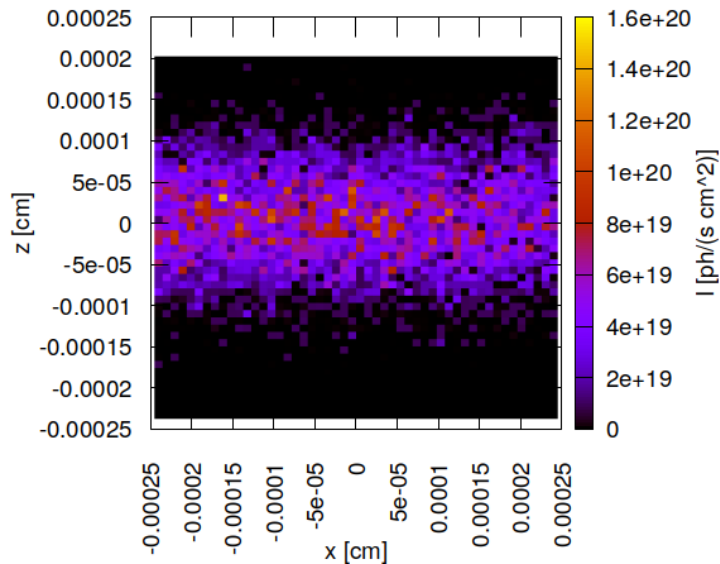


Figure 52.22: Photon irradiance in beam cross section of optical element #09 (sample) for case #1 for 21800 eV photon energy setting.

"fig/Defocus\_C111\_Bragg/plot023.png" Lbl.:Defocus\_C111\_Bragg\_false\_colour\_plot\_I\_foc\_oe09\_c2\_21800eV

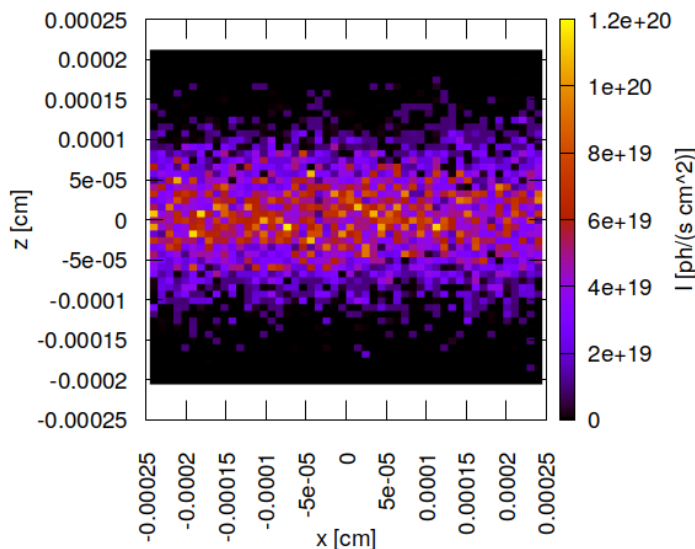


Figure 52.23: Photon irradiance in beam cross section of optical element #09 (sample) for case #2 for 21800 eV photon energy setting.

```
"fig/Defocus_C111_Bragg/plot024.png" Lbl.:Defocus_C111_Bragg_false_colour_plot_I_foc_oe09_c3_21800eV
```

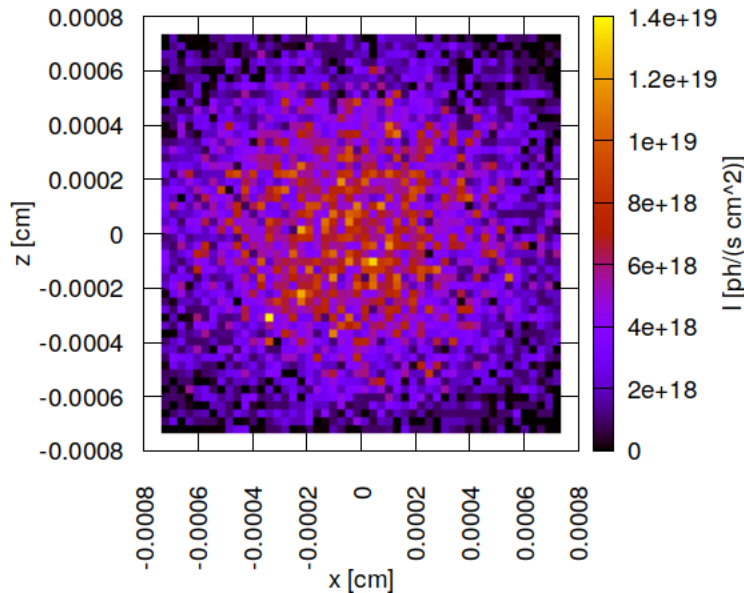


Figure 52.24: Photon irradiance in beam cross section of optical element #09 (sample) for case #3 for 21800 eV photon energy setting.

```
"fig/Defocus_C111_Bragg/plot025.png" Lbl.:Defocus_C111_Bragg_false_colour_plot_I_foc_oe09_c4_21800eV
```

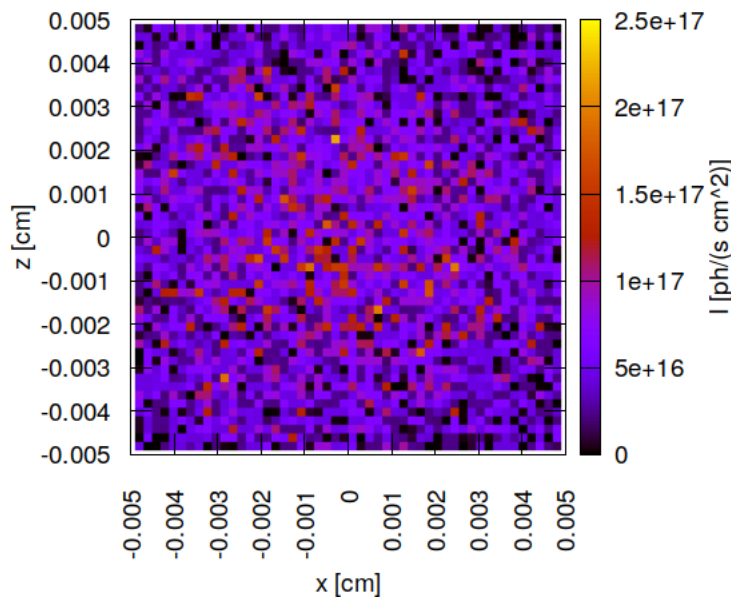


Figure 52.25: Photon irradiance in beam cross section of optical element #09 (sample) for case #4 for 21800 eV photon energy setting.

"fig/Defocus\_C111\_Bragg/plot026.png" Lbl.:Defocus\_C111\_Bragg\_false\_colour\_plot\_I\_foc\_oe09\_c5\_21800eV

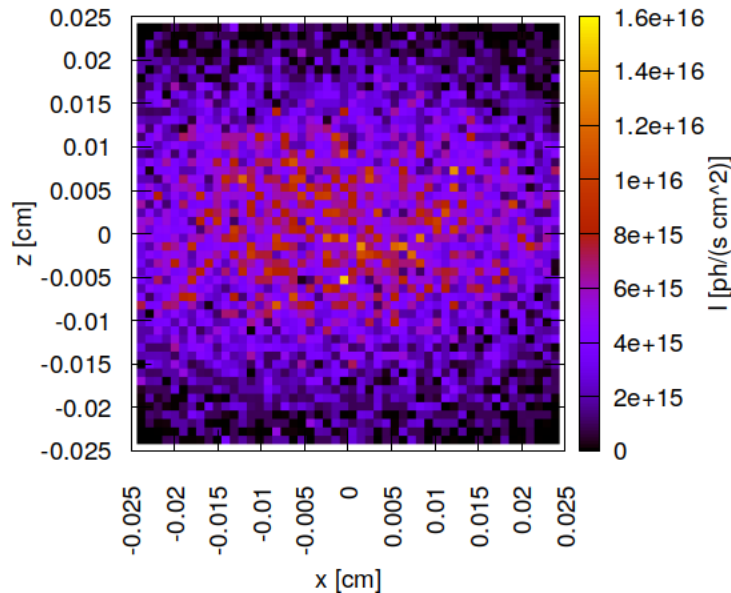


Figure 52.26: Photon irradiance in beam cross section of optical element #09 (sample) for case #5 for 21800 eV photon energy setting.

## 52.5 Spectral photon flux in beam cross section

"fig/Defocus\_C111\_Bragg/plot027.png" Lbl.:Defocus\_C111\_Bragg\_2d\_plot\_I\_bandfoc\_oe09\_c1\_21800eV

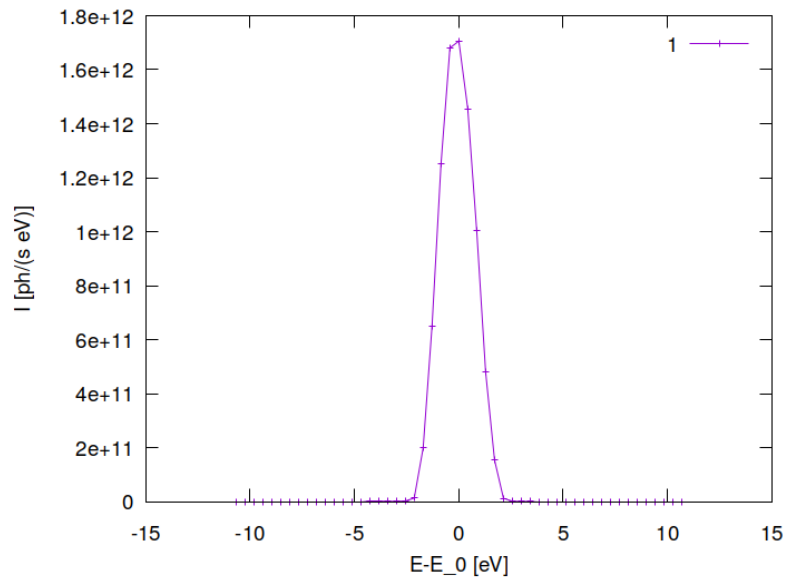


Figure 52.27: Spectral photon flux in beam cross section of optical element #09 (sample) for case #1 for 21800 eV photon energy setting.

"fig/Defocus\_C111\_Bragg/plot028.png" Lbl.:Defocus\_C111\_Bragg\_2d\_plot\_I\_bandfoc\_oe09\_c2\_21800eV

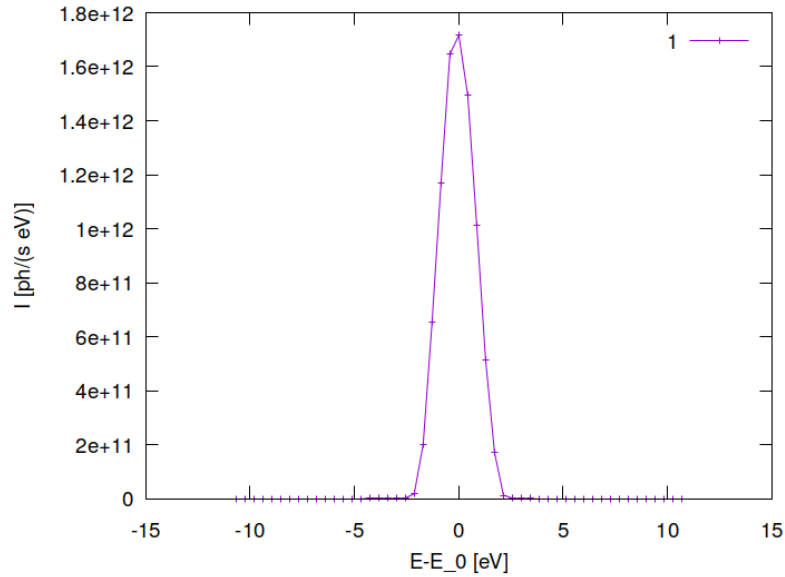


Figure 52.28: Spectral photon flux in beam cross section of optical element #09 (sample) for case #2 for 21800 eV photon energy setting.

"fig/Defocus\_C111\_Bragg/plot029.png" Lbl.:Defocus\_C111\_Bragg\_2d\_plot\_I\_bandfoc\_oe09\_c3\_21800eV

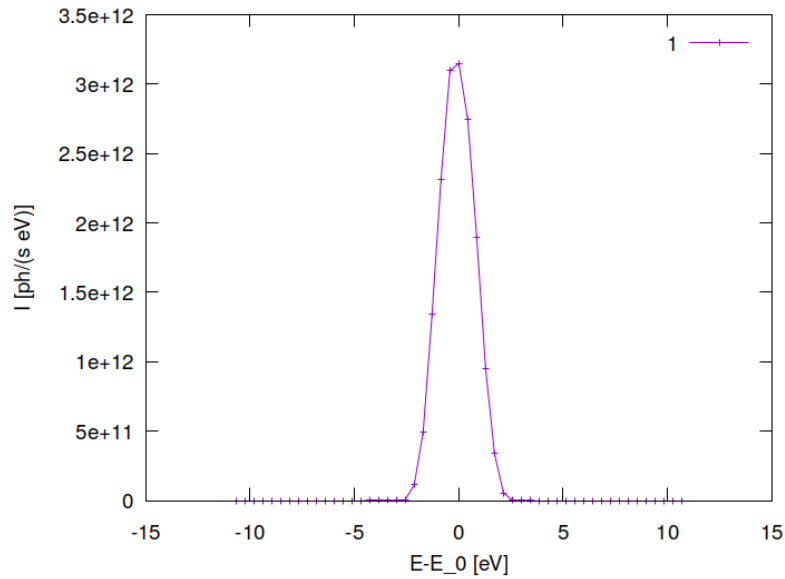


Figure 52.29: Spectral photon flux in beam cross section of optical element #09 (sample) for case #3 for 21800 eV photon energy setting.

"fig/Defocus\_C111\_Bragg/plot030.png" Lbl.:Defocus\_C111\_Bragg\_2d\_plot\_I\_bandfoc\_oe09\_c4\_21800eV

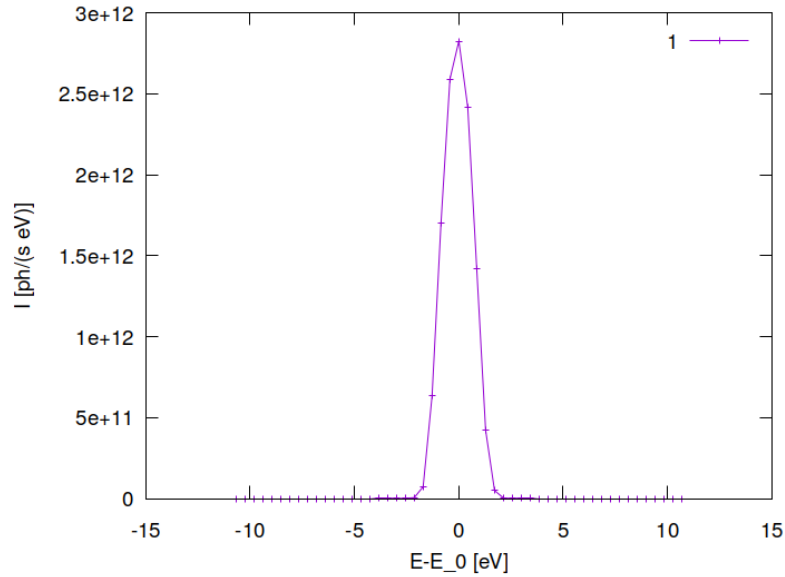


Figure 52.30: Spectral photon flux in beam cross section of optical element #09 (sample) for case #4 for 21800 eV photon energy setting.

"fig/Defocus\_C111\_Bragg/plot031.png" Lbl.:Defocus\_C111\_Bragg\_2d\_plot\_I\_bandfoc\_oe09\_c5\_21800eV

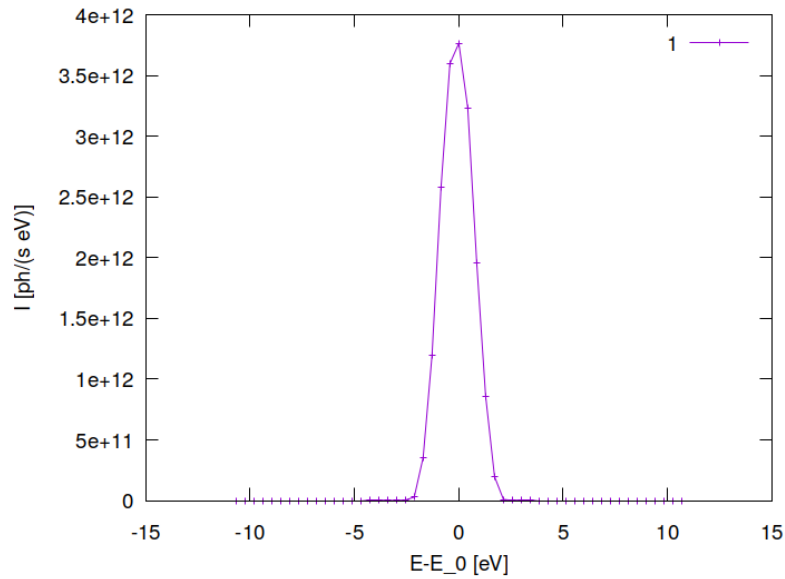


Figure 52.31: Spectral photon flux in beam cross section of optical element #09 (sample) for case #5 for 21800 eV photon energy setting.

# Chapter 53

## Discussion of results

### 53.1 Horizontal beam size

Due to the larger aberrations of the beam splitter in Laue geometry, the horizontal<sup>1</sup> focal spot size of about 50 microns exceeds that for the beam splitter in Bragg geometry by more than a factor of three. Therefore, in Laue geometry but also in Bragg geometry a horizontal aperture is required to get down to five microns implying a considerable loss of flux.

### 53.2 Vertical beam size

In the vertical, due to smaller source size and fewer aberrations, beam diameter at the sample position is much smaller, around two to five microns at best focus, both for the beam splitter in Laue and in Bragg geometry. Hence, no apertures are required to limit the illuminated spot size. Defocussing alone is sufficient.

### 53.3 Flux

For the beam splitter in Laue geometry the flux loss caused by the aperture required to limit the horizontal beam size is more severe due to the larger incident beam size. This lowers the flux even more, that is already down by a factor of two before the aperture compared to the beam splitter in Bragg geometry. The total flux at the sample position for an illuminated spot of five microns is thus by a factor of six lower for a Laue beam splitter, i.e.  $7 \times 10^{11}$  as compared to  $4 \times 10^{12}$  photons per second for a Bragg one.

This is a strong argument for a beam splitter in Bragg geometry. It remains to be shown in a later part of the report that a Bragg beam splitter is not deteriorating the transmitted main beam to DanMAX more than a Laue one. Due to the shallower angle of incidence in this geometry, the main beam is more sensitive to deformations and it's pathlength through the beam splitter is longer.

---

<sup>1</sup>sagittal in both Laue and Bragg geometry. In Bragg geometry the sample was rotated by -90°, in order to be consistent with Laue geometry

**Part V**

**High harmonic  
contamination**

## Chapter 54

# Higher harmonic test setup with diamond 111 beam splitter in Laue geometry

A thin CVD diamond crystal is employed as a diffractive beam splitter, using the 111 reflection in Laue geometry. The diamond 111 reflection diverts radiation within a narrow bandwidth of

$$\delta E/E = \delta\theta/\tan\theta$$

to the SinCrys side station. The thickness of the diamond crystal slab has been optimised in order to maximise 111 reflectivity under the constraint of keeping absorption of the transmitted main beam low.

Subsequent reflection from a second crystal of the same material using the same set of diffracting planes which are parallel to the first is required to provide the necessary stability of the exit beam which has to hit the very small acceptance aperture of the CRLs (see chapter 23.3).

Putting the second crystal at a distance of around 3.66 metres behind the first provides the required offset of more than one metre between the twice deflected beam and the main beam.

Compound refractive lenses (CRL) are used to focus the monochromatised beam onto the sample. A stack of two-dimensionally focussing lenses has to be complemented by a stack of vertically focussing one-dimensional lenses in order to compensate for the astigmatism generated by the asymmetry and the Laue geometry of the beam splitter and its deformation under the heat load from absorption. Furthermore, the beam splitter is bent meridionally to a concave cylindrical shape with radius  $R = 41.77$  m to partially compensate for aberrations introduced by the beam splitter.

The aim of this particular setup is to test on how much flux from higher undulator harmonics is slipping through the beam splitter, via the diamond 333 diffraction order, and the CRLs further downstream. The focussing scheme with fewest lenses was chosen which also has the largest beam cross section at the sample position, namely  $100 \times 100$  micrometres, as these are both conditions that are favouring higher harmonic slip through.

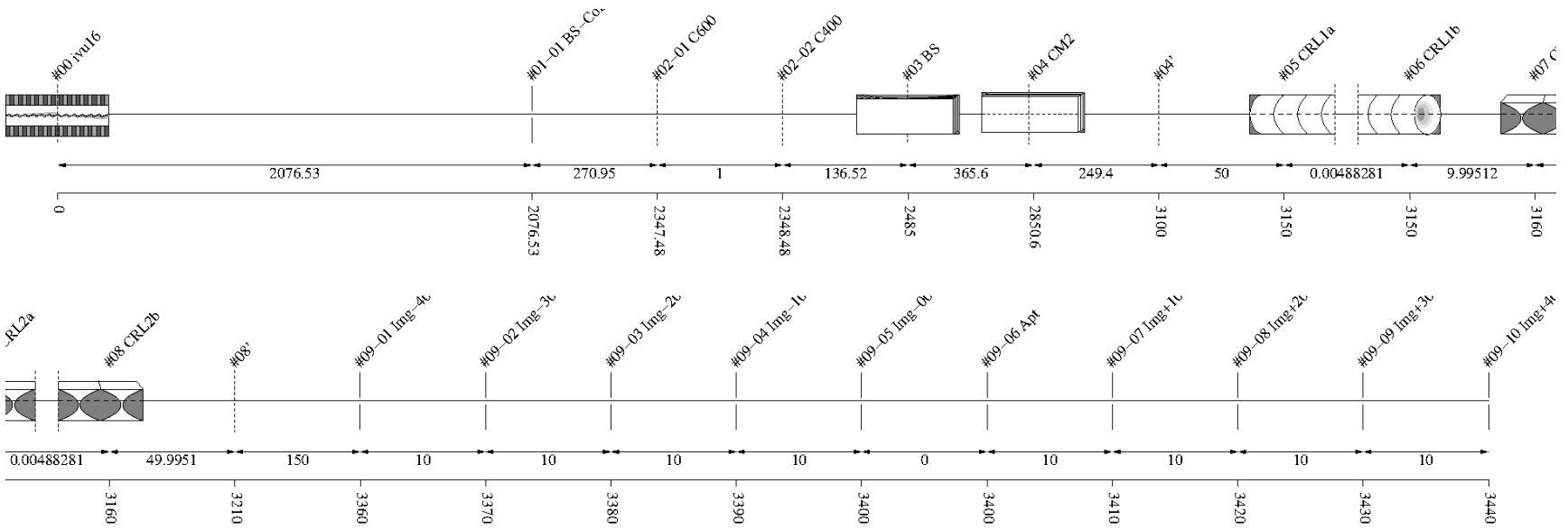


Figure 54.1: Schematic of optical setup

#	Name	Pathlen. cm	Descript.	Shape	Pitch* deg	Roll deg	Yaw deg	x_min cm	x_max cm	y_min cm	y_max cm	Thick. cm	Surface
<b>0</b>	ivu16	0	undulator	auto	0	0	0	-0.0027	0.0027	-0.0002	0.0002	auto	
<b>1</b>		2076.53	none	plane	0	0	0	-inf	inf	-inf	inf		perfect
<b>1-1</b>	BS-Collim	2076.53	aperture	rectangle	0	0	0	-0.035	0.035	-0.035	0.035		
<b>2</b>	Filter	2347.48	none	plane	0	0	0	-inf	inf	-inf	inf		perfect
<b>2-1</b>	C600	2347.48	C-filter	rectangle	0	0	0	-inf	inf	-inf	inf	0.06	
<b>2-2</b>	C400	2348.48	C-filter	rectangle	0	0	0	-inf	inf	-inf	inf	0.04	

<b>3</b>	BS	2485	C(1,1,1)-crystal	cylinder	133.197	90	0	-0.15	0.15	-0.15	0.15			heat bump
<b>4</b>	CM2	2850.6	C(1,1,1)-crystal	plane	7.93694+0	180+0	0+0	-inf	inf	-inf	inf			perfect
<b>4'</b>		3100	continuation plane		0	0	0							
<b>5</b>	CRL1a	3150	vac/Be-lens surface	parabola	0	0	0	-0.03	0.03	-0.03	0.03			perfect
<b>6</b>	CRL1b	3150	Be/vac-lens surface	parabola	0	0	0	-0.03	0.03	-0.03	0.03			perfect
<b>7</b>	CRL2a	3160	vac/Be-lens surface	extruded parabola	0	-90	0	-0.1	0.1	-0.03	0.03			perfect
<b>8</b>	CRL2b	3160	Be/vac-lens surface	extruded parabola	0	0	0	-0.1	0.1	-0.03	0.03			perfect
<b>8'</b>		3210	continuation plane		0	0	0							
<b>9</b>	sample	3400	none	plane	0	0	0	-inf	inf	-inf	inf			perfect
<b>9-1</b>	Img-40	3360	aperture	rectangle	0	0	0	-0.025	0.025	-0.025	0.025			
<b>9-2</b>	Img-30	3370	aperture	rectangle	0	0	0	-0.025	0.025	-0.025	0.025			
<b>9-3</b>	Img-20	3380	aperture	rectangle	0	0	0	-0.025	0.025	-0.025	0.025			
<b>9-4</b>	Img-10	3390	aperture	rectangle	0	0	0	-0.025	0.025	-0.025	0.025			
<b>9-5</b>	Img-00	3400	aperture	rectangle	0	0	0	-0.025	0.025	-0.025	0.025			
<b>9-6</b>	Apt	3400	aperture	rectangle	0	0	0	-0.025	0.025	-0.025	0.025			
<b>9-7</b>	Img+10	3410	aperture	rectangle	0	0	0	-0.025	0.025	-0.025	0.025			
<b>9-8</b>	Img+20	3420	aperture	rectangle	0	0	0	-0.025	0.025	-0.025	0.025			
<b>9-9</b>	Img+30	3430	aperture	rectangle	0	0	0	-0.025	0.025	-0.025	0.025			
<b>9-10</b>	Img+40	3440	aperture	rectangle	0	0	0	-0.025	0.025	-0.025	0.025			

Table 54.1: Setup parameters common to all components. (\*Glancing angle for mirrors, multilayers and crystals. Angle to surface normal otherwise.)

**Rays:** Polar type = total

Polar phase = 0 deg

Polar degree = 0

Is coherent = no

**Spectrum:** E min = 500 eV

E max = 80000 eV

Relative linewidth = 1

**Band:** Bandwidth = 0.0005

**Insertion Device:** lambda period = 1.6 cm

n period = 187

I electron = 0.5 A

E electron = 3 GeV

y horizontal waist = 0 cm

y vertical waist = 0 cm

epsilon x = 3.2E-08 cm rad

epsilon z = 8E-10 cm rad

K y = 1.66

K ymax = 1.7

Divergence limit = 5E-05 rad

**Undulator:** n harmonic max = 99

Tuning type = fixed gap

l aperture = 2076.53 cm

dx aperture = 0.07 cm

dz aperture = 0.07 cm

#1

**Screen:** Is absorbing[1] = no

**Shape:** Thickness = 0 cm

#2 Filter

**Screen:** Is absorbing[1] = yes

Is absorbing[2] = yes

Molecular formula[1] = C

Molecular formula[2] = C

Mass density[1] = 3.5 g/cm^3

Mass density[2] = 3.5 g/cm^3

Thickness[1] = 0.06 cm

Thickness[2] = 0.04 cm

**Shape:** Thickness = 0 cm

### #3 BS

**Grating:** n order = -1

**Crystal:** Structure type = zincblende

Lattice constant[1] = 3.567 Angstrom  
Lattice constant[2] = 3.567 Angstrom  
Lattice constant[3] = 3.567 Angstrom  
Debye Waller factor = 1  
Is absorbing = yes  
Is asymmetric = yes  
Angle asymmetry = 125.26 deg  
Is inclined = no  
Is Johansson geometry = no  
Is mosaic = no

**Geometry:** Is thin = yes

Tune automatic = no

**Shape:** Defined by = user

Is convex = no  
Is extruded = yes  
Radius = 4.177E+06 cm  
Thickness = 0.01 cm

**Boundary:** Type = rectangle

x rim = 0.5 cm  
y rim = 0.5 cm

**Extruded:** Angle z = 0 deg

**Surface:** Is rough = no

**FEA:** Design type = type specific

Crystal design = laue with cooling loop  
Is isotropic = no  
Angle x = 0 deg  
Angle y = 0 deg  
Angle z = 0 deg  
Mass density = 3.516 g/cm<sup>3</sup>

**Heat:** Heat transfer type[1] = insulated

Heat transfer type[2] = heat transfer  
Heat transfer type[3] = insulated  
Heat transfer type[4] = insulated  
Heat transfer type[5] = heat transfer  
Heat transfer type[6] = flux  
Heat transfer type[7] = insulated

Heat transfer type[8] = heat transfer  
 Heat transfer type[9] = heat sink  
 Heat transfer coefficient = 1 W/(cm^2K)  
 Heat sink coefficient = 10 W/(cm^2K)  
 T reference = 293.15 K  
 T cooling = 293.15 K  
 Heat capacity = 0.54 J/(gK)  
 Thermal conductivity[1] = 25 W/(cmK^n)

**Stress and strain:** Constraint[1] = free  
 Constraint[2] = kinematic  
 Constraint[3] = free  
 Constraint[4] = free  
 Constraint[5] = free  
 Constraint[6] = free  
 Constraint[7] = free  
 Constraint[8] = free  
 Constraint[9] = free  
 Thermal expansion tensor[1] = 1.1E-06 1/K  
 Thermal expansion tensor[2] = 1.1E-06 1/K  
 Thermal expansion tensor[3] = 1.1E-06 1/K  
 Thermal expansion tensor[4] = 0 1/K  
 Thermal expansion tensor[5] = 0 1/K  
 Thermal expansion tensor[6] = 0 1/K  
 Stiffness tensor(1)(1) = 1.07861E+12 Pa  
 Stiffness tensor(2)[1] = 1.2663E+11 Pa  
 Stiffness tensor(2)[2] = 1.07861E+12 Pa  
 Stiffness tensor(3)[1] = 1.2663E+11 Pa  
 Stiffness tensor(3)[2] = 1.2663E+11 Pa  
 Stiffness tensor(3)[3] = 1.07861E+12 Pa  
 Stiffness tensor(4)[1] = 0 Pa  
 Stiffness tensor(4)[2] = 0 Pa  
 Stiffness tensor(4)[3] = 0 Pa  
 Stiffness tensor(4)[4] = 5.7756E+11 Pa  
 Stiffness tensor(5)[1] = 0 Pa  
 Stiffness tensor(5)[2] = 0 Pa  
 Stiffness tensor(5)[3] = 0 Pa  
 Stiffness tensor(5)[4] = 0 Pa  
 Stiffness tensor(5)[5] = 5.7756E+11 Pa  
 Stiffness tensor(6)[1] = 0 Pa  
 Stiffness tensor(6)[2] = 0 Pa  
 Stiffness tensor(6)[3] = 0 Pa  
 Stiffness tensor(6)[4] = 0 Pa  
 Stiffness tensor(6)[5] = 0 Pa  
 Stiffness tensor(6)[6] = 5.7756E+11 Pa

#### #4 CM2

**Crystal:** Structure type = zincblende  
 Lattice constant[1] = 3.567 Angstrom  
 Lattice constant[2] = 3.567 Angstrom  
 Lattice constant[3] = 3.567 Angstrom  
 Debye Waller factor = 1

Is absorbing = yes  
Is asymmetric = no  
Is inclined = no  
Is Johansson geometry = no  
Is mosaic = no

**Geometry:** Is thin = no  
Tune automatic = no

**Boundary:** Type = none

**Surface:** Is rough = no

### #5 CRL1a

**Dielectric:** Reflectivity type = polarisation  
Is constant = no  
Mass density = 1.85 g/cm<sup>3</sup>

**Geometry:** g = 3150 cm  
b = 250 cm  
Is thin = yes  
n clones = 5  
Focus automatically = no

**Shape:** Defined by = user  
Is convex = no  
Is extruded = no  
Radius = 0.01 cm  
Thickness = 0.005 cm

**Boundary:** Type = ellipse

**Parabola:** Is source in infinity = no  
p semi = 0.01 cm

**Surface:** Is rough = no

### #6 CRL1b

**Dielectric:** Reflectivity type = polarisation  
Is constant = yes  
delta refraction = 0  
beta absorption = 0

**Geometry:** g = 3150 cm  
b = 250 cm  
Is thin = yes  
n clones = 5  
Focus automatically = no

**Shape:** Defined by = user  
Is convex = yes  
Is extruded = no  
Radius = 0.01 cm  
Thickness = 0.005 cm

**Boundary:** Type = ellipse

**Parabola:** Is source in infinity = no  
p semi = 0.01 cm

**Surface:** Is rough = no

## #7 CRL2a

**Dielectric:** Reflectivity type = polarisation  
Is constant = no  
Mass density = 1.85 g/cm<sup>3</sup>

**Geometry:** g = -255 cm  
b = 240 cm  
Is thin = yes  
n clones = 6  
Focus automatically = no

**Shape:** Defined by = user  
Is convex = no  
Is extruded = yes  
Radius = 0.02 cm  
Thickness = 0.005 cm

**Boundary:** Type = rectangle

**Parabola:** Is source in infinity = no  
p semi = 0.02 cm

**Extruded:** Angle z = 0 deg

**Surface:** Is rough = no

## #8 CRL2b

**Dielectric:** Reflectivity type = polarisation

Is constant = yes  
delta refraction = 0  
beta absorption = 0

**Geometry:** g = -255 cm

b = 240 cm  
Is thin = yes  
n clones = 6  
Focus automatically = no

**Shape:** Defined by = user

Is convex = yes  
Is extruded = yes  
Radius = 0.02 cm  
Thickness = 0.005 cm

**Boundary:** Type = rectangle

**Parabola:** Is source in infinity = no

p semi = 0.02 cm

**Extruded:** Angle z = 0 deg

**Surface:** Is rough = no

## #9 sample

**Screen:** Is absorbing[1] = no

Is absorbing[2] = no  
Is absorbing[3] = no  
Is absorbing[4] = no  
Is absorbing[5] = no  
Is absorbing[6] = no  
Is absorbing[7] = no  
Is absorbing[8] = no  
Is absorbing[9] = no  
Is absorbing[10] = no

**Shape:** Thickness = 0 cm

# Chapter 55

## Parameter scan cases

There are three cases in total. Case #1 is simply a repetition of the focusing scheme test in case #4 from section 36, i.e. using the 9th undulator harmonic the setup is designed for. It's purpose is to make comparison with the following cases easier using the same optical setups but with the diamond 333 reflection and the 27th harmonic instead, thus providing the higher harmonic contamination. Finally, case #3 is a small modification of case #2 where the second crystal's pitch has been tweaked. Without tweaking the reflectivity of the second crystal was unexpectedly low. That reflectivity could be restored by small pitch adjustments provides an explanation that will be discussed later.

Case	Bandwidth	Miller_indices(1)_03	dangle_x_04 deg	Miller_indices(1)_04	E_max eV	E_min eV	E_step eV	Has_slope_error
1	0.0005	1	0	1	23500.0	20000.0	100	no
2	0.0005	3	0	3	70500.0	60000.0	300	no
3	0.0005	3	0.000525	3	70500.0	60000.0	300	no

Table 55.1: Parameter values for different cases in parameter scan

### Legend

**Case:** Case number in parameter scan

**Bandwidth:** Band.Bandwidth (Bandwidth that should be covered by ray tracing.

It should be large enough to fill out the throughput of your monochromator. For a Si111 double crystal monochromator this could be 0.0002. For a multilayer or a grating monochromator it should be something considerably larger. In the ray-tracing, twice the width is actually used. Hence, using the Darwin width covers probably most of the photons. Nowadays, I do not like this doubling, as it is in-transparent, but keep it for the sake of continuity.)

**Miller\_indices(1)\_03:** Optical\_element\_#3.Type.Crystal.Miller\_indices(1) (Miller indices of crystal reflection.)

**dangle\_x\_04:** Optical\_element\_#4.Move.Source.dangle\_x (Source rotation angle around x-axis (ccw).)

**Miller\_indices(1)\_04:** Optical\_element\_#4.Type.Crystal.Miller\_indices(1) (Miller indices of crystal reflection.)

**E\_max:** Scan.E\_max (Highest photon energy in scan.)

**E\_min:** Scan.E\_min (Smallest photon energy in scan.)

**E\_step:** Scan.E\_step (Energy scan step.)

**Has\_slope\_error\_03:** Optical\_element\_#3.Surface.Has\_slope\_error (Has surface slope error?)

**b\_05:** Optical\_element\_#5.Geometry.b (Distance from optical element's pole to meridional image focus.)

**b\_06:** Optical\_element\_#6.Geometry.b (Distance from optical element's pole to meridional image focus.)

**g\_07:** Optical\_element\_#7.Geometry.g (Distance btw. meridional object focus and optical element's pole.)

**g\_08:** Optical\_element\_#8.Geometry.g (Distance btw. meridional object focus and optical element's pole.)

# Chapter 56

## Photon energy scan

The  $K_y$ -values in the table below are those for optimized flux in the 7th harmonic between 15.6 and 18.3 keV used by the DanMAX main branch. The number of 2D and 1D focusing lens elements needed for the required beam properties in the SinCrys side branch for the 9th harmonic are provided, too.

E eV	K_y	n_harm/step	theta_i03 deg	theta_r03 deg	theta_i04 deg	nMult_05	nMult_07
<b>20000</b>	1.67551	9	-43.9164	206.603	81.3428	18	0
<b>20100</b>	1.66836	9	-43.873	206.647	81.3862	18	0
<b>20200</b>	1.66125	9	-43.8301	206.69	81.4291	18	0
<b>20300</b>	1.65418	9	-43.7875	206.732	81.4717	18	0
<b>20400</b>	1.64714	9	-43.7454	206.774	81.5138	18	0
<b>20500</b>	1.64015	9	-43.7037	206.816	81.5555	19	0
<b>20600</b>	1.63319	9	-43.6625	206.857	81.5968	19	0
<b>20700</b>	1.62628	9	-43.6216	206.898	81.6377	19	0
<b>20800</b>	1.6194	9	-43.5811	206.939	81.6782	19	0
<b>20900</b>	1.61255	9	-43.541	206.979	81.7182	19	0
<b>21000</b>	1.60575	9	-43.5013	207.019	81.758	19	0
<b>21100</b>	1.59898	9	-43.462	207.058	81.7973	20	0
<b>21200</b>	1.59224	9	-43.423	207.097	81.8363	20	0
<b>21300</b>	1.58554	9	-43.3844	207.135	81.8748	20	0
<b>21400</b>	1.57887	9	-43.3462	207.174	81.9131	20	0
<b>21500</b>	1.57224	9	-43.3083	207.212	81.9509	20	0
<b>21600</b>	1.56564	9	-43.2708	207.249	81.9884	21	0
<b>21700</b>	1.55908	9	-43.2337	207.286	82.0256	21	0
<b>21800</b>	1.55255	9	-43.1969	207.323	82.0624	21	0
<b>21900</b>	1.54605	9	-43.1604	207.359	82.0989	21	0
<b>22000</b>	1.53958	9	-43.1243	207.396	82.135	21	0
<b>22100</b>	1.53315	9	-43.0885	207.431	82.1708	22	0
<b>22200</b>	1.52674	9	-43.053	207.467	82.2063	22	0
<b>22300</b>	1.52037	9	-43.0178	207.502	82.2415	22	0
<b>22400</b>	1.51402	9	-42.983	207.537	82.2763	22	0
<b>22500</b>	1.50771	9	-42.9484	207.571	82.3109	22	0
<b>22600</b>	1.50143	9	-42.9142	207.606	82.3451	23	0
<b>22700</b>	1.49517	9	-42.8803	207.64	82.379	23	0
<b>22800</b>	1.48895	9	-42.8467	207.673	82.4127	23	0
<b>22900</b>	1.48275	9	-42.8133	207.707	82.446	23	0
<b>23000</b>	1.47658	9	-42.7803	207.74	82.479	23	0
<b>23100</b>	1.47044	9	-42.7476	207.772	82.5117	24	0
<b>23200</b>	1.46433	9	-42.7151	207.805	82.5442	24	0
<b>23300</b>	1.45824	9	-42.6829	207.837	82.5764	24	0
<b>23400</b>	1.45218	9	-42.651	207.869	82.6083	24	0
<b>23500</b>	1.44615	9	-42.6194	207.9	82.6399	24	0

Table 56.1: Scan values for the 9th harmonic energy scan

## Legend

**E:** photon energy

**K\_y:** deflection parameter for vertical field component of insertion device

**n\_harm/step:** number of undulator harmonic or number of energy slot for continuous source (e.g. wiggler)

**theta\_i03:** Optical\_element\_#3.Geometry.angle\_incident (Incidence angle w.r.t. surface normal defining optical axis.)

**theta\_r03:** Optical\_element\_#3.Geometry.angle\_reflect (Reflection angle w.r.t. surface normal.)

**theta\_i04:** Optical\_element\_#4.Geometry.angle\_incident (Incidence angle w.r.t. surface normal defining optical axis.)

**nMult\_05:** Optical\_element\_#5.Geometry.n\_clones (Clone optical element 'nMult' times.)

**nMult\_07:** Optical\_element\_#7.Geometry.n\_clones (Clone optical element 'nMult' times.)

# Chapter 57

## Plots

### 57.1 Flux at sample position with higher harmonic contamination

```
"fig/High_harm_C111_Laue/plot001.png" Lbl.:High_harm_C111_Laue_2d_plot_I_int_focstatavg_oe09
```

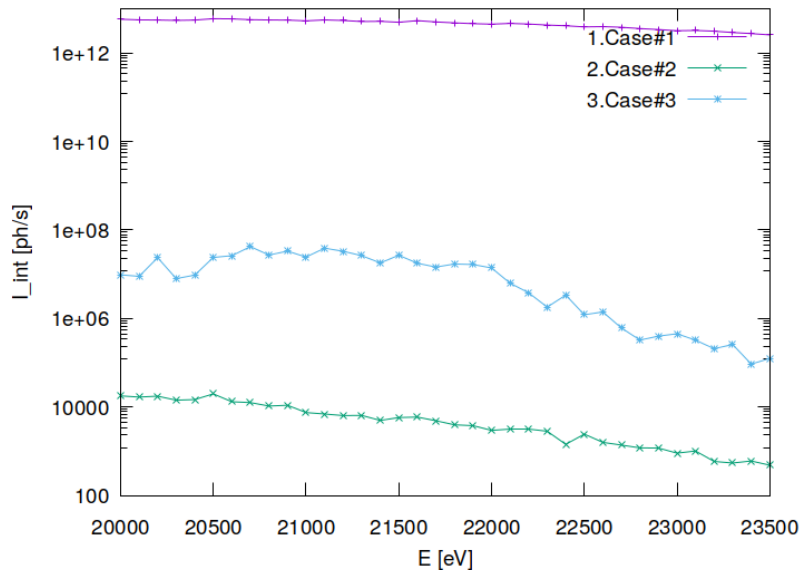


Figure 57.1: Photon flux in beam cross section of optical element #09 (sample). Case #1 represents the useful signal from the undulator's 9th harmonic. Case #2 is the higher harmonic contamination that would occur naturally, whilst case #3 is harmonic contamination artificially increased by tweaking the pitch of the second diamond 111 crystal. The latter merely serves as an explanation for the unexpectedly low high harmonic throughput in Laue geometry. More about this in the text. The photon energy in the abscissa of the higher harmonic curves has been divided by three to match that of the useful signal from the 9th undulator harmonic.

## Chapter 58

# Higher harmonic test setup with diamond 111 beam splitter in Bragg geometry

A thin CVD diamond crystal is employed as a diffractive beam splitter, using the 111 reflection in Bragg geometry. The diamond 111 reflection diverts radiation within a narrow bandwidth of

$$\delta E/E = \delta\theta/\tan\theta$$

to the SinCrys side station.

Subsequent reflection from a second crystal of the same material using the same set of diffracting planes which are parallel to the first is required to provide the necessary stability of the exit beam which has to hit the very small acceptance aperture of the CRLs (see chapter 23.3).

Putting the second crystal at a distance of around 3.66 metres behind the first provides the required offset of more than one metre between the twice deflected beam and the main beam.

Compound refractive lenses (CRL) are used to focus the monochromatised beam onto the sample. A stack of two-dimensionally focussing lenses has to be complemented by a stack of one-dimensional lenses in order to compensate for the astigmatism generated by the deformation of the beam splitter under the heat load from absorption.

The focussing scheme with fewest lenses was chosen which also has the largest beam cross section at the sample position, namely  $100 \times 100$  micrometres, as these are both conditions that are favouring higher harmonic slip through.

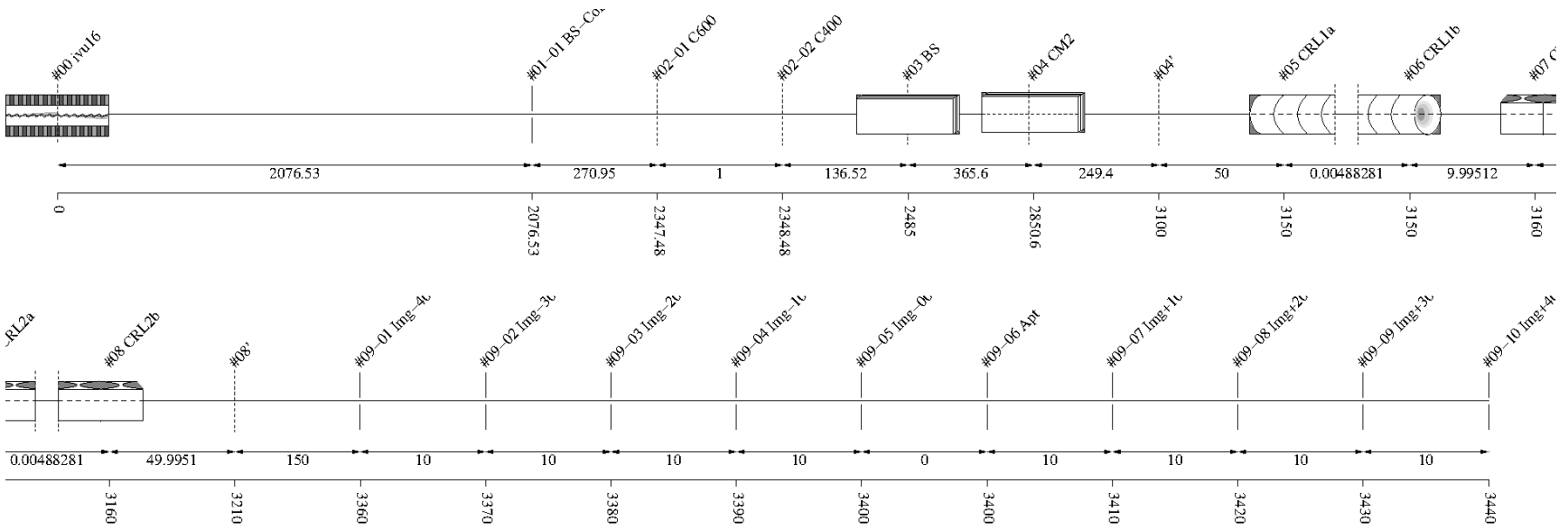


Figure 58.1: Schematic of optical setup

#	Name	Pathlen. cm	Descript.	Shape	Pitch* deg	Roll deg	Yaw deg	x_min cm	x_max cm	y_min cm	y_max cm	Thick. cm	Surface
<b>0</b>	ivu16	0	undulator	auto	0	0	0	-0.0027	0.0027	-0.0002	0.0002	auto	
<b>1</b>		2076.53	none	plane	0	0	0	-inf	inf	-inf	inf		perfect
<b>1-1</b>	BS-Collim	2076.53	aperture	rectangle	0	0	0	-0.035	0.035	-0.035	0.035		
<b>2</b>	Filter	2347.48	none	plane	0	0	0	-inf	inf	-inf	inf		perfect
<b>2-1</b>	C600	2347.48	C-filter	rectangle	0	0	0	-inf	inf	-inf	inf	0.06	
<b>2-2</b>	C400	2348.48	C-filter	rectangle	0	0	0	-inf	inf	-inf	inf	0.04	

<b>3</b>	BS	2485	C(1,1,1)-crystal	plane	7.93694	90	0	-0.15	0.15	-0.5	0.5		heat bump
<b>4</b>	CM2	2850.6	C(1,1,1)-crystal	plane	7.93694+0	180+0	0+0	-inf	inf	-inf	inf		perfect
<b>4'</b>		3100	continuation plane		0	0	0						
<b>5</b>	CRL1a	3150	vac/Be-lens surface	parabola	0	0	0	-0.03	0.03	-0.03	0.03		perfect
<b>6</b>	CRL1b	3150	Be/vac-lens surface	parabola	0	0	0	-0.03	0.03	-0.03	0.03		perfect
<b>7</b>	CRL2a	3160	vac/Be-lens surface	extruded parabola	0	0	0	-0.1	0.1	-0.03	0.03		perfect
<b>8</b>	CRL2b	3160	Be/vac-lens surface	extruded parabola	0	0	0	-0.1	0.1	-0.03	0.03		perfect
<b>8'</b>		3210	continuation plane		0	0	0						
<b>9</b>	sample	3400	none	plane	0	-90	0	-inf	inf	-inf	inf		perfect
<b>9-1</b>	Img-40	3360	aperture	rectangle	0	0	0	-0.025	0.025	-0.025	0.025		
<b>9-2</b>	Img-30	3370	aperture	rectangle	0	0	0	-0.025	0.025	-0.025	0.025		
<b>9-3</b>	Img-20	3380	aperture	rectangle	0	0	0	-0.025	0.025	-0.025	0.025		
<b>9-4</b>	Img-10	3390	aperture	rectangle	0	0	0	-0.025	0.025	-0.025	0.025		
<b>9-5</b>	Img-00	3400	aperture	rectangle	0	0	0	-0.025	0.025	-0.025	0.025		
<b>9-6</b>	Apt	3400	aperture	rectangle	0	0	0	-0.025	0.025	-0.025	0.025		
<b>9-7</b>	Img+10	3410	aperture	rectangle	0	0	0	-0.025	0.025	-0.025	0.025		
<b>9-8</b>	Img+20	3420	aperture	rectangle	0	0	0	-0.025	0.025	-0.025	0.025		
<b>9-9</b>	Img+30	3430	aperture	rectangle	0	0	0	-0.025	0.025	-0.025	0.025		
<b>9-10</b>	Img+40	3440	aperture	rectangle	0	0	0	-0.025	0.025	-0.025	0.025		

Table 58.1: Setup parameters common to all components. (\*Glancing angle for mirrors, multilayers and crystals. Angle to surface normal otherwise.)

**Rays:** Polar type = total

Polar phase = 0 deg

Polar degree = 0

Is coherent = no

**Spectrum:** E min = 500 eV

E max = 80000 eV

Relative linewidth = 1

**Band:** Bandwidth = 0.0005

**Insertion Device:** lambda period = 1.6 cm

n period = 187

I electron = 0.5 A

E electron = 3 GeV

y horizontal waist = 0 cm

y vertical waist = 0 cm

epsilon x = 3.2E-08 cm rad

epsilon z = 8E-10 cm rad

K y = 1.66

K ymax = 1.7

Divergence limit = 5E-05 rad

**Undulator:** n harmonic max = 99

Tuning type = fixed gap

l aperture = 2076.53 cm

dx aperture = 0.07 cm

dz aperture = 0.07 cm

#1

**Screen:** Is absorbing[1] = no

**Shape:** Thickness = 0 cm

#2 Filter

**Screen:** Is absorbing[1] = yes

Is absorbing[2] = yes

Molecular formula[1] = C

Molecular formula[2] = C

Mass density[1] = 3.5 g/cm^3

Mass density[2] = 3.5 g/cm^3

Thickness[1] = 0.06 cm

Thickness[2] = 0.04 cm

**Shape:** Thickness = 0 cm

### #3 BS

**Crystal:** Structure type = zinblend

Lattice constant[1] = 3.567 Angstrom  
Lattice constant[2] = 3.567 Angstrom  
Lattice constant[3] = 3.567 Angstrom  
Debye Waller factor = 1  
Is absorbing = yes  
Is asymmetric = no  
Is inclined = no  
Is Johansson geometry = no  
Is mosaic = no

**Geometry:** Is thin = yes

Tune automatic = no

**Shape:** Thickness = 0.01 cm

**Boundary:** Type = rectangle

x rim = 0.5 cm  
y rim = 0.5 cm

**Surface:** Is rough = no

**FEA:** Design type = type specific

Crystal design = laue with cooling loop  
Is isotropic = no  
Angle x = 0 deg  
Angle y = 0 deg  
Angle z = 0 deg  
Mass density = 3.516 g/cm<sup>3</sup>

**Heat:** Heat transfer type[1] = insulated

Heat transfer type[2] = heat transfer  
Heat transfer type[3] = insulated  
Heat transfer type[4] = insulated  
Heat transfer type[5] = heat transfer  
Heat transfer type[6] = flux  
Heat transfer type[7] = insulated  
Heat transfer type[8] = heat transfer  
Heat transfer type[9] = heat sink  
Heat transfer coefficient = 1 W/(cm<sup>2</sup>K)  
Heat sink coefficient = 10 W/(cm<sup>2</sup>K)  
T reference = 293.15 K  
T cooling = 293.15 K  
Heat capacity = 0.54 J/(gK)  
Thermal conductivity[1] = 25 W/(cmK<sup>n</sup>)

**Stress and strain:** Constraint[1] = free  
 Constraint[2] = kinematic  
 Constraint[3] = free  
 Constraint[4] = free  
 Constraint[5] = free  
 Constraint[6] = free  
 Constraint[7] = free  
 Constraint[8] = free  
 Constraint[9] = free  
 Thermal expansion tensor[1] = 1.1E-06 1/K  
 Thermal expansion tensor[2] = 1.1E-06 1/K  
 Thermal expansion tensor[3] = 1.1E-06 1/K  
 Thermal expansion tensor[4] = 0 1/K  
 Thermal expansion tensor[5] = 0 1/K  
 Thermal expansion tensor[6] = 0 1/K  
 Stiffness tensor(1)(1) = 1.07861E+12 Pa  
 Stiffness tensor(2)[1] = 1.2663E+11 Pa  
 Stiffness tensor(2)[2] = 1.07861E+12 Pa  
 Stiffness tensor(3)[1] = 1.2663E+11 Pa  
 Stiffness tensor(3)[2] = 1.2663E+11 Pa  
 Stiffness tensor(3)[3] = 1.07861E+12 Pa  
 Stiffness tensor(4)[1] = 0 Pa  
 Stiffness tensor(4)[2] = 0 Pa  
 Stiffness tensor(4)[3] = 0 Pa  
 Stiffness tensor(4)[4] = 5.7756E+11 Pa  
 Stiffness tensor(5)[1] = 0 Pa  
 Stiffness tensor(5)[2] = 0 Pa  
 Stiffness tensor(5)[3] = 0 Pa  
 Stiffness tensor(5)[4] = 0 Pa  
 Stiffness tensor(5)[5] = 5.7756E+11 Pa  
 Stiffness tensor(6)[1] = 0 Pa  
 Stiffness tensor(6)[2] = 0 Pa  
 Stiffness tensor(6)[3] = 0 Pa  
 Stiffness tensor(6)[4] = 0 Pa  
 Stiffness tensor(6)[5] = 0 Pa  
 Stiffness tensor(6)[6] = 5.7756E+11 Pa

#### #4 CM2

**Crystal:** Structure type = zinblend  
 Lattice constant[1] = 3.567 Angstrom  
 Lattice constant[2] = 3.567 Angstrom  
 Lattice constant[3] = 3.567 Angstrom  
 Debye Waller factor = 1  
 Is absorbing = yes  
 Is asymmetric = no  
 Is inclined = no  
 Is Johansson geometry = no  
 Is mosaic = no

**Geometry:** Is thin = no  
 Tune automatic = no

**Boundary:** Type = none

**Surface:** Is rough = no

### #5 CRL1a

**Dielectric:** Reflectivity type = polarisation

Is constant = no

Mass density = 1.85 g/cm<sup>3</sup>

**Geometry:** g = 3150 cm

b = 250 cm

Is thin = yes

n clones = 5

Focus automatically = no

**Shape:** Defined by = user

Is convex = no

Is extruded = no

Radius = 0.01 cm

Thickness = 0.005 cm

**Boundary:** Type = ellipse

**Parabola:** Is source in infinity = no

p semi = 0.01 cm

**Surface:** Is rough = no

### #6 CRL1b

**Dielectric:** Reflectivity type = polarisation

Is constant = yes

delta refraction = 0

beta absorption = 0

**Geometry:** g = 3150 cm

b = 250 cm

Is thin = yes

n clones = 5

Focus automatically = no

**Shape:** Defined by = user

Is convex = yes

Is extruded = no

Radius = 0.01 cm

Thickness = 0.005 cm

**Boundary:** Type = ellipse

**Parabola:** Is source in infinity = no  
p semi = 0.01 cm

**Surface:** Is rough = no

### #7 CRL2a

**Dielectric:** Reflectivity type = polarisation  
Is constant = no  
Mass density = 1.85 g/cm<sup>3</sup>

**Geometry:** g = -255 cm  
b = 240 cm  
Is thin = yes  
n clones = 6  
Focus automatically = no

**Shape:** Defined by = user  
Is convex = no  
Is extruded = yes  
Radius = 0.02 cm  
Thickness = 0.005 cm

**Boundary:** Type = rectangle

**Parabola:** Is source in infinity = no  
p semi = 0.02 cm

**Extruded:** Angle z = 0 deg

**Surface:** Is rough = no

### #8 CRL2b

**Dielectric:** Reflectivity type = polarisation  
Is constant = yes  
delta refraction = 0  
beta absorption = 0

**Geometry:** g = -255 cm  
b = 240 cm  
Is thin = yes  
n clones = 6  
Focus automatically = no

**Shape:** Defined by = user

Is convex = yes

Is extruded = yes

Radius = 0.02 cm

Thickness = 0.005 cm

**Boundary:** Type = rectangle

**Parabola:** Is source in infinity = no

p semi = 0.02 cm

**Extruded:** Angle z = 0 deg

**Surface:** Is rough = no

### #9 sample

**Screen:** Is absorbing[1] = no

Is absorbing[2] = no

Is absorbing[3] = no

Is absorbing[4] = no

Is absorbing[5] = no

Is absorbing[6] = no

Is absorbing[7] = no

Is absorbing[8] = no

Is absorbing[9] = no

Is absorbing[10] = no

**Shape:** Thickness = 0 cm

# Chapter 59

## Parameter scan cases

There are three cases in total. Case #1 is simply a repetition of the focusing scheme test in case #4 from section 40, i.e. using the 9th undulator harmonic the setup is designed for. Its purpose is to make comparison with the following cases easier. Case #2 and #3 use the same optical setup but with the diamond 333 reflection and the 27th harmonic instead, thus providing the higher harmonic contamination. Case #3 differs from case #2 in that the pitch of the second diamond crystal is misaligned by just one microradian from perfect parallelism. This is in order to see how sensitive the high harmonic contamination is to very specific – and somewhat unrealistic – conditions.

Case	Bandwidth	Miller_indices(1)_03	dangle_x_04 deg	Miller_indices(1)_04	E_max eV	E_min eV	E_step eV	Has_slope_error
1	0.0005	1	0	1	23500.0	20000.0	100	no
2	0.001	3	0	3	70500.0	60000.0	300	no
3	0.001	3	0.0000573	3	70500.0	60000.0	300	no

Table 59.1: Parameter values for different cases in parameter scan

### Legend

**Case:** Case number in parameter scan

**Bandwidth:** Band.Bandwidth (Bandwidth that should be covered by ray tracing.

It should be large enough to fill out the throughput of your monochromator. For a Si111 double crystal monochromator this could be 0.0002. For a multilayer or a grating monochromator it should be something considerably larger. In the ray-tracing, twice the width is actually used. Hence, using the Darwin width covers probably most of the photons. Nowadays, I do not like this doubling, as it is in-transparent, but keep it for the sake of continuity.)

**Miller\_indices(1)\_03:** Optical\_element\_#3.Type.Crystal.Miller\_indices(1) (Miller indices of crystal reflection.)

**dangle\_x\_04:** Optical\_element\_#4.Move.Source.dangle\_x (Source rotation angle around x-axis (ccw).)

**Miller\_indices(1)\_04:** Optical\_element\_#4.Type.Crystal.Miller\_indices(1) (Miller indices of crystal reflection.)

**E\_max:** Scan.E\_max (Highest photon energy in scan.)

**E\_min:** Scan.E\_min (Smallest photon energy in scan.)

**E\_step:** Scan.E\_step (Energy scan step.)

**Has\_slope\_error\_03:** Optical\_element\_#3.Surface.Has\_slope\_error (Has surface slope error?)

**b\_05:** Optical\_element\_#5.Geometry.b (Distance from optical element's pole to meridional image focus.)

**b\_06:** Optical\_element\_#6.Geometry.b (Distance from optical element's pole to meridional image focus.)

**g\_07:** Optical\_element\_#7.Geometry.g (Distance btw. meridional object focus and optical element's pole.)

**g\_08:** Optical\_element\_#8.Geometry.g (Distance btw. meridional object focus and optical element's pole.)

# Chapter 60

## Photon energy scan

The  $K_y$ -values in the table below are those for optimized flux in the 7th harmonic between 15.6 and 18.3 keV used by the DanMAX main branch. The number of 2D and 1D focusing lens elements needed for the required beam properties in the SinCrys side branch for the 9th harmonic are provided, too.

E eV	K_y	n_harm/step	theta_i03 deg	theta_r03 deg	theta_i04 deg	nMult_05	nMult_07
<b>20000</b>	1.67551	9	81.3428	81.3428	81.3428	16	7
<b>20100</b>	1.66836	9	81.3862	81.3862	81.3862	16	7
<b>20200</b>	1.66125	9	81.4291	81.4291	81.4291	16	7
<b>20300</b>	1.65418	9	81.4717	81.4717	81.4717	17	7
<b>20400</b>	1.64714	9	81.5138	81.5138	81.5138	17	7
<b>20500</b>	1.64015	9	81.5555	81.5555	81.5555	17	7
<b>20600</b>	1.63319	9	81.5968	81.5968	81.5968	17	7
<b>20700</b>	1.62628	9	81.6377	81.6377	81.6377	17	7
<b>20800</b>	1.6194	9	81.6782	81.6782	81.6782	17	8
<b>20900</b>	1.61255	9	81.7182	81.7182	81.7182	18	8
<b>21000</b>	1.60575	9	81.758	81.758	81.758	18	8
<b>21100</b>	1.59898	9	81.7973	81.7973	81.7973	18	8
<b>21200</b>	1.59224	9	81.8363	81.8363	81.8363	18	8
<b>21300</b>	1.58554	9	81.8748	81.8748	81.8748	18	8
<b>21400</b>	1.57887	9	81.9131	81.9131	81.9131	18	8
<b>21500</b>	1.57224	9	81.9509	81.9509	81.9509	19	8
<b>21600</b>	1.56564	9	81.9884	81.9884	81.9884	19	8
<b>21700</b>	1.55908	9	82.0256	82.0256	82.0256	19	8
<b>21800</b>	1.55255	9	82.0624	82.0624	82.0624	19	8
<b>21900</b>	1.54605	9	82.0989	82.0989	82.0989	19	8
<b>22000</b>	1.53958	9	82.135	82.135	82.135	20	8
<b>22100</b>	1.53315	9	82.1708	82.1708	82.1708	20	9
<b>22200</b>	1.52674	9	82.2063	82.2063	82.2063	20	9
<b>22300</b>	1.52037	9	82.2415	82.2415	82.2415	20	9
<b>22400</b>	1.51402	9	82.2763	82.2763	82.2763	20	9
<b>22500</b>	1.50771	9	82.3109	82.3109	82.3109	20	9
<b>22600</b>	1.50143	9	82.3451	82.3451	82.3451	21	9
<b>22700</b>	1.49517	9	82.379	82.379	82.379	21	9
<b>22800</b>	1.48895	9	82.4127	82.4127	82.4127	21	9
<b>22900</b>	1.48275	9	82.446	82.446	82.446	21	9
<b>23000</b>	1.47658	9	82.479	82.479	82.479	21	9
<b>23100</b>	1.47044	9	82.5117	82.5117	82.5117	22	9
<b>23200</b>	1.46433	9	82.5442	82.5442	82.5442	22	9
<b>23300</b>	1.45824	9	82.5764	82.5764	82.5764	22	9
<b>23400</b>	1.45218	9	82.6083	82.6083	82.6083	22	10
<b>23500</b>	1.44615	9	82.6399	82.6399	82.6399	22	10

Table 60.1: Scan values for different photon energies in energy scan

## Legend

**E:** photon energy

**K\_y:** deflection parameter for vertical field component of insertion device

**n\_harm/step:** number of undulator harmonic or number of energy slot for continuous source (e.g. wiggler)

**theta\_i03:** Optical\_element\_#3.Geometry.angle\_incident (Incidence angle w.r.t. surface normal defining optical axis.)

**theta\_r03:** Optical\_element\_#3.Geometry.angle\_reflect (Reflection angle w.r.t. surface normal.)

**theta\_i04:** Optical\_element\_#4.Geometry.angle\_incident (Incidence angle w.r.t. surface normal defining optical axis.)

**nMult\_05:** Optical\_element\_#5.Geometry.n\_clones (Clone optical element 'nMult' times.)

**nMult\_07:** Optical\_element\_#7.Geometry.n\_clones (Clone optical element 'nMult' times.)

# Chapter 61

## Plots

### 61.1 Flux at sample position with higher harmonic contamination

```
"fig/High_harm_C111_Bragg/plot001.png" Lbl.:High_harm_C111_Bragg_2d_plot_I_int_focstatavg_oe09
```

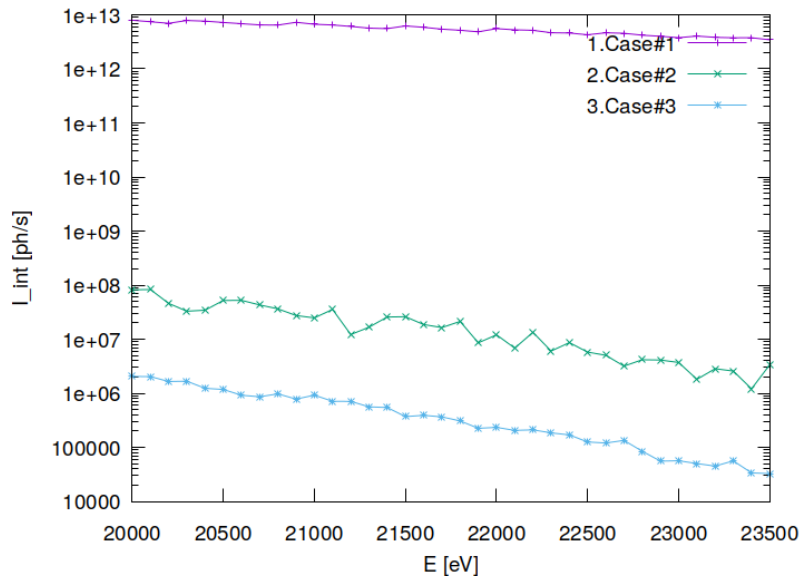


Figure 61.1: Photon flux in beam cross section of optical element #09 (sample). Case #1 represents the useful signal from the undulator's 9th harmonic. Case #2 and #3 are the higher harmonic contaminations with perfect alignment and with a relative misalignment by one microradian respectively. The photon energy in the abscissa of the higher harmonic curve has been divided by three to match that of the useful signal from the 9th undulator harmonic.

# Chapter 62

## Discussion of results

### 62.1 Beam splitter in Laue geometry

The high harmonic contamination from the 27th undulator harmonic reflected twice via diamond 333, first in Laue geometry and a second time in Bragg geometry, is exceptionally low. It is by eight orders of magnitude lower than the signal from the 9th undulator harmonic. Explanation are the slightly different refraction corrections to the deflection angles at the two consecutive diamond crystals, due to their different asymmetry. The diamond 333 rocking curve at 60 keV is narrower than half a microradians. Therefore even small angular deviations prevent their overlap.

Tweaking the pitch of the second diamond crystal in order to reinstate overlap increases high harmonic throughput to a similar level than with two crystals in identical geometry, like e.g. twice symmetrical Bragg geometry in the following section. This would be of course counter productive, as it would not only increase high harmonic contamination but would also deteriorate overlap of the diamond 111 rocking curves for the useful signal.

### 62.2 Beam splitter in Bragg geometry

High harmonic contamination for two perfectly aligned diamond crystals in symmetric Bragg geometry is down by five orders of magnitude in comparison to the useful signal. In reality it will be most likely even weaker. As the diamond 333 rocking curve width is smaller than half a microradian the two consecutive diamond crystals would need to be aligned with respect to each other with an accuracy better than that in order to match the high harmonic throughput of the model. This is shown in case #3, where a relative misalignment of the pitch angles between first and second crystal of just one microradian makes the high harmonic contamination weaker by another two orders of magnitude.

# Bibliography

- [1] Hyperphysics, hosted by the Department of Physics and Astronomy at Georgia State University, 2021. <http://hyperphysics.phy-astr.gsu.edu/hbase/hframe.html>.
- [2] Inscribed angle, 2022. [https://en.wikipedia.org/wiki/Inscribed\\_angle](https://en.wikipedia.org/wiki/Inscribed_angle).
- [3] Sweden Comsol AB, Stockholm. Comsol Multiphysics, 2014. <http://www.comsol.com/>.
- [4] P. Elleaume. Optimization of compound refractive lenses for x-rays. *Nucl. Inst. Meth. Phys. Res. A*, 412:483–506, 1998.
- [5] Jack Philip Holman. *Heat Transfer (SI Units)*. McGraw Hill, 2008.
- [6] Frank P. Incropera and David P. DeWitt. *Fundamentals of Heat and Mass Transfer*. Hoboken: Wiley, 5th edition, 2002.
- [7] Bruno Lengeler, Christian Schroer, Johannes Tümmler, Boris Benner, Matthias Richwin, Anatoly Snigirev, Irina Snigirevab, and Michael Drakopoulos. Imaging by parabolic refractive lenses in the hard x-ray range. *J. Synchrotron Rad.*, 6:1153–67, 1999.
- [8] C.B. Mammen, T. Ursby, M. Thunnissen, and J. Als-Nielsen. Bent diamond crystals and multilayer based optics at the new 5-station protein crystallography beamline Cassiopeia at max-lab. *AIP Conf.Proc.*, 705:808–811, 2004.
- [9] J.R. Meyer-Arendt. *Introduction to Classical and Modern Optics*. Prentice Hall, 1989.
- [10] A.G. Michette and C.J. Buckley, editors. *X-ray science and technology*. Institute of Physics Publishing, Bristol and Philadelphia, 1 edition, 1993.
- [11] Gregory Nelis and Sanford Klein. *Heat Transfer*. Cambridge University Press New York, 2009.
- [12] J.F. Nye. *Physical properties of crystals*. Oxford University Press, 1957.
- [13] H. Onuki and P. Elleaume, editors. *Undulators, wigglers and their applications*. Taylor & Francis Inc., London, New York, 2003.
- [14] M. Necati Özisik. *Heat Conduction*. Wiley, John & Sons, Inc, 1993.
- [15] Manuel Sanchez del Rio, Niccolo Canestrari, Fan Jiangc, and Franco Cerrina. Shadow3: a new version of the synchrotron x-ray optics modelling package. *J. Synchrotron Rad.*, 18:708–16, 2011.

- [16] S. Stoupin, S. A. Terentyev, V. D. Blank, Yu. V. Shvyd'ko, K. Goetze, L. Assoufid, S. N. Polyakov, M. S. Kuznetsov, N. V. Kornilov, J. Katsoudas, R. Alonso-Mori, M. Chollet, Y. Feng, J. M. Glownia, H. Lemke, A. Robert, M. Sikorski, S. Song, and D. Zhu. All-diamond optical assemblies for a beam-multiplexing x-ray monochromator at the linac coherent light source. *J.Appl.Crystallography*, 47(4):1329–1336, 2014.
- [17] S. Sundin, M. Bässler, R. Deneche, M. Weiss, P. Väterlein, A. Nilsson, and S. Svensson. Imaging properties of beam line optics for undulator based third generation synchrotron facilities. *Rev.Sci.Instrum.*, 70:14, 1999.
- [18] H.U. Svedrup, M.W. Johnson, and R.H. Fleming. *The Oceans Their Physics, Chemistry and General Biology*. Prentice Hall, New York, 1942.
- [19] T. Tanaka and H. Kitamura. Spectra – a synchrotron radiation calculation code. *J. Synchrotron Radiation*, 8:1221, 2001.
- [20] S. Wakatsuki, H. Belrhali, E.P. Mitchell, W.P. Burmeister, S.M. McSweeney, R. Kahn, D. Bourgeois, M. Yao, T. Tomizakia, and P. Theveneau. ID14 ‘Quadriga’, a beamline for protein crystallography at the ESRF. *J.Synchrotron Rad.*, 5:215–221, 1998.